Constraining New Physics with Colliders and Neutrinos

Chen Sun

Dissertation submitted to the Faculty of the
Virginia Polytechnic Institute and State University
in partial fulfillment of the requirements for the degree of

Doctor of Philosophy
in
Physics

Tatsu Takeuchi, Chair
Djordje Minic
Leo Piilonen
Eric Sharpe

May 12, 2017
Blacksburg, Virginia

Keywords: New Physics, Collider, Neutrino, Noncommutative Geometry

Constraining New Physics with Neutrino and Collider

Chen Sun

(ABSTRACT)

In this work, we examine how neutrino and collider experiments can each and together put constraints on new physics more stringently than ever. Constraints arise in three ways. First, possible new theoretical frameworks are reviewed and analyzed for the compatibility with collider experiments. We study alternate theories such as the superconnection formalism and non-commutative geometry (NCG) and show how these can be put to test, if any collider excess were to show up. In this case, we use the previous diboson and diphoton statistical excess as examples to do the analysis. Second, we parametrize low energy new physics in the neutrino sector in terms of non-standard interactions (NSI), which are constrained by past and proposed future neutrino experiments. As an example, we show the capability of resolving such NSI with the OscSNS, a detector proposed for Oak Ridge National Lab and derive interesting new constraints on NSI at very low energy ($\lesssim 50$ MeV). Apart from this, in order to better understand the NSI matter effect in long baseline experiments such as the future DUNE experiment, we derive a new compact formula to describe the effect analytically, which provides a clear physical picture of our understanding of the NSI matter effect compared to numerical computations. Last, we discuss the possibility of combining neutrino and collider data to get a better understanding of where the new physics is hidden. In particular, we study a model that produces sizable NSI to show how they can be constrained by past collider data, which covers a distinct region of the model parameter space from the DUNE experiment. In combining the two, we show that neutrino experiments are complementary to collider searches in ruling out models such as the ones that utilize a light mediator particle. More general procedures in constructing such models relevant to neutrino experiments are also described.

This work was partially support by U.S. Department of Energy grant DE-FG05-92ER40677, task A, by Virginia Tech Sigma Xi PhD Research Award, and by the Clayton D. Williams Graduate Fellowship in Theoretical Physics, Virginia Tech.

Constraining New Physics with Neutrino and Collider

Chen Sun

(GENERAL AUDIENCE ABSTRACT)

As we know, all matter in our daily life is made of particles called atoms and molecules, which are in turn formed by subatomic particles: protons, neutrons, and electrons. If one further divides the former two with certain technology, such as using a proton collider to smash one into another, it goes to the regime of elementary particles. It is shown experimentally that all matter we know is made of elementary particles that cannot be further divided. They include quarks and leptons. Together with the force carrier particles (also called gauge bosons) and the Higgs scalar, they form the Standard Model of particle physics. In this work, we study the properties of elementary particles and the way they interact with each other that are different from the Standard Model predictions. We conduct the research study in the following two aspects: collider phenomena and neutrino phenomena. These two aspects cover the high energy regime of particle scattering process and low energy regime of neutrino propagation, which are two important sectors of great interest recently. As a result of the analysis, we discuss possible ways that the new physics is hidden yet can be detected with next generation experiments.

Dedication

TO MY PARENTS
for raising me to believe that anything was possible.

AND TO ZHULIN
for making everything possible.

Acknowledgments

I would like to thank my advisor, Prof. Tatsu Takeuchi. This work would not have been done without his continuous help and encouragement. When my research slows or even halts by unexpected difficulties, Prof. Takeuchi is always there to work it out with me, to guide me through details to see the big picture, as a mentor and also a reliable friend. During the years of studying with him, I learned much more than just physics expertise.

I am grateful for insightful discussions with Prof. Djordje Minic on various advanced topics and physics history, on which I had little knowledge otherwise. In addition to the shared experience as a researcher, this exposure to real world research is valuable in helping me decide and plan my future career. Special thanks go to Profs. Lay Nam Chang and Patrick Huber, both of whom lent helping hands and gave me solid support during the time of job search. I am grateful for their wisdom on making choices, and the initiative to interact with people. I would also like to thank my committee members for reviewing this work in such a short notice and the comments for revision.

I would like to acknowledge the ideas and inspirations from communications with Profs. Sajib Agarwalla, Pilar Coloma, James Gray, Peter Haskell, Yee Kao, Cecilia Lunardini, Irina Mocioiu, Leo Piilonen, Eric Sharpe, Uwe Täuber, Devin Walker, and Hanqing Zheng. In particular, I appreciate the advice received from Prof. Kyungwha Park, which paved my way to finishing the study.

Among the students and research fellows, I would like to thank Ufuk Aydemir, Sofiane Boucenna, John Cherry, David Forero, Xin Gao, Wei Gu, Yun Jiang, Vishvas Pandey, Graham White, and Zhong-Zhi Xianyu for productive discussions over the years on topics we either agreed upon or not. I am grateful for the help from Jirui Guo during the beginning years of Ph.D. study and stimulating discussions and friendship with Ron Wu.

Last but definitely not least, I would like to express my gratitude for my family. I would not be pursuing my dream without the understanding from my parents, nor would I be making progress toward it without the support from my wife. You make my world a meaningful and colorful place to live in.

Contents

List of Figures

List of Tables

Introduction

After decades of experimentation, the Standard Model (SM) of particle physics is verified to unprecedented precision. At this point, two questions remain particularly intriguing. 1) In which sector might new physics be hidden? 2) What principle requires the SM to be a gauge theory of the given form with the observed parameters? For the first question, the neutrino sector has large uncertainty in regards to determining the SM parameters due to the nature of the weak interaction. A thorough study of these parameters and the possible non-standard interaction (NSI) is crucial for any constraints or probes of physics beyond the SM. However, for the second question, although the gauge field theory framework is verified by data from various experiments during the past few decades, the fundamental reason that fixes the SM to the specific form we observe remains unexplained. For example, it is not understood what theory fixes the boundary value of Yukawa couplings; what the source of baryon asymmetry of the universe is; why the gauge group is chosen to be $U(1) \times SU(2) \times SU(3)$; how the hypercharge is quantized, which in turn leads to anomaly cancellation; what principle determines the number of families of fermionic particles; and whether the SM Higgs is the only scalar responsible for spontaneous symmetry breaking (SSB). In short, an understanding of the principle that dictates the SM does not yet exist. On the other hand, although the origin of the SM remains unclear, past attempts show that an arbitrary modification of the SM will likely cause problems either experimentally or theoretically, which hints for the existence of a fundamental theory that leads to the SM.

At this point, a different perspective may provide us with new insights that are not available with conventional approaches. Different from most formal theories, as a reformulation of the SM in terms of geometry, noncommutative geometry (NCG) provides a new way of looking at the SM while building directly upon low energy particle data. Because of its geometric structure, this approach leads to more restrictive model building than other approaches, and implicitly proposes some relations between different sectors, relations which are not visible in the SM itself. In addition, because the geometry is built directly on particle data, models derived from NCG usually share specific collider signatures. Therefore, a good understanding of the collider data may help us understand the structure of new physics and finally shed some light on the origin of the SM.

With two sets of data, one from neutrino experiments and the other from collider experiments, one may ask how to combine them to get extra information which otherwise would

remain obscure. In particular, whenever a new particle model is proposed, one should be able to constrain the new model with both sets of particle data. To address this question, an example is worked out explicitly. Our message is that, even from a practical viewpoint, particle models motivated by specific problems should still be tested with all available data. In particular, collider experiments put strong bound on models that predict sizable NSI. As a result, it is non-trivial to build a model that generate flavor changing NSI large enough to be observed at long baseline neutrino experiments such as DUNE using light mediator particles, while it survives all the current bounds from particle data. In this analysis, we list possible constraints for such model building for future reference.

To summarize, in this work constraints on new physics are studied from two directions: neutrino measurements and collider signals. On the collider side we consider the signature of physics from exotic structures, e.g., NCG; on the neutrino side, we study constraints on the NSI. In the end, we use collider data to constrain neutrino models. Data from complementary sources such as current and future colliders and long-baseline neutrino experiments will guide future model building.

The rest of the thesis is organized as follows. In Part I, collider experiments are applied to constrain NCG-motivated models. In Chapters 2 and 3, collider signatures of superconnections and NCG motivated models are discussed. In each chapter we start with a brief review on the superconnection formalism and the NCG respectively. Without going into details of the formalism, we investigate the phenomenological consequences based on each approach, and compare with current bounds from various process. Inspired by the previous statistical excess from LHC, Chapter 4 serves as an example of using collider signals to test such NCG motivated models. In Part II, neutrino experiments are studied to constrain NSI. In Chapter 6, a previously-proposed neutrino detector, OscSNS at Oak Ridge National Lab is studied. Constraints on ε_{ee} are worked out explicitly based on the proposal. In Chapter 7, an analytic way to understand the neutrino matter effect in the presence of $\varepsilon_{\mu\tau}$ NSI is proposed. As a check of the validity of the formula, it is demonstrated how to use it to understand the NSI matter effect at long-baseline neutrino experiments such as DUNE. In Chapter 8 of Part III, we list some of the models that reproduce sizable NSI. We investigate the constraints on one particular model and show the relevant channels for model building of this type.

Part I

Constraining New Physics with Collider Experiments

Chapter 1

Evidence for the Standard Model and Beyond

1.1 The Standard Model and Why We Believe It

Although we still have a lot of unanswered questions such as the solution of QCD at low energy [10–15] and naturalness of the SM [16–20], etc., the SM packaged in effective field theory (EFT) [21–25] language is verified to high precision at low energy. We will elaborate on the SM, after first explaining what it means to verify a theory.

Any theory comes with a certain number of free parameters as input and makes predictions of certain number of observables as output. The difference of these two numbers[1] describes the predictive power. If one is not concerned about the predictive power of the theory but only cares about the viability of the theory, he/she can cook up a theory with infinite free parameters so that, in principle, this theory can accommodate any experimental outcome – it works as the 'theory of everything'. However, in reality a theory like that requires infinitely many terms to describe thus will take infinite amount of time to reach. To make it worse, the number of free parameters being infinity makes the theory neither falsifiable nor able to predict anything; hence, it cannot be counted as a real theory in the context of science.

With a finite number of free parameters and a finite number of observables, a theory expresses the latter in terms of the former. In a simplified situation, if each experiment measures one observable, we need P independent measurements to determine the theory with P free parameters. Suppose the theory predicts O independent observables; if $O > P$, it is possible to over-constrain the theory with independent experiments. In this case we say the theory is *verifiable*. In this case, we are able to fit the parameters of the theory with a set of P

[1] Actually we should only count the number of independent free parameters and observables. Therefore it is the difference in dimensions of the parameter space and the 'observable space' that amounts to the capability of making predictions.

observables and to make predictions for the remaining $(O - P)$ observables. By comparing these predictions with the independent measurement of each observable, we can either verify or rule out the theory. Equivalently, when $O > P$, what a theory does is to find P observables and express the $(O-P)$ variables in terms of them. Therefore, it is safe to think of a theory as a set of relations among observables. Whether it 'explains' the relations well is a philosophical question and we refrain ourselves from further discussion on it. In general, only verifiable theories ($O > P$) are of interest.

In the real world, verifiability is also limited by experimental conditions. At any certain point of time only certain experiments are complete, in progress, or being planned in the near future. Our ability to verify theories is thus limited by the experimental conditions. Therefore, we phenomenologists are more interested in the type of theories that can be verified with data from past, current or near-future experiments. The SM is a theory that is commonly believed for particle physics at or below a few TeV. To show why we believe the SM to be true, let us take the electroweak sector of the SM as an example.

The electroweak sector of SM is verified to a high precision by several precision measurements. In this sector, we have the following very well measured observables:

$$\hat{\alpha}, \hat{G}_F, \hat{m}_Z, \hat{m}_W, \hat{\Gamma}_{\ell^+\ell^-}, \hat{s}^2_{\text{eff}}, \text{etc...} \tag{1.1}$$

where they are, in order of appearance: the fine structure constant from $\gamma^* \to e^+e^-$, the Fermi constant from muon decay, the Z boson mass, the W boson mass, the leptonic partial width of Z boson, and the effective $\sin^2\theta_W$ from the left-right asymmetry $\hat{A}_{LR}$. For electroweak theory, we have three (most relevant) free parameters:

$$g, g', v, \tag{1.2}$$

viz., the $U(1)_Y$ coupling, $SU(2)_L$ coupling, and the vacuum expectation value (VEV) of the Standard Model (SM) Higgs. In electroweak analysis, it is easier to express two of these in terms of the QED coupling e and the weak angle θ_W by

$$\begin{aligned} e &\equiv \frac{gg'}{\sqrt{g^2 + g'^2}}, \\ s &\equiv \sin\theta_W = \frac{g'}{\sqrt{g^2 + g'^2}}, \end{aligned} \tag{1.3}$$

with v unchanged. The relation among the observables and the SM parameters, up to one

loop, are given as

$$
\begin{aligned}
(\hat{\alpha})^{th} &= \frac{e^2}{4\pi}\left[1+\frac{\Pi_{\gamma\gamma}(m_Z^2)}{m_Z^2}\right], \\
(\hat{G}_F)^{th} &= \frac{1}{\sqrt{2}v^2}\left[1-\frac{\Pi_{WW}(0)}{m_W^2}\right], \\
(\hat{m}_Z^2)^{th} &= \frac{e^2v^2}{4s^2c^2}+\Pi_{ZZ}(m_Z^2), \\
(\hat{m}_W^2)^{th} &= \frac{e^2v^2}{4s^2}+\Pi_{WW}(m_W^2), \\
(\hat{s}^2_{\rm eff})^{th} &= s^2 - sc\frac{\Pi_{\gamma Z}(m_Z^2)}{m_Z^2}, \\
(\hat{\Gamma}_{\ell^+\ell^-})^{th} &\approx \frac{e^2}{48\pi s^2c^2}m_Z\left(1+\frac{\Pi_{ZZ}(m_Z^2)}{2m_Z^2}\right) \\
&\quad\times\left[\left(-\frac{1}{2}+2s^2-2sc\frac{\Pi_{\gamma Z}(m_Z^2)}{m_Z^2}\right)^2+\frac{1}{4}\right]\left(1+\Pi'_{ZZ}(m_Z^2)\right),
\end{aligned}
\tag{1.4}
$$

where the parts involving a vacuum polarization amplitude Π are the one-loop corrections. In order to test the SM, we need to fit g, g', and v in terms of three of the observables, say $\hat{\alpha}, \hat{G}_F$, and $\hat{m}_Z^2$ [2], predict the remaining observables, and then compare the predictions with the measurements[3].

In Table 1.1, we show the measured and the SM-predicted values of a few observables. As we can see, the deviation between them is small in general, and the SM is verified to great precision. Part of this can also be seen from Fig. 1.2 of the uncertainty in the plane of Higgs mass vs the top-quark mass, which is verified by the discovery of Higgs boson [32, 33]. As a result, theoretically it is reasonable to ask about the origin of the SM. There are theoretical structures that beg for an explanation, such as what dictates the SM gauge group, whether the coupling constants of the three gauge sectors unify at a certain scale as hinted in Fig. 1.1, what guarantees the anomaly cancellation of the SM, without which the theory would be rendered invalid, etc. The structure of the SM seems unnatural if all of this is just a coincidence without further fundamental reasons [16–20]. This motivates a number of ingenious ideas perceived to explain the naturalness of the SM, which will be discussed in the next section.

[2] These three observables are usually chosen because of their small uncertainties.

[3] This is essentially using observables $\hat{\alpha}, \hat{G}_F$, and $\hat{m}_Z^2$ to express the rest of observables and check this relation predicted by the SM and measured by experiments. That is the reason that in literature such as Ref. [26–31] it is often mentioned to 'expression observables in terms of observables' to test the theory.

Quantity	Value	Standard Model	Pull
m_t [GeV]	173.34 ± 0.81	173.76 ± 0.76	-0.5
M_W [GeV]	80.387 ± 0.016	80.361 ± 0.006	1.6
	80.376 ± 0.033		0.4
Γ_W [GeV]	2.046 ± 0.049	2.089 ± 0.001	-0.9
	2.195 ± 0.083		1.3
M_H [GeV]	125.09 ± 0.24	125.11 ± 0.24	0.0
$g_V^{\nu e}$	-0.040 ± 0.015	-0.0397 ± 0.0002	0.0
$g_A^{\nu e}$	-0.507 ± 0.014	-0.5064	0.0
M_Z [GeV]	91.1876 ± 0.0021	91.1880 ± 0.0020	-0.2
Γ_Z [GeV]	2.4952 ± 0.0021	91.1880 ± 0.0020	0.4
$\Gamma(had)$ [GeV]	1.7444 ± 0.0020	1.7420 ± 0.0008	–
$\Gamma(inv)$ [MeV]	449.0 ± 1.5	501.66 ± 0.05	–
$\Gamma(\ell^+\ell^-)$ [MeV]	83.984 ± 0.086	83.995 ± 0.010	–

Table 1.1: Observables compared with the SM best fit predictions. Result is taken from PDG.

1.2 Energy vs. Intensity and What Has Been Attempted

According to the Wilsonian picture, in the IR limit the set of physically relevant operators is formed by normalizable operators whose mass dimension is lower than four. Any effects from higher dimensional operators are suppressed. Taking scalar theory as an example,

$$\mathcal{L} = \underbrace{\frac{1}{2}(\partial_\mu\phi)^2 - \frac{1}{2}m^2\phi^2 - \frac{\lambda_3}{3!}\phi^3 - \frac{\lambda_4}{4!}\phi^4}_{\mathcal{L}_{\text{renorm}}} + \underbrace{\sum_{n>4}\frac{\lambda_n}{n!}\frac{\phi^n}{\Lambda^{n-4}}}_{\mathcal{L}_{\text{non-renorm}}}, \tag{1.5}$$

where Λ is the cutoff of the theory. The non-renormalizable part of the Lagrangian gets suppressed by powers of $\frac{1}{\Lambda}$. To study the non-renormalizable part of the Lagrangian, experimentally two directions are pursued: One either goes to the high energy regime in the hope of resolving the non-renormalizable operator in terms of renormalizable pieces as suggested in Ref. [34–38], or one generates an enormous amount of data hoping to see the suppressed effect from the high-dimensional operators in $\mathcal{L}_{\text{non-renorm}}$ as attempted in Ref. [39–47]. These two directions correspond to the so-called 'energy frontier' and 'intensity frontier,' respectively. These two methods both played important roles in the history of particle physics: in 1934, Enrico Fermi proposed 'An attempt of a theory of beta radiation' in Ref. [48, 49], and 'characteristically swept what was unknowable at that time under the rug, and focused on what can be calculated.' [50] Because the energy scale at which the β decay happens is so low, the W propagator is impossible to resolve. Therefore, a contact interaction model that uses non-renormalizable high dimensional operators explains nuclear β decay to a good precision and inspired later studies on weak interaction and the proposal of $V-A$ structure.

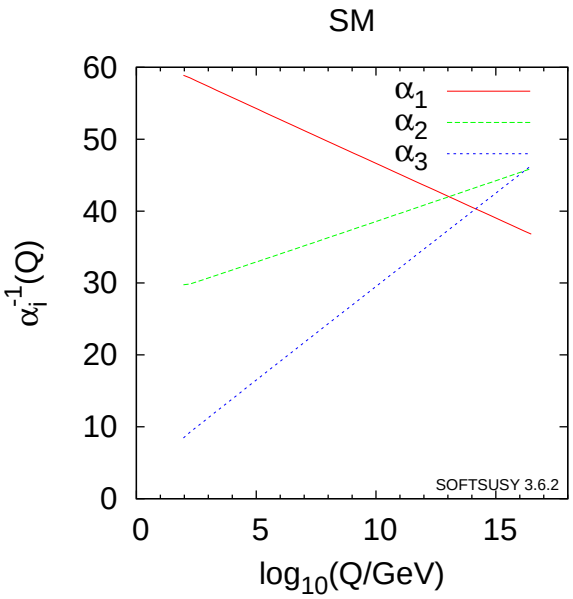

Figure 1.1: The running of the Standard Model gauge coupling. Plot is used with permission of PDG [1].

[51–53] It remains a nice approximation and a good tool for calculation until the modern formulation of gauge theory was proposed [54–56] and verified by the W and Z discoveries at CERN [57, 58].

Besides the success in gauge sector, another important part of the SM is the Yukawa interaction. A similar story happened in formulating the Yukawa interaction: it was proposed in 1935 by Hideki Yukawa [59] that the nuclear binding energy is dominated by exchanging a 'new' particle, the pion, where the energy potential characteristic length of the potential is interpreted as m_π^{-1}. By fitting data of the nuclei binding energy, one could estimate the mass of the pion, which was later verified by the discovery of the pion [60, 61], which is itself explained as a bound state of more fundamental particles – the quarks.

This motivates people to focus on the following 'standard' procedures of modeling new physics: a) describe the new physics in terms of high-dimensional operators such as in Ref. [62–77] and constrain these effective operators with data from experiments; or, b) construct models based on local quantum field theories to generate such operators and avoid the bounds from a), and maybe also provide features such as grand unification theory (GUT) and answers to the hierarchy problem, with examples such as SUSY [78–80]; small, large, or non-compact extra dimension [81–85]; conformity [86, 87]; technicolor [88–99]; and other paradigms [100]. However, with null observation of any above models, it revives a few interesting old questions rather than providing answers to them, namely

- Does grand unification occur?

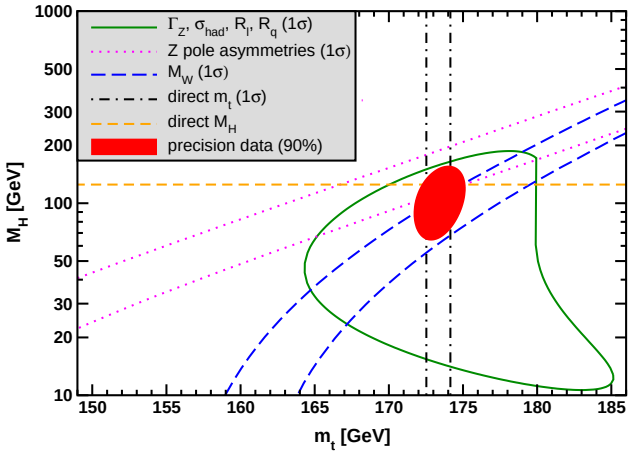

Figure 1.2: The fit result of (M_H, m_t) and one-standard deviation uncertainty, with various input. Plot is used with permission of PDG [1].

- Is the hierarchy problem a (well-defined) problem?
- If grand unification does occur and hierarchy problem is a real problem, then why do we not see the extra degrees of freedom after the breaking of the extra structure (e.g. GUT gauge fields, SUSY partners, etc.)?
- Without the number of extra degrees of freedom, how do we ever (elegantly) address the naturalness of the Higgs mass?

In this work, we take a different philosophy to address the questions raised above and the questions on the origin of the SM raised in section 1.1, which is to be elaborated in the next section.

1.3 Physics Beyond the Standard Model and Where to Find It

The aforementioned attempts are mostly based on the assumption that the new physics responsible for generating the SM and perhaps addressing the hierarchy problem and grand unification can also be described in terms of effective field theory. However, this is not necessarily true from either the experimental or the theoretical viewpoint. Although effective field theory works surprisingly well at the current energy scale, it is expected to break down ultimately due to the non-local effect of quantum gravity [101–119] and the breaking scale is $\Lambda_{NP} \lesssim \Lambda_{Pl}$. Therefore, there remains the possibility that the theory that describes the new physics above the scale Λ_{NP} is not a local quantum field theory, and below Λ_{NP} effective field theory works just fine.

According to the Wilsonian picture, there are two ways an 'advanced' theory above a certain scale controls the effective field theories below that scale: either through directly fixing the degrees of freedom below the cut off scale, i.e., affecting the renormalization group equation (RGE); or by imposing boundary conditions of the RGE. Since effective field theory works well below Λ_{NP} and the structure is fairly rigid against arbitrary modifications, it must be determined in both ways.

In this scenario, the effect of the new physics above Λ_{NP} is not described by local operators nor usual renormalization group equation (RGE) flow. As a consequence, the non-renormalizable effective operators below Λ_{NP} is not a direct result of any local operators above Λ_{NP}. This is no longer an analog of, say, resolving Fermi interaction in terms of the W propagator. As a result, a theory built in this fashion usually does not have the large number of extra degrees of freedom as in SUSY or $SU(5)/SO(10)$ GUT theories, where the extra degrees of freedom below Λ_{NP} are inevitable since the theory above Λ_{NP} is a local quantum field theory and the degrees of freedom just propagate through Λ_{NP}. This is not true in our case.

Now that new physics does not manifest itself through a direct generation of local operators below Λ_{NP}, the only way it controls low energy effective field theory is via the boundary relations imposed at Λ_{NP}. Given the evidence of the SM being so robust against any modification at the electroweak (EW) scale and the almost unification of the coupling constants at some higher scale as shown in Fig. 1.1, we conjecture that the boundary condition[4] at Λ_{NP} is the SM spectrum itself with a GUT relation, plus a minimal extension in order to reconcile the GUT relation with EW measurements at low energy. In this context, the questions raised in section 1.1 and section 1.2 indicate answers to each other: the robustness of the SM against modifications with arbitrary local quantum field operators hints at a theory that may not be Wilsonian, which is why we do not observe the extra degrees of freedom inherited from any local field theory extension. On the other hand, because of the lack of observation of extra quantum field theoretical degrees of freedom, the advanced theory can only dictates the low energy theory through some boundary relation, which itself is the SM up to a minimal extension at a certain scale. We call this picture a *quasi-desert* picture.

To summarize, here is the logic we follow. Being an effective theory, the SM plus any extension can only be explained by the advanced theory from which it is derived. In the past, the full theory is conjectured to be also a local quantum field theory; therefore, a large number of degrees of freedom propagate into the SM as an extension to it. Due to the null observation of any of these degrees of freedom, we provide a picture different from the above one. Instead of having the full theory as another local quantum field theory, we argue that it is possible the theory above Λ_{NP} is not fully describable in terms of local quantum operators. Thus new physics manifests itself only through a set of relations dictated at Λ_{NP}, i.e., the SM-like spectrum plus the GUT relation. As a result, we can predict the extra degrees of

[4]We take the broader meaning of boundary condition as a constraint imposed at a certain scale, which is not necessarily a formal boundary condition of a differential equation.

freedom we need to maintain the compatibility between the GUT relation at $\Lambda_{NP} \lesssim \Lambda_{Pl}$ and the low energy phenomena at Λ_{EW}. Please note that, in this picture, the GUT relation is not the result of a local quantum field theory with GUT gauge group. Instead, it is the result of the theory above Λ_{NP}. We can therefore look at theories below Λ_{NP} that contains SM but do not have a GUT gauge group since the GUT gauge group itself is no longer the reason of the unification.

1.4 Noncommutative Theories as a Framework for Potential Candidates

To understand possible candidate theories above Λ_{NP}, let us look at the requirement we have so far. Because of the non-locality due to aforementioned quantum gravity effects and the possible breakdown of effective field theory, the full theory above Λ_{NP} is unknown. However, just as the Fermi interaction provides a good low energy approximation of the weak interaction, the theory that approximates the full theory should at least share some features of the full theory, such as non-locality. On the other hand, as we discussed it should give a SM-like spectrum as the boundary condition, which includes the GUT relation, anomaly cancellation, a different way of looking at the hierarchy problem, and an indication of the extension needed to achieve the above. As examples, we try two theories here: the super-connection formalism and the NCG, both of which share a non-commutative nature and accommodate the particle spectrum of the SM yet provide interesting boundary conditions for the coupling constants. In addition, both indicate a left-right symmetric completion of the SM as the extension to maintain the compatibility between the boundary conditions and the low energy phenomena. With details to be discussed at length in the following chapters, we briefly summarize the features of these two theories.

The super-connection formalism is applied to non-supersymmetric particle physics in Ref. [120–146]. Although it resembles usual gauge theories in many ways, the main differences are the following.

- Instead of being Lie-algebra valued, the connection is now valued in super Lie algebra, such as $su(2|1)$ or $su(2|2)$.
- A 'matrix derivative' is introduced due to the non-commutativity of the matrix basis, as an analog of the usual derivative. It is shown to be responsible for the spontaneous symmetry breaking.
- The SM Higgs field is part of the gauge field, in order to maintain the gauge invariance of terms involving the matrix derivative.
- The super-connection generates the usual Yang-Mills sector of the SM plus the Higgs potential.

- The super-connection only provides an emergent structure at a certain scale to encode the non-commutativity and the spectrum. It is an effective way of parametrizing our ignorance of new physics above Λ_{NP}. It does not necessarily lead to an extra symmetry. As a result, no redundant degrees of freedom are needed.
- As we articulated in previous sections, interesting boundary conditions for the gauge couplings are imposed.
- The proper prediction for the Higgs mass necessitates a minimal extension of the SM.

The NCG is applied to particle physics by Connes *et al.* in Ref. [147–156]. Similar to the super-connection formalism, NCG has the following features.

- Instead of using the super algebra to encode the non-commutativity, we use an almost commutative geometry defined by $\mathbb{C} \oplus \mathbb{H} \oplus M_3(\mathbb{C})$. Again, it does not directly lead to extra unobserved degrees of freedom but merely works as a framework at a certain scale to describe how physics above Λ_{NP} determines the effective field theory below it.
- The geometry related to $\mathbb{C} \oplus \mathbb{H} \oplus M_3(\mathbb{C})$ is interpreted physically as a structure with two sheets. In general, fermions of one chirality live on one sheet and fermions of the opposite chirality live on the other[5]. The sheet separation determines the electroweak scale. The discrete derivative resulting from the non-commutativity connects the two sheets.
- In addition to the ordinary Dirac operator, a matrix derivative is included. In order to retain gauge invariance of terms involving the discrete derivative, a gauge field in the discrete direction must be included, which serves as the Higgs field. Similarly, a regular gauge field is needed due to the regular derivative in the continuous direction. As a result, both the Higgs field and the (non-abelian) gauge fields are the result of non-commutativity.
- The GUT relation arises from the geometry.
- Because the Higgs and regular gauge fields are the results of gauge invariance in two different directions, the hierarchy problem is reformulated as relating the characteristic lengths in the discrete and continuous directions. This is similar to asking why the speed of light is $\sim 3 \times 10^8$ m/s in Minkowski spacetime, which is essentially a constant that relates the time and space directions.
- The NCG also provides extra relations beyond the SM such as a mass relation between the fermionic and bosonic sectors.

[5]This depends on how the spectrum is embedded and the specific representation being used. There are more complicated versions such as fermions living on one sheet and anti-fermions on the other. However, in this case there is no gauge field in the discrete direction, i.e., Majorana mass naturally remains a c-number until manually promoted to a field as in Refs. [2, 156].

- It seems that the NCG dictates anomaly cancellation [142, 157, 158]. Whether this is a general feature of the NCG remains an open question worthy of future investigation.

Compared to the super-connection formalism, the algebraic structure of the connection is relaxed. There is no demand of the Higgs sector being part of a superalgebra. Also, the super traceless condition is replaced to regular traceless condition of $\mathbb{C}\oplus\mathbb{H}\oplus M_3(\mathbb{C})$ (unimodularity condition).

With the nice features of the super-connection and the NCG satisfying the requirements posed in section 1.3, we take the two approaches seriously and study the physics consequences of imposing such structures. Since the NP above Λ_{NP} is unknown and likely to require drastic modification of current theories, we mainly focus on the phenomenological aspects of such frameworks. We hope to shed light on possible ways of looking for NP and indications of modification of current theories. The rest of this part is organized as follows. Chapter 2 is dedicated to superconnection formalism and its physical interpretation, as well as its indication of a left-right completion. In Chapter 3, the collider signature of NCG by Connes *et al.* is studied. Chapter 4 serves as an example to show the restrictive feature of NCG and hint for new physics in case some collider signal shows up. This part is based on our published work in Refs. [159–161] and our in-preparation work in Ref. [162].

Chapter 2

Left-right symmetric model motivated by super-connection

In this chapter, we review the superconnection formalism and its application to particle physics as discussed in our work, Ref. [159] published in Physical Review D. The phenomenology bounds on the superconnection formalism are also discussed in length. In particular, we observe the necessity of including a matrix derivative and the effect of that in generating SSB. This hints at a geometric structure that fixes the SM particle spectrum at a certain scale.

2.1 Introduction to the Superconnection Formalism

2.1.1 A Brief Review

In Ref. [163], the authors investigated the possibility of reviving the superconnection formalism first discussed in 1979 by Ne'eman [164], Fairlie [165, 166], and others [167–169]. The original observation of Ne'eman was that the $SU(2)_L \times U(1)_Y$ gauge fields and the Higgs doublet in the SM could be embedded into a single $su(2/1)$ superconnection [170, 171] with the $SU(2)_L \times U(1)_Y$ gauge fields constituting the even part of the superconnection and the Higgs doublet ϕ constituting the odd part, to wit:

$$\mathcal{J} \;=\; i \begin{bmatrix} \mathcal{W} - \frac{1}{\sqrt{3}} B \cdot \mathbf{1}_{2\times 2} & \sqrt{2}\,\phi \\ \sqrt{2}\,\phi^\dagger & -\frac{2}{\sqrt{3}} B \end{bmatrix}, \tag{2.1}$$

where $\mathcal{W} = W_i \tau_i$. This embedding predicts $\sin^2\theta_W = 1/4$ as well as the Higgs quartic coupling, the latter leading to a prediction for the Higgs mass [172–174]. The leptons and quarks could also be embedded into irreducible representations of $su(2/1)$ [175–178], thereby

fixing their electroweak quantum numbers in a natural fashion. Fairlie started from a six-dimensional gauge-Higgs unified theory reduced to four dimensions and arrived at a similar observation.[1] Subsequently, suggestions have been made to incorporate QCD into the formalism by extending the superalgebra to $su(5/1)$ [180–182].

Though the appearance of the $su(2/1)$ superconnection suggested an underlying 'internal' $SU(2/1)$ supersymmetry, gauging this supersymmetry to obtain the superconnection proved problematic as discussed in Refs. [183, 184]. For instance, the Higgs doublet is a boson whereas an $SU(2/1)$ supersymmetry would demand the off-diagonal scalar components of the superconnection be fermionic with the wrong spin-statistics. Interpreting these degrees of freedom as ghosts would render the model non-unitary, and though attempts have been made to deal with this problem [185, 186] the issue has never been completely resolved. It is also clear that the quarks and leptons placed in $SU(2/1)$ representations cannot all be fermions [185, 187]. The $SU(2/1)$ supersymmetry must also be broken by hand to give the gauge boson kinetic terms the correct signs [188]. Due to these, and various other problems, interest in the approach waned.

2.1.2 Relation to Noncommutative Geometry

It was subsequently recognized, however, that the appearance of a superconnection does not necessarily require the involvement of the familiar boson↔fermion supersymmetry. This development follows the 1990 paper of Connes and Lott [147] who constructed a new description of the SM using the framework of noncommutative geometry (NCG) in which the Higgs doublet appears as part of the Yang-Mills field (i.e. connection) in a spacetime with a modified geometry. The full Yang-Mills field in this approach was described by a superconnection, the off-diagonal elements of which were required to be bosonic.

The NCG-superconnection approach to the SM was studied by many authors and a vast literature on the subject exists, *e.g.* Refs. [120–145] to give just a representative list.[2] Though these works differ from each other in detail, the basic premise is the same. The models are all of the Kaluza-Klein type in which the extra dimension is discrete and consists of only two points. In other words, the model spacetime consists of two $3+1$ dimensional 'branes.' In such a setup, the connection must be generalized to connect not just points within each brane, but also to bridge the gap between the two. If the left-handed fermions live on one brane and the right-handed fermions on the other, then the connections within each brane, *i.e.* the even part of the superconnection, will involve the usual SM gauge fields which couple to fermions of that chirality. In contrast, the connection across the gap, *i.e.* the odd part of the superconnection, connects fermions of opposite chirality and can be identified with the Higgs doublet.

[1] See also Ref. [179].

[2] See Ref. [146] for a collection of lectures from 1999 by various authors.

In this approach, both the even and odd parts of the superconnection are bosonic, the $\mathbb{Z}_2$-grading of the superalgebra resulting not from fermionic degrees of freedom but from the existence of the two 'branes' (on which the chirality γ_5 provides the $\mathbb{Z}_2$ grading operator), and the definition of the generalized exterior derivative d in the discrete direction.[3] That is, the superconnection emerges from the 'geometry' of the discrete extra dimension.

In algebraic geometry, the geometric properties of a manifold M are studied via the algebraic properties of the commutative algebra of smooth functions $C^\infty(M)$ defined on it. If this algebra is allowed to be noncommutative in general, one has a NCG [147–149, 152–156, 189, 190]. In the discrete extra dimension case, one usually starts with the algebra $\mathcal{A} = C^\infty(M) \otimes (\mathbb{C} \oplus \mathbb{H})$, and the fermions on the branes are required to lie in representations of this algebra. Gauge transformations correspond to the unitary inner automorphisms of the algebra,[4] which in this case is $U(1) \times SU(2)$. The exterior derivative d is defined via

$$d\alpha \;=\; [D, \alpha]_s \;, \qquad \alpha \in \mathcal{A} \;, \tag{2.2}$$

where $[\cdot, \cdot]_s$ is the super-commutator, and the operator D includes the usual exterior derivative acting on the $C^\infty(M)$ part of the algebra, as well as a 'matrix derivative' [120, 121, 130] which acts on the $\mathbb{C} \oplus \mathbb{H}$ part. QCD can be included in the model by extending the algebra to $\mathcal{A} = C^\infty(M) \otimes (\mathbb{C} \oplus \mathbb{H} \oplus M_3(\mathbb{C}))$, where $M_3(\mathbb{C})$ is the algebra of 3×3 matrices with elements in $\mathbb{C}$. Indeed, Connes *et al.* have shown that the entire SM can be rewritten in the NCG language [147, 153].

The extra-discrete-dimension interpretation of the superconnection model also solves the problem that the prediction $\sin^2\theta_W = 1/4$ is not stable under renormalization group running and can only be imposed at one scale [191, 192]. That scale can be interpreted as the scale at which the SM with $\sin^2\theta_W = 1/4$ emerges from the underlying discrete extra dimension model. The same scale should also characterize the separation of the two 'branes' in the discrete direction. Given the current experimental knowledge of the SM, this scale turns out to be ~ 4 TeV [163], suggesting a phenomenology that could potentially be explored at the LHC, as well as the existence of a new fundamental scale of nature at those energies. We will have more to say about this later.

These developments notwithstanding, a definitive recipe for constructing a NCG Kaluza-Klein model for a given algebra still seems to be in the works. Different authors use different definitions of the exterior derivative d, which, naturally, lead to different Higgs sectors and different predictions. In the Spectral SM of Connes *et al.* [149, 152–156], for instance, the prediction for the $U(1) \times SU(2) \times SU(3)$ gauge couplings are of the $SO(10)$ GUT type, pushing up the scale of emergence to the GUT scale. The Spectral SM is not particularly predictive, either: the fermionic masses and mixings must all be put by hand into the operator D. Thus, the NCG-superconnection approach still leaves much to be desired and further development is needed.

[3] Since $d^2 = 0$, the exterior derivative is intrinsically 'fermionic.'

[4] The unitary condition renders the resulting gauge theory anomaly free [142].

Despite the still incomplete nature of the NCG-superconnection approach, one can still make predictions and assessments based on the SM which we assume to emerge from it at the emergence scale. We have already commented on the fact that the prediction $\sin^2\theta_W = 1/4$ leads to an emergence scale of $\sim$4 TeV. The $su(2/1)$ superconnection also predicts the Higgs quartic coupling at that scale, from which in turn one can predict the Higgs boson mass to be $\sim$170 GeV. As discussed in Ref. [163], lowering this prediction down to $\sim$126 GeV requires the introduction of extra scalar degrees of freedom which modify the renormalization group equations (RGE) of the Higgs couplings. Those degrees of freedom would be available, for instance, if the $su(2/1)$ superconnection were extended to $su(2/2)$. The extra-discrete-dimensional $su(2/2)$ model shares the same prediction for $\sin^2\theta_W$ as the $su(2/1)$ version, and therefore the same scale ($\sim$4 TeV) at which an effective $SU(2)_L \times SU(2)_R \times U(1)_{B-L}$ gauge theory can be expected to emerge. Thus, explaining the Higgs mass within the NCG-superconnection formalism seems to demand an extension of the SM gauge group.

Curiously, Connes *et al.*'s Spectral SM with a GUT emergence scale also predicts the Higgs mass to be $\sim$170 GeV. Lowering this to $\sim$126 GeV requires the introduction of extra scalar degrees of freedom as discussed above [155, 156]. See also Refs. [193, 194]. Here, too, the Higgs mass seems to suggest that the SM gauge group needs to be extended to $SU(2)_L \times SU(2)_R \times U(1)_{B-L}$, or, including the QCD sector, to $SU(2)_L \times SU(2)_R \times SU(4)$.

Thus, the NCG-superconnection formalism already requires the extension of the SM gauge group to that of the left-right symmetric model (LRSM), or that of Pati-Salam [195].[5] Here, we will take a look at some of the phenomenological consequences of a NCG-superconnection motivated LRSM, in anticipation of the start of the upgraded LHC program in 2015, and various experiments at the intensity frontier which will be able to constrain new physics via rare decay processes.

This chapter is organized as follows. In section 2.2, we first review the $su(2/1)$ superconnection approach to the SM. We follow the bottom-up approach of Ne'eman *et al.* [129, 164, 173], Coquereaux *et al.* [120], and Haussling *et al.* [121], in which we start with the superconnection and build up the theory around it. This review goes into some pedagogical detail, and also shows where the Higgs mass prediction of $\sim$170 GeV comes from. In section 2.3, we extend the formalism developed in section 2.2 to the $su(2/2)$ superconnection into which the LRSM gauge group $SU(2)_L \times SU(2)_R \times U(1)_{B-L}$ is embedded. Again, the model is reviewed in some detail to clearly present the assumptions that go into its construction, and the resulting predictions including that of the Higgs mass. Section 2.4 discusses how fermion masses and mixings can be incorporated into the model. Section 2.5 discusses whether the new particles predicted by the $su(2/2)$ superconnection motivated LRSM are accessible at the LHC and other experiments. Section 2.6 concludes with a summary of what was discovered, a review of the remaining questions, and some speculation on what all this could mean. The review of the Spectral SM of Connes *et al.* is relegated to a subsequent paper [162].

[5] Coincidentally, the analysis of possible string compactifications by Dienes [196] also finds frequent occurrence of the Pati-Salam group.

2.2 The $su(2/1)$ Superconnection Formalism of the Standard Model

We begin by reviewing the $su(2/1)$ superconnection formalism of Ne'eman *et al.* [129, 164, 173], supplemented by the matrix derivative of Coquereaux *et al.* [120] and Haussling *et al.* [121], and some of our own observations. This will be done in some detail to dispel many misconceptions that exist concerning the formalism, while at the same time to expose its weaknesses. For a pedagogical introduction to superconnections, we point the reader to Ref. [171] by Sternberg.

2.2.1 Superalgebras

Let K be a field such as $\mathbb{R}$ or $\mathbb{C}$. A superalgebra A over K is a vector space over K with a direct sum decomposition

$$A \;=\; A_0 \oplus A_1 \;, \tag{2.3}$$

together with a bilinear multiplication $A \times A \to A$ such that

$$A_i \cdot A_j \;\subseteq\; A_{(i+j) \bmod 2} \;. \tag{2.4}$$

The subscripts 0 and 1 of A_0 and A_1 are known as the 'grading' of each space and its elements. The above relation indicates that when two elements of A are multiplied together, the gradings of the elements add as elements of the group $\mathbb{Z}_2$. Consequently, superalgebras are also known as $\mathbb{Z}_2$-graded algebras. If we call the elements of A_0 and A_1 respectively 'even' and 'odd,' then $A_i \cdot A_j \subseteq A_{(i+j) \bmod 2}$ means that

$$\begin{aligned} \text{even} \cdot \text{even} &= \text{even} \;, \\ \text{even} \cdot \text{odd} &= \text{odd} \;, \\ \text{odd} \cdot \text{even} &= \text{odd} \;, \\ \text{odd} \cdot \text{odd} &= \text{even} \;. \end{aligned} \tag{2.5}$$

Some texts use the symbols $+$ and $-$ instead of 0 and 1 for the $\mathbb{Z}_2$ gradings

$$A \;=\; A_+ \oplus A_- \;, \tag{2.6}$$

so that

$$A_i \cdot A_j \;\subseteq\; A_{ij} \;, \tag{2.7}$$

in which case Eq. (2.5) can also be written

$$\begin{aligned} + \cdot + &= + \;, \\ + \cdot - &= - \;, \\ - \cdot + &= - \;, \\ - \cdot - &= + \;, \end{aligned} \tag{2.8}$$

and the analogy with regular multiplication is manifest. Here, we will stick to 0 and 1 for notational convenience.

2.2.2 The Commutative Superalgebra of Differential Forms

Consider the vector space of differential forms $\Omega(M)$ on the manifold M, which decomposes as:

$$\Omega(M) \;=\; \Omega_0(M) \oplus \Omega_1(M)\;, \tag{2.9}$$

where

$$\begin{aligned} \Omega_0(M) &= \bigoplus_{n=\text{even}} \Omega^n(M)\;, \\ \Omega_1(M) &= \bigoplus_{n=\text{odd}} \Omega^n(M)\;. \end{aligned} \tag{2.10}$$

Here, $\Omega^n(M)$ is the vector space of n-forms on M. $\Omega_0(M)$ is the vector space of even-order differential forms, while $\Omega_1(M)$ is the vector space of odd-order differential forms. $\Omega(M) = \Omega_0(M) \oplus \Omega_1(M)$ is a superalgebra under the wedge product $\wedge$ since, clearly,

$$\Omega^i(M) \wedge \Omega^j(M) \;\subseteq\; \Omega^{i+j}(M) \tag{2.11}$$

implies

$$\Omega_i(M) \wedge \Omega_j(M) \;\subseteq\; \Omega_{(i+j) \bmod 2}(M)\;. \tag{2.12}$$

Furthermore, for any $a, b \in \Omega(M)$ with definite gradings $|a|$ and $|b|$, we have

$$a \wedge b \;=\; (-1)^{|a||b|}\, b \wedge a\;, \tag{2.13}$$

that is,

$$a \wedge b - (-1)^{|a||b|}\, b \wedge a \;=\; 0\;. \tag{2.14}$$

For generic superalgebras, when

$$a \cdot b - (-1)^{|a||b|}\, b \cdot a \;=\; 0\;, \tag{2.15}$$

the superalgebra is said to be commutative. Thus, $\Omega(M)$ is a commutative superalgebra.

2.2.3 The Lie Superalgebra $su(2/1)$

Formally, a Lie superalgebra is a superalgebra whose product $a \cdot b$ satisfies the relations

$$\begin{aligned} a \cdot b &= -(-1)^{|a||b|}\, b \cdot a\;, \\ a \cdot (b \cdot c) &= (a \cdot b) \cdot c + (-1)^{|a||b|}\, b \cdot (a \cdot c)\;. \end{aligned} \tag{2.16}$$

Elements of the real Lie superalgebra $su(N/M)$ are represented by $(N+M) \times (N+M)$ supertraceless Hermitian matrices of the form [177, 178]

$$\mathcal{H} \;=\; \begin{bmatrix} H^{(N)} & \theta \\ \theta^\dagger & H^{(M)} \end{bmatrix} \;=\; \underbrace{\begin{bmatrix} H^{(N)} & 0 \\ 0 & H^{(M)} \end{bmatrix}}_{\mathcal{H}_0} + \underbrace{\begin{bmatrix} 0 & \theta \\ \theta^\dagger & 0 \end{bmatrix}}_{\mathcal{H}_1}\;,$$

(2.17)

where $H^{(N)}$ and $H^{(M)}$ are, respectively, $N\times N$ and $M\times M$ Hermitian matrices and constitute the even (grading 0) part of the superalgebra, while θ ($\theta^\dagger$) is an $N\times M$ ($M\times N$) matrix and constitutes the odd (grading 1) part. The 'supertrace' of $\mathcal{H}$ is defined as

$$\mathrm{STr}\,\mathcal{H} \;=\; \mathrm{Tr}\,H^{(N)} - \mathrm{Tr}\,H^{(M)}\;, \tag{2.18}$$

and the elements of $su(N/M)$ all have vanishing supertrace. Note that the traceless parts of $H^{(N)}$ and $H^{(M)}$ respectively generate $SU(N)$ and $SU(M)$, while the non-vanishing trace part generates $U(1)$. Therefore, the even part of the $su(N/M)$ superalgebra generates $SU(N)\times SU(M)\times U(1)$ upon exponentiation.

The product of $X, Y \in su(N/M)$ in the matrix representation is given by

$$\begin{array}{ll} \dfrac{1}{i}[\,X,\,Y\,] & \text{if } |X||Y| = 0\;, \\ \{\,X,\,Y\,\} & \text{if } |X||Y| = 1\;, \end{array} \tag{2.19}$$

where $[*,*]$ and $\{*,*\}$ respectively denote the standard commutator and anti-commutator between two matrices. Note that the factor of i^{-1} for the $|X||Y| = 0$ case is necessary to render the product Hermitian. Ref. [121] denotes the two cases collectively as

$$\frac{1}{i}[\,X,\,Y\,]_s \tag{2.20}$$

where $[X,Y]_s$ is the 'supercommutator.' Given the even-odd decompositions $X = X_0 + X_1$ and $Y = Y_0 + Y_1$, it is defined as [121]

$$\begin{array}{l} [\,X,\,Y\,]_s \\ \quad = \;\; [\,X_0 + X_1,\,Y_0 + Y_1\,]_s \\ \quad = \;\; [\,X_0,\,Y_0\,] + [\,X_0,\,Y_1\,] + [\,X_1,\,Y_0\,] + i\{\,X_1,\,Y_1\,\}\;. \end{array} \tag{2.21}$$

In the literature, the supercommutator is also defined as

$$[\,X,\,Y\,]_s \;=\; XY - (-1)^{|X||Y|}\,YX\;, \tag{2.22}$$

which, when written out explicitly, reads

$$\begin{array}{l} [\,X,\,Y\,]_s \\ \quad = \;\; [\,X_0 + X_1,\,Y_0 + Y_1\,]_s \\ \quad = \;\; [\,X_0,\,Y_0\,] + [\,X_0,\,Y_1\,] + [\,X_1,\,Y_0\,] + \{\,X_1,\,Y_1\,\}\;. \end{array} \tag{2.23}$$

Though we will be using the first definition to express multiplication in Lie superalgebras, we will also have a use for the latter definition later in the text, so we request the reader to keep

in mind that the i in front of the anti-commutator terms may or may not be there depending on the context. It is straightforward to check that both definitions of the supercommutator satisfy Eq. (2.16), that is:

$$\begin{aligned} [X,Y]_s &= -(-1)^{|X||Y|}\,[Y,X]_s\,, \\ [X,[Y,Z]_s]_s &= [[X,Y]_s,Z]_s + (-1)^{|X||Y|}\,[Y,[X,Z]_s]_s\,. \end{aligned} \tag{2.24}$$

Let us look at a specific case. The Lie superalgebra $su(2/1)$ is the algebra of 3×3 supertraceless Hermitian matrices, the basis for which can be chosen as

$$\begin{aligned} \lambda_1^s &= \begin{bmatrix} 0 & 1 & 0 \\ 1 & 0 & 0 \\ 0 & 0 & 0 \end{bmatrix},\ \lambda_2^s = \begin{bmatrix} 0 & -i & 0 \\ i & 0 & 0 \\ 0 & 0 & 0 \end{bmatrix},\ \lambda_3^s = \begin{bmatrix} 1 & 0 & 0 \\ 0 & -1 & 0 \\ 0 & 0 & 0 \end{bmatrix}, \\ \lambda_4^s &= \begin{bmatrix} 0 & 0 & 1 \\ 0 & 0 & 0 \\ 1 & 0 & 0 \end{bmatrix},\ \lambda_5^s = \begin{bmatrix} 0 & 0 & -i \\ 0 & 0 & 0 \\ i & 0 & 0 \end{bmatrix},\ \lambda_6^s = \begin{bmatrix} 0 & 0 & 0 \\ 0 & 0 & 1 \\ 0 & 1 & 0 \end{bmatrix}, \\ \lambda_7^s &= \begin{bmatrix} 0 & 0 & 0 \\ 0 & 0 & -i \\ 0 & i & 0 \end{bmatrix},\ \lambda_8^s = \frac{1}{\sqrt{3}} \begin{bmatrix} -1 & 0 & 0 \\ 0 & -1 & 0 \\ 0 & 0 & -2 \end{bmatrix}. \end{aligned} \tag{2.25}$$

These are the usual $su(3)$ Gell-mann matrices except for the eighth (λ_8^s) due to the requirement of vanishing supertrace. Of these, $\lambda_1^s, \lambda_2^s, \lambda_3^s, \lambda_8^s$ span the even part of the superalgebra while $\lambda_4^s, \lambda_5^s, \lambda_6^s, \lambda_7^s$ span the odd part. They close under commutation and anti-commutation relations as [164]

$$\begin{aligned} \frac{1}{i}\left[\lambda_i^s,\,\lambda_j^s\right] &= 2\,f_{ijk}\lambda_k^s\,, \\ \left[\lambda_i^s,\,\lambda_8^s\right] &= 0\,, \\ \frac{1}{i}\left[\lambda_i^s,\,\lambda_m^s\right] &= 2\,f_{iml}\lambda_l^s\,, \\ \frac{1}{i}\left[\lambda_8^s,\,\lambda_m^s\right] &= \frac{2}{3} f_{8ml}\lambda_l^s\,, \\ \left\{\lambda_m^s,\,\lambda_n^s\right\} &= 2\,d_{mnk}\lambda_k^s - \sqrt{3}\,\delta_{mn}\lambda_8^s\,, \end{aligned} \tag{2.26}$$

where i,j,k denote the even indices $1,2,3,8$ and m,n,l denote the odd indices $4,5,6,7$. The f's and the d's are the same as the $su(3)$ structure constants defined in Ref. [197]. Note that the odd matrices close into the even ones under anti-commutation (instead of commutation), which is the main difference from the $su(3)$ case. Note also that we have chosen to normalize the above matrices, including λ_8^s, in the usual way

$$\mathrm{Tr}(\lambda_a^s\lambda_b^s) \;=\; 2\delta_{ab}\,, \tag{2.27}$$

and not via the supertrace.

2.2.4 Tensor Product of Superalgebras

If A and B are superalgebras, then the tensor product $A \otimes B$ is also a superalgebra under the multiplication

$$(a \otimes b) \cdot (a' \otimes b') \equiv (-1)^{|b||a'|}(a \cdot a') \otimes (b \cdot b') , \tag{2.28}$$

where $a, a' \in A$ and $b, b' \in B$. In constructing this product, elements of A and B are assumed to (super)commute, *cf.* Eq. (2.15). The grading of the element $a \otimes b \in A \otimes B$ is given by

$$|a \otimes b| = |a| + |b| \mod 2 , \tag{2.29}$$

and the even-odd decomposition $A \otimes B = (A \otimes B)_0 \oplus (A \otimes B)_1$ is

$$\begin{aligned} (A \otimes B)_0 &= (A_0 \otimes B_0) \oplus (A_1 \otimes B_1) , \\ (A \otimes B)_1 &= (A_0 \otimes B_1) \oplus (A_1 \otimes B_0) , \end{aligned} \tag{2.30}$$

where $A = A_0 \oplus A_1$ and $B = B_0 \oplus B_1$.

In particular, the tensor product of a commutative superalgebra of differential forms $\Omega(M)$ and a Lie superalgebra L is again a Lie superalgebra with product

$$[\, a \otimes X,\, b \otimes Y \,]_S = (-1)^{|X||b|}(a \wedge b) \otimes [\, X,\, Y \,]_s , \tag{2.31}$$

where $a, b \in \Omega(M)$ and $X, Y \in L$. The tensor product $\Omega(M) \otimes L$ is the space of L valued differential forms.

2.2.5 Superconnection

Just as the gauge connection in QCD is given by $G = i \sum_{a=1}^{8} G_a \lambda_a$, where $G_a = G_a^\mu dx_\mu$ are one-forms corresponding to the gluon fields, we construct the $su(2/1)$ superconnection $\mathcal{J}$ using the λ^s matrices as[6]

$$\begin{aligned} \mathcal{J} &= i \sum_{a=1}^{8} J_a \lambda_a^s \\ &= i \sum_{i=1,2,3,8} J_i \, \lambda_i^s + i \sum_{m=4,5,6,7} J_m \lambda_m^s . \end{aligned} \tag{2.32}$$

For the terms multiplying the even $su(2/1)$ matrices, we make the identifications $J_i = W_i$ $(i = 1, 2, 3)$ and $J_8 = B$, where $W_i = W_i^\mu dx_\mu$ and $B = B^\mu dx_\mu$ are respectively the one-form

[6] We take the elements of $su(2/1)$ to be Hermitian, but the superconnection $\mathcal{J}$ and the supercurvature $\mathcal{F}$, to be defined in section 2.2.6, are taken to be anti-Hermitian.

fields corresponding to the $SU(2)_L$ and $U(1)_Y$ gauge fields. The terms multiplying the odd $su(2/1)$ matrices are identified with zero-form fields corresponding to the Higgs doublet:

$$J_4 \mp i J_5 = \sqrt{2}\,\phi^{\pm}\,, \tag{2.33}$$
$$J_6 - i J_7 = \sqrt{2}\,\phi^{0}\,, \tag{2.34}$$
$$J_6 + i J_7 = \sqrt{2}\,\phi^{0*}\,. \tag{2.35}$$

Then, the superconnection can be written as

$$\mathcal{J} = i \begin{bmatrix} \mathcal{W} - \frac{1}{\sqrt{3}} B \cdot \mathbf{1}_{2\times 2} & \sqrt{2}\phi \\ \sqrt{2}\phi^{\dagger} & -\frac{2}{\sqrt{3}} B \end{bmatrix}\,, \tag{2.36}$$

where, $\mathcal{W} = W_i\,\tau_i$ (where τ_i are the Pauli matrices), and

$$\phi = \begin{bmatrix} \phi^{+} \\ \phi^{0} \end{bmatrix}\,. \tag{2.37}$$

Note that the superconnection $\mathcal{J}$ is an odd element of $\Omega(M)\otimes su(2/1)$, where M is the (3+1) dimensional spacetime manifold. Though ϕ by itself is a zero-form, the superconnection $\mathcal{J}$ as a whole is actually a generalized one-form, the odd grading of λ^s_m ($m = 4, 5, 6, 7$) supplying the extra grading associated with every application of the exterior derivative operator.

Note also that the one-forms $W_i = W_i^{\mu} dx_{\mu}$ and $B = B^{\mu} dx_{\mu}$ are dimensionless, so the zero-form ϕ which appears together with them in the superconnection must also be dimensionless. To give ϕ its usual mass dimension of one, some authors replace ϕ with ϕ/μ, where μ is a mass scale. However, for notational simplicity we will not do this. We request the reader to assume that, not just ϕ, but all dimensionful quantities are multiplied by the appropriate (but invisible) powers of μ to make them dimensionless, *e.g.*, $B^{\nu} \to B^{\nu}/\mu$, $dx^{\nu} \to \mu\, dx^{\nu}$. In particular, the Hodge dual should not change the dimension of the operand: $*1 = \mu^4 d^4x$, $*(\mu\, dx^{\nu}) = \frac{1}{6}\mu^3\, \varepsilon^{\kappa\lambda\mu\nu} dx_{\kappa} \wedge dx_{\lambda} \wedge dx_{\mu}$, etc. Once all the dust has settled, the powers of μ will disappear from the final expression for the action, and we will then be free to think of all quantities to have their usual dimensions.

As stated in the introduction, we are considering a model space consisting of two $3+1$ dimensional branes separated by a gap. We interpret the even part of the superconnection $\mathcal{J}$ as connecting points within the two $3+1$ dimensional branes, the one-form $\mathcal{W} - \frac{1}{\sqrt{3}} B \cdot \mathbf{1}_{2\times 2}$ acting on the left-handed brane, and the one-form $-\frac{2}{\sqrt{3}} B$ acting on the right. The zero-form $\sqrt{2}\phi$ connects the left-handed brane to the right, and $\sqrt{2}\phi^{\dagger}$ the right-handed brane to the left.

2.2.6 Supercurvature

Extension of the Exterior Derivative

In usual differential geometry, the curvature of the connection ω is given by $(d\omega) + \omega \wedge \omega$, and in QCD the curvature of the gauge connection G is given by $F_G = (dG) + \frac{1}{2}[G, G]$. We would like to calculate the supercurvature from the superconnection $\mathcal{J}$ via the analogous expression

$$\mathcal{F} \;=\; (\mathbf{d}_S\, \mathcal{J}) + \frac{1}{2}\,[\,\mathcal{J},\, \mathcal{J}\,]_S \;, \tag{2.38}$$

where $\mathbf{d}_S$ is the extension of the usual exterior derivative operator d to the superalgebra $\Omega(M) \otimes su(2/1)$. Let us define it.

The exterior derivative operator $d = dx^\mu \wedge \partial_\mu$ is a map from $\Omega^i(M)$ to $\Omega^{i+1}(M)$:

$$\Omega^i(M) \;\stackrel{d}{\longrightarrow}\; \Omega^{i+1}(M) \;, \tag{2.39}$$

or in terms of the $\mathbb{Z}_2$-grading decomposition $\Omega(M) = \Omega_0(M) + \Omega_1(M)$, it maps from one grading to the other:

$$\Omega_0(M) \;\stackrel{d}{\longleftrightarrow}\; \Omega_1(M) \;. \tag{2.40}$$

Since it changes the $\mathbb{Z}_2$ grading of differential forms by 1, it carries grading 1 itself. Its characteristic properties are that it satisfies the super-Leibniz rule

$$d(a \wedge b) \;=\; (da) \wedge b + (-1)^{|a|} a \wedge (db) \;. \tag{2.41}$$

and that it is nilpotent:

$$d^2 \;=\; 0 \;. \tag{2.42}$$

The extension $\mathbf{d}_S$ operating on $\Omega(M) \otimes su(2/1)$ should also be a grading-switching operator

$$[\Omega(M) \otimes su(2/1)]_0 \;\stackrel{\mathbf{d}_S}{\longleftrightarrow}\; [\Omega(M) \otimes su(2/1)]_1 \;, \tag{2.43}$$

and should possess the same properties of obeying the super-Leibniz rule and nilpotency. To this end, let us write

$$\mathbf{d}_S \;=\; \mathbf{d} + \mathbf{d}_M \;, \tag{2.44}$$

where

$$\begin{aligned} \Omega_0(M) \otimes su(2/1) \;&\stackrel{\mathbf{d}}{\longleftrightarrow}\; \Omega_1(M) \otimes su(2/1) \;, \\ \Omega(M) \otimes su(2/1)_0 \;&\stackrel{\mathbf{d}_M}{\longleftrightarrow}\; \Omega(M) \otimes su(2/1)_1 \;, \end{aligned} \tag{2.45}$$

that is, $\mathbf{d}$ switches the grading of the $\Omega(M)$ part while $\mathbf{d}_M$ switches the grading of the $su(2/1)$ part, and consider the two operators separately. Since the operators themselves have grading 1 in $\Omega(M) \otimes su(2/1)$, they should anti-commute:

$$\mathbf{d}\mathbf{d}_M + \mathbf{d}_M\mathbf{d} \;=\; 0 \;. \tag{2.46}$$

From the model building perspective, the $\mathbf{d}$ operator generates translations within each of the two $3+1$ dimensional branes while the 'matrix derivative' $\mathbf{d}_M$ [120, 121] accounts for transitions between the two branes.

The operator d

We define the action of the operator $\mathbf{d}$ on $a \otimes X \in \Omega(M) \otimes su(2/1)$ by

$$\mathbf{d}(a \otimes X) \;=\; (da) \otimes X \;. \tag{2.47}$$

It is straightforward to show that $\mathbf{d}$ satisfies the super-Leibniz rule given by

$$\begin{aligned} &\mathbf{d}\Big(\big[\, a \otimes X,\, b \otimes Y \,\big]_S \Big) \\ &= \;\; \big[\, \mathbf{d}(a \otimes X),\, b \otimes Y \,\big]_S \\ &\quad\; + (-1)^{|a|+|X|} \big[\, a \otimes X,\, \mathbf{d}(b \otimes Y) \big]_S \;. \end{aligned} \tag{2.48}$$

Nilpotency $\mathbf{d}^2(a \otimes X) = 0$ also follows immediately from $(d^2 a) = 0$. From Eqs. (2.41) and (2.47), we infer

$$\begin{aligned} \mathbf{d}(a \otimes X) &= \big[da - (-1)^{|a|} a d \big] \otimes X \\ &= da \otimes X - (-1)^{|a|} a d \otimes X \\ &= da \otimes X - (-1)^{|a|+|X|} a \otimes X d \;, \end{aligned} \tag{2.49}$$

or using the second definition of the supercommutator, Eq. (2.23), we can write

$$\mathbf{d}(a \otimes X) \;=\; \big[\, \mathbf{d},\, a \otimes X \,\big]_S \;. \tag{2.50}$$

The Matrix Derivative $\mathbf{d}_M$

Let us first find an operator d_M which acts on $su(2/1)$ such that

$$su(2/1)_0 \;\overset{d_M}{\longleftrightarrow}\; su(2/1)_1 \tag{2.51}$$

with the required properties. For $X, Y \in su(2/1)$, the super-Leibniz rule demands

$$(d_M[\, X,\, Y \,]_s) \;=\; [\,(d_M X),\, Y \,]_s + (-1)^{|X|} [\, X,\, (d_M Y)\,]_s \;. \tag{2.52}$$

Comparing with the second line of Eq. (2.24), we see that such an operator can be realized as [7]

$$(d_M X) \;=\; i\,[\,\eta,\, X\,]_s \;, \tag{2.53}$$

[7] The supercommutator that appears here is that of the first definition, Eq. (2.21).

where η is any odd element of $su(2/1)$. It is clear that this operator switches the grading of X.

Nilpotency is more difficult to realize and how it is treated is an important consideration of the entire formalism. It was shown in Ref. [121] that for a generic Lie superalgebra $su(N/M)$, demanding $d_M^2(X) = 0$ with d_M defined as above for all $X \in su(N/M)$ leads to the condition $N = M$. Indeed, since η is an odd element of $su(N/M)$ it has the form

$$\eta \;=\; \begin{bmatrix} \mathbf{0}_{N\times N} & \zeta \\ \zeta^\dagger & \mathbf{0}_{M\times M} \end{bmatrix} \tag{2.54}$$

where ζ is an $N \times M$ matrix. To impose $(d_M^2 X) = 0$ we must have

$$(d_M^2 X) \;=\; -[\,\eta,\,[\,\eta,\,X\,]_s\,]_s \;=\; -i[\,\eta^2,\,X\,] \;=\; 0\,, \tag{2.55}$$

which means that

$$\eta^2 \;=\; \begin{bmatrix} \zeta\zeta^\dagger & \mathbf{0}_{N\times M} \\ \mathbf{0}_{M\times N} & \zeta^\dagger\zeta \end{bmatrix} \tag{2.56}$$

must commute with all elements of $su(N/M)$. This requires η^2 to be a multiple of a unit matrix, that is

$$\zeta\zeta^\dagger \;=\; v^2\mathbf{1}_{N\times N}\,, \qquad \zeta^\dagger\zeta \;=\; v^2\mathbf{1}_{M\times M}\,, \tag{2.57}$$

with v^2 a constant, which is possible only when $N = M$.

Because of this, Coquereaux *et al.* in Ref. [120] work in 4 dimensions by adding an extra row and column of zeroes to the $su(2/1)$ matrices to make them into 4×4 $su(2/2)$ matrices. The η-matrix for $su(2/2)$ will have the form of Eq. (2.54) with ζ a multiple of a 2×2 unitary matrix. The supercommutator of η and a generic $su(2/1)$ matrix embedded into $su(2/2)$ will have non-zero elements in the fourth row and fourth column, but these are dropped, projecting the result back into $su(2/1)$.

Haussling *et al.* in Ref. [121] take a different approach and work in 3 dimensions throughout by dropping the fourth row and fourth column from the η matrix for $su(2/2)$.[8] Writing the first column of ζ as ξ, the η-matrix used in Ref. [121] is

$$\eta \;=\; \begin{bmatrix} \mathbf{0}_{2\times 2} & \xi \\ \xi^\dagger & 0 \end{bmatrix}\,, \tag{2.58}$$

where $\xi^\dagger\xi = v^2$. Since the condition $N = M$ is not met, d_M defined with this η is not nilpotent.

Thus, to define a matrix derivative for $su(2/1)$, one must either work in $su(2/2)$ and project back into $su(2/1)$, or forgo nilpotency. However, it turns out that, either way, the resulting

[8] In the representation, we use for $su(2/2)$ in a later section, so it is more precise to say that Ref. [121] drops the third row and third column corresponding to the right-handed neutrino.

supercurvature and other physical quantities will be the same, so we will adopt the three dimensional version, Eq. (2.58), in our definition of d_M on $su(2/1)$.

We extend d_M acting on $su(2/1)$ to $\mathbf{d}_M$ acting on $\Omega(M) \otimes su(2/1)$ by defining the operation of $\mathbf{d}_M$ on $a \otimes X \in \Omega(M) \otimes su(2/1)$ to be given by

$$\mathbf{d}_M(a \otimes X) \;=\; (-1)^{|a|} a \otimes (d_M X) \;, \tag{2.59}$$

which can also be written as

$$\mathbf{d}_M(a \otimes X) \;=\; \big[\, \mathbf{d}_M,\, a \otimes X \,\big]_S \;, \tag{2.60}$$

where the supercommutator here is that of Eq. (2.21). It is straightforward to show that $\mathbf{d}_M$ satisfies the super-Leibniz rule.

Short note on nilpotency

At this point, we would like to bring to the reader's attention the fact that the statements $d_M^2 = 0$ and $(d_M^2 X) = 0$ are not equivalent. While the first guarantees the second, the converse is not true. Indeed, using Eq. (2.24), we can rewrite Eq. (2.55) as

$$(d_M^2 X) \;=\; \big[d_M, \big[d_M, X\big]_s\big]_s \;=\; \frac{1}{2}\big[\big[d_M, d_M\big]_s, X\big]_s \;, \tag{2.61}$$

and we can make the identification

$$\frac{1}{2}\big[d_M, d_M\big]_s \;=\; d_M^2 \;=\; -i\eta^2 \;, \tag{2.62}$$

where η^2 is a non-zero even element of $su(N/M)$. For the $N = M$ case, it becomes a multiple of the unit matrix which constitutes the center of the superalgebra (λ_{15}^s in the case of $su(2/2)$ to be discussed later). Thus, it is not clear whether d_M as defined here truly qualifies as a generalization of the 'exterior derivative' operator. Furthermore, whether d_M^2, and consequently $\mathbf{d}_M^2$, can be considered to vanish or not is an important consideration when calculating the supercurvature, as we will see in the following.

Derivation of $\mathcal{F}$

Let us now look at the terms contributing to Eq. (2.38) one by one. $(\mathbf{d}\mathcal{J})$ is simply[9]

$$(\mathbf{d}\mathcal{J}) \;=\; i\begin{bmatrix} d\mathcal{W} - \frac{1}{\sqrt{3}}\, dB\cdot \mathbf{1}_{2\times 2} & \sqrt{2}\, d\phi \\ \sqrt{2}\, d\phi^\dagger & -\frac{2}{\sqrt{3}}\, dB \end{bmatrix}. \tag{2.64}$$

while $(\mathbf{d}_M\mathcal{J})$ is given by

$$\begin{aligned}(\mathbf{d}_M\mathcal{J}) \;&=\; i\big[\,\eta,\,\mathcal{J}\,\big]_S \\ &=\; i\begin{bmatrix} -\sqrt{2}\left(\xi\phi^\dagger + \phi\xi^\dagger\right) & i\Big(\mathcal{W}\xi + \frac{1}{\sqrt{3}}B\xi\Big) \\ -i\Big(\xi^\dagger\mathcal{W} + \frac{1}{\sqrt{3}}\xi^\dagger B\Big) & -\sqrt{2}\left(\xi^\dagger\phi + \phi^\dagger\xi\right)\end{bmatrix}.\end{aligned} \tag{2.65}$$

To calculate the supercommutator of $\mathcal{J}$ with itself, we decompose $\mathcal{J}$ into two parts as

$$\mathcal{J} \;=\; \underbrace{i\begin{bmatrix}\mathcal{W} - \frac{1}{\sqrt{3}}B\cdot\mathbf{1}_{2\times 2} & \mathbf{0}_{2\times 1} \\ \mathbf{0}_{1\times 2} & -\frac{2}{\sqrt{3}}B\end{bmatrix}}_{\mathcal{J}_{10}} + \underbrace{i\begin{bmatrix}\mathbf{0}_{2\times 2} & \sqrt{2}\phi \\ \sqrt{2}\phi^\dagger & 0\end{bmatrix}}_{\mathcal{J}_{01}}, \tag{2.66}$$

where the two subscripts refer to the gradings in $\Omega(M)$ and $su(2/1)$, respectively, in that order. Keeping in mind the product rule given in Eq. (2.31) for $\Omega(M)\otimes su(2/1)$, we find

$$\begin{aligned}\big[\,\mathcal{J}_{10},\,\mathcal{J}_{10}\,\big]_S \;&=\; -2i\begin{bmatrix}\varepsilon_{ijk}(W_i\wedge W_j)\tau_k & \mathbf{0}_{2\times 1} \\ \mathbf{0}_{1\times 2} & 0\end{bmatrix}, \\ \big[\,\mathcal{J}_{01},\,\mathcal{J}_{01}\,\big]_S \;&=\; -4i\begin{bmatrix}\phi\phi^\dagger & \mathbf{0}_{2\times 1} \\ \mathbf{0}_{1\times 2} & \phi^\dagger\phi\end{bmatrix},\end{aligned} \tag{2.67}$$

and[10]

$$\big[\,\mathcal{J}_{10},\,\mathcal{J}_{01}\,\big]_S \;=\; \big[\,\mathcal{J}_{01},\,\mathcal{J}_{10}\,\big]_S$$

[9] If the superconnection $\mathcal{J}$ is considered an element of $su(2/1)\otimes\Omega(M)$ instead of $\Omega(M)\otimes su(2/1)$, then the result of $\mathbf{d}$ acting on $\mathcal{J}$ will be

$$(\mathbf{d}\mathcal{J}) \;=\; i\begin{bmatrix} d\mathcal{W} - \frac{1}{\sqrt{3}}\, dB\cdot \mathbf{1}_{2\times 2} & -\sqrt{2}\, d\phi \\ -\sqrt{2}\, d\phi^\dagger & -\frac{2}{\sqrt{3}}\, dB \end{bmatrix}. \tag{2.63}$$

Note the minus signs on the off diagonal terms which results when $\mathbf{d}$ commutes through the odd $su(2/1)$ matrix multiplying the zero-form fields. This choice is a matter of convention and does not affect the final results.

[10] As mentioned in footnote 9, we are assuming that the supercurvature is an element of $\Omega(M)\otimes su(2/1)$, not $su(2/1)\otimes\Omega(M)$. The latter choice would reverse the signs of $[\,\mathcal{J}_{10},\,\mathcal{J}_{01}\,]_S$ and $[\,\mathcal{J}_{01},\,\mathcal{J}_{10}\,]_S$. Again, this is a matter of convention and does not affect the final result as long as the convention is consistently applied.

$$= \sqrt{2}i \begin{bmatrix} \mathbf{0}_{2\times 2} & i\left(\mathcal{W}\phi + \frac{1}{\sqrt{3}}B\phi\right) \\ -i\left(\phi^\dagger\mathcal{W} + \frac{1}{\sqrt{3}}\phi^\dagger B\right) & 0 \end{bmatrix} . \tag{2.68}$$

Therefore,[11]

$$\begin{aligned} &[\,\mathcal{J},\,\mathcal{J}\,]_S \\ &= [\,\mathcal{J}_{10},\,\mathcal{J}_{10}\,]_S + [\,\mathcal{J}_{10},\,\mathcal{J}_{01}\,]_S \\ &\qquad +[\,\mathcal{J}_{01},\,\mathcal{J}_{10}\,]_S + [\,\mathcal{J}_{01},\,\mathcal{J}_{01}\,]_S \\ &= 2i \begin{bmatrix} -\varepsilon_{ijk}(W_i \wedge W_j)\tau_k - 2\phi\phi^\dagger & +\sqrt{2}i\left(\mathcal{W}\phi + \frac{1}{\sqrt{3}}B\phi\right) \\ -\sqrt{2}i\left(\phi^\dagger\mathcal{W} + \frac{1}{\sqrt{3}}\phi^\dagger B\right) & -2\phi^\dagger\phi \end{bmatrix} . \end{aligned} \tag{2.69}$$

Putting everything together, the supercurvature reads as

$$\begin{aligned} \mathcal{F} &= \mathbf{d}\mathcal{J} + \mathbf{d}_M\mathcal{J} + \frac{1}{2}[\,\mathcal{J},\,\mathcal{J}\,]_S \\ &= i \begin{bmatrix} F_W - \frac{1}{\sqrt{3}}F_B\cdot\mathbf{1}_{2\times 2} - 2\phi\phi^\dagger - \sqrt{2}\left(\xi\phi^\dagger + \phi\xi^\dagger\right) & \sqrt{2}\,D\phi + \left(i\mathcal{W}\xi + \frac{i}{\sqrt{3}}B\xi\right) \\ \sqrt{2}(D\phi)^\dagger - \left(i\xi^\dagger\mathcal{W} + \frac{i}{\sqrt{3}}\xi^\dagger B\right) & -\frac{2}{\sqrt{3}}F_B - 2\phi^\dagger\phi - \sqrt{2}\left(\xi^\dagger\phi + \phi^\dagger\xi\right) \end{bmatrix} \\ &= i \begin{bmatrix} F_W - \frac{1}{\sqrt{3}}F_B\cdot\mathbf{1}_{2\times 2} - 2\hat{\phi}\hat{\phi}^\dagger + \xi\xi^\dagger & \sqrt{2}\,D\hat{\phi} \\ \sqrt{2}(D\hat{\phi})^\dagger & -\frac{2}{\sqrt{3}}F_B - 2\hat{\phi}^\dagger\hat{\phi} + v^2 \end{bmatrix} , \end{aligned} \tag{2.70}$$

where we have introduced the shifted zero-form field

$$\hat{\phi} = \phi + \frac{\xi}{\sqrt{2}} , \tag{2.71}$$

and

$$D\phi = d\phi + \left(i\mathcal{W}\phi + \frac{i}{\sqrt{3}}B\phi\right) ,$$

[11] Instead of calculating the supercommutator $\frac{1}{2}[\mathcal{J},\mathcal{J}]_S$ as we have done here, some papers treat the superconnection $\mathcal{J}$ as a super-endomorphism of a superspace and calculate the product $\mathcal{J}\odot\mathcal{J}$, using the Ne'eman-Sternberg rule for supermatrix multiplication [129, 171, 173]:

$$\begin{aligned} &\begin{bmatrix} A & C \\ D & B \end{bmatrix} \odot \begin{bmatrix} A' & C' \\ D' & B' \end{bmatrix} \\ &= \begin{bmatrix} A\wedge A' + (-1)^{|D'|}C\wedge D' & A\wedge C' + (-1)^{|B'|}C\wedge B' \\ (-1)^{|A'|}D\wedge A' + B\wedge D' & (-1)^{|C'|}D\wedge C' + B\wedge B' \end{bmatrix} . \end{aligned}$$

The resulting supercurvature $\mathcal{F}$ is not an element of $\Omega(M)\otimes su(2/1)$, and the definition of the inner product of $\mathcal{F}$ with itself must be changed accordingly in the calculation of the action. However, the resulting action turns out to be the same. The above multiplication rule is derived in Appendix A.1.

$$
\begin{aligned}
D\hat{\phi} &= d\hat{\phi} + \left(i\mathcal{W}\hat{\phi} + \frac{i}{\sqrt{3}} B\hat{\phi} \right) , \\
F_W &= (F_W)_k \, \tau_k \;=\; (dW_k - \epsilon_{ijk} W_i \wedge W_j) \, \tau_k \; , \\
F_B &= dB \; .
\end{aligned} \tag{2.72}
$$

We have also used $\xi^\dagger \xi = v^2$.

Gauge Transformation Properties

Recall that, in the case of QCD, the curvature $F_G = dG + \frac{1}{2}[G, G]$ transforms as

$$
F_G \;\rightarrow U F_G U^\dagger \tag{2.73}
$$

under $SU(3)$ gauge transformations:

$$
U \;=\; \exp\left[i \sum_{j=1}^{8} \theta_j \lambda_j \right] \; . \tag{2.74}
$$

Let us see whether the supercurvature $\mathcal{F}$ derived above transforms in an analogous fashion under $SU(2)_L \times U(1)_Y$ gauge transformations generated by the even part of the $su(2/1)$ superalgebra:

$$
U \;=\; \exp\left[i \sum_{j=1,2,3,8} \theta_j \lambda_j^s \right] \;=\; \begin{bmatrix} u \, e^{-i\theta/\sqrt{3}} & \mathbf{0}_{2\times 1} \\ \mathbf{0}_{1\times 2} & e^{-2i\theta/\sqrt{3}} \end{bmatrix} \; , \tag{2.75}
$$

where

$$
u \;=\; \exp\left[i \sum_{j=1,2,3} \theta_j \tau_j \right] \;\in\; SU(2)_L \; , \quad \theta \;=\; \theta_8 \; . \tag{2.76}
$$

The one-form gauge fields transform as

$$
\begin{aligned}
\mathcal{W} &\rightarrow u\mathcal{W}u^\dagger + i \, du \, u^\dagger \; , \\
B &\rightarrow B - d\theta \; .
\end{aligned} \tag{2.77}
$$

For the zero-form field, we assume that it is the shifted field $\hat{\phi} = \phi + \xi/\sqrt{2}$ which transforms as

$$
\hat{\phi} \;\rightarrow\; u \, e^{i\theta/\sqrt{3}} \, \hat{\phi} \; . \tag{2.78}
$$

The interpretation is that $\xi/\sqrt{2}$ is the vacuum expectation value (VEV) of $\hat{\phi}$ and ϕ is the fluctuation around that VEV. Then,

$$
\begin{aligned}
F_W &\rightarrow u F_W u^\dagger \; , \\
F_B &\rightarrow F_B \; , \\
D\hat{\phi} &\rightarrow u \, e^{i\theta/\sqrt{3}} \, D\hat{\phi} \; .
\end{aligned} \tag{2.79}
$$

Unfortunately, the $\xi\xi^\dagger$ term in the upper-left block of $\mathcal{F}$ is a constant projection matrix which does not transform under gauge transformations. This term prevents $\mathcal{F}$ from transforming analogously to Eq. (2.73) as $\mathcal{F} \to U\mathcal{F}U^\dagger$. Since this transformation law would guarantee the gauge invariance of the action, which we will derive in the next subsection, the lack of such a law is somewhat problematic (though, in fact, it is found that the problem cures itself in the sense that the action derived from this supercurvature is still manifestly gauge invariant). In the following, we trace this problem back to the non-nilpotency of the matrix derivative d_M in $su(2/1)$. However, this can already be seen by noticing that the problem would not exist if we could replace $\xi\xi^\dagger$ with $v^2\mathbf{1}_{2\times 2}$.

Covariant Derivative

Given $\mathbf{d}$, $\mathbf{d}_M$, and the superconnection $\mathcal{J}$, we can construct a covariant derivative operator via

$$\mathcal{D} \;=\; \mathbf{d} + \mathbf{d}_M + \mathcal{J}\;. \tag{2.80}$$

Let $\alpha \in \Omega(M) \otimes su(2/1)$ be an object which gauge transforms as $\alpha \to \alpha' = U\alpha U^\dagger$. Then, $(\mathbf{d}\alpha)$ transforms as

$$\begin{aligned}
(\mathbf{d}\alpha) \;&\to\; (\mathbf{d}\alpha') \\
&=\; \mathbf{d}(U\alpha U^\dagger) \\
&=\; (\mathbf{d}U)\alpha U^\dagger + U(\mathbf{d}\alpha)U^\dagger + (-1)^{|\alpha|}U\alpha(\mathbf{d}U^\dagger) \\
&=\; (\mathbf{d}U)U^\dagger\alpha' + U\mathbf{d}U^\dagger(\alpha') + (-1)^{|\alpha'|}\alpha' U(\mathbf{d}U^\dagger) \\
&=\; (\mathbf{d}U)U^\dagger\alpha' + U\mathbf{d}U^\dagger(\alpha') - (-1)^{|\alpha'|}\alpha'(\mathbf{d}U)U^\dagger \\
&=\; \left[U\mathbf{d}U^\dagger + (\mathbf{d}U)U^\dagger,\, \alpha'\right]_S\,,
\end{aligned} \tag{2.81}$$

and we can see that $\mathbf{d}$ transforms as

$$\mathbf{d} \;\to\; \mathbf{d}' = U\mathbf{d}U^\dagger + (\mathbf{d}U)U^\dagger\;. \tag{2.82}$$

On the other hand, from the gauge transformation properties we introduced in Eqs. (2.77) and (2.78), we can infer that the combination

$$\begin{aligned}
\mathbf{d}_M + \mathcal{J} \;&=\; i\eta + \mathcal{J} \\
&=\; i\begin{bmatrix} \mathcal{W} - \frac{1}{\sqrt{3}}B\cdot\mathbf{1}_{2\times 2} & \sqrt{2}\,\hat{\phi} \\ \sqrt{2}\,\hat{\phi}^\dagger & -\frac{2}{\sqrt{3}}B \end{bmatrix}\,,
\end{aligned} \tag{2.83}$$

transforms as

$$\mathbf{d}_M + \mathcal{J} \;\to\; U(\mathbf{d}_M + \mathcal{J})U^\dagger - (\mathbf{d}U)U^\dagger\;. \tag{2.84}$$

Therefore, the covariant derivative $\mathcal{D} = \mathbf{d} + \mathbf{d}_M + \mathcal{J}$ transforms as

$$\mathcal{D} \;\to\; U\mathcal{D}U^\dagger\,, \tag{2.85}$$

and consequently, if $\alpha \to U\alpha U^\dagger$ then

$$(\mathcal{D}\alpha) \;\to U(\mathcal{D}\alpha)U^\dagger\;. \tag{2.86}$$

Supercurvature from the Covariant Derivative

The supercurvature can be defined as the supercommutator of the covariant derivative with itself:

$$\begin{aligned}\mathcal{F} &= \frac{1}{2}\big[\,\mathcal{D},\,\mathcal{D}\,\big]_S \\ &= \frac{1}{2}\big[\,\mathbf{d}_S+\mathcal{J},\,\mathbf{d}_S+\mathcal{J}\,\big]_S \\ &= \mathbf{d}_S^2+(\mathbf{d}_S\,\mathcal{J})+\frac{1}{2}\big[\,\mathcal{J},\,\mathcal{J}\,\big]_S\,. \end{aligned} \tag{2.87}$$

From Eq. (2.85), we can infer that $\mathcal{F}$ gauge transforms as $\mathcal{F}\to U\mathcal{F}U^\dagger$.

In the above expression for $\mathcal{F}$, it is usually assumed that

$$\mathbf{d}_S^2 \;=\; (\mathbf{d}+\mathbf{d}_M)^2 \;=\; \mathbf{d}^2+\mathbf{d}_M^2 \;=\; 0\,, \tag{2.88}$$

and the $\mathbf{d}_S^2$ term is dropped, recovering Eq. (2.38). However, we have found that the supercurvature calculated without the first term in the $su(2/1)$ case did not gauge transform as $\mathcal{F}\to U\mathcal{F}U^\dagger$. This can be understood as due to the non-vanishing of $\mathbf{d}_M^2$, and the mixing of $\mathbf{d}_M$ and $\mathcal{J}$ under gauge transformations as shown in Eq. (2.84). Indeed, in the current case, $\mathbf{d}_M^2$ is represented by the matrix

$$\mathbf{d}_M^2 \;=\; -i\eta^2 \;=\; -i\begin{bmatrix}\xi\xi^\dagger & 0\\ 0 & v^2\end{bmatrix}\,, \tag{2.89}$$

which precisely cancels the problematic terms if added to Eq. (2.70):

$$\begin{aligned}&\mathcal{F}+\mathbf{d}_M^2 \\ &\quad= \; i\begin{bmatrix}F_W-\frac{1}{\sqrt{3}}F_B\cdot\mathbf{1}_{2\times2}-2\hat\phi\hat\phi^\dagger & \sqrt{2}\,D\hat\phi\\ \sqrt{2}(D\hat\phi)^\dagger & -\frac{2}{\sqrt{3}}F_B-2\hat\phi^\dagger\hat\phi\end{bmatrix}\,.\end{aligned} \tag{2.90}$$

Thus, keeping the $\mathbf{d}_M^2$ term will give us a supercurvature with the desired gauge transformation property. However, we nevertheless argue that the $\mathbf{d}_M^2$ term should be dropped. In the following, we calculate the action for $\mathcal{F}$ of Eq. (2.70), without the addition of $\mathbf{d}_M^2$, and find that adding $\mathbf{d}_M^2$ will lead to inconsistencies which we would like to avoid.

Before continuing, we note that the situation is somewhat different in the $su(2/2)$ case to be considered in section 2.3. There, the matrix derivative is nilpotent in the sense that $(\mathbf{d}_M^2X)=0$ for all $X\in su(2/2)$, and $\mathbf{d}_M^2\propto\lambda_{15}^s=-\frac{1}{\sqrt{2}}\mathbf{1}_{4\times4}$ which belongs to the center of the superalgebra. Despite the mixing between $\mathbf{d}_M$ and $\mathcal{J}$ as given in Eq. (2.84), $\mathbf{d}_M^2\propto\mathbf{1}_{4\times4}$ is invariant under gauge transformations by itself and can be dropped without any ill effects.

2.2.7 Inner Product and the Action

In QCD, the action is given by the inner product of the gauge connection $F_G = dG + \frac{1}{2}[G, G]$ with itself:

$$S_{\rm QCD} \;=\; \frac{1}{4}\langle F_G, F_G\rangle \;. \tag{2.91}$$

Note that F_G is an element of $\Omega(M) \otimes su(3)$. For $a, b \in \Omega(M)$ and $X, Y \in su(3)$, the inner product of the elements $a \otimes X$ and $b \otimes Y$ is given by

$$\langle a \otimes X, b \otimes Y\rangle \;=\; \langle a, b\rangle_{\Omega(M)}\langle X, Y\rangle_{su(3)} \;. \tag{2.92}$$

The inner product in $su(3)$ is simply

$$\langle X, Y\rangle_{su(3)} \;=\; {\rm Tr}(XY) \;. \tag{2.93}$$

For $\Omega(M) = \oplus_{i=0}^{4}\Omega^i(M)$, the inner product in each of the subspaces $\Omega^i(M)$ is given by

$$\langle a_i, b_i\rangle_{\Omega^i(M)} \;=\; \int *a_i \wedge b_i \;, \tag{2.94}$$

where $*$ indicates the Hodge dual, that is:

$$\begin{aligned}
*1 \;&=\; \frac{1}{24}\,\varepsilon^{\kappa\lambda\mu\nu} dx_\kappa \wedge dx_\lambda \wedge dx_\mu \wedge dx_\nu \;=\; d^4x \;, \\
*dx^\nu \;&=\; \frac{1}{6}\,\varepsilon^{\kappa\lambda\mu\nu} dx_\kappa \wedge dx_\lambda \wedge dx_\mu \;, \\
*(dx^\mu \wedge dx^\nu) \;&=\; \frac{1}{2}\,\varepsilon^{\kappa\lambda\mu\nu} dx_\kappa \wedge dx_\lambda \;, \\
*(dx^\lambda \wedge dx^\mu \wedge dx^\nu) \;&=\; \varepsilon^{\kappa\lambda\mu\nu} dx_\kappa \;, \\
*(dx^\kappa \wedge dx^\lambda \wedge dx^\mu \wedge dx^\nu) \;&=\; \varepsilon^{\kappa\lambda\mu\nu} \;,
\end{aligned} \tag{2.95}$$

where we assume the metric $g^{\mu\nu} = {\rm diag}(1, -1, -1, -1)$ and $\varepsilon_{0123} = 1$. For $a, b \in \Omega(M)$, we decompose $a = \sum_i a_i$, $b = \sum_i b_i$, where $a_i, b_i \in \Omega^i(M)$, and define

$$\langle a, b\rangle_{\Omega(M)} \;=\; \sum_i \langle a_i, b_i\rangle_{\Omega^i(M)} \;=\; \int \sum_i *a_i \wedge b_i \;. \tag{2.96}$$

In the case of F_G, which is an $su(3)$ valued two-form, we can write (with a slight abuse of notation)

$$\langle F_G, F_G\rangle \;=\; \int {\rm Tr}\Big[*F_G \wedge F_G\Big] \;. \tag{2.97}$$

Note that ${\rm Tr}[\,*F_G \wedge F_G\,]$ is a real scalar-valued 4-form which is gauge invariant. This guarantees the Lorentz and gauge invariance of the action $S_{\rm QCD}$.

Let us rewrite the above action in terms of the field strength tensor. Since $G = iG^a\lambda_a = i(G^a_\mu\, dx^\mu)\lambda_a$, we have

$$\begin{aligned} F_G &= dG + \frac{1}{2}[\,G,\,G\,] \;=\; \frac{i}{2}\left(G^a_{\mu\nu}\, dx^\mu \wedge dx^\nu\right)\lambda_a\;, \\ *F_G &= \frac{i}{4}\left(G^b_{\rho\sigma}\,\varepsilon^{\rho\sigma}{}_{\kappa\lambda} dx^\kappa \wedge dx^\lambda\right)\lambda_b\;, \end{aligned} \tag{2.98}$$

with

$$G^a_{\mu\nu} \;=\; \partial_\mu G^a_\nu - \partial_\nu G^a_\mu + i f^{abc} G^b_\mu G^c_\nu\;, \tag{2.99}$$

from which we find

$$*F_G \wedge F_G \;=\; -\frac{1}{2}\left(G^a_{\mu\nu} G^{b\mu\nu} d^4x\right)\lambda_a\lambda_b\;. \tag{2.100}$$

Recalling the normalization $\mathrm{Tr}(\lambda_a\lambda_b) = 2\delta_{ab}$ for the $su(3)$ Gell-Mann matrices, we obtain

$$\mathrm{Tr}\Big[*F_G \wedge F_G\Big] \;=\; -G^a_{\mu\nu} G^{a\mu\nu}\, d^4x\;, \tag{2.101}$$

and therefore

$$S_{\mathrm{QCD}} \;=\; -\frac{1}{4}\int G^a_{\mu\nu} G^{a\mu\nu}\, d^4x\;, \tag{2.102}$$

which is the more familiar form.

In an analogous fashion, let us write the action for $\mathcal{F}$, Eq. (2.70), as

$$\mathcal{S} \;=\; \frac{1}{4}\langle \mathcal{F}, \mathcal{F}\rangle_S\;. \tag{2.103}$$

Note that $\mathcal{F}$ is an element of $\Omega(M)\otimes su(2/1)$. For $a, b \in \Omega(M)$ and $X, Y \in su(2/1)$, the inner product of the elements $a\otimes X$ and $b\otimes Y$ is given by

$$\begin{aligned} &\langle a\otimes X, b\otimes Y\rangle_S \\ &\quad= \;(-1)^{|b||X|}\langle a, b\rangle_{\Omega(M)}\langle X, Y\rangle_{su(2/1)}\;. \end{aligned} \tag{2.104}$$

The inner product in $\Omega(M)$ is the same as before. For the inner product on $su(2/1)$, we define it to be

$$\langle X, Y\rangle_{su(2/1)} \;=\; \mathrm{Tr}(XY)\;, \tag{2.105}$$

just as in $su(3)$. Note that our use of a trace instead of a supertrace here in this definition has phenomenological significance. First, it would break any internal $SU(2/1)$ symmetry that may exist, but maintain the diagonal $SU(2)_L \times U(1)_Y$ gauge invariance. But, more significantly, it provides all the gauge boson kinetic terms with the correct signs, and also demands ϕ to be bosonic (commuting) instead of fermionic (anti-commuting) to prevent the

ϕ-dependent terms in the action from vanishing. Had a supertrace been used, ϕ would have been required to be fermionic.[12]

Unlike F_G of QCD, $\mathcal{F}$ is a linear combination of $su(2/1)$ valued zero-, one-, and two-forms. Let us write

$$\mathcal{F} \;=\; \sum_{i=0}^{2} \mathcal{F}^i \;, \tag{2.106}$$

where $\mathcal{F}^i \in \Omega^i(M) \otimes su(2/1)$. Then,

$$\begin{aligned} \langle \mathcal{F}, \mathcal{F} \rangle_S &= \int \mathrm{Tr} \left[\sum_{i=0}^{2} * \mathcal{F}^i \wedge \mathcal{F}^i \right] \\ &= \sum_{i=0}^{2} \langle \mathcal{F}^i, \mathcal{F}^i \rangle_S \;. \end{aligned} \tag{2.107}$$

Explicitly, we have

$$\begin{aligned} \mathcal{F}^0 &= i \begin{bmatrix} (-2\hat{\phi}\hat{\phi}^\dagger + \xi\xi^\dagger) & \mathbf{0}_{2\times 1} \\ \mathbf{0}_{1\times 2} & (-2\hat{\phi}^\dagger\hat{\phi} + v^2) \end{bmatrix} \;, \\ \mathcal{F}^1 &= \sqrt{2} i \begin{bmatrix} \mathbf{0}_{2\times 2} & (D\hat{\phi}) \\ (D\hat{\phi})^\dagger & 0 \end{bmatrix} \;, \\ \mathcal{F}^2 &= i \begin{bmatrix} F_W - \frac{1}{\sqrt{3}} F_B \cdot \mathbf{1}_{2\times 2} & \mathbf{0}_{2\times 1} \\ \mathbf{0}_{1\times 2} & -\frac{2}{\sqrt{3}} F_B \end{bmatrix} \;, \end{aligned} \tag{2.108}$$

and

[12] We have been unable to find any mention in the literature of the connection between the choice of trace or supertrace in the inner product with the bosonic or fermionic nature of ϕ. Perhaps this is a new observation. Mathematically, the choice of trace or supertrace is related to the KO dimension of the cyclic (co-)homology. See, for example, Refs. [157, 189, 198] for a mathematical description.

$$
\begin{aligned}
\mathrm{Tr}\Big[*\mathcal{F}^0\wedge\mathcal{F}^0\Big] &= -\mathrm{Tr}\begin{bmatrix}*(-2\hat\phi\hat\phi^\dagger+\xi\xi^\dagger) & \mathbf{0}_{2\times1}\\ \mathbf{0}_{1\times2} & *(-2\hat\phi^\dagger\hat\phi+v^2)\end{bmatrix}\wedge\begin{bmatrix}(-2\hat\phi\hat\phi^\dagger+\xi\xi^\dagger) & \mathbf{0}_{2\times1}\\ \mathbf{0}_{1\times2} & (-2\hat\phi^\dagger\hat\phi+v^2)\end{bmatrix}\\
&= -\mathrm{Tr}\begin{bmatrix}*(-2\hat\phi\hat\phi^\dagger+\xi\xi^\dagger)\wedge(-2\hat\phi\hat\phi^\dagger+\xi\xi^\dagger) & \mathbf{0}_{2\times1}\\ \mathbf{0}_{1\times2} & *(-2\hat\phi^\dagger\hat\phi+v^2)\wedge(-2\hat\phi^\dagger\hat\phi+v^2)\end{bmatrix}\\
&= -8\left(\hat\phi^\dagger\hat\phi-\frac{v^2}{2}\right)^2 d^4x\ ,\\
\mathrm{Tr}\Big[*\mathcal{F}^1\wedge\mathcal{F}^1\Big] &= +2\,\mathrm{Tr}\begin{bmatrix}\mathbf{0}_{2\times2} & *(D\hat\phi)\\ *(D\hat\phi)^\dagger & 0\end{bmatrix}\wedge\begin{bmatrix}\mathbf{0}_{2\times2} & (D\hat\phi)\\ (D\hat\phi)^\dagger & 0\end{bmatrix}\\
&= +2\,\mathrm{Tr}\begin{bmatrix}*(D\hat\phi)\wedge(D\hat\phi)^\dagger & \mathbf{0}_{2\times1}\\ \mathbf{0}_{1\times2} & *(D\hat\phi)^\dagger\wedge(D\hat\phi)\end{bmatrix}\\
&= +4(D_\mu\hat\phi)^\dagger(D^\mu\hat\phi)\ d^4x\ ,\\
\mathrm{Tr}\Big[*\mathcal{F}^2\wedge\mathcal{F}^2\Big] &= -\mathrm{Tr}\begin{bmatrix}*F_W-\frac{1}{\sqrt3}*F_B\cdot\mathbf{1}_{2\times2} & \mathbf{0}_{2\times1}\\ \mathbf{0}_{1\times2} & -\frac{2}{\sqrt3}*F_B\end{bmatrix}\wedge\begin{bmatrix}F_W-\frac{1}{\sqrt3}F_B\cdot\mathbf{1}_{2\times2} & \mathbf{0}_{2\times1}\\ \mathbf{0}_{1\times2} & -\frac{2}{\sqrt3}F_B\end{bmatrix}\\
&= -\mathrm{Tr}\begin{bmatrix}\left(*F_W-\frac{1}{\sqrt3}*F_B\cdot\mathbf{1}_{2\times2}\right)\wedge\left(F_W-\frac{1}{\sqrt3}F_B\cdot\mathbf{1}_{2\times2}\right) & \mathbf{0}_{2\times1}\\ \mathbf{0}_{1\times2} & \frac{4}{3}*F_B\wedge F_B\end{bmatrix}\\
&= -\mathrm{Tr}\begin{bmatrix}*F_W\wedge F_W-\frac{1}{\sqrt3}(*F_B\wedge F_W+*F_W\wedge F_B)+\frac{1}{3}*F_B\wedge F_B\cdot\mathbf{1}_{2\times2} & \mathbf{0}_{2\times1}\\ \mathbf{0}_{1\times2} & \frac{4}{3}*F_B\wedge F_B\end{bmatrix}\\
&= -\left(F^i_{W\mu\nu}F_W^{i\mu\nu}+F_{B\mu\nu}F_B^{\mu\nu}\right)d^4x\ . \qquad (2.109)
\end{aligned}
$$

Notice that, when calculating the traces of the 0- and 1- form contributions, one respectively needs to commute $\hat\phi$ through $\hat\phi^\dagger\hat\phi\hat\phi^\dagger$, and $(D\hat\phi)$ through $(D\hat\phi)^\dagger$, and $\hat\phi$ must be bosonic to prevent the trace from vanishing.

Putting everything together, we find:

$$
\begin{aligned}
\mathcal{S} &= \frac{1}{4}\langle\mathcal{F},\mathcal{F}\rangle_S\\
&= \int d^4x\Big[-\frac{1}{4}\left(F^i_{W\mu\nu}F_W^{i\mu\nu}+F_{B\mu\nu}F_B^{\mu\nu}\right)\\
&\qquad +(D_\mu\hat\phi)^\dagger(D^\mu\hat\phi)-V(\hat\phi,\hat\phi^\dagger)\Big]\ , \qquad (2.110)
\end{aligned}
$$

where

$$
\begin{aligned}
F^i_{W\mu\nu} &= \partial_\mu W^i_\nu-\partial_\nu W^i_\mu+2i\varepsilon^{ijk}W^j_\mu W^k_\nu\ ,\\
F_{B\mu\nu} &= \partial_\mu B_\nu-\partial_\nu B_\mu\ ,\\
D_\mu\hat\phi &= \partial_\mu\hat\phi-i\left(\boldsymbol{\tau}\cdot\boldsymbol{W}_\mu\right)\hat\phi-\frac{i}{\sqrt3}B_\mu\hat\phi\ . \qquad (2.111)
\end{aligned}
$$

and

$$
V(\hat\phi,\hat\phi^\dagger) = 2\left(\hat\phi^\dagger\hat\phi-\frac{v^2}{2}\right)^2\ . \qquad (2.112)
$$

Note that the above action is manifestly $SU(2)_L \times U(1)_Y$ gauge invariant as required, even though $\mathcal{F}$ did not have the desired gauge transformation property. Furthermore, the Higgs potential is minimized when $\phi^\dagger\phi = v^2/2$, consistent with our assumption that

$$\langle\hat{\phi}\rangle \;=\; \frac{\xi}{\sqrt{2}}\,, \tag{2.113}$$

and that ϕ is the fluctuation around it. Had we used $\mathcal{F}+\mathbf{d}_M^2$ instead of $\mathcal{F}$, the Higgs potential would have been $2(\hat{\phi}^\dagger\hat{\phi})^2$ and $\hat{\phi}$ would not have developed a VEV. So, for the consistency of the formalism, we will drop the $\mathbf{d}_M^2$ term from our supercurvature.

The resulting model is quite interesting in that spontaneous symmetry breaking is built into the model from the beginning. The ϕ field appearing in the superconnection is already the fluctuation around a symmetry-breaking vacuum. In other words, as emphasized in Refs. [120, 121], the superconnection $\mathcal{J}$ already 'knows' about the breaking of the symmetry. Eq. (2.84) suggests that the development of the Higgs VEV can be interpreted as due to the separation of the matrix derivative $\mathbf{d}_M$ from the superconnection $\mathcal{J}$, which would be the consequence of the two branes separating from each other. Thus, the spontaneous breaking of the gauge symmetry could be the result of the brane dynamics at work.

2.2.8 Symmetry Breaking

Let us analyze the model further. We take

$$\langle\hat{\phi}\rangle \;=\; \frac{\xi}{\sqrt{2}} \;=\; \frac{v}{\sqrt{2}}\begin{bmatrix}0\\1\end{bmatrix}\,, \tag{2.114}$$

so that

$$\langle\hat{\phi}^\dagger\tau^1\hat{\phi}\rangle \;=\; \langle\hat{\phi}^\dagger\tau^2\hat{\phi}\rangle \;=\; 0\,, \qquad \langle\hat{\phi}^\dagger\tau^3\hat{\phi}\rangle \;=\; -\frac{v^2}{2}\,. \tag{2.115}$$

Then, the linear combinations

$$W^\pm \;=\; \frac{W^1 \mp W^2}{\sqrt{2}}\,, \qquad Z \;=\; \frac{\sqrt{3}\,W^3 - B}{2} \tag{2.116}$$

obtain masses given by

$$M_W \;=\; v\,, \qquad M_Z \;=\; \frac{2v}{\sqrt{3}}\,, \tag{2.117}$$

while the linear combination

$$A \;=\; \frac{W^3 + \sqrt{3}\,B}{2} \tag{2.118}$$

remains massless and couples to

$$\frac{\lambda_3^s + \sqrt{3}\lambda_8^s}{2} \;=\; \begin{bmatrix}0 & 0 & 0\\ 0 & -1 & 0\\ 0 & 0 & -1\end{bmatrix} \;=\; Q\,, \tag{2.119}$$

which corresponds to the electromagnetic charge. Comparison with the SM will be made after the introduction of the coupling constant in the next subsection.

2.2.9 The Coupling Constants and the Value of $\sin^2\theta_W$

The Higgs Quartic Coupling and the Higgs Mass

We introduce the $SU(2)_L$ coupling constant g by rescaling the superconnection $\mathcal{J}$, the action $\mathcal{S}$, and the matrix-derivative matrix η as

$$\mathcal{J} \;\to\; \frac{g}{2}\mathcal{J}\,, \qquad \mathcal{S} \;\to\; \frac{g^2}{4}\mathcal{S}\,, \qquad \eta \;\to\; \frac{g}{2}\eta\,. \tag{2.120}$$

Extracting the Lagrangian from the action, we find

$$\begin{aligned}\mathcal{L} \;&=\; -\frac{1}{4}F^i_{W\,\mu\nu}\,F_W^{i\,\mu\nu} - \frac{1}{4}F_{B\,\mu\nu}F_B^{\mu\nu} \\ &\quad + \left(D_\mu\hat{\phi}\right)^\dagger\left(D^\mu\hat{\phi}\right) - \frac{g^2}{2}\left(\hat{\phi}^\dagger\hat{\phi} - \frac{v^2}{2}\right)^2\,,\end{aligned} \tag{2.121}$$

with

$$\begin{aligned}F^i_{W\,\mu\nu} \;&=\; \partial_\mu W^i_\nu - \partial_\nu W^i_\mu + ig\varepsilon^{ijk}W^j_\mu W^k_\nu\,, \\ F_{B\,\mu\nu} \;&=\; \partial_\mu B_\nu - \partial_\nu B_\mu\,, \\ D_\mu\hat{\phi} \;&=\; \partial_\mu\hat{\phi} - i\frac{g}{2}\left(\boldsymbol{\tau}\cdot\boldsymbol{W}_\mu\right)\hat{\phi} - i\frac{g}{2\sqrt{3}}B_\mu\hat{\phi}\,.\end{aligned} \tag{2.122}$$

The Higgs quartic coupling, which we normalize to

$$V(\hat{\phi}^\dagger,\hat{\phi}) \;=\; \lambda(\hat{\phi}^\dagger\hat{\phi})^2 + \cdots\,, \tag{2.123}$$

can be read off from Eq. (2.121) to be

$$\lambda \;=\; \frac{g^2}{2}\,. \tag{2.124}$$

Rewriting the Higgs field $\hat{\phi}$ as

$$\hat{\phi} \;=\; \begin{bmatrix}\pi^+ \\ \dfrac{v+h+i\pi^0}{\sqrt{2}}\end{bmatrix}\,, \tag{2.125}$$

we find

$$V(\hat{\phi}^\dagger,\hat{\phi}) \;=\; \frac{1}{2}(2\lambda v^2)h^2 + \cdots \tag{2.126}$$

so the Higgs mass (at tree level) is

$$M_h \;=\; \sqrt{2\lambda}\,v \;=\; gv\,. \tag{2.127}$$

$\sin^2\theta_W$ from the Coupling to Higgs

Since the Higgs doublet $\hat{\phi}$ has hypercharge +1, we can make the identification

$$g' \;=\; \frac{g}{\sqrt{3}}\,, \tag{2.128}$$

so that

$$D_\mu\hat{\phi} \;=\; \partial_\mu\hat{\phi} - i\frac{g}{2}\,(\boldsymbol{\tau}\cdot\boldsymbol{W}_\mu)\,\hat{\phi} - i\frac{g'}{2}B_\mu\hat{\phi}\,. \tag{2.129}$$

Also, after symmetry breaking, the photon field A couples to $(g/2)Q$, where Q is given in Eq. (2.119). Therefore,

$$e \;=\; \frac{g}{2} \;=\; g\sin\theta_W\,. \tag{2.130}$$

This relation can also be confirmed from the matching condition of the gauge couplings:

$$\frac{1}{e^2} \;=\; \frac{1}{g^2} + \frac{1}{g'^2} \;=\; \frac{4}{g^2}\,. \tag{2.131}$$

Thus, this formalism predicts

$$\sin^2\theta_W \;=\; \frac{g'^2}{g^2+g'^2} \;=\; \frac{e^2}{g^2} \;=\; \frac{1}{4}\,. \tag{2.132}$$

Using g and g', the masses of the W and Z we listed earlier in Eq. (2.117) can be written

$$M_W \;=\; \frac{gv}{2}\,, \qquad M_Z \;=\; \frac{\sqrt{g^2+g'^2}\,v}{2}\,, \tag{2.133}$$

while the linear combinations of W^3 and B that constitute the Z and the photon listed in Eqs. (2.116) and (2.118) can be written

$$\begin{aligned} Z &= W^3\cos\theta_W - B\sin\theta_W\,,\\ A &= W^3\sin\theta_W + B\cos\theta_W\,, \end{aligned} \tag{2.134}$$

just as in the SM. Note that, together with Eq. (2.127), this model predicts

$$\frac{M_h}{M_W} \;=\; 2\,. \tag{2.135}$$

This is clearly problematic, since it leads to the prediction $M_h \approx 160\,\mathrm{GeV}$. However, we could argue that these tree level predictions are those that are valid at the scale at which the SM emerges from the underlying NCG theory. The question is whether renormalization group running from this emergence scale to the electroweak scale will cure the Higgs mass. This will be addressed in the next subsection.

$\sin^2\theta_W$ from the Coupling to Fermions

The value of $\sin^2\theta_W$ can also be checked by looking at the gauge couplings of the fermions [164]. The interaction of the leptons with the $SU(2)_L \times U(1)_Y$ gauge bosons in the SM is given by

$$\begin{aligned} -\mathcal{L}_\ell^{\rm SM} &= \frac{g}{2}\big(\,\overline{\ell}_L\gamma^\mu\tau_i\ell_L\,\big)W_\mu^i \\ &\quad -\frac{g'}{2}\big(\,\overline{\ell}_L\gamma^\mu\ell_L + 2\,\overline{\ell}_R\gamma^\mu\ell_R\,\big)B_\mu, \end{aligned} \tag{2.136}$$

where

$$\ell_L \;=\; \begin{bmatrix}\nu_L\\ \ell_L^-\end{bmatrix}\;, \qquad \ell_R \;=\; \ell_R^-\;. \tag{2.137}$$

In the $su(2/1)$ embedding, we demand invariance only under transformations generated by the even part of the superalgebra, which leads to the interaction

$$\mathcal{L}_\ell^{\rm even} \;=\; -\frac{g}{2}\sum_{i=1,2,3,8}\big(\,\overline{\psi}\gamma^\mu\lambda_i^s\psi\,\big)\,J_\mu^i \tag{2.138}$$

where

$$\psi \;=\; \begin{bmatrix}\ell_L\\ \ell_R\end{bmatrix} \;=\; \begin{bmatrix}\nu_L\\ \ell_L^-\\ \ell_R^-\end{bmatrix} \tag{2.139}$$

is a triplet under $su(2/1)$, and J_μ^i is the vector field associated with the one-form $J^i = J_\mu^i dx^\mu$. Recalling that $J^{1,2,3}$ are identified with $W^{1,2,3} = W_\mu^{1,2,3}dx^\mu$, while J^8 is identified with $B = B_\mu dx^\mu$, this interaction can be written out as

$$\begin{aligned} -\mathcal{L}_\ell^{\rm even} &= \frac{g}{2}\,\big(\,\overline{\ell}_L\gamma^\mu\tau_i\ell_L\,\big)\,W_\mu^i \\ &\quad -\frac{g}{2\sqrt{3}}\,\big(\,\overline{\ell}_L\gamma^\mu\ell_L + 2\,\overline{\ell}_R\gamma^\mu\ell_R\,\big)\,B_\mu\;. \end{aligned} \tag{2.140}$$

Comparing Eqs. (2.136) and (2.140) we reproduce Eq. (2.128).

Here the requirement of $SU(2)_L\times U(1)_Y$ gauge invariance was used to determine the couplings between the even part of the $su(2/1)$ superconnection and the fermion fields. The couplings between the odd part of the superconnection, namely the Higgs doublet ϕ, and the fermion fields must reproduce the SM Yukawa couplings. How these can be accommodated within the superconnection formalism will be discussed in section 2.4.

2.2.10 The Emergence Scale and the Higgs Boson Mass from $su(2/1)$

Let us now address the prediction for the Higgs mass including radiative corrections. In what follows, we assume the relation

$$\frac{M_h^2}{M_W^2} \;=\; \frac{8\lambda}{g^2} \tag{2.141}$$

to be invariant under renormalization group flow, and follow the evolutions of the coupling constants λ and g assuming the SM particle content below the scale at which the SM emerges from some underlying NCG theory.

The renormalization group equation (RGE) for λ is coupled to those of the fermion Yukawa couplings, of which we only take that of the top quark to be relevant. The RGE's for λ and the top Yukawa coupling h_t are [199]

$$\begin{aligned}
\mu\frac{dh_t}{d\mu} &= \frac{h_t}{(4\pi)^2}\left[\frac{9}{2}h_t^2 - \left(\frac{17}{12}g'^2 + \frac{9}{4}g^2 + 8g_s^2\right)\right] , \\
\mu\frac{d\lambda}{d\mu} &= \frac{1}{(4\pi)^2}\Bigg[\left\{12h_t^2 - \left(3g'^2 + 9g^2\right)\right\}\lambda - 6h_t^4 \\
&\qquad +24\lambda^2 + \frac{3}{8}\left(g'^4 + 2g'^2g^2 + 3g^4\right)\Bigg] ,
\end{aligned} \tag{2.142}$$

where g', g, and g_s are the $U(1)_Y$, $SU(2)_L$ and $SU(3)_c$ coupling constants, respectively, and the top Yukawa coupling h_t is normalized to

$$m_t = \frac{h_t v}{\sqrt{2}} . \tag{2.143}$$

The most recent value of the top quark mass is $m_t = 173.21 \pm 0.51 \pm 0.71$ GeV [1].

We follow Ref. [164] to find the boundary condition on λ. To fix the scale of emergence Λ_s of the $su(2/1)$ structure, we look for the scale at which the relation $g = \sqrt{3}g'$ (*i.e.*, $\sin^2\theta_W = 1/4$) holds. We use the 1-loop relations

$$\frac{1}{[g_i(\Lambda_s)]^2} = \frac{1}{[g_i(\Lambda_0)]^2} - 2b_i \ln\frac{\Lambda_s}{\Lambda_0} \qquad (i = 1, 2, 3) \tag{2.144}$$

where $g_1 = g'$, $g_2 = g$, $g_3 = g_s$, and the respective constants b_i read as [200]:

$$\begin{aligned}
b_1 &= \frac{1}{16\pi^2}\left(\frac{20\,n_f}{9} + \frac{n_H}{6}\right) , \\
b_2 &= -\frac{1}{16\pi^2}\left(-\frac{4\,n_f}{3} - \frac{n_H}{6} + \frac{22}{3}\right) , \\
b_3 &= -\frac{1}{16\pi^2}\left(-\frac{4\,n_f}{3} + 11\right) .
\end{aligned} \tag{2.145}$$

We will only need to look at the runnings of g_1 and g_2 to find Λ_s, but will also need to look at the running of g_3 in the RGE's listed in Eq. (2.142). Setting the number of fermion families to $n_f = 3$, and the number of Higgs doublets to $n_H = 1$, we have

$$b_1 = \frac{1}{16\pi^2}\left(\frac{41}{6}\right) , \quad b_2 = \frac{1}{16\pi^2}\left(-\frac{19}{6}\right) , \quad b_3 = -\frac{7}{16\pi^2} . \tag{2.146}$$

The numerical values ($\overline{\text{MS}}$) of the coupling constants at the scale $\Lambda_0 = M_Z$ are given in Ref. [1] as $\alpha_1^{-1}(M_Z) = 98.36$, $\alpha_2^{-1}(M_Z) = 29.58$, and $\alpha_3^{-1}(M_Z) = 8.45$, where $\alpha_i^{-1} = 4\pi/g_i^2$. Note that $\alpha_1^{-1}(M_Z)/\alpha_2^{-1}(M_Z) = 3.325$. Running this ratio up to where $\alpha_1^{-1}(\Lambda_s)/\alpha_2^{-1}(\Lambda_s) = 3$, we find the scale of emergence to be

$$\Lambda_s \simeq 4\,\text{TeV} . \tag{2.147}$$

Since this is the energy where the structure associated with $su(2/1)$ emerges, the constraint Eq. (2.124), $\lambda = g_2^2/2$, is also expected to hold at this energy. This predicts the Higgs mass value as $M_h = 2M_W \simeq 160$ GeV, which should also be interpreted as the Higgs mass value at $\Lambda_s \simeq 4$ TeV. Using Eq. (2.142) with the boundary conditions $\lambda = g_2^2/2$ at 4 TeV and $h_t = \sqrt{2}m_t/v$ at M_Z, we find $\lambda(M_Z) \simeq 0.24$ (Fig. 2.1) and

$$M_h(M_Z) \simeq 170\,\text{GeV} . \tag{2.148}$$

Thus, the predicted Higgs mass is incorrect and it cannot be remedied within the $su(2/1)$ superconnection framework. However, as we will show in the next section, lowering it to 126 GeV can be realized in the $su(2/2)$ extension which predicts the emergence of the left-right symmetric model (already broken to the SM) at the TeV scale.

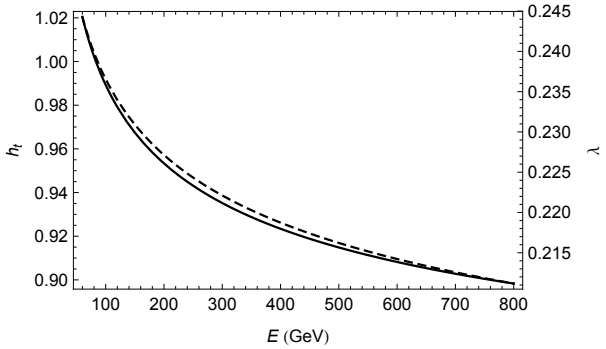

Figure 2.1: The behavior of the top Yukawa coupling (h_t), which is represented as the dashed line, and the Higgs quartic coupling (λ).

2.2.11 $su(2/1)$ Summary

In this section, we have reviewed the $su(2/1)$ superconnection formalism into which the SM is embedded in some detail, including some sticking points, and looked at its predictions. The embedding enforces the relations $\sin^2\theta_W = 1/4$ and $\lambda = g^2/2$. The first is valid at the scale of $\Lambda_s \sim 4\,\text{TeV}$, which we interpret as the scale at which the $su(2/1)$ formalism emerges from a yet unknown underlying NCG theory. Assuming the second relation is also valid at that scale, we obtain $M_h \sim 170\,\text{GeV}$ as the prediction for the Higgs mass.

Though the Higgs mass prediction is clearly problematic, the formalism has a couple of interesting and attractive features which deserve attention. First and foremost, we note that the generalized exterior derivative in the discrete direction, *i.e.*, the matrix derivative, carries in it information on the Higgs VEV $\langle\hat{\phi}\rangle = \xi/\sqrt{2}$. The zero-form field ϕ which appears in the superconnection $\mathcal{J}$ is the fluctuation of $\hat{\phi}$ around this VEV: $\hat{\phi} = \langle\hat{\phi}\rangle + \phi$. Thus, the $SU(2)_L \times U(1)_Y$ gauge symmetry is spontaneously broken to $U(1)_{em}$ from the beginning, and there is, in fact, no need to shift the field from ϕ to $\hat{\phi}$, only to shift it back again to account for the physical degrees of freedom in the broken phase. Since the matrix derivative is necessitated by the existence of the discrete extra dimension, one could argue that it is the dynamical separation of the two branes itself that broke the symmetry and shifted the Higgs field. In other words, it is the dynamics of the discrete geometry of the two branes that is responsible for spontaneous symmetry breaking, and the Higgs field is just one manifestation of the phenomenon. This is in contrast to the usual SM point of view in which the Higgs dynamics is independent of any dynamics of the background geometry.

Second, since the formalism fails to predict the correct Higgs mass, it begs an extension to a formalism that would. This can be viewed as an advantage instead of a drawback of the model since it points us to new directions. As it has been pointed out in Ref. [155, 156, 163], an additional singlet scalar degree of freedom in the Higgs sector would mix with the Higgs boson to brings its mass down, and a simple way to introduce such a degree of freedom would be to extend the SM electroweak gauge group to $SU(2)_L \times SU(2)_R \times U(1)_{B-L}$. In the superconnection formalism, this gauge group can be embedded into $su(2/2)$. Thus, despite the absence of our understanding on how these structures arise from an underlying NCG theory, the data already suggest an extension from $su(2/1)$ to $su(2/2)$.

2.3 Embedding of the Left-Right Symmetric Model into $su(2/2)$

Given the limitations of the $su(2/1)$ superconnection model outlined above, here we explore the possibility of using an $su(2/2)$ superconnection to embed the SM electroweak gauge fields and the Higgs. The gauge group embedded will be $SU(2)_L \times SU(2)_R \times U(1)_{B-L}$ with the same gauge couplings for $SU(2)_L$ and $SU(2)_R$. Thus, we are working with the left-right symmetric model (LRSM) [201–214]. We will assume the breaking of $SU(2)_L \times SU(2)_R \times U(1)_{B-L}$ down to $U(1)_{em}$ so that the electromagnetic charge Q will be given by

$$Q \;=\; I_{L3} + I_{R3} + \frac{B-L}{2}\,, \tag{2.149}$$

where I_{L3} and I_{R3} are respectively the third components of the left- and right-handed isospins.

We follow the same route as in the previous section: we will first work out the superconnection $\mathcal{J}$ of the model and find that an bi-doublet scalar field Φ appears in the odd part. The

supercurvature $\mathcal{F}$ and action $\mathcal{S}$ are derived from the superconnection $\mathcal{J}$; in the process, it is discovered that the matrix derivative $\mathbf{d}_M$ in this case can be made nilpotent, and as a consequence, the supercurvature $\mathcal{F}$ has a simple gauge transformation property, which guarantees the gauge invariance of the action $\mathcal{S}$. To achieve the breaking of $SU(2)_L \times SU(2)_R \times U(1)_{B-L}$ down to $U(1)_{em}$, two complex triplet scalar fields Δ_L and Δ_R are introduced as matter fields living, respectively, on the left- and right-handed branes. We find that $\Delta_{L,R}$ can naturally be placed in an $su(2/2)$ representation, suggesting that their introduction is not entirely ad-hoc. The formalism predicts the ratios of gauge coupling constants, and thus the value of $\sin^2\theta_W$, and the self-couplings of the Φ, but not the various couplings involving $\Delta_{L,R}$ in the most generic Higgs potential [208]. However, this is sufficient to fix the scale Λ_s at which the structure is expected to emerge from an underlying NCG theory, and also suggests that the measured Higgs mass can be accommodated within the framework.

2.3.1 $su(2/2)$ Superalgebra

The superalgebra $su(2/2)$ consists of 4×4 supertraceless Hermitian matrices, in which the even and odd parts are 2×2 submatrices. The basis for $su(2/2)$ can be chosen to be

$$
\begin{aligned}
\lambda_1^s &= \begin{bmatrix} 0 & 1 & 0 & 0 \\ 1 & 0 & 0 & 0 \\ 0 & 0 & 0 & 0 \\ 0 & 0 & 0 & 0 \end{bmatrix}, \ \lambda_2^s = \begin{bmatrix} 0 & -i & 0 & 0 \\ i & 0 & 0 & 0 \\ 0 & 0 & 0 & 0 \\ 0 & 0 & 0 & 0 \end{bmatrix}, \\
\lambda_3^s &= \begin{bmatrix} 1 & 0 & 0 & 0 \\ 0 & -1 & 0 & 0 \\ 0 & 0 & 0 & 0 \\ 0 & 0 & 0 & 0 \end{bmatrix}, \ \lambda_4^s = \begin{bmatrix} 0 & 0 & 1 & 0 \\ 0 & 0 & 0 & 0 \\ 1 & 0 & 0 & 0 \\ 0 & 0 & 0 & 0 \end{bmatrix}, \\
\lambda_5^s &= \begin{bmatrix} 0 & 0 & -i & 0 \\ 0 & 0 & 0 & 0 \\ i & 0 & 0 & 0 \\ 0 & 0 & 0 & 0 \end{bmatrix}, \ \lambda_6^s = \begin{bmatrix} 0 & 0 & 0 & 0 \\ 0 & 0 & 1 & 0 \\ 0 & 1 & 0 & 0 \\ 0 & 0 & 0 & 0 \end{bmatrix}, \\
\lambda_7^s &= \begin{bmatrix} 0 & 0 & 0 & 0 \\ 0 & 0 & -i & 0 \\ 0 & i & 0 & 0 \\ 0 & 0 & 0 & 0 \end{bmatrix}, \ \lambda_8^s = \begin{bmatrix} 0 & 0 & 0 & 0 \\ 0 & 0 & 0 & 0 \\ 0 & 0 & 1 & 0 \\ 0 & 0 & 0 & -1 \end{bmatrix}, \\
\lambda_9^s &= \begin{bmatrix} 0 & 0 & 0 & 1 \\ 0 & 0 & 0 & 0 \\ 0 & 0 & 0 & 0 \\ 1 & 0 & 0 & 0 \end{bmatrix}, \ \lambda_{10}^s = \begin{bmatrix} 0 & 0 & 0 & -i \\ 0 & 0 & 0 & 0 \\ 0 & 0 & 0 & 0 \\ i & 0 & 0 & 0 \end{bmatrix}, \\
\lambda_{11}^s &= \begin{bmatrix} 0 & 0 & 0 & 0 \\ 0 & 0 & 0 & 1 \\ 0 & 0 & 0 & 0 \\ 0 & 1 & 0 & 0 \end{bmatrix}, \ \lambda_{12}^s = \begin{bmatrix} 0 & 0 & 0 & 0 \\ 0 & 0 & 0 & -i \\ 0 & 0 & 0 & 0 \\ 0 & i & 0 & 0 \end{bmatrix},
\end{aligned}
$$

$$\lambda^s_{13} = \begin{bmatrix} 0 & 0 & 0 & 0 \\ 0 & 0 & 0 & 0 \\ 0 & 0 & 0 & 1 \\ 0 & 0 & 1 & 0 \end{bmatrix}, \ \lambda^s_{14} = \begin{bmatrix} 0 & 0 & 0 & 0 \\ 0 & 0 & 0 & 0 \\ 0 & 0 & 0 & -i \\ 0 & 0 & i & 0 \end{bmatrix},$$
$$\lambda^s_{15} = -\frac{1}{\sqrt{2}} \begin{bmatrix} 1 & 0 & 0 & 0 \\ 0 & 1 & 0 & 0 \\ 0 & 0 & 1 & 0 \\ 0 & 0 & 0 & 1 \end{bmatrix}. \tag{2.150}$$

These matrices are normalized to satisfy the orthogonality condition

$$\mathrm{Tr}(\lambda^s_a \lambda^s_b) = 2\delta_{ab}, \quad \text{where } a, b = 1, 2, \cdots 15. \tag{2.151}$$

The even elements of the superalgebra are spanned by λ^s_1, λ^s_2, λ^s_3, λ^s_8, λ^s_{13}, λ^s_{14}, λ^s_{15}, while the odd elements are spanned by λ^s_4, λ^s_5, λ^s_6, λ^s_7, λ^s_9, λ^s_{10}, λ^s_{11}, λ^s_{12}. The only matrix different from its $su(4)$ counterpart is λ^s_{15} due to the supertracelessness condition. These matrices close under commutation and anti-commutation relations as

$$\begin{aligned} \frac{1}{i}[\lambda^s_i, \lambda^s_j] &= 2 f_{ijk} \lambda^s_k , \\ \frac{1}{i}[\lambda^s_i, \lambda^s_m] &= 2 f_{iml} \lambda^s_l , \\ \{\lambda^s_m, \lambda^s_n\} &= 2 d_{mnk} \lambda^s_k - \sqrt{2}\, \delta_{mn} \lambda^s_{15} , \end{aligned} \tag{2.152}$$

where i, j, k denote the even indices $1, 2, 3, 8, 13, 14, 15$, while m, n, l denote the odd indices $4, 5, 6, 7, 9, 10, 11, 12$. The f's and d's are the same as the structure constants for $su(4)$:

$$\begin{aligned} \frac{1}{i}[\lambda_a, \lambda_b] &= 2 f_{abc} \lambda_c , \\ \{\lambda_a, \lambda_b\} &= 2 d_{abc} \lambda_c + \delta_{ab} , \end{aligned} \tag{2.153}$$

where $\lambda_a = \lambda^s_a$ for $a = 1, 2, \cdots 14$, and

$$\lambda_{15} = \frac{1}{\sqrt{2}} \begin{bmatrix} 1 & 0 & 0 & 0 \\ 0 & 1 & 0 & 0 \\ 0 & 0 & -1 & 0 \\ 0 & 0 & 0 & -1 \end{bmatrix}. \tag{2.154}$$

2.3.2 $su(2/2)$ Superconnection

The superconnection $\mathcal{J}$ of this model is expressed as $\mathcal{J} = iJ_a\lambda_a^s$, where $a = 1, 2, \cdots 15$. We make the identifications[13]

$$\begin{array}{lcllcl} J_{1,2,3} & = & W_L^{1,2,3}\,, & J_{13,14,8} & = & W_R^{1,2,3}\,, \\ J_4 - iJ_5 & = & \sqrt{2}\phi_1^0\,, & J_4 + iJ_5 & = & \sqrt{2}\phi_1^{0*}\,, \\ J_6 - iJ_7 & = & \sqrt{2}\phi_1^-\,, & J_6 + iJ_7 & = & \sqrt{2}\phi_1^+\,, \\ J_9 - iJ_{10} & = & \sqrt{2}\phi_2^+\,, & J_9 + iJ_{10} & = & \sqrt{2}\phi_2^-\,, \\ J_{11} - iJ_{12} & = & \sqrt{2}\phi_2^0\,, & J_{11} + iJ_{12} & = & \sqrt{2}\phi_2^{0*}\,, \\ J_{15} & = & W_{BL}\,, & & & \end{array} \tag{2.155}$$

where $W_L^i = W_L^{i\mu}dx_\mu$, $W_R^i = W_R^{i\mu}dx_\mu$, and $W_{BL} = W_{BL}^\mu dx_\mu$ are one-form fields while the ϕ's are zero-form fields, corresponding, respectively, to the $SU(2)_L \times SU(2)_R \times U(1)_{B-L}$ gauge fields and the bi-doublet Higgs field:[14]

$$\Phi \;=\; \begin{bmatrix} \phi_1^0 & \phi_2^+ \\ \phi_1^- & \phi_2^0 \end{bmatrix}\,. \tag{2.156}$$

The resulting superconnection has the form

$$\mathcal{J} \;=\; i\begin{bmatrix} \mathcal{W}_L - \frac{1}{\sqrt{2}}W_{BL}\cdot\mathbf{1}_{2\times2} & \sqrt{2}\,\Phi \\ \sqrt{2}\,\Phi^\dagger & \mathcal{W}_R - \frac{1}{\sqrt{2}}W_{BL}\cdot\mathbf{1}_{2\times2} \end{bmatrix}\,, \tag{2.157}$$

where

$$\mathcal{W}_L \;=\; W_L^i\,\tau^i\,, \qquad \mathcal{W}_R \;=\; W_R^i\,\tau^i\,. \tag{2.158}$$

In this assignment, we have assumed that the ordering of the rows of the $su(2/2)$ matrix, from top to bottom, correspond to left-handed isospin up, left-handed isospin down, right-handed isospin up, then right-handed isospin down. So the leptons will be placed in a 4 dimensional representation of $su(2/2)$ in the order

$$\psi \;=\; \begin{bmatrix} \ell_L \\ \ell_R \end{bmatrix} \;=\; \begin{bmatrix} \nu_L \\ \ell_L^- \\ \nu_R \\ \ell_R^- \end{bmatrix}\,. \tag{2.159}$$

[13] We switch from subscripts to superscripts for the $SU(2)$ indices to make room for the subscripts L and R.

[14] Here, we use the subscripts 1 and 2 to label the two $SU(2)_L$ doublets embedded in Φ. Some papers in the literature use subscripts to label $SU(2)_R$ doublets, *e.g.*, Refs. [207, 208], so care is necessary when comparing formulae.

2.3.3 $su(2/2)$ Supercurvature

As reviewed in the discussion of the $su(2/1)$ case, the supercurvature is given by

$$\mathcal{F} \;=\; (\mathbf{d}\mathcal{J}) + (\mathbf{d}_M\mathcal{J}) + \frac{1}{2}[\,\mathcal{J},\,\mathcal{J}\,]_S\;, \tag{2.160}$$

where the $\mathbf{d}_M^2$ term has been assumed not to contribute and has been dropped.

The $(\mathbf{d}\mathcal{J})$ term is

$$\begin{aligned}&(\mathbf{d}\mathcal{J})\\ &\quad=\;\; i\begin{bmatrix} d\mathcal{W}_L - \frac{1}{\sqrt{2}}\,dW_{BL}\cdot\mathbf{1}_{2\times2} & \sqrt{2}\,d\Phi \\ \sqrt{2}\,d\Phi^\dagger & d\mathcal{W}_R - \frac{1}{\sqrt{2}}\,dW_{BL}\cdot\mathbf{1}_{2\times2}\end{bmatrix}\;.\end{aligned} \tag{2.161}$$

The matrix derivative is defined with the 4×4 η-matrix given by

$$\eta \;=\; \begin{bmatrix}\mathbf{0}_{2\times2} & \zeta \\ \zeta^\dagger & \mathbf{0}_{2\times2}\end{bmatrix}\;, \tag{2.162}$$

where ζ is a multiple of a 2×2 unitary matrix, that is $\zeta^\dagger\zeta = \zeta\zeta^\dagger = v^2\mathbf{1}_{2\times2}$. This time, the matrix derivative is nilpotent: $(\mathbf{d}_M^2 X) = 0$ for all $X \in su(2/2)$. We find

$$\begin{aligned}&(\mathbf{d}_M\mathcal{J})\\ &\quad=\;\; i[\,\eta,\,\mathcal{J}\,]_S\\ &\quad=\;\; i\begin{bmatrix}-\sqrt{2}(\zeta\Phi^\dagger + \Phi\zeta^\dagger) & +i(\mathcal{W}_L\zeta - \zeta\mathcal{W}_R)\\ -i(\zeta^\dagger\mathcal{W}_L - \mathcal{W}_R\zeta^\dagger) & -\sqrt{2}(\zeta^\dagger\Phi + \Phi^\dagger\zeta)\end{bmatrix}\;.\end{aligned} \tag{2.163}$$

To calculate the supercommutator of $\mathcal{J}$ with itself, we separate it into the 1-0 and 0-1 parts as before:

$$\begin{aligned}\mathcal{J} \;\;=\;\; &\underbrace{i\begin{bmatrix}\mathcal{W}_L - \frac{1}{\sqrt{2}}W_{BL}\cdot\mathbf{1}_{2\times2} & \mathbf{0}_{2\times2}\\ \mathbf{0}_{2\times2} & \mathcal{W}_R - \frac{1}{\sqrt{2}}W_{BL}\cdot\mathbf{1}_{2\times2}\end{bmatrix}}_{\mathcal{J}_{10}}\\ &+\underbrace{i\begin{bmatrix}\mathbf{0}_{2\times2} & \sqrt{2}\,\Phi\\ \sqrt{2}\,\Phi^\dagger & \mathbf{0}_{2\times2}\end{bmatrix}}_{\mathcal{J}_{01}}\;.\end{aligned} \tag{2.164}$$

We find:

$$[\,\mathcal{J}_{10},\,\mathcal{J}_{10}\,]_S$$

$$
\begin{aligned}
&= -2i \begin{bmatrix} \varepsilon^{ijk}(W_L^i \wedge W_L^j)\tau^k & \mathbf{0}_{2\times 2} \\ \mathbf{0}_{2\times 2} & \varepsilon_{ijk}(W_R^i \wedge W_R^j)\tau^k \end{bmatrix} , \\
[\,\mathcal{J}_{01},\,\mathcal{J}_{01}\,]_S &= -4i \begin{bmatrix} \Phi\Phi^\dagger & \mathbf{0}_{2\times 2} \\ \mathbf{0}_{2\times 2} & \Phi^\dagger\Phi \end{bmatrix} , \\
[\,\mathcal{J}_{10},\,\mathcal{J}_{01}\,]_S &= [\,\mathcal{J}_{01},\,\mathcal{J}_{10}\,]_S \\
&= \sqrt{2}i \begin{bmatrix} \mathbf{0}_{2\times 2} & +i(\mathcal{W}_L\Phi - \Phi\mathcal{W}_R) \\ -i(\Phi^\dagger\mathcal{W}_L - \mathcal{W}_R\Phi^\dagger) & \mathbf{0}_{2\times 2} \end{bmatrix} .
\end{aligned}
\tag{2.165}
$$

Putting everything together, we obtain

$$
\begin{aligned}
\mathcal{F} &= i \begin{bmatrix} F_L - \frac{1}{\sqrt{2}}F_{BL} - 2\Phi\Phi^\dagger - \sqrt{2}(\zeta\Phi^\dagger + \Phi\zeta^\dagger) & \sqrt{2}\,D\Phi + i(\mathcal{W}_L\zeta - \zeta\mathcal{W}_R) \\ \sqrt{2}(D\Phi)^\dagger - i(\zeta^\dagger\mathcal{W}_L - \mathcal{W}_R\zeta^\dagger) & F_R - \frac{1}{\sqrt{2}}F_{BL} - 2\Phi^\dagger\Phi - \sqrt{2}(\zeta^\dagger\Phi + \Phi^\dagger\zeta) \end{bmatrix} \\
&= i \begin{bmatrix} F_L - \frac{1}{\sqrt{2}}F_{BL} - 2\hat{\Phi}\hat{\Phi}^\dagger + v^2\mathbf{1}_{2\times 2} & \sqrt{2}\,D\hat{\Phi} \\ \sqrt{2}(D\hat{\Phi})^\dagger & F_R - \frac{1}{\sqrt{2}}F_{BL} - 2\hat{\Phi}^\dagger\hat{\Phi} + v^2\mathbf{1}_{2\times 2} \end{bmatrix} ,
\end{aligned}
\tag{2.166}
$$

where we have introduced the shifted Higgs field

$$
\hat{\Phi} = \Phi + \frac{\zeta}{\sqrt{2}} , \tag{2.167}
$$

and

$$
\begin{aligned}
F_{L,R} &= (F_{L,R})^a\tau^a = (dW_{L,R}^i - (W_{L,R} \wedge W_{L,R})^i)\tau^i \\
&\qquad = (dW_{L,R}^i - \varepsilon^{ijk}W_{L,R}^j \wedge W_{L,R}^k)\tau^i , \\
F_{BL} &= dW_{BL} \cdot \mathbf{1}_{2\times 2} , \\
D\Phi &= d\Phi + i\mathcal{W}_L\Phi - i\Phi\mathcal{W}_R , \\
D\hat{\Phi} &= d\hat{\Phi} + i\mathcal{W}_L\hat{\Phi} - i\hat{\Phi}\mathcal{W}_R .
\end{aligned}
\tag{2.168}
$$

We have also used $\zeta^\dagger\zeta = \zeta\zeta^\dagger = v^2\mathbf{1}_{2\times 2}$.

2.3.4 Gauge Transformation Properties

The even part of $su(2/2)$ generate the gauge transformations in $SU(2)_L \times SU(2)_R \times U(1)_{B-L}$:

$$
U = \exp\left[i \sum_{i=1,2,3,8,13,14,15} \theta_i \lambda_i^s \right]
$$

$$= \begin{bmatrix} u_L\, e^{-i\theta/\sqrt{2}} & \mathbf{0}_{2\times 2} \\ \mathbf{0}_{2\times 2} & u_R\, e^{-i\theta/\sqrt{2}} \end{bmatrix} , \tag{2.169}$$

where

$$\begin{aligned} u_L &= \exp\Big[\, i(\theta_1\tau_1 + \theta_2\tau_2 + \theta_3\tau_3)\Big] \;\in\; SU(2)_L \,, \\ u_R &= \exp\Big[\, i(\theta_{13}\tau_1 + \theta_{14}\tau_2 + \theta_8\tau_3)\Big] \;\in\; SU(2)_R \,, \\ \theta &= \theta_{15} \,. \end{aligned} \tag{2.170}$$

The one-form gauge fields transform as

$$\begin{aligned} \mathcal{W}_L &\to u_L \mathcal{W}_L u_L^\dagger + i\, du_L u_L^\dagger \,, \\ \mathcal{W}_R &\to u_R \mathcal{W}_R u_R^\dagger + i\, du_R u_R^\dagger \,, \\ W_{BL} &\to W_{BL} - d\theta \,. \end{aligned} \tag{2.171}$$

For the zero-form field, we assume that it is the shifted field $\hat{\Phi}$ which transforms as

$$\hat{\Phi} \;\to\; u_L \hat{\Phi}\, u_R^\dagger \,. \tag{2.172}$$

$\zeta/\sqrt{2}$ is interpreted as the VEV of $\hat{\Phi}$, and Φ as the fluctuation around it. Thus,

$$\begin{aligned} F_L &\to u_L F_L u_L^\dagger \,, \\ F_R &\to u_R F_R u_R^\dagger \,, \\ F_{BL} &\to F_{BL} \,, \\ D\hat{\Phi} &\to u_L (D\hat{\Phi}) u_R^\dagger \,. \end{aligned} \tag{2.173}$$

This time, the terms coming from ζ causes no problems due to $\zeta^\dagger\zeta = \zeta\zeta^\dagger = v^2\mathbf{1}_{2\times 2}$, and $\mathcal{F}$ can be seen to transform as

$$\mathcal{F} \;\to\; U\mathcal{F}U^\dagger \,. \tag{2.174}$$

2.3.5 The Action

Following the same procedure as the $su(2/1)$ case, we find that the action in the $su(2/2)$ case is given by

$$\begin{aligned} \mathcal{S} &= \frac{1}{4}\langle \mathcal{F}, \mathcal{F}\rangle_S \\ &= \int d^4x \Big[-\frac{1}{4}\left(F^i_{L\mu\nu} F_L^{i\mu\nu} + F^i_{R\mu\nu} F_R^{i\mu\nu} + F_{BL\mu\nu} F_{BL}^{\mu\nu} \right) \\ &\qquad + \mathrm{Tr}\Big[(D_\mu\hat{\Phi})^\dagger (D^\mu\hat{\Phi}) \Big] - V(\hat{\Phi}^\dagger, \hat{\Phi}) \Big] \,, \end{aligned} \tag{2.175}$$

where

$$\begin{aligned} F_L^{i\mu\nu} &= \partial^\mu W_L^{i\nu} - \partial^\nu W_L^{i\mu} + 2i\varepsilon^{ijk} W_L^{j\mu} W_L^{k\nu} \,, \\ F_R^{i\mu\nu} &= \partial^\mu W_R^{i\nu} - \partial^\nu W_R^{i\mu} + 2i\varepsilon^{ijk} W_R^{j\mu} W_R^{k\nu} \,, \\ F_{BL}^{\mu\nu} &= \partial^\mu W_{BL}^{\nu} - \partial^\nu W_{BL}^{\mu} \,, \\ D^\mu \hat{\Phi} &= \partial^\mu \hat{\Phi} - i W_L^{i\mu} \tau^i \hat{\Phi} + i W_R^{i\mu}\, \hat{\Phi}\, \tau^i \,, \\ V(\hat{\Phi}^\dagger, \hat{\Phi}) &= 2\,\mathrm{Tr}\left[\left(\hat{\Phi}^\dagger \hat{\Phi} \; - \frac{v^2}{2} \mathbf{1}_{2\times 2} \right)^2 \right] . \end{aligned} \tag{2.176}$$

Thus, we obtain a manifestly gauge invariant action as required. The Higgs potential is minimized when

$$\hat{\Phi}^\dagger \hat{\Phi} \;=\; \frac{v^2}{2} \mathbf{1}_{2\times 2} \,, \tag{2.177}$$

which is consistent with our interpretation that the VEV of $\hat{\Phi}$ is given by

$$\langle \hat{\Phi} \rangle \;=\; \frac{\zeta}{\sqrt{2}} \,. \tag{2.178}$$

2.3.6 Symmetry Breaking

Breaking with the Bi-doublet

It is a well known fact that the bidoublet $\hat{\Phi}$ alone acquiring a vacuum expectation value (VEV) will not break $SU(2)_L \times SU(2)_R \times U(1)_{B-L}$ all the way down to $U(1)_{em}$. Indeed, if we assume non-zero VEV's for the (would-be) neutral components of Φ as

$$\langle \hat{\Phi} \rangle \;=\; \frac{\zeta}{\sqrt{2}} \;=\; \frac{1}{\sqrt{2}} \begin{bmatrix} \kappa_1 & 0 \\ 0 & \kappa_2 \end{bmatrix} \,, \tag{2.179}$$

where κ_1 and κ_2 are in general complex, then the unitarity of ζ demands

$$|\kappa_1| \;=\; |\kappa_2| \;=\; v \,. \tag{2.180}$$

So, up to a possible relative phase between κ_1 and κ_2, we have

$$\langle \hat{\Phi} \rangle \;=\; \frac{v}{\sqrt{2}} \begin{bmatrix} 1 & 0 \\ 0 & 1 \end{bmatrix} \,. \tag{2.181}$$

Since $\hat{\Phi}$ transforms as $\hat{\Phi} \to u_L \hat{\Phi} u_R^\dagger$ under local gauge transformations, this VEV remains invariant under $U(1)_{B-L}$, and under the vectorial combination of $SU(2)_L$ and $SU(2)_R$, that is, when $u_L = u_R$. Thus $\langle \hat{\Phi} \rangle$ only breaks $SU(2)_L \times SU(2)_R \times U(1)_{B-L}$ down to $SU(2)_V \times U(1)_{B-L}$, providing only three massive gauge bosons.

Introduction of Triplets

To achieve the symmetry breaking we need, we follow Mohapatra and Senjanovic [204] and introduce the scalar fields $\Delta_L(3,1,2)$ and $\Delta_R(1,3,2)$, where the first two numbers indicate the dimensions of the $SU(2)_L$ and $SU(2)_R$ representations these fields belong to, and the third number is the $B-L$ charge. We advocate the picture that Δ_L lives on the left-handed brane while Δ_R lives on the right-handed brane as matter fields and are not part of a generalized connection.

These triplet fields are often represented in the literature as 2×2 complex traceless matrices:

$$\begin{aligned}\Delta_{L,R} &= \frac{1}{\sqrt{2}}\left(\delta^1_{L,R}\,\tau^1+\delta^2_{L,R}\,\tau^2+\delta^3_{L,R}\,\tau^3\right)\\ &= \begin{bmatrix}\delta^+_{L,R}/\sqrt{2} & \delta^{++}_{L,R}\\ \delta^0_{L,R} & -\delta^+_{L,R}/\sqrt{2}\end{bmatrix}\,,\end{aligned} \tag{2.182}$$

where

$$\begin{aligned}\delta^{++}_{L,R} &= \frac{1}{\sqrt{2}}\left(\delta^1_{L,R}-i\delta^2_{L,R}\right)\,,\\ \delta^+_{L,R} &= \delta^3_{L,R}\,,\\ \delta^0_{L,R} &= \frac{1}{\sqrt{2}}\left(\delta^1_{L,R}+i\delta^2_{L,R}\right)\,.\end{aligned} \tag{2.183}$$

These fields transform as

$$\begin{aligned}\Delta_L &\to e^{+i\sqrt{2}\theta}u_L\Delta_L u_L^\dagger\,,\\ \Delta_R &\to e^{+i\sqrt{2}\theta}u_R\Delta_R u_R^\dagger\,,\end{aligned} \tag{2.184}$$

where the $U(1)_{B-L}$ phase will be shown to correspond to $B-L=2$ later.

It is instructive to rewrite the $\Delta_{L,R}$ fields as complex symmetric matrices:

$$\begin{aligned}\widetilde{\Delta}_{L,R} &\equiv i\tau^2\Delta^*_{L,R}\\ &= \begin{bmatrix}\delta^{0*}_{L,R} & -\delta^-_{L,R}/\sqrt{2}\\ -\delta^-_{L,R}/\sqrt{2} & -\delta^{--}_{L,R}\end{bmatrix}\,.\end{aligned} \tag{2.185}$$

These fields transform as

$$\begin{aligned}\widetilde{\Delta}_L &\to e^{-i\sqrt{2}\theta}u_L\widetilde{\Delta}_L u_L^{\mathrm{T}}\,,\\ \widetilde{\Delta}_R &\to e^{-i\sqrt{2}\theta}u_R\widetilde{\Delta}_R u_R^{\mathrm{T}}\,.\end{aligned} \tag{2.186}$$

Let us place these fields into a single 4×4 matrix as

$$\widetilde{\Delta} = \begin{bmatrix}\widetilde{\Delta}_L & \mathbf{0}_{2\times 2}\\ \mathbf{0}_{2\times 2} & \widetilde{\Delta}_R\end{bmatrix}\,. \tag{2.187}$$

Then under $SU(2)_L \times SU(2)_R \times U(1)_{B-L}$ gauge transformations, Eq. (2.169), it transforms as

$$\widetilde{\Delta} \;\rightarrow\; U\widetilde{\Delta}U^{\mathrm{T}}\,, \tag{2.188}$$

which shows that $\widetilde{\Delta}$ provides a module for an $su(2/2)$ representation. The even elements of $su(2/2)$ correspond to the gauge transformations, while the odd elements would interchange $\widetilde{\Delta}_L$ and $\widetilde{\Delta}_R$. Since the leptons ψ and its charge conjugate $\psi^c = C\bar{\psi}^{\mathrm{T}}$ transform as

$$\psi \;\rightarrow\; U\psi\,, \qquad \psi^c \;\rightarrow\; U^*\psi^c\,, \tag{2.189}$$

we can construct the gauge invariant interaction

$$\begin{aligned}\mathcal{L}_M &= y_M\left(\bar{\psi}^c\,\widetilde{\Delta}^\dagger\,\psi + \bar{\psi}\,\widetilde{\Delta}\,\psi^c\right)\\ &= y_M\left[\left(\ell_L^{\mathrm{T}}\,C\,\Delta_L i\tau^2\ell_L + \ell_R^{\mathrm{T}}\,C\,\Delta_R i\tau^2\ell_R\right) + h.c.\right]\,,\end{aligned} \tag{2.190}$$

which will lead to Majorana masses for the neutrinos after symmetry breaking. Thus, the triplet scalars have a natural place in the $su(2/2)$ framework, as do Majorana neutrinos.

The Higgs Potential

Reverting to the original traceless matrix representation, the Lagrangian for the $\Delta_{L,R}$ is given by

$$\begin{aligned}\mathcal{L} &= \mathrm{Tr}\Big[(D^\mu\Delta_L)^\dagger(D_\mu\Delta_L) + (D^\mu\Delta_R)^\dagger(D_\mu\Delta_R)\Big]\\ &\quad -V(\Delta_L^\dagger,\Delta_L,\Delta_R^\dagger,\Delta_R,\hat{\Phi}^\dagger,\hat{\Phi})\,,\end{aligned} \tag{2.191}$$

where the covariant derivatives are given by

$$\begin{aligned}D^\mu\Delta_L &= \partial^\mu\Delta_L - iW_L^{i\mu}\left[\tau^i,\Delta_L\right] - i\sqrt{2}W_{BL}^\mu\Delta_L\,,\\ D^\mu\Delta_R &= \partial^\mu\Delta_R - iW_R^{i\mu}\left[\tau^i,\Delta_R\right] - i\sqrt{2}W_{BL}^\mu\Delta_R\,.\end{aligned} \tag{2.192}$$

The most general form of the Higgs potential $V(\Delta_L^\dagger,\Delta_L,\Delta_R^\dagger,\Delta_R,\hat{\Phi}^\dagger,\hat{\Phi})$ which respects the $SU(2)_L \times SU(2)_R \times U(1)_{B-L}$ gauge symmetry and the discrete left-right symmetry under the interchanges

$$\Delta_L \;\leftrightarrow\; \Delta_R\,, \qquad \hat{\Phi} \;\leftrightarrow\; \hat{\Phi}^\dagger\,, \tag{2.193}$$

and is at most quartic in the fields is given in Ref. [208] as

$$V \;=\; -\mu_1^2\mathrm{Tr}\Big[\Phi^\dagger\Phi\Big] - \mu_2^2\left(\mathrm{Tr}\Big[\Phi^\dagger\widetilde{\Phi}\Big] + \mathrm{Tr}\Big[\widetilde{\Phi}^\dagger\Phi\Big]\right) - \mu_3^2\left(\mathrm{Tr}\Big[\Delta_L^\dagger\Delta_L\Big] + \mathrm{Tr}\Big[\Delta_R^\dagger\Delta_R\Big]\right)$$

$$
\begin{aligned}
&+\lambda_1\left(\mathrm{Tr}\Big[\Phi^\dagger\Phi\Big]\right)^2+\lambda_2\left\{\left(\mathrm{Tr}\Big[\Phi^\dagger\widetilde{\Phi}\Big]\right)^2+\left(\mathrm{Tr}\Big[\widetilde{\Phi}^\dagger\Phi\Big]\right)^2\right\}\\
&+\lambda_3\,\mathrm{Tr}\Big[\Phi^\dagger\widetilde{\Phi}\Big]\mathrm{Tr}\Big[\widetilde{\Phi}^\dagger\Phi\Big]+\lambda_4\,\mathrm{Tr}\Big[\Phi^\dagger\Phi\Big]\left(\mathrm{Tr}\Big[\Phi^\dagger\widetilde{\Phi}\Big]+\mathrm{Tr}\Big[\widetilde{\Phi}^\dagger\Phi\Big]\right)\\
&+\rho_1\left\{\left(\mathrm{Tr}\Big[\Delta_L^\dagger\Delta_L\Big]\right)^2+\left(\mathrm{Tr}\Big[\Delta_R^\dagger\Delta_R\Big]\right)^2\right\}+\rho_2\left(\mathrm{Tr}\Big[\Delta_L\Delta_L\Big]\mathrm{Tr}\Big[\Delta_L^\dagger\Delta_L^\dagger\Big]+\mathrm{Tr}\Big[\Delta_R\Delta_R\Big]\mathrm{Tr}\Big[\Delta_R^\dagger\Delta_R^\dagger\Big]\right)\\
&+\rho_3\,\mathrm{Tr}\Big[\Delta_L^\dagger\Delta_L\Big]\mathrm{Tr}\Big[\Delta_R^\dagger\Delta_R\Big]+\rho_4\left(\mathrm{Tr}\Big[\Delta_L\Delta_L\Big]\mathrm{Tr}\Big[\Delta_R^\dagger\Delta_R^\dagger\Big]+\mathrm{Tr}\Big[\Delta_L^\dagger\Delta_L^\dagger\Big]\mathrm{Tr}\Big[\Delta_R\Delta_R\Big]\right)\\
&+\alpha_1\,\mathrm{Tr}\Big[\Phi^\dagger\Phi\Big]\left(\mathrm{Tr}\Big[\Delta_L^\dagger\Delta_L\Big]+\mathrm{Tr}\Big[\Delta_R^\dagger\Delta_R\Big]\right)+\alpha_2\left(\mathrm{Tr}\Big[\Phi^\dagger\tilde{\Phi}\Big]\mathrm{Tr}\Big[\Delta_L^\dagger\Delta_L\Big]+\mathrm{Tr}\Big[\tilde{\Phi}^\dagger\Phi\Big]\mathrm{Tr}\Big[\Delta_R^\dagger\Delta_R\Big]\right)\\
&+\alpha_2^*\left(\mathrm{Tr}\Big[\Phi^\dagger\tilde{\Phi}\Big]\mathrm{Tr}\Big[\Delta_R^\dagger\Delta_R\Big]+\mathrm{Tr}\Big[\tilde{\Phi}^\dagger\Phi\Big]\mathrm{Tr}\Big[\Delta_L^\dagger\Delta_L\Big]\right)+\alpha_3\left(\mathrm{Tr}\Big[\Phi\Phi^\dagger\Delta_L\Delta_L^\dagger\Big]+\mathrm{Tr}\Big[\Phi^\dagger\Phi\Delta_R\Delta_R^\dagger\Big]\right)\\
&+\beta_1\left(\mathrm{Tr}\Big[\Phi\Delta_R\Phi^\dagger\Delta_L^\dagger\Big]+\mathrm{Tr}\Big[\Phi^\dagger\Delta_L\Phi\Delta_R^\dagger\Big]\right)+\beta_2\left(\mathrm{Tr}\Big[\widetilde{\Phi}\Delta_R\Phi^\dagger\Delta_L^\dagger\Big]+\mathrm{Tr}\Big[\widetilde{\Phi}^\dagger\Delta_L\Phi\Delta_R^\dagger\Big]\right)\\
&+\beta_3\left(\mathrm{Tr}\Big[\Phi\Delta_R\widetilde{\Phi}^\dagger\Delta_L^\dagger\Big]+\mathrm{Tr}\Big[\Phi^\dagger\Delta_L\widetilde{\Phi}\Delta_R^\dagger\Big]\right)\,, \qquad (2.194)
\end{aligned}
$$

where we have denoted $\hat{\Phi}$ simply as Φ, and $\widetilde{\Phi}=\tau^2\Phi^*\tau^2$. As we can see, it is fairly complicated with 18 free parameters: 3 negative mass-squared parameters μ_i^2 $(i=1,2,3)$, 4 parameters λ_i $(i=1,2,3,4)$ for the quartic self-couplings of Φ, 4 parameters ρ_i $(i=1,2,3,4)$ for the quartic couplings of $\Delta_{L,R}$, 4 parameters α_i ($i=1,2,3$ with α_2 complex) that couple Φ to Δ_L or Δ_R, and 3 parameters β_i $(i=1,2,3)$ which couple all three. The possible phase of α_2 breaks CP explicitly.

Using the identity[15]

$$
\mathrm{Tr}\Big[(\Phi^\dagger\Phi)^2\Big] \;=\; \left(\mathrm{Tr}\Big[\Phi^\dagger\Phi\Big]\right)^2-\frac{1}{2}\mathrm{Tr}\Big[\Phi^\dagger\widetilde{\Phi}\Big]\mathrm{Tr}\Big[\widetilde{\Phi}^\dagger\Phi\Big]\,, \qquad (2.195)
$$

we can see that the Higgs potential of Eq. (2.176) corresponds to

$$
\lambda_1\;=\;2\,,\quad \lambda_3\;=\;-1\,,\quad \lambda_2\;=\;\lambda_4\;=\;0\,, \qquad (2.196)
$$

with

$$
\mu_1^2\;=\;2v^2\,,\qquad \mu_2^2\;=\;0\,. \qquad (2.197)
$$

We envision that the NCG theory from which the effective $su(2/2)$ model emerges will determine all the other parameters in the potential as well. For now, we follow Ref. [204] and simply assume that the (would be) neutral components of the triplets acquire VEV's given by

$$
\langle\Delta_L\rangle\;=\;\frac{1}{\sqrt{2}}\begin{bmatrix}0&0\\ v_L&0\end{bmatrix}\,,\quad \langle\Delta_R\rangle\;=\;\frac{1}{\sqrt{2}}\begin{bmatrix}0&0\\ v_R&0\end{bmatrix}\,, \qquad (2.198)
$$

where we set $v_L=0$ to avoid it from breaking $SU(2)_L$. This breaks $SU(2)_R\times U(1)_{B-L}$ down to $U(1)_Y$. The linear combinations

$$
W_R^\pm\;=\;\frac{W_R^1\mp W_R^2}{\sqrt{2}}\,,\quad Z'\;=\;\frac{\sqrt{2}\,W_R^3-W_{BL}}{\sqrt{3}} \qquad (2.199)
$$

[15] See Appendix B.1 for a collection of useful identities of this type.

obtain masses given by

$$M_{W_R} \;=\; \sqrt{2}v_R\,, \qquad M_{Z'} \;=\; \sqrt{6}v_R\,, \tag{2.200}$$

while the linear combination

$$B \;=\; \frac{W_R^3 + \sqrt{2}\,W_{BL}}{\sqrt{3}} \tag{2.201}$$

remains massless and couples to

$$\frac{\lambda_8^s + \sqrt{2}\,\lambda_{15}^s}{\sqrt{3}} \;=\; \frac{1}{\sqrt{3}}\begin{bmatrix} -1 & 0 & 0 & 0 \\ 0 & -1 & 0 & 0 \\ 0 & 0 & 0 & 0 \\ 0 & 0 & 0 & -2 \end{bmatrix} \;=\; \frac{Y}{\sqrt{3}}\,, \tag{2.202}$$

which corresponds to the hypercharge Y embedded in $su(2/1)$.

The presence of the VEV of $\hat{\Phi}$, Eq. (2.179), breaks the remaining $SU(2)_L \times U(1)_Y$ down to $U(1)_{em}$. We have noted earlier that the nilpotency of the matrix derivative demands the unitarity of the ζ matrix, which in turn would demand $|\kappa_1| = |\kappa_2|$. If the underlying NCG requires this condition to be maintained under the introduction of the triplet fields, it would constitute a robust prediction of the formalism and provide an extra condition on the emergent LRSM. However, such a condition is phenomenologically problematic. If we generate the quark masses via Yukawa couplings with the bi-doublet field Φ, that is, the interaction of the form

$$\mathcal{L}_Y \;=\; \overline{q}_{Li}\left(y_{ij}\Phi + \tilde{y}_{ij}\widetilde{\Phi}\right) q_{Rj} + h.c.\,, \tag{2.203}$$

where y_{ij} and $\tilde{y}_{ij}$ are the Yukawa coupling matrices, it would lead to mass matrices of the form

$$\begin{aligned} \sqrt{2}M_u \;&=\; \kappa_1\, y + \kappa_2^*\,\tilde{y} \;=\; |\kappa_1|\, y + |\kappa_2| e^{-i\alpha}\tilde{y}\,, \\ \sqrt{2}M_d \;&=\; \kappa_2\, y + \kappa_1^*\,\tilde{y} \;=\; |\kappa_2| e^{i\alpha} y + |\kappa_1|\,\tilde{y}\,, \end{aligned} \tag{2.204}$$

where α is a possible CP violating phase difference between κ_1 and κ_2. The condition $|\kappa_1| = |\kappa_2|$ would imply

$$M_u \;=\; e^{-i\alpha} M_d\,, \tag{2.205}$$

leading to both M_u and M_d being diagonalized in the same basis with the same eigenvalues. For this reason, it is normally assumed that $|\kappa_1| \gg |\kappa_2|$, which would provide an explanation of $m_t \gg m_b$, and CKM mixing[16]. Moreover, $|\kappa_1|$ and $|\kappa_2|$ being hierarchical is also required by the suppression of the flavor changing neutral-currents (FCNC) [208]. Therefore, we will allow for $|\kappa_1| \neq |\kappa_2|$ though the nilpotency of the matrix derivative is destroyed.

We have seen in the $su(2/1)$ case that the lack of nilpotency of the matrix derivative could lead to the gauge transformation property of the supercurvature $\mathcal{F}$ becoming non-standard,

[16]The assumption $|\kappa_1| \gg |\kappa_2|$ is not mandatory in order to realize $m_t \gg m_b$. The smallness of the CP violating parameter can be established by the interplay of $\sin\alpha$, $|\kappa_1|$, and $|\kappa_2|$ [215].

though otherwise it did not seem to have any ill effects. However, it is somewhat worrisome that an exterior derivative is not nilpotent. We conjecture a couple of reasons why this may be permissible. First, the dynamics necessary for the breaking of the gauge symmetries may be accompanied by some type of 'phase' transition in the NCG from one in which the matrix derivative is nilpotent to one in which it is not. Second, the $su(2/2)$ formalism is not a complete description of the NCG (we are yet to include $SU(3)$ color or the generational structure) and needs to be extended to a larger superalgebra in which the matrix derivative maintains nilpotency even after symmetry breaking, just as the $su(2/1)$ formalism needed to be extended to $su(2/2)$. The two possibilities we have listed here could actually be compatible. Recalling that the exterior derivative operator d in standard differential geometry is the dual of the boundary operator ∂ [216], $d^2 \neq 0$ would imply $\partial^2 \neq 0$, that is, the boundary of a boundary does not vanish. That could imply the appearance of some type of singularity in the geometry, which can be removed by going to higher dimensions.

The massive gauge bosons are now linear combinations of $W_L^\pm$, Z, $W_R^\pm$, and Z' defined in Eqs. (2.116) and (2.199). Taking both κ_1 and κ_2 to be real for the moment, and setting $\kappa_+ = \sqrt{\kappa_1^2 + \kappa_2^2}$, they are

$$\begin{aligned} W_2^\pm &= W_R^\pm \cos\chi - W_L^\pm \sin\chi \,, \\ W_1^\pm &= W_R^\pm \sin\chi + W_L^\pm \cos\chi \,, \end{aligned} \tag{2.206}$$

where

$$\tan 2\chi = \frac{2\kappa_1\kappa_2}{v_R^2} \,, \tag{2.207}$$

with masses

$$M^2_{W_{1,2}} = (v_R^2 + \kappa_+^2) \mp \sqrt{v_R^4 + 4\kappa_1^2\kappa_2^2} \,, \tag{2.208}$$

and

$$\begin{aligned} Z_2 &= Z' \cos\varphi - Z \sin\varphi \,, \\ Z_1 &= Z' \sin\varphi + Z \cos\varphi \,, \end{aligned} \tag{2.209}$$

where

$$\tan 2\varphi = \frac{4\sqrt{2}\kappa_+^2}{9v_R^2 - 2\kappa_+^2} \,, \tag{2.210}$$

with masses

$$\begin{aligned} M^2_{Z_1} &= \left(3v_R^2 + \kappa_+^2\right) - \sqrt{9v_R^4 - 2v_R^2\kappa_+^2 + \kappa_+^4} \,, \\ M^2_{Z_2} &= \left(3v_R^2 + \kappa_+^2\right) + \sqrt{9v_R^4 - 2v_R^2\kappa_+^2 + \kappa_+^4} \,. \end{aligned} \tag{2.211}$$

When $v_R \gg \kappa_+$, the masses are approximately

$$M^2_{W_1} = \kappa_+^2 - \frac{2\kappa_1^2\kappa_2^2}{v_R^2} + \cdots \,,$$

$$
\begin{aligned}
M_{W_2}^2 &= 2v_R^2 + \kappa_+^2 + \frac{2\kappa_1^2\kappa_2^2}{v_R^2} + \cdots \,, \\
M_{Z_1}^2 &= \frac{4\kappa_+^2}{3} - \frac{4\kappa_+^4}{27v_R^2} + \cdots \,, \\
M_{Z_2}^2 &= 6v_R^2 + \frac{2\kappa_+^2}{3} + \frac{4\kappa_+^4}{27v_R^2} + \cdots \,.
\end{aligned} \tag{2.212}
$$

The remaining massless gauge boson is

$$
A \;=\; \frac{W_L + \sqrt{3}B}{2} \;=\; \frac{W_L^3 + W_R^3 + \sqrt{2}W_{BL}}{2} \,, \tag{2.213}
$$

coupled to

$$
\frac{\lambda_3^s + \lambda_8^s + \sqrt{2}\lambda_{15}^s}{2} \;=\; \begin{bmatrix} 0 & 0 & 0 & 0 \\ 0 & -1 & 0 & 0 \\ 0 & 0 & 0 & 0 \\ 0 & 0 & 0 & -1 \end{bmatrix} \;=\; Q \,. \tag{2.214}
$$

For the model to be phenomenologically viable, we need $v_R \gg \kappa_+ \approx 246\,\mathrm{GeV}$ to suppress the mixing between W_L and W_R, and that between Z and Z'. The current experimental bounds on the LRSM parameters will be discussed in section 2.5.

2.3.7 The Coupling Constants and the Value of $\sin^2\theta_W$

Introduction of the Coupling Constant and $\sin^2\theta_W$ from the Coupling to Triplet Higgs

We introduce the gauge coupling constant g by rescaling the superconnection $\mathcal{J}$, the action $\mathcal{S}$, and the matrix-derivative matrix η as in Eq. (2.120). The expression for the resulting action is the same as before except with the following replacements:

$$
\begin{aligned}
F_L^{i\mu\nu} &= \partial^\mu W_L^{i\nu} - \partial^\nu W_L^{i\mu} + ig\varepsilon^{ijk} W_L^{j\mu} W_L^{k\nu} \,, \\
F_R^{i\mu\nu} &= \partial^\mu W_R^{i\nu} - \partial^\nu W_R^{i\mu} + ig\varepsilon^{ijk} W_R^{j\mu} W_R^{k\nu} \,,
\end{aligned}
$$

$$
\begin{aligned}
D^\mu\hat{\Phi} &= \partial^\mu\hat{\Phi} - i\frac{g}{2} W_L^{i\mu}\tau^i\hat{\Phi} + i\frac{g}{2} W_R^{i\mu}\,\hat{\Phi}\,\tau^i \,, \\
V(\hat{\Phi}^\dagger, \hat{\Phi}) &= \frac{g^2}{2}\,\mathrm{Tr}\left[\left(\hat{\Phi}^\dagger\hat{\Phi} \;- \frac{v^2}{2}\right)^2\right] .
\end{aligned} \tag{2.215}
$$

Note that the gauge couplings for $SU(2)_L$ and $SU(2)_R$ are the same. Thus, we have a left-right symmetric model (LRSM). The ratio of the $U(1)_{B-L}$ coupling to the $SU(2)_{L,R}$ couplings cannot be determined from the gauge couplings of the bi-doublet $\hat{\Phi}$ since it does

not couple to W_{BL}. It can, however, be read off from the covariant derivatives of the triplet fields which are changed to:

$$\begin{aligned} D^\mu \Delta_L &= \partial^\mu \Delta_L - i\frac{g}{2} W_L^{i\mu} \left[\tau^i, \Delta_L\right] - i\frac{g}{\sqrt{2}} W_{BL}^\mu \Delta_L \,, \\ D^\mu \Delta_R &= \partial^\mu \Delta_R - i\frac{g}{2} W_R^{i\mu} \left[\tau^i, \Delta_R\right] - i\frac{g}{\sqrt{2}} W_{BL}^\mu \Delta_R \,. \end{aligned} \tag{2.216}$$

Since the triplets are assigned the charge $B - L = 2$, these need to be compared with the expressions

$$\begin{aligned} D^\mu \Delta_L &= \partial^\mu \Delta_L - i\frac{g}{2} W_L^{i\mu} \left[\tau^i, \Delta_L\right] - i g_{BL} W_{BL}^\mu \Delta_L \,, \\ D^\mu \Delta_R &= \partial^\mu \Delta_R - i\frac{g}{2} W_R^{i\mu} \left[\tau^i, \Delta_R\right] - i g_{BL} W_{BL}^\mu \Delta_R \,, \end{aligned} \tag{2.217}$$

from which we conclude[17]

$$\frac{g_{BL}}{g} \;=\; \frac{1}{\sqrt{2}} \,. \tag{2.218}$$

The Z' and B fields in Eqs. (2.199) and (2.201) can then be written as

$$\begin{aligned} Z' &= \frac{g W_R^3 - g_{BL} W_{BL}}{\sqrt{g^2 + g_{BL}^2}} \,, \\ B &= \frac{g_{BL} W_R^3 + g W_{BL}}{\sqrt{g^2 + g_{BL}^2}} \,. \end{aligned} \tag{2.219}$$

The value of g' can then be obtained from the matching condition associated with the breaking $SU(2)_R \times U(1)_{B-L} \to U(1)_Y$:

$$\frac{1}{g'^2} \;=\; \frac{1}{g^2} + \frac{1}{g_{BL}^2} \;=\; \frac{3}{g^2} \quad \to \quad \frac{g'}{g} \;=\; \frac{1}{\sqrt{3}} \,. \tag{2.220}$$

Note also that the B field couples to $(g/2)(Y/\sqrt{3})$, where $Y/\sqrt{3}$ is defined in Eq. (2.202), and the photon field of Eq. (2.213) couples to $(g/2)Q$, where Q is defined in Eq. (2.214). Therefore,

$$g' \;=\; \frac{g}{\sqrt{3}} \,, \qquad e \;=\; \frac{g}{2} \,, \tag{2.221}$$

[17] Where this relation comes from can also seen by the requirement that the mass of Z,

$$M_{Z_1}^2 \;\simeq\; \frac{g^2}{4}\kappa_+^2 \Big[1 + 4v_L^2/\kappa_+^2 + O(\kappa_+^2/v_R^2)\Big] \left(\frac{g^2 + 2g_{BL}^2}{g^2 + g_{BL}^2}\right)$$

should match the SM one $M_Z^2 = (g^2 + g'^2)v^2/4$ at the scale where $SU(2)_R$ is broken. Basically, the Weinberg angle in the LRSM is defined as $\cos^2\theta_W = \frac{g^2 + g_{BL}^2}{g^2 + 2g_{BL}^2}$, which is matched to the SM definition $\cos^2\theta_W = \frac{g^2}{g^2 + g'^2}$ [207].

and thus $\sin^2\theta_W = 1/4$, just as in the $su(2/1)$ case. Perhaps this is not surprising given that our $su(2/1)$ embedding is a sub-embedding of the $su(2/2)$ embedding.

The masses of the massive gauge bosons are now expressed as

$$\begin{aligned} M_{W_1}^2 &= \frac{g^2\kappa_+^2}{4} - \frac{g^2\kappa_1^2\kappa_2^2}{2v_R^2} + \cdots , \\ M_{W_2}^2 &= \frac{g^2(2v_R^2+\kappa_+^2)}{4} + \frac{g^2\kappa_1^2\kappa_2^2}{2v_R^2} + \cdots , \\ M_{Z_1}^2 &= \frac{(g^2+g'^2)\kappa_+^2}{4} - \frac{g^2\kappa_+^4}{27v_R^2} + \cdots , \\ M_{Z_2}^2 &= \frac{g^2(9v_R^2+\kappa_+^2)}{6} + \frac{g^2\kappa_+^4}{27v_R^2} + \cdots , \end{aligned} \tag{2.222}$$

and we can see that κ_+ plays the role of the SM Higgs VEV and thus $\kappa_+ \approx 246\,\mathrm{GeV}$.

$\sin^2\theta_W$ from the Coupling to Fermions

The value of $\sin^2\theta_W$ can also be determined from the gauge coupling of the fermions. Collecting the lepton fields into an $su(2/2)$ quartet as shown in Eq. (2.159), the requirement of $SU(2)_L \times SU(2)_R \times U(1)_{B-L}$ gauge invariance leads to the interaction

$$\begin{aligned} -\mathcal{L}_\ell^{\text{even}} &= \frac{g}{2} \sum_{i=1,2,3,8,13,14,15} \left(\overline{\psi}\gamma^\mu \lambda_i^s \psi \right) J_\mu^i \\ &= \frac{g}{2}\Big[\overline{\ell}_L\gamma_\mu \left(\boldsymbol{\tau}\cdot\boldsymbol{W}_L^\mu\right)\ell_L + \overline{\ell}_R\gamma_\mu\left(\boldsymbol{\tau}\cdot\boldsymbol{W}_R^\mu\right)\ell_R \\ &\qquad -\frac{1}{\sqrt{2}}\,\overline{\ell}_L\gamma_\mu W_{BL}^\mu \ell_L - \frac{1}{\sqrt{2}}\,\overline{\ell}_R\gamma_\mu W_{BL}^\mu \ell_R \Big] . \end{aligned} \tag{2.223}$$

This should be compared with the leptonic part of the $SU(2)_L \times SU(2)_R \times U(1)_{B-L}$ Lagrangian in which the left- and right-handed leptons are assigned the representations $\ell_L(2,1,-1)$ and $\ell_R(1,2,-1)$:

$$\begin{aligned} -\mathcal{L}_\ell^{221} &= \overline{\ell}_L\gamma_\mu\left[\frac{g_L}{2}\boldsymbol{\tau}\cdot\boldsymbol{W}_L^\mu - \frac{g_{BL}}{2}W_{BL}^\mu\right]\ell_L \\ &\quad + \overline{\ell}_R\gamma_\mu\left[\frac{g_R}{2}\boldsymbol{\tau}\cdot\boldsymbol{W}_R^\mu - \frac{g_{BL}}{2}W_{BL}^\mu\right]\ell_R . \end{aligned} \tag{2.224}$$

Identifying $g = g_L$, we find $g_R = g$ and $\sqrt{2}g_{BL} = g$, leading to the same result as above.

The Higgs Quartic Couplings and the Higgs Mass

With a bi-doublet $\hat{\Phi}$ and two complex triplets $\Delta_{L,R}$, the Higgs sector of the model has 20 degrees of freedom, of which 6 are absorbed into the massive gauge bosons, while 14 remain physical [207, 208]. Of these, 4 are doubly charged, 4 are singly charged, and 6 are neutral. We identify the observed Higgs boson with the lightest neutral member.

The masses of the physical Higgs sector particles naturally depend on the parameters in the Higgs potential, Eq. (2.194). Of these, we are aware of the self-couplings of $\hat{\Phi}$, which, due to the introduction of the coupling constant, are rescaled from Eq. (2.196) to

$$\lambda_1 \;=\; \frac{g^2}{2}\,, \quad \lambda_3 \;=\; -\frac{g^2}{4}\,, \quad \lambda_2 \;=\; \lambda_4 \;=\; 0\,, \tag{2.225}$$

as are the mass parameters to

$$\mu_1^2 \;=\; \frac{g^2 v^2}{2}\,, \qquad \mu_2^2 \;=\; 0\,. \tag{2.226}$$

The other parameters are unknown except for requirement that they must lead to $v_R \gg \kappa_+ = \sqrt{\kappa_1^2 + \kappa_2^2} \approx 246\,\text{GeV} \gg v_L \approx 0$, and $\kappa_1 \gg \kappa_2$. Let us approximate $\kappa_2 \approx 0$. In this case, the mass of the lightest neutral scalar, which consists mostly of the real part of ϕ_1^0, is given approximately by [207, 208]

$$M_h^2 \;\approx\; \kappa_1^2 \left(2\lambda_1 - \frac{\alpha_1^2}{2\rho_1}\right)\,. \tag{2.227}$$

The first term is what the Higgs mass would be if the couplings to the triplets were non-existent:

$$M_h \;=\; \sqrt{2\lambda_1}\kappa_1 \;=\; g\kappa_1\,. \tag{2.228}$$

Given that the prediction for the left-handed W mass would be $M_{W_L} = M_{W_1} = g\kappa_1/2$ in this case, this would lead to the prediction $M_h/M_W = 2$ as in the $su(2/1)$ case. The existence of the second term shows that mixing with the neutral components of $\Delta_{L,R}$ could lower the mass to a more realistic value. Renormalization group running could further lower M_h toward 126 GeV. We examine this possibility in subsection 2.3.9.

2.3.8 The Emergence Scale and the Right-Handed Breaking Scale

Let us now determine the scale Λ_s at which we envision the $su(2/2) \sim SU(2)_L \times SU(2)_R \times U(1)_{B-L}$ structure to emerge from an underlying NCG theory. This is the scale at which we expect the relation $g_{BL}/g = 1/\sqrt{2}$ to hold.

When one imagines the emergence of an LRSM from an underlying UV theory at some scale Λ_s, one usually thinks of the subsequent breaking of the gauge symmetry down to $U(1)_{em}$

to occur in steps at several scales, a schematic diagram of which would be:

$$\begin{aligned} \text{NCG} \quad & \text{theory?} \\ & \downarrow \Lambda_s \\ su(2/2) \quad & \sim \; SU(2)_L \times SU(2)_R \times U(1)_{B-L} \\ & \downarrow \Lambda_R \sim g v_R \\ su(2/1) \quad & \sim \; SU(2)_L \times U(1)_Y \\ & \downarrow M_W \sim g v \\ & U(1)_{em} \end{aligned}$$

Thus, the theory would be effectively $SU(2)_L \times SU(2)_R \times U(1)_{B-L}$ between Λ_s and Λ_R, and $SU(2)_L \times U(1)_Y$ between Λ_R and M_W, that is, the gauge couplings would run with the LRSM particle content between Λ_s and Λ_R, and with the SM particle content below Λ_R. The boundary condition we would like to impose at Λ_s is

$$\frac{g_{BL}(\Lambda_s)}{g(\Lambda_s)} \;=\; \frac{1}{\sqrt{2}} \,, \tag{2.229}$$

while the matching condition at Λ_R requires

$$\frac{1}{g'^2(\Lambda_R)} \;=\; \frac{1}{g^2(\Lambda_R)} + \frac{1}{g_{BL}^2(\Lambda_R)} \,. \tag{2.230}$$

Therefore, we have, up to one-loop, the relations

$$\begin{aligned} \frac{1}{g_L^2(\Lambda_s)} &= \frac{1}{g_2^2(\Lambda_R)} - 2b_L \ln \frac{\Lambda_s}{\Lambda_R} \\ &= \left(\frac{1}{g_2^2(M_W)} - 2b_2 \ln \frac{\Lambda_R}{M_W} \right) - 2b_L \ln \frac{\Lambda_s}{\Lambda_R} \,, \\ \frac{1}{g_{BL}^2(\Lambda_s)} &= \frac{1}{g_{BL}^2(\Lambda_R)} - 2b_{BL} \ln \frac{\Lambda_s}{\Lambda_R} \\ &= \left(\frac{1}{g'^2(\Lambda_R)} - \frac{1}{g_2^2(\Lambda_R)} \right) - 2b_{BL} \ln \frac{\Lambda_s}{\Lambda_R} \,, \\ \frac{1}{g'^2(\Lambda_R)} &= \frac{1}{g'^2(M_W)} - 2b_1 \ln \frac{\Lambda_R}{M_W} \,. \end{aligned} \tag{2.231}$$

The b_i's are given by Ref. [200]

$$b_i \;=\; \frac{1}{16\pi^2} \left[-\frac{11}{3} C_2(G_i) + \frac{2}{3} \sum_f T_i(f) + \frac{1}{3} \sum_s T_i(s) \right] , \tag{2.232}$$

where the summation is over Weyl fermions in the second term and over scalars in the third. The index i labels the gauge groups and we have $i = 1, 2$ below Λ_R, and $i = L, R, BL$ above

it, and $i = 3$ for QCD. $C_2(G_i)$ is the quadratic Casimir for the adjoint representation of the group G_i, and T_i is the Dynkin index of each representation. For $SU(N)$, $C_2(G) = N$, $T = 1/2$ for doublet representations and $T = 2$ for triplets. For $U(1)$, $C_2(G) = 0$ and

$$\sum_{f,s} T \;=\; \sum_{f,s} \left(\frac{Y}{2}\right)^2 \;, \tag{2.233}$$

where $Y/2$ is the $U(1)$ charge, the factor of $1/2$ coming from the traditional normalizations of the hypercharge Y and $B - L$ charges. In the LRSM, we have, for each generation, 6 left-handed and 6 right-handed quarks with $B - L = 1/3$, 2 left-handed and 2 right-handed leptons with $B - L = -1$, 6 complex scalars (coming from the two triplets) with $B - L = 2$, and a bi-doublet with $B - L = 0$.

Therefore, we have

$$b_L \;=\; b_R \;=\; \frac{1}{16\pi^2}\left(-\frac{7}{3}\right) \;, \quad b_{BL} \;=\; \frac{1}{16\pi^2}\left(\frac{14}{3}\right) \;. \tag{2.234}$$

The values of b_1, b_2, and b_3 for the SM particle content have been listed earlier in Eq. (2.146). Using the above RGE relations Eq. (2.231), we look for the scale Λ_s at which the constraint Eq. (2.229) is satisfied as a function Λ_R. The results are shown in Fig. 2.2.

One possible solution is, of course, $\Lambda_s = \Lambda_R \approx 4\,\text{TeV}$ since that was the scale at which $g'/g = 1/\sqrt{3}$ when the couplings run with the SM particle content, and this automatically leads to $g_{BL}/g = 1/\sqrt{2}$. When Λ_R is increased above 4 TeV, however, as we can see from Fig. 2.2, we find that the scale Λ_s at which Eq. (2.229) is satisfied is actually lower than Λ_R. That is, we must run the couplings up to Λ_R with the SM particle content, and then run back down to a lower energy with the LRSM particle content to satisfy the required boundary condition. Obviously, this is an unphysical situation. So we are led to conclude that our formalism demands $\Lambda_s = \Lambda_R \approx 4\,\text{TeV}$. That is, the $SU(2)_L \times SU(2)_R \times U(1)_{B-L}$ gauge theory emerges already broken to $SU(2)_L \times U(1)_Y$ of the SM at that scale. In fact, it is already broken all the way down to $U(1)_{em}$ due to the non-zero VEV of the bi-doublet field Φ, though it may not necessarily be manifest at Λ_s due to $\Lambda_s = \Lambda_R \gg M_W$.

This result is not inconsistent with the view we have been advocating based on our $su(2/1) \sim SU(2)_L \times U(1)_Y$ model. There, the theory emerged already broken to $U(1)_{em}$ at the emergence scale Λ_s, with the Higgs field already shifted to fluctuations around its non-zero VEV. So schematically, we had:

$$\text{NCG theory?}$$

$$\downarrow \Lambda_s \approx 4\,\text{TeV}$$

$$\text{Broken } SU(2)_L \times U(1)_Y \xrightarrow{M_W} U(1)_{em}$$

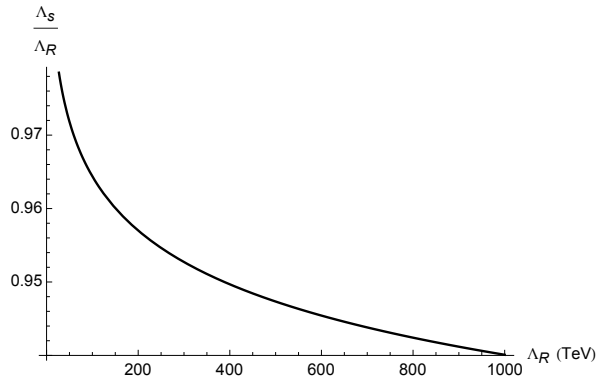

Figure 2.2: The behavior of $\frac{\Lambda_s}{\Lambda_R}$ above 4 TeV, where it is exactly equal to unity.

For the $su(2/2)$ case, the breaking schematic is

$$\text{NCG theory?}$$
$$\downarrow \Lambda_s = \Lambda_R \approx 4\,\text{TeV}$$
$$\text{Broken } SU(2)_L \times SU(2)_R \times U(1)_{B-L} \xrightarrow{M_W} U(1)_{em}$$

These schematics suggest that the physics responsible for the emergence of the $su(2/1)$ or $su(2/2)$ patterns from the underlying theory may also be responsible for the spontaneous breaking of the chiral gauge symmetries. A possible and attractive scenario would be that this new physics is geometric in nature and is triggered by the separation of the two branes from each other, as evidenced in the fact that the matrix derivative encodes information on the Higgs VEV.

Another attractive point about the scale Λ_R being on the order of 4 TeV is that it would place the masses of all the new particles associated with the LRSM at that scale, perhaps light enough to be discovered just beyond their current experimental limits. We will return to this observation in section 2.5.

2.3.9 The Higgs Boson Mass from $su(2/2)$

Let us now discuss how the observed Higgs mass can be accommodated in our $su(2/2)$ framework. We have seen that both $su(2/1)$ and $su(2/2)$ embeddings place the emergence scale at ~ 4 TeV. Moreover, they demand the same boundary condition on the Higgs quartic coupling (λ for $su(2/1)$, λ_1 for $su(2/2)$) at that scale. In the $su(2/1)$ case, this led to a prediction of the Higgs mass of $M_h(M_Z) \sim 170\,\text{GeV}$. In the $su(2/2)$ case, however, the Higgs mass prediction can be lowered due to the mixing of the Higgs with other neutral scalars available in the model.

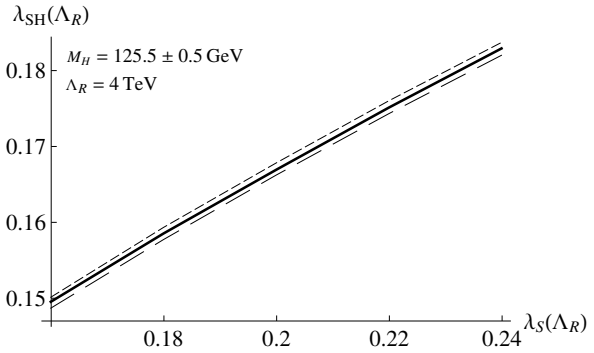

Figure 2.3: A patch of the parameter space which gives the observed Higgs mass.

In this section, we will investigate the simplest option as an example. We will assume that only a SM singlet scalar S survives dominantly at low energies ($\sim M_Z$), which is responsible for the mass of the right handed neutrino. In our $su(2/2)$ embedding, this can be taken to be the real part of δ_R^0:

$$\delta_R^0 \;=\; \frac{v_R + S + iT}{\sqrt{2}} \;. \tag{2.235}$$

We assume that S couples to the SM Higgs field H via

$$\mathcal{L}_S \;=\; \frac{1}{2}\partial_\mu S \partial^\mu S - \frac{m^2}{2}S^2 - \frac{\lambda_S}{4}S^4 - \lambda_{HS} H^\dagger H S^2 \;. \tag{2.236}$$

This model, in which the SM is extended with a singlet scalar S, has been analyzed in detail previously in the contexts of the vacuum stability of the SM [217, 218], and dark matter [219, 220]. In the $su(2/2)$ framework, terms in the above Lagrangian result from the terms with coefficients ρ_1 and α_1 in Eq. (2.194), provided that

$$\lambda_S \;=\; \rho_1 \;, \qquad \lambda_{HS} \;=\; \frac{\alpha_1}{2} \;. \tag{2.237}$$

A similar singlet field is found in the Spectral SM [155]. See also Refs. [193, 194].

Assuming that in addition to S, the right-handed neutrino survives a low energies, we obtain the following renormalization group equations (RGE's) for the evolution of the relevant parameters [219, 221]:

$$\begin{aligned}
\mu\frac{dh_t}{d\mu} &= \frac{h_t}{(4\pi)^2}\left[\frac{9}{2}h_t^2 + h_\nu^2 - \left(\frac{17}{12}g'^2 + \frac{9}{4}g^2 + 8g_s^2\right)\right] \;, \\
\mu\frac{dh_\nu}{d\mu} &= \frac{h_\nu}{(4\pi)^2}\left[3h_t^2 + \frac{5}{2}h_\nu^2 - \left(\frac{3}{4}g'^2 + \frac{9}{4}g^2\right)\right] \;, \\
\mu\frac{d\lambda}{d\mu} &= \frac{1}{(4\pi)^2}\Big[\Big\{12h_t^2 + 4h_\nu^2 - \left(3g'^2 + 9g^2\right)\Big\}\lambda
\end{aligned}$$

$$
\begin{aligned}
& -2h_\nu^4 - 6h_t^4 + 24\lambda^2 + 2\lambda_{HS}^2 \\
& + \frac{3}{8}\left(g'^4 + 2g'^2 g^2 + 3g^4\right)\Bigg] , \\
\mu\frac{d\lambda_{HS}}{d\mu} &= \frac{\lambda_{HS}}{(4\pi)^2}\Bigg[6h_t^2 + 2h_\nu^2 - \left(\frac{3}{2}g'^2 + \frac{9}{2}g^2\right) \\
& + 2\left(6\lambda + 3\lambda_S + 4\lambda_{HS}\right)\Bigg] , \\
\mu\frac{d\lambda_S}{d\mu} &= \frac{1}{(4\pi)^2}\left(8\lambda_{HS}^2 + 18\lambda_S^2\right) ,
\end{aligned}
\tag{2.238}
$$

where h_t and h_ν are the top-quark and right-handed neutrino Yukawa couplings, λ and λ_S are the Higgs and the singlet quartic couplings, and λ_{HS} is the Higgs-singlet coupling. The boundary conditions we use are $h_t(M_Z) = 0.997$, obtained from $h_t(M_Z) = \sqrt{2}m_t/v$, and $\lambda(\Lambda_R) = g^2(\Lambda_R)/2$, where the latter is fixed by our $su(2/2)$ construction. We also assume $h_\nu \sim 10^{-6}$, which is necessary to generate the correct light neutrino mass from the TeV scale seesaw, if the Dirac mass $M_D \approx M_e$. We also need the values of $\lambda_S(\Lambda_R)$ and $\lambda_{HS}(\Lambda_R)$ as boundary conditions for our RGE's, but these are not fixed by our $su(2/2)$ framework (yet). Thus, we allow these values to float to find the conditions that lead to the correct Higgs mass. The mass of the Higgs is determined from [155]

$$
\begin{aligned}
M_h^2 &= \lambda v^2 + \lambda_S v_R^2 - \sqrt{\left(\lambda v^2 - \lambda_S v_R^2\right)^2 + 4\lambda_{HS}^2 v^2 v_R^2} \\
&\simeq 2v^2\lambda\left(1 - \frac{\lambda_{HS}^2}{\lambda\lambda_S}\right) ,
\end{aligned}
\tag{2.239}
$$

consistent with Eq. (2.227). We have also set $v_R = \Lambda_R \simeq 4$ TeV in this calculation.

The resulting range of values for $\lambda_S(\Lambda_R)$ and $\lambda_{HS}(\Lambda_R)$ which reproduce the correct Higgs mass is shown in Fig. 2.3. The plot shows the range of values $(0.15 \sim 0.25)$ in the perturbative region, but larger values for these couplings are also possible as long as $(1 - \lambda_{HS}^2/\lambda\,\lambda_S) \geq 0$, while λ remains small. Thus, the $su(2/2)$ structure can accommodate the correct Higgs mass, provided the parameters in the Higgs potential are in the appropriate ranges.

2.3.10 *su*(2/2)ummary

In this section, we have applied the formalism developed for the $su(2/1)$ embedding of the SM in the previous section to an $su(2/2)$ superconnection into which the $SU(2)_L \times SU(2)_R \times U(1)_{B-L}$ gauge bosons of the LRSM were embedded in its diagonal even part, and a bi-doublet Higgs field Φ in its off-diagonal odd part. Unlike the $su(2/1)$ case, the matrix derivative could be made nilpotent, and the supercurvature $\mathcal{F}$ followed a simple transformation law under gauge transformations. To the gauge invariant but spontaneously broken (to $SU(2)_V \times U(1)_{B-L}$) action derived from $\mathcal{F}$, in which the bi-doublet Φ was already

the shifted field fluctuating around the VEV $\zeta/\sqrt{2}$, we introduced two triplet fields $\Delta_{L,R}$ to achieve the breaking sequence $SU(2)_L \times SU(2)_R \times U(1)_{B-L} \to SU(2)_L \times U(1)_Y \to U(1)_{em}$.

The predictions of the formalism were $g_{BL}/g = 1/\sqrt{2}$ (or, equivalently, $g'/g = 1/\sqrt{3}$) and $\lambda_1 = -2\lambda_3 = g^2/2$, $\lambda_2 = \lambda_4 = 0$, where the λ_i's are quartic self couplings of the bi-doublet Φ. Of these, λ_1 corresponds to the quartic self coupling λ of the SM Higgs. Assuming the above symmetry breaking sequence, it was found that the condition $g_{BL}/g = 1/\sqrt{2}$ could only be imposed if the emergence scale Λ_s of the $su(2/2)$ structure and the breaking scale Λ_R of the LRSM down to the SM were the same and at $\sim 4\,\text{TeV}$. Thus, the formalism demands that the LRSM emerge from the hypothetical underlying NCG theory already fully broken. Despite the formalism's predictions including the emergence scale being essentially the same as in the $su(2/1)$ case, the observed Higgs mass could still be accommodated due to the availability of other neutral scalar degrees of freedom in the model which mixed with the Higgs.

2.4 Fermions

For the superconnection formalism presented here to be taken seriously, we must have the freedom to couple fermions to the Higgs field with arbitrary Yukawa couplings, or the formalism must be able to predict what these Yukawa couplings should be. This is a difficult problem given that the superconnection formalism is essentially a gauge-Higgs unified theory, and, as with any such scenario, if one naively couples the superconnection $\mathcal{J}$ to the fermions, the Yukawa couplings are forced to be equal to the gauge couplings [222–228].

To see how this comes about in the $su(2/1)$ case, let us assume that the Lagrangian of the lepton $su(2/1)$ triplet ψ coupled to the superconnection $\mathcal{J}$ is given, schematically, by

$$\mathcal{L}_\ell \;=\; i\bar{\psi}\mathcal{D}\psi \;=\; i\bar{\psi}\left[\mathbf{d} + \frac{g}{2}\left(\mathbf{d}_M + \mathcal{J}\right)\right]\psi\,, \tag{2.240}$$

where all the operators within the parentheses must be placed in the appropriate representations. In the spinorial representation, the one-form dx^μ is represented by the Dirac matrix γ^μ [229–232]. Thus, we have the replacements

$$\begin{aligned} d &= dx^\mu \wedge \partial_\mu \;\to\; \gamma^\mu\partial_\mu \;=\; \not{\partial}\,, \\ W^i &= W^i_\mu dx^\mu \;\to\; W^i_\mu\gamma^\mu \;=\; \not{W}^i\,, \\ B &= B_\mu dx^\mu \;\to\; B_\mu\gamma^\mu \;=\; \not{B}\,, \end{aligned} \tag{2.241}$$

and consequently,

$$\begin{aligned} \mathbf{d} &\to \not{\partial}\cdot\mathbf{1}_{3\times3}\,, \\ \mathcal{J} &\to i\begin{bmatrix} \boldsymbol{\tau}\cdot\not{\mathbf{W}} - \frac{1}{\sqrt{3}}\not{B}\cdot\mathbf{1}_{2\times2} & \sqrt{2}\phi \\ \sqrt{2}\phi^\dagger & -\frac{2}{\sqrt{3}}\not{B} \end{bmatrix} \;\equiv\; J\,. \end{aligned}$$

(2.242)

We define the Dirac operator D as

$$D \;=\; \not{\phi}\cdot \mathbf{1}_{3\times 3} + i\frac{g}{2}\eta\,, \tag{2.243}$$

to represent the generalized exterior derivative $\mathbf{d}_S = \mathbf{d} + \frac{g}{2}\mathbf{d}_M$. Then, the Lagrangian is found to be

$$\begin{aligned}
\mathcal{L}_\ell \;&\to\; i\bar{\psi}\left(D + \frac{g}{2}J\right)\psi \\
&=\; \overline{\ell}_L i\not{\partial}\,\ell_L + \overline{\ell}_R i\not{\partial}\,\ell_R \\
&\quad -\frac{g}{2}\left(\overline{\ell}_L\xi\,\ell_R + \overline{\ell}_R\xi^\dagger\,\ell_L\right) - \frac{g}{\sqrt{2}}\left(\overline{\ell}_L\phi\,\ell_R + \overline{\ell}_R\phi^\dagger\,\ell_L\right) \\
&\quad -\frac{g}{2}\left[(\overline{\ell}_L\gamma^\mu\tau_i\,\ell_L)W^i_\mu - \frac{1}{\sqrt{3}}\left(\,\overline{\ell}_L\gamma^\mu\ell_L + 2\,\overline{\ell}_R\gamma^\mu\ell_R\,\right)B_\mu\right] \\
&=\; \overline{\ell}_L i\not{\partial}\,\ell_L + \overline{\ell}_R i\not{\partial}\,\ell_R - \frac{g}{\sqrt{2}}\left(\overline{\ell}_L\hat{\phi}\,\ell_R + \overline{\ell}_R\hat{\phi}^\dagger\,\ell_L\right) \\
&\quad -\frac{g}{2}\left[(\overline{\ell}_L\gamma^\mu\tau_i\,\ell_L)W^i_\mu - \frac{1}{\sqrt{3}}\left(\,\overline{\ell}_L\gamma^\mu\ell_L + 2\,\overline{\ell}_R\gamma^\mu\ell_R\,\right)B_\mu\right]\,,
\end{aligned} \tag{2.244}$$

where we have defined $\hat{\phi} = \phi + \xi/\sqrt{2}$ as before. Thus, in addition to $g'/g = 1/\sqrt{3}$, we find that the lepton Yukawa coupling is fixed to $g/\sqrt{2}$, and the matrix derivative terms couple the leptons to the Higgs VEV and yield the charged lepton mass. Note also that this Lagrangian is manifestly $SU(2)\times U(1)_Y$ gauge invariant when written in terms of the shifted field $\hat{\phi}$, but the invariance is already spontaneously broken with fermion mass terms when written in terms of the ϕ field appearing in the superconnection.

In order to be able to change the Yukawa coupling to an arbitrary value, one must have the freedom to multiply ξ in the matrix derivative, which determines $\langle\hat{\phi}\rangle$, and ϕ in the superconnection $\mathcal{J}$ by the same constant for each fermion flavor to maintain the gauge invariance of the Lagrangian when written in terms of $\hat{\phi}$. This is essentially one of the fundamental reason we have to turn to NCG approach to have multiple lengths in the separation. Essentially, one copy of the two sheets is 'fuzzed up' and multiple characteristic lengths can be 'measured out' if projected to the commutative c numbers.[18] In the Spectral SM approach [147–149, 152–156, 189], this is accomplished by writing the Dirac operator D in full fermion flavor space, including all three generations, and inserting the complete fermion mass-mixing matrix into the off-diagonal matrix derivative part. This is in accordance with the idea that the matrix derivative encodes information on symmetry breaking. The superconnection J is also defined via the generalized exterior derivative using D, which passes on the information

[18] We note this also shares some interesting features with quantum mechanics and quantum measurement process as discussed in Refs. [233, 234].

included in the matrix derivative to the couplings of the ϕ. The information also feeds into the supercurvature, from which one determines the gauge-Higgs action and the Higgs VEV. This procedure allows for the introduction of arbitrary masses and mixings into the fermion sector.

Thus, the Spectral SM shows that it is possible to embed the required masses and mixings of the fermions to reproduce the SM into the 'geometry' of the NCG discrete direction. The interesting point is that in the Spectral SM approach, it is the fermion masses that are the input and the Yukawa couplings the output, and not the other way around as in the standard approach. The breaking of the gauge symmetry is encoded in the geometry, which is given in terms of the fermion masses and from which one extracts the Higgs VEV, and one could say that the Yukawa interactions themselves are consequences rather than the reason for fermion mass.

It must be said, though, that this is actually a highly unsatisfactory state of affairs. One wishes the NCG to determine the fermion masses and mixings, and not the other way around. But, for that, a full theory of NCG dynamics would be necessary. So, for the time being, we leave the prediction of the fermion masses and mixings to a possible future theory, and simply deal with the problem by assuming that when the $su(2/1)$ (or $su(2/2)$) structure emerges from the underlying NCG theory at the emergence scale, the geometry, a full description of which could be fairly complicated, in addition to breaking the gauge symmetries, also fixes the fermion masses and mixings to the observed values.

2.5 TeV Collider Signal and Constraints

We have been led to the possibility that a LRSM emerges from an underlying NCG theory at the scale of $\Lambda_s \approx 4\,\text{TeV}$, which also breaks to $SU(2)_L \times U(1)_Y$ with a triplet VEV of $v_R = O(\Lambda_R/g)$ with $\Lambda_R = \Lambda_s$. An additional constraint that the model predicts is that the Higgs quartic coupling λ_1 and the $SU(2)$ coupling g are related by $\lambda_1 = g^2/2$ at that scale. In this section, let us look at what the phenomenological consequences are of such a scenario.

Since we envision that the UV theory above the emergence scale of $\Lambda_s = 4\,\text{TeV}$ is a NCG theory with a discrete extra dimension, the existence of the extra dimension at such a low scale should have observable consequences beyond predicting a LRSM with a particular boundary condition. However, since the extra dimension is also discrete, it is not at all clear what it means to have a 'scale' associated with it. Having zero measure, it cannot be populated by extra degrees of freedom, which, for a continuum extra dimension model, would lead to Kaluza-Klein states. Lacking an understanding of the hypothetical UV NCG theory, it is difficult to state what to expect, so we will, for now, concentrate on the more conventional phenomenology of the effective LRSM the formalism predicts. Considerations of more exotic 'smoking gun' signatures will be left to future work.

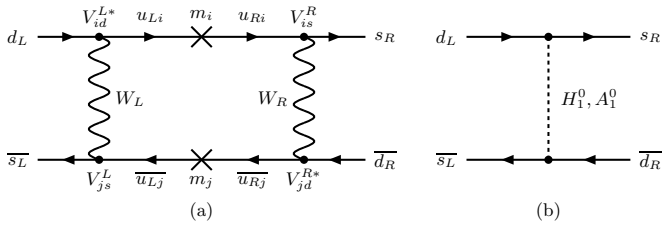

Figure 2.4: Processes that contribute to K^0-$\overline{K^0}$ mixing in the LRSM. In (a), the indices i and j run over the three generations of up-type quarks u, c, and t. Diagrams rotated by 90°, 180°, and 270° also contribute.

2.5.1 New Particles

First and foremost, the LRSM we have been considering predicts a plethora of new and heavy particles: $W_2^\pm$ (which are mostly $W_R^\pm$), Z_2 (which is mostly Z'), and a variety of neutral, singly charged, and doubly charged scalars originating in the Higgs sector that are denoted H_1^0, H_2^0, H_3^0, A_1^0, A_2^0, $H_1^\pm$, $H_2^\pm$, $\delta_L^{\pm\pm}$ and $\delta_R^{\pm\pm}$ in Ref. [235].[19] The coupling of the triplet to the leptons, Eq. (2.190), will also generate massive Majorana neutrinos, which we will denote N or N_R (since they are mostly ν_R) with a possible flavor index.

All these new particles will receive masses from the same triplet VEV, $v_R = O(\Lambda_R/g)$, so we can expect them all to have masses in the multi-TeV range, placing some of them, hopefully, within LHC reach. The actual masses will depend on the many parameters of the model, e.g., those appearing in the Higgs potential. One concrete prediction we can make is that $M_{Z_2}/M_{W_2} \approx \sqrt{3}$, so, for instance, if $M_{W_2} = 4\,\text{TeV}$ then $M_{Z_2} \approx \sqrt{3}\,M_{W_2} \approx 7\,\text{TeV}$. Thus, the actual particle masses need not all be concentrated at 4 TeV, and one expects a spread-out spectrum. The TeV scale Majorana masses of the N_R's will also allow us to invoke a TeV scale see-saw mechanism to suppress regular neutrino masses.

Bounds on these new particle masses exist from various low energy observables and from direct searches at the LHC. Let us take a look at what they are.

2.5.2 Bounds from Low Energy Processes

Constraints on the LRSM from low energy processes have been heavily studied in the literature for both the non-supersymmetric LRSM [235–266] and its supersymmetric extension [267–270]. Processes and observables that have been considered include muon decay $\mu \to e\overline{\nu}_e\nu_\mu$, neutron beta decay $n \to p\,e^-\overline{\nu}_e$, the neutron electric dipole moment (nEDM), $K^0\overline{K^0}$ mixing (*i.e.*, the K_L^0-K_S^0 mass difference $\Delta M_K = M_{K_L^0} - M_{K_S^0}$ and the K-decay CP violation parameters ϵ and ϵ', *c.f.* Fig. 2.4), $D^0\overline{D^0}$ mixing, $B^0\overline{B^0}$ mixing (ΔM_{B_d}, ΔM_{B_s}, and

[19] The lightest neutral Higgs particle, denoted h^0 in Ref. [235], is identified with the SM Higgs and is not included in this list.

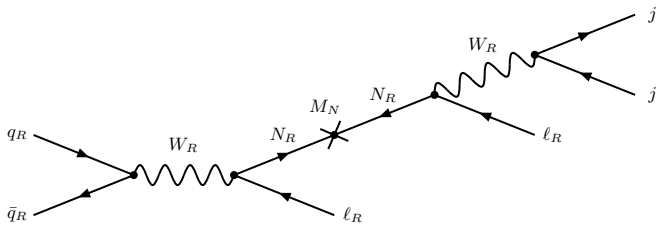

Figure 2.5: The Feynman diagram for the production of a heavy right-handed neutrino and its decay to a dilepton and a dijet through W_R exchange. M_N is the Majorana mass of N_R.

CP violation in hadronic B decays), b semileptonic decay, and $b \to s\gamma$.

Of the constraints thus obtained, those on the mass of W_2, which is mostly W_R, are fairly robust and independent of the detailed form of the Higgs potential. This is due to the $SU(2)_R$ gauge coupling being well known in the LRSM, and for the quark sector, if one assumes the Yukawa interaction with the bi-doublet Φ, Eq. (2.203), to be solely responsible for the quark masses and mixings, then the right-handed CKM matrix V^R can be fairly well constrained from quark masses and the usual left-handed CKM matrix V^L. According to the analysis of Ref. [235], ΔM_K yields 2.5 TeV, while the combination of ϵ and nEDM yields 4 TeV, respectively, as the lower bound of M_{W_2}. The 4 TeV bound matches precisely our right-handed scale Λ_R where we expect typical new particle masses to be.

Bounds on scalar masses are more model dependent, and can be much stronger than that on M_{W_R}. For instance, H_1^0 and A_1^0 exchange can contribute to $K^0\overline{K^0}$ mixing at tree-level (see Fig. 2.4(b)), and Ref. [235] uses ΔM_K to place a lower bound of 15 TeV on their masses.

2.5.3 LHC Signatures

CMS and ATLAS have looked for BSM signals including W_R, Z', and $\delta_{L,R}^{\pm\pm}$'s of the LRSM in proton-proton collisions of energies up to $\sqrt{s} = 8\,\text{TeV}$, and continued their searches at the center of mass energy of $\sqrt{s} = 13\,\text{TeV}$. Here, we cite some of their current bounds.

W_R and N_R

Since the heavy neutrino N_R has a large Majorana mass in our construction, a distinctive signature for the model at the LHC is a same-sign dilepton + dijet final state with no missing energy via $W_R^\pm \to N_R\ell^\pm \to \ell^\pm\ell^\pm jj$ [271]. The Drell-Yan diagram for this lepton number violating process is shown in Fig. 2.5, the violation due to the Majorana mass insertion on the N_R line. Since a Dirac mass does not violate lepton number, a Dirac neutrino would only allow oppositely-charged dileptons in the final state. Therefore, LHC searches for the same-sign channel are important in determining whether the heavy neutrino N_R is Majorana or Dirac.

The cross section of the process naturally depends on both W_R and N_R masses, so the searches exclude correlated regions in M_{W_R}-M_N space. In particular, if $M_{W_R} < M_N$ then the process will be highly suppressed and be undetectable, so certain regions cannot be probed. If the intermediate state is N_e (N_μ), then the dilepton in the final state will be ee ($\mu\mu$). However, if the N_e and N_μ mix, then one can also have $e\mu$ final states. Thus, the bounds could also depend on which channels are included in the analysis.

In Ref. [272], ATLAS reports that for both no-mixing and maximal-mixing scenarios (between N_e and N_μ), they have excluded W_R of mass up to 1.8 TeV (2.3 TeV) at 95% C.L., assuming a mass difference between W_R and N_ℓ larger than 0.3 TeV (0.9 TeV).

In Ref. [273], CMS reports that W_R of mass up to 3.0 TeV have been excluded at 95% C.L. for the ee and $\mu\mu$ channels separately, and also with the two channels combined assuming degenerate N_e and N_μ masses.

Doubly Charged Higgs

Another signature of the LRSM which could be observed at the LHC comes from the triplet Higgs channel. In particular, the doubly-charged Higgs of the triplet decaying to two same-sign leptons

$$\delta^{\pm\pm}_{L,R} \;\rightarrow\; e^\pm e^\pm,\, \mu^\pm\mu^\pm, e^\pm\mu^\pm \tag{2.245}$$

via the Majorana interaction, Eq. (2.190), will present a very clear and distinctive signal.

In Ref. [274], ATLAS reports that $\delta^{\pm\pm}_L$ of masses up to 409 GeV, 398 GeV, and 375 GeV, and $\delta^{\pm\pm}_R$ of masses up to 322 GeV, 306 GeV, and 310 GeV have been excluded at 95% C.L. for the ee, $\mu\mu$, and $e\mu$ final states, respectively. These results assume a branching fraction of 100% for each final state. For smaller branching fractions, the bounds will be weaker.

In Ref. [275], CMS reports the mass bounds on the doubly charged Higgs in the left-handed triplet extension of the SM (type II seesaw model). At the 95% C.L., the bounds are 444 GeV, 453 GeV, 373 GeV, 459 GeV, 375 GeV, and 204 GeV respectively when 100% decay to ee, $e\mu$, $e\tau$, $\mu\mu$, $\mu\tau$, and $\tau\tau$ final states are assumed.

2.5.4 Neutrinoless Double-β Decay

Since the Majorana masses of the neutrinos violate lepton number by two units, their presence will lead to lepton number violating processes such as neutrinoless double-β decay ($0\nu\beta\beta$):

$$(A, Z) \;\rightarrow\; (A, Z+2) \,+\, e^- \,+\, e^- \,. \tag{2.246}$$

The rate of $0\nu\beta\beta$ can be written generically as

$$\frac{\Gamma_{0\nu\beta\beta}}{\ln 2} \;=\; G\,\frac{|\mathcal{M}|^2}{m_e^2}\left|m_\nu^{\beta\beta}\right|^2 \,, \tag{2.247}$$

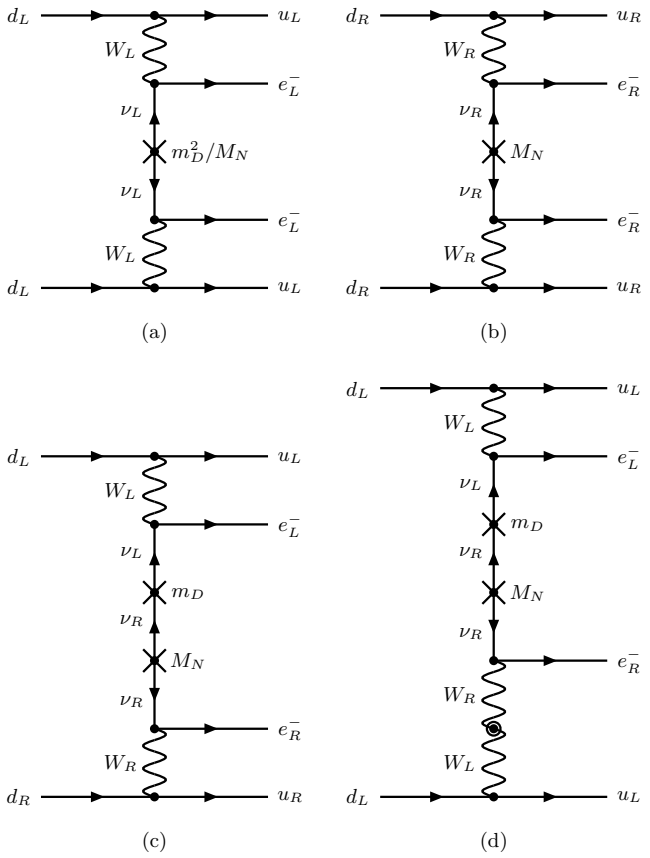

Figure 2.6: Neutrinoless double-beta decay in the LRSM via the exchange of W_L, W_R with ν_L and ν_R intermediate states. m_D and M_N are respectively the Dirac and Majorana masses of the neutrino. Mass eigenstates are linear combinations of ν_L and ν_R, with the light state ν consisting mostly of ν_L, and the heavy state N consisting mostly of ν_R. The double-circle on the W propagator in (d) indicates W_L-W_R mixing.

where G denotes the kinematic factor, $\mathcal{M}$ the nuclear matrix element, m_e the electron mass, and $|m_\nu^{\beta\beta}|$ the effective neutrino mass:

$$m_\nu^{\beta\beta} \;=\; \sum_i U_{ei}^2\, m_i\,. \tag{2.248}$$

Here, U is the PMNS mixing matrix, and m_i the mass of the i-th mass eigenstate.

In the LRSM, $0\nu\beta\beta$ would occur via the W_L and W_R exchange processes with ν_L and ν_R intermediate states as shown in Fig. 2.6. The dominant contributions are more likely to come from pure left-handed currents with light neutrino intermediate states, Fig. 2.6(a), and pure right-handed current with heavy neutrino intermediate states, Fig. 2.6(b). Contributions from left-right mixed currents, Figs. 2.6(c) and 2.6(d), involve a suppression factor due to the small left-right mixing ($m_D/M_N \sim 10^{-6}$ for the TeV scale LRSM with generic Yukawa

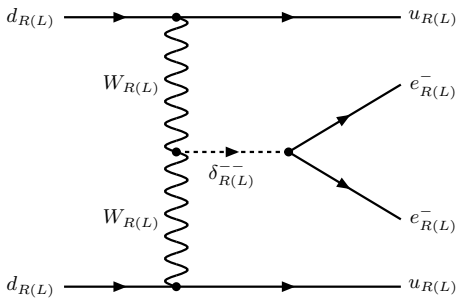

Figure 2.7: Doubly-charged Higgs contributions to $0\nu\beta\beta$ in LRSM.

couplings) [276–281]. However, there is still room in the parameter space which allows significant contributions from the mixed diagrams, as discussed in Ref. [282].

In addition, there exist contributions to $0\nu\beta\beta$ from the doubly-charged Higgs mediated diagrams shown in Fig. 2.7. While those involving the left-handed currents and δ_L are suppressed by a factor of p^2/M_δ^2, those involving the right-handed currents and δ_R are proportional to M_N/M_δ^2, which may give significant contributions, depending on the masses in question.

The present limits on $0\nu\beta\beta$ are not in contradiction with the TeV scale LRSM. As stated in Ref. [259], the current signal on $0\nu\beta\beta$ can be accounted by, for example, $M_{W_2} = 3$ TeV and $M_N = 10$ GeV, where some fine-tuning is required but not by an unacceptable amount.

2.5.5 Lepton Flavor Violating Processes

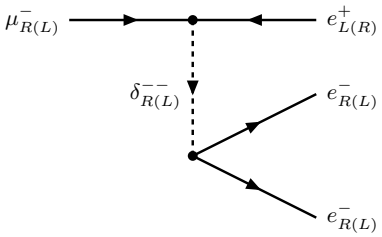

Figure 2.8: Doubly-charged Higgs contribution to $\mu^- \to e^-e^-e^+$ in LRSM.

The LRSM also allows for the lepton flavor violating (LFV) processes $\mu \to e\gamma$ [283–285], $\mu \to 3e$ [285, 286], and $\mu \to e$ conversion in nuclei [285, 287–290], though the predictions for these processes are dependent on how much LFV is built into the Majorana interaction between the leptons and the triplet scalars [277, 279, 281, 285, 291]. Current experimental bounds on the branching fractions are [1]

$$\begin{aligned} B(\mu \to e\gamma) &< 5.7 \times 10^{-13} , \\ B(\mu \to eee) &< 1.0 \times 10^{-12} , \\ \frac{\sigma(\mu^- \mathrm{Au} \to e^- \mathrm{Au})}{\sigma(\mu^- \mathrm{Au} \to \mathrm{capture})} &< 7 \times 10^{-13} , \end{aligned} \tag{2.249}$$

all at 90% C.L.

Among these processes, $\mu \to 3e$ is mediated by the doubly charged Higgses ($\delta^{\pm\pm}_{L,R}$) at tree level, Fig. 2.8, and can be expected to have a relatively large branching fraction. Since the Majorana couplings at the vertices of Fig. 2.8 are proportional to the scale of the Majorana masses of the N's, the diagram is roughly proportional to M_N^2/M_δ^2, and the branching fraction to M_N^4/M_δ^4. So the process provides a bound on M_N/M_δ. In the analysis of Ref. [277], the left-right symmetry operator of the model is taken to be charge conjugation C [259] which restricts the form of the Majorana interaction and allows one to constrain the right-handed PMNS matrix from the left-handed PMNS matrix, just as in the case of the Yukawa interaction for quarks, providing some predictability. Assuming $M_{W_2} = 3.5\,\text{TeV}$ and $M_N^{\max} = 0.5\,\text{TeV}$, and taking all of the above LFV processes into account, Ref. [277] reports $M_N^{\max}/M_\delta < 0.1$, which places a lower bound on M_δ of 5 TeV, right in the ballpark of our $\Lambda_R = 4\,\text{TeV}$.

Belle, Babar, and LHCb have also searched for the LFV decays $\tau \to \ell\gamma$ [292, 293] and $\tau \to \ell\ell\ell$ [294–296], where $\ell = e$ or μ and have placed bounds on the branching fractions to these decays at around a few times 10^{-8} at 90% C.L. According to the analysis of Ref. [297], the LRSM with W_2, $H_1^\pm$, and $\delta^{\pm\pm}_{L,R}$ masses all set to 3 TeV can accommodate a branching fraction of $\tau \to \ell\ell\ell$ as large as 10^{-9} which would be accessible at the next generation of super B factories [298, 299].

2.5.6 Phenomenological Outlook

Based on these conventional phenomenological analyses, we conclude that the TeV scale LRSM predicted by the $su(2/2)$ superconnection formalism, possibly with an underlying NCG, provides a wealth of new particles and predictions within reach of LHC and other experiments. The fact that the current experimental bounds on the LRSM and the corresponding predictions of the superconnection formalism are suspiciously close may be a sign that LHC is on the brink of discovering something new and exciting.

With the center of mass energy of $\sqrt{s} = 13\,\text{TeV}$ for its second run, the LHC is well capable of observing the new particles of the model among which the most important are the right-handed gauge bosons ($W_R^\pm$, Z') whose masses are fixed by the formalism and range within the TeV scale. With the scale of 4 TeV, selected by the formalism itself, these masses will be within reach of the LHC, provided that the right handed neutrinos (N_R) are light enough to make the corresponding channels accessible.[20]

A number of relevant and important observations could be delivered in the LFV branch as

[20]There is nothing in the model which constraints the right-handed neutrinos N_R to be light. With N_R heavier than $W_R^\pm$, the Drell-Yan interactions will be highly suppressed and thus, although theoretically the TeV scale LRSM could still be viable, it will be very difficult for the LHC to detect its signature through the $W_R^\pm$ channels.

well, especially in $\mu \to e$ conversion in nuclei, which we briefly discussed in an earlier section. With the next generation of machines, the COMET [300] and Mu2e [301] collaborations target to increase their sensitivity for this process from 10^{-13} to 10^{-17}, which will significantly improve the limits on new physics including LRSM. Moreover, the next generation of super B factories aim to increase the limit on LFV τ decays to a level of 10^{-9} [298, 299], which will also provide useful information on the nature of new physics.

Thus, the early disappointments of the LHC (lack of other discoveries except for the discovery of the Higgs) could have been nothing but the calm before the storm.

2.6 Summary and Outlook for Superconnection Formalism

2.6.1 Strengths and Weaknesses of the NCG-Superconnection Approach

Here, we have reviewed the $su(2/1)$ superconnection approach to the SM of Ne'eman *et al.* [129, 164, 173], supplemented by later developments by Coquereaux *et al.* [120] and Haussling *et al.* [121]. The superconnection describes the connection in a model space in which our $3+1$ dimensional spacetime is extended by a discrete extra dimension consisting of only two points, *i.e.*, the model space consists of two $3+1$ dimensional branes separated by a gap. The left-handed fermions are assumed to inhabit one brane, and the right-handed fermions the other. The even part of the superconnection describes the usual gauge connection within each $3+1$ dimensional brane, while the odd part of the superconnection, identified with the Higgs doublet, describes the connection in the discrete direction bridging the gap between the two branes. Contrary to early misconceptions about the approach, the Higgs doublet enters as a bosonic scalar, and does not violate the spin-statistics theorem.

The $su(2/1)$ superconnection model predicts $\sin^2\theta_W = 1/4$, a condition which can only be imposed on the $SU(2)_L \times U(1)_Y$ gauge couplings at ~ 4 TeV. We interpret this to mean that the SM emerges from the underlying discrete extra dimension theory at that scale. The model also predicts the Higgs mass, which, including RGE running down from 4 TeV, is ~ 170 GeV.

To remedy this problem, we extended the model to $su(2/2)$, in which the $SU(2)_L \times SU(2)_R \times U(1)_{B-L}$ gauge bosons and a bi-doublet field Φ were embedded into the superconnection. This extended the SM to the LRSM, for which the emergence scale also turned out to be 4 TeV. In this case, additional gauge triplet scalars were introduced to break $SU(2)_R \times U(1)_{B-L}$ down to $U(1)_Y$, and the scale of this breaking was also required to be at 4 TeV. The bi-doublet field then broke the $SU(2)_L \times U(1)_Y$ symmetry down to $U(1)_{em}$. It was shown that the lightest neutral scalar in the Higgs sector could have mass as light as ~ 126 GeV.

The model also predicts a plethora of new particles with masses in the multi-TeV range, within reach of the LHC run 2.

Of the several salient features of the approach, the most interesting is that the generalized exterior derivative in the discrete direction, *i.e.*, the matrix derivative, shifts the VEV of the off-diagonal zero-forms to non-zero values, effectively breaking the gauge symmetries. Thus, gauge symmetry breaking is intimately connected to the geometry of the model spacetime, in particular, to the separation of the two branes. We envision a scenario in which the two branes, originally overlapping, separate from each other dynamically and trigger gauge symmetry breaking. In other words, the Higgs mechanism is not due to the Higgs dynamics which is independent of any underlying geometry, but an integral part of the geometry itself, and is quantum gravitational in character.

Many problems still remain for the formalism to mature into a full fledged model building paradigm. First, the Lie superalgebra structure is assumed to emerge from some underlying NCG theory, but we have not clarified how the geometry enforces the structure yet. We would also like to incorporate QCD, and fermion generations into the structure. The Spectral SM of Connes *et al.* supposedly has already done this, but, as commented on earlier, the Spectral SM approach does not have much predictive power. Also, after the incorporation of QCD into the model, we would like to unify it with the LRSM via the Pati-Salam group. The $U(1)_{B-L}$ gauge boson being part of the $su(2/2)$ superconnection, this suggests that QCD cannot be simply tacked on to the model.

There is also the subtle problem of how the nilpotency of the matrix derivative should be treated. In the $su(2/1)$ case, the term $\mathbf{d}_M^2$ in the definition of the supercurvature could not be ignored for gauge invariance, but including it led to internal inconsistencies. In the $su(2/2)$ case, $\mathbf{d}_M^2$ belongs to the center of the superalgebra, so it can be added or subtracted from the super curvature without changing its algebraic properties. This suggests that one can decide to ignore $\mathbf{d}_M^2$ based on consistency requirements, but one cannot shake the impression that the treatment is ad hoc. Furthermore, in the $su(2/2)$ case, phenomenological requirements demanded that the nilpotency of the matrix derivative be broken. Whether this is another indication of a deep connection between spontaneous symmetry breaking and the geometry of the underlying theory remains to be seen.

These and other questions will be addressed in future work.

2.6.2 Comment on the Hierarchy Problem and the Unification of Couplings

The major appeal of the more traditional approaches to BSM model building such as supersymmetry (as well as technicolor, extra dimensions, etc.) is that they address the hierarchy problem, and that they shed light on the apparent unification of couplings, both within the context of local effective field theory (EFT).

However, this apparent theoretical appeal of supersymmetry does not exclude approaches that do not necessarily follow the local EFT paradigm. For example, in the Spectral SM approach of Connes *et al.* [147–149, 152–156, 189] the hierarchy problem can be addressed in a completely different fashion [154]. The crucial NCG (and thus in some sense non-local) aspect of the SM is found in the Higgs sector, which in principle comes with an extra (second) scale, to be distinguished from the usual UV scale of local EFT. The hierarchy between the Higgs and the UV (Planck) scale can be associated (as shown by Chamseddine and Connes in Ref. [154]) with the natural exponential factor that comes from the dynamical discrete geometry of the Higgs sector. Similarly, the apparent gauge unification (in the guise of an effective $SO(10)$ relation between the gauge couplings) is also incorporated into the Spectral SM. These aspects of the NCG approach to the SM are almost completely unknown in the particle physics community, and at the moment, almost completely undeveloped from a phenomenological viewpoint.

One of our aims in our upcoming review of the Spectral SM [162] is to clarify these interesting features of the NCG approach to the SM and make them palatable to the wider phenomenological community. We are also motivated by a deeper need to understand the limitations of the local EFT paradigm from the point of view of the physics of quantum gravity, which is usually, rather naively, ignored at the currently interesting particle physics scales, by invoking the concept of decoupling, which represents another central feature of the local EFT and which is also challenged by the NCG approach to the SM. Finally, as we discuss in the next concluding subsection of this paper, the usual RG analysis of the local EFT should be re-examined in the new light of the non-commutative/non-local structure of the SM, and the apparent existence of two natural (and naturally related) physics scales.

2.6.3 The Violation of Decoupling and the Possibility for UV/IR Mixing

In this concluding subsection we would like to comment on the observation made in Ref. [302] regarding the violation of decoupling in the Higgs sector, and how this violation may point to the more fundamental possibility of mixing of UV and IR degrees of freedom, given our view that a NCG underlies the Higgs sector. Such UV/IR mixing is known in the simpler context of non-commutative field theory [303], which we review below.

First, let us briefly recall the argument made in Ref. [302]: Essentially, Senjanovic and Sokorac found within the LRSM that the Higgs scalars do not decouple at low energy due to the essential relation between the gauge couplings and the Higgs mass. Note that this violation of decoupling will affect the scales of the electroweak breaking (taken as the low energy scale) and the TeV scale (taken as the high energy scale of new physics).

Such a violation of decoupling might point to a more fundamental phenomenon of the UV/IR mixing of the short and long distance physics. Here, we briefly recall in slightly more

detail the UV/IR mixing found in non-commutative field theory [303]. In this particular toy-model case (to be distinguished from NCG of Connes relevant for our discussion), the non-commutative spatial coordinates are assumed to satisfy

$$[\, x_a,\, x_b \,] \;=\; i\theta_{ab}\;, \tag{2.250}$$

where θ_{ab} is real and antisymmetric. Note that when this relation is taken together with the fundamental commutation relation

$$[\, x_a,\, p_b \,] \;=\; i\delta_{ab}\;, \tag{2.251}$$

they imply the possibility of a fundamentally new effect: UV/IR mixing, *i.e.*,

$$\delta x_a \;\sim\; \theta_{ab}\,\delta p_b\;. \tag{2.252}$$

This would mean, contrary to the usual intuition from local effective field theory, that high energy processes are related to low energy distances. We have argued elsewhere that the UV/IR mixing should be a fundamental feature of quantum gravity and string theory [118, 304].

At the moment, we are not aware of an explicit UV/IR relation in the context of the NCG of Connes that underlies the superconnection formalism and the new viewpoint on the SM and the physics beyond it, as advocated here. However, there exists a very specific toy model of non-commutative field theory in which such UV/IR mixing has been explicitly demonstrated. The nice feature of this toy model is that it can be realized in a fundamental short distance theory, such as string theory [303].

The non-commutative field theory is defined by the effective action

$$S_{nc} \;=\; \int d^4x\; L[\phi] \tag{2.253}$$

where the product of the fields ϕ is given by the Moyal (or star) product

$$(\phi_1 \star \phi_2)(x) \;\equiv\; \exp\left[\frac{i}{2}\theta^{ab}\partial_a^y\partial_b^z\right]\phi_1(y)\phi_2(z)\Big|_{y=z=x}\;. \tag{2.254}$$

In what follows, motivated by the form of the Higgs Lagrangian, we take $L[\phi]$ to describe the massive $\lambda\phi^4$ non-commutative field theory.

The main point made in Ref. [303] is that, in the simplest case of the ϕ^4 theory, the 1PI two point function has the non-trivial leading form (up to an overall coefficient)

$$\Lambda_{\rm eff}^2 - m^2\log\left(\frac{\Lambda_{\rm eff}^2}{m^2}\right)\;, \tag{2.255}$$

where m is the mass of the ϕ field, and the effective cut-off $\Lambda_{\rm eff}$ is given by the following expression:

$$\Lambda_{\rm eff}^2 \;=\; \left(\frac{1}{\Lambda^2} - p_a\theta_{ab}^2 p_b\right)^{-1}\;. \tag{2.256}$$

Here, Λ is the usual UV cut-off. Note that the non-commutativity scale θ plays the role of the natural IR cut-off.

The UV/IR mixing, characteristic of this type of non-commutative field theory leads to the question of the existence of the proper continuum limit for non-commutative field theory. This question can be examined from the point of view of non-perturbative Renormalization Group (RG). The proper Wilsonian analysis of this type of non-commutative theory has been done in Ref. [305]. The UV/IR mixing leads to a new kind of the RG flow: a double RG flow, in which one flows from the UV to IR and the IR to the UV and ends up, generically, at a self-dual fixed point. It would be tantalizing if the NCG set-up associated with the SM, and in particular, the LRSM generalization discussed here, would lead to the phenomenon of the UV/IR mixing and the double RG flow with a self-dual fixed point. Finally, we remark that it has been argued in a recent work on quantum gravity and string theory that such UV/IR mixing and the double RG might be a generic feature of quantum gravity coupled to matter [118, 304].

Even though the NCG in our case is different from this toy example, the lesson in the essential physics of the UV/IR mixing is present in our situation as well: the Higgs field can be associated with the natural scale of non-commutativity and thus the natural IR scale, and, therefore, even in our situation we might reasonably expect that the the Higgs scale is mixed with the UV cut-off defined by some more fundamental theory. Needless to say, at the moment this is only an exciting conjecture.

If this conjecture is true, given the results presented here one could expect that the appearance of the LRSM degrees of freedom (as well as the embedded SM degrees of freedom) at low energy is essentially a direct manifestation of some effective UV/IR mixing, and thus that, on one hand, the remnants of the UV physics can be expected at a low energy scale of 4 TeV, and, conversely, that the LRSM structure point to some unique features of the high energy physics of quantum gravity. In this context, we recall the observations made in Ref. [196] about the special nature of the Pati-Salam model, which unifies the LRSM with QCD, in certain constructions of string vacua. Even though this observation is mainly based on "groupology" and it is not deeply understood, this observation might be indicative that the Pati-Salam model is the natural completion of the SM, as suggested here, in which the infrared physics associated with the Higgs sector is mixed with the ultraviolet physics of some more fundamental physics, such as string theory.

Chapter 3

Left-right Symmetric Model Motivated by Non-Commutative Geometry

In the last chapter, we studied the superconnection formalism, which implies a geometry responsible for the structure of the SM particle spectrum. It was shown by Connes *et al.* [190] that, in order to describe all the symmetries we observe in terms of diffeomorphisms of a single geometric structure, the geometry cannot be a regular geometry but instead must be NCG. In this chapter, we briefly review NCG as studied in our previous work [160] published in International Journal of Modern Physics A, and study the phenomenology related to it. In particular, we study the LRSM extension hinted by the NCG structure and point out that the model would have been in tension with the previous LHC diboson excess had the signal persisted.

3.1 Introduction and Overview of NCG Approach

Canonical discussions on possible new physics beyond the Standard Model (SM) have been centered around the hierarchy problem and the unifications of couplings. The current favorites among various approaches to stabilizing the low Higgs mass (126 GeV, as found at the LHC [306, 307]) are supersymmetry, technicolor, and extra dimensions. These approaches also incorporate the philosophy of coupling unification in Grand Unified Theories (GUT's).

To this list, we seek to add another contender, namely models based on the NCG of Connes [152, 189]. In a series of papers starting from 1990 [147–156], Connes and collaborators have argued that the SM action could be derived from a particular NCG via the construction of what they call the "spectral" action [149], in essence geometrizing the SM and placing it on a similar footing to gravity. Several of the predictions that result from the

approach, according to our current understanding, are quite remarkable:[1]

- The $SU(2)_L$ gauge bosons and the Higgs doublet are unified into a single "superconnection," one of the consequences being that the $SU(2)_L$ gauge coupling g_L and the Yukawa couplings are related in a particular way [147, 150–152].
- The $SU(2)_L \times U(1)_Y \times SU(3)_C$ gauge couplings satisfy an $SO(10)$ GUT-like relation, even though the particle content of the model is that of the SM [149, 154].
- Anomaly cancellation requires the presence of both electroweak and QCD sectors, another GUT-like feature [150].
- The smallness of the Higgs boson mass can potentially be explained via an extra-dimension-like mechanism involving a 'warp'-factor [154].

The approach, of course, is not without its problems:

- The GUT-like relations on the gauge couplings can only be imposed at a single scale, so one must interpret the NCG spectral action as that which 'emerges' from an underlying NCG theory at the 'unification' scale.
- Quantization of the model within the NCG framework (in the sense of path integrals) is yet to be fully explored [152, 189], so one usually treats the NCG spectral action as an effective QFT action at the unification scale, and evolve it down to lower energies using the usual Renormalization Group (RG) equations to work out the infrared consequences.
- The minimal version of the NCG model which describes the SM predicts a Higgs mass of ~ 170 GeV, in clear contradiction with experiment [154]. This issue could be remedied by turning one of the off-diagonal entries of the Dirac operator, which is responsible for the neutrino Majorana mass, into a field. With this singlet field coupled to the SM Higgs field, the model accommodates a 126 GeV Higgs boson [155]. This could also be accomplished by extending the NCG to that which leads to a left-right symmetric Pati-Salam type action with coupling unification which automatically involves this singlet field [156].

In addition, the NCG spectral action approach to particle physics is under continued development by Connes and collaborators, and sorting out the various versions can be difficult.

Despite these caveats, however, or any other reservation one may have about the entire approach, it is not without its merits, as explained above, and we feel that it may have the potential to develop into a full-fledged paradigm. In particular, from the phenomenological

[1] We are currently working on a review article explaining how these predictions come about [162].

standpoint, the necessity to enlarge the gauge symmetry (via an enlargement of the underlying NCG) to accommodate the Higg mass can be considered a strength rather than a weakness. It tells us that the approach is restrictive enough for the models to be confronted by experiment, and point us in new directions to explore.

Indeed, in a recent paper [2], Chamseddine, Connes, and van Suijlekom have proposed a new formulation of an NCG based unified left-right symmetric Pati-Salam model, which comes in three different versions differing in Higgs content. In all three, the gauge theory which emerges from the underlying NCG at the unification scale, which we will call M_U, is that with gauge symmetry $G_{224} = SU(2)_L \times SU(2)_R \times SU(4)_C$ with unified couplings:

$$g_L(M_U) \;=\; g_R(M_U) \;=\; g_4(M_U)\;. \tag{3.1}$$

In one version, the symmetry is actually $G_{224D} = G_{224} \times D$, where D denotes parity which maintains left-right symmetry.[2]

G_{224} or G_{224D} is assumed to break down to $G_{213} = SU(2)_L \times U(1)_Y \times SU(3)_C$ of the SM at scale M_R with matching conditions

$$\begin{aligned}
\frac{1}{[g_1(M_R)]^2} &= \frac{2}{3}\frac{1}{[g_4(M_R)]^2} + \frac{1}{[g_R(M_R)]^2}\;,\\
\frac{1}{[g_2(M_R)]^2} &= \frac{1}{[g_L(M_R)]^2}\;,\\
\frac{1}{[g_3(M_R)]^2} &= \frac{1}{[g_4(M_R)]^2}\;.
\end{aligned} \tag{3.2}$$

For all three versions, which differ in particle content, Ref. [2] argues that both boundary conditions can be satisfied if $M_U \sim 10^{15}\,\mathrm{GeV}$ and $M_R \sim 10^{13}\,\mathrm{GeV}$.

Here, we will not attempt to review or justify the derivation of these models, but look at their consequences purely phenomenologically. From that viewpoint, the high value of M_R is problematic in light of recent hints of a W_R with a mass of around 2 TeV at the LHC. [308–313] If the LHC signal is indeed the gauge boson of the $SU(2)_R$ group, then M_R on the order of a few TeV would be more compatible with that possibility. For instance, in Refs. [159, 163] we proposed an $su(2/2)$ superconnection-based left-right symmetric model for which $M_R = 4\,\mathrm{TeV}$, placing the mass of W_R in the correct range. We address the question whether M_R for Chamseddine *et al.*'s NCG models can be lowered by the addition of intermediate breaking scales between M_U and M_R at which the symmetry breaks down from G_{224D}/G_{224} to G_{213} via several intermediate steps. In other words, is any symmetry-breaking pattern compatible with a unified left-right symmetric Pati-Salam model at M_U, and the SM below $M_R \sim$ few TeV? We will demand that M_U stay below the Planck mass

[2] D-parity is slightly different from the usual Lorentz (P) parity in that the former interchanges the $SU(2)_L$ and $SU(2)_R$ sectors completely (including the scalars), while the latter does not transform the scalars. For example, the D-parity interchanges the $SU(2)_L$ Higgs fields and their $SU(2)_R$ counterparts, and transforms the bidoublet ϕ into $\phi^\dagger$ (and vice versa), while the P-parity leaves them unchanged.

at 10^{19} GeV. Similar analyses have been carried out in the context of non-supersymmetric $SO(10)$ GUT models in Refs. [314–321] for a variety of symmetry breaking chains.[3] Our analysis differs from these due to the NCG models considered here differing in Higgs content since NCG does not require the Higgs fields to fall into $SO(10)$ multiplets.

While originally motivated by the desire to confront the viability of NCG derived unified left-right symmetric Pati-Salam models, we note in passing that similar models may emerge in a large class of string compactifications as discovered by Dienes. [326] So the results presented here may have a wider range of applicability.

This chapter is organized as follows. In section 2, we briefly review the current status of the W_R-like signal seen at the LHC, and phenomenological constraints. In section 3, we cover various symmetry breaking chains from G_{224D}/G_{224} down to G_{213}, and solve the renormalization group evolution equations for breaking scales which would satisfy the boundary/matching conditions for the given particle content. The list includes those that were considered by Chamseddine, Connes, and van Suijlekom in Ref. [2]. We conclude in section 4 with a discussion of what was discovered.

3.2 Example: The W_R Signal at the LHC

In 2015, ATLAS reported on a search for narrow resonances hadronically decaying into a pair of SM gauge bosons WW, WZ, or ZZ [308]. The largest excess occurs in the WZ channel at around 2 TeV with a local significance of 3.4σ and a global 2.5σ. Moreover, both CMS [309] and ATLAS [310] notice an excess at around 1.8 TeV in the dijet distributions, albeit with low significance (2.2σ and 1σ). In addition, CMS observes an excess, again at around 2 TeV, both in their search for massive WH production in the $\ell\nu b\bar{b}$ final state [311] and in massive-resonance production decaying into two SM vector bosons (one of which is leptonically tagged [312]), both of which have lower significance than 2σ.

It is discussed in Refs. [327–330] that these results may be interpreted in the context of the left-right model with the gauge group $SU(2)_L \times SU(2)_R \times U(1)'$ and it is shown that a heavy right-handed gauge boson W_R with a single coupling $g_R(M_R) \simeq 0.4$ can explain the current measurements. Note that this coupling is different from the SM left-handed W_L coupling $g_L(5\text{ TeV}) \simeq 0.63$. [1, 331] Many other authors have also discussed possible phenomenological consequences of the W_R interpretation, e.g. Refs. [332–343] to list just a few, but we refrain from reviewing them here.

Although the collider excess goes away later, we nevertheless use it as an example to demonstrate how exotic high energy physics such as NCG can be put into test in a collider experiment.

[3] For analyses of supersymmetric $SO(10)$ GUT, see Refs. [322–325].

3.3 TeV-Scale Left-Right Model in the Light of Latest LHC Searches

3.3.1 Setup of the Problem

We would like to see whether such a W_R can be accommodated within an NCG induced unified left-right symmetric Pati-Salam model. The left-right symmetric model naturally has $g_R = g_L$. However, one can have an asymmetry between g_R and g_L if one separates the D-parity [259] breaking scale M_D from the the scale M_R where $SU(2)_R$ is broken [206, 344].

As an intermediate symmetry between G_{224D}/G_{224} and G_{213} of the SM, we introduce

$$G_{2213} \;=\; SU(2)_L \times SU(2)_R \times U(1)_{B-L} \times SU(3)_C \;, \tag{3.3}$$

with gauge couplings g_L, g_R, g_{BL}, and g_3. The most general breaking sequence will then be

$$\text{NCG} \;\overset{M_U}{\Longrightarrow}\; G_{224D} \;\overset{M_D}{\longrightarrow}\; G_{224} \;\overset{M_C}{\longrightarrow}\; G_{2213} \;\overset{M_R}{\longrightarrow}\; G_{213} \;\overset{M_Z}{\longrightarrow}\; G_{13} \;, \tag{3.4}$$

where the double-line arrow indicates the emergence of the G_{224D} theory from the underlying NCG, and $G_{13} = U(1)_{\text{EM}} \times SU(3)_C$ is the unbroken group which remains below the electroweak scale with couplings e and g_3.

We label the energy intervals in between symmetry breaking scales starting from $[M_Z, M_R]$ up to $[M_D, M_U]$ with Roman numerals as:

$$\begin{aligned} \text{I} \;&:\; [M_Z,\, M_R] \;, \quad G_{213}\,(\text{SM}) \;, \\ \text{II} \;&:\; [M_R,\, M_C] \;, \quad G_{2213} \;, \\ \text{III} \;&:\; [M_C,\, M_D] \;, \quad G_{224} \;, \\ \text{IV} \;&:\; [M_D,\, M_U] \;, \quad G_{224D} \;. \end{aligned} \tag{3.5}$$

The ordering of the breaking scales must be strictly maintained, that is

$$M_Z \;\leq\; M_R \;\leq\; M_C \;\leq\; M_D \;\leq\; M_U \;. \tag{3.6}$$

However, adjacent scales can be set equal, which collapses the corresponding energy interval and skips the intermediate step. For instance, if $M_R = M_C$, then G_{224} breaks directly to G_{213}, and interval III will be followed by interval I, skipping interval II.

In the following, we investigate whether it is possible to set $M_R \sim 5\,\text{TeV}$ while maintaining M_U below the Planck scale. The IR data which we will keep fixed as boundary conditions to the RG running are [1, 331]

$$\begin{aligned} \alpha(M_Z) \;&=\; 1/127.9 \;, \\ \alpha_s(M_Z) \;&=\; 0.118 \;, \\ \sin^2\theta_W(M_Z) \;&=\; 0.2312 \;, \end{aligned} \tag{3.7}$$

at $M_Z = 91.1876\,\mathrm{GeV}$, which translates to

$$g_1(M_Z) \;=\; 0.36\,, \quad g_2(M_Z) \;=\; 0.65\,, \quad g_3(M_Z) \;=\; 1.22\,. \tag{3.8}$$

The coupling constants are all required to remain in the perturbative regime during the evolution from M_U down to M_Z.

3.3.2 One-Loop Running and the Extended Survival Hypothesis

For a given particle content, the gauge couplings are evolved according to the 1-loop RG relation

$$\frac{1}{g_i^2(M_A)} - \frac{1}{g_i^2(M_B)} \;=\; \frac{a_i}{8\pi^2} \ln \frac{M_B}{M_A}\,, \tag{3.9}$$

where the RG coefficients a_i are given by [7, 200]

$$\begin{aligned} a_i \;=\; -\frac{11}{3} C_2(G_i) \;&+\; \frac{2}{3} \sum_{R_f} T_i(R_f) \cdot d_1(R_f) \cdots d_n(R_f) \\ &+\; \frac{1}{3} \sum_{R_s} T_i(R_s) \cdot d_1(R_s) \cdots d_n(R_s)\,. \end{aligned} \tag{3.10}$$

Here, the summation is over irreducible chiral representations of fermions (R_f) in the second term and those of scalars (R_s) in the third. $C_2(G_i)$ is the quadratic Casimir for the adjoint representation of the group G_i, and T_i is the Dynkin index of each (complex) representation.[4] For $SU(2)$, $C_2(G) = 2$, $T = 1/2$ for doublet representations and $T = 2$ for triplets. See Table 3.1 for the Dynkin indexes of other representations. For $U(1)$, $C_2(G) = 0$ and

$$\sum_{f,s} T \;=\; \sum_{f,s} \left(\frac{Y}{2}\right)^2\,, \tag{3.11}$$

where $Y/2$ is the $U(1)$ charge, the factor of $1/2$ coming from the traditional normalizations of the hypercharge Y and $B - L$ charges. The a_i's will differ depending on the particle content, which changes every time symmetry breaking occurs. We will distinguish the a_i's in different energy intervals with the corresponding roman numeral superscript, cf. Eq. (3.5).

For the particle content in each energy interval we impose the *Extended Survival Hypothesis* (ESH) [345]. The ESH states that at every step of the symmetry breaking chain, the only scalars which survive below the symmetry breaking scale are the ones which acquire vacuum expectation values (VEV's) at the subsequent levels of the symmetry breaking. For instance, the only scalar assumed to survive below M_R would be the SM Higgs doublet which acquires a VEV to break G_{213} further down to G_{13} under the ESH.

[4] If the representation is real a factor of $\frac{1}{2}$ comes about in the third term.

3.3.3 Non-Unified Left-Right Symmetric Pati-Salam

We begin by looking at the Pati-Salam model [195, 201–203] without the unification of all three couplings as demanded in the NCG approach. We impose left-right symmetry $g_L = g_R$ at scale M_D, which we identify as the scale at which G_{224D} breaks to G_{224}, and evolve our couplings down from M_D:

$$G_{224D} \xrightarrow{M_D} G_{224} \xrightarrow{M_C} G_{2213} \xrightarrow{M_R} G_{213} \xrightarrow{M_Z} G_{13} \,. \tag{3.12}$$

Note that energy interval IV is absent. In addition to Eq. (3.8), the boundary/matching conditions we impose on the couplings at the symmetry breaking scales are:

$$M_D \;:\; g_L(M_D) \;=\; g_R(M_D) \,, \tag{3.13}$$

$$M_C \;:\; \sqrt{\frac{2}{3}}\, g_{BL}(M_C) \;=\; g_3(M_C) = g_4(M_C) \,, \tag{3.14}$$

$$M_R \;:\; \frac{1}{g_1^2(M_R)} \;=\; \frac{1}{g_R^2(M_R)} + \frac{1}{g_{BL}^2(M_R)} \,, \quad g_2(M_R) \;=\; g_L(M_R) \,, \tag{3.15}$$

$$M_Z \;:\; \frac{1}{e^2(M_Z)} \;=\; \frac{1}{g_1^2(M_Z)} + \frac{1}{g_2^2(M_Z)} \,. \tag{3.16}$$

Note that if $M_C = M_R$, then the conditions at those scales reduce to those given in Eq. (3.2).

We assume that the above breaking sequence is accomplished by a Higgs sector consisting of scalars which transform under G_{224} as

$$\phi(2,2,1) \,, \quad \Delta_R(1,3,10) \,, \quad \Sigma(1,1,15) \,. \tag{3.17}$$

These fields decompose into irreducible representations of G_{2213} as:

$$\begin{aligned}
\Sigma(1,1,15) &= \Sigma_1(1,1,0,1) \oplus \Sigma_3\left(1,1,\frac{4}{3},3\right) \oplus \Sigma_{\bar{3}}\left(1,1,\frac{-4}{3},\bar{3}\right) \oplus \Sigma_8(1,1,0,8) \,, \\
\Delta_R(1,3,10) &= \Delta_{R1}(1,3,2,1) \oplus \Delta_{R3}\left(1,3,\frac{2}{3},3\right) \oplus \Delta_{R6}\left(1,3,\frac{-2}{3},6\right) \,, \\
\phi(2,2,1) &= \phi(2,2,0,1) \,.
\end{aligned} \tag{3.18}$$

The breaking of G_{224} down to G_{2213} would be accomplished by the field Σ_1 acquiring a VEV. Σ_3, $\Sigma_{\bar{3}}$, Σ_8, Δ_{R3}, Δ_{R6} are all colored, so they will not be acquiring VEV's in the subsequent steps. Thus, under ESH, all these fields will become heavy at M_C and decouple from the RG equations below M_C. The remaining fields decompose into irreducible representations of G_{213} as:

$$\Delta_{R1}(1,3,2,1) \;=\; \Delta_{R1}^0(1,0,1) \oplus \Delta_{R1}^+(1,2,1) \oplus \Delta_{R1}^{++}(1,4,1) \,,$$

$$\phi(2,2,0,1) \;=\; \phi_2(2,1,1) \oplus \phi_2'(2,-1,1)\;. \tag{3.19}$$

The breaking of G_{2213} down to G_{213} would be accomplished by the field Δ^0_{R1}, while that of G_{213} down to G_{13} would be realised by the neutral (diagonal) components of $\phi_2(2,2,0,1)$, acquiring VEVs. The fields Δ^+_{R1} and Δ^{++}_{R1} would be both charged under electromagnetism, so they will not be acquiring VEV's in the subsequent steps. Thus, under the ESH, these fields will become heavy at M_R. In addition, only one of the two physical states (which are linear combinations of ϕ_2 and ϕ_2') remains light while the other picks a mass at M_R, unless we apply fine-tuning [346]. The left-over field, the SM Higgs (which can be identified without loss of generality as $\phi_2(2,1,1)$) is left to be the only field in the Higgs spectrum below M_R. Finally, with ESH, the particle content (other than the fermions and gauge bosons) of our model in the three energy intervals I through III are:

$$\begin{aligned}
\text{III} \;&:\; \phi(2,2,1)\;,\; \Delta_R(1,3,10)\;,\; \Sigma(1,1,15)\;,\\
\text{II} \;&:\; \phi(2,2,0,1)\;,\; \Delta_{R1}(1,3,2,1)\;,\\
\text{I} \;&:\; \phi_2(2,1,1)\;.
\end{aligned} \tag{3.20}$$

The values of the RG coefficients for this Higgs content are listed in Table 3.2.

Taking advantage of the boundary/matching conditions, the following relations can be derived between the boundary values $\alpha(M_Z)$, $\alpha_s(M_Z)$, $\sin^2\theta_W(M_Z)$, $g_R(M_R)$, and the ratios of the successive symmetry breaking scales:

$$\begin{aligned}
&2\pi\left[\frac{3-6\sin^2\theta_W(M_Z)}{\alpha(M_Z)} - \frac{2}{\alpha_s(M_Z)}\right]\\
&\quad= \underbrace{(3a_1-3a_2-2a_3)^{\text{I}}}_{44}\,\ln\frac{M_R}{M_Z} + \underbrace{(-3a_L+3a_R+3a_{BL}-2a_3)^{\text{II}}}_{27}\,\ln\frac{M_C}{M_R}\\
&\qquad\quad + \underbrace{(-3a_L+3a_R)^{\text{III}}}_{20}\,\ln\frac{M_D}{M_C}\;,\\
&2\pi\left[\frac{4\pi}{g_R^2(M_R)} - \frac{\sin^2\theta_W(M_Z)}{\alpha(M_Z)}\right]\\
&\quad= \underbrace{(-a_2)^{\text{I}}}_{19/6}\,\ln\frac{M_R}{M_Z} + \underbrace{(a_R-a_L)^{\text{II}}}_{2/3}\,\ln\frac{M_C}{M_R} + \underbrace{(a_R-a_L)^{\text{III}}}_{20/3}\,\ln\frac{M_D}{M_C}\;.
\end{aligned} \tag{3.21}$$

The derivation is shown in the Appendix B.1. To maintain the ordering of the mass scales, all logarithms in these expressions must be non-negative. Numerically, we have

$$\begin{aligned}
517 \;&=\; 44\,x + 27\,y + 20\,z\;,\\
\frac{206}{g_R^2(M_R)} - 484 \;&=\; 19\,x + \;4\,y + 40\,z\;,
\end{aligned} \tag{3.22}$$

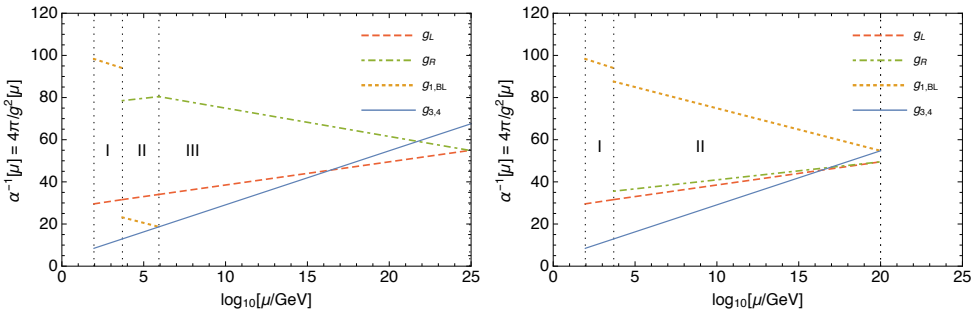

(a) $g_R(M_R) = 0.4$ (b) $g_R(M_R) = 0.59$

Figure 3.1: Running of the gauge couplings for the left-right symmetric Pati-Salam model. The vertical dotted lines from left to right correspond to the symmetry breaking scales M_Z, M_R, and M_C. M_R is fixed at 5 TeV. For the $U(1)_{B-L}$ coupling between M_R and M_C, we plot $\dfrac{3}{2}\alpha_{BL}^{-1}(\mu) = \dfrac{6\pi}{g_{BL}^2(\mu)}$ so that it agrees with $\alpha_4^{-1}(\mu)$ at $\mu = M_C$. The two cases shown are (a) $g_R(M_R) = 0.4$ is imposed, and (b) M_D is minimized by collapsing the energy interval III.

where

$$x \;=\; \log_{10}\frac{M_R}{M_Z}\,, \qquad y \;=\; \log_{10}\frac{M_C}{M_R}\,, \qquad z \;=\; \log_{10}\frac{M_D}{M_C}\,. \tag{3.23}$$

If we fix $M_R = 5\,\text{TeV}$, then $x = \log_{10}(M_R/M_Z) = 1.74$, and the above system of linear equations yields

$$y \;=\; 27.9 - \frac{4.11}{g_R^2(M_R)}\,, \qquad z \;=\; -15.7 + \frac{5.56}{g_R^2(M_R)}\,. \tag{3.24}$$

Since both y and z must be positive, we must have

$$0.38 \;<\; g_R(M_R) \;<\; 0.59\,. \tag{3.25}$$

We would also like to impose the condition

$$x + y + z \;=\; 14.0 + \frac{1.44}{g_R^2(M_R)} \;=\; \log_{10}\frac{M_D}{M_Z} \;<\; \log_{10}\frac{10^{19}\,\text{GeV}}{M_Z} \;=\; 17.0\,, \tag{3.26}$$

which constrains $g_R(M_R)$ to

$$g_R(M_R) \;>\; 0.69\,, \tag{3.27}$$

which is incompatible with Eq. (3.25). Thus, the system does not allow for a parity breaking scale M_D lower than the Planck mass.

Indeed, if we set $g_R(M_R) = 0.4$, as preferred by experiment [327–330], we obtain $y = 2.2$, $z = 19.0$, which translates to

$$M_R \;=\; 5\,\text{TeV}\,, \quad M_C \;=\; 8\times10^5\,\text{GeV}\,, \quad M_D \;=\; 8\times10^{24}\,\text{GeV}\,, \tag{3.28}$$

with

$$g_L(M_D) \;=\; g_R(M_D) \;=\; 0.48\,, \qquad g_4(M_D) \;=\; 0.43\,. \tag{3.29}$$

If we allow $g_R(M_R)$ to be as large as 0.59, we obtain $y = 16.3$, $z = 0$, which translates to

$$M_R \;=\; 5\,\text{TeV}\,, \quad M_C \;=\; M_D \;=\; 1\times 10^{20}\,\text{GeV}\,, \tag{3.30}$$

with

$$g_L(M_D) \;=\; g_R(M_D) \;=\; 0.50\,, \qquad g_4(M_D) \;=\; 0.48\,. \tag{3.31}$$

The evolution of the couplings for these choices of scales is shown in Fig. 3.1. For each choice of $g_R(M_R)$, the value of $g_{BL}(M_R)$ is determined from the known value of the hypercharge coupling $g_1(M_R)$ and the matching condition Eq. (3.15). Larger values of $g_R(M_R)$ closer to $g_L(M_R)$ will lower the scale M_D at which the RG flow of the two couplings separate. At the same time, larger values of $g_R(M_R)$ demand smaller values of $g_{BL}(M_R)$, which pushes up the scale M_C where the RG flow of g_{BL} bifurcates from that of g_3. Since the order $M_C \leq M_D$ cannot be violated, M_D cannot be lowered further by increasing $g_R(M_R)$ once the two scales meet.

Looking at Fig. 3.1(b), however, we notice that in energy interval II g_L and g_R do flow apart, but not as much as in energy interval III. A larger difference between g_L and g_R could be generated in interval II if $(a_L - a_R)^{\text{II}}$ could be enhanced. To this end, let us relax the ESH and allow some of the colored Δ_R fields to survive into interval II. The RG coefficients for three Higgs-content scenarios in interval II that differ from the ESH case are listed in Table 3.3. Clearly, the addition of extra Δ_R fields enhances $(a_L - a_R)^{\text{II}}$.

We perform the same analyses as above for the three ESH-breaking cases, namely, the calculation of the symmetry breaking scales to reproduce $g_R(M_R) = 0.4$, and then by allowing the value of $g_R(M_R)$ to float in order to find the lowest value of M_D:

1. Δ_{R1} and Δ_{R3} survive:
   To reproduce $g_R(M_R) = 0.4$, we find

   $$M_R \;=\; 5\,\text{TeV}\,, \quad M_C \;=\; 8\times 10^{5}\,\text{GeV}\,, \quad M_D \;=\; 2\times 10^{24}\,\text{GeV}\,, \tag{3.32}$$

   with

   $$g_L(M_D) \;=\; g_R(M_D) \;=\; 0.48\,, \qquad g_4(M_D) \;=\; 0.44\,. \tag{3.33}$$

   If $g_R(M_R)$ is allowed to float, the minimum of M_D is achieved when $g_R(M_R) = 0.53$ with

   $$M_R \;=\; 5\,\text{TeV}\,, \quad M_C \;=\; M_D \;=\; 1\times 10^{17}\,\text{GeV}\,, \tag{3.34}$$

   with

   $$g_L(M_D) \;=\; g_R(M_D) \;=\; 0.52\,, \qquad g_4(M_D) \;=\; 0.53\,. \tag{3.35}$$

   The runnings of the couplings for these cases are shown in Fig. 3.2(a) and (b).

2. Δ_{R1} and Δ_{R6} survive:
   To reproduce $g_R(M_R) = 0.4$, we find

$$M_R \;=\; 5\,\text{TeV}\;, \quad M_C \;=\; 2\times 10^6\,\text{GeV}\;, \quad M_D \;=\; 5\times 10^{23}\,\text{GeV}\;, \tag{3.36}$$

   with

$$g_L(M_D) \;=\; g_R(M_D) \;=\; 0.48\;, \qquad g_4(M_D) \;=\; 0.45\;. \tag{3.37}$$

   If $g_R(M_R)$ is allowed to float, the minimum of M_D is achieved when $g_R(M_R) = 0.49$ with

$$M_R \;=\; 5\,\text{TeV}\;, \quad M_C \;=\; M_D \;=\; 8\times 10^{15}\,\text{GeV}\;, \tag{3.38}$$

   with

$$g_L(M_D) \;=\; g_R(M_D) \;=\; 0.53\;, \qquad g_4(M_D) \;=\; 0.62\;. \tag{3.39}$$

   The runnings of the couplings for these cases are shown in Fig. 3.2(c) and (d).

3. All three multiplets Δ_{R1}, Δ_{R3}, and Δ_{R6} survive:
   To reproduce $g_R(M_R) = 0.4$, we find

$$M_R \;=\; 5\,\text{TeV}\;, \quad M_C \;=\; 2\times 10^6\,\text{GeV}\;, \quad M_D \;=\; 8\times 10^{22}\,\text{GeV}\;, \tag{3.40}$$

   with

$$g_L(M_D) \;=\; g_R(M_D) \;=\; 0.49\;, \qquad g_4(M_D) \;=\; 0.46\;. \tag{3.41}$$

   If $g_R(M_R)$ is allowed to float, the minimum of M_D is achieved when $g_R(M_R) = 0.47$ with

$$M_R \;=\; 5\,\text{TeV}\;, \quad M_C \;=\; M_D \;=\; 2\times 10^{14}\,\text{GeV}\;, \tag{3.42}$$

   with

$$g_L(M_D) \;=\; g_R(M_D) \;=\; 0.54\;, \qquad g_4(M_D) \;=\; 0.67\;. \tag{3.43}$$

   The runnings of the couplings for these cases are shown in Fig. 3.2(e) and (f).

These results indicate that achieving a value of $g_R(M_R) = 0.4$ at $M_R = 5\,\text{TeV}$ is not trivial in this model, requiring a very high value of the parity breaking scale M_D. Lowering this scale below the Planck mass cannot be achieved with the minimal Higgs content in energy interval II as required by the ESH even if the value of $g_R(M_R)$ were allowed to float. If one relaxes the ESH, then M_D lower than the Planck mass is possible, provided $g_R(M_R)$ is allowed to be as large as ~ 0.5. It is also preferable for M_C and M_D to be degenerate, that is, for G_{224D} to break directly to G_{2213}.

3.3.4 Unified Left-Right Symmetric Pati-Salam from NCG

With the above results in mind, let us now look at the unified left-right symmetric Pati-Salam model which we expect to emerge from an underlying NCG. The breaking pattern now includes an emergence/unification scale as in Eq. (3.4), and all four energy intervals listed in Eq. (3.5) must be taken into account with an extra boundary condition at M_U:

$$M_U \quad : \quad g_L(M_U) \;=\; g_R(M_U) \;=\; g_4(M_U)\;. \tag{3.44}$$

This leads to the relations

$$\begin{aligned}
&2\pi\left[\frac{3-8\sin^2\theta_W(M_Z)}{\alpha(M_Z)}\right] \\
&= \;(3a_1-5a_2)^{\mathrm{I}}\,\ln\frac{M_R}{M_Z}+(-5a_L+3a_R+3a_{BL})^{\mathrm{II}}\,\ln\frac{M_C}{M_R} \\
&\quad +(-5a_L+3a_R+2a_4)^{\mathrm{III}}\,\ln\frac{M_D}{M_C}+(-5a_L+3a_R+2a_4)^{\mathrm{IV}}\,\ln\frac{M_U}{M_D}\;, \qquad (3.45)\\
&2\pi\left[\frac{3}{\alpha(M_Z)}-\frac{8}{\alpha_s(M_Z)}\right] \\
&= \;(3a_1+3a_2-8a_3)^{\mathrm{I}}\,\ln\frac{M_R}{M_Z}+(3a_L+3a_R+3a_{BL}-8a_3)^{\mathrm{II}}\,\ln\frac{M_C}{M_R} \\
&\quad +(3a_L+3a_R-6a_4)^{\mathrm{III}}\,\ln\frac{M_D}{M_C}+(3a_L+3a_R-6a_4)^{\mathrm{IV}}\,\ln\frac{M_U}{M_D}\;, \qquad (3.46)\\
&2\pi\left[\frac{4\pi}{g_R^2(M_R)}-\frac{\sin^2\theta_W(M_Z)}{\alpha(M_Z)}\right] \\
&= \;(-a_2^{\mathrm{I}})\,\ln\frac{M_R}{M_Z}+(a_R-a_L)^{\mathrm{II}}\,\ln\frac{M_C}{M_R}+(a_R-a_L)^{\mathrm{III}}\,\ln\frac{M_D}{M_C}\;. \qquad (3.47)
\end{aligned}$$

The derivation is given in the Appendix B.1. Note that there is no $\ln M_U/M_D$ term in the last line since parity is not broken in energy interval IV and $a_L^{\mathrm{IV}}=a_R^{\mathrm{IV}}$. We will now look at the three models of Chamseddine, Connes, and van Suijlekom in Ref. [2], one by one.

A. Pati-Salam with "composite" Higgs fields[5]

The first model of Ref. [2] emerges with symmetry G_{224} at $M_U=M_D$, which breaks directly to G_{213} of the SM at $M_C=M_R$. Only energy intervals I and III are present. The Higgs content of this model in interval III, as specified in Ref. [2], is shown in Table 3.4. We make a slight modification by taking the $\Sigma(1,1,15)$ field to be real, conforming to standard Pati-Salam literature, whereas Ref. [2] assumes it to be complex.

[5]The terminology of Ref. [2] may cause confusion with the standard concept of compositeness that is found in the literature. What the authors of Ref. [2] call a "composite" field seems to be a field which does not transform under a single irreducible representation.

In this case, Eqs. (3.45) through (3.47) simply reduce to those with the II and IV terms missing. Then, the system of three equations has three unknowns, namely $\ln \frac{M_D}{M_C}$, $\ln \frac{M_R}{M_Z}$, and $g_R(M_R)$, which allows us to determine all three. We find:

$$\begin{aligned} g_R(M_R) &= 0.54 \,, \\ M_R = M_C &= 4.1 \times 10^{13}\,\mathrm{GeV} \,, \\ M_U = M_D &= 3.5 \times 10^{15}\,\mathrm{GeV} \,, \end{aligned} \tag{3.48}$$

in agreement with Ref. [2]. The unified coupling in this case is $g_L(M_U) = g_R(M_U) = g_4(M_U) = 0.53$. The running of the couplings for this case is shown in Fig. 3.3(a).

We now allow for $M_C \neq M_R$ and insert the energy interval II with symmetry G_{2213}. To determine the Higgs content in this interval, we again invoke the ESH. The decomposition of $\Sigma(1,1,15)$ into irreducible representations of G_{2213} was given in Eq. (3.18) and it was concluded that all the components of $\Sigma(1,1,15)$ become heavy and decouple from the RG equations at M_C. The decomposition of $\Delta_R(1,2,4)$ into irreducible representations of G_{2213} is given by

$$\Delta_R(1,2,4) \;=\; \Delta_{R1}(1,2,1,1) \oplus \Delta_{R3}\left(1,2,\frac{-1}{3},3\right) \,. \tag{3.49}$$

Δ_{R3} is colored so again, by ESH, it will become heavy and only Δ_{R1} will survive into II. The decomposition of Δ_{R1} into irreducible representations of G_{213} is given by

$$\Delta_{R1}(1,2,1,1) \;=\; \Delta^0_{R1}(1,0,1) \oplus \Delta^+_{R1}(1,1,1) \,. \tag{3.50}$$

The breaking of G_{2213} down to G_{213} would be accomplished by the field Δ^0_{R1} acquiring a VEV, while Δ^+_{R1} has electromagnetic charge so it must become heavy. The survival of $\phi_2(2,1,1)$ into I is as before. Thus, the Higgs content of the model is as shown in Table 3.4.

Eqs. (3.45) through (3.47) now has four unknowns instead of three. Numerically, they are given by

$$\begin{aligned} 401 &= \frac{109}{3}x + \frac{13}{2}y - \frac{34}{3}z \,, \\ 862 &= 67x + \frac{77}{2}y + 42z \,, \\ \frac{206}{g_R^2(M_R)} - 484 &= 19x - 16y + 4z \,, \end{aligned} \tag{3.51}$$

where x, y, and z are defined as in Eq. (3.23). Solving this system for x, y, and z we find

$$x \;=\; 2.3 + \frac{2.71}{g_R^2(M_R)} \,,$$

$$\begin{aligned} y &= 30.2 - \frac{8.72}{g_R^2(M_R)} \,, \\ z &= -10.8 + \frac{3.68}{g_R^2(M_R)} \,. \end{aligned} \tag{3.52}$$

Demanding that both y and z be positive restricts $g_R(M_R)$ to the range

$$0.54 \;<\; g_R(M_R) \;<\; 0.58 \,. \tag{3.53}$$

The lower bound corresponds to the case considered in Ref. [2] at which $y = 0$. Since we would like to minimize x, and thereby M_R, we set $g_R(M_R)$ to the upper bound of this range where $x = 10.2$, $y = 4.6$, and $z = 0$. This corresponds to

$$M_R \;=\; 1.5 \times 10^{12}\,\text{GeV} \,, \qquad M_C \;=\; M_D \;=\; M_U \;=\; 6 \times 10^{14}\,\text{GeV} \,. \tag{3.54}$$

The unified coupling in this case is $g_L(M_U) = g_R(M_U) = g_4(M_U) = 0.52$. The running of the couplings for this case is shown in Fig. 4.2(b).

Comparing the two cases, allowing $M_R \neq M_C$ has lowered M_R from $10^{13}\,\text{GeV}$ to $10^{12}\,\text{GeV}$. This is due to the bifurcation of g_4 into g_3 and g_{BL} at M_C. The hypercharge coupling at M_R must be matched to g_R and g_4 if $M_R = M_C$, but it will be matched to g_R and g_{BL} if $M_R \neq M_C$. Since g_{BL} decreases in II, one can allow g_R to increase further to generate the numerically correct value for g_1. This lowers the scale M_R. However, $10^{12}\,\text{GeV}$ is still too large compared to the TeV scale. This lowering is also at the expense of G_{224} breaking immediately to G_{2213} as the model emerges from the underlying NCG theory.

B. Pati-Salam with fundamental Higgs fields

The Higgs content of Model B of Ref. [2] is shown in Table 3.5, together with what the Higgs content in interval II would be under the ESH if the condition $M_C = M_R$ were relaxed. As in Model A, it is assumed that $M_U = M_D$. We first follow Ref. [2] and also assume $M_C = M_R$ and find

$$\begin{aligned} g_R(M_R) &= 0.48 \,, \\ M_R \;=\; M_C &= 1.5 \times 10^{11}\,\text{GeV} \,, \\ M_U \;=\; M_D &= 5.4 \times 10^{16}\,\text{GeV} \,. \end{aligned} \tag{3.55}$$

The unified coupling is $g_L(M_U) = g_R(M_U) = g_4(M_U) = 0.59$. The running of the couplings for this case is shown in Fig. 3.4(a).

Let us now relax the condition $M_C = M_R$ and insert the energy interval II with symmetry G_{2213} between intervals I and III. Without going into detail, we list the

Higgs fields that survive via the ESH into II from III in Table 3.5. Note that the Higgs content in I and II are exactly the same as the non-unified Pati-Salam model we considered earlier. In the exact repeat of our analysis of Model A, it can be shown that, for the ordering of the symmetry breaking scale to be maintained, $g_R(M_R)$ is restricted to the range

$$0.48 \ < \ g_R(M_R) \ < \ 0.56 \,, \tag{3.56}$$

with the higher bound giving the smallest possible M_R. This is found to be

$$M_R \ = \ 1.1 \times 10^9 \,\mathrm{GeV} \,, \qquad M_C \ = \ M_D \ = \ M_U \ = \ 4.4 \times 10^{16} \,\mathrm{GeV} \,, \tag{3.57}$$

with the unified coupling $g_L(M_U) = g_R(M_U) = g_4(M_U) = 0.52$. The running of the couplings for this case is shown in Fig. 3.4(b).

While this result is somewhat more promising than Model A, M_R is still to large, as is the value of $g_R(M_R)$ necessary for M_R to be pushed down to this scale. Let us see if the situation may be improved by relaxing the ESH as we did for the non-unified Pati-Salam case. We will allow some or all of the colored Δ_R fields to survive into interval II to enhance the difference between g_L and g_R. We consider the same three cases listed in Table 3.3.

(i) Δ_{R1} and Δ_{R3} survive:
To maintain the ordering of the symmetry breaking scales, it is found that $g_R(M_R)$ is restricted to the narrow range

$$0.48 \ < \ g_R(M_R) \ < \ 0.51 \,. \tag{3.58}$$

As $g_R(M_R)$ is increased, M_R/M_Z and M_D/M_C decrease while M_C/M_R increases. In terms of scale, M_R decreases while both M_C and M_D increase. The upper bound of this range is when $M_R/M_Z = 1$, so this case actually allows for $M_R = 5\,\mathrm{TeV}$. The other parameters in this case is

$$\begin{aligned} g_R(M_R) \ &= \ 0.51 \,, \\ M_R \ &= \ 5 \times 10^3 \,\mathrm{GeV} \,, \\ M_C \ &= \ 5 \times 10^{15} \,\mathrm{GeV} \,, \\ M_U \ = \ M_D \ &= \ 8 \times 10^{17} \,\mathrm{GeV} \,, \end{aligned} \tag{3.59}$$

with the unified coupling $g_L(M_U) = g_R(M_U) = g_4(M_U) = 0.54$. The running of the couplings for this case is shown in Fig. 3.5(a).

(ii) Δ_{R1} and Δ_{R6} survive:
To maintain the ordering of the symmetry breaking scales, it is found that $g_R(M_R)$ is restricted to the range

$$0.42 \ < \ g_R(M_R) \ < \ 0.48 \,, \tag{3.60}$$

with smaller $g_R(M_R)$ associated with smaller M_R, which drops down to M_Z at the lower bound. Imposing $M_R = 5\,\text{TeV}$ we obtain:

$$\begin{aligned} g_R(M_R) &= 0.43\,, \\ M_R &= 5\times 10^3\,\text{GeV}\,, \\ M_C &= 2\times 10^{10}\,\text{GeV}\,, \\ M_U = M_D &= 3\times 10^{20}\,\text{GeV}\,, \end{aligned} \tag{3.61}$$

with the unified coupling $g_L(M_U) = g_R(M_U) = g_4(M_U) = 0.63$. The running of the couplings for this case is shown in Fig. 3.5(b). Maintaining M_D below 10^{19} requires

$$0.45 \;<\; g_R(M_R)\,. \tag{3.62}$$

Selecting this boundary value for $g_R(M_R)$, we find

$$\begin{aligned} g_R(M_R) &= 0.45\,, \\ M_R &= 5\times 10^6\,\text{GeV}\,, \\ M_C &= 4\times 10^{10}\,\text{GeV}\,, \\ M_U = M_D &= 1\times 10^{19}\,\text{GeV}\,, \end{aligned} \tag{3.63}$$

with the unified coupling $g_L(M_U) = g_R(M_U) = g_4(M_U) = 0.62$. The running of the couplings for this case is shown in Fig. 3.5(c).

(iii) Δ_{R1}, Δ_{R3}, and Δ_{R6} all survive:
To maintain the ordering of the symmetry breaking scales, it is found that $g_R(M_R)$ is restricted to the range

$$0.41 \;<\; g_R(M_R) \;<\; 0.48\,, \tag{3.64}$$

while to maintain $M_U = M_D$ below $10^{19}\,\text{GeV}$ we must have

$$0.44 \;<\; g_R(M_R)\,. \tag{3.65}$$

If we demand $M_R = 5\,\text{TeV}$, we find

$$\begin{aligned} g_R(M_R) &= 0.42\,, \\ M_R &= 5\times 10^3\,\text{GeV}\,, \\ M_C &= 5\times 10^8\,\text{GeV}\,, \\ M_U = M_D &= 2\times 10^{20}\,\text{GeV}\,, \end{aligned} \tag{3.66}$$

with the unified coupling $g_L(M_U) = g_R(M_U) = g_4(M_U) = 0.66$. The running of the couplings for this case is shown in Fig. 3.5(d). If we demand $M_U = M_D = 10^{19}\,\text{GeV}$, we find

$$g_R(M_R) \;=\; 0.44\,,$$

$$\begin{aligned} M_R &= 2\times 10^6\,\text{GeV}\,, \\ M_C &= 4\times 10^9\,\text{GeV}\,, \\ M_U = M_D &= 1\times 10^{19}\,\text{GeV}\,, \end{aligned} \tag{3.67}$$

with the unified coupling $g_L(M_U) = g_R(M_U) = g_4(M_U) = 0.63$. The running of the couplings for this case is shown in Fig. 3.5(e).

C. Left-right symmetric Pati-Salam with fundamental Higgs fields

Finally, the last and most general scenario of Ref. [2] is where G_{224D} instead of G_{224} is the emergent symmetry of the spectral action. The assumed Higgs content of the model is shown in Table 3.6.

First, assuming $M_D = M_C = M_R$ as in Ref. [2], we solve Eqs. (3.45) through (3.47) and find

$$\begin{aligned} g_R(M_R) &= 0.54\,, \\ M_D = M_C = M_R &= 5\times 10^{13}\,\text{GeV}\,, \\ M_U &= 3\times 10^{15}\,\text{GeV}\,, \end{aligned} \tag{3.68}$$

with the unified coupling $g_L(M_U) = g_R(M_U) = g_4(M_U) = 0.58$. The running of the couplings for this case is shown in Fig. 3.6(a).

We next relax the relation $M_D = M_C = M_R$ and insert energy intervals II and III in between intervals I and IV with the Higgs content listed in Table 3.6. Eqs. (3.45) through (3.47) now read

$$\begin{aligned} 401 &= \frac{109}{3}x + 19y + \frac{34}{3}z - \frac{44}{3}w\,, \\ 862 &= 67x + 51y + 46z + 44w\,, \\ \frac{206}{g_R^2(M_R)} - 484 &= 19x + 4y + 40z\,, \end{aligned} \tag{3.69}$$

where x, y, and z are defined as in Eq. (3.23), and $w = \log_{10} M_U/M_D$. Solving this system for y, z, and w we find:

$$\begin{aligned} y &= 30.3 - 1.38x - \frac{4.11}{g_R^2(M_R)}\,, \\ z &= 15.1 + 0.34x - \frac{5.56}{g_R^2(M_R)}\,, \\ w &= 0.24 + 0.43x - \frac{1.04}{g_R^2(M_R)}\,. \end{aligned} \tag{3.70}$$

Demanding that y, z, and w are all positive restricts $x = \log_{10} M_R/M_Z$ and $g_R^{-2}(M_R)$ to the triangular region shown in Fig. 3.7(a). It is clear from the figure that M_R is

minimized when $M_U = M_D = M_C$, that is, energy regions III and IV are collapsed and only I and II remain. On the other hand, $g_R(M_R)$ is minimized when $M_U = M_D$ and $M_C = M_R$, that is, energy regions II and IV are collapsed and only I and III remain.

For the $M_U = M_D = M_C$ case, we find

$$\begin{aligned} g_R(M_R) &= 0.56\,, \\ M_R &= 1 \times 10^9\,\text{GeV}\,, \\ M_U = M_D = M_C &= 4 \times 10^{16}\,\text{GeV}\,, \end{aligned} \tag{3.71}$$

with the unified coupling $g_L(M_U) = g_R(M_U) = g_4(M_U) = 0.52$. The running of the couplings for this case is shown in Fig. 3.6(b).

For the $M_U = M_D$, $M_C = M_R$ case, we find

$$\begin{aligned} g_R(M_R) &= 0.49\,, \\ M_C = M_R &= 3 \times 10^{11}\,\text{GeV}\,, \\ M_U = M_D &= 2 \times 10^{16}\,\text{GeV}\,, \end{aligned} \tag{3.72}$$

with the unified coupling $g_L(M_U) = g_R(M_U) = g_4(M_U) = 0.52$. The running of the couplings for this case is shown in Fig. 3.6(c).

Again, the values of M_R and $g_R(M_R)$ thus obtained are more promising than what could be achieved in Model A, but nevertheless both are still too large. So let us relax the ESH in energy interval II again to see whether things are improved. As we did for Model B, we consider the three cases listed in Table 3.3. The allowed regions in (x, g_R^{-2}) space are shown in Fig. 3.7(b)-(d). Taking M_R to be as close to 5 TeV as possible while minimizing $g_R(M_R)$ and maintaining $M_U \leq 10^{19}\,\text{GeV}$ leads to the following optimum solutions:

(i) Δ_{1R} and Δ_{3R} survive:

$$\begin{aligned} g_R(M_R) &= 0.51\,, \\ M_R &= 5 \times 10^3\,\text{GeV}\,, \\ M_C &= 8 \times 10^{15}\,\text{GeV}\,, \\ M_U = M_D &= 6 \times 10^{17}\,\text{GeV}\,, \end{aligned} \tag{3.73}$$

with the unified coupling $g_L(M_U) = g_R(M_U) = g_4(M_U) = 0.52$. The running of the couplings for this case is shown in Fig. 3.6(d).

(ii) Δ_{1R} and Δ_{6R} survive:

$$\begin{aligned} g_R(M_R) &= 0.45\,, \\ M_R &= 8 \times 10^5\,\text{GeV}\,, \end{aligned}$$

$$\begin{aligned} M_C &= 9\times10^{10}\,\text{GeV}\,, \\ M_U = M_D &= 1\times10^{19}\,\text{GeV}\,, \end{aligned} \tag{3.74}$$

with the unified coupling $g_L(M_U) = g_R(M_U) = g_4(M_U) = 0.51$. The running of the couplings for this case is shown in Fig. 3.6(e).

(iii) Δ_{1R}, Δ_{3R}, and Δ_{6R} survive:

$$\begin{aligned} g_R(M_R) &= 0.43\,, \\ M_R &= 2\times10^{5}\,\text{GeV}\,, \\ M_C &= 4\times10^{9}\,\text{GeV}\,, \\ M_U = M_D &= 1\times10^{19}\,\text{GeV}\,, \end{aligned} \tag{3.75}$$

with the unified coupling $g_L(M_U) = g_R(M_U) = g_4(M_U) = 0.51$. The running of the couplings for this case is shown in Fig. 3.6(f).

3.3.5 Summary of Results

In this section, we have looked at whether the IR conditions $M_R = 5\,\text{TeV}$ and $g_R(M_R) = 0.4$ could be realized within the left-right symmetric and the unified left-right symmetric Pati-Salam models in which the unification/emergence scale is below the Planck mass. The left-right symmetric Pati-Salam demands the unification of g_L and g_R, while the unified left-right symmetric Pati-Salam demands further unification of g_L and g_R with g_4. The requirements that these couplings unify at a single scale, and the matching conditions between g_1, g_{BL}, and g_R at M_R, and that between g_{BL}, g_3 and g_4 at M_C, place conflicting demands on the various symmetry breaking scales, and it is found that the target IR conditions cannot be realized so easily. In particular, if the Higgs content at various energy intervals is determined based on the Extended Survival Hypothesis (ESM), M_R and $g_R(M_R)$ tend to be much larger than our target values. Lowering these values requires the breaking of ESH. The most promising cases are Models B and C of Ref. [2] with the colored Δ_{3R} field surviving below M_C. We note that this may put the Δ_{3R} particles within reach of the LHC. But, even for those cases, $g_R(M_R)$ cannot be made as low as 0.4. In all cases, the optimum conditions for minimum M_R and/or minimum $g_R(M_R)$ require degeneracies of some of the symmetry breaking scales.

3.4 Discussion and Conclusions

In this chapter, we have initiated a purely phenomenological analysis of Connes' NCG approach to the SM and beyond, in the light of the 2015 statistical fluctuation from the LHC. In particular, we have concentrated on the remarkable left-right symmetric structure that is inherent in the NCG of the SM, embodied in the unified left-right symmetric Pati-Salam

models of Ref. [2], and explored its phenomenological consequences by concentrating on the possible existence of a TeV scale W_R boson. We find that generating a TeV scale W_R boson with the small coupling of $g_R = 0.4$ within NCG motivated models is not trivial and places strong constraints on the particle content and symmetry breaking scales. In this sense, the naive version of NCG motivated LRSM would be unnatural had any signal persisted.

We note that we have also conducted a preliminary analysis of the constraints imposed by proton stability [347], the $\Delta B = 2$ neutron-antineutron and hydrogen-antihydrogen oscillations [346] as well as the constraints coming from the inflationary cosmological models [317]. In principle, these constraints are not prohibitive of the phenomenological analysis carried out here.

While our analysis could suggest that the NCG motivated unified left-right Pati-Salam model is not favored phenomenologically by the current LHC data, we note the possibility that the current approach of grafting the NCG spectral action to RG evolution of standard QFT at the GUT scale may not capture the true nature and predictions of NCG theories.

Finally, we address the closely related question of the hierarchy problem. One of the most interesting aspects of the NCG of the SM and its Pati-Salam-like completion is the existence of the GUT scale which can be found in the close proximity to the Planck scale, *i.e.*, the scale of quantum gravity. Given this fact as well as the presence of a hidden fundamental non-commutative structure in this approach, this suggests that the hierarchy problem should get a quantum gravitational rather than an effective field theory treatment. The more convincing physical meaning of this GUT scale also comes after one realizes that Connes' approach also produces a gravity sector in parallel with the standard model (and its Pati-Salam completion) and thus the GUT scale should be viewed as being close to the natural scale of gravity, *i.e.*, the Planck scale, and indeed the two scales are not that far apart in the non-commutative approach. In particular, if one views quantum gravity as having origins in metastring theory [118, 304, 348], then one finds the fundamental non-commutative structure, and also, the two-scale renormalization group, which sheds new light on such fundamental issues as the hierarchy problem: the two scales that featured in Refs. [118, 304, 348] are both the UV and the IR scales and thus the stability of the Higgs mass becomes two-fold, both with respect to the UV and to the IR. In other words, the question is now not only why the Higgs mass is not of the Planck scale (or the GUT scale) but also why the Higgs mass is not of the Hubble (vacuum energy) scale. It is well known that, numerologically, the Higgs scale ($\sim 1\,\text{TeV}$) is the geometric mean between these two scales, at the point of a UV/IR invariant energy scale. The Higgs scale also naturally appears as a geometric scale in Connes' non-commutative geometry approach, in complete analogy with the geometric meaning of the Planck and the Hubble scales. Actually, because of the appearance of gravity and the standard model Lagrangians in the Connes's spectral action, and because of the discrete nature of the Higgs dimension, there is a natural Higgs-like degree of freedom on the gravity side – a Brans-Dicke-Jordan-like scalar – which can be argued to contribute to the geometric warping of the Higgs discrete dimension. This is similar to the infinite extra dimensional scenarios, however, without infinite extra dimensions [152, 154].

In our view, the approach based on NCG (and its related proposal based on the superconnection approach [159, 163]) offers a new and, phenomenologically, almost completely unexplored view on the rationale for the SM and also for its natural completion. This approach also offers a possibly exciting relation with the fundamental physics of quantum gravity, thus relating the infrared physics of the current exciting experimental searches conducted at the LHC to the hidden ultraviolet physics of quantum theory of space and time.

Table 3.1: Dynkin index T_i for several irreducible representations of $SU(2)$, $SU(3)$, and $SU(4)$. Different normalization conventions are used in the literature. For example, there is a factor of 2 difference between those given in Refs. [7] and [8]. Our convention follows the former. For $SU(3)$, there exist two inequivalent 15 dimensional irreducible representations.

Representation	$SU(2)$	$SU(3)$	$SU(4)$
2	$\frac{1}{2}$	–	–
3	2	$\frac{1}{2}$	–
4	5	–	$\frac{1}{2}$
6	$\frac{35}{2}$	$\frac{5}{2}$	1
8	42	3	–
10	$\frac{165}{2}$	$\frac{15}{2}$	3
15	280	$10, \frac{35}{2}$	4

Table 3.2: The Higgs content and RG coefficients in the three energy intervals for the non-unified left-right symmetric Pati-Salam model under the Extended Survival Hypothesis (ESH).

Interval	Higgs content	RG coefficients
III	$\phi(2,2,1),\ \Delta_R(1,3,10),\ \Sigma(1,1,15)$	$(a_L, a_R, a_4)^{\rm III} = \left(-3, \frac{11}{3}, -7\right)$
II	$\phi(2,2,0,1),\ \Delta_{R1}(1,3,2,1)$	$(a_L, a_R, a_{BL}, a_3)^{\rm II} = \left(-3, \frac{-7}{3}, \frac{11}{3}, -7\right)$
I	$\phi_2(2,1,1)$	$(a_1, a_2, a_3)^{\rm I} = \left(\frac{41}{6}, \frac{-19}{6}, -7\right)$

Table 3.3: The dependence of the RG coefficients on the Higgs content in energy interval II where the symmetry is G_{2213}. Relaxing the ESH will lead to different Higgs content and different RG coefficients.

Interval	Higgs content	$(a_L, a_R, a_{BL}, a_3)^{\rm II}$
II	$\phi(2,2,0,1),\ \Delta_{R1}(1,3,2,1)$	$\left(-3, \frac{-7}{3}, \frac{11}{3}, -7\right)$
	$\phi(2,2,0,1),\ \Delta_{R1}(1,3,2,1),\ \Delta_{R3}\left(1,3,\frac{2}{3},3\right)$	$\left(-3, \frac{-1}{3}, 4, \frac{-13}{2}\right)$
	$\phi(2,2,0,1),\ \Delta_{R1}(1,3,2,1),\ \Delta_{R6}\left(1,3,\frac{-2}{3},6\right)$	$\left(-3, \frac{5}{3}, \frac{13}{3}, \frac{-9}{2}\right)$
	$\phi(2,2,0,1),\ \Delta_{R1}(1,3,2,1),\ \Delta_{R3}\left(1,3,\frac{2}{3},3\right),\ \Delta_{R6}\left(1,3,\frac{-2}{3},6\right)$	$\left(-3, \frac{11}{3}, \frac{14}{3}, -4\right)$

Table 3.4: Higgs content of Model A of Ref. [2]. In Ref. [2], the model emerges with symmetry G_{224} at $M_U = M_D$. This breaks directly to G_{213} of the SM at $M_C = M_R$. We modify this process by allowing $M_C \neq M_R$, inserting energy interval II with symmetry G_{2213} between intervals III and I. The Higgs content in interval II is based on the ESH.

Interval	Higgs content	RG coefficients
III	$\phi(2,2,1),\ \Delta_R(1,2,4),\ \Sigma(1,1,15)$	$(a_L, a_R, a_4)^{\rm III} = \left(-3, \frac{-7}{3}, \frac{-29}{3}\right)$
II	$\phi(2,2,0,1),\ \Delta_{R1}(1,2,1,1)$	$(a_L, a_R, a_{BL}, a_3)^{\rm II} = \left(-3, \frac{-17}{6}, \frac{17}{6}, -7\right)$
I	$\phi_2(2,1,1)$	$(a_1, a_2, a_3)^{\rm I} = \left(\frac{41}{6}, \frac{-19}{6}, -7\right)$

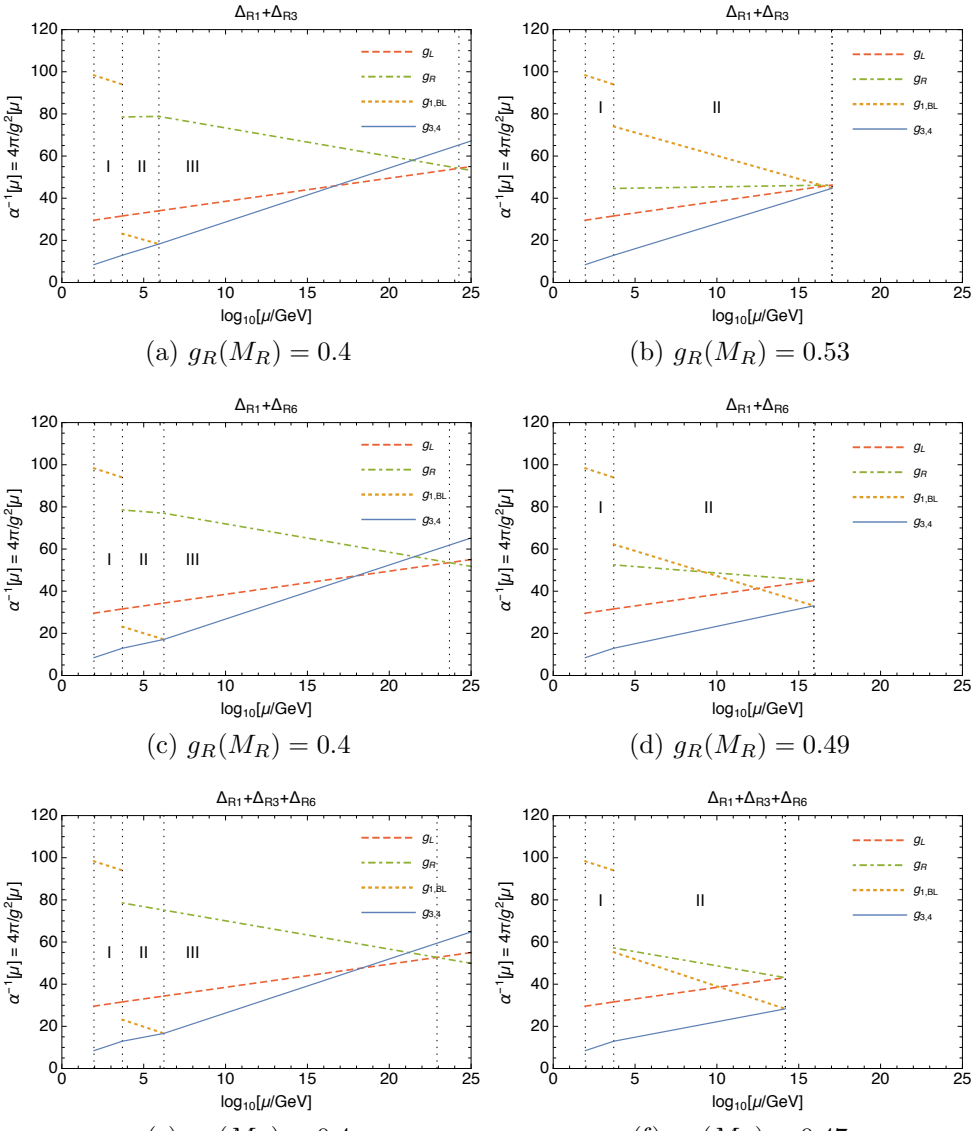

(a) $g_R(M_R) = 0.4$ (b) $g_R(M_R) = 0.53$

(c) $g_R(M_R) = 0.4$ (d) $g_R(M_R) = 0.49$

(e) $g_R(M_R) = 0.4$ (f) $g_R(M_R) = 0.47$

Figure 3.2: Running of the gauge couplings for the left-right symmetric Pati-Salam model with more than Δ_{R1} surviving into energy interval II. Vertical dotted lines indicate symmetry breaking scales. M_R is fixed at 5 TeV. In (a), (c), and (e) $g_R(M_R) = 0.4$ is imposed, while in (b), (d), and (d) M_D is minimized by collapsing the energy interval III.

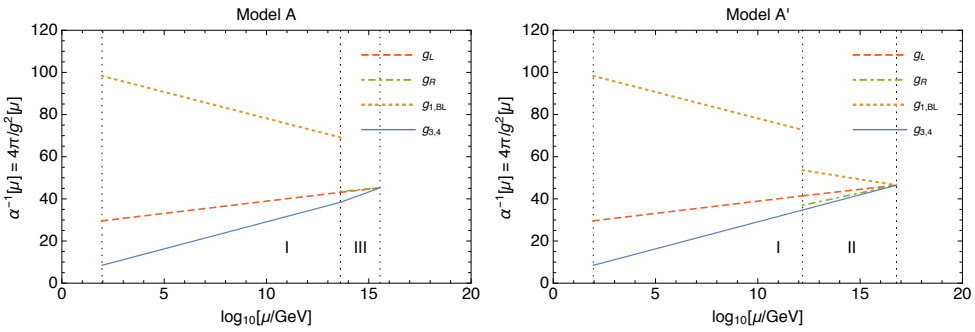

(a) $g_R(M_R) = 0.54$ (b) $g_R(M_R) = 0.58$

Figure 3.3: Running of the gauge couplings for Model A of Ref. [2]. with (a) G_{224} breaking directly into G_{213}, and (b) G_{224} breaks immediately to G_{2213} as it emerges. In (a), the dashed line indicating g_L and the dot-dashed line indicating g_R are almost overlapping in interval III.

Table 3.5: Higgs content of Model B of Ref. [2]. In Ref. [2], the model emerges with symmetry G_{224} at $M_U = M_D$. This breaks directly to G_{213} of the SM at $M_C = M_R$. We modify this process by allowing $M_C \neq M_R$, inserting energy interval II with symmetry G_{2213} between intervals III and I. The Higgs content in interval II is based on the ESH. The particle content and RG coefficients in intervals I and II are the same as those listed in Table 3.2.

Interval	Higgs content	RG coefficients
III	$\phi(2,2,1),\ H(1,1,6),\ \Delta_R(1,3,10),$ $\widetilde{\Sigma}(2,2,15)$	$(a_L, a_R, a_4)^{\text{III}} = \left(2, \frac{26}{3}, -2\right)$
II	$\phi(2,2,0,1),\ \Delta_{R1}(1,3,2,1)$	$(a_L, a_R, a_{BL}, a_3)^{\text{II}} = \left(-3, \frac{-7}{3}, \frac{11}{3}, -7\right)$
I	$\phi_2(2,1,1)$	$(a_1, a_2, a_3)^{\text{I}} = \left(\frac{41}{6}, \frac{-19}{6}, -7\right)$

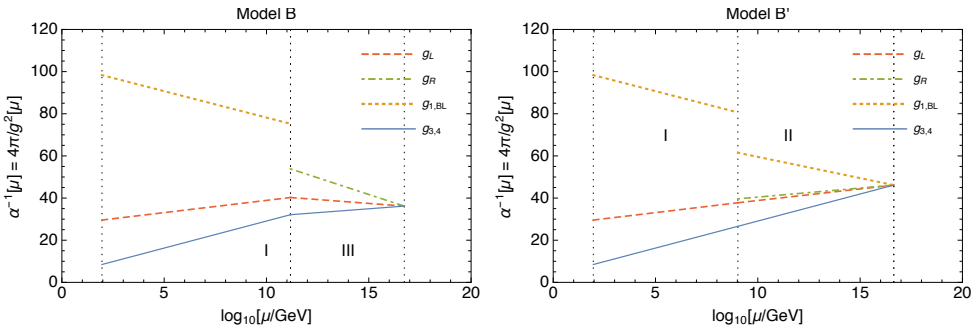

(a) $g_R(M_R) = 0.59$ (b) $g_R(M_R) = 0.52$

Figure 3.4: Running of the gauge couplings for Model B of Ref. [2]. with (a) G_{224} breaking directly into G_{213}, and (b) G_{224} breaks immediately to G_{2213} as it emerges.

Table 3.6: Higgs content of Model C of Ref. [2]. In Ref. [2], the model emerges with symmetry G_{224D} at M_U. This breaks directly to G_{213} of the SM at $M_D = M_C = M_R$. We modify this process by allowing $M_D \neq M_C \neq M_R$, inserting energy intervals II and III with symmetries G_{2213} and G_{224}, respectively, between intervals I and IV. The Higgs content in intervals I, II, and III are based on the ESH. An extra D-parity singlet field $\sigma(1,1,1)$ is introduced in interval IV to break parity spontaneously. The particle content and RG coefficients in intervals I and II are the same as those listed in Table 3.2.

Interval	Higgs content	RG coefficients
IV	$\phi(2,2,1),\ H(1,1,6)\times 2,\ \widetilde{\Sigma}(2,2,15)$ $\Delta_R(1,3,10),\ \Delta_L(3,1,10),\ \sigma(1,1,1)$	$(a_L,a_R,a_4)^{\text{IV}} = \left(\frac{26}{3},\frac{26}{3},\frac{4}{3}\right)$
III	$\phi(2,2,1),\ H(1,1,6),\ \Delta_R(1,3,10)$	$(a_L,a_R,a_4)^{\text{III}} = \left(-3,\frac{11}{3},\frac{-22}{3}\right)$
II	$\phi(2,2,0,1),\ \Delta_{R1}(1,3,2,1)$	$(a_L,a_R,a_{BL},a_3)^{\text{II}} = \left(-3,\frac{-7}{3},\frac{11}{3},-7\right)$
I	$\phi_2(2,1,1)$	$(a_1,a_2,a_3) = \left(\frac{41}{6},\frac{-19}{6},-7\right)$

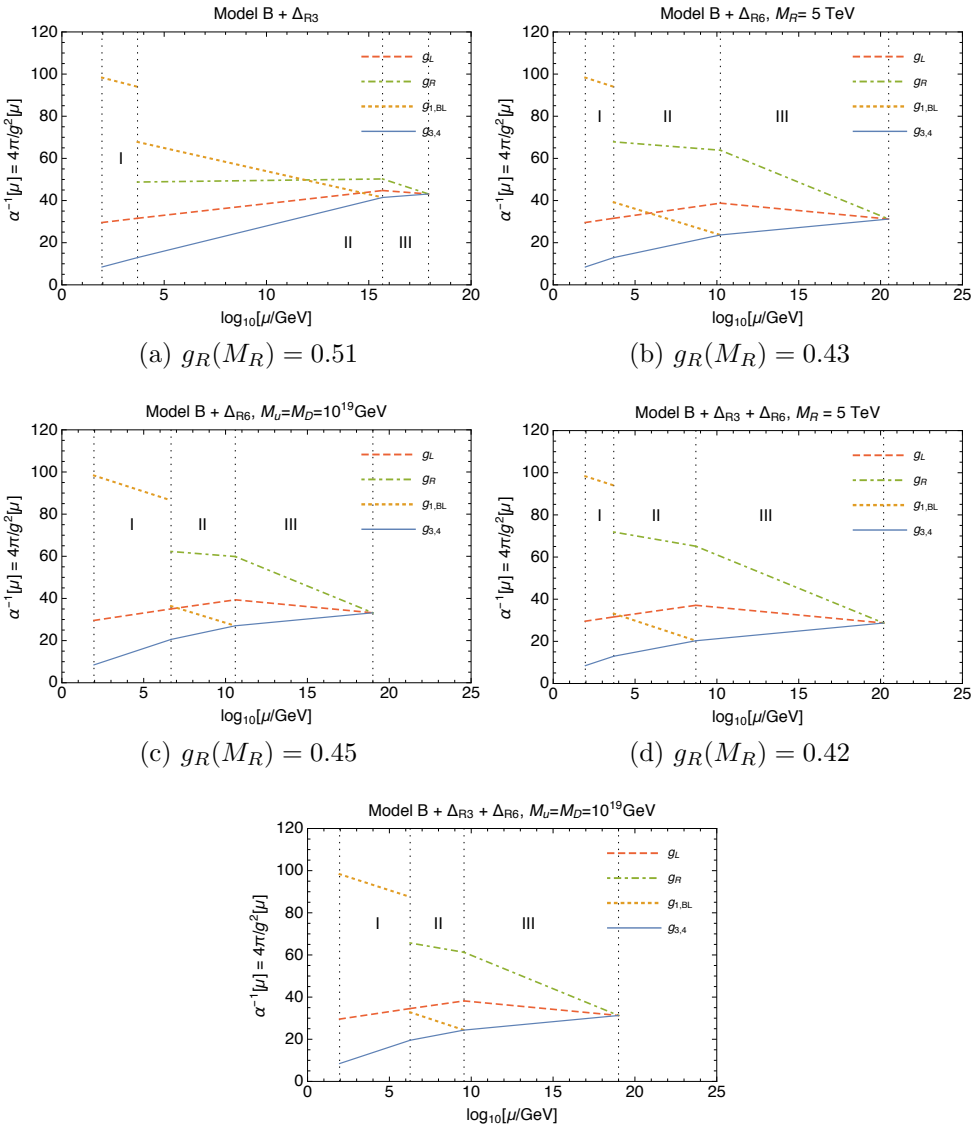

(a) $g_R(M_R) = 0.51$ (b) $g_R(M_R) = 0.43$

(c) $g_R(M_R) = 0.45$ (d) $g_R(M_R) = 0.42$

(e) $g_R(M_R) = 0.44$

Figure 3.5: Running of the gauge couplings for Model B of Ref. [2] with extended Higgs content in energy interval II. In addition to Δ_{R1}, the field Δ_{R3} survives into II in (a), (d), and (e), while the field Δ_{R6} also survives into II in (b), (c), (d) and (e). In (a), (b), and (d) we impose $M_R = 5\,\text{TeV}$. In (c) and (e) we impose $M_U = M_D = 10^{19}\,\text{GeV}$.

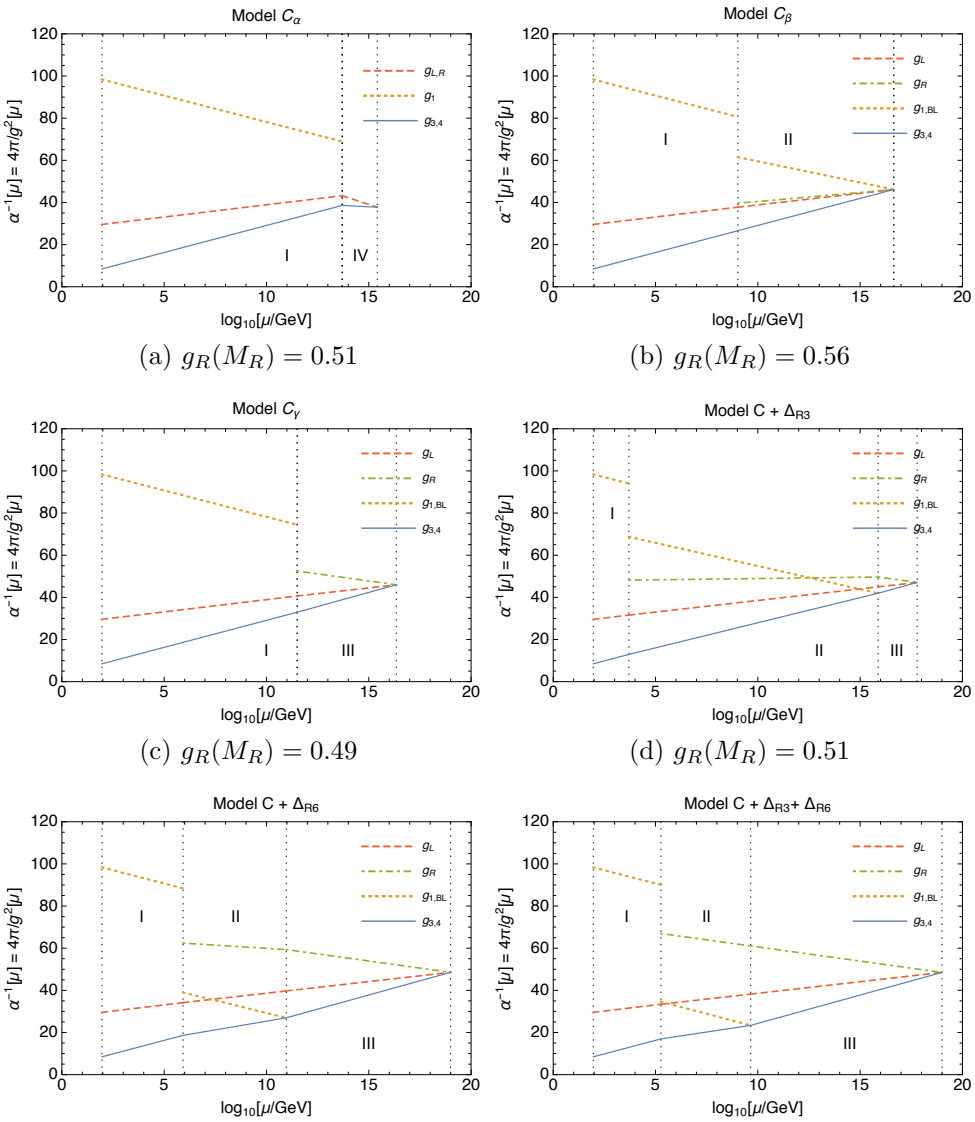

(a) $g_R(M_R) = 0.51$ (b) $g_R(M_R) = 0.56$

(c) $g_R(M_R) = 0.49$ (d) $g_R(M_R) = 0.51$

(e) $g_R(M_R) = 0.45$ (f) $g_R(M_R) = 0.43$

Figure 3.6: (a) Running of the gauge couplings for Model C of Ref. [2] where $M_D = M_C = M_R$, (b) $M_U = M_D = M_C$, (c) $M_U = M_D$, $M_C = M_R$, (d) with Δ_{R3} surviving in II, (e) with Δ_{R6} surviving in II, and (f) with Δ_{R3} and Δ_{R6} surviving in II.

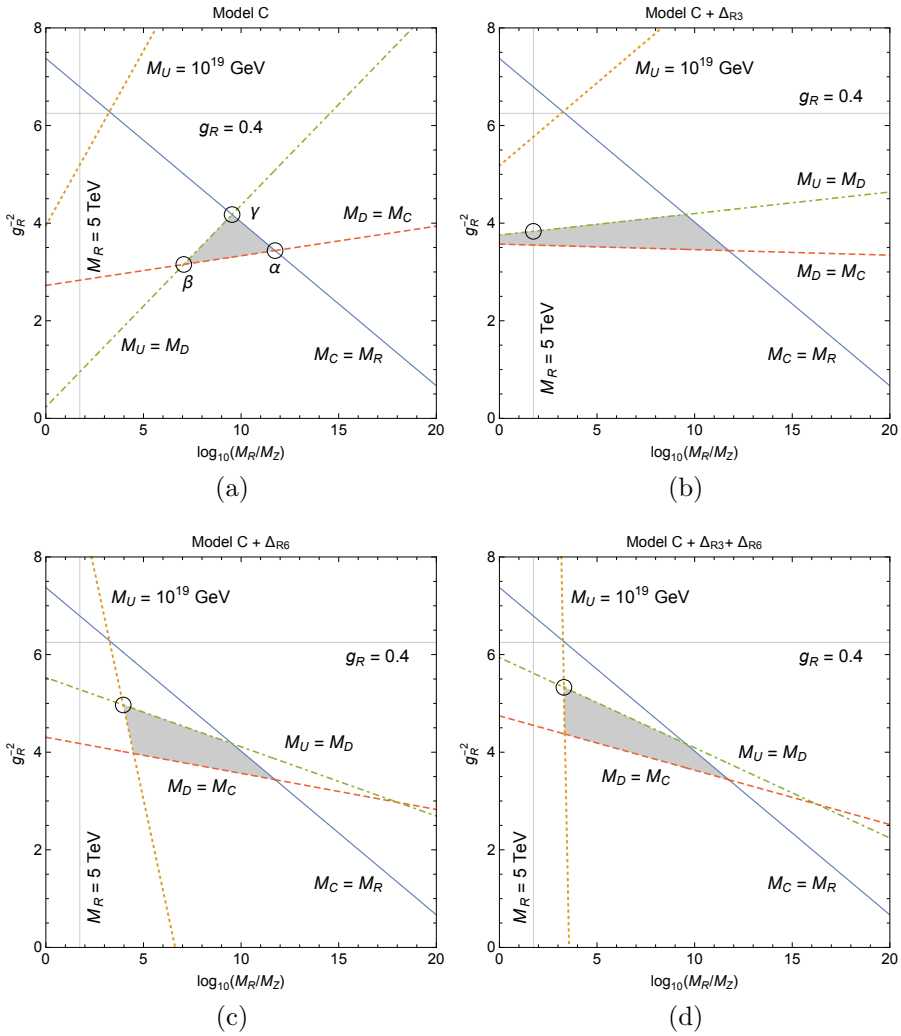

Figure 3.7: (a) For Model C, the values of $x = \log_{10} M_R/M_Z$ and $g_R^{-2}(M_R)$ must lie inside the shaded triangle shown to maintain the ordering of the symmetry breaking scales. Ref. [2] selects the values at point α, where $M_D = M_C = M_R$. M_R is minimized at point β where $M_U = M_D = M_C$, while $g_R(M_R)$ is minimized at point γ where $M_U = M_D$ and $M_C = M_R$. (b), (c), and (d) show how the allowed region changes with the addition of extra colored Δ_R fields in energy interval II. The requirement that $M_U \leq 10^{19}\,\mathrm{GeV}$ demands that one stay to the right of the dotted line, and this restricts us to the interiors of the shaded quadrangles. Consequently, only case (b) allows for $M_R = 5\,\mathrm{GeV}$. In all three cases, $g_R(M_R)$ is minimized for a given choice of M_R when $M_U = M_D$. The optimum points for each case discussed in the text are indicated by circles.

Chapter 4

Example: Addressing Potential Collider Excess with Unified $SU(2)_L \times SU(2)_R \times SU(4)$ Models from NCG

In this chapter, we continue the investigation of the NCG motivated extensions of the SM, in particular the LRSM. After it was shown in Chapter 3 that accommodating the collider excess in the diboson channel is non-trivial, we study the 750 GeV resonance in the diphoton channel and check the compatibility with the NCG. We stress that the tension between the low energy phenomenology provides an effective way to test models fixed at very high energy scale, hence the new physics. This is partly due to the restrictive nature of the NCG. This chapter is based on our work [161] published in Modern Physics Letters A.

4.1 Introduction

In 2015, ATLAS [349] and CMS [350] both reported a resonance in the diphoton channel with an invariant mass around 750 GeV. The local significances were, respectively, 3.6σ and 2.6σ, assuming a narrow-width resonance. These signals were thought to be the first hint associated with the long-anticipated physics beyond the SM. The 95% CL cross section upper limit around 750 GeV set by ATLAS (CMS) is roughly 10 ± 2.8 fb (6.5 ± 3.5 fb) using 3.2 fb^{-1} (2.6 fb^{-1}) of data at $\sqrt{s} = 13\,\text{TeV}$, assuming the resonance is a scalar produced through gluon-gluon fusion. When the width of the resonance is allowed to vary, a maximum local significance of 3.9σ is attained by ATLAS at a width of 45 GeV. On the other hand, the local significance attains its maximum for a narrow width resonance in the CMS results. Unfortunately, the significance of the signal decreased, leaving many disappointed at the

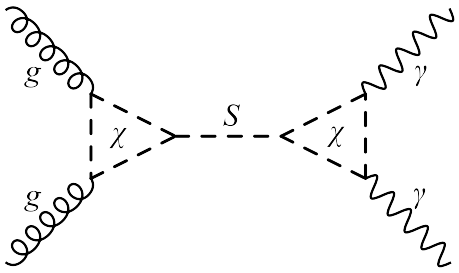

Figure 4.1: The Feynman diagram of the production and decay of the SM-singlet scalar $\mathcal{S}$ at the LHC through colored-scalar χ in the loop.

non-discovery of new physics. However, we can still gain knowledge of what is not working. In this chapter, we use this statistical fluctuation as another example to show how the machinery of NCG-motivated LRSM can be tested with collider signals.

We discuss a possible identification of this resonance with SM-singlet scalars in the NCG motivated unified G_{224} models [2, 156]. A plausible and economical way to realize the LHC diphoton signal in the unified G_{224} context is to couple this SM-singlet scalar to gluons and photons via loops of colored scalars, as recently discussed in Ref. [351] in the context of $SO(10)$ GUT, *cf.* Fig. 4.1.[1] The NCG models we consider have either an $SU(2)_R$ triplet $\Delta_R(1,3,10)$, or an $SU(2)_R$ doublet $\widetilde{\Delta}_R(1,2,4)$ in their scalar content, where the three numbers refer to the dimensions of the $G_{224} = SU(2)_L \times SU(2)_R \times SU(4)_C$ irreducible representations. The SM-singlet scalar $\mathcal{S}$, which we identify with the 750 GeV resonance, is assumed to be the excitation of the electrically neutral component Δ^0_{R1} of $\Delta_R(1,3,10)$, or that of $\widetilde{\Delta}_R(1,2,4)$ (denoted as $\widetilde{\Delta}^0_{R1}$), depending on the model considered. Δ^0_{R1} (or $\widetilde{\Delta}^0_{R1}$) is also the field that breaks the gauge symmetry of the G_{224} model to that of the SM, by acquiring a vacuum expectation value (VEV) at the scale M_C where G_{224} breaks to $G_{213} = SU(2)_L \times U(1)_Y \times SU(3)_C$ of the SM. A color-triplet components of $\Delta_R(1,3,10)$ (or $\widetilde{\Delta}_R(1,2,4)$) is assumed to survive down to low energies (TeV-scale) to take on the role of the χ-field in Fig. 4.1. This is but one way that one could embed the 750 GeV diphoton resonance into the NCG G_{224} framework, and we use this as a demonstrative example.

While this identification itself is fairly straightforward, and it can already be inferred from the similar $SO(10)$ analysis of Ref. [351] that the cross section and width can be made to come out in the right ballpark, the question is whether the assumed symmetry breaking and scalar survival scenario can actually be realized in the NCG G_{224} models, given the gauge-coupling-unification requirement and restricted scalar content which limit our ability to adjust the renormalization group running of those couplings. Indeed, we have demonstrated in Chapter 3 that realizing a 2 TeV W_R, which had been suggested by the LHC data [308–310, 312, 353, 354], in the same NCG models highly non-trivial due to the uni-

[1] Dasgupta *et al.* in Ref. [352] have shown that coupling the SM-singlet scalar to quarks and photons via mixing with the SM Higgs boson would lead to too small a cross section.

fication requirement applying conflicting pressure on the symmetry breaking scales. Thus, we subject our scenarios to renormalization group equation (RGE) analyses to check their feasibilities.

The main message of this chapter is that, even though the 750 GeV diphoton resonance can be accommodated within the NCG motivated unified G_{224} models, the price one has to pay is a certain amount of fine tuning in the sector involving the necessary colored scalars. This is somewhat similar to the main message of last chapter, and points to the underlying rigidity of the NCG framework. However, this conclusion is based on effective-field-theory reasoning, which could fail in the NCG framework due to the possible mixing between the short-distance and long-distance physics as discussed in our previous work [159, 160, 163].

This chapter is organized as follows. In section 2, we present the list of the NCG-based unified G_{224} models that are analyzed, and discuss how the 750 GeV diphoton resonance could be explained within their framework. In section 3, we address the question of whether the unification of gauge couplings can be achieved naturally in those models. We conclude in section 4 with an outlook on the rigid phenomenological aspects of the NCG framework. In the process, we follow the technology discussed in our previous paper [160] to which we refer the reader for further technical details.

4.2 Diphoton resonance in NCG based unified G_{224} models

Table 4.1: The scalar content of the three NCG based unified G_{224} models proposed by Chamseddine, Connes, and van Suijlekom in Refs. 4 and 5, compared to the scalar content of the $SO(10)$ based G_{224} model, discussed in Ref. 16, below its unification scale where the $SO(10)$ symmetry is broken to G_{224}.

Model	Symmetry	Higgs Content
A	G_{224}	$\phi(2,2,1)$, $\widetilde{\Delta}_R(1,2,4)$, $\Sigma(1,1,15)$
B	G_{224}	$\phi(2,2,1)$, $H(1,1,6)$, $\Delta_R(1,3,10)$, $\widetilde{\Sigma}(2,2,15)$
C	G_{224D}	$\phi(2,2,1)$, $H(1,1,6)\times 2$, $\Delta_R(1,3,10)$, $\Delta_L(3,1,10)$, $\widetilde{\Sigma}(2,2,15)$
$SO(10)$	G_{224}	$\phi(2,2,1)$, $\Delta_R(1,3,10)$, $\Sigma(1,1,15)$

In this section, we list the three unified G_{224} models proposed by Chamseddine, Connes, and van Suijlekom in Refs. [156] and [2], and specify how we fit the diphoton resonance into their

particle content. These models emerge from an underlying NCG, which is an extension of the NCG of the SM to that of left-right symmetric models. The three versions differ in the scalar sector content, and the unbroken symmetry structure as listed in Table 4.1. We use the following notation for the symmetries:

$$\begin{aligned} G_{224D} &= SU(2)_L \otimes SU(2)_R \otimes SU(4)_C \otimes D \ , \\ G_{224} &= SU(2)_L \otimes SU(2)_R \otimes SU(4)_C \ , \\ G_{213} &= SU(2)_L \otimes U(1)_Y \otimes SU(3)_C \ , \\ G_{13} &= U(1)_Q \otimes SU(3)_C \ , \end{aligned} \tag{4.1}$$

where D in G_{224D} refers to the left-right symmetry, a Z_2 symmetry which keeps the left and the right sectors equivalent. The last row of Table 4.1 lists the scalar content of an $SO(10)$ based G_{224} model studied in Ref. [351], below its unification scale where the $SO(10)$ had broken to G_{224}. The scalars $\phi(2,2,1)$, $\Delta_R(1,3,10)$, $\Sigma(1,1,15)$ are respectively obtained from the $SO(10)$ multiplets **10** (or **120**), **126**, and **210**. The **210** also includes a $(1,1,1)$ representation, whose VEV breaks $SO(10)$ down to G_{224} [8].

As in Chapter 3 we do not attempt to review the NCG foundations of these models nor to justify their derivation, but simply look at their consequences from a purely phenomenological viewpoint in the light of the possible 750 GeV diphoton resonance. The distinguishing feature of NCG motivated versions of the SM [154, 155] as well as its G_{224} completion discussed here is that they come with GUT-like coupling unification conditions, due to the underlying spectral action having only one overall coupling. This is not the case for the canonical G_{224} constructions found in the literature [195, 201–203, 355].

The decompositions of the various scalar fields, which appear in Table 4.1, into irreducible representations of the subgroups as the symmetry breaks from G_{224} (or G_{224D}) to G_{2213} and then to G_{213} are shown in Table 4.2. In model A, we assume that G_{224} is broken directly to G_{213} by $\widetilde{\Delta}^0_{R1}(1,0,1)$ acquiring a VEV, and $\mathcal{S}$ is identified with the excitation of $\widetilde{\Delta}^0_{R1}$. In models B and C, we assume that G_{224}/G_{224D} is broken directly to G_{213} by $\Delta^0_{R1}(1,0,1)$ acquiring a VEV, while $\mathcal{S}$ is identified with the excitation of Δ^0_{R1}. In all three models, the colored field $\Delta^{-2/3}_{R3}(1,-4/3,3)$, which is contained in the decompositions of both $\widetilde{\Delta}_R(1,2,4)$ and $\Delta_R(1,3,10)$, is assumed to survive below the symmetry breaking scale.

The advantage of this choice of the surviving colored scalar is that it exists in all three models, and that it is similar to the one considered in the $SO(10)$ context in Ref. [351], where the reproducibility of the reported LHC signal has been demonstrated with such a new degree of freedom. The other colored components of $\widetilde{\Delta}_R(1,2,4)$ and $\Delta_R(1,3,10)$ could also serve this end. Single-step breaking from G_{224} to G_{213} is assumed for the sake of simplicity,[2] and also due to our experience in Ref. [160] telling us that introducing multi-step breaking does

[2]In models B and C, the breaking sequence $G_{224} \to G_{2213} \to G_{213}$ considered in Ref. [160] requires scalar composites acquiring a VEV in the intermediate steps.

Table 4.2: The decomposition of various G_{224} representations into those of G_{2213} and G_{213} (SM).

G_{224}	G_{2213}	G_{213}
$\phi(2,2,1)$	$\phi(2,2,0,1)$	$\phi_2(2,1,1)$, $\phi_2'(2,-1,1)$
$\widetilde{\Delta}_R(1,2,4)$	$\widetilde{\Delta}_{R1}(1,2,1,1)$	$\widetilde{\Delta}^0_{R1}(1,0,1)$, $\widetilde{\Delta}^+_{R1}(1,2,1)$
	$\widetilde{\Delta}_{R3}\left(1,2,-\frac{1}{3},3\right)$	$\widetilde{\Delta}^{1/3}_{R3}\left(1,\frac{2}{3},3\right)$, $\widetilde{\Delta}^{-2/3}_{R3}\left(1,-\frac{4}{3},3\right)$
$\Delta_R(1,3,10)$	$\Delta_{R1}(1,3,2,1)$	$\Delta^0_{R1}(1,0,1)$, $\Delta^+_{R1}(1,2,1)$, $\Delta^{++}_{R1}(1,4,1)$
	$\Delta_{R3}\left(1,3,\frac{2}{3},3\right)$	$\Delta^{+4/3}_{R3}\left(1,\frac{8}{3},3\right)$, $\Delta^{+1/3}_{R3}\left(1,\frac{2}{3},3\right)$, $\Delta^{-2/3}_{R3}\left(1,-\frac{4}{3},3\right)$
	$\Delta_{R6}\left(1,3,-\frac{2}{3},6\right)$	$\Delta^{+2/3}_{R6}\left(1,\frac{4}{3},6\right)$, $\Delta^{-1/3}_{R6}\left(1,-\frac{2}{3},6\right)$, $\Delta^{-4/3}_{R6}\left(1,-\frac{8}{3},6\right)$
$\Delta_L(3,1,10)$	$\Delta_{L1}(3,1,2,1)$	$\Delta_{L1}(3,2,1)$
	$\Delta_{L3}\left(3,1,\frac{2}{3},3\right)$	$\Delta_{L3}\left(3,\frac{2}{3},3\right)$
	$\Delta_{L6}\left(3,1,-\frac{2}{3},6\right)$	$\Delta_{L6}\left(3,-\frac{2}{3},6\right)$
$H(1,1,6)$	$H_3\left(1,1,\frac{2}{3},3\right)$	$H^{1/3}_3\left(1,\frac{2}{3},3\right)$
	$H_{\bar{3}}\left(1,1,-\frac{2}{3},\bar{3}\right)$	$H^{-1/3}_{\bar{3}}\left(1,-\frac{2}{3},\bar{3}\right)$
$\Sigma(1,1,15)$	$\Sigma_1(1,1,0,1)$	$\Sigma^0_1(1,0,1)$
	$\Sigma_3\left(1,1,-\frac{4}{3},3\right)$	$\Sigma^{-2/3}_3\left(1,-\frac{4}{3},3\right)$
	$\Sigma_{\bar{3}}\left(1,1,\frac{4}{3},\bar{3}\right)$	$\Sigma^{2/3}_{\bar{3}}\left(1,\frac{4}{3},\bar{3}\right)$
	$\Sigma_8(1,1,0,8)$	$\Sigma^0_8(1,0,8)$
$\widetilde{\Sigma}(2,2,15)$	$\widetilde{\Sigma}_1(2,2,0,1)$	$\widetilde{\Sigma}_1(2,1,1)$, $\widetilde{\Sigma}_1'(2,-1,1)$
	$\widetilde{\Sigma}_3\left(2,2,-\frac{4}{3},3\right)$	$\widetilde{\Sigma}_3\left(2,-\frac{7}{3},3\right)$, $\widetilde{\Sigma}_3'\left(2,-\frac{1}{3},3\right)$
	$\widetilde{\Sigma}_{\bar{3}}\left(2,2,\frac{4}{3},\bar{3}\right)$	$\widetilde{\Sigma}_{\bar{3}}\left(2,\frac{7}{3},\bar{3}\right)$, $\widetilde{\Sigma}_{\bar{3}}'\left(2,\frac{1}{3},\bar{3}\right)$
	$\widetilde{\Sigma}_8(2,2,0,8)$	$\widetilde{\Sigma}_8(2,1,8)$, $\widetilde{\Sigma}_8'(2,-1,8)$

not necessarily facilitate the grafting of the NCG models to the SM at low energies.

In the $SO(10)$ model of Ref. [351], the 750 GeV resonance $\mathcal{S}$ was identified with the excitation of the charge neutral component Δ^0_{R3} of $\Delta_R(1,3,10)$, which acquires a VEV breaking G_{2213}

down to G_{213} at $M_R = 5\,\text{TeV}$, and only one of the colored components, $\chi = \Delta_{R3}^{-2/3}(1, -4/3, 3)$, was assumed to survive below this breaking. This is the exact same identification as in models B and C, except the assumed symmetry breaking pattern is different. Since $\mathcal{S}$ is a singlet under the SM gauge group G_{213}, it cannot directly couple to gluons or photons. The coupling is induced by χ-loops as shown in Fig. 4.1. Assuming a coupling between $\mathcal{S}$ and χ of the form

$$\kappa M_R \mathcal{S} \chi^\dagger \chi \,, \qquad M_R \,=\, 5\,\text{TeV} \,, \tag{4.2}$$

where κ is a dimensionless parameter, and $M_\chi > M_\mathcal{S}/2$ so that $\mathcal{S}$ does not decay into a χ pair, it has been shown in Ref. [351] that the LHC signal can be reproduced for a wide range of (κ, M_χ) values around $\kappa = O(1)$ and $M_\chi = O(1\,\text{TeV})$. Thus, without repeating the analysis, we conclude that our NCG models can also reproduce the LHC signal provided a similar coupling exists between $\mathcal{S}$ and χ, and the assumed particle content allows the required unification of gauge couplings at a high scale.

Several comments are in order. The $\Delta_R(1, 3, 10)$ scalar is associated with a rich phenomenology, as discussed by Mohapatra and Marshak in Ref. [347], including the generation of Majorana neutrino mass and neutron-anti-neutron oscillations. These depend on the Yukawa couplings of the $\Delta_R(1, 3, 10)$ to the fermions, and the quartic coupling of the $\Delta_R(1, 3, 10)$ to itself. In the NCG approach, the Dirac operator, which includes the Yukawa couplings, is the input from which the entire model is constructed. The scalar content of the model as well as their quartic couplings are derived from the Dirac operator.[3] Therefore, the NCG approach can, in principle, make predictions in regards to neutron-anti-neutron oscillations. However, it is necessary to check the viability of the model before performing such detailed analyses, so this will not be discussed further here.

4.3 Unification of the Couplings

As discussed in the introduction, the unification of couplings in the NCG based G_{224} models imposes non-trivial requirements on the symmetry breaking scales, given that the scalar content of each model is restricted and cannot be changed at will. In this section, we discuss whether the unification of the couplings can be achieved in the NCG based G_{224} models with the assumed particle content and scalar survival assumptions. In contrast to our work in Ref. [160], we assume direct breaking of G_{224} to G_{213} at a single scale M_C, between the unification scale M_U and the electroweak symmetry breaking (EWSB) scale M_Z. Between the scales M_C and M_Z, in addition to the usual SM particle content we have the $\chi = \Delta_{R3}^{-2/3}\,(1, -4/3, 3)$ field contributing to the RGE, which we assume is the only colored scalar to survive below M_C, and possess a mass of around a TeV. The 750 GeV scalar $\mathcal{S}$ is an SM singlet and consequently does not contribute to the RG running of the SM gauge couplings.

[3] See the appendix of Ref. [156].

4.3.1 Boundary and Matching Conditions

The symmetry breaking chain of the model considered in this chapter has been discussed in detail in our previous papers [160, 321]. The ordering of the breaking scales must be strictly maintained in the computations, *i.e.*,

$$M_U \geq M_C \geq M_Z \ . \tag{4.3}$$

We label the energy intervals between symmetry breaking scales $[M_Z, M_C]$ and $[M_C, M_U]$ with Roman numerals as

$$\begin{array}{rcl} \mathrm{I} & : & [M_Z,\ M_C]\ , \quad G_{213}\ (\mathrm{SM})\ , \\ \mathrm{II} & : & [M_C,\ M_U]\ , \quad G_{224} \quad \mathrm{or} \quad G_{224D}\ . \end{array} \tag{4.4}$$

The boundary/matching conditions we impose on the couplings at the symmetry breaking scales are:

$$\begin{aligned} M_U \quad &: \quad g_L(M_U) \ = \ g_R(M_U) \ = \ g_4(M_U)\ , \\ M_C \quad &: \quad \sqrt{\frac{2}{3}}\, g_{BL}(M_C) \ = \ g_3(M_C) = g_4(M_C)\ , \quad g_2(M_C) \ = \ g_L(M_C)\ , \\ &\qquad \frac{1}{g_1^2(M_C)} \ = \ \frac{1}{g_R^2(M_C)} + \frac{2}{3}\frac{1}{g_4^2(M_C)}\ , \\ M_Z \quad &: \quad \frac{1}{e^2(M_Z)} \ = \ \frac{1}{g_1^2(M_Z)} + \frac{1}{g_2^2(M_Z)}\ . \end{aligned} \tag{4.5}$$

The low energy data which we will use as boundary conditions to the RG running are [1, 331]

$$\alpha(M_Z) \ = \ 1/127.9\ , \quad \alpha_s(M_Z) \ = \ 0.118\ , \quad \sin^2\theta_W(M_Z) \ = \ 0.2312\ , \tag{4.6}$$

at $M_Z = 91.1876\,\mathrm{GeV}$, which translates to

$$g_1(M_Z) \ = \ 0.36\ , \quad g_2(M_Z) \ = \ 0.65\ , \quad g_3(M_Z) \ = \ 1.22\ . \tag{4.7}$$

Note that the coupling constants are all required to remain in the perturbative regime during the evolution from M_U down to M_Z.

4.3.2 One-Loop Renormalization Group Running

For a given particle content; the gauge couplings, in an energy interval $[M_A, M_B]$, are evolved according to the 1-loop RG relation

$$\frac{1}{g_i^2(M_A)} - \frac{1}{g_i^2(M_B)} \ = \ \frac{a_i}{8\pi^2}\ln\frac{M_B}{M_A}\ , \tag{4.8}$$

where the RG coefficients a_i are given by [7, 200]

$$\begin{aligned} a_i &= -\frac{11}{3}C_2(G_i) + \frac{2}{3}\sum_{R_f} T_i(R_f)\cdot d_1(R_f)\cdots d_n(R_f) \\ &\quad + \frac{\eta}{3}\sum_{R_s} T_i(R_s)\cdot d_1(R_s)\cdots d_n(R_s)\ . \end{aligned} \tag{4.9}$$

The summation in Eq. (4.9) is over irreducible chiral representations of fermions (R_f) in the second term and those of scalars (R_s) in the third. The coefficient η is either 1 or 1/2, depending on whether the corresponding representation is complex or real, respectively. $C_2(G_i)$ is the quadratic Casimir for the adjoint representation of the group G_i, and T_i is the Dynkin index of each representation. For $U(1)$ group, $C_2(G) = 0$ and

$$\sum_{f,s} T = \sum_{f,s}\left(\frac{Y}{2}\right)^2\ , \tag{4.10}$$

where $Y/2$ is the $U(1)$ charge, the factor of 1/2 coming from the traditional normalizations of the hypercharge and $B-L$ charges.

The RG coefficients, a_i, differ depending on the particle content in each energy interval, changing every time symmetry breaking occurs. We will distinguish the a_i's in different intervals with the corresponding roman numeral superscript, *cf.* Eq. (4.4). Together with the matching and boundary conditions of Eqs. (4.5), (4.6), and (4.7), 1-loop RG running leads to the following conditions on the symmetry breaking scales M_U and M_C:

$$\begin{aligned} 2\pi\left[\frac{3-8\sin^2\theta_W(M_Z)}{\alpha(M_Z)}\right] &= (3a_1-5a_2)^{\rm I}\ln\frac{M_C}{M_Z} + (-5a_L+3a_R+2a_4)^{\rm II}\ln\frac{M_U}{M_C}\ , \\ 2\pi\left[\frac{3}{\alpha(M_Z)}-\frac{8}{\alpha_s(M_Z)}\right] &= (3a_1+3a_2-8a_3)^{\rm I}\ln\frac{M_C}{M_Z} + (3a_L+3a_R-6a_4)^{\rm II}\ln\frac{M_U}{M_C}\ . \end{aligned} \tag{4.11}$$

The unified coupling α_U at scale M_U can then be obtained from

$$\frac{2\pi}{\alpha_U} = \frac{2\pi}{\alpha_s(M_Z)} - \left(a_4^{\rm II}\ \ln\frac{M_U}{M_C} + a_3^{\rm I}\ \ln\frac{M_C}{M_Z}\right)\ . \tag{4.12}$$

Thus, once the RG coefficients in each interval are specified, the scales M_U and M_C, and the value of α_U are uniquely determined. For the computations to be meaningful, however, M_U must stay below the Planck scale, and α_U must be in the perturbative regime.

4.3.3 Results

The particle content and the RG coefficients for the three models in the two energy intervals are listed in Tables. 4.3, 4.4, and 4.5. As stated above, though $\mathcal{S}$ survives in the energy

interval I, being an SM singlet, it does not contribute to the RG coefficients. The values of M_U, M_C, and α_U obtained using the formalism above are listed in Table 4.6. The running of the gauge couplings for the three models are shown in Figure 4.2.

We see that, for all three models, M_U is below the Planck scale and α_U is perturbative, as are all the gauge couplings during their course of running. The value of the symmetry breaking scale M_C is high in the $10^{10\sim13}$ GeV range, suggesting that providing $\mathcal{S}$ and $\chi = \Delta_{R3}^{-2/3}(1, -4/3, 3)$ with TeV scale masses, and the TeV scale coupling $\kappa M_R \mathcal{S}\chi^\dagger\chi$ between them would involve fine tuning.

Table 4.3: The Higgs content and the RG coefficients in the energy intervals for model A.

Interval	Higgs content	RG coefficients
II	$\phi(2,2,1),\ \widetilde{\Delta}_R(1,2,4),\ \Sigma(1,1,15)$	$(a_L, a_R, a_4)^{\rm II} = \left(-3, \frac{-7}{3}, \frac{-29}{3}\right)$
I	$\phi_2(2,1,1),\ \mathcal{S}(1,0,1),\ \widetilde{\Delta}_{R3}^{-2/3}\left(1, \frac{-4}{3}, 3\right)$	$(a_1, a_2, a_3)^{\rm I} = \left(\frac{131}{18}, \frac{-19}{6}, \frac{-41}{6}\right)$

Table 4.4: The Higgs content and the RG coefficients in the energy intervals for model B.

Interval	Higgs content	RG coefficients
II	$\phi(2,2,1),\ H(1,1,6),\ \Delta_R(1,3,10),$ $\widetilde{\Sigma}(2,2,15)$	$(a_L, a_R, a_4)^{\rm II} = \left(2, \frac{26}{3}, -2\right)$
I	$\phi_2(2,1,1),\ \mathcal{S}(1,0,1),\ \Delta_{R3}^{-2/3}\left(1, \frac{-4}{3}, 3\right)$	$(a_1, a_2, a_3)^{\rm I} = \left(\frac{131}{18}, \frac{-19}{6}, \frac{-41}{6}\right)$

Table 4.5: The Higgs content and the RG coefficients in the energy intervals for model C.

Interval	Higgs content	RG coefficients
II	$\phi(2,2,1),\ H(1,1,6)\times 2,\ \widetilde{\Sigma}(2,2,15)$ $\Delta_R(1,3,10),\ \Delta_L(3,1,10)$	$(a_L, a_R, a_4)^{\rm II} = \left(\frac{26}{3}, \frac{26}{3}, \frac{4}{3}\right)$
I	$\phi_2(2,1,1),\ \mathcal{S}(1,0,1),\ \Delta_{R3}^{-2/3}\left(1, \frac{-4}{3}, 3\right)$	$(a_1, a_2, a_3)^{\rm I} = \left(\frac{131}{18}, \frac{-19}{6}, \frac{-41}{6}\right)$

Table 4.6: The predictions of Models A, B, and C.

Model	A	B	C
Unbroken Symmetry	G_{224}	G_{224}	G_{224D}
$\log_{10}(M_U/\text{GeV})$	15.7	17.1	15.6
$\log_{10}(M_C/\text{GeV})$	13.3	10.5	13.4
α_U^{-1}	45.4	34.7	36.2

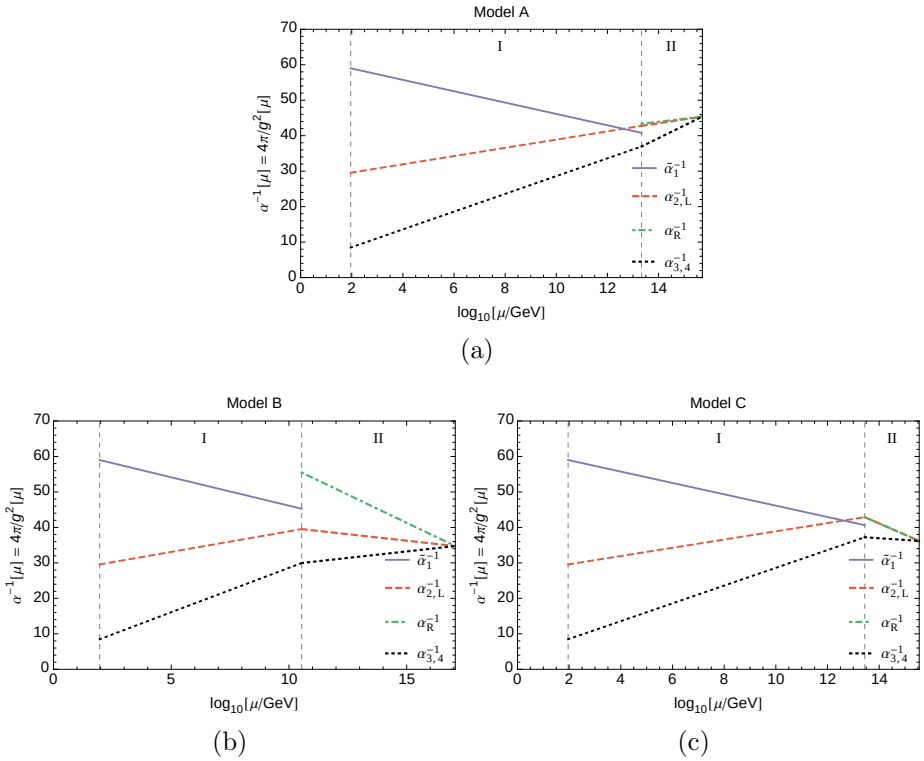

(a)

(b)

(c)

Figure 4.2: Running of the gauge couplings for models A, B, and C. The vertical dotted lines from left to right correspond to the symmetry breaking scales M_Z and M_C, which also indicate the beginning of the energy intervals I and II, respectively. For α_1^{-1}, we plot the redefined quantity $\widetilde{\alpha}_1^{-1} \equiv \frac{3}{5}\alpha_1^{-1}$. Note that, in interval II of panel (a), α_L^{-1} and α_R^{-1} evolve very closely but not identically.

4.4 Discussion

In this chapter, we have discussed a possible interpretation of the 750 GeV diphoton resonance in the framework of unified G_{224} models derived in the context of a left-right symmetric extension of non-commutative geometry (NCG) of the Standard Model (SM). Our framework is a grand unified version of G_{224} models, within which the corresponding Higgs content is restrictively determined (or uniquely determined for each model) from the underlying non-commutative geometry. This should be contrasted to the regular G_{224} models, discussed in the literature, in which the corresponding Higgs context is arbitrarily selected.

We have argued that the observed cross sections involving the 750 GeV diphoton resonance could be realized through a SM singlet scalar field and colored scalars in the NCG of unified G_{224} models. However, the color scalars are light and thus fine tuned from the usual effective field theory point of view. This indicates a certain rigidity of the NCG approach to the Standard Model and its natural completion in the context of the unified G_{224} models. As already emphasized, this conclusion is based on the effective field theory reasoning, which might fail in the NCG framework due to the possible mixing between the short- and long-distance physics as we have discussed in Chapter 3 and Ref. [160], as well as Refs. [159, 163]. In this chapter, we have discussed three different scenarios and their implications for the physics beyond the Standard Model. We have concentrated on the purely phenomenological aspects of the NCG unified G_{224} models without relying on their deep mathematical structure or various novel physics aspects that go beyond the effective field theory framework.

We believe that the discussion presented in this chapter gives extra evidence to the underlying phenomenological rigidity of the NCG approach towards understanding of the origins of the Standard Model and the physics beyond the Standard Model. However, this phenomenological rigidity might be the price one has to pay for the non-commutative nature of the approach, and it might be indicative of a possibly exciting relation to the non-particle sector of high energy physics that is to be found in the context of the underlying quantum structure of space and time.

Part II

Constraining New Physics with Neutrino Experiments

Chapter 5

Constraints on New Physics at Low Energy

5.1 Bounds of Different Sectors

In Part I, we discussed the alternative viewpoint of how new physics fundamentally incompatible with EFT determines the EFT, and studied the possibility of finding clues of new physics at LHC. Since EFT works very well below Λ_{NP} as we show in Section 1.1, in this part, we take a step back and focus purely on the phenomenological aspect of the EFT at an energy scale much lower than Λ_{NP}. Let us first examine the room for new physics in this regime.

After years of experimentation, we have set stringent bounds on various processes. In Section 1.1, we have seen the precision electroweak measurements matches the QED predictions extremely well. Let us examine the bounds derived from other sectors. For the flavor sector, the bounds for unitarity of the CKM matrix are also very tight. If we denote the CKM matrix as

$$V = \begin{bmatrix} V_{ud} & V_{us} & V_{ub} \\ V_{cd} & V_{cs} & V_{cb} \\ V_{td} & V_{ts} & V_{tb} \end{bmatrix}, \tag{5.1}$$

then checking unitarity of first two rows and first two columns of matrix V gives the following relations [1]:

$$VV^\dagger = \begin{bmatrix} 0.9996 \pm 0.0005 & - & - \\ - & 1.002 \pm 0.027 & - \\ - & - & - \end{bmatrix},$$

and

$$V^\dagger V = \begin{bmatrix} 0.9975 \pm 0.0022 & - & - \\ - & 1.042 \pm 0.032 & - \\ - & - & - \end{bmatrix}. \tag{5.2}$$

which mean the CKM matrix is extremely close to unitary. Therefore, a simple fourth-generation quark that mixes with the first three generations is largely constrained. Taking the Wolfenstein parametrization of the CKM matrix as [356]

$$V_{CKM} = \begin{bmatrix} 1-\lambda^2/2 & \lambda & A\lambda^3(\rho - i\eta) \\ -\lambda & 1-\lambda^2/2 & A\lambda^2 \\ A\lambda^3(1-\rho-i\eta) & -A\lambda^2 & 1 \end{bmatrix} + \mathcal{O}(\lambda^4), \tag{5.3}$$

geometrically we can parametrize each unitarity constraint with a triangle in a complex plain. Using the first and third columns of V_{CKM}, this is shown in Fig. 5.1. Therefore,

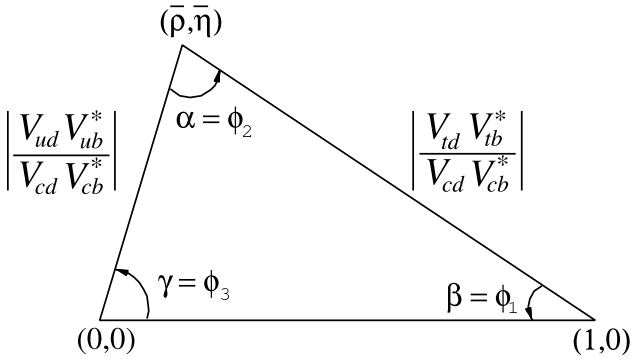

Figure 5.1: The 'unitarity triangle'. Plot is used with permission of PDG [1].

independent measurements of the CKM matrix by various experiments can be characterized by their consistency with this triangle. In Fig. 5.2, the results from different experiments are combined and the global bounds are given in the $(\overline{\rho}, \overline{\eta})$ plane.

Next, let us look at the constraints of the charged lepton sector. In many models [76, 318, 357–367], lepton flavor violation (LFV) emerges as a result of new physics beyond the SM.

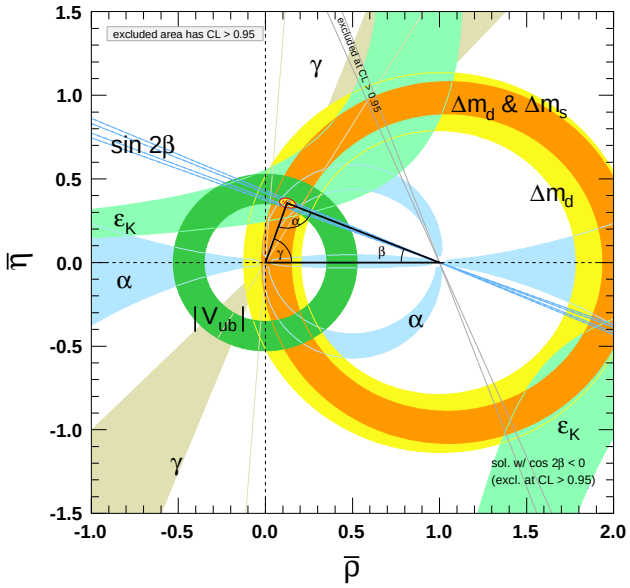

Figure 5.2: The global fit results (shaded region) v.s. the constraints of the unitarity triangle. Plot is used with permission of PDG. For more details of the plot see Refs. [3] and [1].

Bounds on some of these processes are summarized in the following list:

$$
\begin{aligned}
&\frac{\Gamma_i}{\Gamma}(\tau^- \to e^-\gamma) < 3.3 \times 10^{-8}\ [293],\\
&\frac{\Gamma_i}{\Gamma}(\tau^- \to \mu^-\gamma) < 4.4 \times 10^{-8}\ [293],\\
&\frac{\Gamma_i}{\Gamma}(\tau^- \to e^-\mu^+\mu^-) < 2.7 \times 10^{-8}\ [368],\\
&\frac{\Gamma_i}{\Gamma}(\tau^- \to \mu^- e^+ e^-) < 1.8 \times 10^{-8}\ [368],\\
&\frac{\Gamma_i}{\Gamma}(\mu^- \to e\gamma) < 2.4 \times 10^{-12}\ [369],\\
&\frac{\Gamma_i}{\Gamma}(\mu^- \to e\gamma\gamma) < 7.2 \times 10^{-11}\ [370\text{–}372],\\
&\frac{\Gamma_i}{\Gamma}(\mu^- \to e^- e^+ e^-) < 1 \times 10^{-12}\ [286],\\
&\ldots
\end{aligned}
\tag{5.4}
$$

which give stringent constraints on any extra particle that directly couples to charged leptons and causes LFV, such as the ones shown in Ref. [373].

Besides these bounds, since some models allow amplitudes that potentially cause proton decay, the bound of proton decay is carefully studied over the past a few decades. The

current bounds are [1, 374]

$$\begin{aligned}\tau_p/\mathrm{Br}(p \to e^+\pi^0) &> 1.6 \times 10^{34}\ \mathrm{yrs},\\ \tau_p/\mathrm{Br}(p \to \mu^+\pi^0) &> 7.7 \times 10^{33}\ \mathrm{yrs},\\ \tau_p/\mathrm{Br}(p \to K^+\overline{\nu}) &> 6.6 \times 10^{33}\ \mathrm{yrs}.\end{aligned} \tag{5.5}$$

which makes the suppression of proton decay a non-trivial practice that requires extra care in many model building, such as demonstrated in Refs. [76, 318, 357–367]. Contrary to the tight bounds shown above, constraints on the neutrino sector are not comparably strong yet. For example, the allowed region of some of the standard-neutrino oscillation parameters are shown in Fig. 5.3. The parameters relevant to the oscillation are listed in Table 5.1. With new data from various current neutrino experiments and from others being planned for the near future, these bounds are likely to improve. As a result, there is a significant possibility

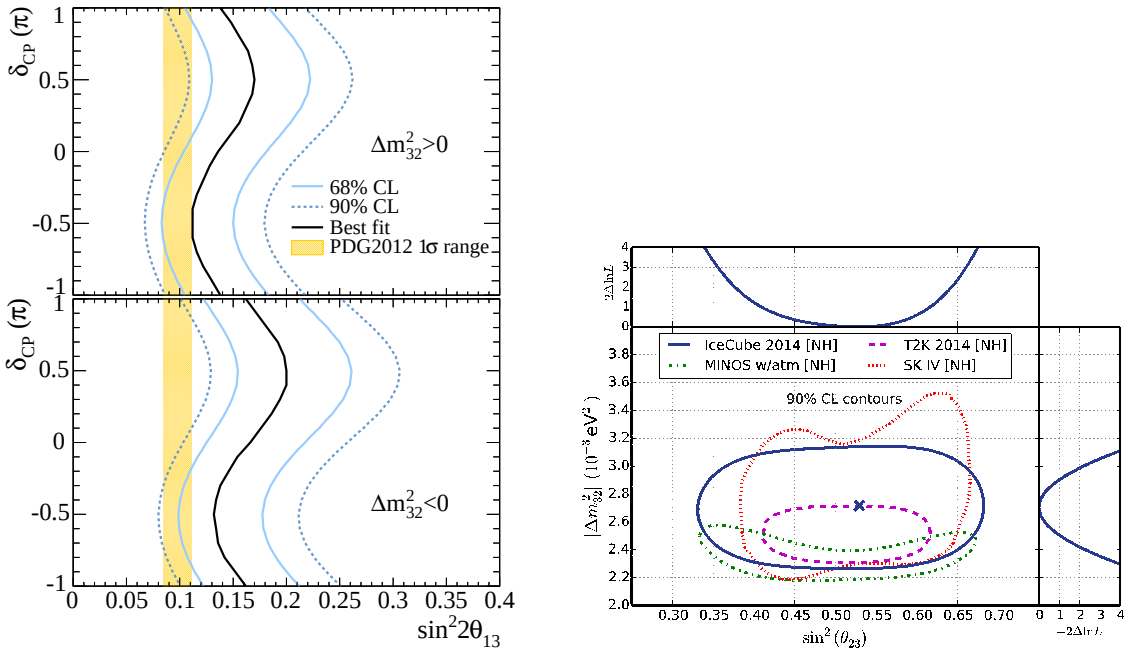

Figure 5.3: The uncertainty on $\sin^2(2\theta_{13}) - \delta_{CP}$ plane and $\sin^2(\theta_{23}) - |\Delta m^2_{32}|$ plane. Plot is used with permission of PDG [1].

to reveal new physics beyond the SM in the neutrino sector, which will be addressed in the next section.

5.2 What Is of Interest in the Neutrino Sector

It is known that the existing uncertainties of the measurements provide room for higher-dimensional operators. These operators potentially arise as a result of new physics at higher

Parameter	Best-fit Value & 1σ Range	Benchmark Value
δm^2_{21}	$(7.50 \pm 0.185) \times 10^{-5}$ eV^2	7.50×10^{-5} eV^2
δm^2_{31}	$(2.47^{+0.069}_{-0.067}) \times 10^{-3}$ eV^2	2.47×10^{-3} eV^2
$\sin^2\theta_{23}$	$0.41^{+0.037}_{-0.025} \oplus 0.59^{+0.021}_{-0.022}$	0.41
$\theta_{23}/^\circ$	$40.0^{+2.1}_{-1.5} \oplus 50.4^{+1.2}_{-1.3}$	
θ_{23}/rad	$0.698^{+0.037}_{-0.026} \oplus 0.880^{+0.021}_{-0.023}$	
$\sin^2\theta_{12}$	0.30 ± 0.013	0.30
$\theta_{12}/^\circ$	33.3 ± 0.8	
θ_{12}/rad	0.580 ± 0.014	
$\sin^2\theta_{13}$	0.023 ± 0.0023	0.023
$\theta_{13}/^\circ$	$8.6^{+0.44}_{-0.46}$	
θ_{13}/rad	0.15 ± 0.01	
$\delta/^\circ$	300^{+66}_{-138}	0
δ/π	$1.67^{+0.37}_{-0.77}$	

Table 5.1: Second column shows the best-fit values and 1σ uncertainties on the oscillation parameters taken from Ref. [9]. We use the values listed in the third column as benchmark values for which we calculate our oscillation probabilities in this work.

scale and can be parameterized by the non-standard interaction parameters (NSI). As a direct analog of the Fermi-interaction development, any discovery of the NSI would be definite evidence of new physics deviating from the SM expectations. Therefore, searching for nsi in the neutrino sector is of theoretical interest. For a recent analysis on the bounds of NSI, see Ref. [375].

Besides, measuring the SM parameters precisely is important in pointing to the direction of new physics in a broader context. For example, the neutrinos are the only fermions of which only one chirality is observed. On the other hand, neutrino oscillation experiments show that the mass of neutrinos is non-zero albeit tiny. Therefore, it is natural to ask about the origin of this smallness [204, 283, 376–378]. Models such as the see-saw mechanism provide solutions to address the smallness of the SM neutrino using new physics. In order to form a mass term, a right handed partner is needed. If this right handed neutrino is not charged under any gauge group, it is allowed to have a Majorana mass without directly breaking any gauge symmetry, which makes the see-saw mechanism possible. As a result, a sub-eV SM neutrino mass requires the right handed partner to be $\sim$ TeV to 10^{16} GeV, depending on the Dirac coupling chosen. On the other hand, as an alternative to regular see-saw models, if the right handed particle is not Majorana, it is a hint for some new symmetry beyond the SM that forbids it, such as the left-right symmetry models we studied in Part I and the inverse see-saw in Refs. [379–384].

Experimentally, a light sterile neutrino that has large mixing with the active neutrinos are subject to the constraints from unitarity [385–387]. Possible observables related to the

unitarity violation due to the extra particle content is also studied in Refs. [388, 389]. As a result, models in this class will be affected by the measurement of the oscillation angles and the mass parameters. It is known that the phenomenological effect of NSI and different values of the standard parameters are degenerate in many processes [375, 390–397]. In this context, understanding the effect of NSI's is important in determining the standard parameters of the neutrino sector. A careful study of the effects of NSI gives us insight on what the degeneracy is and under what circumstances it gets lifted, as shown in Fig. 5.4. In short, a good understanding of the effect of NSI helps us interpret the experimental outcome correctly.

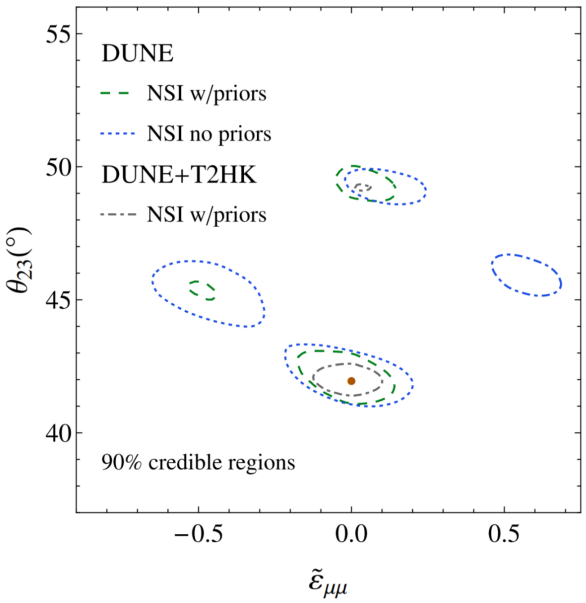

Figure 5.4: The degeneracy between $\epsilon_{\mu\mu}$ and θ_{23} gets partially lifted after combining the DUNE and T2HK data. This figure is from Ref. [4], courtesy of Pilar Coloma.

With this in mind, we study a specific proposed neutrino detector in Chapter 6, which is specifically sensitive to $e-\nu_e$ NSI. We point out the advantage of such a detector and also the issues of potential backgrounds, which should be considered with care. In order to better understand the effect of NSI in neutrino-oscillation experiments, we develop a theoretical tool in Chapter 7 to analytically parametrize the matter effect with the presence of NSI by modifying the vacuum oscillation parameters to run. In this formalism, the physics of NSI is more transparent with little loss of accuracy – at a level that is negligible for experiments such as DUNE. This part is based on our work [398–400] to appear as future publications.

Chapter 6

Constraining Neutrino Non-standard Interaction with OscSNS

In this chapter, we work out the capability of constraining NSI with the proposed OscSNS neutrino detector. We point out the advantage of this detector and possible backgrounds. A goodness-of-fit analysis is performed with projections of one and two years of data.

6.1 Introduction

The proposed OscSNS experiment [401–405] aims to use the Spallation Neutron Source (SNS) [406] at the Oak Ridge National Laboratory (ORNL) in Oak Ridge, Tennessee, USA, as a neutrino source to search for oscillations of the active neutrinos to sterile ones [386, 407–409]. Though the main stated objective of OscSNS is the search for sterile neutrinos, the setup can be utilized to measure the neutrino cross sections on electrons and carbon as well. In this chapter, we analyze the potential of the OscSNS experiment to constrain the coupling of the neutrino via the measurement of the neutrino-electron elastic cross section. If one assumes the SM, a precise measurement of the νe^- cross section would allow one to determine the effective value of $\sin^2\theta_W$ at low momentum transfer. If one fixes the value of $\sin^2\theta_W$ to that determined from other experiments, then the measurement will constrain the sizes of possible non-standard interactions (NSI's) of the neutrino. One should note that the analysis is only valid if all backgrounds are known and under control. In particular, there is a potential background from the non-detection of the excited nitrogen final state in the process

$$\nu_e + {}^{12}C \to e + {}^{12}N^*. \tag{6.1}$$

This can be suppressed through an angular cut of the electron events, as the ones from ν_e scattering are strongly forward peaked. Therefore, in this work we assume this background is under control. More details about this are shown in Section 6.4.3.

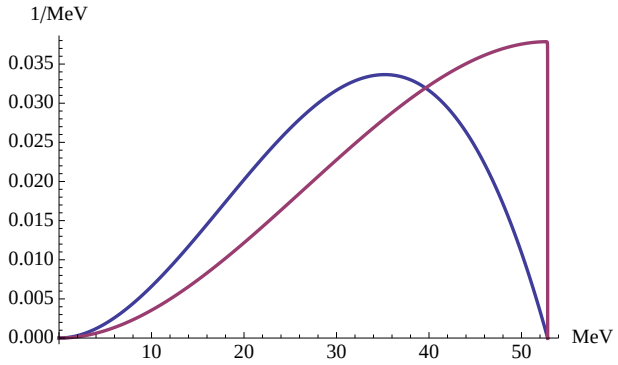

Figure 6.1: The energy spectra of ν_e (blue) and $\overline{\nu}_\mu$ (purple) in μ^+ decay at rest.

We will not consider the neutrino magnetic dipole moment (MDM) since its presence can only be detected via a steep increase in the νe^- cross section at low energies, and OscSNS cannot compete with other detectors that have a much lower detection threshold.

6.2 Neutrinos at the SNS

The SNS at ORNL consists of an H^- ion source, a linear accelerator system for accelerating the H^- ions to 1 GeV a stripper that removes the two electrons, and a proton accumulator ring which stores the resulting 1 GeV protons and releases them in short 695 ns-long pulses at a rate of 60 Hz onto a liquid Hg target.[1]

In addition to 20 to 30 neutrons being spalled from the Hg nuclei per proton on target (POT), the collisions produce charged pions. The π^- are attracted to nuclei and quickly absorbed, while the π^+ come to rest inside the target and decay predominantly via

$$\pi^+ \;\to\; \mu^+ + \nu_\mu \tag{6.2}$$

with a lifetime of $\tau_\pi \;=\; (2.6033 \pm 0.0005) \times 10^{-8}$ sec. Being a two-body decay at rest, the μ^+ and ν_μ from this decay are mono-energetic, with energies

$$\begin{aligned} E_\mu \;&=\; \frac{m_\pi^2 + m_\mu^2}{2m_\pi} \;=\; 109.778 \text{ MeV} \quad\to\quad T_\mu \;=\; E_\mu - m_\mu \;=\; 4.120 \text{ MeV} \,, \\ E_{\nu_\mu} \;&=\; \frac{m_\pi^2 - m_\mu^2}{2m_\pi} \;=\; 29.792 \text{ MeV} \,. \end{aligned} \tag{6.3}$$

The positive muons from this π^+ decay-at-rest then come to rest inside the Hg target[2] and decay themselves via,

$$\mu^+ \;\to\; e^+ + \nu_e + \overline{\nu}_\mu \,, \tag{6.4}$$

[1] About 20 tons of liquid Hg is continuously circulated inside a stainless steel target vessel.

[2] Ref. [401] claims that the μ^+ stop within 0.2 g/cm^2 from the point of π^+ decay. Refs. [410, 411] give tables

with a lifetime of $\tau_\mu = (2.1969811 \pm 0.0000022) \times 10^{-6}$ sec. The ν_e and $\overline{\nu}_\mu$ from this μ^+ decay-at-rest are distributed isotropically with energy spectra given by

$$\begin{aligned} \lambda_{\nu_e}(E_{\nu_e})\, dE_{\nu_e} &= \frac{192}{f(\eta)}\, \frac{x^2(x_{\max}-x)^2}{\left(\frac{1}{2}-x\right)}\, \theta(x_{\max}-x)\, dx\ , \\ \lambda_{\overline{\nu}_\mu}(E_{\overline{\nu}_\mu})\, dE_{\overline{\nu}_\mu} &= \frac{64}{f(\eta)}\, \frac{y^2(y_{\max}-y)^2\left(y^2-\frac{5+\eta}{4}y+\frac{3(1+\eta)}{8}\right)}{\left(\frac{1}{2}-y\right)^3}\, \theta(y_{\max}-y)\, dy\ , \end{aligned} \tag{6.5}$$

where $x = E_{\nu_e}/m_\mu$, $y = E_{\overline{\nu}_\mu}/m_\mu$, $\eta = m_e^2/m_\mu^2 = 2.339 \times 10^{-5}$, and

$$f(\eta) = \left(1 - 8\eta + 8\eta^3 - \eta^4 - 12\eta^2 \ln \eta\right) \approx 1\ . \tag{6.6}$$

The maximum of the neutrino energies is

$$E_{\nu_e,\max} = E_{\overline{\nu}_\mu,\max} = \frac{m_\mu^2 - m_e^2}{2m_\mu} = 52.828\ \text{MeV}\ , \tag{6.7}$$

and thus $x_{\max} = y_{\max} = (1-\eta)/2 \approx 0.5$. These distributions are shown in Fig. 6.1.

At its design power of 1.44 MW,[3] the SNS delivers

$$\frac{1.44\,\text{MW}}{1\,\text{GeV}} = 9.0 \times 10^{15}\,\text{POT/second} = 1.5 \times 10^{14}\,\text{POT/pulse}\ . \tag{6.8}$$

A Geant4 [412, 413] simulation places the number of each of the neutrino flavors ν_μ, ν_e, and $\overline{\nu}_\mu$ produced per 1 GeV POT at 0.09 [401][4]. Thus, in addition to being a neutron source, the SNS produces an equal number of the three neutrino flavors ν_μ, ν_e, and $\overline{\nu}_\mu$ emitted isotropically from the target at the rate of

$$(9.0 \times 10^{15}\,\text{POT/second}) \times (0.09/\text{POT}) = 8 \times 10^{14}/\text{second}\ . \tag{6.9}$$

Due to the large difference between τ_π and τ_μ, the ν_μ flux from π^+ decay and the ν_e and $\overline{\nu}_\mu$ fluxes from the subsequent μ^+ decay are temporally separated. Assuming a uniform pion production rate while the proton beam is on, the time-dependence of the ν_μ, ν_e, and $\overline{\nu}_\mu$ fluxes from the instant that the proton beam is turned on is shown in Fig. 6.2. Of the total ν_μ flux, 96.3% is emitted during the 695 ns while the proton beam is on, and the remaining 3.7% is emitted after the proton beam is turned off. For the ν_e and $\overline{\nu}_\mu$ fluxes, the corresponding

of the muon stopping power of Hg for various muon energies, but they only go down as far as $T_\mu = 10.0$ MeV where the range is given as $1.5\,\text{g/cm}^2$. Given the mass density of Hg, which is $\rho = 13.5\,\text{g/cm}^3$, the range $0.2\,\text{g/cm}^2$ corresponds to $0.015\,\text{cm} = 0.15\,\text{mm}$.

[3]The SNS has not reached its design power yet; in April 2013, it was operating at a power of about 0.85 MW [406].

[4]Ref. [401] quotes two different numbers for this production rate: 0.12 on page 10, and 0.09 on page 23. We use the latter value here since it seems to be the one used in the flux calculations in Chapter 8 of Ref. [401].

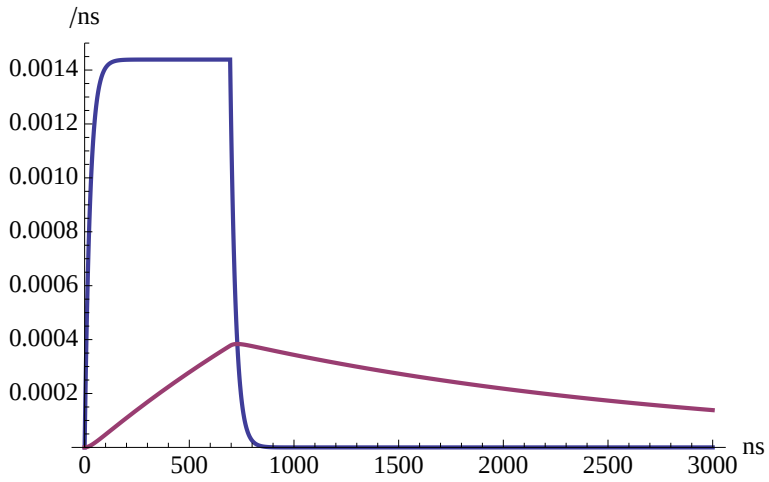

Figure 6.2: The time-dependence of the neutrino fluxes. The proton beam is on during the initial 695 ns. The blue line indicates the time-dependence of the ν_μ flux, while the purple line indicates that of the ν_e and $\bar{\nu}_\mu$ fluxes. The total integrated fluxes are normalized to one. Note that the ν_e and $\bar{\nu}_\mu$ fluxes share the exact same time dependence indicated by the purple line, which is NOT the sum of the two fluxes.

percentages are, respectively, 13.3% and 86.7%. Consequently, when the proton beam is on, the ν_μ's make up 78% of the total neutrino flux while ν_e's and $\overline{\nu}_\mu$'s contribute 11% each.[5] When the beam is off, the ν_μ's constitute 2% while ν_e and $\overline{\nu}_\mu$ contribute 49% each. If we wait a few times τ_π after the proton beam is turned off, the pions will all have decayed and the ν_μ component in the flux will be completely eliminated. We take advantage of this temporal separation later.

6.3 The OscSNS Detector

The OscSNS detector is envisioned to be a liquid scintillation detector, one similar to MiniBooNE, filled with mineral oil and surrounded by photomultiplier tubes (PMT's). The size and shape of the detector are yet to be finalized, but its location will be 60 meters away from the Hg target, at an angle of 160 degrees from the direction of the proton beam. Since the three neutrino flavors are emitted isotropically, the flux of each flavor at a distance of

[5]Ref. [401] on page 10 states that the ν_μ flux has 14% contamination of ν_e and $\overline{\nu}_\mu$ each while the proton beam is on. This should be understood as 14% each relative to the ν_μ flux, that is, the ratio of the fluxes of the three flavors ν_μ, ν_e, and $\overline{\nu}_\mu$ is $100 : 14 : 14$, or $78 : 11 : 11$.

60 meters would be

$$\Phi_\nu(60\,\mathrm{m}) \;=\; \frac{8\times10^{14}/\mathrm{second}}{4\pi(6\times10^3\,\mathrm{cm})^2} \;=\; 1.8\times10^6/\mathrm{second/cm^2} \;=\; 1.8\times10^{13}/\,10^7\,\mathrm{seconds/cm^2}\;. \tag{6.10}$$

Assuming that the liquid scintillator in the detector is pseudocumene[6], C_9H_{12}, with mass density $0.8761\,\mathrm{g/cm^3}$, molar weight $120.19\,\mathrm{g/mol}$, and 66 electrons per molecule, the number of pseudocumene molecules in 100 tons of the material is

$$\begin{aligned} N_{C_9H_{12}} &= \left(\frac{100\,\mathrm{tons}}{120.19\,\mathrm{g/mol}}\right)\times N_A \\ &= (8.32\times10^5\,\mathrm{mols})\times(6.022\times10^{23}/\mathrm{mol}) \\ &= 5.0\times10^{29}\;, \end{aligned} \tag{6.11}$$

and the number densities of electrons, free protons (those not in the carbon), and carbon nuclei are

$$\begin{aligned} \rho_e &= N_e/100\text{ tons} = 66\times N_{C_9H_{12}}/100\text{ tons} = 3.3\times10^{31}/100\text{ tons}\;, \\ \rho_p &= N_p/100\text{ tons} = 12\times N_{C_9H_{12}}/100\text{ tons} = 6.0\times10^{30}/100\text{ tons}\;, \\ \rho_C &= N_\mathrm{C}/100\text{ tons} = 9\times N_{C_9H_{12}}/100\text{ tons} = 4.5\times10^{30}/100\text{ tons}\;. \end{aligned} \tag{6.12}$$

Multiplying by the flux from Eq. (6.10), we find

$$\begin{aligned} \rho_e\Phi_\nu(60\,\mathrm{m}) &= 5.9\times10^{44}/100\text{ tons}/10^7\,\mathrm{seconds/cm^2}\;, \\ \rho_p\Phi_\nu(60\,\mathrm{m}) &= 1.1\times10^{44}/100\text{ tons}/10^7\,\mathrm{seconds/cm^2}\;, \\ \rho_\mathrm{C}\Phi_\nu(60\,\mathrm{m}) &= 8.1\times10^{43}/100\text{ tons}/10^7\,\mathrm{seconds/cm^2}\;. \end{aligned} \tag{6.13}$$

Given that neutrino cross sections with single electrons (nuclei) are on the order of $10^{-44}\,\mathrm{cm^2}$ ($10^{-42}\,\mathrm{cm^2}$), we need the (detector mass) $\times$ (exposure time) to be at least one order of magnitude beyond 10^9 ton $\cdot$ seconds to obtain useful events yields.

In the original OscSNS White Paper [401], the detector is assumed to be spherical, with the central part of radius 5 meters constituting the fiducial volume. The mass of pseudocumene in the fiducial volume is

$$M_\mathrm{fid} \;=\; \frac{4\pi(5.0\times10^2\,\mathrm{cm})^3}{3}\times(0.8761\,\mathrm{g/cm^3}) \;=\; 4.6\times10^8\,\mathrm{g} \;=\; 4.6\times10^2\,\mathrm{ton}\;. \tag{6.14}$$

The number of estimated events in Ref. [401] is given for a flux-exposure of one full calendar year, which is

$$\begin{aligned} T_\mathrm{exp} &= (60\,\mathrm{seconds/minute})\times(60\,\mathrm{minutes/hour})\times(24\,\mathrm{hours/day})\times(365\,\mathrm{days}) \\ &= 3.2\times10^7\,\mathrm{seconds}\;. \end{aligned} \tag{6.15}$$

So the reference value of (detector mass) $\times$ (exposure time) for OscSNS is

$$(M_\mathrm{fid}T_\mathrm{exp})_\mathrm{ref} \;=\; (4.6\times10^2\,\mathrm{ton})\times(3.2\times10^7\,\mathrm{seconds}) \;=\; 1.5\times10^{10}\,\mathrm{ton\cdot seconds}\;. \tag{6.16}$$

We use this value to calculate the benchmark constraints that we place on $\sin^2\theta_W$ and the neutrino NSI's using OscSNS.

[6] Aka 1,2,4-Trimethylbenzene.

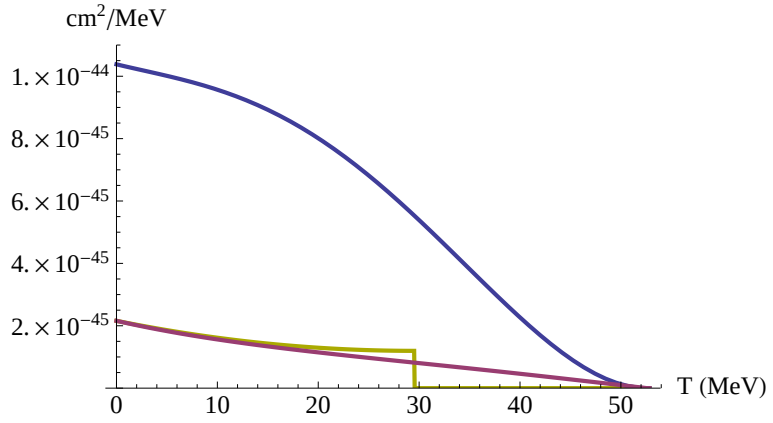

Figure 6.3: The ES differential cross sections as functions of the electron recoil energy T for ν_μ (yellow), ν_e (blue) and $\overline{\nu}_\mu$ (purple).

6.4 The Interactions

The neutrinos will interact with the electrons, free protons, and carbon nuclei in the scintillator via both charged current (CC) and neutral current (NC) interactions. In the following, we will look at the interactions of the neutrino with the three types of target particles, one by one.

6.4.1 Interactions with Electrons

Elastic Scattering

In the SM, the interaction between neutrino flavor α ($\alpha = e, \mu, \tau$) and the electron is described at low energies by the effective four fermion interaction

$$\mathcal{L}_{\rm SM} \;=\; -2\sqrt{2}\,G_F(\bar{\nu}_\alpha\gamma^\mu P_L\nu_\alpha)\Big[\,g_{\alpha L}(\bar{e}\gamma_\mu P_L e) + g_{\alpha R}(\bar{e}\gamma_\mu P_R e)\,\Big]. \tag{6.17}$$

The coupling constants at tree level are given by $g_{\alpha R} = \sin^2\theta_W$ and $g_{\alpha L} = \sin^2\theta_W \pm \frac{1}{2}$, where the lower sign applies for $\alpha = \mu$ and τ (from Z exchange only) and the upper sign applies for $\alpha = e$ (from both Z and W exchange). For anti-neutrinos, the values of $g_{\alpha L}$ and $g_{\alpha R}$ will be reversed.

The differential cross section for neutrino-electron elastic scattering (ES) due to this interaction is given by

$$\frac{d\sigma_{\nu_\alpha}(E_{\nu_\alpha}, T)}{dT} = \frac{2G_F^2 m_e}{\pi}\left[g_{\alpha L}^2 + g_{\alpha R}^2\left(1 - \frac{T}{E_{\nu_\alpha}}\right)^2 - g_{\alpha L}g_{\alpha R}\frac{m_e T}{E_{\nu_\alpha}^2}\right]. \tag{6.18}$$

Here, m_e is the electron mass, E_{ν_α} is the initial energy of neutrino flavor α, and T is the kinetic energy of the recoil electron, which has the range

$$0 \;\le\; T \;\le\; T_{\max}(E_{\nu_\alpha}) \;=\; \frac{E_{\nu_\alpha}}{1 + m_e/2E_{\nu_\alpha}} \; . \tag{6.19}$$

Since the ν_μ from π^+ decay at rest is mono-energetic, the scattering cross section is given simply by the above expression. For the ν_e and $\overline{\nu}_\mu$ from μ^+ decay at rest, however, we must convolute the above expression with the energy spectra given in Eq. (6.5):

$$\begin{aligned} \frac{d\overline{\sigma}_{\nu_e}(T)}{dT} &= \int_0^{E_{\nu_e,\max}} dE_{\nu_e}\; \lambda_{\nu_e}(E_{\nu_e})\; \frac{d\sigma_{\nu_e}(E_{\nu_e},T)}{dT}\; \theta(T_{\max}(E_{\nu_e}) - T) \; , \\ \frac{d\overline{\sigma}_{\overline{\nu}_\mu}(T)}{dT} &= \int_0^{E_{\overline{\nu}_\mu,\max}} dE_{\overline{\nu}_\mu}\; \lambda_{\overline{\nu}_\mu}(E_{\overline{\nu}_\mu})\; \frac{d\sigma_{\overline{\nu}_\mu}(E_{\overline{\nu}_\mu},T)}{dT}\; \theta(T_{\max}(E_{\overline{\nu}_\mu}) - T) \; . \end{aligned} \tag{6.20}$$

The shapes of these differential cross sections are shown in Fig. 6.3.

The total cross sections for ν_μ is given by

$$\begin{aligned} \sigma_{\nu_\mu}(\mathrm{ES}) &= \int_0^{T_{\max}(E_{\nu_\mu})} \frac{d\sigma_{\nu_\mu}(E_{\nu_\mu},T)}{dT}\, dT \\ &= \frac{2G_F^2 m_e T_{\max}}{\pi} \left[g_{\mu L}^2 + g_{\mu R}^2 \left(1 - \frac{T_{\max}}{E_{\nu_\mu}} + \frac{T_{\max}^2}{3E_{\nu_\mu}^2} \right) - g_{\mu L} g_{\mu R} \frac{m_e T_{\max}}{2E_{\nu_\mu}^2} \right] \\ &= 4.48 \times 10^{-44}\, \mathrm{cm}^2 \; , \end{aligned} \tag{6.21}$$

where we have used the value $\sin^2\theta_W = 0.2386$ for the coupling constants. Similarly,

$$\begin{aligned} \sigma_{\nu_e}(\mathrm{ES}) &= \int_0^{T_{\max}(E_{\nu_e,\max})} \frac{d\overline{\sigma}_{\nu_e}(T)}{dT}\, dT \;=\; 3.05 \times 10^{-43}\, \mathrm{cm}^2 \; , \\ \sigma_{\overline{\nu}_\mu}(\mathrm{ES}) &= \int_0^{T_{\max}(E_{\overline{\nu}_\mu,\max})} \frac{d\overline{\sigma}_{\overline{\nu}_\mu}(T)}{dT}\, dT \;=\; 5.08 \times 10^{-44}\, \mathrm{cm}^2 \; . \end{aligned} \tag{6.22}$$

Inverse Muon Decay

For an initial ν_μ, the CC process,

$$\nu_\mu + e^- \;\rightarrow\; \mu^- + \nu_e \; , \tag{6.23}$$

is also possible if the ν_μ is energetic enough. However, the threshold energy is

$$E_{\nu_\mu,\mathrm{thres}} \;=\; \frac{m_\mu^2 - m_e^2}{2m_e} \;=\; 10.923\,\mathrm{GeV} \; , \tag{6.24}$$

so this reaction cannot occur in the present context.

6.4.2 Interactions with Protons

Elastic Scattering

Neutrinos can scatter elastically against the protons via Z exchange, but the recoil protons are not energetic enough to be dissociated from the pseudocumene molecules and cause scintillation light. So the ES events against protons, and similarly those against carbon, are invisible.

Inverse Beta Decay

Anti-neutrinos can undergo the reactions

$$\begin{array}{lcl} \overline{\nu}_e + p & \rightarrow & e^+ + n \ , \\ \overline{\nu}_\mu + p & \rightarrow & \mu^+ + n \ , \end{array} \tag{6.25}$$

with the resulting neutron detected via $n + p \rightarrow D + \gamma\,(2.2\,\mathrm{MeV})$. These reactions have thresholds of

$$\begin{array}{rcl} E_{\overline{\nu}_e,\mathrm{thres}} & = & \dfrac{(m_n + m_e)^2 - m_p^2}{2m_p} \ = \ 1.806\,\mathrm{MeV} \ , \\ E_{\overline{\nu}_\mu,\mathrm{thres}} & = & \dfrac{(m_n + m_\mu)^2 - m_p^2}{2m_p} \ = \ 113.05\,\mathrm{MeV} \ , \end{array} \tag{6.26}$$

so the second reaction cannot occur. The first will be used by OscSNS to detect $\overline{\nu}_e$ appearance. For our purpose, we will simply assume that the $\overline{\nu}_e$ contamination in the flux (from μ^- decay) is negligible and ignore this reaction.

6.4.3 Interactions with Carbon

Elastic Scattering

The elastic scattering of the neutrinos against the carbon nuclei from Z exchange cannot be detected, as discussed above.

CC Inelastic Scattering

The ν_e can undergo the CC process

$$\nu_e + {}^{12}C \ \rightarrow \ e^- + {}^{12}N \tag{6.27}$$

where the ^{12}N in the final state can either be in the ground state $^{12}N_{gs}$, or one of the short-lived, broad excited states $^{12}N^*$.

The cross section to the ground state $^{12}N_{gs}$ can be calculated fairly reliably, since the form factors necessary can be determined from other experiments [414, 415]. The reaction to the ground state $\nu_e + {}^{12}C \to e^- + {}^{12}N_{gs}$ has a Q value 17.33 MeV, so the ν_e energy threshold is

$$E_{\nu_e,\text{thres}} \;=\; \frac{(m_N + m_e)^2 - m_C^2}{2m_C} \;=\; \frac{Q(Q+2m_C)}{2m_C} \;=\; 17.35\,\text{MeV}\;. \tag{6.28}$$

The ground state $^{12}N_{gs}$ decays with a lifetime of $\tau(^{12}N_{gs}) \;=\; 15.9\,\text{ms}$ into[7]

$$^{12}N_{gs} \;\to\; \begin{cases} {}^{12}C + e^+ + \nu_e & (96.5\%) \\ {}^{12}C^* + e^+ + \nu_e \;\to\; {}^{8}Be + \alpha + e^+ + \nu_e \;\to\; 3\alpha + e^+ + \nu_e & (3.5\%) \end{cases} \tag{6.29}$$

The positrons from these decays have a maximum kinetic energy of $Q - 2m_e = 16.33\,\text{MeV}$. The process is identified via the detection of the initial prompt electron, and the delayed coincident detection of the positron. The three α's in the second decay cannot be detected. The excited states $^{12}N^*$ are short-lived and decay mostly via proton emission (Table 12.22 of Ref. [416])

$$^{12}N^* \;\to\; {}^{11}C + p\;. \tag{6.30}$$

This is a potential background unless a) the proton is detected to identify this reaction, or b) the cross section of this process is well understood theoretically through calculation. Otherwise, this process will be a background to νe elastic scattering process. According to Ref. [417], this proton is detectable, *c.f.* Fig. 21-22 therein. In the case of OscSNS, without the direct detection of the proton, there are several ways to control the background from this process. First, it is observed by LSND that the electrons from Eq. (6.27) with a $^{12}N^*$ final state are backward peaked. On the other hand, the differential cross section of $\nu_e + e$ in Eq. (6.31) is forward peaked as plotted in and Fig. 6.4 and measured in Fig. 9 of Ref. [418],

$$\begin{aligned} \frac{\mathrm{d}\sigma}{\mathrm{d}\cos\theta} = \frac{G_F^2 m_e}{2\pi}\Bigg\{ &(c_V + c_A)^2 + (c_V - c_A)^2 m_e^2 \left(1 - \frac{2m_e E_\nu \cos^2\theta}{\sin^2\theta E_\nu^2 + 2m_e E_\nu + m_e^2}\right)^2 \\ &\times -(c_V^2 - c_A^2)\frac{2m_e^2\cos^2\theta}{\sin^2\theta E_\nu^2 + 2m_e E_\nu + m_e^2}\Bigg\} \times \frac{4m_e E_\nu^2 (E_\nu + m_e)^2 \cos\theta}{(E_\nu + m_e)^2 - E_\nu^2\cos^2\theta}, \end{aligned} \tag{6.31}$$

where c_V and c_A are the vector and axial charge of the electron. Therefore, it is possible to perform an angular cut to suppress this background if $\frac{\mathrm{d}^2\sigma}{\mathrm{d}E\mathrm{d}\cos\theta}(\nu_e + {}^{12}C \to e + {}^{12}N^*)$ is known. Alternatively, we can subtract altogether the events from Eq. (6.27) if the cross section is known to sufficient accuracy. In either case, it is necessary to have a cross section profile of the process in Eq. (6.27) through theoretical estimate or measurement. The differential cross section is not included in Ref. [417]. At the moment, we have contacted one of the authors

[7] See Table 12.21 of Ref. [416]. The decay to the ground state $^{12}C_{gs}$ is 94.6% and to the first excited state $^{12}C^*(4.44)$ is 1.9%, which add up to 96.5%. Decays to higher excited states of ^{12}C result in 3α break-up.

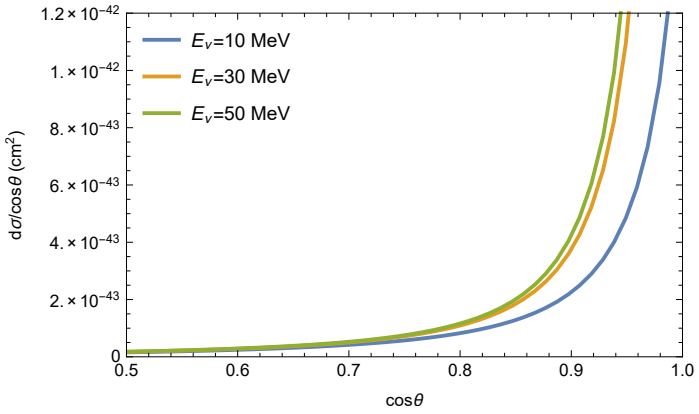

Figure 6.4: Differential cross section of $\nu_e + e \to \nu_e + e$ scattering

of Ref. [419] for further study of this background. In the rest of the chapter, we perform the analysis assuming this background is well-controlled.

The total cross section of the process $\nu_e + {}^{12}C \to e^- + {}^{12}N_{gs}$, convoluted with the initial neutrino energy spectrum, is given as

$$\begin{aligned} \sigma({}^{12}C(\nu_e, e^-){}^{12}N_{gs}) &= 9.2 \times 10^{-42}\,\mathrm{cm}^2 \quad \text{Ref. [414]} \\ &= 9.1 \times 10^{-42}\,\mathrm{cm}^2 \quad \text{Ref. [415]} \end{aligned} \tag{6.32}$$

These agree very well, though the methods used are different. The experimental values are

$$\begin{aligned} \sigma({}^{12}C(\nu_e, e^-){}^{12}N_{gs}) &= (9.1 \pm 0.5 \pm 0.8) \times 10^{-42}\,\mathrm{cm}^2 \quad \text{KARMEN [420, 421]} \\ &= (8.9 \pm 0.3 \pm 0.9) \times 10^{-42}\,\mathrm{cm}^2 \quad \text{LSND [422]} \\ &= (10.5 \pm 1.0 \pm 1.0) \times 10^{-42}\,\mathrm{cm}^2 \quad \text{E225 [423]} \end{aligned} \tag{6.33}$$

so the agreement is good. We can conclude that the cross section is around

$$\sigma({}^{12}C(\nu_e, e^-){}^{12}N_{gs}) \approx 9 \times 10^{-42}\,\mathrm{cm}^2\ . \tag{6.34}$$

Using this value, we estimate the number of events for the reference value of the detector mass and flux exposure, Eq. (6.16), to be:

$$\rho_C \Phi_\nu(60\,\mathrm{m}) \times (M_{\mathrm{fid}} T_{\mathrm{exp}})_{\mathrm{ref}} \sigma({}^{12}C(\nu_e, e^-){}^{12}N_{gs}) \approx 11,000\ . \tag{6.35}$$

Given the large number of expected events, it is tempting to to use this channel to constrain the neutrino flux. However, Ref. [414] warns that the uncertainty in its result could be as large as 12% so it is far from clear whether the theoretical errors are completely under control. Rather, it would better to use νe ES to constrain the flux, and use it to determine $\sigma({}^{12}C(\nu_e, e^-){}^{12}N_{gs})$. The corresponding reaction for $\overline{\nu}_e$ would be

$$\overline{\nu}_e + {}^{12}C \to e^+ + {}^{12}B\ . \tag{6.36}$$

The $\overline{\nu}_e$ energy threshold of this reaction to the ground state of ^{12}B is

$$E_{\overline{\nu}_e,\text{thres}} \;=\; \frac{(m_B+m_e)^2-m_C^2}{2m_C} \;=\; 14.40\,\text{MeV}\;. \tag{6.37}$$

The ground state of ^{12}B decays with a lifetime of $\tau(^{12}B_{gs}) = 29.1\,\text{ms}$ into[8]

$$^{12}B_{gs} \;\rightarrow\; \begin{cases} ^{12}C + e^- + \overline{\nu}_e & (98.4\%) \\ ^{12}C^* + e^- + \overline{\nu}_e \;\rightarrow\; ^8Be + \alpha + e^- + \overline{\nu}_e \;\rightarrow\; 3\alpha + e^- + \overline{\nu}_e & (1.6\%) \end{cases} \tag{6.38}$$

Together with inverse beta decay, this process can be used to detect $\overline{\nu}_e$ appearance. The CC reactions that can be obtained by changing the lepton flavor from electron to muon in the above interactions, *i.e.*

$$\begin{array}{rcl} \nu_\mu + ^{12}C & \rightarrow & \mu^- + ^{12}N \\ \overline{\nu}_\mu + ^{12}C & \rightarrow & \mu^+ + ^{12}B \end{array} \tag{6.39}$$

have thresholds given by

$$\begin{aligned} E_{\nu_\mu,\text{thres}} &= \frac{(m_N+m_\mu)^2-m_C^2}{2m_C} \;=\; 123.15\,\text{MeV}\;, \\ E_{\overline{\nu}_\mu,\text{thres}} &= \frac{(m_B+m_\mu)^2-m_C^2}{2m_C} \;=\; 120.18\,\text{MeV}\;, \end{aligned} \tag{6.40}$$

so these reactions cannot occur.

NC Inelastic Scattering

All neutrino and anti-neutrino flavors can undergo the following NC processes:

$$\nu + ^{12}C \;\rightarrow\; \nu + ^{12}C^*\;. \tag{6.41}$$

The cross section to the first $(J^P, I) = (1^+, 1)$ excited state of Carbon-12 is well understood. In the process

$$\begin{array}{rcl} \nu + ^{12}C & \longrightarrow & \nu + ^{12}C^*(15.11)\;, \\ ^{12}C^*(15.11) & \longrightarrow & ^{12}C + \gamma\;, \end{array} \tag{6.42}$$

So the signature of this process is the mono-energetic 15.11 MeV gamma ray. Theoretical calculations of the cross section are

$$\begin{array}{rcll} \sigma &=& 4.47\times10^{-42}\,\text{cm}^2 & \text{for } \nu_e\text{, Ref. [414]} \\ &=& 5.40\times10^{-42}\,\text{cm}^2 & \text{for } \overline{\nu}_\mu\text{, Ref. [414]} \end{array}$$

[8] See Table 12.14 of Ref. [416]. The decay to the ground state $^{12}C_{gs}$ is 97.2% and to the first excited state $^{12}C^*(4.44)$ is 1.2%, which add up to 98.4%. Decays to higher excited states of ^{12}C result in 3α break-up.

$$\begin{aligned} &= 2.74 \times 10^{-42}\,\mathrm{cm}^2 \qquad \text{for } \nu_\mu, \text{ Ref. [414]} \\ &= 9.8 \times 10^{-42}\,\mathrm{cm}^2 \qquad \text{for } \nu_e + \overline{\nu}_\mu, \text{ Ref. [415]} \end{aligned} \tag{6.43}$$

while the experimental values are

$$\begin{aligned} \sigma &= (3.2 \pm 0.5 \pm 0.4) \times 10^{-42}\,\mathrm{cm}^2 \qquad \nu_\mu, \text{ KARMEN [424]} \\ &= (11 \pm 1.0 \pm 0.9) \times 10^{-42}\,\mathrm{cm}^2 \qquad \nu_e + \overline{\nu}_\mu, \text{ KARMEN [425, 426].} \end{aligned} \tag{6.44}$$

These are consistent with the theoretical calculations, but not that accurate yet.

6.5 Neutrino-Electron Elastic Scattering

To constrain neutrino NSI's, we use neutrino-electron elastic scattering:

$$\nu_\alpha + e^- \longrightarrow \nu_\alpha + e^- \,. \tag{6.45}$$

The signal will be scintillation light from the recoil electrons. The energy of the electrons can be reconstructed from the collected energy of the scintillation photons as in Borexino and MiniBooNE. Since the kinetic energy of the recoil electrons will be in the 10's of MeV range, backgrounds due to the β-decay of radioactive nuclei do not have to be considered since their energies are all around an MeV or below.

6.5.1 The Interaction

In the SM, the interaction between neutrino flavor α ($\alpha = e, \mu, \tau$) and the electron is described at low energies by the effective four-fermion interaction

$$\mathcal{L}_{\mathrm{SM}} \;=\; -2\sqrt{2}\,G_F(\bar{\nu}_\alpha \gamma^\mu P_L \nu_\alpha)\Big[\, g_{\alpha L}(\bar{e}\gamma_\mu P_L e) + g_{\alpha R}(\bar{e}\gamma_\mu P_R e)\,\Big]. \tag{6.46}$$

The coupling constants at tree level are given by $g_{\alpha R} = \sin^2\theta_W$ and $g_{\alpha L} = \sin^2\theta_W \pm \frac{1}{2}$, where the lower sign applies for $\alpha = \mu$ and τ (from Z exchange only) and the upper sign applies for $\alpha = e$ (from both Z and W exchange). For anti-neutrinos, the values of $g_{\alpha L}$ and $g_{\alpha R}$ are reversed.

6.5.2 Differential Cross Section

The differential cross section for elastic neutrino-electron scattering due to this interaction is given by

$$\frac{d\sigma_{\nu_\alpha}(E_{\nu_\alpha}, T)}{dT} = \frac{2G_F^2 m_e}{\pi}\left[g_{\alpha L}^2 + g_{\alpha R}^2\left(1 - \frac{T}{E_{\nu_\alpha}}\right)^2 - g_{\alpha L} g_{\alpha R}\frac{m_e T}{E_{\nu_\alpha}^2}\right] \,. \tag{6.47}$$

Here, m_e is the electron mass, E_{ν_α} is the initial neutrino energy, and T is the kinetic energy of the recoil electron which has the range

$$0 \;\leq\; T \;\leq\; T_{\rm max}(E_{\nu_\alpha}) \;=\; \frac{E_{\nu_\alpha}}{1 + m_e/2E_{\nu_\alpha}} \; . \tag{6.48}$$

Since the ν_μ from π^+ decay is mono-energetic, the scattering cross section is given simply by the above expression. For the ν_e and $\overline{\nu}_\mu$ from μ^+ decay, however, we must convolute the above expression with the energy spectra:

$$\begin{aligned}
\frac{d\overline{\sigma}_{\nu_e}(T)}{dT} &= \int_0^{E_{\nu e,\rm max}} dE_{\nu_e} \; \lambda_{\nu_e}(E_{\nu_e}) \; \frac{d\sigma_{\nu_e}(E_{\nu_e},T)}{dT} \; \theta(T_{\rm max}(E_{\nu_e}) - T) \; , \\
\frac{d\overline{\sigma}_{\overline{\nu}_\mu}(T)}{dT} &= \int_0^{E_{\overline{\nu}_\mu,\rm max}} dE_{\overline{\nu}_\mu} \; \lambda_{\overline{\nu}_\mu}(E_{\overline{\nu}_\mu}) \; \frac{d\sigma_{\overline{\nu}_\mu}(E_{\overline{\nu}_\mu},T)}{dT} \; \theta(T_{\rm max}(E_{\overline{\nu}_\mu}) - T) \; .
\end{aligned} \tag{6.49}$$

The shapes of these differential cross sections are shown in Fig. 6.3.

6.5.3 Total Cross Section

The total cross sections for ν_μ is given by

$$\begin{aligned}
\sigma_{\nu_\mu} &= \int_0^{T_{\rm max}(E_{\nu_\mu})} \frac{d\sigma_{\nu_\mu}}{dT} \, dT \\
&= \frac{2G_F^2 m_e T_{\rm max}}{\pi} \left[g_L^2 + g_R^2 \left(1 - \frac{T_{\rm max}}{E_{\nu_\mu}} + \frac{T_{\rm max}^2}{3E_{\nu_\mu}^2} \right) - g_L g_R \frac{m_e T_{\rm max}}{2E_{\nu_\mu}^2} \right] \\
&= 4.48 \times 10^{-44} \, {\rm cm}^2 \; ,
\end{aligned} \tag{6.50}$$

where we have used the value $\sin^2\theta_W = 0.2386$ for the coupling constants. Similarly,

$$\begin{aligned}
\sigma_{\nu_e} &= \int_0^{T_{\rm max}(E_{\nu e,\rm max})} \frac{d\overline{\sigma}_{\nu_e}}{dT} \, dT \;=\; 3.05 \times 10^{-43} \, {\rm cm}^2 \; , \\
\sigma_{\overline{\nu}_\mu} &= \int_0^{T_{\rm max}(E_{\overline{\nu}_\mu,\rm max})} \frac{d\overline{\sigma}_{\overline{\nu}_\mu}}{dT} \, dT \;=\; 5.08 \times 10^{-44} \, {\rm cm}^2 \; .
\end{aligned} \tag{6.51}$$

6.5.4 Expected Number of Events

According to Eq. (8.3) of Ref. [401], the expected neutrino fluxes at the OscSNS detector are

$$\begin{aligned}
\Phi(\nu_\mu) &= (5.48 \pm 0.05) \times 10^{13} \, /{\rm year}/{\rm cm}^2 \; , \\
\Phi(\nu_e) &= (5.45 \pm 0.05) \times 10^{13} \, /{\rm year}/{\rm cm}^2 \; , \\
\Phi(\bar{\nu}_\mu) &= (5.51 \pm 0.05) \times 10^{13} \, /{\rm year}/{\rm cm}^2 \; .
\end{aligned} \tag{6.52}$$

The number of electrons inside a 6 meter radius (12 meter diameter) detector is estimated to be $N_e = 2.68 \times 10^{32}$. To calculate this number, we need the total mass of the mineral oil inside the detector. Ref. [401] says that this is 800 tons. The "mineral oil" used in Borexino experiment is $C_6H_3(CH_3)_3$, or C_9H_{12}, with a density of 0.8761 g/cm^3 and a molar weight of 120.19 g/mol . Suppose the OscSNS detector uses the same type of material. With this data, and considering that each molecule has 66 electrons, 800 tons would contain a total number of electrons of:

$$66 \times N_A\,(\mathrm{mol}^{-1}) \times \frac{1}{120.19\,(\mathrm{g/mol})} \times (800 \times 10^6\,(\mathrm{g})) \;=\; 2.6455 \times 10^{32},$$

where N_A is Avogadro's number. In Borexino, they also add some ($1.5\,\mathrm{g}/\ell$) scintillator, $C_{15}H_{11}NO$. Using the size of the detector, we get a total of 1.37×10^6 g of scintillator in the detector. One can easily compute that the total number of extra electrons introduced by the scintillator is 4.33×10^{29}. The correction is small, so we use the number for pure mineral oil, $N_e = 2.65 \times 10^{32}$, for the rest of the calculation. The expected total number of events per year is, therefore,

$$\begin{aligned} N(\nu_\mu) &= N_e\,\Phi(\nu_\mu)\,\sigma_{\nu_\mu} = 658\,/\mathrm{year}\,, \\ N(\nu_e) &= N_e\,\Phi(\nu_\mu)\,\sigma_{\nu_\mu} = 4458\,/\mathrm{year}\,, \\ N(\bar\nu_\mu) &= N_e\,\Phi(\nu_\mu)\,\sigma_{\nu_\mu} = 750\,/\mathrm{year}\,. \end{aligned} \tag{6.53}$$

Ref. [401] claims 4491/year for ν_e events, so we are close. The difference could be due to our choice of the value of $\sin^2\theta_W$, and rounding off errors. Assuming a 50% detector efficiency, $\varepsilon_{\mathrm{det}} = 0.5$, the observed yields are reduced to

$$\begin{aligned} N(\nu_\mu) &= N_e\,\Phi(\nu_\mu)\,\sigma_{\nu_\mu}\,\varepsilon_{\mathrm{det}} = 329\,/\mathrm{year}\,, \\ N(\nu_e) &= N_e\,\Phi(\nu_e)\,\sigma_{\nu_e}\,\varepsilon_{\mathrm{det}} = 2228\,/\mathrm{year}\,, \\ N(\bar\nu_\mu) &= N_e\,\Phi(\bar\nu_\mu)\,\sigma_{\bar\nu_\mu}\,\varepsilon_{\mathrm{det}} = 375\,/\mathrm{year}\,. \end{aligned} \tag{6.54}$$

Ref. [401] also claims a reduction by a factor of $\varepsilon_{\mathrm{fid}} = (5/6)^3 \approx 0.5787$ due to fiducial volume cuts.

$$\begin{aligned} N(\nu_\mu) &= N_e\,\Phi(\nu_\mu)\,\sigma_{\nu_\mu}\,\varepsilon_{\mathrm{det}}\,\varepsilon_{\mathrm{fid}} = 190\,/\mathrm{year}\,, \\ N(\nu_e) &= N_e\,\Phi(\nu_e)\,\sigma_{\nu_e}\,\varepsilon_{\mathrm{det}}\,\varepsilon_{\mathrm{fid}} = 1290\,/\mathrm{year}\,, \\ N(\bar\nu_\mu) &= N_e\,\Phi(\bar\nu_\mu)\,\sigma_{\bar\nu_\mu}\,\varepsilon_{\mathrm{det}}\,\varepsilon_{\mathrm{fid}} = 217\,/\mathrm{year}\,. \end{aligned} \tag{6.55}$$

These numbers are for a full Julian year, so for a Snowmass year of 10^7 seconds we will only get one-third of these numbers.

6.5.5 Detector Response

An actual detector cannot measure the recoil electron energy to arbitrary precision, and one must take its finite energy resolution into account. If we denote the probability of detecting

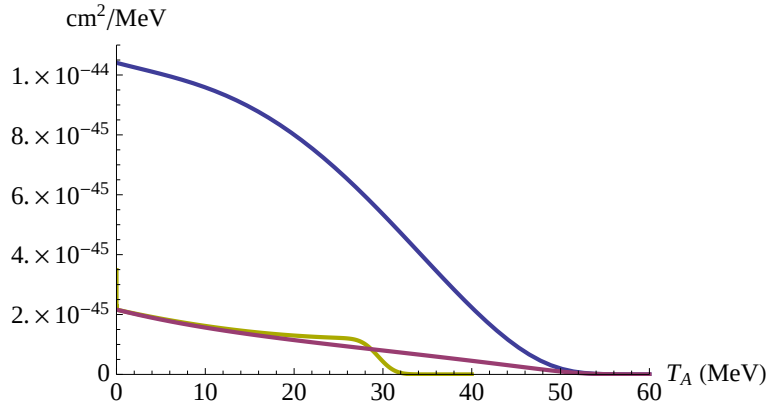

Figure 6.5: The differential cross sections as with the detector energy resolution included. T_A is the reconstructed electron recoil energy. The three curves are for ν_μ (yellow), ν_e (blue) and $\overline{\nu}_\mu$ (purple).

energy T_A for an electron with kinetic energy T by $R(T_A, T)$, the differential cross section as a function of the actual detection energy T_A is given by

$$\frac{d\overline{\sigma}_{\nu_\alpha}(T_A)}{dT_A} \;=\; \int_0^{T_{\rm max}} R(T_A, T)\, \frac{d\tilde{\sigma}_{\nu_\alpha}(T)}{dT}\, dT \;. \tag{6.56}$$

For Borexino, we take the energy resolution function $R(T_A, T)$ to be a Gaussian with a T-dependent standard deviation

$$R(T_A, T) \;=\; \frac{1}{\sqrt{2\pi}\,\sigma(T)} \exp\left[-\frac{(T_A - T)^2}{2\,[\,\sigma(T)\,]^2}\right] . \tag{6.57}$$

For Borexino analyses, the following form is used [427]:

$$\sigma(T) \;=\; \sigma_0 \left(\frac{T}{\rm MeV}\right)^{1/2} , \qquad \sigma_0 \;=\; 50\,{\rm keV} \;. \tag{6.58}$$

This gives a 5% error at $T = 1\,{\rm MeV}$. We use a uniform 5% error, which corresponds to

$$\sigma(T) \;=\; 0.05\,T \;. \tag{6.59}$$

Performing the integral of Eq. (6.56), we obtain the differential cross sections as functions of T_A shown in Fig. 6.5.

6.5.6 Energy Bins

The calibrated range of OscSNS is expected to be $1 \sim 50\,{\rm MeV}$. With a 5% error on the energy, a 50 MeV electron will have an energy uncertainty of 2.5 MeV, so we should make

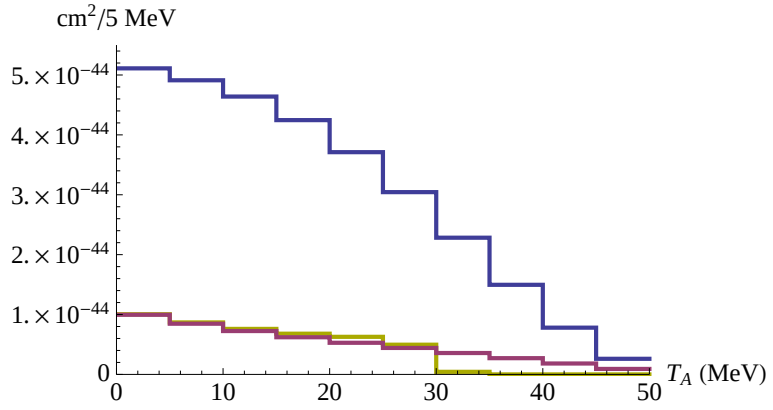

Figure 6.6: The cross sections per 5 MeV energy bin. T_A is the reconstructed electron recoil energy. The three histograms are for ν_μ (yellow), ν_e (blue) and $\overline{\nu}_\mu$ (purple).

the widths of the energy bins larger than this. We just use 5 MeV and divide the range $0 \sim 50$ MeV into 10 bins. We ignore the 1 MeV cutoff for now. Integrating the cross sections in these energy bins, we obtain the graph shown in Fig. 6.6. Multiplying these cross sections per bin with

$$\begin{aligned} N_e \Phi \varepsilon_{\rm det} \varepsilon_{\rm fid} &= (2.68 \times 10^{32}) \times (5.5 \times 10^{13}/{\rm year}/{\rm cm}^2) \times (0.5) \times (5/6)^3 \\ &= 4.3 \times 10^{45}/{\rm year}/{\rm cm}^2 \ , \end{aligned} \tag{6.60}$$

we find the event yields per bin per Julian year. The result is plotted in Fig. 6.7. The error bars indicate the statistical error, assuming a Poisson distribution.

6.6 NSIs

6.6.1 Effect of NSIs on the ν_e-electron Scattering Spectrum

With Non-Standard Interactions (NSIs), the couplings of neutrinos of flavor α are shifted:

$$g_{\alpha L} \ \to \ \tilde{g}_{\alpha L} \ = \ g_{\alpha L} + \varepsilon_{\alpha L} \ , \qquad g_{\alpha R} \ \to \ \tilde{g}_{\alpha R} \ = \ g_{\alpha R} + \varepsilon_{\alpha R} \ . \tag{6.61}$$

The shifts in the couplings of the muon neutrino and its anti-particle are already constrained fairly strongly by CHARM II data, so we will only consider shifts in the electron neutrino couplings.

As we can see from Eq. (6.47), the neutrino-electron scattering cross section consists of three terms which are, respectively, proportional to $\tilde{g}_{eL}^2$, $\tilde{g}_{eR}^2$, and the product $\tilde{g}_{eL}\tilde{g}_{eR}$. The $\tilde{g}_{eL}\tilde{g}_{eR}$ term is proportional to the electron mass so it is suppressed compared to the other terms.

We just neglect it for now. We can calculate the parts of the cross section proportional to $\tilde{g}_{eL}^2$ and $\tilde{g}_{eR}^2$ separately:

$$\sigma_{\nu_e} \;=\; \tilde{g}_{eL}^2\,\sigma_L + \tilde{g}_{eR}^2\,\sigma_R\;. \tag{6.62}$$

Calculating σ_L and σ_R separately, including convolution with the neutrino energy spectrum, energy smearing due to detector resolution, and energy binning, we obtain the graphs shown in Fig. 6.8.

Using σ_L and σ_R, we can calculate the cross section for arbitrary values of $\tilde{g}_L = g_L + \varepsilon_L$ and $\tilde{g}_L = g_R + \varepsilon_R$. In Fig. 6.9, we show how the cross section changes when the left and right handed couplings are respectively shifted by ± 0.1. If we convert these cross sections into the numbers of events expected after one full Julian year of data taking, the result is shown in Fig. 6.10. The blue and red cases can be clearly distinguished provided that the neutrino flux uncertainty can be well constrained. To distinguish between the blue and green cases clearly needs more data.

The graph only shows the total number of ν_e-electron scattering events, but does not show what is actually measured. We need to take the timing information into account and ask whether the neutrino flux can be well constrained by the ν_μ events even though the number of events is quite limited, and there is contamination from ν_e which has a much larger cross section with electrons.

6.6.2 Expected Events with Protons On and Off

We calculated earlier that 96.3% of the ν_μ's will be emitted while the proton beam is on, while 3.7% will be emitted after the proton beam is turned off. For ν_e and $\bar{\nu}_\mu$, the percentages are 13.3% while the proton beam is on, and 86.7% after it is turned off.

The cross section is calculated for the energy spectra of events collected while the proton beam is on and while it is off, as shown in Fig. 6.11. There is a significant ν_e contribution while the proton beam is on due to the much larger cross section that ν_e has compared to ν_μ. On the other hand, the contribution of ν_μ while the proton beam is off is negligible.

To see how these cross sections are changed in the presence of NSI's, g_L and g_R are shifted again by ± 0.1 and the resulting cross sections are plotted in Fig. 6.12. The corresponding event yields are shown in Fig. 6.13. Due to ν_e contamination when the proton beam is on, a goodness-of-fit analysis is needed to see how well we can constrain the neutrino flux using the ν_μ contribution. This is performed in the next section.

6.7 Computation of the χ^2

First, let's compute the total number of events due to standard interactions only. We do it assuming that the beam has already been turned off, including the different weights mentioned in the previous section for the neutrino flavors:

$$N_i^{SM} = 0.867 \times (N_{\nu_e,i}^{SM} + N_{\bar{\nu}_\mu,i}^{SM}) + 0.037 \times N_{\nu_\mu,i}^{SM}, \tag{6.63}$$

where i denotes each 5 MeV bin.

Then, we do the same for the events in presence of NSI, for each pair of values (ϵ_L, ϵ_R):

$$N_i^{NSI}(\epsilon_L, \epsilon_R) = 0.867 \times \left(N_{\nu_e,i}^{SM+NSI}(\epsilon_L, \epsilon_R) + N_{\bar{\nu}_\mu,i}^{SM}\right) + 0.037 \times N_{\nu_\mu,i}^{SM},$$

where the exact cross section is used to compute $N_{\nu,e}^{SM+NSI}$, *i.e.*, the third term in Eq. 6.47 is not neglected.

Then we build a Poissonian χ^2:

$$\begin{aligned} \chi^2(\epsilon_L, \epsilon_R) &= \sum_i \chi_i^2(\epsilon_L, \epsilon_R) = \\ &= \sum_i 2\left(N_i^{SM} - N_i^{NSI}(\epsilon_L, \epsilon_R) + N_i^{NSI}(\epsilon_L, \epsilon_R) \ln\left[\frac{N_i^{NSI}(\epsilon_L, \epsilon_R)}{N_i^{SM}}\right]\right). \end{aligned} \tag{6.64}$$

The physical interpretation of the above χ^2 is understood as follows. First, we assume that the prediction is based on the cross section given purely by the SM. In the end, a different number of events is observed due to the presence of NSI. The significance is then depicted by the above χ^2 expression. The plot of χ^2 in the (ϵ_L, ϵ_R) plane will tell us at which point the NSI are so large that the observed number of events are incompatible with the prediction by the SM. The shape of this χ^2 is shown in Figs. 6.14 and 6.15. As can be seen from Fig. 6.14 the χ^2 is asymmetric. This is due to the interference terms between the standard and non-standard couplings in Eq. 6.47. Since both $g_{L,e}$ and $g_{R,e}$ are defined positive, negative values of ϵ_L or ϵ_R can, in principle, be better accommodated by the data. Fig. 6.15 shows the contours at 1, 2 and 3σ (for 2 d.o.f.) drawn in the (ϵ_L, ϵ_R) plane. Systematic errors are to be included in the next subsection.

6.7.1 Inclusion of a Systematic Error over the Flux

The flux uncertainty is included as an overall normalization error over the predicted number of events from the SM, so we have to replace:

$$N_i^{SM} \to (1 + \xi)\, N_i^{SM}.$$

Now the NSI contribution can be better accommodated by simply varying this nuisance parameter, ξ, which is unknown. As a result, the χ^2 profile is degraded. The χ^2_i (per bin) is obtained as in Eq. 6.64, but now depends on $(\epsilon_L, \epsilon_R, \xi)$. A penalty term needs to be added to the total χ^2 in Eq. 6.64, too:

$$\chi^2(\epsilon_L, \epsilon_R, \xi) = \sum_i \chi^2_i(\epsilon_L, \epsilon_R, \xi) + \left(\frac{\xi}{\sigma_\xi}\right)^2 , \tag{6.65}$$

where ξ is the nuisance parameter (unknown) while σ_ξ is the prior knowledge for the flux uncertainty (an estimate). We assume 10%, for instance. However, we can use this χ^2 to estimate the constraint that the experiment itself would be able to put on the neutrino flux. In order to do so, we use the first 690 ns of the pulse. The beam composition in this time window is mainly ν_μ (96.3%), which can be used to normalize the flux. In this case ($t < 690$ ns), the χ^2 profile is built following Eq. 6.65 with:

$$\begin{aligned} N_i^{SM} &= (1+\xi)\left[0.133 \times \left(N_{\nu_e,i}^{SM} + N_{\bar{\nu}_\mu,i}^{SM}\right) + 0.963 \times N_{\nu_\mu,i}^{SM}\right], \\ N_i^{NSI}(\epsilon_L, \epsilon_R) &= 0.133 \times \left(N_{\nu_e,i}^{SM+NSI}(\epsilon_L, \epsilon_R) + N_{\bar{\nu}_\mu,i}^{SM}\right) + 0.963 \times N_{\nu_\mu,i}^{SM}. \end{aligned} \tag{6.66}$$

Ideally, we have to marginalize over ϵ_L and ϵ_R, and then plot the result as a function of ξ in order to get an accurate value. However, we do not expect a great difference in the χ^2 due to the NSI[9], since they are now just a small portion of the total number of events (only 13.3% come from ν_e events in this time window). Therefore, we choose a pair of values and plot the χ^2 along the ξ axis. Several values of (ϵ_L, ϵ_R) are checked and they result in more or less the same result, as shown in Fig. 6.16. As can be seen from this plot, if we cut at 1 σ (for 1 d.o.f.), we obtain $\sigma_\xi \sim 0.05$. In the following, this value is used for σ_ξ as the prior knowledge of the flux.

In order to have a χ^2 in the (ϵ_L, ϵ_R) plane, we need to marginalize over the nuisance parameter:

$$\chi^2_{min}(\epsilon_L, \epsilon_R) = \min_\xi \left\{ \sum_i \chi^2_i(\epsilon_L, \epsilon_R, \xi) + \left(\frac{\xi}{\sigma_\xi}\right)^2 \right\} . \tag{6.67}$$

The resulting profile is shown in Figs. 6.17 and 6.18, as we did in the previous section. The χ^2 plot with 30% systematic error is also included for comparison. In this case, the results are worsened, as expected, but we still have some sensitivity to the non-standard couplings. On the other hand, this shows that the systematic error strongly affects the sensitivity. Therefore, a good control of the flux uncertainty is critical.

[9]This is valid only under the assumption that NSI only enter in the ν_e couplings.

6.8 Conclusion and Outlook

In this chapter, we estimate the capability of a then-proposed detector, OscSNS at Oak Ridge National Laboratory, to constrain ν_e-electron NSI. The time structure of the pulsed proton beam allows us to constrain the neutrino flux uncertainty more accurately. Because of the different life-time of π^+ and μ^+, the neutrino content is quite different when the beam is on and off. When the proton beam is turned on, a produced π^+ goes through a two body decay at rest and produces mono-energetic ν_μ and μ^+. Because the π^+ decays roughly 100 times faster than the μ^+, the ν_e content is negligible when the beam is on. Similarly, during the beam-off period, because most of π decay quickly, the neutrino flux is dominated by the μ^+ decay, which produces ν_e and $\overline{\nu}_\mu$.

Because of this feature, it is possible to constrain the neutrino flux with data from beam-on period since ν_μ-electron NSI is well constrained already. As a result, this type of design has great potential to constrain ν_e-electron scattering. In our note, we show the χ^2 analysis on the (ϵ_L, ϵ_R) plane with one and two years data taking. The result is comparable to other experiments even though the number of events is limited. On the other hand, we also observe a degradation of sensitivity when the systematic error is included. We point out that both the control and the estimate of systematics strongly affect the result of the analysis, hence the capability of constraining NSI.

During the study of this topic, we noticed a technical issue which should be addressed in the future. The material of the OscSNS detector is mineral oil, which is similar to Borexino and MiniBooNE. Therefore, the $\nu - {}^{12}C$ scattering should be well understood; otherwise, it is a background. Due to the difficulty in calculating ν-nuclei scattering at very low energy [419, 428], this needs to be treated carefully to suppress the background.

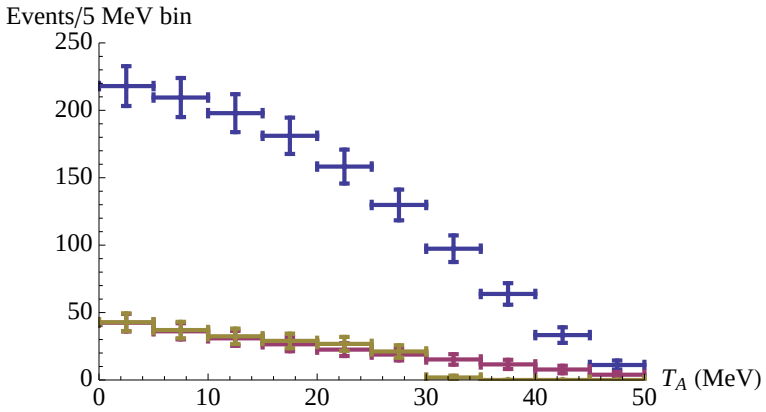

Figure 6.7: Expected number of events per 5 MeV energy bin per year. The three plots are for ν_μ (yellow), ν_e (blue) and $\overline{\nu}_\mu$ (purple).

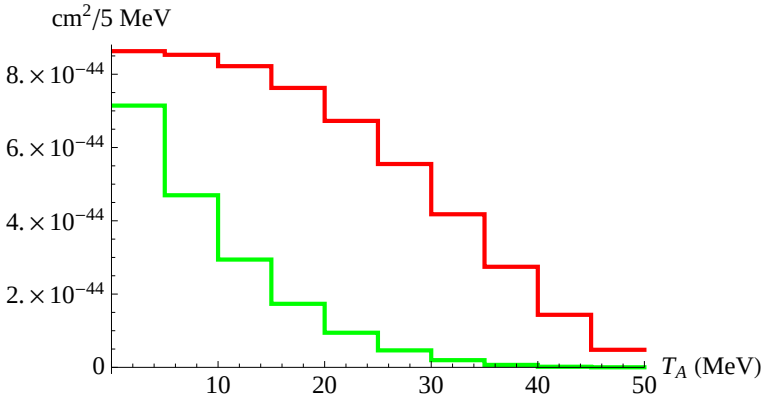

Figure 6.8: The left (red) and right handed (green) cross sections per 5 MeV energy bin.

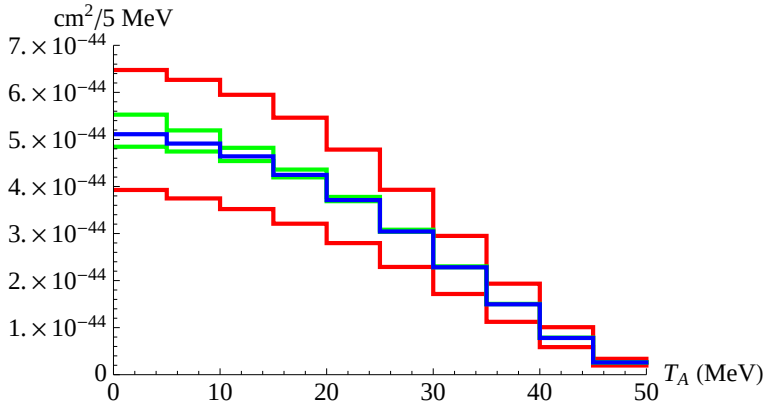

Figure 6.9: The ν_e-electron cross section per 5 MeV energy bin when g_L is shifted by ± 0.1 (red graphs) and when g_R is shifted by ± 0.1 (green graphs). The blue graph is when the NSIs are all zero.

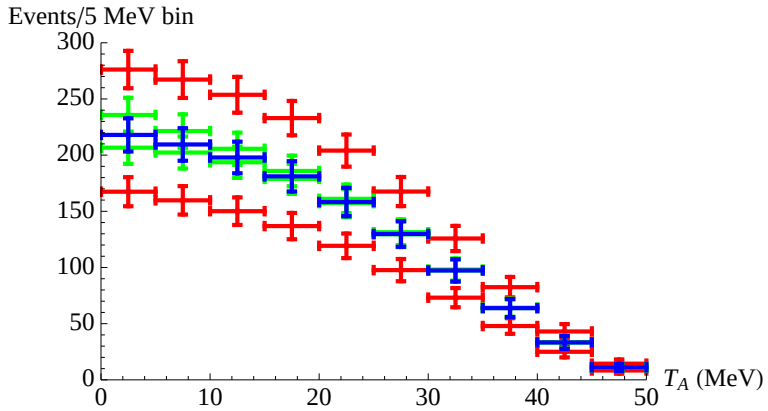

Figure 6.10: Number of expected ν_e-electron scattering events per 5 MeV energy bin after one full Julian year of data taking when g_L is shifted by ± 0.1 (red graphs) and when g_R is shifted by ± 0.1 (green graphs). The blue graph is when the NSIs are all zero.

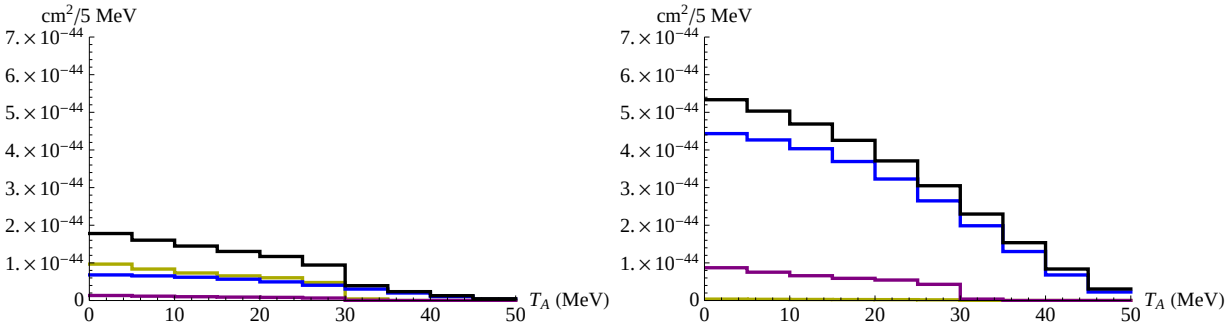

Figure 6.11: Total cross section of $\nu_\mu + \nu_e + \bar{\nu}_\mu$ scattering against electrons per 5 MeV energy bin with proton beam on (left) and off (right). The black graph is the total cross sections, while the blue, purple, and yellow graphs indicate the contributions of ν_e, $\bar{\nu}_\mu$, and ν_μ, respectively. Note that there is a significant ν_e contribution when the proton beam is on.

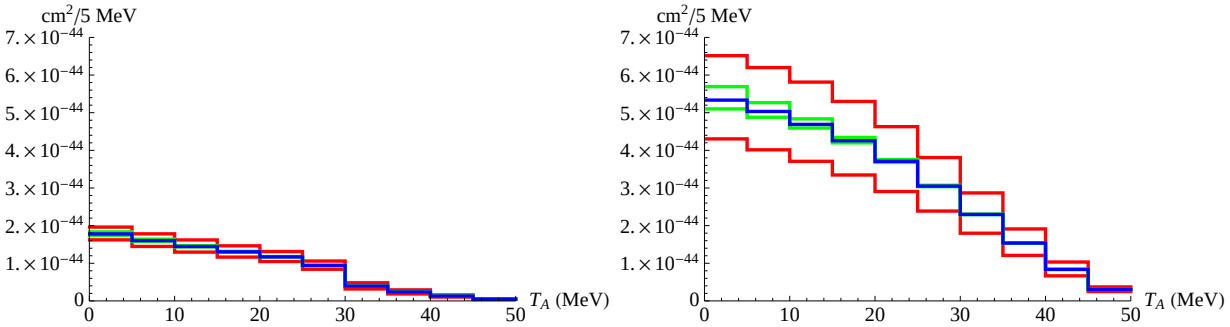

Figure 6.12: Total cross section of $\nu_\mu + \nu_e + \bar{\nu}_\mu$ scattering against electrons per 5 MeV energy bin with proton beam on (left) and off (right). The red graphs indicate the cases in which g_L is shifted by ± 0.1 while the green graphs indicate the cases in which g_R is shifted by ± 0.1. The blue graphs are when the NSIs are all zero.

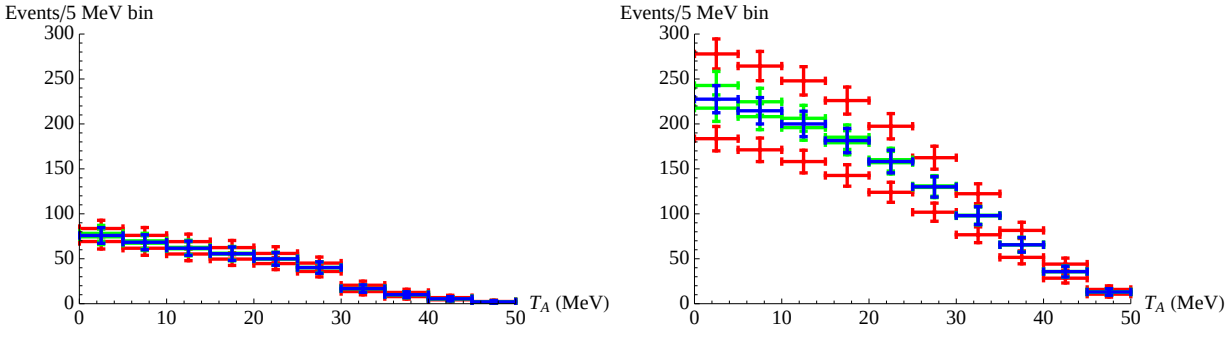

Figure 6.13: Expected total number of $(\nu_\mu + \nu_e + \bar{\nu}_\mu)e^-$ scattering events per 5 MeV energy bin with proton beam on (left) and off (right) after one full Julian year of data taking. The red graphs indicate the cases in which g_L is shifted by ± 0.1 while the green graphs indicate the cases in which g_R is shifted by ± 0.1. The blue graphs are when the NSIs are all zero.

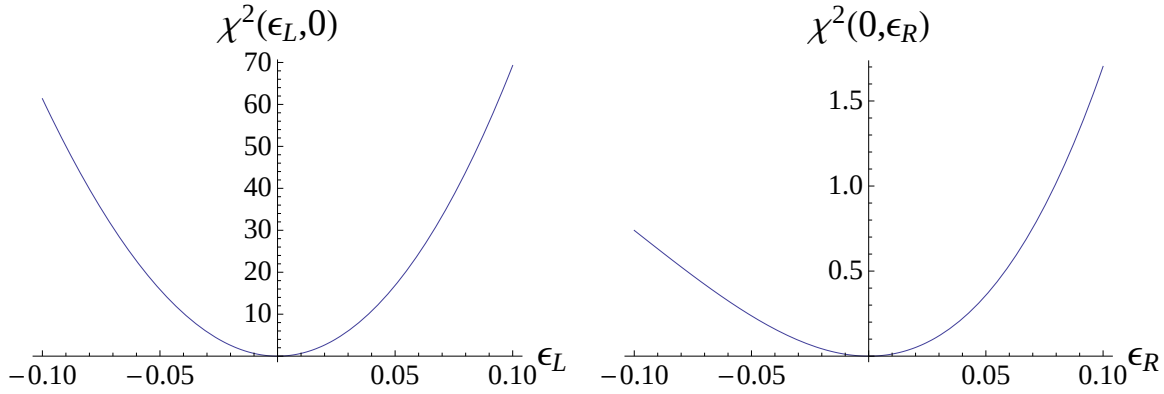

Figure 6.14: Cut of the two-dimensional χ^2 in the ϵ_L (left) and ϵ_R (right) directions, assuming the other parameter to be zero. No systematics have been included.

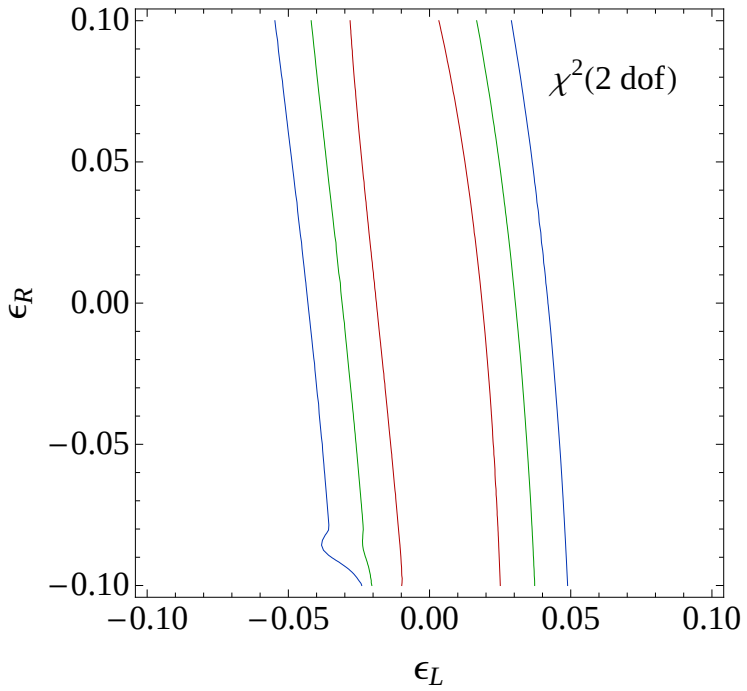

Figure 6.15: $\Delta\chi^2$ contours at 1,2 and 3σ (2 d.o.f.) in the (ϵ_L,ϵ_R) plane after one year of exposure. No systematics have been included.

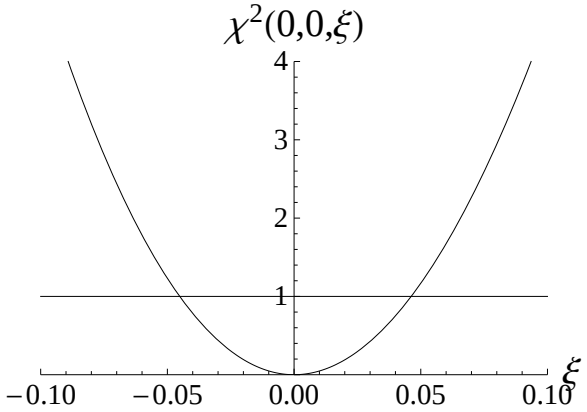

Figure 6.16: $\Delta\chi^2$ profile in the ξ direction for $\epsilon_L = \epsilon_R$=0.

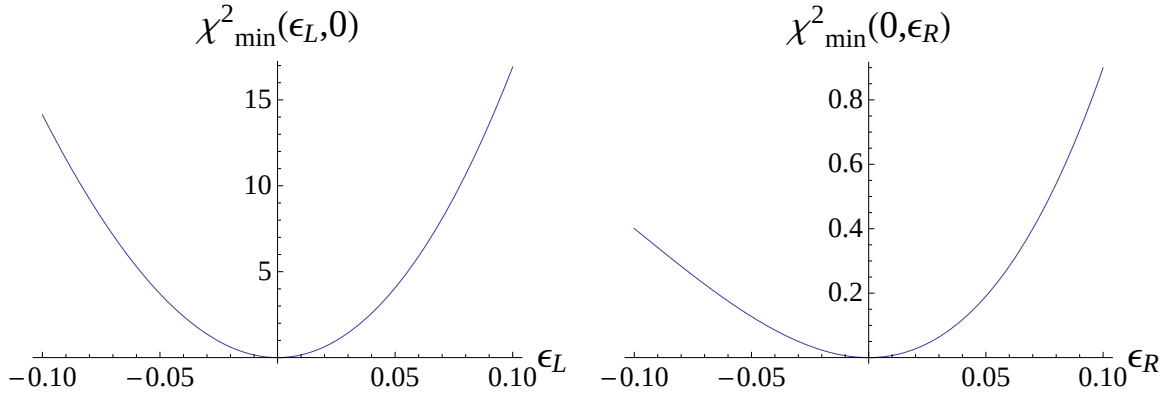

Figure 6.17: Cut of the two-dimensional χ^2 in the ϵ_L (left) and ϵ_R (right) directions with one year data, assuming the other parameter to be zero and for a 5% flux uncertainty.

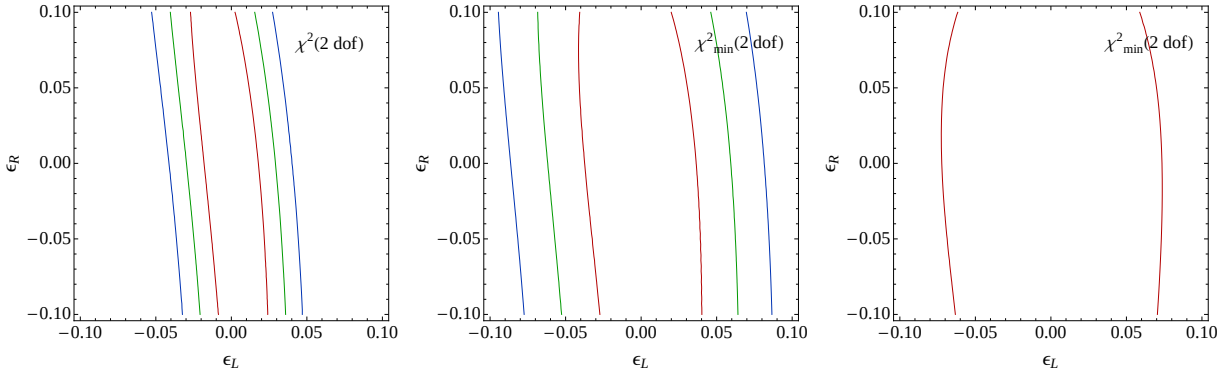

(a) χ^2 contour with one year exposure.

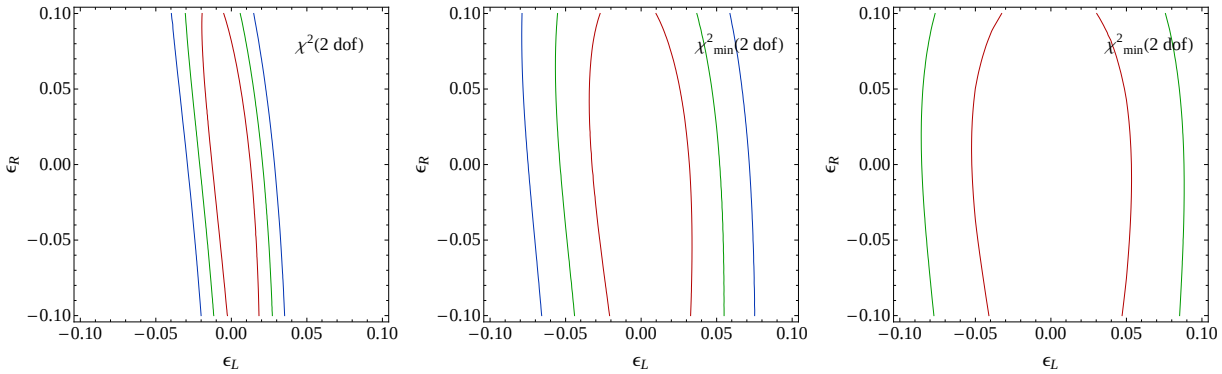

(b) χ^2 contour with two years exposure.

Figure 6.18: $\Delta\chi^2$ contours at 1,2 and 3σ (2 d.o.f.) in the (ϵ_L,ϵ_R) plane, after one year of exposure (upper panel) and two year exposure (lower panel). The systematic uncertainty is assumed to be $0, 5\%, 30\%$ over the flux from left column to right column respectively.

Chapter 7

Constraining Neutrino Non-standard Interaction with Long Baseline Oscillation Experiments

In this chapter, we study the neutrino matter effect in the presence of non-zero $\varepsilon_{\mu\tau}$ NSI. In particular, we parametrize the Hamiltonian with a matter potential in the same form as the vacuum Hamiltonian, by changing of the vacuum parameters into running parameters that are functions of the matter parameter a. In this approach, we get a better understanding of the effect of the NSI, and the degeneracy with the standard oscillation parameters.

7.1 Introduction

In this chapter, we perform an analytical investigation of matter effect on neutrino oscillation in the presence of non-standard interactions (NSI's) of the form

$$\mathcal{L}_{\text{NC}-\text{NSI}} \;=\; -\sum_{\alpha\beta f} 2\sqrt{2} G_F \varepsilon^{fC}_{\alpha\beta} \big(\overline{\nu_\alpha}\gamma^\mu P_L \nu_\beta\big)\big(\overline{f}\gamma_\mu P_C f\big)\;, \tag{7.1}$$

where the subscripts $\alpha, \beta = e, \mu, \tau$ label the neutrino flavor, $f = e, u, d$ indicates the matter fermions, $C = L, R$ denotes the chirality of the ff current, and $\varepsilon^{fC}_{\alpha\beta}$ are dimensionless quantities which parametrize the strengths of the interactions relative to the Fermi constant G_F. Hermiticity of the interaction demands

$$\varepsilon^{fC}_{\beta\alpha} \;=\; (\varepsilon^{fC}_{\alpha\beta})^*\;. \tag{7.2}$$

For neutrino propagation through matter, the relevant combinations are

$$\varepsilon_{\alpha\beta} \;\equiv\; \sum_{f=e,u,d} \varepsilon^{f}_{\alpha\beta} \frac{N_f}{N_e} \;\equiv\; \sum_{f=e,u,d} \left(\varepsilon^{fL}_{\alpha\beta} + \varepsilon^{fR}_{\alpha\beta}\right) \frac{N_f}{N_e}\;, \tag{7.3}$$

where N_f denotes the density of fermion f. These combinations enter into the effective Hamiltonian governing the propagation of neutrinos through matter as

$$H \;=\; \frac{1}{2E}\left(U \begin{bmatrix} m_1^2 & 0 & 0 \\ 0 & m_2^2 & 0 \\ 0 & 0 & m_3^2 \end{bmatrix} U^\dagger + a \begin{bmatrix} 1+\varepsilon_{ee} & \varepsilon_{e\mu} & \varepsilon_{e\tau} \\ \varepsilon_{e\mu}^* & \varepsilon_{\mu\mu} & \varepsilon_{\mu\tau} \\ \varepsilon_{e\tau}^* & \varepsilon_{\mu\tau}^* & \varepsilon_{\tau\tau} \end{bmatrix} \right) \;, \tag{7.4}$$

where U is the vacuum Pontecorvo-Maki-Nakagawa-Sakata (PMNS) matrix [429–431], $a = 2\sqrt{2}G_F N_e E$ is the matter-effect parameter, N_e is the electron density, and E is the neutrino energy. In the Earth, we assume $N_n \approx N_p = N_e$, in which case $N_u \approx N_d \approx 3N_e$. Therefore,

$$\varepsilon_{\alpha\beta} \;=\; \varepsilon_{\alpha\beta}^{\oplus} \;\approx\; \varepsilon_{\alpha\beta}^{e} + 3\,\varepsilon_{\alpha\beta}^{u} + 3\,\varepsilon_{\alpha\beta}^{d} \;, \tag{7.5}$$

and[1]

$$a \;=\; 2\sqrt{2}G_F N_e E \;=\; 7.63\times 10^{-5}(\mathrm{eV}^2)\left(\frac{\rho}{\mathrm{g/cm}^3}\right)\left(\frac{E}{\mathrm{GeV}}\right) \;. \tag{7.6}$$

In Ref. [432], the off-diagonal terms of the above matter-effect matrix are set to zero, and the effect of lepton-flavor diagonal NSI's is studied, *i.e.* all matrix elements of Eq. (7.4) are set to zero except for ε_{ee}, $\varepsilon_{\mu\mu}$, and $\varepsilon_{\tau\tau}$. In this chapter, we look at the effect of flavor off-diagonal NSI's, in particular, the case in which only $\varepsilon_{\mu\tau}$ is allowed to deviate from zero. The cases of non-zero $\varepsilon_{e\mu}$ and $\varepsilon_{e\tau}$ will be discussed in a separate paper [399]. We adopt the approach in which the matter effect is absorbed into the "running" of the effective oscillation parameters (mass-squared differences, mixing angles, and CP violating phase) with the parameter $a = 2\sqrt{2}G_F N_e E$ [432–438]. The approximate analytical expressions for the a-dependent effective oscillation parameters are derived using the Jacobi method [439], as demonstrated in Refs. [432, 437, 438]. The oscillation probabilities in matter can then be obtained by simply replacing the vacuum-oscillation parameters in the expressions for the corresponding probabilities with their respective in-matter counterparts. The resulting expressions simplify considerably in certain ranges of a as the result of the "running" of the oscillation parameters, facilitating the analysis of NSI effects.

This chapter is organized as follows. In section 7.2, we review the current experimental bounds on $\varepsilon_{\mu\tau}$ and point out that the phase of $\varepsilon_{\mu\tau}$ has heretofore not been the focus of much attention. The theoretical expectation on the possible size of $\varepsilon_{\mu\tau}$ is also discussed. In section 7.3, we present the derivation of our approximate expressions using the Jacobi method and then compare the resulting approximation to the oscillation probabilities for constant density matter with numerical calculations, and the approximation of Asano and Minakata [5]. The approximation for the anti-neutrino case is presented in section 7.4. We verify our approximation formula in section 7.5. We conclude in section 7.6 with a summary and outlook for future study.

[1]This formula for a here assumes $N_e = \rho/2m_N$ where m_N is the average nucleon mass.

7.2 Current Experimental Bound and Theoretical Expectation

7.2.1 Experimental Bound

Bounds on the parameters $\varepsilon_{\mu\tau}^{fC}$ ($f = e, u, d$, $C = L, R$) have been placed by a variety of experiments as analyzed and reviewed in Refs. [440–444]. The data used include those on $\nu_\mu e$ scattering from CHARM II [445, 446], $\nu_\mu q$ scattering from NuTeV [447–449], $e^+e^- \to \nu\bar{\nu}\gamma$ from the LEP experiments ALEPH [450–452], L3 [453–455] OPAL [456–459], and DELPHI [460], and neutrino oscillation data from Super-Kamiokande [461], MACRO [462], KamLAND [463], SNO [464], MINOS [465], and IceCube DeepCore [466, 467].

Ref. [442] combines the bounds on $\varepsilon_{\mu\tau}^{fC}$ from various analyses to derive the 90% C.L. bound of

$$|\varepsilon_{\mu\tau}| \ < \ 0.33 \, . \tag{7.7}$$

Refs. [468–470], in turn, place bounds on $\varepsilon_{\mu\tau}$ directly by looking at the matter effect on neutrino oscillation. In Ref. [468], a 3σ bound of

$$-\, 0.03 \ \leq \ \varepsilon_{\mu\tau}^{d} \ \leq \ 0.02 \, , \tag{7.8}$$

is obtained from the atmospheric neutrino data assuming that only the NSI with the d-quarks in Earth matter exist. This result can be reinterpreted as the 90% C.L. bound of

$$-\, 0.05 \ \leq \ \varepsilon_{\mu\tau} \ \leq \ 0.03 \, . \tag{7.9}$$

In that analysis, $\varepsilon_{\mu\tau}$ was assumed to be real and no phase seems to have been considered. The analysis of Ref. [469] allows $\varepsilon_{\mu\tau}$ to be complex but marginalizes over its phase to obtain the 90% C.L. bound of

$$|\varepsilon_{\mu\tau}| \ \leq \ 0.035 \, . \tag{7.10}$$

Ref. [470] uses the high energy neutrino data ($E > 20\,\text{GeV}$) from IceCube DeepCore to place the 90% C.L.

$$|\varepsilon_{\mu\tau}| \ \leq \ 0.006 \, . \tag{7.11}$$

Bounds direct from experimental collaborations include that from Super-Kamiokande [461] which reports

$$|\varepsilon_{\mu\tau}| \ \leq \ 0.011 \, , \tag{7.12}$$

and MINOS [465] which reports

$$-\, 0.20 \ < \ \varepsilon_{\mu\tau} \ < \ 0.07 \, . \tag{7.13}$$

While these results suggest a 90% C.L. upper bound on $|\varepsilon_{\mu\tau}|$ of $\mathcal{O}(0.01)$, we will show later that this bound could be highly sensitive to the phase of $\varepsilon_{\mu\tau}$. Since all the above analyses have either assumed $\varepsilon_{\mu\tau}$ to be real or marginalized the bound over its phase, the actual bound on $|\varepsilon_{\mu\tau}|$ for particular choices of phase could be much larger. With this caveat in mind, we allow $|\varepsilon_{\mu\tau}|$ to be as large as $\mathcal{O}(0.1)$ in the following.

7.2.2 Theoretical Considerations

Another caveat one should keep in mind is that, if one attempts to generate the $\varepsilon_{\mu\tau}$ NSI from an $SU(2)_L \times U(1)_Y$ gauge invariant interaction, stringent bounds will be introduced from existing data involving the charged-leptons. For instance, if the interaction

$$\mathcal{L} \;=\; -2\sqrt{2}G_F\varepsilon^{eL}_{\mu\tau}\big(\overline{\nu_\mu}\gamma^\mu P_L\nu_\tau\big)\big(\overline{e}\gamma_\mu P_L e\big) \tag{7.14}$$

arose as part of the interaction

$$\begin{aligned}&\big(\overline{L_\mu}\gamma^\mu L_\tau\big)\big(\overline{L_e}\gamma_\mu L_e\big)\\ &= \Big[\big(\overline{\nu_{\mu L}}\gamma^\mu\nu_{\tau L}\big)\big(\overline{\nu_{eL}}\gamma_\mu\nu_{eL}\big) + \big(\overline{\nu_{\mu L}}\gamma^\mu\nu_{\tau L}\big)\big(\overline{e_L}\gamma_\mu e_L\big)\\ &\qquad +\big(\overline{\mu_L}\gamma_\mu\tau_L\big)\big(\overline{\nu_{eL}}\gamma^\mu\nu_{eL}\big) + \big(\overline{\mu_L}\gamma^\mu\tau_L\big)\big(\overline{e_L}\gamma_\mu e_L\big)\Big]\;,\end{aligned} \tag{7.15}$$

where

$$L_\alpha \;=\; \begin{bmatrix}\nu_{\alpha L}\\ \ell_{\alpha L}\end{bmatrix}\;, \qquad \ell_e = e\;,\;\; \ell_\mu = \mu\;,\;\; \ell_\tau = \tau\;, \tag{7.16}$$

then the strength of this interaction would be constrained by the bounds on the four-charged-lepton processes $\tau \to \mu ee$. According to Ref. [444], the current 90% C.L. bound is $|\varepsilon^{eL}_{\mu\tau}| < 9.9 \times 10^{-5}$.

Alternatively, the same interaction could also arise from an interaction of the form [75, 471]

$$\begin{aligned}&\big(\overline{L_\mu}i\sigma_2 L^c_e\big)\big(\overline{L^c_\tau}i\sigma_2 L_e\big)\\ &= \frac{1}{2}\big(\overline{\nu_\mu}\gamma^\mu P_L\nu_\tau\big)\big(\overline{e}\gamma_\mu P_L e\big) - \frac{1}{2}\big(\overline{\nu_e}\gamma^\mu P_L\nu_\tau\big)\big(\overline{\mu}\gamma_\mu P_L e\big)\\ &\quad -\frac{1}{2}\big(\overline{\nu_\mu}\gamma^\mu P_L\nu_e\big)\big(\overline{e}\gamma_\mu P_L\tau\big) + \frac{1}{2}\big(\overline{\nu_e}\gamma^\mu P_L\nu_e\big)\big(\overline{\mu}\gamma_\mu P_L\tau\big)\;.\end{aligned} \tag{7.17}$$

The three extra terms lead, respectively, to the processes $\mu \to e\nu_e\nu_\tau$, $\tau \to e\nu_e\nu_\mu$, and $\tau \to \mu\nu_e\nu_e$, which add incoherently to the SM lepton-flavor conserving processes $\mu \to e\nu_e\nu_\mu$, $\tau \to e\nu_e\nu_\tau$, and $\tau \to \mu\nu_\mu\nu_\tau$. The current 90% C.L. bound from μ and τ decay is $|\varepsilon^{eL}_{\mu\tau}| < 1.9 \times 10^{-3}$ [471]. Note also that the extra interactions in Eq. (7.17) will give rise to NSI's at the source and detector.

Thus, while the actual bound on $|\varepsilon^{eL}_{\mu\tau}|$ will depend strongly on the underlying interaction, the NSI is generically more stringently bound by orders of magnitude compared to current direct experimental bounds. So we should be mindful of the possibility that $|\varepsilon^{eL}_{\mu\tau}|$, and consequently $|\varepsilon_{\mu\tau}|$, is actually of order 10^{-3} or smaller.

7.3 Effective Mixing Angles and Effective Mass-Squared Differences – Neutrino Case

We now derive our approximate expressions for the "running" effective oscillation parameters in the presence of $\varepsilon_{\mu\tau}$ utilizing the Jacobi method [439]. The process follows closely

Parameter	Best-fit Value & 1σ Range	Benchmark Value
δm^2_{21}	$(7.50 \pm 0.185) \times 10^{-5}$ eV^2	7.50×10^{-5} eV^2
δm^2_{31}	$(2.47^{+0.069}_{-0.067}) \times 10^{-3}$ eV^2	2.47×10^{-3} eV^2
$\sin^2\theta_{23}$	$0.41^{+0.037}_{-0.025} \oplus 0.59^{+0.021}_{-0.022}$	0.41
$\theta_{23}/^\circ$	$40.0^{+2.1}_{-1.5} \oplus 50.4^{+1.2}_{-1.3}$	
θ_{23}/rad	$0.698^{+0.037}_{-0.026} \oplus 0.880^{+0.021}_{-0.023}$	
$\sin^2\theta_{12}$	0.30 ± 0.013	0.30
$\theta_{12}/^\circ$	33.3 ± 0.8	
θ_{12}/rad	0.580 ± 0.014	
$\sin^2\theta_{13}$	0.023 ± 0.0023	0.023
$\theta_{13}/^\circ$	$8.6^{+0.44}_{-0.46}$	
θ_{13}/rad	0.15 ± 0.01	
$\delta/^\circ$	300^{+66}_{-138}	0
δ/π	$1.67^{+0.37}_{-0.77}$	

Table 7.1: Second column shows the best-fit values and 1σ uncertainties on the oscillation parameters, taken from Ref. [9]. We use the values listed in the third column as benchmark values for which we calculate our oscillation probabilities in this work.

that already presented in Refs. [432, 437, 438], so the reader is requested to refer to those publications for further details.

When presenting graphs showing how our effective parameters run with a, we find it convenient to introduce the log-scale variable

$$\beta \;=\; -\log_\epsilon \frac{a}{|\delta m^2_{31}|}\;, \tag{7.18}$$

where

$$\epsilon \;=\; \sqrt{\frac{\delta m^2_{21}}{|\delta m^2_{31}|}} \;\approx\; 0.17\;. \tag{7.19}$$

Note that we are using a different ϵ here to distinguish from the NSI's. $\beta = -2$ corresponds to $a = \delta m^2_{21}$, while $\beta = 0$ corresponds to $a = |\delta m^2_{31}|$. Instead of plotting the dependence on a, we will plot the dependence on β. We also use ϵ as an order parameter for the Jacobi method. When all the rotation angles necessary to diagonalize a matrix further is $\mathcal{O}(\epsilon^3)$ or smaller, we consider the matrix approximately diagonal. For the vacuum values of the oscillation parameters that are necessary as input, we use the numbers listed in the third column of Table 7.1 as benchmark values. Note that at these benchmark values $\theta_{13} = \mathcal{O}(\epsilon)$, and $\cos(2\theta_{23}) = \mathcal{O}(\epsilon)$. We will also assume $|\varepsilon_{\mu\tau}| = \mathcal{O}(\epsilon^2) = \mathcal{O}(0.03)$ in the derivation of our formulae, but allow it to be as large as 0.1 in our plots with the caveat mentioned in section 2 in mind, and also to magnify its effects to make them visible. We allow the phase of $\varepsilon_{\mu\tau}$ to be arbitrary.

7.3.1 Setup of the Problem

Let us write

$$\varepsilon_{\mu\tau} \;=\; |\varepsilon_{\mu\tau}|\, e^{i\omega} \;\equiv\; \varepsilon\, e^{i\omega}\;. \tag{7.20}$$

In the presence of $\varepsilon_{\mu\tau}$, the effective Hamiltonian (times $2E$) for neutrino propagation in Earth matter in the flavor-eigenbasis is given by

$$H_{\mu\tau} \;=\; \tilde{U} \begin{bmatrix} \lambda_1 & 0 & 0 \\ 0 & \lambda_2 & 0 \\ 0 & 0 & \lambda_3 \end{bmatrix} \tilde{U}^\dagger \;=\; \underbrace{U \begin{bmatrix} 0 & 0 & 0 \\ 0 & \delta m^2_{21} & 0 \\ 0 & 0 & \delta m^2_{31} \end{bmatrix} U^\dagger + a \underbrace{\begin{bmatrix} 1 & 0 & 0 \\ 0 & 0 & 0 \\ 0 & 0 & 0 \end{bmatrix}}_{\equiv\, M_a}}_{\equiv\, H_a} + a\varepsilon \underbrace{\begin{bmatrix} 0 & 0 & 0 \\ 0 & 0 & e^{i\omega} \\ 0 & e^{-i\omega} & 0 \end{bmatrix}}_{\equiv\, M_{\mu\tau}}\;. \tag{7.21}$$

The problem is to find the diagonalization matrix $\tilde{U}$, and the eigenvalues λ_i $(i = 1, 2, 3)$.

In the previous paper dealing with flavor-diagonal NSI's [432], the Standard Model part H_a is diagonalized with two Jacobi rotations first, and then the NSI part is tacked on, which is diagonalized by a third Jacobi rotation. While it is possible to take a similar approach here, we elect to perform a slightly more sophisticated procedure in which $M_{\mu\tau}$ is separated into two parts, one of which is diagonalized together with H_a, and the other which is tacked on later to be diagonalized by further rotations. This separation of $M_{\mu\tau}$ into two parts is as follows:

$$\begin{aligned} M_{\mu\tau} \;&=\; c_\omega \begin{bmatrix} 0 & 0 & 0 \\ 0 & 0 & 1 \\ 0 & 1 & 0 \end{bmatrix} + s_\omega \begin{bmatrix} 0 & 0 & 0 \\ 0 & 0 & i \\ 0 & -i & 0 \end{bmatrix} \\ &=\; \underbrace{c_\omega \sin(2\theta_{23}) \begin{bmatrix} 0 & 0 & 0 \\ 0 & -\cos(2\theta_{23}) & \sin(2\theta_{23}) \\ 0 & \sin(2\theta_{23}) & \cos(2\theta_{23}) \end{bmatrix}}_{\equiv\, M^c_{\mu\tau}} \\ &\quad \underbrace{+\, c_\omega \cos(2\theta_{23}) \begin{bmatrix} 0 & 0 & 0 \\ 0 & \sin(2\theta_{23}) & \cos(2\theta_{23}) \\ 0 & \cos(2\theta_{23}) & -\sin(2\theta_{23}) \end{bmatrix} + s_\omega \begin{bmatrix} 0 & 0 & 0 \\ 0 & 0 & i \\ 0 & -i & 0 \end{bmatrix}}_{\equiv\, M^s_{\mu\tau}}\;, \end{aligned} \tag{7.22}$$

where $c_\omega = \cos\omega$ and $s_\omega = \sin\omega$. In the following, we diagonalize $H_a + a\varepsilon M^c_{\mu\tau}$ first, and then deal with $M^s_{\mu\tau}$ later. Note that when $\theta_{23} = \pi/4$, we have $\sin(2\theta_{23}) = 1$ and $\cos(2\theta_{23}) = 0$. Therefore, in that limit

$$M^c_{\mu\tau} \;=\; c_\omega \begin{bmatrix} 0 & 0 & 0 \\ 0 & 0 & 1 \\ 0 & 1 & 0 \end{bmatrix}\;, \qquad M^s_{\mu\tau} \;=\; s_\omega \begin{bmatrix} 0 & 0 & 0 \\ 0 & 0 & i \\ 0 & -i & 0 \end{bmatrix}\;. \tag{7.23}$$

In particular, if $\omega = 0$ or π, we have

$$M^c_{\mu\tau} \;=\; \pm \begin{bmatrix} 0 & 0 & 0 \\ 0 & 0 & 1 \\ 0 & 1 & 0 \end{bmatrix} \;, \qquad M^s_{\mu\tau} \;=\; 0 \;. \tag{7.24}$$

7.3.2 Diagonalization of the Effective Hamiltonian

Review of SM case

We begin with a brief recap of the $\varepsilon = 0$ case discussed in Refs. [437, 438]. Define

$$V \;\equiv\; \begin{bmatrix} c_\varphi & s_\varphi & 0 \\ -s_\varphi & c_\varphi & 0 \\ 0 & 0 & 1 \end{bmatrix} , \quad W \;\equiv\; \begin{bmatrix} 1 & 0 & 0 \\ 0 & c_\phi & s_\phi \\ 0 & -s_\phi & c_\phi \end{bmatrix} , \quad Q_3 \;\equiv\; \begin{bmatrix} 1 & 0 & 0 \\ 0 & 1 & 0 \\ 0 & 0 & e^{i\delta} \end{bmatrix} , \tag{7.25}$$

where

$$\begin{aligned} c_\varphi \;&=\; \cos\varphi \,, \quad s_\varphi \;=\; \sin\varphi \,, \quad \tan 2\varphi \;\equiv\; \frac{a c_{13}^2 \sin(2\theta_{12})}{\delta m^2_{21} - a c^2_{13}\cos(2\theta_{12})} \,, \quad \left(0 \le \varphi \le \frac{\pi}{2} - \theta_{12}\right) \,, \\ c_\phi \;&=\; \cos\phi \,, \quad s_\phi \;=\; \sin\phi \,, \quad \tan 2\phi \;\equiv\; \frac{a \sin(2\theta_{13})}{(\delta m^2_{31} - s^2_{12}\delta m^2_{21}) - a\cos(2\theta_{13})} \,. \end{aligned} \tag{7.26}$$

As demonstrated in Ref. [437, 438],

$$\begin{aligned} H'''_a \;&=\; W^\dagger V^\dagger Q_3^\dagger U^\dagger H_a U Q_3 V W \\ &=\; \begin{bmatrix} \lambda'_- & -a c'_{12} c_{13} s_{13} s_\phi & a c'_{12} c_{13} s_{13} c_\phi \\ -a c'_{12} c_{13} s_{13} s_\phi & \lambda''_\mp & 0 \\ a c'_{12} c_{13} s_{13} c_\phi & 0 & \lambda''_\pm \end{bmatrix} , \end{aligned} \tag{7.27}$$

where the upper (lower) sign corresponds to normal (inverted) hierarchy, with

$$\begin{aligned} \lambda'_\pm \;&\equiv\; \frac{(a c^2_{13} + \delta m^2_{21}) \pm \sqrt{(a c^2_{13} - \delta m^2_{21})^2 + 4 a c^2_{13} s^2_{12} \delta m^2_{21}}}{2} \,, \\ \lambda''_\pm \;&\equiv\; \frac{[\lambda'_+ + (\delta m^2_{31} + a s^2_{13})] \pm \sqrt{[\lambda'_+ - (\delta m^2_{31} + a s^2_{13})]^2 + 4 (a s'_{12} c_{13} s_{13})^2}}{2} \,, \end{aligned} \tag{7.28}$$

and $s'_{12} = \sin\theta'_{12}$, $c'_{12} = \cos\theta'_{12}$, $\theta'_{12} = \theta_{12} + \varphi$. The off-diagonal elements of H'''_a in Eq. (7.27) can be shown to be $|\delta m^2_{31}| \mathcal{O}(\epsilon^3)$, which is negligibly small and H'''_a can be considered approximately diagonal.

The corresponding effective mixing matrix is then $\tilde{U} = U Q_3 V W$ and can be approximated by absorbing the extra rotations into the "running" parameters $\theta'_{12} = \theta_{12} + \varphi$ and $\theta'_{13} = \theta_{13} + \phi$:

$$\tilde{U} \approx R_{23}(\theta_{23}, 0) Q_3 R_{13}(\theta'_{13}, 0) R_{12}(\theta'_{12}, 0) = R_{23}(\theta_{23}, 0) R_{13}(\theta'_{13}, \delta) R_{12}(\theta'_{12}, 0) Q_3 \;, \tag{7.29}$$

where θ'_{12} and θ'_{13} can be calculated directly via

$$\begin{aligned}\tan 2\theta'_{12} &= \frac{\delta m^2_{21}\sin 2\theta_{12}}{\delta m^2_{21}\cos 2\theta_{12} - ac^2_{13}}\,, \qquad \left(\theta_{12} \le \theta'_{12} \le \frac{\pi}{2}\right)\,,\\ \tan 2\theta'_{13} &= \frac{(\delta m^2_{31} - \delta m^2_{21}s^2_{12})\sin 2\theta_{13}}{(\delta m^2_{31} - \delta m^2_{21}s^2_{12})\cos 2\theta_{13} - a}\,. \end{aligned} \tag{7.30}$$

In Eq. (7.29), the expression $R_{ij}(\theta,\delta)$ denotes an ij-rotation matrix such that its ij submatrix is of the form

$$\begin{bmatrix} \cos\theta & \sin\theta\, e^{-i\delta} \\ -\sin\theta\, e^{i\delta} & \cos\theta \end{bmatrix}\,. \tag{7.31}$$

Note the signs of the off-diagonal sines and those of the phases in the exponents.

Change to the Mass Eigenbasis in Vacuum

Let us now look at the $\varepsilon \neq 0$ case. We begin by partially diagonalizing $H_{\mu\tau} = H_a + a\varepsilon(M^c_{\mu\tau} + M^s_{\mu\tau})$ by going from the flavor-eigenbasis to the vacuum-mass-eigenbasis:

$$\begin{aligned} H'_{\mu\tau} &= Q_3^\dagger U^\dagger H_{\mu\tau} U Q_3 \\ &= \underbrace{\begin{bmatrix} 0 & 0 & 0 \\ 0 & \delta m^2_{21} & 0 \\ 0 & 0 & \delta m^2_{31} \end{bmatrix} + a\, Q_3^\dagger U^\dagger \underbrace{\begin{bmatrix} 1 & 0 & 0 \\ 0 & 0 & 0 \\ 0 & 0 & 0 \end{bmatrix}}_{M_a} U Q_3}_{\equiv M'_a} + a\varepsilon\, Q_3^\dagger U^\dagger \underbrace{\begin{bmatrix} 0 & 0 & 0 \\ 0 & 0 & e^{i\omega} \\ 0 & e^{-i\omega} & 0 \end{bmatrix}}_{M^c_{\mu\tau} + M^s_{\mu\tau}} U Q_3\,. \end{aligned} \tag{7.32}$$

Note that the matrix Q_3 introduced in Eq. (7.25) allows us to write

$$\begin{aligned} UQ_3 &= R_{23}(\theta_{23},0) R_{13}(\theta_{13},\delta) R_{12}(\theta_{12},0) Q_3 \\ &= R_{23}(\theta_{23},0) Q_3 R_{13}(\theta_{13},0) R_{12}(\theta_{12},0)\,. \end{aligned} \tag{7.33}$$

Given that the lower-right 2×2 block of M_a is zero, it is straightforward to see that M'_a only depends on θ_{12} and θ_{13}, and is given by

$$M'_a \;=\; Q_3^\dagger U^\dagger M_a U Q_3 \;=\; \begin{bmatrix} c^2_{12}c^2_{13} & s_{12}c_{12}c^2_{13} & c_{12}s_{13}c_{13} \\ s_{12}c_{12}c^2_{13} & s^2_{12}c^2_{13} & s_{12}s_{13}c_{13} \\ c_{12}s_{13}c_{13} & s_{12}s_{13}c_{13} & s^2_{13} \end{bmatrix}\,. \tag{7.34}$$

Looking at how $M^c_{\mu\tau}$ and $M^s_{\mu\tau}$ transform, after the first 23-rotation we find

$$R^\dagger_{23}(\theta_{23},0) M^c_{\mu\tau} R_{23}(\theta_{23},0) \;=\; \begin{bmatrix} 0 & 0 & 0 \\ 0 & -c_\omega \sin(2\theta_{23}) & 0 \\ 0 & 0 & c_\omega \sin(2\theta_{23}) \end{bmatrix}\,,$$

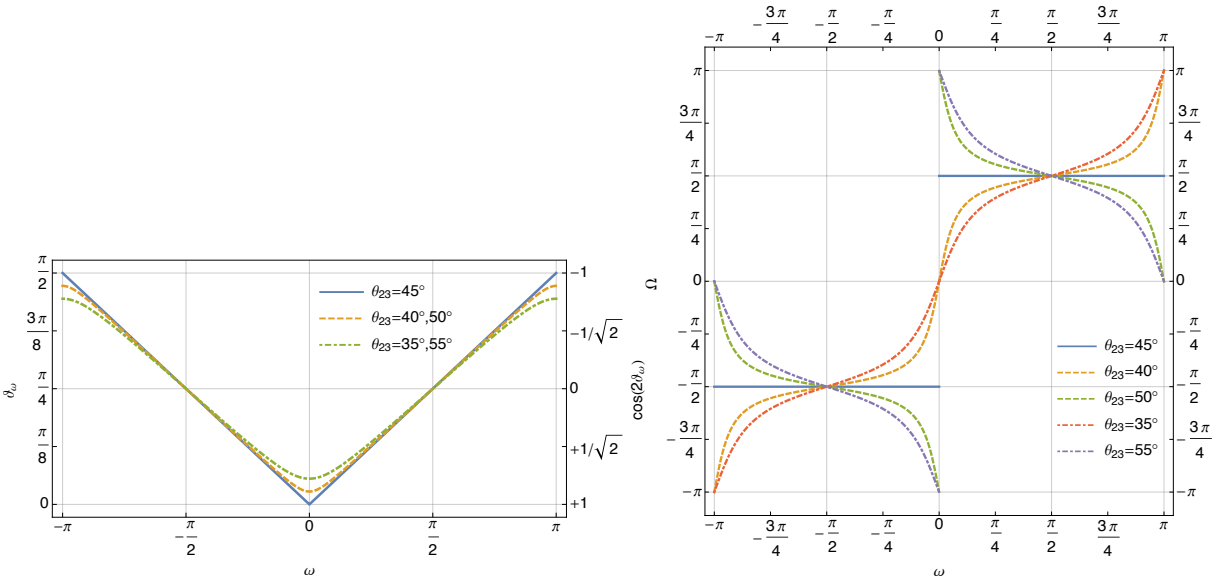

(a) (b)

Figure 7.1: The ω-dependence of (a) ϑ_ω and (b) Ω.

$$R_{23}^\dagger(\theta_{23},0)M_{\mu\tau}^s R_{23}(\theta_{23},0) \;=\; \begin{bmatrix} 0 & 0 & 0 \\ 0 & 0 & c_\omega\cos(2\theta_{23}) + is_\omega \\ 0 & c_\omega\cos(2\theta_{23}) - is_\omega & 0 \end{bmatrix} . \quad (7.35)$$

We find it convenient to define[2]

$$c_\omega \sin(2\theta_{23}) \;=\; \cos(2\vartheta_\omega)\,, \qquad \left[c_\omega\cos(2\theta_{23}) + is_\omega\right] \;=\; e^{i\Omega}\sin(2\vartheta_\omega)\,. \quad (7.36)$$

Choosing ϑ_ω and Ω in the ranges

$$0 \;\le\; \vartheta_\omega \;\le\; \frac{\pi}{2}\,, \qquad -\pi \;<\; \Omega \;\le\; \pi\,, \quad (7.37)$$

we obtain

$$\tan(2\vartheta_\omega) \;\equiv\; \frac{\sqrt{c_\omega^2\cos^2(2\theta_{23}) + s_\omega^2}}{c_\omega\sin(2\theta_{23})}\,, \qquad \Omega \;\equiv\; \arctan\left[\frac{s_\omega}{\cos(2\theta_{23})c_\omega}\right] . \quad (7.38)$$

The ω-dependence of ϑ_ω and Ω is shown in Fig. 7.1 for several values of θ_{23}. Note that due to our restriction $\Omega \in (-\pi,\pi]$, Ω has a discontinuity of 2π at $\omega = 0$ if $\frac{\pi}{4} < \theta_{23} \le \frac{\pi}{2}$, and at $\omega = \pm\pi$ if $0 \le \theta_{23} < \frac{\pi}{4}$. For the $\theta_{23} = \frac{\pi}{4}$ case, $\Omega = +\frac{\pi}{2}$, $\vartheta_\omega = +\frac{\omega}{2}$ in the range $0 < \omega < \frac{\pi}{2}$, $\Omega = -\frac{\pi}{2}$, $\vartheta_\omega = -\frac{\omega}{2}$ in the range $-\frac{\pi}{2} < \omega < 0$, while at $\omega = 0, \pm\pi$, Ω is indeterminate.

[2]Our notation corresponds to those in Ref. [5] via $\tilde{\varepsilon}_{\tau\tau} = \varepsilon\cos(2\vartheta_\omega)$, $|\tilde{\varepsilon}_{\mu\tau}| = \varepsilon\sin(2\vartheta_\omega)$, and $\tilde{\phi}_{\mu\tau} = \Omega$.

Note also that if $\omega = \pm\frac{\pi}{2}$, that is, $\varepsilon_{\mu\tau}$ is purely imaginary, then $\cos(2\vartheta_\omega) = c_\omega \sin(2\theta_{23}) = 0$. These definitions allow us to write

$$\begin{aligned} R_{23}^\dagger(\theta_{23},0) M^c_{\mu\tau} R_{23}(\theta_{23},0) &= \cos(2\vartheta_\omega) \begin{bmatrix} 0 & 0 & 0 \\ 0 & -1 & 0 \\ 0 & 0 & 1 \end{bmatrix} , \\ R_{23}^\dagger(\theta_{23},0) M^s_{\mu\tau} R_{23}(\theta_{23},0) &= \sin(2\vartheta_\omega) \begin{bmatrix} 0 & 0 & 0 \\ 0 & 0 & e^{i\Omega} \\ 0 & e^{-i\Omega} & 0 \end{bmatrix} . \end{aligned} \tag{7.39}$$

Next, we multiply with Q_3 and its conjugate to find

$$\begin{aligned} Q_3^\dagger R_{23}^\dagger(\theta_{23},0) M^c_{\mu\tau} R_{23}(\theta_{23},0) Q_3 &= \cos(2\vartheta_\omega) \begin{bmatrix} 0 & 0 & 0 \\ 0 & -1 & 0 \\ 0 & 0 & 1 \end{bmatrix} , \\ Q_3^\dagger R_{23}^\dagger(\theta_{23},0) M^s_{\mu\tau} R_{23}(\theta_{23},0) Q_3 &= \sin(2\vartheta_\omega) \begin{bmatrix} 0 & 0 & 0 \\ 0 & 0 & e^{i(\delta+\Omega)} \\ 0 & e^{-i(\delta+\Omega)} & 0 \end{bmatrix} . \end{aligned} \tag{7.40}$$

From this, we can see that $M^{c\prime}_{\mu\tau} = Q_3^\dagger U^\dagger M^c_{\mu\tau} U Q_3$ will not have any δ dependence, while $M^{s\prime}_{\mu\tau} = Q_3^\dagger U^\dagger M^s_{\mu\tau} U Q_3$ will only depend on the sum $\delta + \Omega$. Performing the remaining two rotations, we obtain

$$\begin{aligned} M^{c\prime}_{\mu\tau} &= Q_3^\dagger U^\dagger M^c_{\mu\tau} U Q_3 \\ &= \cos(2\vartheta_\omega) \begin{bmatrix} -s_{12}^2 + c_{12}^2 s_{13}^2 & s_{12}c_{12}(1+s_{13}^2) & -c_{12}s_{13}c_{13} \\ s_{12}c_{12}(1+s_{13}^2) & -c_{12}^2 + s_{12}^2 s_{13}^2 & -s_{12}s_{13}c_{13} \\ -c_{12}s_{13}c_{13} & -s_{12}s_{13}c_{13} & c_{13}^2 \end{bmatrix} , \\ M^{s\prime}_{\mu\tau} &= Q_3^\dagger U^\dagger M^s_{\mu\tau} U Q_3 \\ &= \sin(2\vartheta_\omega) \begin{bmatrix} 2s_{12}c_{12}s_{13}\cos(\delta+\Omega) & s_{13}e^{i(\delta+\Omega)} - 2c_{12}^2 s_{13}\cos(\delta+\Omega) & -s_{12}c_{13}e^{i(\delta+\Omega)} \\ s_{13}e^{-i(\delta+\Omega)} - 2c_{12}^2 s_{13}\cos(\delta+\Omega) & -2s_{12}c_{12}s_{13}\cos(\delta+\Omega) & c_{12}c_{13}e^{i(\delta+\Omega)} \\ -s_{12}c_{13}e^{-i(\delta+\Omega)} & c_{12}c_{13}e^{-i(\delta+\Omega)} & 0 \end{bmatrix} \\ &= \sin(2\vartheta_\omega)\cos(\delta+\Omega) \begin{bmatrix} s_{13}\sin(2\theta_{12}) & -s_{13}\cos(2\theta_{12}) & -s_{12}c_{13} \\ -s_{13}\cos(2\theta_{12}) & -s_{13}\sin(2\theta_{12}) & c_{12}c_{13} \\ -s_{12}c_{13} & c_{12}c_{13} & 0 \end{bmatrix} \\ &\quad + i\sin(2\vartheta_\omega)\sin(\delta+\Omega) \begin{bmatrix} 0 & s_{13} & -s_{12}c_{13} \\ -s_{13} & 0 & c_{12}c_{13} \\ s_{12}c_{13} & -c_{12}c_{13} & 0 \end{bmatrix} . \end{aligned} \tag{7.41}$$

So in this vacuum-mass-eigenbasis, the Hamiltonian is given by

$$H'_{\mu\tau} = H'_a + a\varepsilon M^{c\prime}_{\mu\tau} + a\varepsilon M^{s\prime}_{\mu\tau}$$

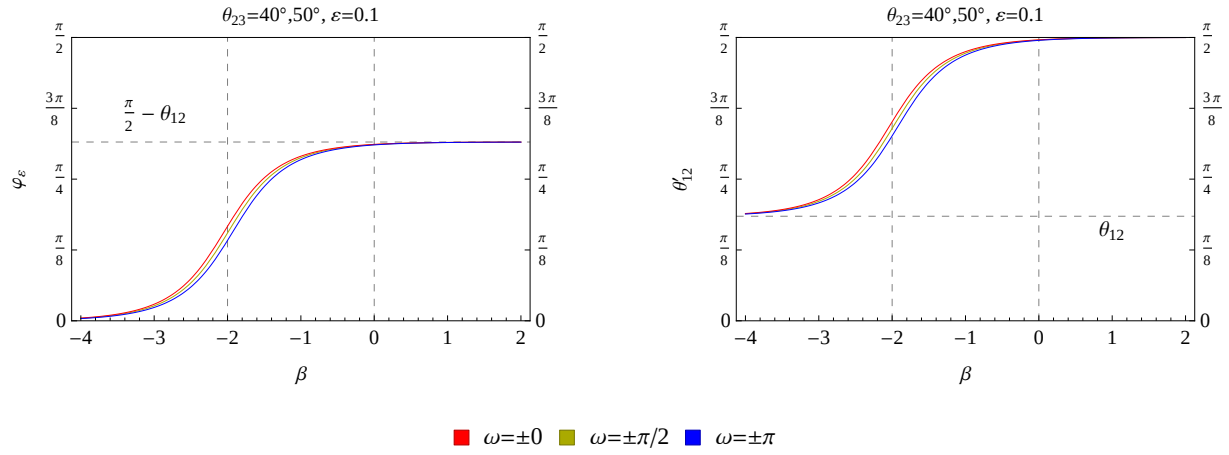

Figure 7.2: The β-dependence of φ_ε (left) and θ'_{12} (right) for the $\varepsilon = 0.1$ case.

$$
\begin{aligned}
&= \begin{bmatrix} a[c_{12}^2c_{13}^2 - \varepsilon_c(s_{12}^2 - c_{12}^2s_{13}^2)] & ac_{12}s_{12}[c_{13}^2 + \varepsilon_c(1+s_{13}^2)] & ac_{12}s_{13}c_{13}(1-\varepsilon_c) \\ ac_{12}s_{12}[c_{13}^2 + \varepsilon_c(1+s_{13}^2)] & \delta m_{21}^2 + a[s_{12}^2c_{13}^2 - \varepsilon_c(c_{12}^2 - s_{12}^2s_{13}^2)] & as_{12}s_{13}c_{13}(1-\varepsilon_c) \\ ac_{12}s_{13}c_{13}(1-\varepsilon_c) & as_{12}s_{13}c_{13}(1-\varepsilon_c) & \delta m_{31}^2 + a(s_{13}^2 + \varepsilon_c c_{13}^2) \end{bmatrix} \\
&\quad + a\varepsilon_s c_{\delta+\Omega} \begin{bmatrix} s_{13}\sin(2\theta_{12}) & -s_{13}\cos(2\theta_{12}) & -s_{12}c_{13} \\ -s_{13}\cos(2\theta_{12}) & -s_{13}\sin(2\theta_{12}) & c_{12}c_{13} \\ -s_{12}c_{13} & c_{12}c_{13} & 0 \end{bmatrix} + ia\varepsilon_s s_{\delta+\Omega} \begin{bmatrix} 0 & s_{13} & -s_{12}c_{13} \\ -s_{13} & 0 & c_{12}c_{13} \\ s_{12}c_{13} & -c_{12}c_{13} & 0 \end{bmatrix} \\
&= \begin{bmatrix} M_{11} & A & B \\ A^\dagger & M_{22} & C \\ B^\dagger & C^\dagger & M_{33} \end{bmatrix},
\end{aligned}
\tag{7.42}
$$

where we have set $\varepsilon_c \equiv \varepsilon\cos(2\vartheta_\omega)$, $\varepsilon_s \equiv \varepsilon\sin(2\vartheta_\omega)$, and

$$
\begin{aligned}
M_{11} &= a[c_{12}^2c_{13}^2 - \varepsilon_c(s_{12}^2 - c_{12}^2s_{13}^2)] + a\varepsilon_s c_{\delta+\Omega}s_{13}\sin(2\theta_{12}), \\
M_{22} &= \delta m_{21}^2 + a[s_{12}^2c_{13}^2 - \varepsilon_c(c_{12}^2 - s_{12}^2s_{13}^2)] - a\varepsilon_s c_{\delta+\Omega}s_{13}\sin(2\theta_{12}), \\
M_{33} &= .\delta m_{31}^2 + a(s_{13}^2 + \varepsilon_c c_{13}^2).
\end{aligned}
\tag{7.43}
$$

We now approximately diagonalize this matrix following the Jacobi diagonalization procedure developed in Refs. [432, 437, 438].

First Rotation

We first perform a 12-rotation to diagonalize the 12 submatrix. The rotation matrix necessary is given by

$$
V_\varepsilon \equiv \begin{bmatrix} c_{\varphi_\varepsilon} & s_{\varphi_\varepsilon} & 0 \\ -s_{\varphi_\varepsilon} & c_{\varphi_\varepsilon} & 0 \\ 0 & 0 & 1 \end{bmatrix},
\tag{7.44}
$$

where $c_{\varphi_\varepsilon} = \cos(\varphi_\varepsilon)$, $s_{\varphi_\varepsilon} = \sin(\varphi_\varepsilon)$, and

$$\tan 2\varphi_\varepsilon \;=\; \frac{a[\{c_{13}^2 + \varepsilon_c(1+s_{13}^2)\}\sin(2\theta_{12})]}{\delta m_{21}^2 - a[\{c_{13}^2 + \varepsilon_c(1+s_{13}^2)\}\cos(2\theta_{12})]}\;. \tag{7.45}$$

Compared to Eq. (7.26), we can see that φ_ϵ evolves more or less similarly to φ but with a small shift in the resonance position. See Fig. 7.2(a). Using V_ε we obtain

$$\begin{aligned} & H_a'' + a\varepsilon M_{\mu\tau}^{c\prime\prime} \\ &= \; V_\varepsilon^\dagger \left(H_a' + a\varepsilon M_{\mu\tau}^{c\prime}\right) V_\varepsilon \\ &= \; \begin{bmatrix} \lambda'_{\varepsilon-} & 0 & ac'_{12}s_{13}c_{13}(1-\varepsilon_c) \\ 0 & \lambda'_{\varepsilon+} & as'_{12}s_{13}c_{13}(1-\varepsilon_c) \\ ac'_{12}s_{13}c_{13}(1-\varepsilon_c) & as'_{12}s_{13}c_{13}(1-\varepsilon_c) & \delta m_{31}^2 + a(s_{13}^2 + \varepsilon_c c_{13}^2) \end{bmatrix}\;, \end{aligned} \tag{7.46}$$

where

$$\begin{aligned} \lambda'_{\varepsilon\pm} \;=\; & \frac{\{(\delta m_{21}^2 - a\varepsilon_c) + a(c_{13}^2 + \varepsilon_c s_{13}^2)\}}{2} \\ & \pm \frac{\sqrt{\{(\delta m_{21}^2 - a\varepsilon_c) - a(c_{13}^2 + \varepsilon_c s_{13}^2)\}^2 + 4as_{12}^2\{c_{13}^2 + \varepsilon_c(1+s_{13}^2)\}\delta m_{21}^2}}{2}\;. \end{aligned} \tag{7.47}$$

and

$$s'_{12} \;=\; \sin\theta'_{12}\;, \qquad c'_{12} \;=\; \cos\theta'_{12}\;, \qquad \theta'_{12} \;\equiv\; \theta_{12} + \varphi_\varepsilon\;. \tag{7.48}$$

The angle θ'_{12}, which is the approximate running θ_{12}, can be calculated directly via

$$\tan 2\theta'_{12} \;=\; \frac{\delta m_{21}^2 \sin 2\theta_{12}}{\delta m_{21}^2 \cos 2\theta_{12} - a[c_{13}^2 + \varepsilon_c(1+s_{13}^2)]}\;. \tag{7.49}$$

Compared to Ref. (7.30), the small correction due to ε_c will lead to a small shift in the solar resonance energy, but the basic a-dependence will be the same. See Fig. 7.2(b).

At small a, the $\lambda'_{\varepsilon\pm}$ behave as

$$\begin{aligned} \lambda'_{\varepsilon+} \;&=\; \delta m_{21}^2 + a\{s_{12}^2 c_{13}^2 - \varepsilon_c(c_{12}^2 - s_{12}^2 s_{13}^2)\} + a\,\mathcal{O}(a/\delta m_{21}^2)\;, \\ \lambda'_{\varepsilon-} \;&=\; a\{c_{12}^2 c_{13}^2 - \varepsilon_c(s_{12}^2 - c_{12}^2 s_{13}^2)\} + a\,\mathcal{O}(a/\delta m_{21}^2)\;, \end{aligned} \tag{7.50}$$

while at large a, we have

$$\begin{aligned} \lambda'_{\varepsilon+} \;&=\; a(c_{13}^2 + \varepsilon_c s_{13}^2) + s_{12}^2\delta m_{21}^2 + \delta m_{21}^2 \mathcal{O}(\delta m_{21}^2/a)\;, \\ \lambda'_{\varepsilon-} \;&=\; -a\varepsilon_c + c_{12}^2\delta m_{21}^2 + \delta m_{21}^2\mathcal{O}(\delta m_{21}^2/a)\;. \end{aligned} \tag{7.51}$$

Compared to the SM case, $\lambda'_{\varepsilon-}$ does not tend asymptotically to a constant except when $\omega = \pm\dfrac{\pi}{2}$, which would render ε_c zero even when $\varepsilon \neq 0$. This behavior is shown in Fig. 7.3.

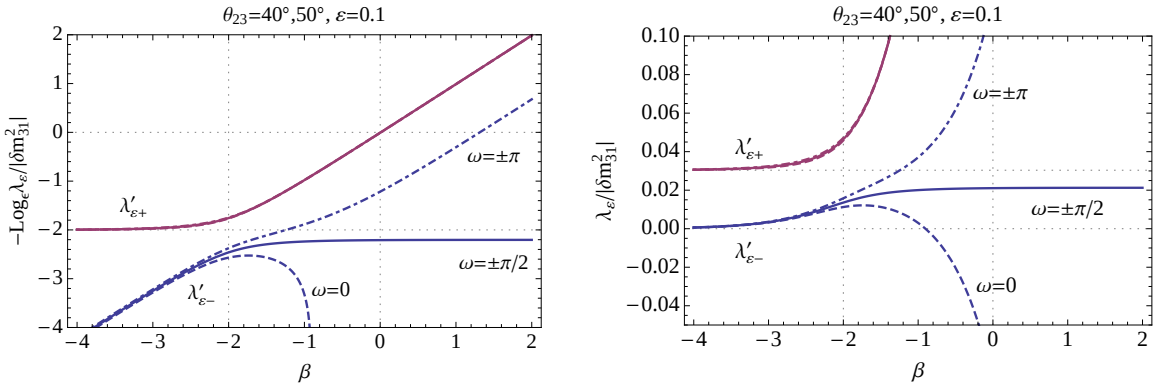

Figure 7.3: The β-dependence of $\lambda'_{\varepsilon\pm}$ for $\theta_{23} = 40°$ and $\varepsilon = 0.1$ with $\omega = 0$ (dashed), $\omega = \pm\dfrac{\pi}{2}$ (solid) and $\omega = \pm\pi$ (dot-dashed) shown in (a) log-scale, and (b) normal scale. The ω-dependence of $\lambda'_{\varepsilon+}$ is weak and the curves for the three cases overlap.

Second Rotation

As a is increased, due to the running of θ'_{12} with a, the product as'_{12} will continue to increase while ac'_{12} stops increasing. Therefore, the (23)-submatrix of $H''_a + a\varepsilon M^{c\prime\prime}_{\mu\tau}$ must be diagonalized next. This requires the rotation matrix

$$W_\varepsilon \;=\; \begin{bmatrix} 1 & 0 & 0 \\ 0 & c_{\phi_\varepsilon} & s_{\phi_\varepsilon} \\ 0 & -s_{\phi_\varepsilon} & c_{\phi_\varepsilon} \end{bmatrix} , \tag{7.52}$$

where $s_{\phi_\varepsilon} = \sin\phi_\varepsilon$, $c_{\phi_\varepsilon} = \cos\phi_\varepsilon$, and

$$\begin{aligned} \tan 2\phi_\varepsilon \;&=\; \frac{as'_{12}(1-\varepsilon_c)\sin(2\theta_{13})}{\delta m^2_{31} + a(s^2_{13} + \varepsilon_c c^2_{13}) - \lambda'_{\varepsilon+}} \\ &\approx\; \frac{a(1-\varepsilon_c)\sin(2\theta_{13})}{(\delta m^2_{31} - s^2_{12}\delta m^2_{21}) - a(1-\varepsilon_c)\cos(2\theta_{13})} \,. \end{aligned} \tag{7.53}$$

Again, compared to Eq. (7.26), we can see that ϕ_ϵ evolves more or less similarly to ϕ but with a small shift in the resonance position. See Fig. 7.4. After the second rotation we have:

$$\begin{aligned} & H'''_a + a\varepsilon M^{c\prime\prime\prime}_{\mu\tau} \\ &= \; W^\dagger_\varepsilon \left(H''_a + a\varepsilon M^{c\prime\prime}_{\mu\tau}\right) W_\varepsilon \\ &= \; \begin{bmatrix} \lambda'_{\varepsilon-} & -ac'_{12}s_{13}c_{13}s_{\phi_\varepsilon}(1-\varepsilon_c) & ac'_{12}s_{13}c_{13}c_{\phi_\varepsilon}(1-\varepsilon_c) \\ -ac'_{12}s_{13}c_{13}s_{\phi_\varepsilon}(1-\varepsilon_c) & \lambda''_{\varepsilon\mp} & 0 \\ ac'_{12}s_{13}c_{13}c_{\phi_\varepsilon}(1-\varepsilon_c) & 0 & \lambda''_{\varepsilon\pm} \end{bmatrix} , \end{aligned} \tag{7.54}$$

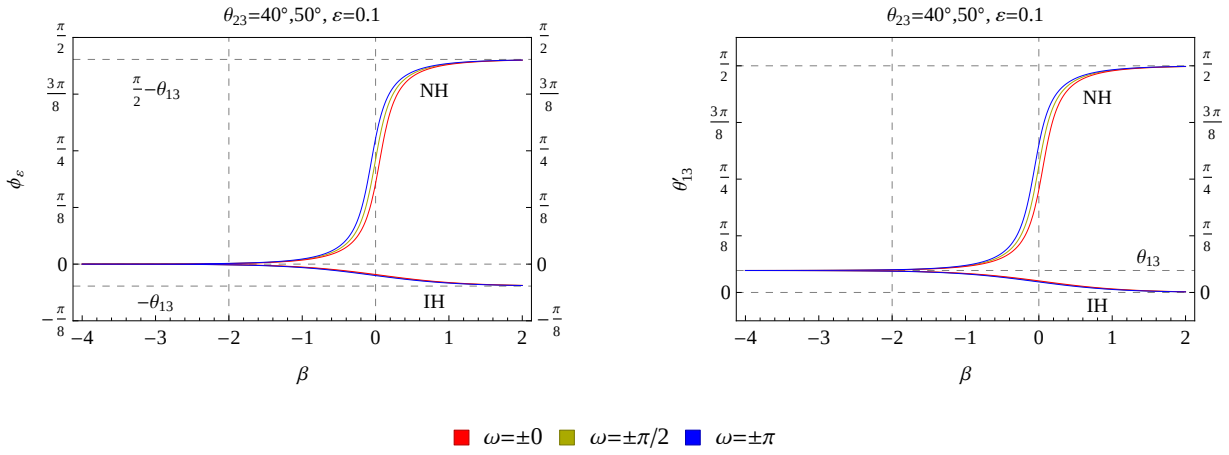

Figure 7.4: The β-dependence of ϕ_ε (left) and θ'_{13} (right) for $\varepsilon = 0.1$ both normal (NH) and inverted (IH) hierarchies. The dependence of ϕ_ε and θ'_{13} on ω for the inverted hierarchy case is weak and the three curves overlap.

where

$$\lambda''_{\varepsilon\pm} = \frac{\lambda'_{\varepsilon+} + \left\{\delta m^2_{31} + a(s^2_{13} + \varepsilon_c c^2_{13})\right\}}{2} \pm \frac{\sqrt{\left[\lambda'_{\varepsilon+} - \left\{\delta m^2_{31} + a(s^2_{13} + \varepsilon_c c^2_{13})\right\}\right]^2 + 4\left\{a s'_{12} s_{13} c_{13}(1-\varepsilon_c)\right\}^2}}{2}, \tag{7.55}$$

and the upper/lower signs correspond to the normal/inverted hierarchies.

For both hierarchies, the asymptotic forms are

$$\begin{aligned} \lambda''_{\varepsilon+} &= a + (s^2_{13}\delta m^2_{31} + s^2_{12}c^2_{13}\delta m^2_{21}) + \delta m^2_{31}\mathcal{O}(\delta m^2_{31}/a), \\ \lambda''_{\varepsilon-} &= a\varepsilon_c + (c^2_{13}\delta m^2_{31} + s^2_{12}s^2_{13}\delta m^2_{21}) + \delta m^2_{31}\mathcal{O}(\delta m^2_{31}/a)\ , \end{aligned} \tag{7.56}$$

with δm^2_{31} taking on the appropriate sign in each case. Note that since $\lambda'_{\varepsilon-} \approx -a\varepsilon_c + c^2_{12}\delta m^2_{21}$, for the normal hierarchy $\lambda'_{\varepsilon-}$ and $\lambda''_{\varepsilon-}$ repel each other with increasing a when $\varepsilon_c = \varepsilon\cos(2\vartheta_\omega) = \varepsilon c_\omega \sin(2\theta_{23}) > 0$, but they will attract each other with increasing a when $\varepsilon_c = \varepsilon\cos(2\vartheta_\omega) = \varepsilon c_\omega \sin(2\theta_{23}) < 0$. For the inverted hierarchy, it is the other way around. This is shown in Fig. 7.5.

Inclusion of $M^s_{\mu\tau}$ part

$H'''_a + a\varepsilon M^{c\prime\prime\prime}_{\mu\tau}$ is approximately diagonalized since the off-diagonal elements are suppressed by ac'_{12}. At this point, we include $M^{s\prime}_{\mu\tau}$. After the first rotation, $M^{s\prime}_{\mu\tau}$ becomes

$$\varepsilon M^{s\prime\prime}_{\mu\tau} = V^\dagger_\varepsilon \left(\varepsilon M^{s\prime}_{\mu\tau}\right) V_\varepsilon$$

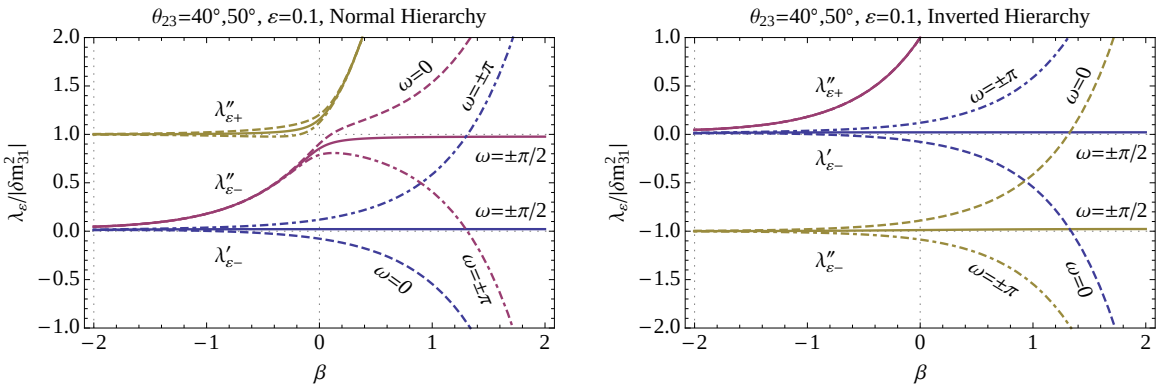

Figure 7.5: The β-dependence of $\lambda''_{\varepsilon\pm}$ and $\lambda'_{\varepsilon-}$ for the (a) normal and (b) inverted hierarchy cases with $\theta_{23} = 40^\circ$ or 50° and $\varepsilon = 0.1$. Shown are the $\omega = 0$ (dashed), $\omega = \pm\dfrac{\pi}{2}$ (solid) and $\omega = \pm\pi$ cases. The ω-dependence of $\lambda''_{\varepsilon+}$ is weak and the curves for the three cases are mostly overlapping.

$$
\begin{aligned}
&= \varepsilon_s \begin{bmatrix} 2s'_{12}c'_{12}s_{13}\cos(\delta+\Omega) & s_{13}e^{i(\delta+\Omega)} - 2c'^2_{12}s_{13}\cos(\delta+\Omega) & -s'_{12}c_{13}e^{i(\delta+\Omega)} \\ s_{13}e^{-i(\delta+\Omega)} - 2c'^2_{12}s_{13}\cos(\delta+\Omega) & -2s'_{12}c'_{12}s_{13}\cos(\delta+\Omega) & c'_{12}c_{13}e^{i(\delta+\Omega)} \\ -s'_{12}c_{13}e^{-i(\delta+\Omega)} & c'_{12}c_{13}e^{-i(\delta+\Omega)} & 0 \end{bmatrix} \\
&\xrightarrow{s'_{12}\approx 1} \varepsilon_s \begin{bmatrix} 0 & s_{13}e^{i(\delta+\Omega)} & -c_{13}e^{i(\delta+\Omega)} \\ s_{13}e^{-i(\delta+\Omega)} & 0 & 0 \\ -c_{13}e^{-i(\delta+\Omega)} & 0 & 0 \end{bmatrix},
\end{aligned}
\tag{7.57}
$$

where we have set $\varepsilon_s = \varepsilon\sin(2\vartheta_\omega)$. After the second rotation, we have

$$
\begin{aligned}
\varepsilon M^{s'''}_{\mu\tau} &= W^\dagger_\varepsilon \left(\varepsilon M^{s''}_{\mu\tau}\right) W_\varepsilon \\
&= \varepsilon_s \begin{bmatrix} 2s'_{12}c'_{12}s_{13}\cos(\delta+\Omega) & & \\ (s_{13}c_{\phi_\varepsilon} + c_{13}s_{\phi_\varepsilon}s'_{12})e^{-i(\delta+\Omega)} - 2c'^2_{12}s_{13}c_{\phi_\varepsilon}\cos(\delta+\Omega) & & \\ -(c_{13}c_{\phi_\varepsilon}s'_{12} - s_{13}s_{\phi_\varepsilon})e^{-i(\delta+\Omega)} - 2c'^2_{12}s_{13}s_{\phi_\varepsilon}\cos(\delta+\Omega) & & \\ (s_{13}c_{\phi_\varepsilon} + c_{13}s_{\phi_\varepsilon}s'_{12})e^{i(\delta+\Omega)} - 2c'^2_{12}s_{13}c_{\phi_\varepsilon}\cos(\delta+\Omega) & & \\ -2c'_{12}c_{\phi_\varepsilon}(s_{13}c_{\phi_\varepsilon}s'_{12} + c_{13}s_{\phi_\varepsilon})\cos(\delta+\Omega) & & \\ c'_{12}[c_{13}e^{-i(\delta+\Omega)} - 2s_{\phi_\varepsilon}(s_{13}c_{\phi_\varepsilon}s'_{12} + c_{13}s_{\phi_\varepsilon})] & & \\ -(c_{13}c_{\phi_\varepsilon}s'_{12} - s_{13}s_{\phi_\varepsilon})e^{i(\delta+\Omega)} - 2c'^2_{12}s_{13}s_{\phi_\varepsilon}\cos(\delta+\Omega) & & \\ c'_{12}[c_{13}e^{i(\delta+\Omega)} - 2s_{\phi_\varepsilon}(s_{13}c_{\phi_\varepsilon}s'_{12} + c_{13}s_{\phi_\varepsilon})] & & \\ 2c'_{12}s_{\phi_\varepsilon}(c_{13}c_{\phi_\varepsilon} - s_{13}s_{\phi_\varepsilon}s'_{12})\cos(\delta+\Omega) & & \end{bmatrix} \\
&\approx \varepsilon_s \begin{bmatrix} 0 & s'_{13}e^{i(\delta+\Omega)} & -c'_{13}e^{i(\delta+\Omega)} \\ s'_{13}e^{-i(\delta+\Omega)} & 0 & 0 \\ -c'_{13}e^{-i(\delta+\Omega)} & 0 & 0 \end{bmatrix},
\end{aligned}
\tag{7.58}
$$

where

$$s'_{13} \;=\; \sin\theta'_{13}\;, \qquad c'_{13} \;=\; \cos\theta'_{13}\;, \qquad \theta'_{13} \;\equiv\; \theta_{13}+\phi_\varepsilon\;. \tag{7.59}$$

The angle θ'_{13}, which is the approximate running θ_{13}, can be calculated directly via

$$\tan 2\theta'_{13} \;=\; \frac{(\delta m^2_{31}-s^2_{12}\delta m^2_{21})\sin(2\theta_{13})}{(\delta m^2_{31}-s^2_{12}\delta m^2_{21})\cos(2\theta_{13})-a(1-\varepsilon_c)}\;. \tag{7.60}$$

Third Rotation

$H'''_a+a\varepsilon M^{c'''}_{\mu\tau}$ is approximately diagonalized since the off-diagonal elements are suppressed by ac'_{12}. At this point, we include $M^{s'}_{\mu\tau}$. After the first rotation, $M^{s'}_{\mu\tau}$ becomes

$$\begin{aligned}
\varepsilon M^{s''}_{\mu\tau} \;&=\; V^\dagger_\varepsilon\left(\varepsilon M^{s'}_{\mu\tau}\right)V_\varepsilon \\
&=\; \varepsilon_s\begin{bmatrix} 2s'_{12}c'_{12}s_{13}\cos(\delta+\Omega) & s'_{13}e^{i(\delta+\Omega)}-2c'^2_{12}s_{13}\cos(\delta+\Omega) & -s'_{12}c_{13}e^{i(\delta+\Omega)} \\ s_{13}e^{-i(\delta+\Omega)}-2c'^2_{12}s_{13}\cos(\delta+\Omega) & -2s'_{12}c'_{12}s_{13}\cos(\delta+\Omega) & c'_{12}c_{13}e^{i(\delta+\Omega)} \\ -s'_{12}c_{13}e^{-i(\delta+\Omega)} & c'_{12}c_{13}e^{-i(\delta+\Omega)} & 0 \end{bmatrix} \\
&\xrightarrow{s'_{12}\approx 1}\; \varepsilon_s\begin{bmatrix} 0 & s_{13}e^{i(\delta+\Omega)} & -c_{13}e^{i(\delta+\Omega)} \\ s_{13}e^{-i(\delta+\Omega)} & 0 & 0 \\ -c_{13}e^{-i(\delta+\Omega)} & 0 & 0 \end{bmatrix}\;,
\end{aligned} \tag{7.61}$$

where we have set $\varepsilon_s=\varepsilon\sin(2\vartheta_\omega)$. After the second rotation, we have

$$\begin{aligned}
\varepsilon M^{s'''}_{\mu\tau} \;&=\; W^\dagger_\varepsilon\left(\varepsilon M^{s''}_{\mu\tau}\right)W_\varepsilon \\
&\approx\; \varepsilon_s\begin{bmatrix} 0 & s'_{13}e^{i(\delta+\Omega)} & -c'_{13}e^{i(\delta+\Omega)} \\ s'_{13}e^{-i(\delta+\Omega)} & 0 & 0 \\ -c'_{13}e^{-i(\delta+\Omega)} & 0 & 0 \end{bmatrix}\;,
\end{aligned} \tag{7.62}$$

where

$$s'_{13} \;=\; \sin\theta'_{13}\;, \qquad c'_{13} \;=\; \cos\theta'_{13}\;, \qquad \theta'_{13} \;\equiv\; \theta_{13}+\phi_\varepsilon\;. \tag{7.63}$$

The angle θ'_{13}, which is the approximate running θ_{13}, can be calculated directly via

$$\tan 2\theta'_{13} \;=\; \frac{(\delta m^2_{31}-s^2_{12}\delta m^2_{21})\sin(2\theta_{13})}{(\delta m^2_{31}-s^2_{12}\delta m^2_{21})\cos(2\theta_{13})-a(1-\varepsilon_c)}\;. \tag{7.64}$$

The running of θ'_{13} depends on the mass hierarchy. For normal hierarchy, θ'_{13} runs to $\dfrac{\pi}{2}$ as a is increased, so $s'_{13}\to 1$, $c'_{13}\to 0$. For inverted hierarchy, θ'_{13} runs to 0 as a is increased, so we have $s'_{13}\to 0$, $c'_{13}\to 1$. Therefore, for the normal hierarchy, we have

$$\varepsilon M^{s'''}_{\mu\tau} \;\xrightarrow{a\gg\delta m^2_{31}}\; \varepsilon_s\begin{bmatrix} 0 & e^{i(\delta+\Omega)} & 0 \\ e^{-i(\delta+\Omega)} & 0 & 0 \\ 0 & 0 & 0 \end{bmatrix}\;, \tag{7.65}$$

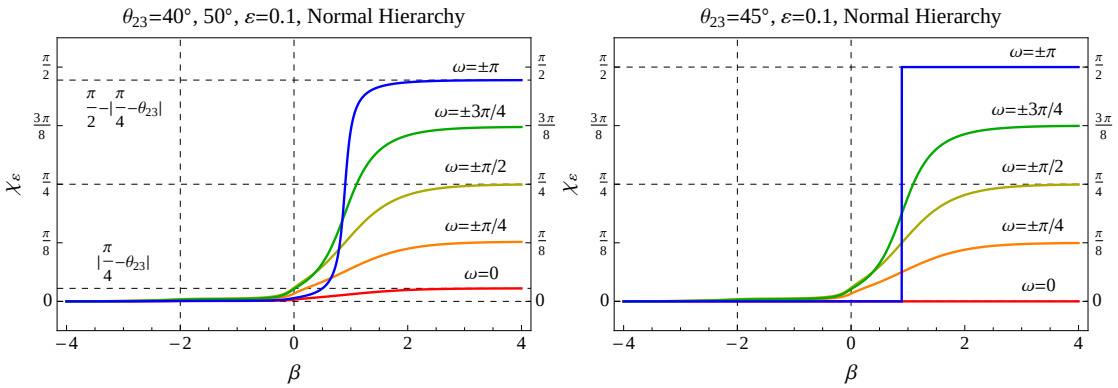

Figure 7.6: The β-dependence of χ_ε for $\varepsilon = 0.1$ and a variety of ω values for the cases (a) $\theta_{23} = 40°$, $50°$ and (b) $\theta_{23} = 45°$ with $\delta m^2_{31} > 0$.

while for the inverted hierarchy we have

$$\varepsilon M^{s'''}_{\mu\tau} \xrightarrow{a \gg |\delta m^2_{31}|} \varepsilon_s \begin{bmatrix} 0 & 0 & -e^{i(\delta+\Omega)} \\ 0 & 0 & 0 \\ -e^{-i(\delta+\Omega)} & 0 & 0 \end{bmatrix} . \tag{7.66}$$

So, for the normal hierarchy case, we need to perform a 12-rotation as the third rotation, and, for the inverted hierarchy case we need to perform a 13-rotation. In either case, $\lambda'_{\varepsilon-}$ and $\lambda''_{\varepsilon-}$ get mixed.

- **$\delta m^2_{31} > 0$ Case**

  For the normal hierarchy, the full matrix is

$$\begin{aligned} H'''_{\mu\tau} &= H'''_a + a\varepsilon M^{c'''}_{\mu\tau} + a\varepsilon M^{s'''}_{\mu\tau} \\ &= \begin{bmatrix} \lambda'_{\varepsilon-} & a\varepsilon_s s'_{13} e^{i(\delta+\Omega)} & 0 \\ a\varepsilon_s s'_{13} e^{-i(\delta+\Omega)} & \lambda''_{\varepsilon-} & 0 \\ 0 & 0 & \lambda''_{\varepsilon+} \end{bmatrix} , \end{aligned} \tag{7.67}$$

  where we have dropped terms of order ac'_{12} and $a\varepsilon c'_{13}$. The rotation matrix necessary to diagonalize this is

$$X_\varepsilon = \begin{bmatrix} c_{\chi_\varepsilon} & s_{\chi_\varepsilon} e^{i(\delta+\Omega)} & 0 \\ -s_{\chi_\varepsilon} e^{-i(\delta+\Omega)} & c_{\chi_\varepsilon} & 0 \\ 0 & 0 & 1 \end{bmatrix} , \tag{7.68}$$

  where

$$\tan 2\chi_\varepsilon = \frac{2a\varepsilon_s s'_{13}}{\lambda''_{\varepsilon-} - \lambda'_{\varepsilon-}}$$

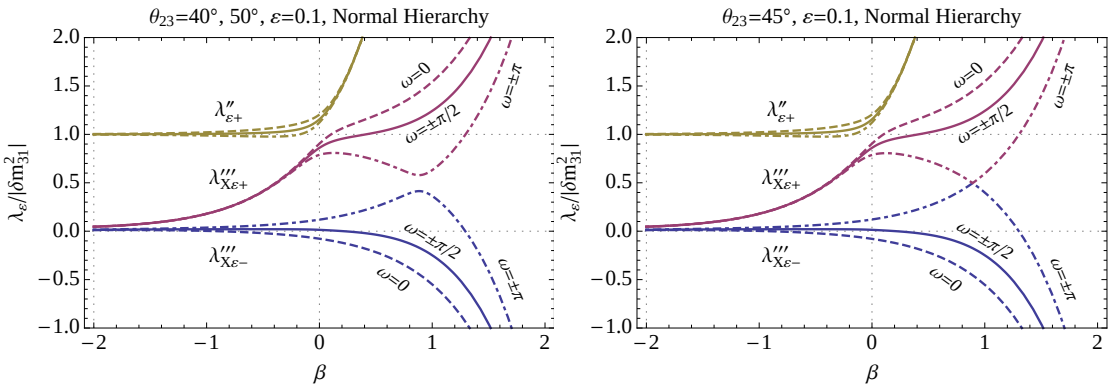

Figure 7.7: The β-dependence of $\lambda'''_{X_\varepsilon\pm}$ for $\varepsilon = 0.1$ and a variety of ω values for the two case (a) $\theta_{23} = 40°, 50°$ and (b) $\theta_{23} = 45°$ with $\delta m^2_{31} > 0$.

$$\approx \frac{2a\varepsilon\sin(2\vartheta_\omega)}{[c^2_{13}\delta m^2_{31} - (c^2_{12} - s^2_{12}s^2_{13})\delta m^2_{21}] + 2a\varepsilon\cos(2\vartheta_\omega)} \,. \tag{7.69}$$

Asymptotically, we have

$$\chi_\varepsilon \xrightarrow{a\varepsilon \gg |\delta m^2_{31}|} \vartheta_\omega \,, \tag{7.70}$$

for each value of ω. This behavior is shown in Fig. 7.6 for the $\theta_{23} = 40°$, $45°$, and $50°$ cases.

After the third rotation,

$$\begin{aligned} H'''' _{\mu\tau} &= X^\dagger_\varepsilon H'''_{\mu\tau} X_\varepsilon \\ &= \begin{bmatrix} \lambda'''_{X_\varepsilon -} & 0 & 0 \\ 0 & \lambda'''_{X_\varepsilon +} & 0 \\ 0 & 0 & \lambda''_{\varepsilon +} \end{bmatrix} \,, \end{aligned} \tag{7.71}$$

where

$$\lambda'''_{X_\varepsilon\pm} = \frac{\left(\lambda''_{\varepsilon-} + \lambda'_{\varepsilon-}\right) \pm \sqrt{\left(\lambda''_{\varepsilon-} - \lambda'_{\varepsilon-}\right)^2 + 4a^2\varepsilon^2_s s'^2_{13}}}{2} \,. \tag{7.72}$$

Thus, after three rotations, our matrix is approximately diagonal. Note that if $\theta_{23} = \dfrac{\pi}{4}$ and $\omega = 0$ or $\pm\pi$, then $\varepsilon_s = \varepsilon\sin(2\vartheta_\omega) = 0$, and we will have

$$\begin{aligned} \lambda'''_{X_\varepsilon +} &= \max(\lambda''_{\varepsilon-}, \lambda'_{\varepsilon-}) \,, \\ \lambda'''_{X_\varepsilon -} &= \min(\lambda''_{\varepsilon-}, \lambda'_{\varepsilon-}) \,. \end{aligned} \tag{7.73}$$

Asymptotically, we have

$\lambda'''_{X_\varepsilon\pm}$

$$
\begin{aligned}
&= \pm\varepsilon a + \frac{1}{2}\Big[(1 \pm \cos 2\vartheta_\omega)(\delta m^2_{31} c^2_{13} + \delta m^2_{21} s^2_{12} s^2_{13}) + (1 \mp \cos 2\vartheta_\omega)\delta m^2_{21} c^2_{12}\Big] + \cdots \\
&= \pm\varepsilon a + \left\{ \begin{array}{c} \cos^2\vartheta_\omega \\ \sin^2\vartheta_\omega \end{array} \right\} (\delta m^2_{31} c^2_{13} + \delta m^2_{21} s^2_{12} s^2_{13}) + \left\{ \begin{array}{c} \sin^2\vartheta_\omega \\ \cos^2\vartheta_\omega \end{array} \right\} \delta m^2_{21} c^2_{12} + \cdots
\end{aligned}
\tag{7.74}
$$

See Fig. 7.7.

- **$\delta m^2_{31} < 0$ Case**

For the inverted hierarchy, the full matrix is

$$
\begin{aligned}
H'''_{\mu\tau} &= H'''_a + a\varepsilon M^{c'''}_{\mu\tau} + a\varepsilon M^{s'''}_{\mu\tau} \\
&= \begin{bmatrix} \lambda'_{\varepsilon-} & 0 & -a\varepsilon_s c'_{13} e^{i(\delta+\Omega)} \\ 0 & \lambda''_{\varepsilon+} & 0 \\ -a\varepsilon_s c'_{13} e^{-i(\delta+\Omega)} & 0 & \lambda''_{\varepsilon-} \end{bmatrix},
\end{aligned}
\tag{7.75}
$$

where we have dropped terms of order ac'_{12} and $a\varepsilon s'_{13}$. The rotation matrix necessary to diagonalize this is

$$
Y_\varepsilon = \begin{bmatrix} c_{\psi_\varepsilon} & 0 & -s_{\psi_\varepsilon} e^{i(\delta+\Omega)} \\ 0 & 1 & 0 \\ s_{\psi_\varepsilon} e^{-i(\delta+\Omega)} & 0 & c_{\psi_\varepsilon} \end{bmatrix},
\tag{7.76}
$$

where

$$
\begin{aligned}
\tan 2\psi_\varepsilon &= \frac{2a\varepsilon_s c'_{13}}{\lambda''_{\varepsilon-} - \lambda'_{\varepsilon-}} \\
&\approx -\frac{2a\varepsilon \sin(2\vartheta_\omega)}{[c^2_{13}|\delta m^2_{31}| + (c^2_{12} - s^2_{12}s^2_{13})\delta m^2_{21}] - 2a\varepsilon\cos(2\vartheta_\omega)}\,.
\end{aligned}
\tag{7.77}
$$

Comparing the approximate expression of $\tan 2\psi_\varepsilon$ given in the second line of this equation to the second line of Eq. (7.69), we see that they differ in only the sign of δm^2_{31}. Therefore, the same approximate expression can be used to define both χ_ε for the $\delta m^2_{31} > 0$ case and ψ_ε for the $\delta m^2_{31} < 0$ case. Asymptotically, we have

$$
\psi_\varepsilon \xrightarrow{a\varepsilon \gg |\delta m^2_{31}|} \vartheta_\omega - \frac{\pi}{2}\,,
\tag{7.78}
$$

for each value of ω. This behavior is shown in Fig. 7.8 for the $\theta_{23} = 40^\circ$, 45°, and 50° cases.

After the third rotation,

$$
\begin{aligned}
H''''_{\mu\tau} &= Y^\dagger_\varepsilon H'''_{\mu\tau} Y_\varepsilon \\
&= \begin{bmatrix} \lambda'''_{Y_\varepsilon+} & 0 & 0 \\ 0 & \lambda''_{\varepsilon+} & 0 \\ 0 & 0 & \lambda'''_{Y_\varepsilon-} \end{bmatrix},
\end{aligned}
\tag{7.79}
$$

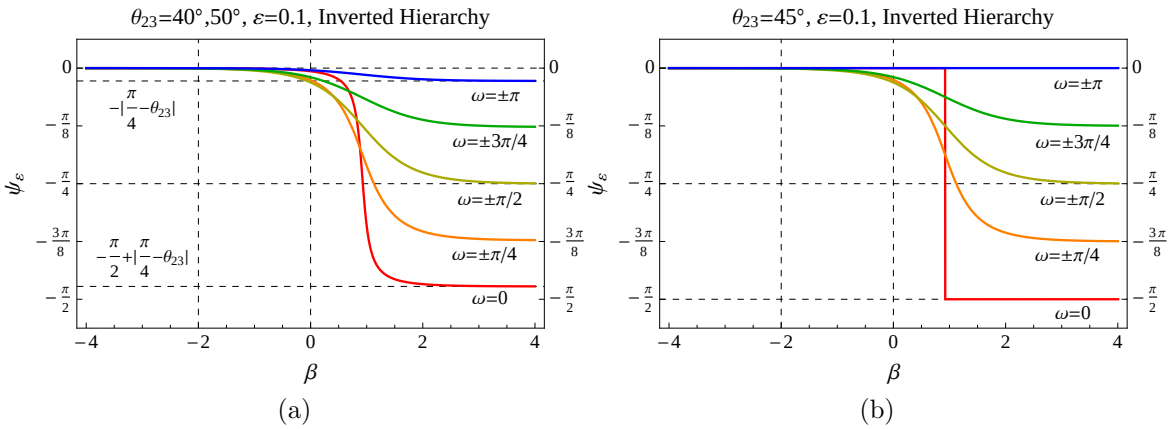

Figure 7.8: The β-dependence of ψ_ε for $\varepsilon = 0.1$ and a variety of ω values for the cases (a) $\theta_{23} = 40°$, $50°$ and (b) $\theta_{23} = 45°$ with $\delta m^2_{31} < 0$.

where

$$\lambda'''_{Y_\varepsilon\pm} = \frac{\left(\lambda''_{\varepsilon-} + \lambda'_{\varepsilon-}\right) \pm \sqrt{\left(\lambda''_{\varepsilon-} - \lambda'_{\varepsilon-}\right)^2 + 4a^2\varepsilon_s^2 c'^2_{13}}}{2} \,. \tag{7.80}$$

Thus, after three rotations, our matrix is approximately diagonal. Note that if $\theta_{23} = \dfrac{\pi}{4}$ and $\omega = 0$ or $\pm\pi$, then $\varepsilon_c = \varepsilon\cos(2\vartheta_\omega) = 0$, and we will have

$$\begin{aligned} \lambda'''_{Y_\varepsilon+} &= \min(\lambda''_{\varepsilon-}, \lambda'_{\varepsilon-}) \,, \\ \lambda'''_{Y_\varepsilon-} &= \max(\lambda''_{\varepsilon-}, \lambda'_{\varepsilon-}) \,. \end{aligned} \tag{7.81}$$

Note that the min and max are inverted from the normal hierarchy case. Asymptotically, we have

$$\begin{aligned} &\lambda'''_{Y_\varepsilon\pm} \\ &= \pm\varepsilon a + \frac{1}{2}\Big[(1 \pm \cos 2\vartheta_\omega)(\delta m^2_{31}c^2_{13} + \delta m^2_{21}s^2_{12}s^2_{13}) + (1 \mp \cos 2\vartheta_\omega)\delta m^2_{21}c^2_{12}\Big] + \cdots \\ &= \pm\varepsilon a + \left\{ \begin{array}{c} \cos^2\vartheta_\omega \\ \sin^2\vartheta_\omega \end{array} \right\}(\delta m^2_{31}c^2_{13} + \delta m^2_{21}s^2_{12}s^2_{13}) + \left\{ \begin{array}{c} \sin^2\vartheta_\omega \\ \cos^2\vartheta_\omega \end{array} \right\}\delta m^2_{21}c^2_{12} + \cdots \end{aligned} \tag{7.82}$$

These expressions are the same as Eq. (7.74), except δm^2_{31} is negative here. This behavior is shown in Fig. 7.9.

Absorption into Effective Mixing Angles

- **$\delta m^2_{31} > 0$ Case**

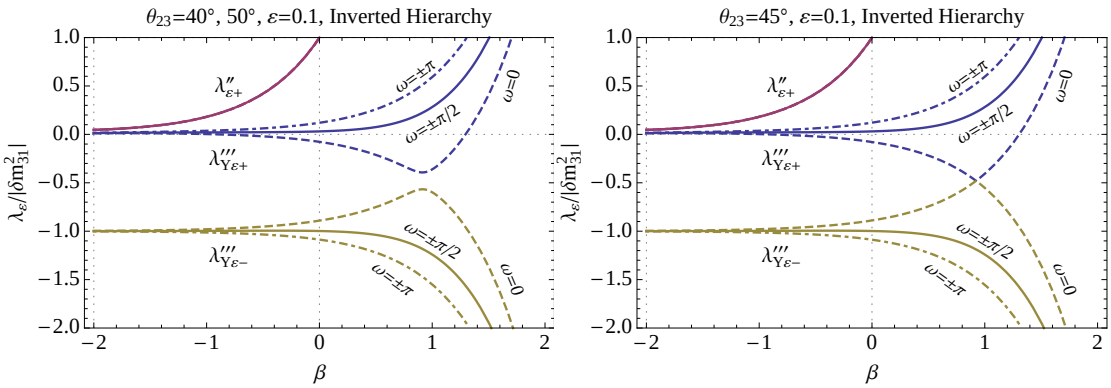

Figure 7.9: The β-dependence of $\lambda'''_{Y_\varepsilon\pm}$ for $\varepsilon = 0.1$ and a variety of ω values for the two case (a) $\theta_{23} = 40°, 50°$ and (b) $\theta_{23} = 45°$ with $\delta m^2_{31} < 0$.

As we have seen above, the effective mixing matrix is well approximated by the product of matrices given by

$$\begin{aligned}
\tilde{U} &= U Q_3 V_\varepsilon W_\varepsilon X_\varepsilon \\
&= \underbrace{R_{23}(\theta_{23},0) Q_3 R_{13}(\theta_{13},0) R_{12}(\theta_{12},0)}_{U Q_3} \underbrace{R_{12}(\varphi_\varepsilon,0)}_{V_\varepsilon} \underbrace{R_{23}(\phi_\varepsilon,0)}_{W_\varepsilon} \underbrace{R_{12}(\chi_\varepsilon,-\delta-\Omega)}_{X_\varepsilon} \\
&\approx R_{23}(\theta_{23},0) Q_3 R_{13}(\theta'_{13},0) R_{12}(\theta'_{12},0) R_{12}(\chi_\varepsilon,-\delta-\Omega) \\
&\approx R_{23}(\theta_{23},0) Q_3 R_{23}(\chi_\varepsilon,-\delta-\Omega) R_{13}(\theta'_{13},0) R_{12}(\theta'_{12},0) \,, \qquad (7.83)
\end{aligned}$$

where, in going from the second to the third line, we use the argument presented in Refs. [437, 438], and, in going from the third to the fourth, we follow the argument in section 3.3 of Ref. [432].

Let us look at the 23 submatrix of the product $R_{23}(\theta_{23},0) Q_3 R_{23}(\chi_\varepsilon,-\delta-\Omega)$. We have

$$\begin{aligned}
&\begin{bmatrix} c_{23} & s_{23} \\ -s_{23} & c_{23} \end{bmatrix} \begin{bmatrix} 1 & 0 \\ 0 & e^{i\delta} \end{bmatrix} \begin{bmatrix} c_{\chi_\varepsilon} & s_{\chi_\varepsilon} e^{i(\delta+\Omega)} \\ -s_{\chi_\varepsilon} e^{-i(\delta+\Omega)} & c_{\chi_\varepsilon} \end{bmatrix} \\
&= \begin{bmatrix} c_{23} & s_{23} \\ -s_{23} & c_{23} \end{bmatrix} \begin{bmatrix} 1 & 0 \\ 0 & e^{-i\Omega} \end{bmatrix} \begin{bmatrix} c_{\chi_\varepsilon} & s_{\chi_\varepsilon} \\ -s_{\chi_\varepsilon} & c_{\chi_\varepsilon} \end{bmatrix} \begin{bmatrix} 1 & 0 \\ 0 & e^{i(\delta+\Omega)} \end{bmatrix} \,. \qquad (7.84)
\end{aligned}$$

The product of the three matrices on the left can be rewritten as

$$\begin{aligned}
&\begin{bmatrix} c_{23} & s_{23} \\ -s_{23} & c_{23} \end{bmatrix} \begin{bmatrix} 1 & 0 \\ 0 & e^{-i\Omega} \end{bmatrix} \begin{bmatrix} c_{\chi_\varepsilon} & s_{\chi_\varepsilon} \\ -s_{\chi_\varepsilon} & c_{\chi_\varepsilon} \end{bmatrix} \\
&= \begin{bmatrix} e^{i\alpha_1} & 0 \\ 0 & e^{i\alpha_2} \end{bmatrix} \begin{bmatrix} c'_{23} & s'_{23} \\ -s'_{23} & c'_{23} \end{bmatrix} \begin{bmatrix} 1 & 0 \\ 0 & e^{i\gamma} \end{bmatrix} \,, \qquad (7.85)
\end{aligned}$$

where

$$c'_{23} = \cos\theta'_{23} = \sqrt{c^2_{23} c^2_{\chi_\varepsilon} - 2 c_{23} s_{23} c_{\chi_\varepsilon} s_{\chi_\varepsilon} \cos\Omega + s^2_{23} s^2_{\chi_\varepsilon}}$$

$$
\begin{aligned}
&= \sqrt{\cos^2(\Omega/2)\cos^2(\theta_{23}+\chi_\varepsilon)+\sin^2(\Omega/2)\cos^2(\theta_{23}-\chi_\varepsilon)}\;,\\
\alpha_1 &= \arctan\left[\frac{s_{23}s_{\chi_\varepsilon}\sin\Omega}{c_{23}c_{\chi_\varepsilon}-s_{23}s_{\chi_\varepsilon}\cos\Omega}\right]\;,\\
\alpha_2 &= \arctan\left[-\frac{c_{23}s_{\chi_\varepsilon}\sin\Omega}{s_{23}c_{\chi_\varepsilon}+c_{23}s_{\chi_\varepsilon}\cos\Omega}\right]\;,\\
\gamma &= \arctan\left[-\frac{\sin(2\theta_{23})\sin\Omega}{\sin(2\chi_\varepsilon)\cos(2\theta_{23})+\cos(2\chi_\varepsilon)\sin(2\theta_{23})\cos\Omega}\right]\\
&= \arctan\left[-\frac{s_\omega\tan(2\theta_{23})}{\cos 2(\chi_\varepsilon-\vartheta_\omega)}\right]\;.
\end{aligned}
\tag{7.86}
$$

The branches of the arctangents must be chosen judiciously for this to work. Using this result, we can write

$$
\begin{aligned}
&\begin{bmatrix} c_{23} & s_{23}\\ -s_{23} & c_{23}\end{bmatrix}\begin{bmatrix}1 & 0\\ 0 & e^{-i\Omega}\end{bmatrix}\begin{bmatrix} c_{\chi_\varepsilon} & s_{\chi_\varepsilon}\\ -s_{\chi_\varepsilon} & c_{\chi_\varepsilon}\end{bmatrix}\begin{bmatrix}1 & 0\\ 0 & e^{i(\delta+\Omega)}\end{bmatrix}\\
&= \begin{bmatrix}e^{i\alpha_1} & 0\\ 0 & e^{i\alpha_2}\end{bmatrix}\begin{bmatrix} c'_{23} & s'_{23}\\ -s'_{23} & c'_{23}\end{bmatrix}\begin{bmatrix}1 & 0\\ 0 & e^{i\delta'}\end{bmatrix}\;,
\end{aligned}
\tag{7.87}
$$

where

$$
\delta' \;=\; \delta+\Omega+\gamma\;. \tag{7.88}
$$

The sum $\Omega+\gamma$ can also be calculated directly via the relation

$$
\tan(\Omega+\gamma) \;=\; \frac{s_\Omega c_\Omega\,[\,\cos 2(\vartheta_\omega-\chi_\varepsilon)-\cos 2\vartheta_\omega\,]}{c_\Omega^2\cos 2(\vartheta_\omega-\chi_\varepsilon)+s_\Omega^2\cos 2\vartheta_\omega}\;. \tag{7.89}
$$

At $a\varepsilon \gg \delta m^2_{31}$ we know that $\chi_\varepsilon \to \vartheta_\omega$, cf. Eq. (7.70), so

$$
\cos 2(\chi_\varepsilon-\vartheta_\omega) \;\xrightarrow{a\varepsilon\gg\delta m^2_{31}}\; 1\;, \tag{7.90}
$$

and

$$
\begin{aligned}
\delta' \;&\xrightarrow{a\varepsilon\gg\delta m^2_{31}}\; \delta+\Omega+\arctan\Big[-s_\omega\tan(2\theta_{23})\Big]\\
&=\; \delta+\arctan\left[\frac{s^2_{\vartheta_\omega}\sin 2\Omega}{c^2_{\vartheta_\omega}+s^2_{\vartheta_\omega}\cos 2\Omega}\right]\;.
\end{aligned}
\tag{7.91}
$$

Let us look at a few specific cases.

A. $\theta_{23}=\dfrac{\pi}{4}$: In this case, we have

$$
\begin{cases}
\vartheta_\omega = +\dfrac{\omega}{2}\;, \quad \Omega = +\dfrac{\pi}{2} \quad \text{for} \quad 0<\omega<\dfrac{\pi}{2}\;,\\
\vartheta_\omega = -\dfrac{\omega}{2}\;, \quad \Omega = -\dfrac{\pi}{2} \quad \text{for} \; -\dfrac{\pi}{2}<\omega<0\;,
\end{cases}
\tag{7.92}
$$

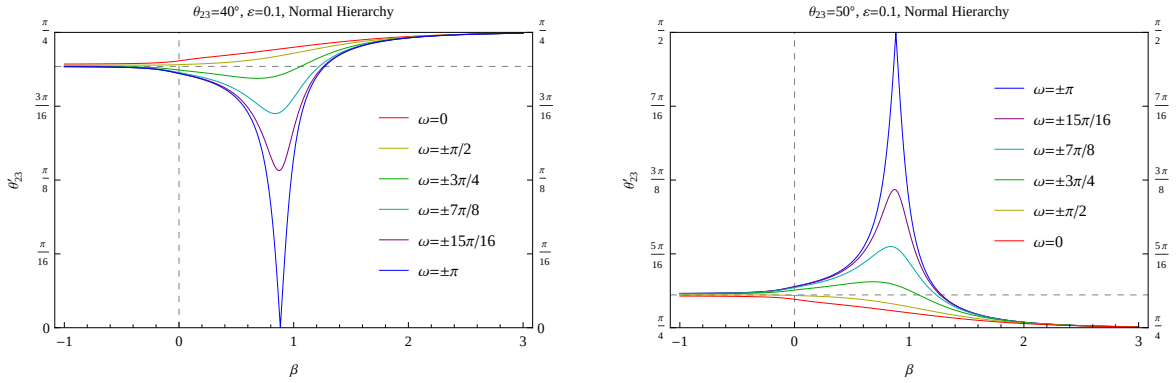

(a) (b)

Figure 7.10: The β-dependence of θ'_{23} for $\varepsilon = 0.1$ and a variety of ω values for the two cases (a) $\theta_{23} = 40^\circ$ and (b) $\theta_{23} = 50^\circ$ with $\delta m^2_{31} > 0$.

and this leads to

$$\begin{aligned}
&\begin{bmatrix} c_{23} & s_{23} \\ -s_{23} & c_{23} \end{bmatrix} \begin{bmatrix} 1 & 0 \\ 0 & e^{-i\Omega} \end{bmatrix} \begin{bmatrix} c_{\chi_\varepsilon} & s_{\chi_\varepsilon} \\ -s_{\chi_\varepsilon} & c_{\chi_\varepsilon} \end{bmatrix} \\
&= \frac{1}{\sqrt{2}} \begin{bmatrix} 1 & 1 \\ -1 & 1 \end{bmatrix} \begin{bmatrix} 1 & 0 \\ 0 & \mp i \end{bmatrix} \begin{bmatrix} c_{\chi_\varepsilon} & s_{\chi_\varepsilon} \\ -s_{\chi_\varepsilon} & c_{\chi_\varepsilon} \end{bmatrix} \\
&= \frac{1}{\sqrt{2}} \begin{bmatrix} e^{\pm i\chi_\varepsilon} & 0 \\ 0 & e^{\mp i\chi_\varepsilon} \end{bmatrix} \begin{bmatrix} 1 & 1 \\ -1 & 1 \end{bmatrix} \begin{bmatrix} 1 & 0 \\ 0 & \mp i \end{bmatrix} \\
&= \begin{bmatrix} e^{\pm i\chi_\varepsilon} & 0 \\ 0 & e^{\mp i\chi_\varepsilon} \end{bmatrix} \begin{bmatrix} c_{23} & s_{23} \\ -s_{23} & c_{23} \end{bmatrix} \begin{bmatrix} 1 & 0 \\ 0 & e^{-i\Omega} \end{bmatrix} . \qquad (7.93)
\end{aligned}$$

Therefore, $\alpha_1 = \pm\chi_\varepsilon$, $\alpha_2 = \mp\chi_\varepsilon$, $\gamma = -\Omega$, and

$$\theta'_{23} \;=\; \theta_{23} \;, \qquad \delta' \;=\; \delta \;, \qquad (7.94)$$

that is, when $\theta_{23} = \dfrac{\pi}{4}$, even though χ_ε runs with a, neither θ_{23} nor δ will run.

B. $\theta_{23} < \dfrac{\pi}{4}$: Let us consider a few specific values for ω :

(a) If $\omega = 0$, then $\Omega = 0$, $\vartheta_\omega = \dfrac{\pi}{4} - \theta_{23}$, and

$$\cos\theta'_{23} \;=\; c_{23}c_{\chi_\varepsilon} - s_{23}s_{\chi_\varepsilon} \;=\; \cos(\theta_{23} + \chi_\varepsilon) \;, \qquad \delta' \;=\; \delta \;. \qquad (7.95)$$

As a is increased χ_ε increased monotonically from 0 to $\vartheta_\omega = \dfrac{\pi}{4} - \theta_{23}$. Therefore, θ'_{23} runs up from θ_{23} to $\dfrac{\pi}{4}$. Looking at $\tan\gamma$, it is zero since $s_\omega = 0$ at $\omega = 0$, and consequently $\gamma = \Omega = 0$ and δ' does not run.

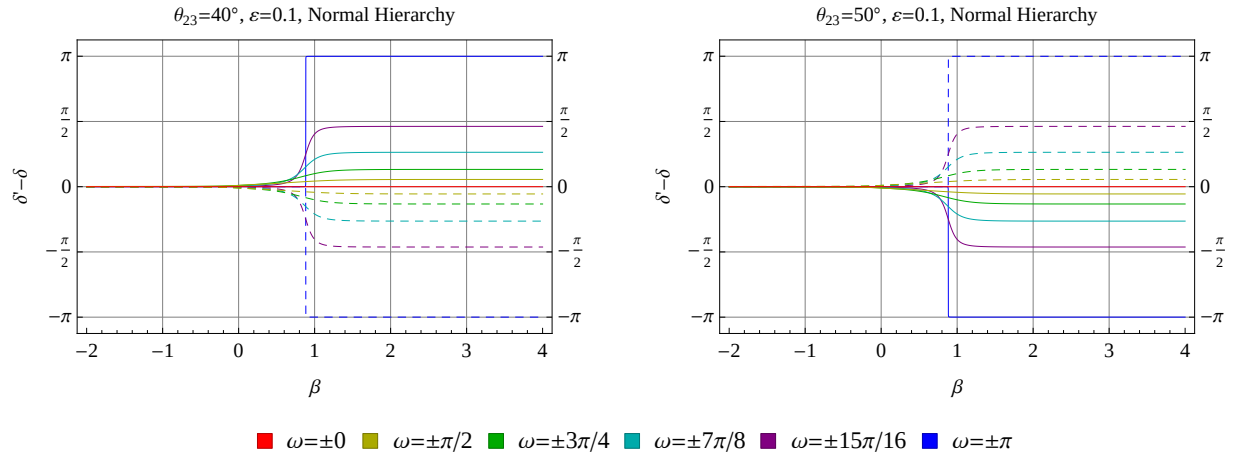

Figure 7.11: The β-dependence of $\delta' - \delta$ for $\varepsilon = 0.1$ and a variety of ω values for the two cases $\theta_{23} = 40°$ (left) and $\theta_{23} = 50°$ (right). with $\delta m^2_{31} > 0$. The solid lines indicate positive ω and the dashed lines indicate negative ω.

(b) If $\omega = \pm\pi/2$, then $\Omega = \pm\pi/2$, $\vartheta_\omega = \dfrac{\pi}{4}$, and

$$\begin{aligned} \cos\theta'_{23} &= \sqrt{c^2_{23}c^2_{\chi_\varepsilon} + s^2_{23}s^2_{\chi_\varepsilon}}\,, \\ \gamma &= \arctan\left[\mp\frac{\tan(2\theta_{23})}{\sin(2\chi_\varepsilon)}\right]\,. \end{aligned} \tag{7.96}$$

Since χ_ε runs from 0 to $\vartheta_\omega = \pi/4$ in this case as β is increased, $\cos\theta'_{23}$ runs from c_{23} to $1/\sqrt{2}$, so, again, θ'_{23} runs from θ_{23} to $\pi/4$.
Looking at $\tan\gamma$, since $\tan(2\theta_{23}) > 0$ when $\theta_{23} < \pi/4$, $\tan\gamma$ runs from $\mp\infty$ to $\mp\tan(2\theta_{23})$. So γ runs from $\mp\pi/2 = -\Omega$ to $\mp 2\theta_{23}$, which in turn means that $\delta' - \delta$ runs from 0 to $\pm 2\left(\dfrac{\pi}{4} - \theta_{23}\right)$.

(c) If $\omega = \pm\pi$, then $\Omega = \pm\pi$, $\vartheta_\omega = \dfrac{\pi}{4} + \theta_{23}$, and

$$\cos(\theta'_{23}) = c_{23}c_{\chi_\varepsilon} + s_{23}s_{\chi_\varepsilon} = \cos(\theta_{23} - \chi_\varepsilon)\,. \tag{7.97}$$

As a is increased, χ_ε increases monotonically from 0 to $\vartheta_\omega = \dfrac{\pi}{4} + \theta_{23}$. So the difference $\theta_{23} - \chi_\varepsilon$ decreases monotonically from θ_{23} to $-\dfrac{\pi}{4}$, going through zero at $\chi_\varepsilon = \theta_{23}$. Since we restrict θ'_{23} to the range $0 \le \theta'_{23} \le \dfrac{\pi}{4}$, it will run from θ_{23} down to zero, and then back up to $\dfrac{\pi}{4}$.
Looking at $\tan\gamma$, since $s_\omega = 0$ at $\omega = \pm\pi$, $\tan\gamma$ is always zero. However, for ω slightly off of $\pm\pi$, yet in the range $-\pi \le \omega \le \pi$, we have $s_\omega = \pm 0$, and since $\tan(2\theta_{23}) > 0$ for $\theta_{23} < \dfrac{\pi}{4}$, when $\cos 2(\chi_\varepsilon - \vartheta_\omega) = \cos 2\left(\chi_\varepsilon - \theta_{23} - \dfrac{\pi}{4}\right) =$

$\sin 2\,(\chi_\varepsilon - \theta_{23})$ goes through zero as χ_ε goes through θ_{23}, $\tan\gamma$ jumps from $\pm\infty$ to $\mp\infty$ thereby jumps from one branch to another. So in the limit $\omega = \pm\pi$, γ at $\chi_\varepsilon = 0$ and $\chi_\varepsilon = \theta_{23} + \dfrac{\pi}{4}$ differ by $\pm\pi$, making the jump at $\chi_\varepsilon = \theta_{23}$.

The behavior of θ'_{23} and δ' for these, and other values of ω are shown in Figs. 7.10(a) and 7.11(a).

C. $\theta_{23} > \dfrac{\pi}{4}$: As above, let us consider a few specific values for ω :

(a) If $\omega = 0$, then $\Omega = \pi$, $\vartheta_\omega = \theta_{23} - \dfrac{\pi}{4}$, and

$$\cos\theta'_{23} \;=\; c_{23}c_{\chi_\varepsilon} + s_{23}s_{\chi_\varepsilon} \;=\; \cos(\theta_{23} - \chi_\varepsilon)\;, \qquad \delta' \;=\; \delta\;. \tag{7.98}$$

As a is increased χ_ε increased monotonically from 0 to $\vartheta_\omega = \theta_{23} - \dfrac{\pi}{4}$. Therefore, θ'_{23} runs from θ_{23} down to $\dfrac{\pi}{4}$. Looking at $\tan\gamma$, it is zero since $s_\omega = 0$ at $\omega = 0$. We take $\gamma = -\pi$ so that $\gamma + \Omega = 0$ and δ' does not run.

(b) If $\omega = \pm\pi/2$, then $\Omega = \pm\pi/2$, $\vartheta_\omega = \dfrac{\pi}{4}$, and

$$\begin{aligned} \cos\theta'_{23} &= \sqrt{c_{23}^2 c_{\chi_\varepsilon}^2 + s_{23}^2 s_{\chi_\varepsilon}^2}\;, \\ \gamma &= \arctan\left[\mp\frac{\tan(2\theta_{23})}{\sin(2\chi_\varepsilon)}\right]\;. \end{aligned} \tag{7.99}$$

Since χ_ε runs from 0 to $\vartheta_\omega = \pi/4$ in this case as β is increased, $\cos\theta'_{23}$ runs from c_{23} to $1/\sqrt{2}$, so, again, θ'_{23} runs from θ_{23} to $\pi/4$.
Looking at $\tan\gamma$, since $\tan(2\theta_{23}) < 0$ when $\theta_{23} > \pi/4$, $\tan\gamma$ runs from $\pm\infty$ to $\mp\tan(2\theta_{23})$. We take γ to run from $\mp\pi/2 = -\Omega$ to $\mp 2\theta_{23}$, which in turn means that $\delta' - \delta$ runs from 0 to $\pm 2\left(\theta_{23} - \dfrac{\pi}{4}\right)$.

(c) If $\omega = \pm\pi$, then $\Omega = 0$, $\vartheta_\omega = \dfrac{3\pi}{4} - \theta_{23}$, and

$$\cos(\theta'_{23}) \;=\; |c_{23}c_{\chi_\varepsilon} - s_{23}s_{\chi_\varepsilon}| \;=\; |\cos(\theta_{23} + \chi_\varepsilon)|\;. \tag{7.100}$$

As a is increased, χ_ε increases monotonically from 0 to $\vartheta_\omega = \dfrac{3\pi}{4} - \theta_{23}$. So the sum $\theta_{23} + \chi_\varepsilon$ increases monotonically from θ_{23} to $\dfrac{3\pi}{4}$, going through $\dfrac{\pi}{2}$ at $\chi_\varepsilon = \dfrac{\pi}{2} - \theta_{23}$. Since we restrict θ'_{23} to the range $0 \le \theta'_{23} \le \dfrac{\pi}{4}$, it will run from θ_{23} down to zero, and then back up to $\dfrac{\pi}{4}$.
Looking at $\tan\gamma$, since $s_\omega = 0$ at $\omega = \pm\pi$, $\tan\gamma$ is always zero. However, for ω slightly off of $\pm\pi$, but in the range $-\pi \le \omega \le \pi$, we have $s_\omega = \pm 0$, and since

$\tan(2\theta_{23}) < 0$ for $\theta_{23} > \dfrac{\pi}{4}$, when $\cos 2(\chi_\varepsilon - \vartheta_\omega) = \cos 2\left(\chi_\varepsilon + \theta_{23} - \dfrac{3\pi}{4}\right) = -\sin 2\left(\chi_\varepsilon + \theta_{23}\right)$ goes through zero as χ_ε goes through $\dfrac{\pi}{2} - \theta_{23}$, $\tan\gamma$ jumps from $\mp\infty$ to $\pm\infty$ thereby jumps from one branch to another. So in the limit $\omega = \pm\pi$, γ at $\chi_\varepsilon = 0$ and $\chi_\varepsilon = \dfrac{3\pi}{4} - \theta_{23}$ differ by $\mp\pi$, making the jump at $\chi_\varepsilon = \dfrac{\pi}{2} - \theta_{23}$.

The behavior of θ'_{23} and δ' for these, and other values of ω are shown in Figs. 7.10(b) and 7.11(b).

- **$\delta m^2_{31} < 0$ Case**

  In this case, the effective mixing matrix is well approximated by the product of matrices given by

$$\begin{aligned}
\tilde{U} &= UQ_3V_\varepsilon W_\varepsilon Y_\varepsilon \\
&= \underbrace{R_{23}(\theta_{23},0)Q_3R_{13}(\theta_{13},0)R_{12}(\theta_{12},0)}_{UQ_3}\underbrace{R_{12}(\varphi_\varepsilon,0)}_{V_\varepsilon}\underbrace{R_{23}(\phi_\varepsilon,0)}_{W_\varepsilon}\underbrace{R_{13}(-\psi_\varepsilon,-\delta-\Omega)}_{Y_\varepsilon} \\
&\approx R_{23}(\theta_{23},0)Q_3R_{13}(\theta'_{13},0)R_{12}(\theta'_{12},0)R_{13}(-\psi_\varepsilon,-\delta-\Omega) \\
&\approx R_{23}(\theta_{23},0)Q_3R_{23}(\psi_\varepsilon,-\delta-\Omega)R_{13}(\theta'_{13},0)R_{12}(\theta'_{12},0)\,, \qquad (7.101)
\end{aligned}$$

  where, in going from the second to the third line, we use the argument presented in Refs. [437, 438], and, in going from the third to the fourth, we follow the argument in section 3.3 of Ref. [432].

  From this point on, we follow the same procedure as the $\delta m^2_{31} > 0$ case discussed above, and we argue that the effective running values of θ_{23} and δ are obtained from

$$\begin{aligned}
\theta'_{23} &= \arccos\left[\sqrt{c^2_{23}c^2_{\psi_\varepsilon} - 2c_{23}s_{23}c_{\psi_\varepsilon}s_{\psi_\varepsilon}\cos\Omega + s^2_{23}s^2_{\psi_\varepsilon}}\right]\,, \\
\delta' &= \delta + \Omega + \arctan\left[-\frac{s_\omega\tan(2\theta_{23})}{\cos 2(\psi_\varepsilon - \vartheta_\omega)}\right]\,.
\end{aligned} \qquad (7.102)$$

  For $a\varepsilon \gg \delta m^2_{31}$, we know from Eq. (7.78) that $\psi_\varepsilon \to \vartheta_\omega - \dfrac{\pi}{2}$. Therefore,

$$\delta' \xrightarrow{a\varepsilon \gg \delta m^2_{31}} \delta + \Omega + \arctan\Big[s_\omega\tan(2\theta_{23})\Big]\,. \qquad (7.103)$$

  As in the $\delta m^2_{31} > 0$ case, we can show that θ'_{23} and δ' do not run when $\theta_{23} = \dfrac{\pi}{4}$, and that θ'_{23} will run toward $\dfrac{\pi}{4}$ for both the $\theta_{23} < \dfrac{\pi}{4}$ and $\theta_{23} > \dfrac{\pi}{4}$ cases. Omitting details, we show the behavior of θ'_{23} and δ' for various values of ω in Figs. 7.12 and 7.13 when $\theta_{23} \neq \dfrac{\pi}{4}$.

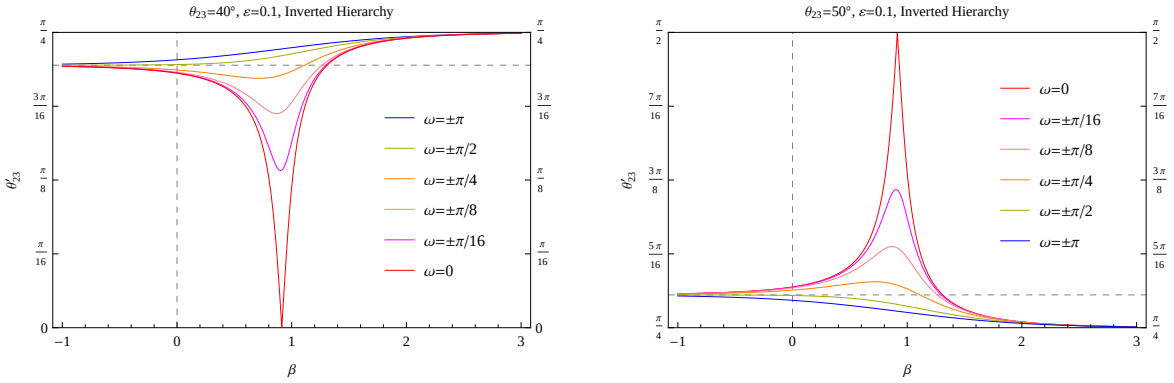

(a) (b)

Figure 7.12: The β-dependence of θ'_{23} for $\varepsilon = 0.1$ and a variety of ω values for the two cases (a) $\theta_{23} = 40^\circ$ and (b) $\theta_{23} = 50^\circ$ with $\delta m^2_{31} < 0$.

7.3.3 Summary of the Neutrino Case

We find that the matter effect due to $\varepsilon_{\mu\tau} = \varepsilon e^{i\omega}$ can be absorbed into the running of the effective mixing angles θ'_{12}, θ'_{13}, θ'_{23}, the effective CP violating phase δ', and the effective mass-squared eigenvalues λ_1, λ_2, and λ_3. The definitions of ϑ_ω and Ω that appear in what follows have been given in Eq. (7.38). First, θ'_{12} and θ'_{13} are given by

$$\begin{aligned} \tan 2\theta'_{12} &= \frac{\delta m^2_{21} \sin 2\theta_{12}}{\delta m^2_{21} \cos 2\theta_{12} - a[c^2_{13} + \varepsilon_c(1 + s^2_{13})]} \,, \\ \tan 2\theta'_{13} &= \frac{(\delta m^2_{31} - s^2_{12}\delta m^2_{21}) \sin(2\theta_{13})}{(\delta m^2_{31} - s^2_{12}\delta m^2_{21}) \cos(2\theta_{13}) - a(1 - \varepsilon_c)} \,, \end{aligned} \tag{7.104}$$

where $\varepsilon_c = \varepsilon \cos(2\vartheta_\omega)$. Next, $\theta'_{23} \in [0, \pi/2]$ and $\delta' \in [-\pi, \pi]$ are given by

$$\begin{aligned} \theta'_{23} &= \arccos\left[\sqrt{c^2_{23}c^2_{\chi_\varepsilon} - 2c_{23}s_{23}c_{\chi_\varepsilon}s_{\chi_\varepsilon}\cos\Omega + s^2_{23}s^2_{\chi_\varepsilon}}\right] \,, \\ \delta' &= \delta + \Omega + \arctan\left[-\frac{s_\omega \tan(2\theta_{23})}{\cos 2(\chi_\varepsilon - \vartheta_\omega)}\right] \,, \end{aligned} \tag{7.105}$$

where

$$\tan 2\chi_\varepsilon = \frac{2a\varepsilon \sin(2\vartheta_\omega)}{[c^2_{13}\delta m^2_{31} - (c^2_{12} - s^2_{12}s^2_{13})\delta m^2_{21}] + 2a\varepsilon\cos(2\vartheta_\omega)} \,. \tag{7.106}$$

Note that the same expression can be used for both the $\delta m^2_{31} > 0$ and $\delta m^2_{31} < 0$ cases, cf. Eqs. (7.69) and (7.77). For the normal hierarchy ($\delta m^2_{31} > 0$), the effective mass-squared eigenvalues are

$$\lambda_1 = \frac{(\lambda''_{\varepsilon-} + \lambda'_{\varepsilon-}) - \sqrt{(\lambda''_{\varepsilon-} - \lambda'_{\varepsilon-})^2 + 4a^2\varepsilon^2_s s'^2_{13}}}{2} \,,$$

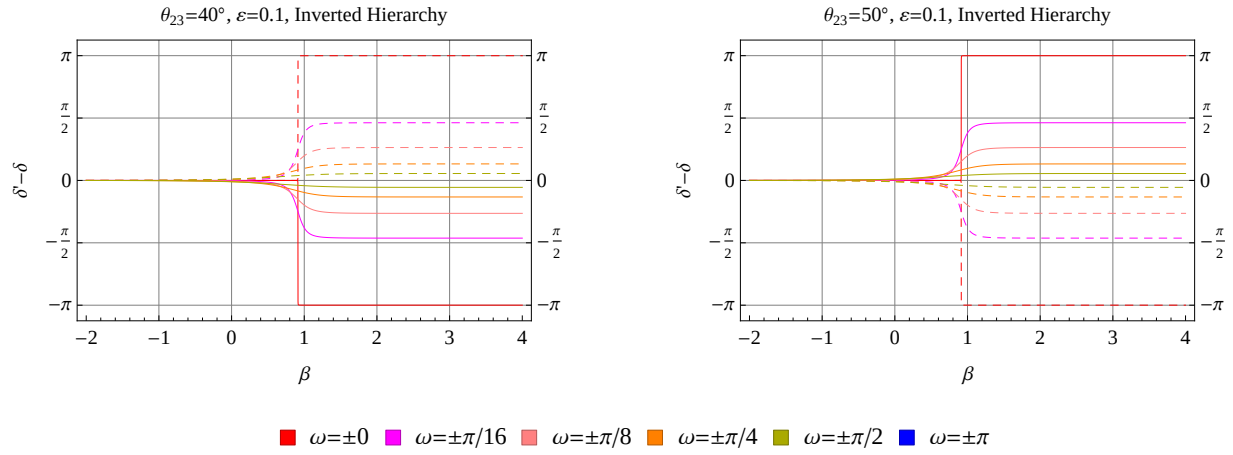

Figure 7.13: The β-dependence of $\delta' - \delta$ for $\varepsilon = 0.1$ and a variety of ω values for the two cases $\theta_{23} = 40°$ (left) and $\theta_{23} = 50°$ (right). with $\delta m^2_{31} < 0$. The solid lines indicate positive ω while the dashed lines indicate negative ω.

$$\begin{aligned} \lambda_2 &= \frac{(\lambda''_{\varepsilon-} + \lambda'_{\varepsilon-}) + \sqrt{(\lambda''_{\varepsilon-} - \lambda'_{\varepsilon-})^2 + 4a^2\varepsilon_s^2 s'^2_{13}}}{2} , \\ \lambda_3 &= \lambda''_{\varepsilon+} , \end{aligned} \tag{7.107}$$

while, for the inverted hierarchy ($\delta m^2_{31} < 0$), they are given by

$$\begin{aligned} \lambda_1 &= \frac{(\lambda''_{\varepsilon-} + \lambda'_{\varepsilon-}) + \sqrt{(\lambda''_{\varepsilon-} - \lambda'_{\varepsilon-})^2 + 4a^2\varepsilon_s^2 c'^2_{13}}}{2} , \\ \lambda_2 &= \lambda''_{\varepsilon+} , \\ \lambda_3 &= \frac{(\lambda''_{\varepsilon-} + \lambda'_{\varepsilon-}) - \sqrt{(\lambda''_{\varepsilon-} - \lambda'_{\varepsilon-})^2 + 4a^2\varepsilon_s^2 c'^2_{13}}}{2} , \end{aligned} \tag{7.108}$$

where $\varepsilon_s = \varepsilon \sin(2\vartheta_\omega)$, and

$$\begin{aligned} \lambda'_{\varepsilon\pm} &= \frac{\{(\delta m^2_{21} - a\varepsilon_c) + a(c^2_{13} + \varepsilon_c s^2_{13})\}}{2} \\ &\quad \pm \frac{\sqrt{\{(\delta m^2_{21} - a\varepsilon_c) - a(c^2_{13} + \varepsilon_c s^2_{13})\}^2 + 4as^2_{12}\{c^2_{13} + \varepsilon_c(1 + s^2_{13})\}\delta m^2_{21}}}{2} , \\ \lambda''_{\varepsilon\pm} &= \frac{\lambda'_{\varepsilon+} + \{\delta m^2_{31} + a(s^2_{13} + \varepsilon_c c^2_{13})\}}{2} \\ &\quad \pm \frac{\sqrt{[\lambda'_{\varepsilon+} - \{\delta m^2_{31} + a(s^2_{13} + \varepsilon_c c^2_{13})\}]^2 + 4\{as'_{12}s_{13}c_{13}(1 - \varepsilon_c)\}^2}}{2} . \end{aligned} \tag{7.109}$$

7.4 Effective Mixing Angles and Effective Mass-Squared Differences – Anti-Neutrino Case

In this section, we study the matter effect due to the anti-neutrino NSI's. We again utilize the Jacobi method to estimate how the NSI parameter η alters the 'running' of the effective mixing angles, effective mass-squared differences, and the effective CP-violating phase δ in matter for the anti-neutrinos.

7.4.1 Differences from the Neutrino Case

For the anti-neutrinos, the effective Hamiltonian is given by

$$\overline{H}_{\mu\tau} = \tilde{U}^* \begin{bmatrix} \overline{\lambda}_1 & 0 & 0 \\ 0 & \overline{\lambda}_2 & 0 \\ 0 & 0 & \overline{\lambda}_3 \end{bmatrix} \tilde{U}^T = \underbrace{U^* \begin{bmatrix} 0 & 0 & 0 \\ 0 & \delta m^2_{21} & 0 \\ 0 & 0 & \delta m^2_{31} \end{bmatrix} U^T - a \underbrace{\begin{bmatrix} 1 & 0 & 0 \\ 0 & 0 & 0 \\ 0 & 0 & 0 \end{bmatrix}}_{\equiv M_a}}_{\equiv \overline{H}_a} - a\varepsilon \underbrace{\begin{bmatrix} 0 & 0 & 0 \\ 0 & 0 & e^{-i\omega} \\ 0 & e^{+i\omega} & 0 \end{bmatrix}}_{\equiv M_{\mu\tau}} . \tag{7.110}$$

The differences from the neutrino case are the reversal of signs of the CP-violating phase δ (and thus the complex conjugation of the PMNS matrix U), the matter interaction parameter a, and the NSI phase ω.

The separation of $M_{\mu\tau}$ into two parts is as follows:

$$\begin{aligned} M_{\mu\tau} &= c_\omega \begin{bmatrix} 0 & 0 & 0 \\ 0 & 0 & 1 \\ 0 & 1 & 0 \end{bmatrix} - s_\omega \begin{bmatrix} 0 & 0 & 0 \\ 0 & 0 & i \\ 0 & -i & 0 \end{bmatrix} \\ &= \underbrace{c_\omega \sin(2\theta_{23}) \begin{bmatrix} 0 & 0 & 0 \\ 0 & -\cos(2\theta_{23}) & \sin(2\theta_{23}) \\ 0 & \sin(2\theta_{23}) & \cos(2\theta_{23}) \end{bmatrix}}_{\equiv M^c_{\mu\tau}} \\ &\quad \underbrace{+ c_\omega \cos(2\theta_{23}) \begin{bmatrix} 0 & 0 & 0 \\ 0 & \sin(2\theta_{23}) & \cos(2\theta_{23}) \\ 0 & \cos(2\theta_{23}) & -\sin(2\theta_{23}) \end{bmatrix} - s_\omega \begin{bmatrix} 0 & 0 & 0 \\ 0 & 0 & i \\ 0 & -i & 0 \end{bmatrix}}_{\equiv M^s_{\mu\tau}} , \end{aligned} \tag{7.111}$$

where $c_\omega = \cos\omega$ and $s_\omega = \sin\omega$. In the following, we diagonalize $\overline{H}_a + a\varepsilon M^c_{\mu\tau}$ first, and then deal with $M^s_{\mu\tau}$ later.

7.4.2 Diagonalization of the Effective Hamiltonian

Change to the Mass Eigenbasis in Vacuum

We begin by partially diagonalizing $H_{\mu\tau}$ by going from the flavor-eigenbasis to the vacuum-mass-eigenbasis:

$$\begin{aligned} H'_{\mu\tau} &= Q_3 U^T H_{\mu\tau} U^* Q_3^* \\ &= \underbrace{\begin{bmatrix} 0 & 0 & 0 \\ 0 & \delta m^2_{21} & 0 \\ 0 & 0 & \delta m^2_{31} \end{bmatrix} - a\, Q_3 U^T \underbrace{\begin{bmatrix} 1 & 0 & 0 \\ 0 & 0 & 0 \\ 0 & 0 & 0 \end{bmatrix}}_{M_a} U^* Q_3^*}_{\equiv \overline{H}'_a} - a\varepsilon\, Q_3 U^T \underbrace{\begin{bmatrix} 0 & 0 & 0 \\ 0 & 0 & e^{-i\omega} \\ 0 & e^{+i\omega} & 0 \end{bmatrix}}_{M^c_{\mu\tau} + M^s_{\mu\tau}} U^* Q_3^* \,. \end{aligned} \tag{7.112}$$

Where $\overline{M}'_a$ only depends on θ_{12} and θ_{13} and is given by

$$\overline{M}'_a \;=\; Q_3 U^T M_a U^* Q_3^* \;=\; \begin{bmatrix} c^2_{12}c^2_{13} & s_{12}c_{12}c^2_{13} & c_{12}s_{13}c_{13} \\ s_{12}c_{12}c^2_{13} & s^2_{12}c^2_{13} & s_{12}s_{13}c_{13} \\ c_{12}s_{13}c_{13} & s_{12}s_{13}c_{13} & s^2_{13} \end{bmatrix} \,. \tag{7.113}$$

Looking at how $M^c_{\mu\tau}$ and $M^s_{\mu\tau}$ transform, after the first 23-rotation we find

$$\begin{aligned} R^\dagger_{23}(\theta_{23},0) M^c_{\mu\tau} R_{23}(\theta_{23},0) &= \begin{bmatrix} 0 & 0 & 0 \\ 0 & -c_\omega \sin(2\theta_{23}) & 0 \\ 0 & 0 & c_\omega \sin(2\theta_{23}) \end{bmatrix} , \\ R^\dagger_{23}(\theta_{23},0) M^s_{\mu\tau} R_{23}(\theta_{23},0) &= \begin{bmatrix} 0 & 0 & 0 \\ 0 & 0 & c_\omega \cos(2\theta_{23}) - i s_\omega \\ 0 & c_\omega \cos(2\theta_{23}) + i s_\omega & 0 \end{bmatrix} . \end{aligned} \tag{7.114}$$

We find it convenient to define

$$c_\omega \sin(2\theta_{23}) \;=\; \cos(2\vartheta_\omega) \,, \qquad \left[c_\omega \cos(2\theta_{23}) - i s_\omega\right] \;=\; e^{-i\Omega} \sin(2\vartheta_\omega) \,. \tag{7.115}$$

Choosing ϑ_ω and Ω in the ranges

$$0 \;\le\; \vartheta_\omega \;\le\; \frac{\pi}{2} \,, \qquad -\pi \;<\; \Omega \;\le\; \pi \,, \tag{7.116}$$

we obtain

$$\tan(2\vartheta_\omega) \;\equiv\; \frac{\sqrt{c^2_\omega \cos^2(2\theta_{23}) + s^2_\omega}}{c_\omega \sin(2\theta_{23})} \,, \qquad \Omega \;\equiv\; \arctan\left[\frac{s_\omega}{\cos(2\theta_{23}) c_\omega}\right] \,. \tag{7.117}$$

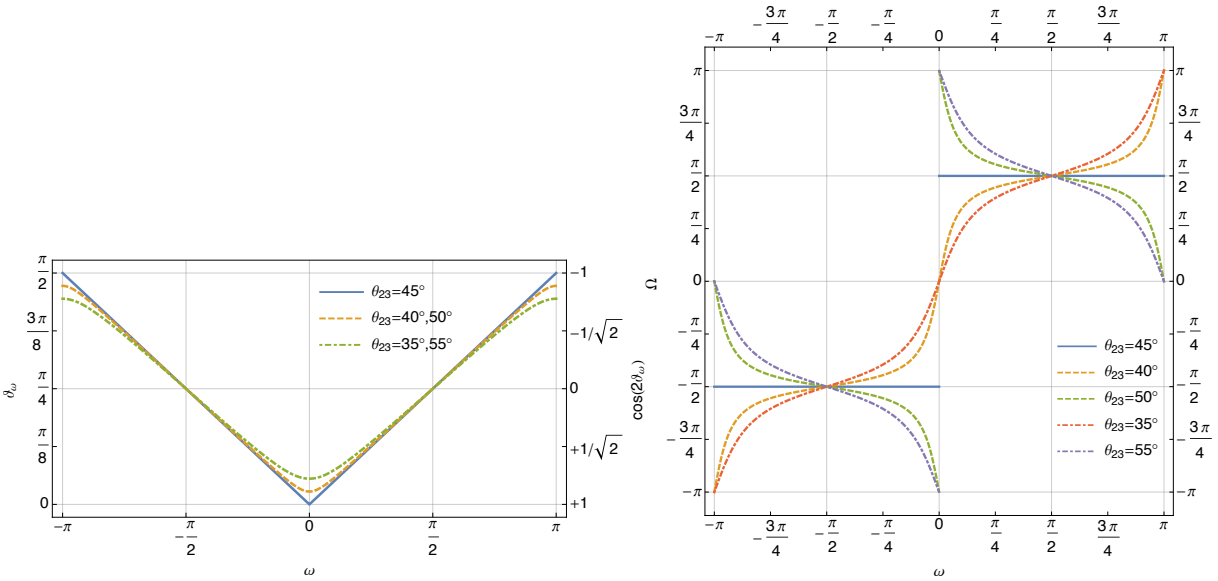

(a) (b)

Figure 7.14: The ω-dependence of (a) ϑ_ω and (b) Ω.

The ω-dependence of ϑ_ω and Ω is shown in Fig. 7.14 for several values of θ_{23}. Note that due to our restriction $\Omega \in (-\pi, \pi]$, Ω has a discontinuity of 2π at $\omega = 0$ if $\frac{\pi}{4} < \theta_{23} \leq \frac{\pi}{2}$, and at $\omega = \pm\pi$ if $0 \leq \theta_{23} < \frac{\pi}{4}$. For the $\theta_{23} = \frac{\pi}{4}$ case, $\Omega = +\frac{\pi}{2}$, $\vartheta_\omega = +\frac{\omega}{2}$ in the range $0 < \omega < \frac{\pi}{2}$, $\Omega = -\frac{\pi}{2}$, $\vartheta_\omega = -\frac{\omega}{2}$ in the range $-\frac{\pi}{2} < \omega < 0$, while at $\omega = 0, \pm\pi$, Ω is indeterminate. Note also that if $\omega = \pm\frac{\pi}{2}$, that is, $\varepsilon_{\mu\tau}$ is purely imaginary, then $\cos(2\vartheta_\omega) = c_\omega \sin(2\theta_{23}) = 0$. These definitions allow us to write

$$\begin{aligned} R_{23}^T(\theta_{23},0) M_{\mu\tau}^c R_{23}^*(\theta_{23},0) &= \cos(2\vartheta_\omega) \begin{bmatrix} 0 & 0 & 0 \\ 0 & -1 & 0 \\ 0 & 0 & 1 \end{bmatrix} , \\ R_{23}^T(\theta_{23},0) M_{\mu\tau}^s R_{23}^*(\theta_{23},0) &= \sin(2\vartheta_\omega) \begin{bmatrix} 0 & 0 & 0 \\ 0 & 0 & e^{-i\Omega} \\ 0 & e^{i\Omega} & 0 \end{bmatrix} . \end{aligned} \tag{7.118}$$

Next, we multiply with Q_3 and its conjugate to find

$$\begin{aligned} Q_3 R_{23}^T(\theta_{23},0) M_{\mu\tau}^c R_{23}^*(\theta_{23},0) Q_3^* &= \cos(2\vartheta_\omega) \begin{bmatrix} 0 & 0 & 0 \\ 0 & -1 & 0 \\ 0 & 0 & 1 \end{bmatrix} , \\ Q_3 R_{23}^T(\theta_{23},0) M_{\mu\tau}^s R_{23}^*(\theta_{23},0) Q_3^* &= \sin(2\vartheta_\omega) \begin{bmatrix} 0 & 0 & 0 \\ 0 & 0 & e^{-i(\delta+\Omega)} \\ 0 & e^{i(\delta+\Omega)} & 0 \end{bmatrix} . \end{aligned} \tag{7.119}$$

From this, we see that $\overline{M}^{c\prime}_{\mu\tau} = Q_3 U^T M^c_{\mu\tau} U^* Q_3^*$ will not have any δ dependence, while $\overline{M}^{s\prime}_{\mu\tau} = Q_3 U^T M^s_{\mu\tau} U^* Q_3^*$ will only depend on the sum $\delta + \Omega$. Performing the remaining two rotations, we obtain

$$\begin{aligned}
\overline{M}^{c\prime}_{\mu\tau} &= Q_3 U^T M^c_{\mu\tau} U^* Q_3^* \\
&= \cos(2\vartheta_\omega) \begin{bmatrix} -s_{12}^2 + c_{12}^2 s_{13}^2 & s_{12}c_{12}(1+s_{13}^2) & -c_{12}s_{13}c_{13} \\ s_{12}c_{12}(1+s_{13}^2) & -c_{12}^2 + s_{12}^2 s_{13}^2 & -s_{12}s_{13}c_{13} \\ -c_{12}s_{13}c_{13} & -s_{12}s_{13}c_{13} & c_{13}^2 \end{bmatrix}, \\
\overline{M}^{s\prime}_{\mu\tau} &= Q_3 U^T M^s_{\mu\tau} U^* Q_3^* \\
&= \sin(2\vartheta_\omega) \begin{bmatrix} 2s_{12}c_{12}s_{13}\cos(\delta+\Omega) & s_{13}e^{-i(\delta+\Omega)} - 2c_{12}^2 s_{13}\cos(\delta+\Omega) & -s_{12}c_{13}e^{-i(\delta+\Omega)} \\ s_{13}e^{i(\delta+\Omega)} - 2c_{12}^2 s_{13}\cos(\delta+\Omega) & -2s_{12}c_{12}s_{13}\cos(\delta+\Omega) & c_{12}c_{13}e^{-i(\delta+\Omega)} \\ -s_{12}c_{13}e^{i(\delta+\Omega)} & c_{12}c_{13}e^{i(\delta+\Omega)} & 0 \end{bmatrix}.
\end{aligned} \tag{7.120}$$

So in this vacuum-mass-eigenbasis, the part of the Hamiltonian we diagonalize first is given by

$$\begin{aligned}
&\overline{H}^{\prime}_a - a\varepsilon \overline{M}^{c\prime}_{\mu\tau} \\
&= \begin{bmatrix} -a[c_{12}^2 c_{13}^2 - \varepsilon_c(s_{12}^2 - c_{12}^2 s_{13}^2)] & -ac_{12}s_{12}[c_{13}^2 + \varepsilon_c(1+s_{13}^2)] & -ac_{12}s_{13}c_{13}(1-\varepsilon_c) \\ -ac_{12}s_{12}[c_{13}^2 + \varepsilon_c(1+s_{13}^2)] & \delta m_{21}^2 - a[s_{12}^2 c_{13}^2 - \varepsilon_c(c_{12}^2 - s_{12}^2 s_{13}^2)] & -as_{12}s_{13}c_{13}(1-\varepsilon_c) \\ -ac_{12}s_{13}c_{13}(1-\varepsilon_c) & -as_{12}s_{13}c_{13}(1-\varepsilon_c) & \delta m_{31}^2 - a(s_{13}^2 + \varepsilon_c c_{13}^2) \end{bmatrix},
\end{aligned} \tag{7.121}$$

where we have set $\varepsilon_c \equiv \varepsilon\cos(2\vartheta_\omega)$. We now approximately diagonalize this matrix following the Jacobi diagonalization procedure.

First Rotation

We first perform a 12-rotation to diagonalize the 12 submatrix. The rotation matrix necessary is given by

$$V_\varepsilon \equiv \begin{bmatrix} \overline{c}_{\varphi_\varepsilon} & \overline{s}_{\varphi_\varepsilon} & 0 \\ -\overline{s}_{\varphi_\varepsilon} & \overline{c}_{\varphi_\varepsilon} & 0 \\ 0 & 0 & 1 \end{bmatrix}, \tag{7.122}$$

where $\overline{c}_{\varphi_\varepsilon} = \cos(\overline{\varphi}_\varepsilon)$, $\overline{s}_{\varphi_\varepsilon} = \sin(\overline{\varphi}_\varepsilon)$, and

$$\tan 2\overline{\varphi}_\varepsilon = \frac{-a[c_{13}^2 + \varepsilon_c(1+s_{13}^2)]\sin(2\theta_{12})}{\delta m_{21}^2 + a[c_{13}^2 + \varepsilon_c(1+s_{13}^2)]\cos(2\theta_{12})}. \tag{7.123}$$

See Fig. 7.15(a). Using V_ε we obtain

$$\overline{H}^{\prime\prime}_a - a\varepsilon \overline{M}^{c\prime\prime}_{\mu\tau}$$

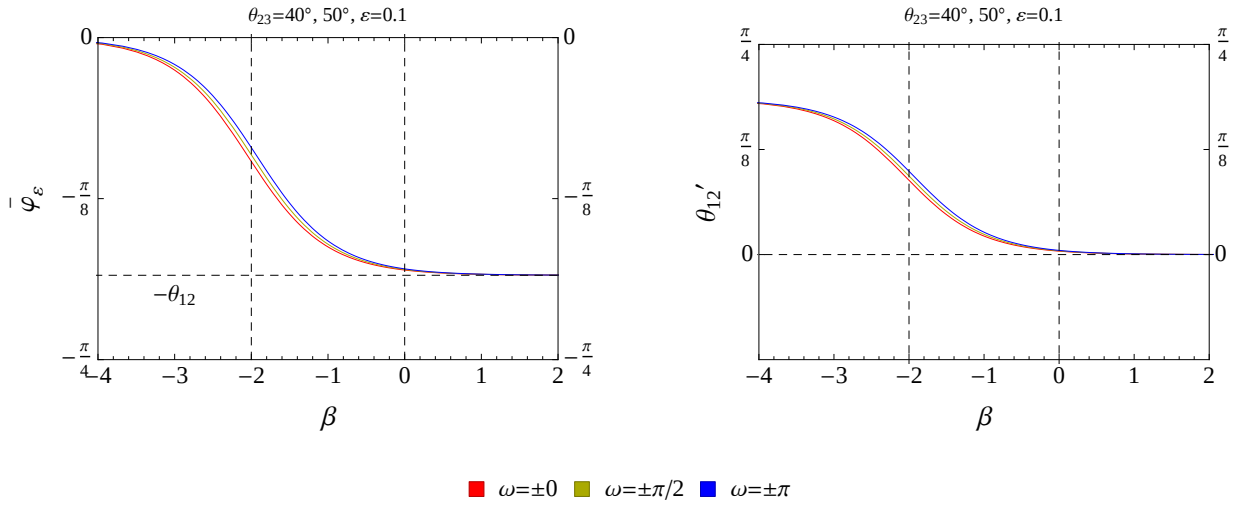

Figure 7.15: The β-dependence of $\overline{\varphi}_\varepsilon$ (left) and θ'_{12} (right) for the $\varepsilon = 0.1$ case.

$$
\begin{aligned}
&= V_\varepsilon^\dagger \left(\overline{H}'_a - a\varepsilon \overline{M}'^{c\prime}_{\mu\tau} \right) V_\varepsilon \\
&= \begin{bmatrix} \overline{\lambda}'_{\varepsilon-} & 0 & -ac'_{12}s_{13}c_{13}(1-\varepsilon_c) \\ 0 & \overline{\lambda}'_{\varepsilon+} & -as'_{12}s_{13}c_{13}(1-\varepsilon_c) \\ -ac'_{12}s_{13}c_{13}(1-\varepsilon_c) & -as'_{12}s_{13}c_{13}(1-\varepsilon_c) & \delta m^2_{31} - a(s^2_{13}+\varepsilon_c c^2_{13}) \end{bmatrix} ,
\end{aligned}
\tag{7.124}
$$

where

$$
\begin{aligned}
\overline{\lambda}'_{\varepsilon\pm} &= \frac{\{(\delta m^2_{21} + a\varepsilon_c) - a(c^2_{13} + \varepsilon_c s^2_{13})\}}{2} \\
&\pm \frac{\sqrt{\{(\delta m^2_{21} + a\varepsilon_c) + a(c^2_{13} + \varepsilon_c s^2_{13})\}^2 - 4as^2_{12}\{c^2_{13} + \varepsilon_c(1+s^2_{13})\}\delta m^2_{21}}}{2} .
\end{aligned}
\tag{7.125}
$$

and

$$
s'_{12} = \sin\theta'_{12} , \qquad c'_{12} = \cos\theta'_{12} , \qquad \theta'_{12} \equiv \theta_{12} + \overline{\varphi}_\varepsilon . \tag{7.126}
$$

The angle θ'_{12}, which is the approximate running θ_{12}, can be calculated directly via

$$
\tan 2\theta'_{12} = \frac{\delta m^2_{21} \sin 2\theta_{12}}{\delta m^2_{21} \cos 2\theta_{12} + a[c^2_{13} + \varepsilon_c(1+s^2_{13})]} , \tag{7.127}
$$

which is shown in Fig. 7.15(b).

At small a, the $\overline{\lambda}'_{\varepsilon\pm}$ behave as

$$
\overline{\lambda}'_{\varepsilon+} = \delta m^2_{21} - a\{s^2_{12}c^2_{13} - \varepsilon_c(c^2_{12} - s^2_{12}s^2_{13})\} - a\,\mathcal{O}(a/\delta m^2_{21}) ,
$$

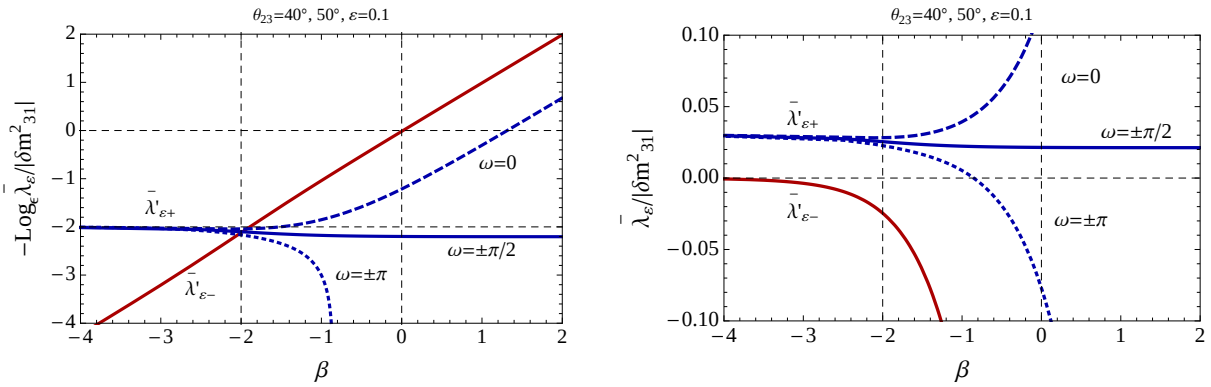

(a) (b)

Figure 7.16: The β-dependence of $\overline{\lambda}'_{\varepsilon\pm}$ for $\theta_{23} = 40^\circ$ and $\varepsilon = 0.1$ with $\omega = 0$ (dashed), $\omega = \pm\frac{\pi}{2}$ (solid) and $\omega = \pm\pi$ (dotted) shown in (a) log-scale, and (b) normal scale. The ω-dependence of $\overline{\lambda}'_{\varepsilon-}$ is weak and the curves for the three cases overlap.

$$\overline{\lambda}'_{\varepsilon-} = -a\{c_{12}^2 c_{13}^2 - \varepsilon_c(s_{12}^2 - c_{12}^2 s_{13}^2)\} - a\,\mathcal{O}(a/\delta m_{21}^2)\,, \tag{7.128}$$

while at large a, we have

$$\begin{aligned} \overline{\lambda}'_{\varepsilon-} &= -a(c_{13}^2 + \varepsilon_c s_{13}^2) + s_{12}^2\delta m_{21}^2 + \delta m_{21}^2\mathcal{O}(\delta m_{21}^2/a)\,, \\ \overline{\lambda}'_{\varepsilon+} &= a\varepsilon_c + c_{12}^2\delta m_{21}^2 + \delta m_{21}^2\mathcal{O}(\delta m_{21}^2/a)\,. \end{aligned} \tag{7.129}$$

Compared to the SM case, $\overline{\lambda}'_{\varepsilon-}$ does not asymptote to a constant except when $\omega = \pm\frac{\pi}{2}$ which would render ε_c zero even when $\varepsilon \neq 0$. This behavior is shown in Fig. 7.16.

Second Rotation

As a is increased, due to the running of θ'_{12} with a, the product as'_{12} will continue to increase while ac'_{12} stops increasing. Therefore, the (23)-submatrix of $\overline{H}''_a - a\varepsilon\overline{M}''_{\mu\tau}$ must be diagonalized next. This requires the rotation matrix

$$W_\varepsilon = \begin{bmatrix} \overline{c}_{\phi_\varepsilon} & 0 & \overline{s}_{\phi_\varepsilon} \\ 0 & 1 & 0 \\ -\overline{s}_{\phi_\varepsilon} & 0 & \overline{c}_{\phi_\varepsilon} \end{bmatrix}\,, \tag{7.130}$$

where $\overline{s}_{\phi_\varepsilon} = \sin\overline{\phi}_\varepsilon$, $\overline{c}_{\phi_\varepsilon} = \cos\overline{\phi}_\varepsilon$, and

$$\begin{aligned} \tan 2\overline{\phi}_\varepsilon &= \frac{-ac'_{12}(1-\varepsilon_c)\sin(2\theta_{13})}{\delta m_{31}^2 - a(s_{13}^2 + \varepsilon_c c_{13}^2) - \lambda'_{\varepsilon-}} \\ &\approx \frac{-a(1-\varepsilon_c)\sin(2\theta_{13})}{(\delta m_{31}^2 - s_{12}^2\delta m_{21}^2) + a(1-\varepsilon_c)\cos(2\theta_{13})}\,. \end{aligned} \tag{7.131}$$

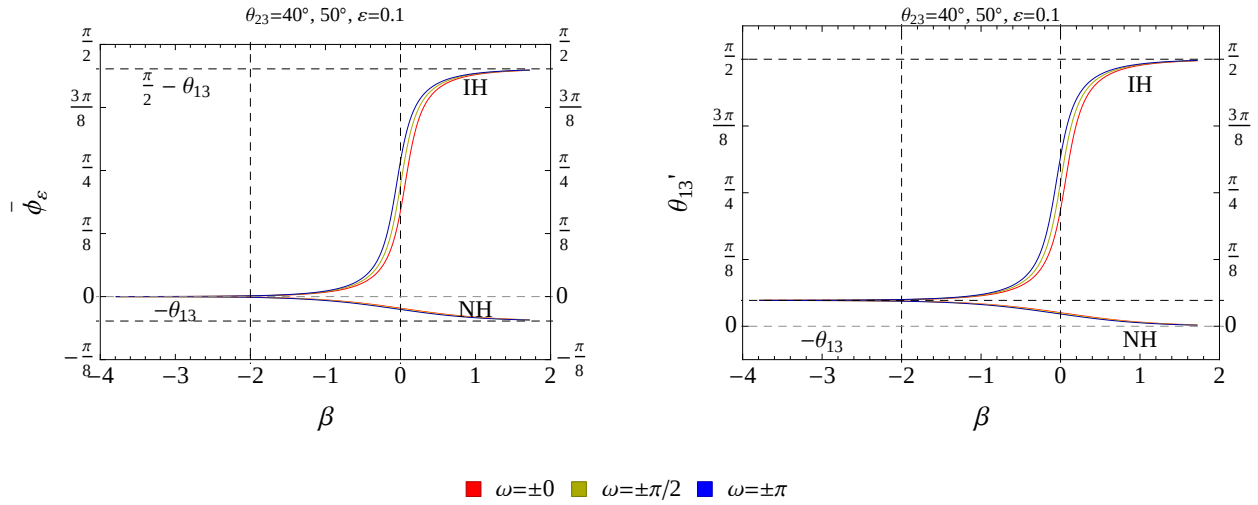

Figure 7.17: The β-dependence of $\overline{\phi}_\varepsilon$ (left) and θ'_{13} (right) for $\varepsilon = 0.1$ both normal (NH) and inverted (IH) hierarchies. The dependence of $\overline{\phi}_\varepsilon$ and θ'_{13} on ω for the inverted hierarchy case is weak and the three curves overlap.

Again, compared to Eq. (7.26), we can see that ϕ_ϵ evolves more or less similarly to ϕ but with a small shift in the resonance position. See Fig. 7.17. After the second rotation we have:

$$\begin{aligned}
&\overline{H}_a''' - a\varepsilon \overline{M}^{c'''}_{\mu\tau} \\
&= W_\varepsilon^\dagger \left(\overline{H}_a'' - a\varepsilon \overline{M}^{c''}_{\mu\tau} \right) W_\varepsilon \\
&= \begin{bmatrix} \overline{\lambda}''_{\varepsilon\mp} & a\overline{s}'_{12} s_{13} c_{13} \overline{s}_{\phi_\varepsilon} (1-\varepsilon_c) & 0 \\ a\overline{s}'_{12} s_{13} c_{13} \overline{s}_{\phi_\varepsilon} (1-\varepsilon_c) & \overline{\lambda}'_{\varepsilon+} & -a\overline{s}'_{12} s_{13} c_{13} \overline{c}_{\phi_\varepsilon} (1-\varepsilon_c) \\ 0 & -a\overline{s}'_{12} s_{13} c_{13} \overline{c}_{\phi_\varepsilon} (1-\varepsilon_c) & \overline{\lambda}''_{\varepsilon\pm} \end{bmatrix},
\end{aligned} \tag{7.132}$$

where

$$\begin{aligned}
\overline{\lambda}''_{\varepsilon\pm} &= \frac{\overline{\lambda}'_{\varepsilon-} + \left\{ \delta m^2_{31} - a(s^2_{13} + \varepsilon_c c^2_{13}) \right\}}{2} \\
&\quad \pm \frac{\sqrt{\left[\overline{\lambda}'_{\varepsilon-} - \left\{ \delta m^2_{31} - a(s^2_{13} + \varepsilon_c c^2_{13}) \right\} \right]^2 + 4 \left\{ a c'_{12} s_{13} c_{13} (1-\varepsilon_c) \right\}^2}}{2},
\end{aligned} \tag{7.133}$$

and the upper/lower signs correspond to the normal/inverted hierarchies.

For both hierarchies, the asymptotic forms are

$$\overline{\lambda}''_{\varepsilon-} = -a + (s^2_{13}\delta m^2_{31} + s^2_{12} c^2_{13} \delta m^2_{21}) + \delta m^2_{31} \mathcal{O}(\delta m^2_{31}/a),$$

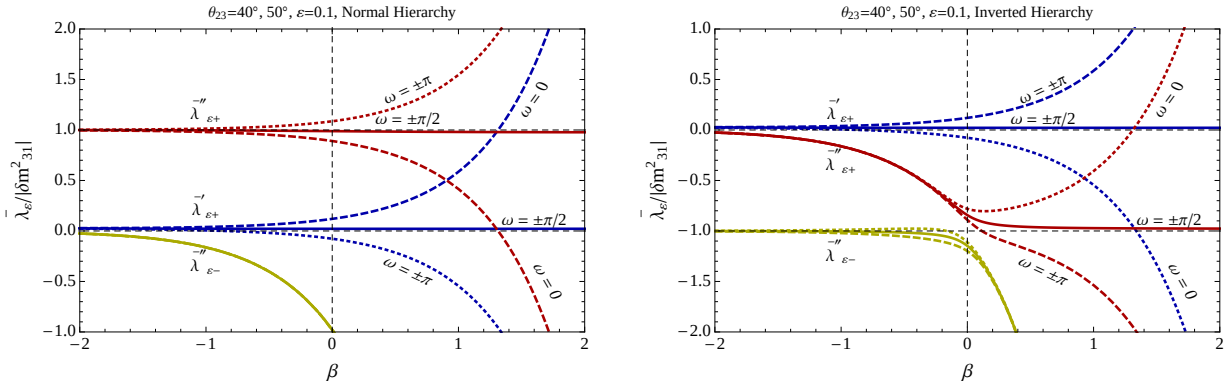

Figure 7.18: The β-dependence of $\overline{\lambda}''_{\varepsilon\pm}$ and $\overline{\lambda}'_{\varepsilon-}$ for the (a) normal and (b) inverted hierarchy cases with $\theta_{23} = 40°$ or $50°$ and $\varepsilon = 0.1$. Shown are the $\omega = 0$ (dashed), $\omega = \pm\dfrac{\pi}{2}$ (solid) and $\omega = \pm\pi$ cases. The ω-dependence of $\overline{\lambda}''_{\varepsilon+}$ is weak and the curves for the three cases are mostly overlapping.

$$\overline{\lambda}''_{\varepsilon+} \;=\; -a\varepsilon_c + (c_{13}^2\delta m_{31}^2 + s_{12}^2 s_{13}^2 \delta m_{21}^2) + \delta m_{31}^2 \mathcal{O}(\delta m_{31}^2/a)\;, \tag{7.134}$$

with δm_{31}^2 taking on the appropriate sign in each case. This is shown in Fig. 7.18.

Third Rotation

$\overline{H}_a''' - a\varepsilon\overline{M}_{\mu\tau}^{c'''}$ is approximately diagonalized since the off-diagonal elements are suppressed by as'_{12}. At this point, we include $\overline{M}_{\mu\tau}^{s'}$. After the first rotation, $\overline{M}_{\mu\tau}^{s'}$ becomes

$$\begin{aligned}
\varepsilon\overline{M}_{\mu\tau}^{s''} \;&=\; V_\varepsilon^\dagger \left(\varepsilon\overline{M}_{\mu\tau}^{s'}\right) V_\varepsilon \\
&=\; \varepsilon_s \begin{bmatrix} 2s'_{12}c'_{12}s_{13}\cos(\delta+\Omega) & s'_{13}e^{-i(\delta+\Omega)} - 2c'^2_{12}s_{13}\cos(\delta+\Omega) & -s'_{12}c_{13}e^{-i(\delta+\Omega)} \\ s_{13}e^{i(\delta+\Omega)} - 2c'^2_{12}s_{13}\cos(\delta+\Omega) & -2s'_{12}c'_{12}s_{13}\cos(\delta+\Omega) & c'_{12}c_{13}e^{-i(\delta+\Omega)} \\ -s'_{12}c_{13}e^{i(\delta+\Omega)} & c'_{12}c_{13}e^{i(\delta+\Omega)} & 0 \end{bmatrix} \\
&\xrightarrow{c'_{12}\approx 1} \varepsilon_s \begin{bmatrix} 0 & -s_{13}e^{i(\delta+\Omega)} & 0 \\ -s_{13}e^{-i(\delta+\Omega)} & 0 & c_{13}e^{-i(\delta+\Omega)} \\ 0 & c_{13}e^{i(\delta+\Omega)} & 0 \end{bmatrix}\;,
\end{aligned} \tag{7.135}$$

where we have set $\varepsilon_s = \varepsilon\sin(2\vartheta_\omega)$. After the second rotation, we have

$$\begin{aligned}
\varepsilon\overline{M}_{\mu\tau}^{s'''} \;&=\; W_\varepsilon^\dagger \left(\varepsilon\overline{M}_{\mu\tau}^{s''}\right) W_\varepsilon \\
&\approx\; \varepsilon_s \begin{bmatrix} 0 & -s'_{13}e^{i(\delta+\Omega)} & 0 \\ -s'_{13}e^{-i(\delta+\Omega)} & 0 & c'_{13}e^{-i(\delta+\Omega)} \\ 0 & c'_{13}e^{i(\delta+\Omega)} & 0 \end{bmatrix}\;,
\end{aligned} \tag{7.136}$$

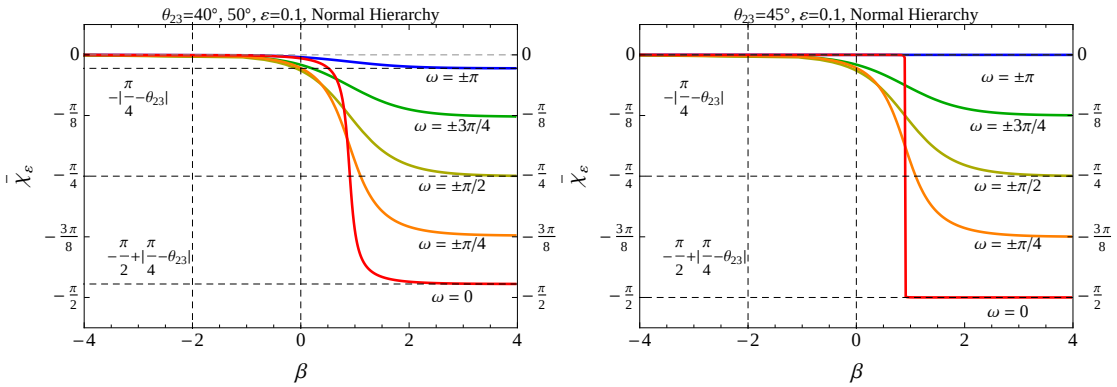

Figure 7.19: The β-dependence of $\overline{\chi}_\varepsilon$ for $\varepsilon = 0.1$ and a variety of ω values for the cases (a) $\theta_{23} = 40°$, $50°$ and (b) $\theta_{23} = 45°$ with $\delta m^2_{31} > 0$.

where

$$s'_{13} \;=\; \sin\theta'_{13}\,, \qquad c'_{13} \;=\; \cos\theta'_{13}\,, \qquad \theta'_{13} \;\equiv\; \theta_{13} + \overline{\phi}_\varepsilon\,. \tag{7.137}$$

The angle θ'_{13}, which is the approximate running θ_{13}, can be calculated directly via

$$\tan 2\theta'_{13} \;=\; \frac{(\delta m^2_{31} - s^2_{12}\delta m^2_{21})\sin(2\theta_{13})}{(\delta m^2_{31} - s^2_{12}\delta m^2_{21})\cos(2\theta_{13}) + a(1-\varepsilon_c)}\,. \tag{7.138}$$

The running of θ'_{13} depends on the mass hierarchy. For inverted hierarchy, θ'_{13} runs to $\dfrac{\pi}{2}$ as a is increased, so $s'_{13} \to 1$, $c'_{13} \to 0$. For the normal hierarchy, θ'_{13} runs to 0 as a is increased, so we have $s'_{13} \to 0$, $c'_{13} \to 1$. Therefore, for the inverted hierarchy, we have

$$\varepsilon M^{s'''}_{\mu\tau} \xrightarrow{a \gg \delta m^2_{31}} \varepsilon_s \begin{bmatrix} 0 & -e^{i(\delta+\Omega)} & 0 \\ -e^{-i(\delta+\Omega)} & 0 & 0 \\ 0 & 0 & 0 \end{bmatrix}, \tag{7.139}$$

while, for the normal hierarchy, we have

$$\varepsilon M^{s'''}_{\mu\tau} \xrightarrow{a \gg |\delta m^2_{31}|} \varepsilon_s \begin{bmatrix} 0 & 0 & 0 \\ 0 & 0 & e^{-i(\delta+\Omega)} \\ 0 & e^{i(\delta+\Omega)} & 0 \end{bmatrix}. \tag{7.140}$$

So, for the normal hierarchy case, we need to perform a 23-rotation as the third rotation, and, for the inverted hierarchy, case we need to perform a 12-rotation. In either case, $\lambda'_{\varepsilon+}$ and $\lambda''_{\varepsilon+}$ get mixed.

- **$\delta m^2_{31} > 0$ Case**

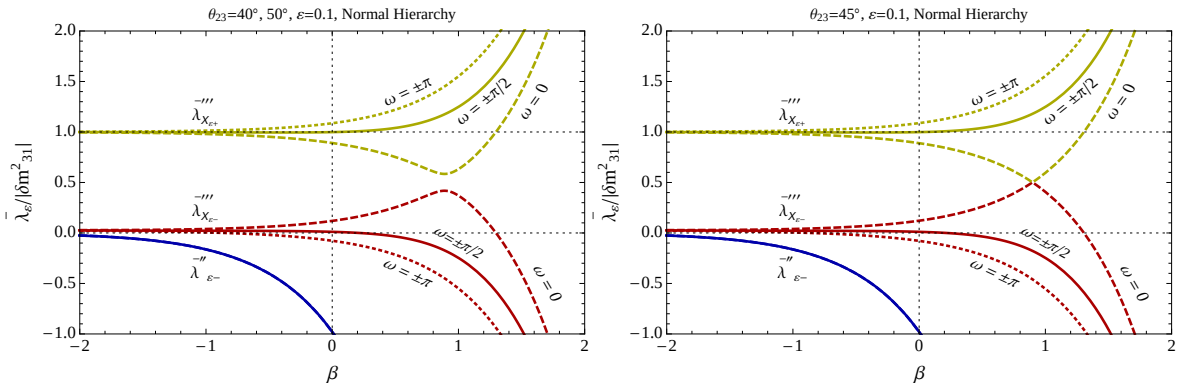

Figure 7.20: The β-dependence of $\overline{\lambda}'''_{X_\varepsilon\pm}$ for $\varepsilon = 0.1$ and a variety of ω values for the two case (a) $\theta_{23} = 40°, 50°$ and (b) $\theta_{23} = 45°$ with $\delta m^2_{31} > 0$.

For the normal hierarchy, the full matrix is

$$\begin{aligned}\overline{H}'''_{\mu\tau} &= \overline{H}'''_a - a\varepsilon\overline{M}^{c'''}_{\mu\tau} - a\varepsilon\overline{M}^{s'''}_{\mu\tau} \\ &= \begin{bmatrix} \overline{\lambda}''_{\varepsilon-} & 0 & 0 \\ 0 & \overline{\lambda}'_{\varepsilon+} & -a\varepsilon_s c'_{13} e^{-i(\delta+\Omega)} \\ 0 & -a\varepsilon_s c'_{13} e^{i(\delta+\Omega)} & \overline{\lambda}''_{\varepsilon+} \end{bmatrix}, \end{aligned} \tag{7.141}$$

where we have dropped terms of order as'_{12} and $a\varepsilon s'_{13}$. The rotation matrix necessary to diagonalize this is

$$X_\varepsilon = \begin{bmatrix} 1 & 0 & 0 \\ 0 & \overline{c}_{\chi_\varepsilon} & \overline{s}_{\chi_\varepsilon} e^{-i(\delta+\Omega)} \\ 0 & -\overline{s}_{\chi_\varepsilon} e^{i(\delta+\Omega)} & \overline{c}_{\chi_\varepsilon} \end{bmatrix}, \tag{7.142}$$

where

$$\begin{aligned}\tan 2\overline{\chi}_\varepsilon &= -\frac{2a\varepsilon_s c'_{13}}{\overline{\lambda}''_{\varepsilon+} - \overline{\lambda}'_{\varepsilon+}} \\ &\approx \frac{-2a\varepsilon\sin(2\vartheta_\omega)}{[c^2_{13}\delta m^2_{31} - (c^2_{12} - s^2_{12}s^2_{13})\delta m^2_{21}] - 2a\varepsilon\cos(2\vartheta_\omega)}\,. \end{aligned} \tag{7.143}$$

Asymptotically, we have

$$\overline{\chi}_\varepsilon \xrightarrow{a\varepsilon \gg |\delta m^2_{31}|} \vartheta_\omega - \frac{\pi}{2}\,, \tag{7.144}$$

for each value of ω. This behavior is shown in Fig. 7.19 for the $\theta_{23} = 40°$, $45°$, and $50°$ cases.

After the third rotation,

$$\overline{H}''''_{\mu\tau} = X^\dagger_\varepsilon \overline{H}'''_{\mu\tau} X_\varepsilon$$

$$= \begin{bmatrix} \overline{\lambda}''_{\varepsilon-} & 0 & 0 \\ 0 & \overline{\lambda}'''_{X_\varepsilon-} & 0 \\ 0 & 0 & \overline{\lambda}'''_{X_\varepsilon+} \end{bmatrix} , \tag{7.145}$$

where

$$\overline{\lambda}'''_{X_\varepsilon\pm} = \frac{\left(\overline{\lambda}''_{\varepsilon+} + \overline{\lambda}'_{\varepsilon+}\right) \pm \sqrt{\left(\overline{\lambda}''_{\varepsilon+} - \overline{\lambda}'_{\varepsilon+}\right)^2 + 4a^2\varepsilon_s^2 c_{13}'^2}}{2} . \tag{7.146}$$

Thus, after three rotations, our matrix is approximately diagonal. Note that if $\theta_{23} = \frac{\pi}{4}$ and $\omega = 0$ or $\pm\pi$, then $\varepsilon_s = \varepsilon \sin(2\vartheta_\omega) = 0$, and we will have

$$\begin{aligned} \overline{\lambda}'''_{X_\varepsilon+} &= \max(\overline{\lambda}''_{\varepsilon-}, \overline{\lambda}'_{\varepsilon-}) , \\ \overline{\lambda}'''_{X_\varepsilon-} &= \min(\overline{\lambda}''_{\varepsilon-}, \overline{\lambda}'_{\varepsilon-}) . \end{aligned} \tag{7.147}$$

Asymptotically, we have

$$\begin{aligned} &\overline{\lambda}'''_{X_\varepsilon\mp} \\ &= \mp\varepsilon a + \frac{1}{2}\Big[(1 \pm \cos 2\vartheta_\omega)(\delta m_{31}^2 c_{13}^2 + \delta m_{21}^2 s_{12}^2 s_{13}^2) + (1 \mp \cos 2\vartheta_\omega)\delta m_{21}^2 c_{12}^2\Big] + \cdots \\ &= \mp\varepsilon a + \left\{ \begin{array}{c} \cos^2\vartheta_\omega \\ \sin^2\vartheta_\omega \end{array} \right\} (\delta m_{31}^2 c_{13}^2 + \delta m_{21}^2 s_{12}^2 s_{13}^2) + \left\{ \begin{array}{c} \sin^2\vartheta_\omega \\ \cos^2\vartheta_\omega \end{array} \right\} \delta m_{21}^2 c_{12}^2 + \cdots \end{aligned} \tag{7.148}$$

See Fig. 7.20.

- **$\delta m_{31}^2 < 0$ Case**

For the inverted hierarchy, the full matrix is

$$\begin{aligned} \overline{H}'''_{\mu\tau} &= \overline{H}'''_a - a\varepsilon\overline{M}^{c\prime\prime\prime}_{\mu\tau} - a\varepsilon\overline{M}^{s\prime\prime\prime}_{\mu\tau} \\ &= \begin{bmatrix} \overline{\lambda}''_{\varepsilon+} & a\varepsilon_s s'_{13} e^{i(\delta+\Omega)} & 0 \\ a\varepsilon_s s'_{13} e^{-i(\delta+\Omega)} & \overline{\lambda}'_{\varepsilon+} & 0 \\ 0 & 0 & \overline{\lambda}''_{\varepsilon-} \end{bmatrix} , \end{aligned} \tag{7.149}$$

where we have dropped terms of order as'_{12} and $a\varepsilon c'_{13}$. The rotation matrix necessary to diagonalize this is

$$Y_\varepsilon = \begin{bmatrix} \overline{c}_{\psi_\varepsilon} & \overline{s}_{\psi_\varepsilon} e^{i(\delta+\Omega)} & 0 \\ -\overline{s}_{\psi_\varepsilon} e^{-i(\delta+\Omega)} & \overline{c}_{\psi_\varepsilon} & 0 \\ 0 & 0 & 1 \end{bmatrix} , \tag{7.150}$$

where

$$\tan 2\overline{\psi}_\varepsilon = \frac{2a\varepsilon_s s'_{13}}{\lambda'_{\varepsilon+} - \lambda''_{\varepsilon+}}$$

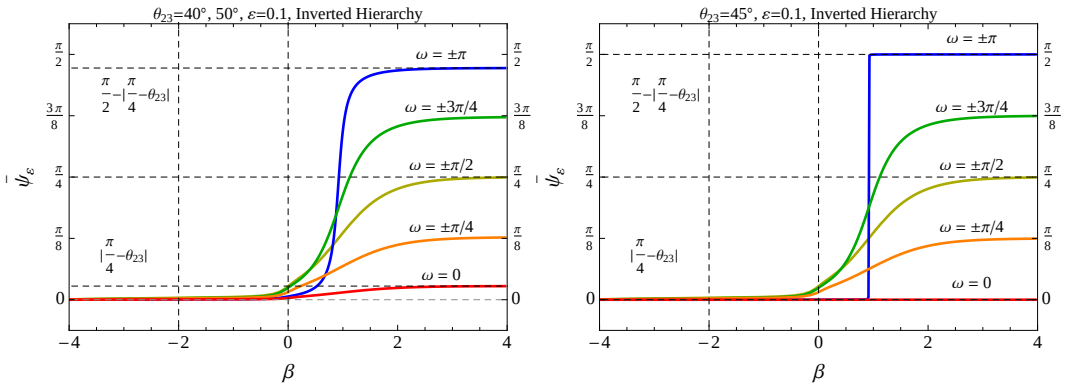

Figure 7.21: The β-dependence of $\overline{\psi}_\varepsilon$ for $\varepsilon = 0.1$ and a variety of ω values for the cases (a) $\theta_{23} = 40°$, $50°$ and (b) $\theta_{23} = 45°$ with $\delta m^2_{31} < 0$.

$$\approx \frac{2a\varepsilon \sin(2\vartheta_\omega)}{[c^2_{13}|\delta m^2_{31}| + (c^2_{12} - s^2_{12}s^2_{13})\delta m^2_{21}] + 2a\varepsilon\cos(2\vartheta_\omega)} \ . \tag{7.151}$$

Comparing the approximate expression of $\tan 2\psi_\varepsilon$ given in the second line of this equation to the second line of Eq. (7.143), we see that they differ in only the sign of δm^2_{31}. Therefore, the same approximate expression can be used to define both χ_ε for the $\delta m^2_{31} > 0$ case and ψ_ε for the $\delta m^2_{31} < 0$ case. Asymptotically, we have

$$\overline{\psi}_\varepsilon \xrightarrow{a\varepsilon \gg |\delta m^2_{31}|} \vartheta_\omega \ , \tag{7.152}$$

for each value of ω. This behavior is shown in Fig. 7.21 for the $\theta_{23} = 40°$, $45°$, and $50°$ cases.

After the third rotation,

$$\begin{aligned} \overline{H}''''_{\mu\tau} &= Y^\dagger_\varepsilon \overline{H}'''_{\mu\tau} Y_\varepsilon \\ &= \begin{bmatrix} \overline{\lambda}'''_{Y_\varepsilon +} & 0 & 0 \\ 0 & \overline{\lambda}'''_{Y_\varepsilon -} & 0 \\ 0 & 0 & \overline{\lambda}''_{\varepsilon -} \end{bmatrix} , \end{aligned} \tag{7.153}$$

where

$$\overline{\lambda}'''_{Y_\varepsilon \pm} = \frac{\left(\overline{\lambda}''_{\varepsilon +} + \overline{\lambda}'_{\varepsilon +}\right) \pm \sqrt{\left(\overline{\lambda}''_{\varepsilon +} - \overline{\lambda}'_{\varepsilon +}\right)^2 + 4a^2\varepsilon^2_s s'^2_{13}}}{2} \ . \tag{7.154}$$

Thus, after three rotations, our matrix is approximately diagonal. Note that if $\theta_{23} = \dfrac{\pi}{4}$ and $\omega = 0$ or $\pm\pi$, then $\varepsilon_c = \varepsilon\cos(2\vartheta_\omega) = 0$, and we will have

$$\overline{\lambda}'''_{Y_\varepsilon +} = \max(\overline{\lambda}''_{\varepsilon +}, \overline{\lambda}'_{\varepsilon +}) \ ,$$

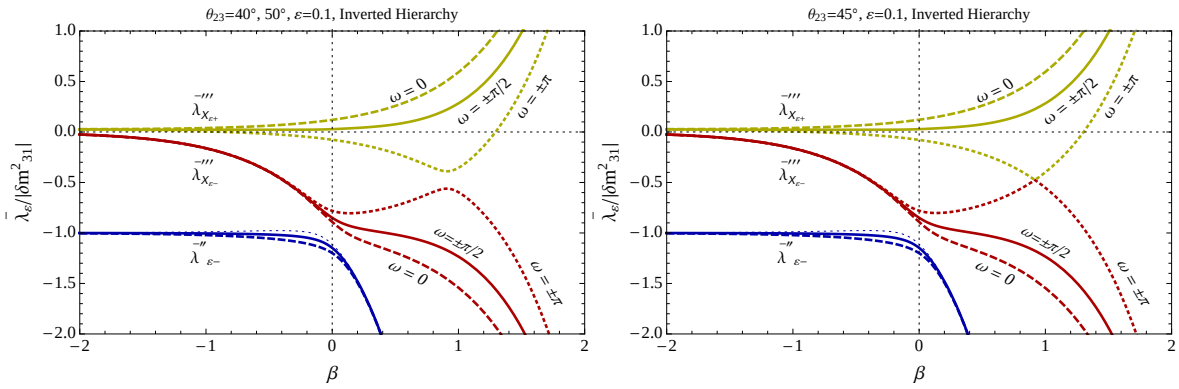

Figure 7.22: The β-dependence of $\overline{\lambda}'''_{Y_\varepsilon\pm}$ for $\varepsilon = 0.1$ and a variety of ω values for the two case (a) $\theta_{23} = 40°, 50°$ and (b) $\theta_{23} = 45°$ with $\delta m^2_{31} < 0$.

$$\overline{\lambda}'''_{Y_\varepsilon -} \;=\; \min(\overline{\lambda}''_{\varepsilon+}, \overline{\lambda}'_{\varepsilon+}) \; . \tag{7.155}$$

Note that the min and max are inverted from the normal hierarchy case. Asymptotically, we have

$$\begin{aligned}
&\overline{\lambda}'''_{Y_\varepsilon \mp} \\
&= \mp\varepsilon a + \frac{1}{2}\Big[(1 \pm \cos 2\vartheta_\omega)(\delta m^2_{31} c^2_{13} + \delta m^2_{21} s^2_{12} s^2_{13}) + (1 \mp \cos 2\vartheta_\omega)\delta m^2_{21} c^2_{12}\Big] + \cdots \\
&= \mp\varepsilon a + \left\{ \begin{array}{c} \cos^2\vartheta_\omega \\ \sin^2\vartheta_\omega \end{array} \right\}(\delta m^2_{31} c^2_{13} + \delta m^2_{21} s^2_{12} s^2_{13}) + \left\{ \begin{array}{c} \sin^2\vartheta_\omega \\ \cos^2\vartheta_\omega \end{array} \right\}\delta m^2_{21} c^2_{12} + \cdots
\end{aligned} \tag{7.156}$$

These expressions are the same as Eq. (7.148), expect δm^2_{31} is negative here. This behavior is shown in Fig. 7.22.

Absorption into Effective Mixing Angles

- **$\delta m^2_{31} > 0$ Case**

  As we have seen above, the effective mixing matrix is well approximated by the product of matrices given by

$$\begin{aligned}
\tilde{U}^* &= U^* Q_3^* V_\varepsilon W_\varepsilon X_\varepsilon \\
&= \underbrace{R_{23}(\theta_{23},0) Q_3^* R_{13}(\theta_{13},0) R_{12}(\theta_{12},0)}_{U^* Q_3^*} \underbrace{R_{12}(\overline{\varphi}_\varepsilon,0)}_{V_\varepsilon} \underbrace{R_{13}(\overline{\phi}_\varepsilon,0)}_{W_\varepsilon} \underbrace{R_{23}(\overline{\chi}_\varepsilon,\delta+\Omega)}_{X_\varepsilon} \\
&\approx R_{23}(\theta_{23},0) Q_3^* R_{13}(\theta'_{13},0) R_{12}(\theta'_{12},0) R_{23}(\overline{\chi}_\varepsilon,\delta+\Omega) \\
&\approx R_{23}(\theta_{23},0) Q_3^* R_{23}(\overline{\chi}_\varepsilon,\delta+\Omega) R_{13}(\theta'_{13},0) R_{12}(\theta'_{12},0) \; .
\end{aligned} \tag{7.157}$$

Let us look at the 23 submatrix of the product $R_{23}(\theta_{23},0)Q_3^* R_{23}(\overline{\chi}_\varepsilon,\delta+\Omega)$. We have

$$\begin{aligned}
&\begin{bmatrix} c_{23} & s_{23} \\ -s_{23} & c_{23} \end{bmatrix} \begin{bmatrix} 1 & 0 \\ 0 & e^{-i\delta} \end{bmatrix} \begin{bmatrix} \overline{c}_{\chi_\varepsilon} & \overline{s}_{\chi_\varepsilon} e^{-i(\delta+\Omega)} \\ -\overline{s}_{\chi_\varepsilon} e^{i(\delta+\Omega)} & \overline{c}_{\chi_\varepsilon} \end{bmatrix} \\
&= \begin{bmatrix} c_{23} & s_{23} \\ -s_{23} & c_{23} \end{bmatrix} \begin{bmatrix} 1 & 0 \\ 0 & e^{i\Omega} \end{bmatrix} \begin{bmatrix} \overline{c}_{\chi_\varepsilon} & \overline{s}_{\chi_\varepsilon} \\ -\overline{s}_{\chi_\varepsilon} & \overline{c}_{\chi_\varepsilon} \end{bmatrix} \begin{bmatrix} 1 & 0 \\ 0 & e^{-i(\delta+\Omega)} \end{bmatrix} . \qquad (7.158)
\end{aligned}$$

The product of the three matrices on the left can be rewritten as

$$\begin{aligned}
&\begin{bmatrix} c_{23} & s_{23} \\ -s_{23} & c_{23} \end{bmatrix} \begin{bmatrix} 1 & 0 \\ 0 & e^{i\Omega} \end{bmatrix} \begin{bmatrix} \overline{c}_{\chi_\varepsilon} & \overline{s}_{\chi_\varepsilon} \\ -\overline{s}_{\chi_\varepsilon} & \overline{c}_{\chi_\varepsilon} \end{bmatrix} \\
&= \begin{bmatrix} e^{-i\alpha_1} & 0 \\ 0 & e^{-i\alpha_2} \end{bmatrix} \begin{bmatrix} c'_{23} & s'_{23} \\ -s'_{23} & c'_{23} \end{bmatrix} \begin{bmatrix} 1 & 0 \\ 0 & e^{-i\gamma} \end{bmatrix} , \qquad (7.159)
\end{aligned}$$

where

$$\begin{aligned}
c'_{23} \;=\; \cos\theta'_{23} \;&=\; \sqrt{c_{23}^2 \overline{c}_{\chi_\varepsilon}^2 - 2c_{23}s_{23}\overline{c}_{\chi_\varepsilon}\overline{s}_{\chi_\varepsilon}\cos\Omega + s_{23}^2\overline{s}_{\chi_\varepsilon}^2} \\
&=\; \sqrt{\cos^2(\Omega/2)\cos^2(\theta_{23}+\overline{\chi}_\varepsilon) + \sin^2(\Omega/2)\cos^2(\theta_{23}-\overline{\chi}_\varepsilon)} \,, \\
\alpha_1 \;&=\; \arctan\left[\frac{s_{23}\overline{s}_{\chi_\varepsilon}\sin\Omega}{c_{23}\overline{c}_{\chi_\varepsilon} - s_{23}\overline{s}_{\chi_\varepsilon}\cos\Omega} \right] , \\
\alpha_2 \;&=\; \arctan\left[-\frac{c_{23}\overline{s}_{\chi_\varepsilon}\sin\Omega}{s_{23}\overline{c}_{\chi_\varepsilon} + c_{23}\overline{s}_{\chi_\varepsilon}\cos\Omega} \right] , \\
\gamma \;&=\; \arctan\left[-\frac{\sin(2\theta_{23})\sin\Omega}{\sin(2\overline{\chi}_\varepsilon)\cos(2\theta_{23}) + \cos(2\overline{\chi}_\varepsilon)\sin(2\theta_{23})\cos\Omega} \right] \\
&=\; \arctan\left[-\frac{s_\omega \tan(2\theta_{23})}{\cos 2(\overline{\chi}_\varepsilon - \vartheta_\omega)} \right] . \qquad (7.160)
\end{aligned}$$

The branches of the arctangents must be chosen judiciously for this to work. Using this result, we can write

$$\begin{aligned}
&\begin{bmatrix} c_{23} & s_{23} \\ -s_{23} & c_{23} \end{bmatrix} \begin{bmatrix} 1 & 0 \\ 0 & e^{i\Omega} \end{bmatrix} \begin{bmatrix} \overline{c}_{\chi_\varepsilon} & \overline{s}_{\chi_\varepsilon} \\ -\overline{s}_{\chi_\varepsilon} & \overline{c}_{\chi_\varepsilon} \end{bmatrix} \begin{bmatrix} 1 & 0 \\ 0 & e^{-i(\delta+\Omega)} \end{bmatrix} \\
&= \begin{bmatrix} e^{-i\alpha_1} & 0 \\ 0 & e^{-i\alpha_2} \end{bmatrix} \begin{bmatrix} c'_{23} & s'_{23} \\ -s'_{23} & c'_{23} \end{bmatrix} \begin{bmatrix} 1 & 0 \\ 0 & e^{-i\delta'} \end{bmatrix} , \qquad (7.161)
\end{aligned}$$

where

$$\delta' \;=\; \delta + \Omega + \gamma \,. \qquad (7.162)$$

At $a\varepsilon \gg \delta m_{31}^2$ we know that $\chi_\varepsilon \to \vartheta_\omega - \dfrac{\pi}{2}$, cf. Eq. (7.144), so

$$\cos 2(\chi_\varepsilon - \vartheta_\omega) \;\xrightarrow{a\varepsilon \gg \delta m_{31}^2}\; -1 \,, \qquad (7.163)$$

and

$$\delta' \;\xrightarrow{a\varepsilon \gg \delta m_{31}^2}\; \delta + \Omega + \arctan\Big[s_\omega \tan(2\theta_{23}) \Big] \,. \qquad (7.164)$$

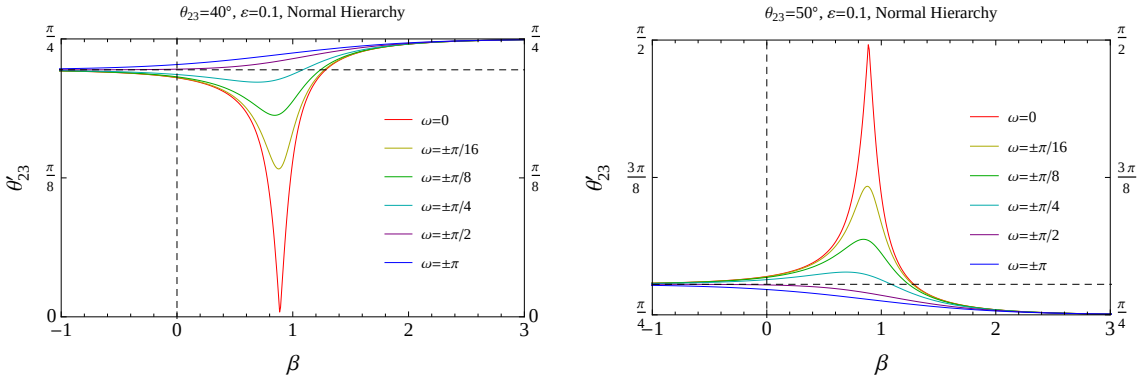

(a) (b)

Figure 7.23: The β-dependence of θ'_{23} for $\varepsilon = 0.1$ and a variety of ω values for the two cases (a) $\theta_{23} = 40^\circ$ and (b) $\theta_{23} = 50^\circ$ with $\delta m^2_{31} > 0$.

The behavior of θ'_{23} and δ' are shown in Figs. 7.23 and 7.24.

- **$\delta m^2_{31} < 0$ Case**

  In this case, the effective mixing matrix is well approximated by the product of matrices given by

$$\begin{aligned}
\tilde{U}^* &= U^* Q_3^* V_\varepsilon W_\varepsilon Y_\varepsilon \\
&= \underbrace{R_{23}(\theta_{23},0) Q_3 R_{13}(\theta_{13},0) R_{12}(\theta_{12},0)}_{U^* Q_3^*} \underbrace{R_{12}(\overline{\varphi}_\varepsilon,0)}_{V_\varepsilon} \underbrace{R_{23}(\overline{\phi}_\varepsilon,0)}_{W_\varepsilon} \underbrace{R_{13}(\overline{\psi}_\varepsilon,-\delta-\Omega)}_{Y_\varepsilon} \\
&\approx R_{23}(\theta_{23},0) Q_3 R_{13}(\theta'_{13},0) R_{12}(\theta'_{12},0) R_{13}(\overline{\psi}_\varepsilon,-\delta-\Omega) \\
&\approx R_{23}(\theta_{23},0) Q_3 R_{23}(\overline{\psi}_\varepsilon,\delta+\Omega) R_{13}(\theta'_{13},0) R_{12}(\theta'_{12},0) \; , \qquad (7.165)
\end{aligned}$$

From this point on, we follow the same procedure as the $\delta m^2_{31} > 0$ case discussed above, and we argue that the effective running values of θ_{23} and δ are obtained from

$$\begin{aligned}
\theta'_{23} &= \arccos\left[\sqrt{c^2_{23} c^2_{\psi_\varepsilon} - 2 c_{23} s_{23} c_{\psi_\varepsilon} s_{\psi_\varepsilon} \cos\Omega + s^2_{23} s^2_{\psi_\varepsilon}}\right] \; , \\
\delta' &= \delta + \Omega + \arctan\left[-\frac{s_\omega \tan(2\theta_{23})}{\cos 2(\psi_\varepsilon - \vartheta_\omega)}\right] \; . \qquad (7.166)
\end{aligned}$$

For $a\varepsilon \gg \delta m^2_{31}$, we know from Eq. (7.152) that $\psi_\varepsilon \to \vartheta_\omega$. Therefore,

$$\delta' \xrightarrow{a\varepsilon \gg \delta m^2_{31}} \delta + \Omega - \arctan\Big[s_\omega \tan(2\theta_{23})\Big] \; . \qquad (7.167)$$

As in the $\delta m^2_{31} > 0$ case, we can show that θ'_{23} and δ' do not run when $\theta_{23} = \dfrac{\pi}{4}$, and that θ'_{23} will run toward $\dfrac{\pi}{4}$ for both the $\theta_{23} < \dfrac{\pi}{4}$ and $\theta_{23} > \dfrac{\pi}{4}$ cases. Omitting details,

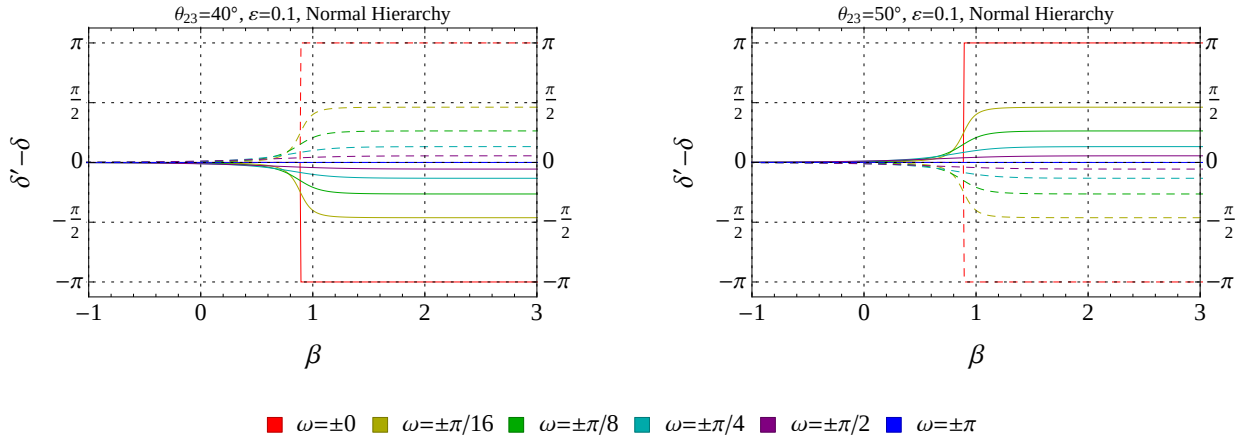

Figure 7.24: The β-dependence of $\delta' - \delta$ for $\varepsilon = 0.1$ and a variety of ω values for the two cases $\theta_{23} = 40°$ (left) and $\theta_{23} = 50°$ (right), both with $\delta m^2_{31} > 0$. The solid lines indicate positive ω and the dashed lines indicate negative ω.

we show the behavior of θ'_{23} and δ' for various values of ω in Figs. 7.25 and 7.26 when $\theta_{23} \neq \dfrac{\pi}{4}$.

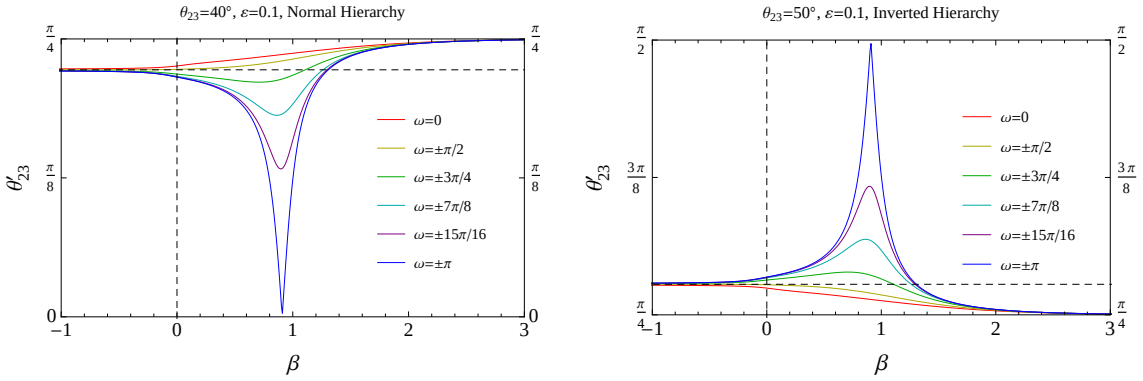

(a) (b)

Figure 7.25: The β-dependence of θ'_{23} for $\varepsilon = 0.1$ and a variety of ω values for the two cases (a) $\theta_{23} = 40^\circ$ and (b) $\theta_{23} = 50^\circ$ with $\delta m^2_{31} < 0$.

7.4.3 Summary of Anti-neutrino Case

We find that the matter effect due to $\varepsilon_{\mu\tau} = \varepsilon e^{i\omega}$ can be absorbed into the running of the effective mixing angles θ'_{12}, θ'_{13}, θ'_{23}, the effective CP violating phase δ', and the effective mass-squared eigenvalues λ_1, λ_2, and λ_3. The definitions of ϑ_ω and Ω that appear in what follows have been given in Eq. (7.117). First, θ'_{12} and θ'_{13} are given by

$$\begin{aligned} \tan 2\theta'_{12} &= \frac{\delta m^2_{21} \sin 2\theta_{12}}{\delta m^2_{21} \cos 2\theta_{12} + a[c^2_{13} + \varepsilon_c(1 + s^2_{13})]} , \\ \tan 2\theta'_{13} &= \frac{(\delta m^2_{31} - s^2_{12}\delta m^2_{21}) \sin(2\theta_{13})}{(\delta m^2_{31} - s^2_{12}\delta m^2_{21}) \cos(2\theta_{13}) + a(1 - \varepsilon_c)} , \end{aligned} \tag{7.168}$$

where $\varepsilon_c = \varepsilon \cos(2\vartheta_\omega)$. Next, $\theta'_{23} \in [0, \pi/2]$ and $\delta' \in [-\pi, \pi]$ are given by

$$\begin{aligned} \theta'_{23} &= \arccos\left[\sqrt{c^2_{23}\overline{c}^2_{\chi_\varepsilon} - 2c_{23}s_{23}\overline{c}_{\chi_\varepsilon}\overline{s}_{\chi_\varepsilon}\cos\Omega + s^2_{23}\overline{s}^2_{\chi_\varepsilon}}\right] , \\ \delta' &= \delta + \Omega + \arctan\left[-\frac{s_\omega \tan(2\theta_{23})}{\cos 2(\chi_\varepsilon - \vartheta_\omega)}\right] , \end{aligned} \tag{7.169}$$

where

$$\tan 2\overline{\chi}_\varepsilon = \frac{-2a\varepsilon \sin(2\vartheta_\omega)}{[c^2_{13}\delta m^2_{31} - (c^2_{12} - s^2_{12}s^2_{13})\delta m^2_{21}] - 2a\varepsilon\cos(2\vartheta_\omega)} . \tag{7.170}$$

Note that the same expression can be used for both the $\delta m^2_{31} > 0$ and $\delta m^2_{31} < 0$ cases, cf. Eqs. (7.143) and (7.151). For the normal hierarchy ($\delta m^2_{31} > 0$), the effective mass-squared eigenvalues are

$$\begin{aligned} \overline{\lambda}_1 &= \overline{\lambda''}_{\varepsilon-} , \\ \overline{\lambda}_2 &= \frac{(\overline{\lambda''}_{\varepsilon+} + \overline{\lambda'}_{\varepsilon+}) - \sqrt{(\overline{\lambda''}_{\varepsilon+} - \overline{\lambda'}_{\varepsilon+})^2 + 4a^2\varepsilon^2_s c'^2_{13}}}{2} , \end{aligned}$$

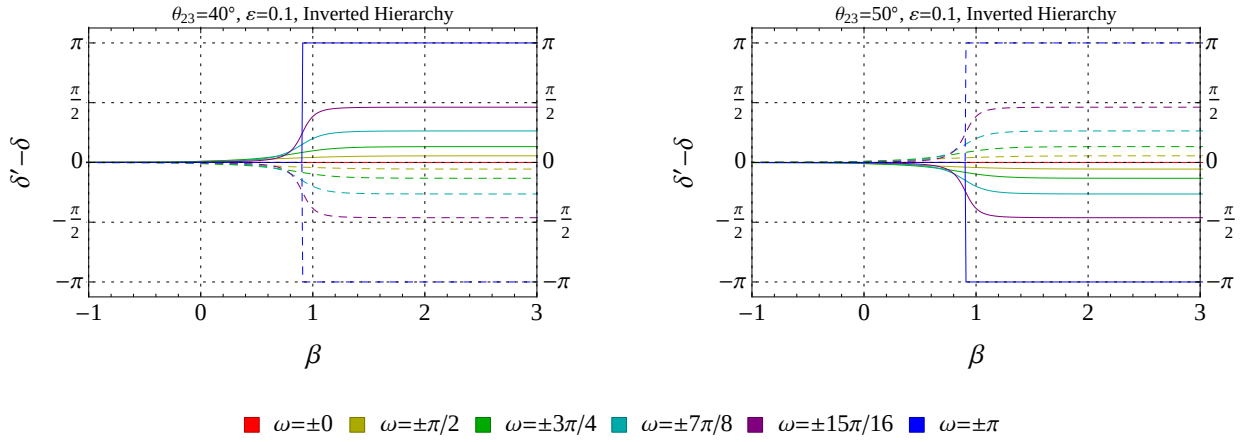

Figure 7.26: The β-dependence of $\delta' - \delta$ for $\varepsilon = 0.1$ and a variety of ω values for the two cases $\theta_{23} = 40°$ (left) and $\theta_{23} = 50°$ (right). with $\delta m^2_{31} < 0$. The solid lines indicate positive ω while the dashed lines indicate negative ω.

$$\overline{\lambda}_3 = \frac{(\overline{\lambda''}_{\varepsilon+} + \overline{\lambda'}_{\varepsilon+}) + \sqrt{(\overline{\lambda''}_{\varepsilon+} - \overline{\lambda'}_{\varepsilon+})^2 + 4a^2\varepsilon_s^2 c_{13}'^2}}{2}\,, \tag{7.171}$$

while, for the inverted hierarchy ($\delta m^2_{31} < 0$), they are given by

$$\begin{aligned}
\overline{\lambda}_1 &= \frac{(\overline{\lambda''}_{\varepsilon+} + \overline{\lambda'}_{\varepsilon+}) + \sqrt{(\overline{\lambda''}_{\varepsilon+} - \overline{\lambda'}_{\varepsilon+})^2 + 4a^2\varepsilon_s^2 s_{13}'^2}}{2}\,, \\
\overline{\lambda}_2 &= \frac{(\overline{\lambda''}_{\varepsilon+} + \overline{\lambda'}_{\varepsilon+}) - \sqrt{(\overline{\lambda''}_{\varepsilon+} - \overline{\lambda'}_{\varepsilon+})^2 + 4a^2\varepsilon_s^2 s_{13}'^2}}{2}\,, \\
\overline{\lambda}_3 &= \overline{\lambda''}_{\varepsilon-}\,,
\end{aligned} \tag{7.172}$$

where $\varepsilon_s = \varepsilon \sin(2\vartheta_\omega)$, and

$$\begin{aligned}
\overline{\lambda'}_{\varepsilon\pm} &= \frac{\{(\delta m^2_{21} + a\varepsilon_c) - a(c^2_{13} + \varepsilon_c s^2_{13})\}}{2} \\
&\quad \pm \frac{\sqrt{\{(\delta m^2_{21} + a\varepsilon_c) + a(c^2_{13} + \varepsilon_c s^2_{13})\}^2 - 4as^2_{12}\left\{c^2_{13} + \varepsilon_c(1 + s^2_{13})\right\}\delta m^2_{21}}}{2}\,, \\
\overline{\lambda''}_{\varepsilon\pm} &= \frac{\overline{\lambda'}_{\varepsilon-} + \left\{\delta m^2_{31} - a(s^2_{13} + \varepsilon_c c^2_{13})\right\}}{2} \\
&\quad \pm \frac{\sqrt{\left[\overline{\lambda'}_{\varepsilon-} - \left\{\delta m^2_{31} - a(s^2_{13} + \varepsilon_c c^2_{13})\right\}\right]^2 + 4\left\{ac'_{12}s_{13}c_{13}(1 - \varepsilon_c)\right\}^2}}{2}\,,
\end{aligned} \tag{7.173}$$

where $\varepsilon_c = \varepsilon \cos(2\vartheta_\omega)$.

7.5 Comparison with the Numerical Result at the Probability Level

To show this approximation works properly, in this section we show the probability calculated with the running parameters and compare this with the probability calculated using numerical diagonalization of the Hamiltonian. In Fig. 7.29, we show the probability of $\nu_\mu \to \nu_e$ for different ω's. In the case of $\omega = \pm\pi$, our approximation is better than Ref. [5] while in the case of $\omega = \pm\frac{\pi}{2}$, our approximation is worse. In other cases, they are about the same. The ν_μ survival probability and the τ appearance probability are shown in Figs. 7.30 and 7.31, respectively. In the case of even longer baseline such CERN to Super-Kamiokande, Fig. 7.32 shows that our approximation formula is significantly better than the one in Ref. [5].

For the specific energy and baseline length of the DUNE experiment, we stress that there is a degeneracy between the δ_{CP} and the NSI phase ω. Our approximation captures this degeneracy very well, as shown in Figs. 7.27 and 7.28. On the other hand, if ε is small, the effect will not be observed at the expected precision of DUNE.

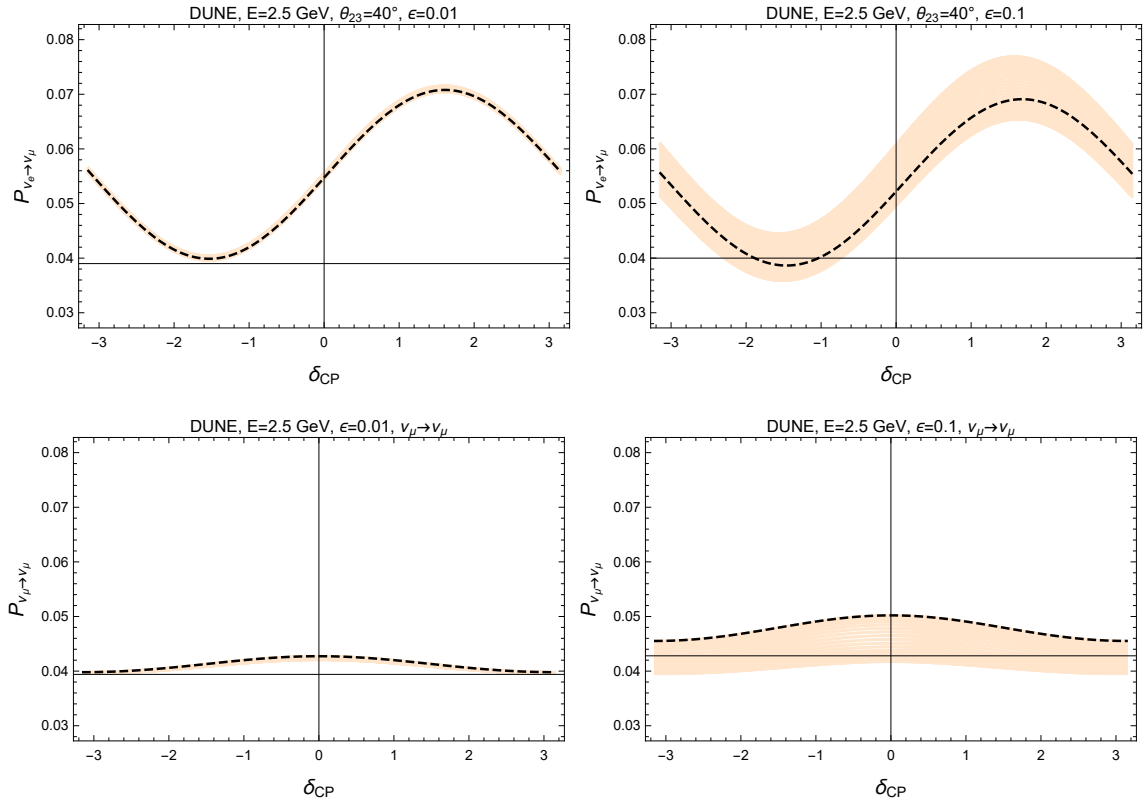

Figure 7.27: The degeneracy band of ω for different ε's. The upper panel is for ν_e appearance and the lower for ν_μ disappearance.

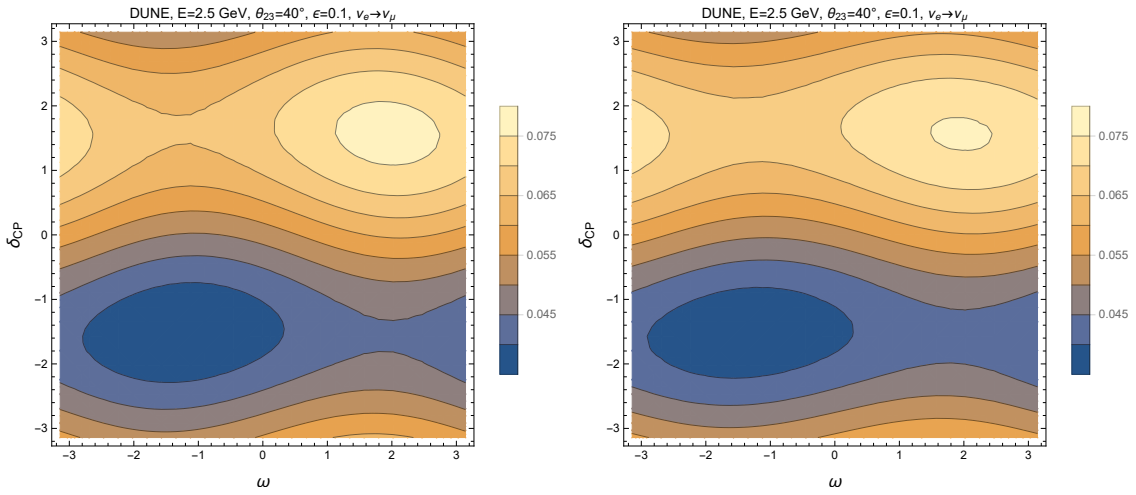

Figure 7.28: Degeneracy contour from this approximation (left) and numerical result (right) for DUNE at $E = 2.5$ GeV, assuming $\varepsilon = 0.1$ and $\theta_{23} = 40°$.

7.6 Summary and Outlook

In this chapter, we studied the analytical expression of the neutrino matter effect with non-zero $\varepsilon_{\mu\tau}$. The idea is similar to renormalization in quantum field theory: first, we write the 'bare' Hamiltonian H_0 for neutrino propagation in the vacuum. Then we add terms for the matter effect to the vacuum Hamiltonian as δH. We then absorb the extra term δH of the matter effect into the 'bare' parameters of H_0. The Jacobi method is used to absorb δH with certain rotations to restore the form of H_0.

The advantage of this method is to make the effect of the neutrino matter interaction transparent. In this formalism, the 'matter effect running' expression shows that θ_{12} and θ_{13} run mostly due to the SM effect while θ_{23} and δ_{CP} run mainly due to the presence of a nonzero $|\varepsilon_{\mu\tau}|$ and its phase. As a result, it is obvious to see which part of $\varepsilon_{\mu\tau}$– norm or phase, affects which parameter, hence which type of experiments. For example, atmospheric neutrinos are able to constrain $\varepsilon_{\mu\tau}$ as long as we do not go to the regime of $a \gg |\delta m^2_{32}|$, *i.e.*, where the energy of atmospheric neutrino is high, which is consistent with the analysis in Refs. [469, 472].

This formalism allows us to study the neutrino–matter effect at the level of modified vacuum parameters instead of solely the probability level. In this sense, the analysis of neutrino long baseline experiments is no longer a 'trial-and-error' type of analysis of probability output for various tweaks of the baseline length, matter density, beam energy, etc. Instead, we can express the oscillation angles as functions of NSI. Once the effect of a type of NSI is understood, deciding which experiment is more sensitive to it is straightforward.

In addition, because the running parameters distinguish between mass hierarchies and also

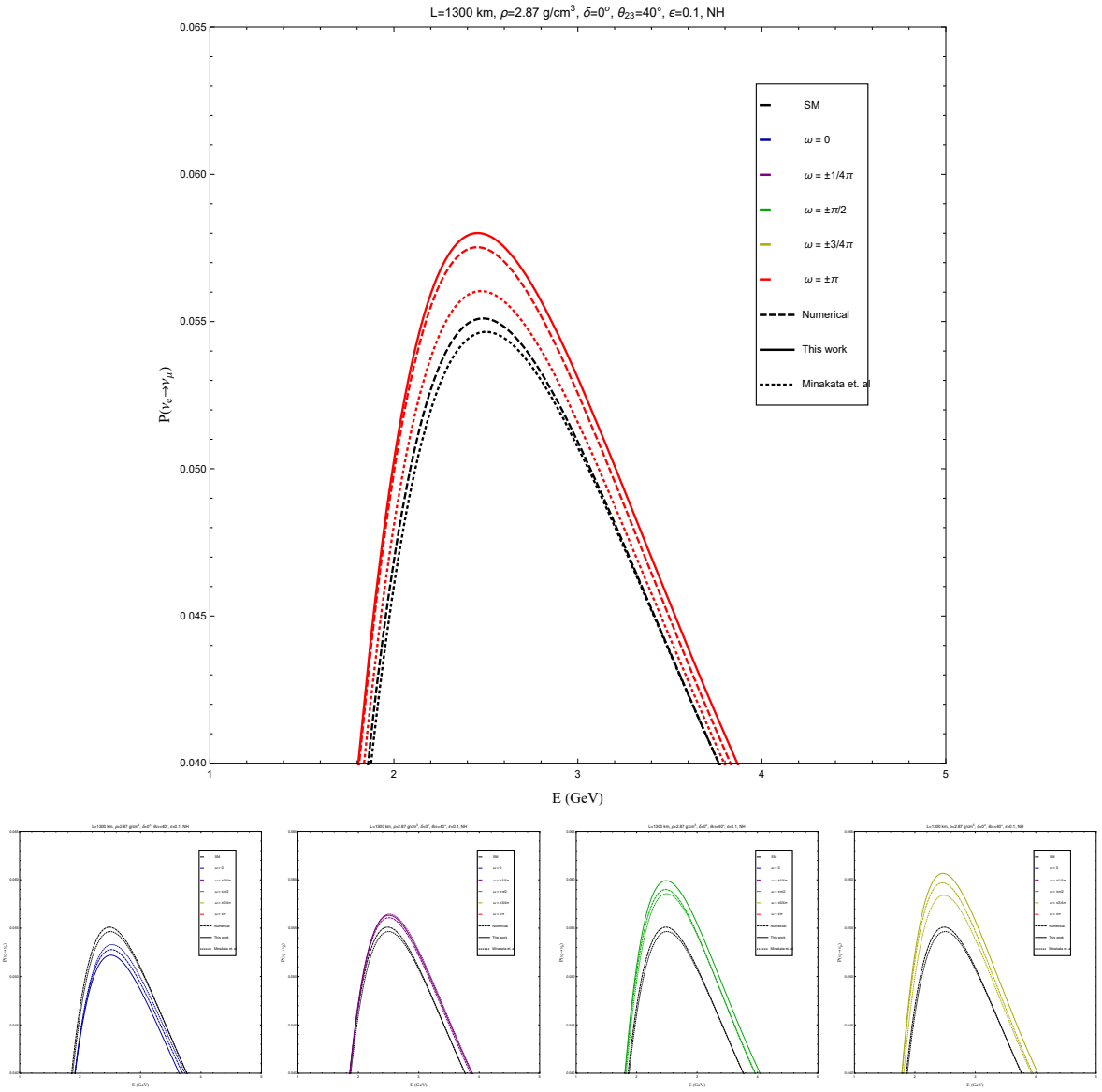

Figure 7.29: Probability of $\nu_\mu \to \nu_e$ at the first oscillation peak of DUNE, assuming $\delta = 0, \theta = 40°, \varepsilon = 0.1$, and normal hierarchy. The dashed curves correspond to the exact value from numerical calculation. The solid curve is our approximation. They are compared with the approximation formula from Ref. [5], which is shown as dotted curves. Different colors correspond to different values of the NSI phase, ω.

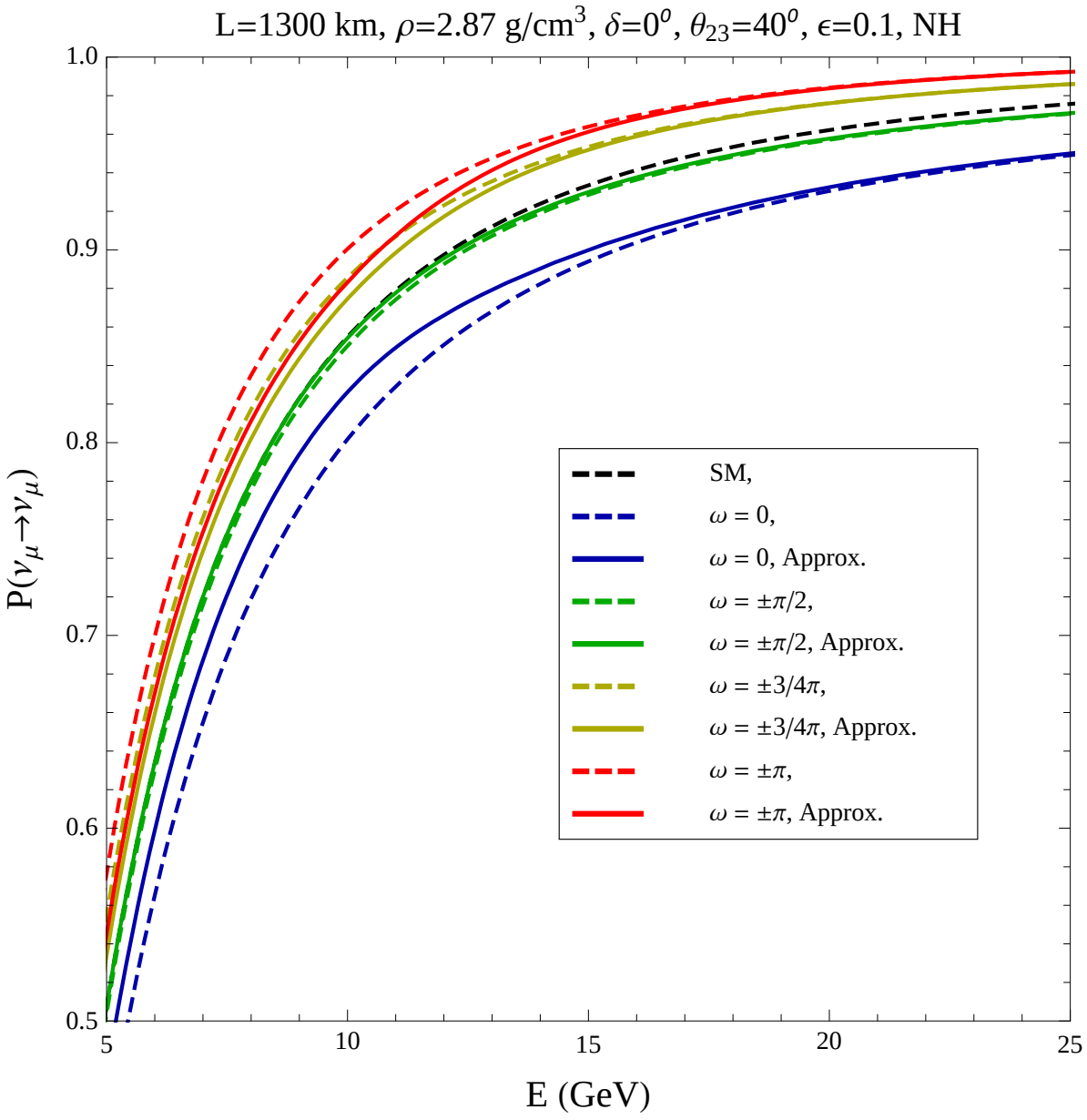

Figure 7.30: Probability of $\nu_\mu \to \nu_\mu$ at DUNE energy, assuming $\delta = 0, \theta = 40°, \varepsilon = 0.1$, normal hierarchy. The dashed curves correspond to the exact value from numerical calculation. The solid curve is our approximation. Different colors corresponds to different NSI phase, ω.

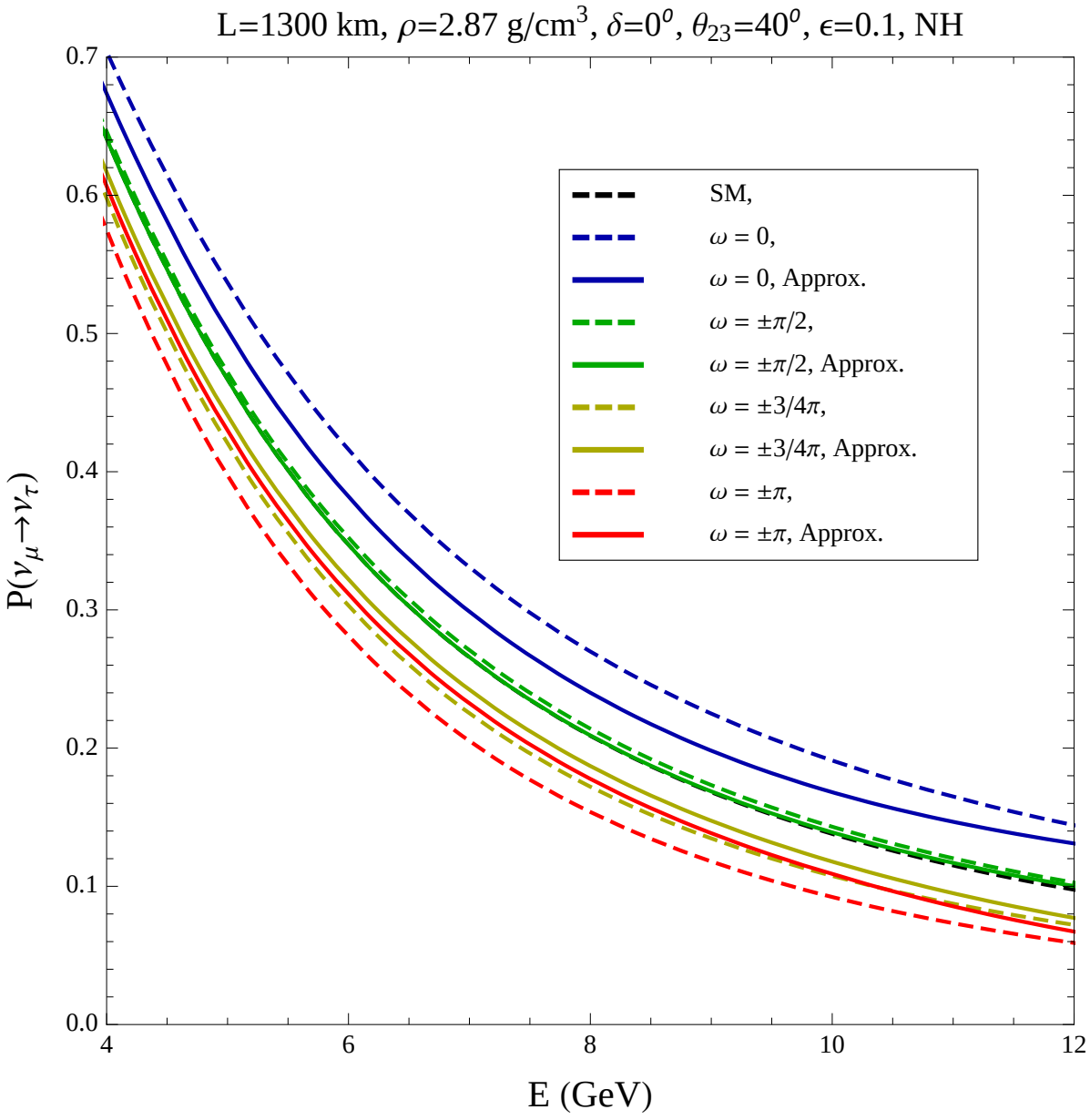

Figure 7.31: Probability of $\nu_\mu \to \nu_\tau$ at DUNE energy, assuming $\delta = 0, \theta = 40°, \varepsilon = 0.1$, normal hierarchy. The dashed curves correspond to the exact value from numerical calculation. The solid curve is our approximation. Different colors correspond to different values of the NSI phase, ω.

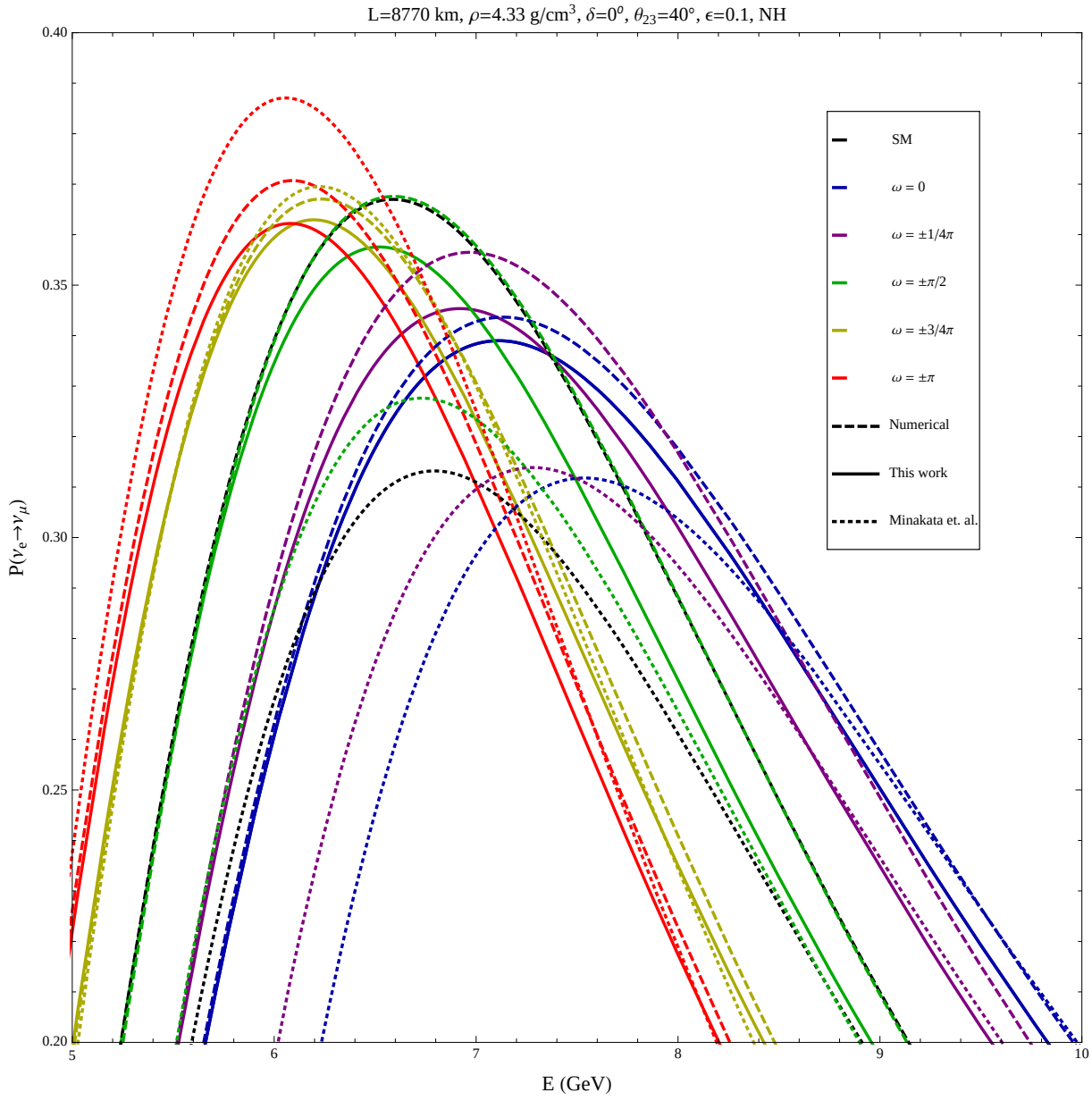

Figure 7.32: Probability of $\nu_\mu \to \nu_e$ at the first oscillation peak of 8770 km baseline, assuming $\delta = 0, \theta = 40°, \varepsilon = 0.1$, and normal hierarchy. The dashed curves correspond to the exact value from numerical calculation. The solid curve is our approximation. They are compared with the approximation formula from Ref. [5], which is shown as dotted curves. Different colors correspond to different values of the NSI phase, ω.

depends on the 'bare' vacuum oscillation angles, it is easier to analyze the degeneracy between uncertainties of the standard oscillation parameters and the effect of NSI. For example, it is observed that the phase of $\varepsilon_{\mu\tau}$ plays an important role in modifying θ_{23} and δ_{CP}. An easy understanding of the large degeneracy of uncertainties between θ_{23}, δ_{CP}, and ε is achieved.

The price we pay for this clean picture is a slight loss of precision due to the approximation where we use the Jacobi method to transform $H_0 + \delta H$ into the form of H_0. The approximation is expected to be improved in future studies. On the other hand, since $\varepsilon_{\mu\tau}$ is already tightly bounded, any error introduced by the approximation is negligible at the current or near-future level of accuracy. Thus, it is more important to focus on understanding of the physics of NSI and its consequences to various experiments using our formalism, which we expect to expand further in a future publication.

Part III

Confronting Neutrino Models with Collider Data

Chapter 8

Constrainting Models of Sizable NSI with Particle Data

In the previous chapters, we have shown the imprints of new physics in collider experiments as TeV-scale signals, and in neutrino oscillation experiments as NSI. In this section, we examine the question of how to combine the treatments of collider and neutrino experiments in order to constrain new physics with more power than ever before. In particular, at one loop level, quantum correction is likely to bring back small or even couplings forbidden at tree level if not protected by any symmetry, which in turn is subject to stringent bounds. On the other hand, if there is no SM process that could generate the quantum correction, the smallness can be stable up to the one-loop correction.

8.1 Introduction

As we showed in previous chapters, the NSI formalism is an efficient way of parametrizing our ignorance of new physics in the effective field theory framework. With the help of the NSI parametrization, we can put bounds on a large class of models in which the deviation from the SM at low energies is described by the size of NSI of the neutrino sector, even though we do not yet know the full theory. On the other hand, with the bounds on NSI improving over the years, we are at a point that the results from neutrino experiments put real constraints on certain particle models. Therefore, it is of importance to look into models that can actually generate such NSI's, thus being testable in neutrino experiments. By this, we gain knowledge of what types of models can be actually constrained by current and future neutrino experiments.

It is shown that gauge invariance, together with low energy particle data, puts severe constraints on the size of NSI's: see, for example, Refs. [75, 440, 444, 473–481]. In particular, models with gauged lepton and baryon number are carefully examined such as in Refs. [482–

496]. Among the proposed models, very light Z's that couple to neutrinos are discussed in Refs. [497–503]. As a result of the loop effects, the light Z's often mix with either the SM photon, the Z boson, or both, through kinetic mixing. This results in effects that are forbidden at tree level. In this chapter, we focus on the model in Ref. [504]. It is noticed that, although NSI parametrizes the forward scattering with zero momentum transfer, the free parameters of the theory are constrained due to the kinetic mixing present in the model, which is strongly scale dependent as opposed to the usual simplification in some analyses. Since collider experiments are sensitive to the squared momentum transfer q^2, we point out that the scale dependence of the kinetic mixing is important when we apply the collider data to constrain NSI. In the end, we briefly mention the constraints from nuclear binding energy, neutron star properties, and accelerator synchrotron radiation. This chapter is based on Ref. [505]. We continue with the same notation of NSI used in previous chapters.

8.2 Model and Notation

In Ref. [504], a model is built to generate sizable non-standard interactions for neutrino scattering. The idea is to gauge the second and third lepton number, $L_{\mu-\tau}$, while all quarks couple to the extra $U(1)'$ diagonally. It is designed this way to avoid stringent bounds from electron scattering measurements. The details of the model, including symmetry breaking and anomaly cancellation, are shown in appendix G. Here we briefly show the field content of the model. The gauge group of the Farzan-Shoemaker model is $SU(3)_C \times SU(2)_L \times U(1)_Y \times U(1)'$. We denote the gauge boson and the gauge coupling of the extra $U(1)'$ respectively as Z' and g'. The $U(1)_Y$ gauge coupling is denoted g_1 to distinguish it from the $U(1)'$ coupling. The charge assignment of the quarks are

$$Q_i = \begin{bmatrix} u_{Li} \\ d_{Li} \end{bmatrix} \sim \left(3, 2, +\frac{1}{6}, \eta\right) \ , \quad u_{Ri} \sim \left(3, 1, +\frac{2}{3}, \eta\right) \ , \quad d_{Ri} \sim \left(3, 1, -\frac{1}{3}, \eta\right) \ , \tag{8.1}$$

for the three generations $i = 1, 2, 3$. For the leptons, we assign

$$L_i = \begin{bmatrix} \nu_{Li} \\ \ell_{Li} \end{bmatrix} \sim \left(1, 2, -\frac{1}{2}, i\zeta\right) \ , \quad \ell_{Ri} \sim (1, 1, -1, i\zeta) \ , \tag{8.2}$$

with $i = 0, +, -$. No right-handed neutrino is introduced. The hypercharge Y is normalized so that the electromagnetic charge is given by

$$Q_{\rm em} \ = \ I_3 + Y \ . \tag{8.3}$$

We need three Higgs fields with charge assignment

$$H \sim \left(1, 2, +\frac{1}{2}, 0\right) \ , \quad H_{++} \sim \left(1, 2, +\frac{1}{2}, +2\zeta\right) \ , \quad H_{--} \sim \left(1, 2, +\frac{1}{2}, -2\zeta\right) \ . \tag{8.4}$$

H is the SM Higgs doublet. Farzan and Shoemaker also introduce two more Higgs doublets which we denote

$$H_{-+} \sim \left(1, 2, +\frac{1}{2}, 0\right) \ , \quad H_{+-} \sim \left(1, 2, +\frac{1}{2}, 0\right) \ , \tag{8.5}$$

but these have the same quantum numbers as the SM Higgs doublet H and are redundant and unnecessary. The coupling of the quarks to Z' is vectorial and is given by

$$g'\eta Z'_\mu \sum_{i=1}^{3} \left(\overline{u_i}\gamma^\mu u_i + \overline{d_i}\gamma^\mu d_i\right) \ , \tag{8.6}$$

while the coupling of the leptons to Z' is chiral and is given by

$$g'\zeta Z'_\mu \left(\overline{L_+}\gamma^\mu L_+ - \overline{L_-}\gamma^\mu L_-\right) + g'\zeta Z'_\mu \left(\overline{\ell_{R+}}\gamma^\mu \ell_{R+} - \overline{\ell_{R-}}\gamma^\mu \ell_{R-}\right) \ . \tag{8.7}$$

Since all the quarks fields have the same $U(1)'$ charge η, the usual Yukawa interaction terms of the quarks with the Higgs doublet H are $U(1)'$ invariant:

$$\sum_{i,j} \left(\lambda_{ij}\overline{d_{Ri}}H^\dagger Q_j + \tilde{\lambda}_{ij}\overline{u_{Ri}}\widetilde{H}^\dagger Q_j\right) + h.c. \tag{8.8}$$

where λ_{ij} and $\tilde{\lambda}_{ij}$ are the Yukawa coupling constants, and

$$H = \begin{bmatrix} H^+ \\ H^0 \end{bmatrix} \ , \quad H^\dagger = \begin{bmatrix} H^- & H^{0*} \end{bmatrix} \ , \quad \widetilde{H} = \begin{bmatrix} H^{0*} \\ -H^- \end{bmatrix} \ , \quad \widetilde{H}^\dagger = \begin{bmatrix} H^0 & -H^+ \end{bmatrix} \ . \tag{8.9}$$

The Yukawa interactions of the leptons to H, on the other hand, are restricted to

$$\sum_{i=0,+,-} \left(f_i\, \overline{\ell_{Ri}}H^\dagger L_i\right) + h.c. \tag{8.10}$$

where f_0, f_+, and f_- are the Yukawa coupling contants. With this interaction alone, we can only generate charged-lepton-mass eigenstates that are also $U(1)'$ charge eigenstates.

In order to generate mixings among the leptons with opposite $U(1)'$ charges, we use the doubly-$U(1)'$-charged Higgs fields H_{++} and H_{--}

$$\left(c_-\overline{\ell_{R+}}H^\dagger_{--}L_- + c_+\overline{\ell_{R-}}H^\dagger_{++}L_+\right) + h.c. \tag{8.11}$$

Farzan and Shoemaker also introduce $U(1)'$-invariant Yukawa interactions of the forms

$$\overline{\ell_{R+}}H^\dagger_{-+}L_+ \ , \qquad \overline{\ell_{R-}}H^\dagger_{+-}L_- \ , \tag{8.12}$$

but these are unnecessary.

After the neutral (under $U(1)_{\rm em}$) components of the Higgs doublets obtain VEV's, the mass matrix of the $+-$ charged lepton sector is given by

$$\begin{bmatrix}\overline{\ell_{R+}} & \overline{\ell_{R-}}\end{bmatrix} M \begin{bmatrix}\ell_{L+} \\ \ell_{L-}\end{bmatrix} + h.c. \tag{8.13}$$

where

$$M \;=\; \begin{bmatrix} f_+\langle H^0\rangle & c_-\langle H^0_{--}\rangle \\ c_+\langle H^0_{++}\rangle & f_-\langle H^0\rangle \end{bmatrix} \;=\; \frac{1}{2}\begin{bmatrix} \sqrt{2}f_+ v & c_- w \\ c_+ w & \sqrt{2}f_- v \end{bmatrix}\,, \tag{8.14}$$

where we have used the notation introduced in the previous section: $v/\sqrt{2} = \langle H^0\rangle$ and $w/2 = \langle H^0_{++}\rangle = \langle H^0_{--}\rangle$. (Note that our definition of v differs from that of Farzan and Shoemaker by a factor of $\sqrt{2}$.)

To find the mass eigenstates, we need to find the unitary matrices U_L and U_R such that

$$U_R M U_L^\dagger \;=\; \begin{bmatrix} m_\alpha & 0 \\ 0 & m_\beta \end{bmatrix}\,, \tag{8.15}$$

so that if we define

$$\begin{bmatrix}\ell_{R\alpha} \\ \ell_{R\beta}\end{bmatrix} \;=\; U_R \begin{bmatrix}\ell_{R+} \\ \ell_{R-}\end{bmatrix}\,, \qquad \begin{bmatrix}\ell_{L\alpha} \\ \ell_{L\beta}\end{bmatrix} \;=\; U_L \begin{bmatrix}\ell_{L+} \\ \ell_{L-}\end{bmatrix}\,, \tag{8.16}$$

we have

$$\begin{bmatrix}\overline{\ell_{R+}} & \overline{\ell_{R-}}\end{bmatrix} M \begin{bmatrix}\ell_{L+} \\ \ell_{L-}\end{bmatrix} \;=\; \begin{bmatrix}\overline{\ell_{R\alpha}} & \overline{\ell_{R\beta}}\end{bmatrix} \begin{bmatrix} m_\alpha & 0 \\ 0 & m_\beta \end{bmatrix} \begin{bmatrix}\ell_{L\alpha} \\ \ell_{L\beta}\end{bmatrix}\,. \tag{8.17}$$

Note that

$$U_L M^\dagger M U_L^\dagger \;=\; U_R M M^\dagger U_R^\dagger \;=\; \begin{bmatrix} m_\alpha^2 & 0 \\ 0 & m_\beta^2 \end{bmatrix}\,. \tag{8.18}$$

$M^\dagger M$ and $M M^\dagger$ are given by

$$\begin{aligned} M^\dagger M &= \begin{bmatrix} f_+^2\langle H^0\rangle^2 + c_+^2\langle H^0_{++}\rangle^2 & \langle H^0\rangle\left(f_+ c_-\langle H^0_{--}\rangle + f_- c_+\langle H^0_{++}\rangle\right) \\ \langle H^0\rangle\left(f_+ c_-\langle H^0_{--}\rangle + f_- c_+\langle H^0_{++}\rangle\right) & f_-^2\langle H^0\rangle^2 + c_-^2\langle H_{--}\rangle^2 \end{bmatrix}\,, \\ M M^\dagger &= \begin{bmatrix} f_+^2\langle H^0\rangle^2 + c_-^2\langle H^0_{--}\rangle^2 & \langle H^0\rangle\left(f_+ c_+\langle H^0_{++}\rangle + f_- c_-\langle H^0_{--}\rangle\right) \\ \langle H^0\rangle\left(f_+ c_+\langle H^0_{++}\rangle + f_- c_-\langle H^0_{--}\rangle\right) & f_-^2\langle H^0\rangle^2 + c_+^2\langle H^0_{++}\rangle^2 \end{bmatrix}\,. \end{aligned} \tag{8.19}$$

Assuming that the elements are all real (for the sake of simplicity), we can set

$$U_L \;=\; \begin{bmatrix}\cos\delta_L & -\sin\delta_L \\ \sin\delta_L & \cos\delta_L\end{bmatrix}\,, \qquad U_R \;=\; \begin{bmatrix}\cos\delta_R & -\sin\delta_R \\ \sin\delta_R & \cos\delta_R\end{bmatrix}\,, \tag{8.20}$$

where

$$\tan(2\delta_L) \;=\; \frac{\langle H^0\rangle\left(f_+ c_-\langle H^0_{--}\rangle + f_- c_+\langle H^0_{++}\rangle\right)}{(f_-^2 - f_+^2)v^2 + c_-^2\langle H_{--}\rangle^2 - c_+^2\langle H_{++}\rangle^2} \;\approx\; \frac{\langle H^0\rangle\left(f_+ c_-\langle H^0_{--}\rangle + f_- c_+\langle H^0_{++}\rangle\right)}{m_\beta^2}\,,$$

$$\tan(2\delta_R) \;=\; \frac{\langle H^0\rangle\left(f_+c_+\langle H^0_{++}\rangle + f_-c_-\langle H^0_{--}\rangle\right)}{(f_-^2-f_+^2)v^2 - c_-^2\langle H_{--}\rangle^2 + c_+^2\langle H_{++}\rangle^2} \;\approx\; \frac{\langle H^0\rangle\left(f_+c_+\langle H^0_{++}\rangle + f_-c_-\langle H^0_{--}\rangle\right)}{m_\beta^2}\,. \tag{8.21}$$

We have assumed that $m_\beta \gg m_\alpha$ to simplify the denominators. Define

$$\begin{bmatrix} L_\alpha \\ L_\beta \end{bmatrix} = U_L \begin{bmatrix} L_+ \\ L_- \end{bmatrix}\,, \qquad \begin{bmatrix} \ell_{R\alpha} \\ \ell_{R\beta} \end{bmatrix} = U_R \begin{bmatrix} \ell_{R+} \\ \ell_{R-} \end{bmatrix}\,, \qquad L_\gamma = L_0\,, \qquad \ell_{R\gamma} = \ell_{R0}\,. \tag{8.22}$$

The subscripts α, β, and γ label charged-lepton mass eigenstates so they correspond to e, μ, and τ (in some order). The coupling of the Z' to the leptons are

$$\begin{aligned}
& g'\zeta Z'_\mu \begin{bmatrix} \overline{L_+} & \overline{L_-} \end{bmatrix} \gamma^\mu\sigma_3 \begin{bmatrix} L_+ \\ L_- \end{bmatrix} + g'\zeta Z'_\mu \begin{bmatrix} \overline{\ell_{R+}} & \overline{\ell_{R-}} \end{bmatrix} \gamma^\mu\sigma_3 \begin{bmatrix} \ell_{R+} \\ \ell_{R-} \end{bmatrix} \\
&= g'\zeta Z'_\mu \begin{bmatrix} \overline{L_\alpha} & \overline{L_\beta} \end{bmatrix} \gamma^\mu U_L\sigma_3 U_L^\dagger \begin{bmatrix} L_\alpha \\ L_\beta \end{bmatrix} + g'\zeta Z'_\mu \begin{bmatrix} \overline{\ell_{R\alpha}} & \overline{\ell_{R\beta}} \end{bmatrix} \gamma^\mu U_R\sigma_3 U_R^\dagger \begin{bmatrix} \ell_{R\alpha} \\ \ell_{R\beta} \end{bmatrix} \\
&= g'\zeta Z'_\mu \begin{bmatrix} \overline{L_\alpha} & \overline{L_\beta} \end{bmatrix} \gamma^\mu \begin{bmatrix} \cos(2\delta_L) & \sin(2\delta_L) \\ \sin(2\delta_L) & -\cos(2\delta_L) \end{bmatrix} \begin{bmatrix} L_\alpha \\ L_\beta \end{bmatrix} \\
&\quad + g'\zeta Z'_\mu \begin{bmatrix} \overline{\ell_{R\alpha}} & \overline{\ell_{R\beta}} \end{bmatrix} \gamma^\mu \begin{bmatrix} \cos(2\delta_R) & \sin(2\delta_R) \\ \sin(2\delta_R) & -\cos(2\delta_R) \end{bmatrix} \begin{bmatrix} \ell_{R\alpha} \\ \ell_{R\beta} \end{bmatrix}\,,
\end{aligned} \tag{8.23}$$

and we can see that flavor-changing couplings to the Z' have been generated. In particular, this interaction includes the neutrino-flavor-changing term

$$g'\zeta Z'_\mu \sin(2\delta_L)\left(\overline{\nu_{L\alpha}}\gamma^\mu\nu_{L\beta} + \overline{\nu_{L\beta}}\gamma^\mu\nu_{L\alpha}\right)\,, \tag{8.24}$$

as well as diagonal couplings to the charged leptons

$$g'\zeta Z'_\mu \left[\cos(2\delta_L)\left(\overline{\ell_{L\alpha}}\gamma^\mu\ell_{L\alpha} - \overline{\ell_{L\beta}}\gamma^\mu\ell_{L\beta}\right) + \cos(2\delta_R)\left(\overline{\ell_{R\alpha}}\gamma^\mu\ell_{R\alpha} - \overline{\ell_{R\beta}}\gamma^\mu\ell_{R\beta}\right)\right]. \tag{8.25}$$

So if $\alpha = \tau$, for instance, Z'-exchange will lead to a NSI of the form

$$\frac{g'^2\zeta^2}{q^2 - M_{Z'}^2}\sin(2\delta_L)\left(\overline{\nu_\tau}\gamma^\mu\nu_\beta + \overline{\nu_\beta}\gamma^\mu\nu_\tau\right)\left[\cos(2\delta_L)\,\overline{\tau_L}\gamma_\mu\tau_L + \cos(2\delta_R)\,\overline{\tau_R}\gamma_\mu\tau_R\right]. \tag{8.26}$$

The NSI matter effect is the result of the following interaction term:

$$\frac{g'^2\zeta\eta}{q^2 - M_{Z'}^2}\sin(2\delta_L)\left(\overline{\nu_\tau}\gamma^\mu\nu_\mu + \overline{\nu_\mu}\gamma^\mu\nu_\tau\right)\left[\overline{u}\gamma_\mu u + \overline{d}\gamma_\mu d\right]. \tag{8.27}$$

Because g' always comes with either ζ or η, without loss of generality we can rescale them and retain only two variables. As in Ref. [504], we let $\eta = 1$. The NSI matter effect is the process with squared momentum transfer $q^2 = 0$. We express the usual NSI parameter as

$$2\sqrt{2}G_F\varepsilon^{qP}_{\mu\tau} = \frac{g'^2\zeta}{M_{Z'}^2}\sin(2\delta_P) \le \frac{g'^2\zeta}{M_{Z'}^2}. \tag{8.28}$$

Next, we focus on the constraints on g', ζ, and $M_{Z'}$. Besides the bounds discussed by Farzan and Shoemaker, which is summarized in appendix G.4, we mainly consider the constraints from the following sectors: $\tau \to Z'\mu$, $\tau \to \mu ee$, and $\tau \to \mu\nu\nu$ processes.

8.3 Constraints from τ Decay

As shown in Ref. [504], the measurement involving the electron final state is very constraining. Therefore, only the $\alpha = \mu, \beta = \tau$ case is viable in this model. Because of the extra coupling with τ, the model is expected to affect the τ decay spectrum, in principle. In this section, we study several τ decay channels to put constraints on the free parameters g', ζ, and $M_{Z'}$. We first look at the $\tau \to \mu Z'$ two body decay bound from ARGUS and Belle in Section 8.3.1, which applies for the long-lived Z'. Next, in Section 8.3.2, we study bounds on the $\tau \to \mu ee$ mode, which applies to the short-lived Z'. Finally, in Section 8.3.3, we study the $\tau \to \mu\nu\nu$ decay mode, which interferes with the W-exchange SM process, and the corresponding constraints.

8.3.1 $\tau \to \mu Z'$ Two Body Decay

If the Z' is fairly stable, then we can have 2-body τ decays $\tau \to \ell_\alpha + Z'$, where Z' is invisible. These processes can be constrained by looking at the energy spectrum of the ℓ_α in the decay product since the more dominant $\tau \to \ell_\alpha \nu\nu$ process is a 3-body decay leading to a different ℓ_α energy spectrum. These were extracted from the $\tau^+\tau^-$ pair creation data in e^+e^- collisions. One of the τ's of the pair is tagged, and the energy of the e or the μ coming from the decay of the other τ in its rest frame is measured.

According to the Review of Particle Properties [1], we have the bounds

$$\begin{aligned} B(\tau \to e + Z') &< 2.7 \times 10^{-3} , \\ B(\tau \to \mu + Z') &< 5 \times 10^{-3} , \end{aligned} \tag{8.29}$$

at 95% C.L., which are based on ARGUS data [506]. This gives

$$\begin{aligned} \frac{\Gamma(\tau \to e + Z')}{\Gamma(\tau \to e\nu\nu)} &< 0.015 , \\ \frac{\Gamma(\tau \to \mu + Z')}{\Gamma(\tau \to \mu\nu\nu)} &< 0.029 , \end{aligned} \tag{8.30}$$

at 95% C.L. for $m_{Z'} = 0$. Looking at Fig. 4 of Ref. [506], we conclude that these bounds are valid for $m_{Z'}$ up to a few 100 MeV. The SM decay widths (without radiative corrections) are

$$\begin{aligned} \Gamma(\tau \to e\nu\nu) &= \frac{G_F^2 m_\tau^5}{192\pi^3} , \\ \Gamma(\tau \to \mu\nu\nu) &= \frac{G_F^2 m_\tau^5}{192\pi^3} f(m_\mu^2/m_\tau^2) , \end{aligned} \tag{8.31}$$

where

$$f(\eta) \equiv 1 - 8\eta + 8\eta^3 - \eta^4 - 12\,\eta^2 \ln \eta . \tag{8.32}$$

Substituting the values we find

$$\begin{aligned}\Gamma(\tau \to e\nu\nu) &= \frac{G_F^2 m_\tau^5}{192\pi^3} = 4.05 \times 10^{-13}\,\mathrm{GeV}\,, \\ \Gamma(\tau \to \mu\nu\nu) &= \frac{G_F^2 m_\tau^5}{192\pi^3} f(m_\mu^2/m_\tau^2) = 3.94 \times 10^{-13}\,\mathrm{GeV}\,,\end{aligned} \tag{8.33}$$

which translates to

$$\begin{aligned}\Gamma(\tau \to e + Z') &< 6.1 \times 10^{-15}\,\mathrm{GeV}\,, \\ \Gamma(\tau \to \mu + Z') &< 1.1 \times 10^{-14}\,\mathrm{GeV}\,.\end{aligned} \tag{8.34}$$

The coupling that would cause the $\tau \to \ell_\alpha + Z'$ decay is

$$g'\zeta Z'_\mu \left[\sin(2\delta_L)\left(\overline{\ell_{L\alpha}}\gamma^\mu \tau_L + \overline{\tau_L}\gamma^\mu \ell_{L\alpha}\right) + \sin(2\delta_R)\left(\overline{\ell_{R\alpha}}\gamma^\mu \tau_R + \overline{\tau_R}\gamma^\mu \ell_{R\alpha}\right)\right]. \tag{8.35}$$

For the sake of simplicity, let us set $\delta_L = \delta_R = \dfrac{\pi}{4}$ so that we have

$$g'\zeta Z'_\mu \left(\overline{\ell_\alpha}\gamma^\mu \tau + \overline{\tau}\gamma^\mu \ell_\alpha\right)\,. \tag{8.36}$$

The decay width will be given by

$$\begin{aligned}&\Gamma(\tau \to \ell_\alpha + Z') \\ &= (g'\zeta)^2 \frac{m_\tau}{16\pi} \frac{\lambda^{1/2}(m_\tau^2, m_\alpha^2, m_{Z'}^2)}{m_\tau^2} \frac{\{(m_\tau + m_\alpha)^2 + 2m_{Z'}^2\}\{(m_\tau - m_\alpha)^2 - m_{Z'}^2\}}{m_{Z'}^2 m_\tau^2}\,,\end{aligned} \tag{8.37}$$

where

$$\lambda(a,b,c) = a^2 + b^2 + c^2 - 2ab - 2bc - 2ca\,. \tag{8.38}$$

If we set $m_\alpha = 0$, we have

$$\Gamma(\tau \to \ell_\alpha + Z') = (g'\zeta)^2 \frac{m_\tau}{16\pi}\left(2 + \frac{m_\tau^2}{m_{Z'}^2}\right)\left(1 - \frac{m_{Z'}^2}{m_\tau^2}\right)^2\,. \tag{8.39}$$

It is argued in Ref. [504] that this places a very strong constraint on ζ due to the $m_\tau^2/m_{Z'}^2$ term enhancing this width. Indeed, for both the $\alpha = e$ and $\alpha = \mu$ cases, we can approximate

$$\Gamma(\tau \to \ell_\alpha + Z') \approx \left(\frac{g'\zeta}{m_{Z'}}\right)^2 \frac{m_\tau^3}{16\pi} \tag{8.40}$$

and also

$$\frac{\Gamma(\tau \to \ell_\alpha + Z')}{\Gamma(\tau \to \ell_\alpha \nu\nu)} \approx \left(\frac{g'\zeta}{m_{Z'}}\right)^2 \frac{12\pi^2}{G_F^2 m_\tau^2} = (2.76 \times 10^{11}\,\mathrm{GeV}^2) \times \left(\frac{g'\zeta}{m_{Z'}}\right)^2\,, \tag{8.41}$$

so we find

$$\begin{aligned} g'\zeta &< 2.3\times10^{-7} m_{Z'}/\text{GeV} \qquad \text{from } \Gamma(\tau\to e+Z), \\ g'\zeta &< 3.2\times10^{-7} m_{Z'}/\text{GeV} \qquad \text{from } \Gamma(\tau\to \mu+Z). \end{aligned} \tag{8.42}$$

Please note that

$$m_{Z'} = 2g'\zeta w\,, \tag{8.43}$$

where w is the VEV of the extra Higgs. See appendix G for more details of the spontaneous symmetry breaking in this model. The above contraints lead to

$$\begin{aligned} w &= \frac{m_{Z'}}{2g'\zeta} > 2.1\times10^6\,\text{GeV} \qquad \text{from } \Gamma(\tau\to e+Z), \\ w &= \frac{m_{Z'}}{2g'\zeta} > 1.5\times10^6\,\text{GeV} \qquad \text{from } \Gamma(\tau\to \mu+Z), \end{aligned} \tag{8.44}$$

which is far too large since we need $\sqrt{v^2+w^2} = 246\,\text{GeV}$ to get the correct W and Z masses. Putting that constraint aside, we draw the following constraints for NSI based on Eq. (8.42). For $\zeta = 10^{-6}$, we have

$$\begin{aligned} \varepsilon^{qP}_{\mu\tau} \le \frac{(\zeta g')^2}{M^2_{Z'}}\left(\zeta^{-1}\frac{1}{2\sqrt{2}G_F}\right) &< 1.6\times10^{-3},\ \text{from } \Gamma(\tau\to e+Z), \\ &< 3.1\times10^{-3},\ \text{from } \Gamma(\tau\to \mu+Z). \end{aligned} \tag{8.45}$$

For $\zeta = 10^{-3}$, we have

$$\begin{aligned} \varepsilon^{qP}_{\mu\tau} \le \frac{(\zeta g')^2}{M^2_{Z'}}\left(\zeta^{-1}\frac{1}{2\sqrt{2}G_F}\right) &< 1.6\times10^{-6},\ \text{from } \Gamma(\tau\to e+Z), \\ &< 3.1\times10^{-6},\ \text{from } \Gamma(\tau\to \mu+Z). \end{aligned} \tag{8.46}$$

This is close to the bounds shown in Ref. [504]. On the other hand, Belle has 2000 times more statistics, which puts a more stringent bound on NSI models with light mediators. In particular, Ref. [507] shows a preliminary result of $B(\Gamma\to\mu+Z') < 1\times10^{-4}$. With this result, we repeat the above analysis for ARGUS, which gives the following bounds on ε. For $\zeta = 10^{-6}$,

$$\varepsilon^{qP}_{\mu\tau} \le 6.1\times10^{-5}, \tag{8.47}$$

and for $\zeta = 10^{-3}$,

$$\varepsilon^{qP}_{\mu\tau} \le 6.1\times10^{-8}, \tag{8.48}$$

which is much stricter and renders the NSI beyond the reach of long-baseline oscillation experiments such as DUNE.

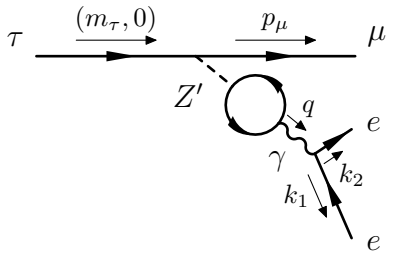

Figure 8.1: Z' coupling to electrons through $Z' - \gamma$ mixing at one loop level that leads to $\tau \to \mu ee$.

8.3.2 $\tau \to \mu ee$ Three Body Decay

As mentioned above, eeZ' coupling at tree level is forbidden to avoid serious bounds on process with electron final states. Even with this, we observe that Z' mixes with γ through hadron loops and couples to electrons anyway, as shown in Fig. 8.1. This process violates lepton flavor and is not allowed in the SM. As a result, we can calculate the partial decay width $\Gamma(\tau \to \mu ee)$ due to the presence of Z' and place bounds on $g', M_{Z'}$, and ζ, hence the NSI ε. Please note there is an caveat for using such bounds. That is, Z' must be short lived so that decays within the detector. In this sense, the analysis of this section is complementary to the two body decay bound in section 8.3.1.

Charge Renormalization up to One-Loop

Let us denote Q'_0 as the bare $U(1)'$ charge of electron. At the tree level, it is chosen to be zero. The running due to the hadron loop correction can be parametrized as follows:

$$\begin{aligned} g'_0 Q'_0 &\mapsto g'_0 (Q'_0 + e^2(q^2) \frac{\Pi_{QQ'}(q^2)}{q^2} \zeta) \\ &= g'_0 (\underbrace{Q'_0 + e^2(q^2) \Pi'_{QQ'}(q^2) \zeta}_{Q'_*}), \end{aligned} \tag{8.49}$$

where Q'_* is the running $U(1)'$ charge of electron, and $\Pi_{QQ'}$ is the vacuum polarization amplitude that mixes Z' with γ. Thus, the problem of solving Q'_* is equivalent to getting the vacuum polarization amplitude $\Pi_{QQ'}$, which can be calculated from the photon self-energy Π_{QQ} by a simple shift of charge from Q' to Q. Let us examine the current structure of Π_{QQ} and $\Pi_{QQ'}$:

$$\begin{aligned} i g^{\mu\nu} \Pi_{IJ} &= (-i)^2 (-1) \int \frac{\mathrm{d}^4 k}{(2\pi)^4} \mathrm{Tr} \left[\gamma^\mu \frac{i}{\not{k} - m} \gamma^\nu \frac{i}{\not{k} + \not{q} - m} \right] \\ &\equiv \langle J^\mu_I J^\nu_J \rangle \,, \end{aligned} \tag{8.50}$$

with I, J being Q or Q'. With $0 < q < m_\tau \approx 1.78$ GeV, the lightest charmed meson being $m_D \approx 1.86$ GeV, only u, d, and c run in the hadron loop. However, based on the calculation in appendix E.1, $\Gamma_{Z'}$ is very small. Therefore, the partial decay width $\Gamma(\tau \to \mu ee)$ receives most of the contribution from process $\tau \to Z'\mu$, followed by $Z' \to ee$ with Z' being on-shell. In this case, the transferred energy is $q \sim m_{Z'} < 200$ MeV, with $m_{Z'}$ chosen in Ref. [504] in order to avoid bounds from processes such as $Z' \to \pi\pi$. With the mass of lightest meson with strangeness being $m_K \approx 0.49$ GeV, we only need to consider the light unflavored mesons running in the loop. The vacuum polarization amplitude of photon propagator is

$$\begin{aligned} ig^{\mu\nu}\Pi_{QQ} &= \left\langle \left(\frac{2}{3}\overline{u}\gamma^\mu u - \frac{1}{3}\overline{d}\gamma^\mu d\right)\left(\frac{2}{3}\overline{u}\gamma^\nu u - \frac{1}{3}\overline{d}\gamma^\nu d\right)\right\rangle \\ &= \left\langle \left[\frac{1}{6}\left(\overline{u}\gamma^\mu u + \overline{d}\gamma^\mu d\right) + \frac{1}{2}\left(\overline{u}\gamma^\mu u - \overline{d}\gamma^\mu d\right)\right]\left[\frac{1}{6}\left(\overline{u}\gamma^\nu u + \overline{d}\gamma^\nu d\right) + \frac{1}{2}\left(\overline{u}\gamma^\nu u - \overline{d}\gamma^\nu d\right)\right]\right\rangle \\ &\approx (\frac{1}{6})^2\left\langle\left(\overline{u}\gamma^\mu u + \overline{d}\gamma^\mu d\right)\left(\overline{u}\gamma^\nu u + \overline{d}\gamma^\nu d\right)\right\rangle + (\frac{1}{2})^2\left\langle\left(\overline{u}\gamma^\mu u - \overline{d}\gamma^\mu d\right)\left(\overline{u}\gamma^\nu u - \overline{d}\gamma^\nu d\right)\right\rangle \\ &\equiv ig^{\mu\nu}\Pi^S_{QQ} + ig^{\mu\nu}\Pi^V_{QQ}, \end{aligned} \tag{8.51}$$

where the isospin symmetry is assumed in the limit of $m_u \approx m_d \approx 0$. We see that the vacuum polarization of the photon self-energy receives contribution from both the isoscalar and isovector currents. Next, let us study the current structure of the vacuum polarization for the $\gamma Z'$ mixing:

$$\begin{aligned} ig^{\mu\nu}\Pi_{QQ'} &= \left\langle \left(\frac{2}{3}\overline{u}\gamma^\mu u - \frac{1}{3}\overline{d}\gamma^\mu d\right)\left(\overline{u}\gamma^\nu u + \overline{d}\gamma^\nu d\right)\right\rangle \\ &\approx \frac{1}{6}\left\langle(\overline{u}\gamma^\mu u + \overline{d}\gamma^\mu d)(\overline{u}\gamma^\mu u + \overline{d}\gamma^\mu d)\right\rangle, \end{aligned} \tag{8.52}$$

which only receives contribution from the isoscalar current. Due to the universal structure of current current correlation function in field theory, $\Pi_{QQ'}$ can be written as a shift of charge of Π^S_{QQ}:

$$\Pi_{QQ'} = 6\Pi^S_{QQ}. \tag{8.53}$$

We show how to get Π^S_{QQ} from electron-positron annihilation data in the next section.

Separating the Isoscalar Contribution of the R Ratio

At the energy range lower than m_τ, we cannot rely on perturbative QCD, so $\Pi_{QQ'}$ cannot be calculated based on first principle. On the other hand, because of the universality of the vacuum polarization amplitude, we can extract Π_{QQ} from electron-positron annihilation data using the following formula:

$$\Pi'_{QQ}(q^2) - \Pi'_{QQ}(0) = -\frac{1}{12\pi^2}\int_{4m_\pi^2}^{\infty}\frac{q^2}{x(x-q^2)}R^{(h)}(\sqrt{x})\mathrm{d}x, \tag{8.54}$$

the derivation of which is shown in appendix D. Then we can shift the charge of Π_{QQ} accordingly to get $\Pi_{QQ'}$. Because we need Π^S_{QQ}, the isoscalar part of photon self-energy, the right hand side of Eq. (8.54) should also be replace with the R ratio due to the isoscalar contribution. We use data taken from Ref. [6] to model the continuous isoscalar contribution to the R ratio, in the energy range $0.81 - 1.39$ GeV, as shown in Table 8.1. This result is compared with the latest R ratio measurement from PDG [1], in Fig. 8.2. Similar to

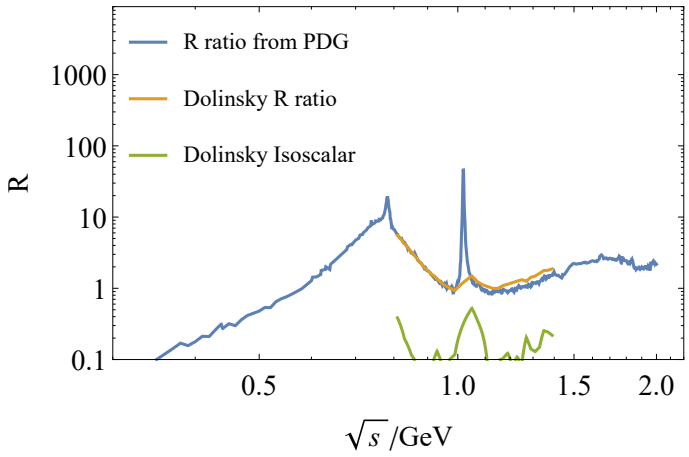

Figure 8.2: The plot is produced with data from the following sources: the total R ratio measurement from PDG (blue curve), the R ratio data from Ref. [6] as listed in the second column of Table 8.1 (orange curve), and the R ratio of the isoscalar contribution from Ref. [6] as shown in third column of Table 8.1 (green curve).

Ref. [508], we add ω and ϕ resonance using the Breit-Wigner approximation to account for the bound-states contribution from ϕ, and ω. This is shown in Fig. 8.3.

Putting this result for the R ratio into Eqs. (8.53) and (8.54), we get the running of the Q'_*, which is shown in Fig. 8.4. We stress that even though the coupling of eeZ' is chosen to be zero in the Lagrangian, it runs up to 10^{-3} due to the $\gamma - Z'$ mixing.

Bounds from $\tau \to \mu ee$

Now that we have the running of $U(1)'$ of the electron, we use it to calculate the partial decay width of $\tau \to \mu ee$. The effective Lagrangian contains the following terms:

$$\mathcal{L}_{eff} \supset (g'Q'_*)(\overline{e}\gamma^\mu e)Z'_\mu + (g'\zeta)(\overline{\tau}\gamma^\mu \mu)Z'_\mu(\sin(2\delta_L) + \sin(2\delta_R)) + h.c. \tag{8.55}$$

Setting $\delta_L = \delta_R = \frac{\pi}{4}$ for simplicity, the amplitude is written as

$$\mathcal{M}_{Z'} = [\overline{u}_\tau(p_\tau)\gamma^\kappa P_L u_\mu(p_\mu)][\overline{u}_e(k_1)\gamma_\mu P_L u_e(k_2)] \left(\frac{g'^2 Q'_* \zeta}{q^2 - M^2_{Z'} + iM_{Z'}\Gamma_{Z'}}\right). \tag{8.56}$$

$\sqrt{q^2}$/GeV	R	R Isoscalar
0.81	5.545	0.385
0.83	4.204	0.196
0.85	3.219	0.117
0.87	2.516	0.081
0.89	1.958	0.085
0.91	1.617	0.071
0.93	1.355	0.131
0.95	1.134	0.075
0.97	1.018	0.098
0.99	0.93	0.118
1.05	1.492	0.526
1.07	1.245	0.358
1.09	1.118	0.228
1.11	1.056	0.079
1.13	0.998	0.096
1.15	0.995	0.097
1.17	1.09	0.103
1.19	1.14	0.123
1.21	1.021	0.082
1.23	1.264	0.109
1.25	1.32	0.084
1.27	1.257	0.204
1.29	1.424	0.141
1.31	1.486	0.129
1.33	1.622	0.149
1.35	1.774	0.255
1.37	1.789	0.243
1.39	1.877	0.219

Table 8.1: The total R ratio and the R ratio from the isoscalar-current contribution. Data is taken from Ref. [6].

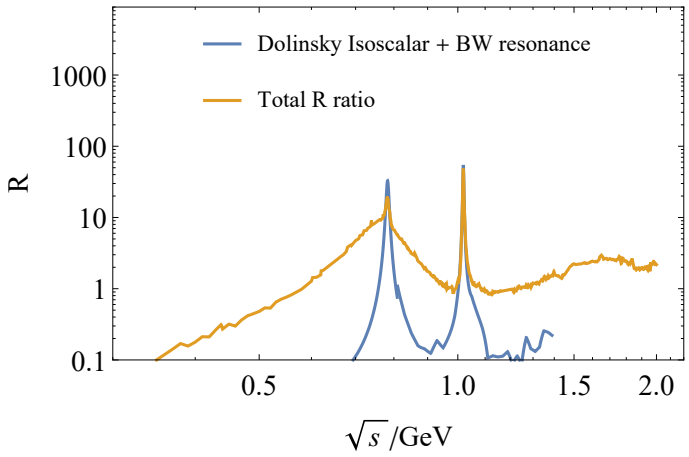

Figure 8.3: The isoscalar contribution to the R ratio (blue), modeled with continuous part from Ref. [6] and bound states using Breit-Wigner resonance formula, compared to the R ratio data from PDG (orange).

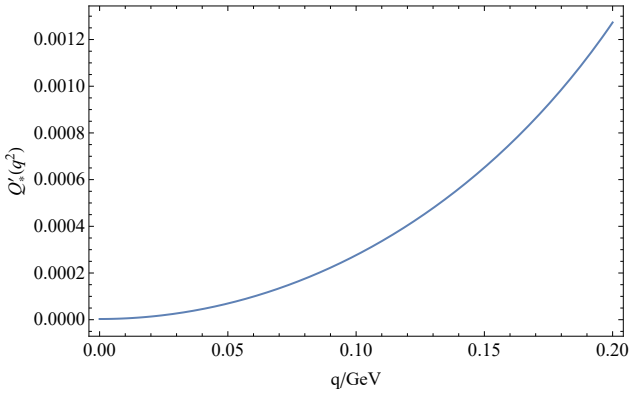

Figure 8.4: Running of Q'_* due to $\gamma Z'$ mixing.

Integrating over momentum, the differential partial width is expressed as follows:

$$\frac{\mathrm{d}\Gamma}{\mathrm{d}E_\mu} = \frac{(g'^2 Q'_* \zeta)^2}{128\pi^3} \frac{1}{q^2 + M_{Z'}^2 \Gamma_{Z'}^2} \left(-\frac{4}{3} m_\tau E_\mu^2 + m_\tau^2 E_\mu - \frac{2}{3} m_\mu^2 m_\tau + m_\mu^2 E_\mu \right) \sqrt{E_\mu^2 - m_\mu^2}, \quad (8.57)$$

where $q^2 = m_\tau + m_\mu^2 - M_{Z'}^2 - 2m_\tau E_\mu$. Obviously, when $\Gamma_{Z'}$ is small, the total partial width is dominated by the region around $q = 0$, which corresponds to Z' being on-shell. From Ref. [368], we find the bound on the rare decay process $\tau \to \mu ee$ is $\Gamma_i/\Gamma \leq 1.8 \times 10^{-8}$ at the 90% confidence level, where Γ_i is the partial width and Γ is the total width. The total width

can be obtained from the τ lifetime:

$$\begin{aligned}\Gamma &= \frac{\hbar}{\tau} \\ &= 1.05 \times 10^{-34}(\mathrm{J}\cdot\mathrm{s})/(2.90 \times 10^{-13}\mathrm{s}) \times (1.60 \times 10^{-19}\mathrm{J/eV})^{-1} \\ &\approx 2.3 \times 10^{-3}\ \mathrm{eV}. \end{aligned} \tag{8.58}$$

Therefore, the bound for the decay width Γ_i is

$$\Gamma_i \leq 1.8 \times 10^{-8}\Gamma = 4.1 \times 10^{-11}\ \mathrm{eV}. \tag{8.59}$$

Based on this bound, we get the bounds on $g', M_{Z'}$, and ζ, shown in the upper panel of Fig. 8.5. The bound on $\varepsilon^{qP}_{\mu\tau}$ is shown in the lower panel of Fig. 8.5.

As we pointed out, the bounds from Sections 8.3.1 and 8.3.2 apply to long-lived and short-lived Z', respectively. To be specific, the bound from Section 8.3.2 is from Belle [509]. The tracking chamber of Belle covers the polar angular range of 17° to 150°, with an outer radius of 0.88 m. The longest reach is about 1.7 m (at the 17° direction). Next, let us look at the lifetime of Z'.

According to the calculation of Appendix E.1, the total decay width of Z' can be estimated as $\Gamma_{Z'} \approx 1.4 \times 10^{-6}$ eV. This translates to $\tau \approx 4.7 \times 10^{-10}$ s. We convert this to a decay length. Since most of Z' is produced on shell due to the mass resonance, the energy is about $E_{Z'} = \frac{m_\tau}{2} = 0.89$ GeV. This gives us the relativistic factor of $\gamma = 4.5 \sim 180$ for 5 MeV $\leq M_{Z'} \leq$ 200 MeV. This translates to a decay length of

$$0.6\ \mathrm{m} \leq (\beta c)(\gamma\tau) \leq 20\ \mathrm{m}. \tag{8.60}$$

This verifies our previous concern of the applicability of the Belle constraint on the LFV three-body decay process. On the other hand, since the bound from either $\tau \to \mu Z'$ or $\tau \to \mu ee$ is strong, we conclude that $\varepsilon^{qP}_{\mu\tau}$ in this model is strongly bounded.

8.3.3 $\tau \to \mu\nu\nu$ Three Body Decay

In this section, we consider the bounds from $\tau \to \mu\overline{\nu}_\mu\nu_\tau$. In the SM, this process happens through a W boson exchange as shown in Fig. 8.6. In this model, the Z' exchange also contributes to the same process, which interferes with the SM process. To be specific, the Lagrangian for the SM $\tau \to \mu\overline{\nu}_\mu\nu_\tau$ process is expressed as follows:

$$\mathcal{L} \supset -2\sqrt{2}G_F\big(\overline{\nu_\tau}\gamma^\mu P_L\tau\big)\big(\overline{\ell_\alpha}\gamma_\mu P_L\nu_\alpha\big), \tag{8.61}$$

which results in the transition amplitude:

$$\mathcal{M}_{\mathrm{SM}} \ = \ -2\sqrt{2}G_F\big[\,\overline{u}_{\nu_\tau}(k_{\nu_\tau})\gamma^\kappa P_L u_\tau(p_\tau)\,\big]\big[\,\overline{u}_\alpha(p_\alpha)\gamma_\kappa P_L v_{\nu_\alpha}(k_{\nu_\alpha})\,\big]\ . \tag{8.62}$$

Adding Z' to the SM will create an extra contribution:

$$\begin{aligned}\mathcal{M}_{\mathrm{Z}'} &= 2\sqrt{2}G_F\frac{\epsilon M_{Z'}^2}{q^2-M_{Z'}^2}\left[\,\overline{u}_\alpha(p_\alpha)\gamma^\kappa P_L u_\tau(p_\tau)\,\right]\left[\,\overline{u}_{\nu_\tau}(k_{\nu_\tau})\gamma_\kappa P_L v_{\nu_\alpha}(k_{\nu_\alpha})\,\right] \\ &= -2\sqrt{2}G_F\frac{\epsilon M_{Z'}^2}{q^2-M_{Z'}^2}\left[\,\overline{u}_{\nu_\tau}(k_{\nu_\tau})\gamma^\kappa P_L u_\tau(p_\tau)\,\right]\left[\,\overline{u}_\alpha(p_\alpha)\gamma_\kappa P_L v_{\nu_\alpha}(k_{\nu_\alpha})\,\right]\,, \qquad (8.63)\end{aligned}$$

where we parametrize the strength of this interaction with the dimensionless parameter ϵ,

$$2\sqrt{2}G_F\frac{\epsilon M_{Z'}^2}{q^2-M_{Z'}^2}=\frac{(\zeta g')^2}{q^2-M_{Z'}^2}, \qquad (8.64)$$

which implies

$$\epsilon=-2\frac{M_W^2}{M_{Z'}^2}\frac{(\zeta g')^2}{g_W^2}. \qquad (8.65)$$

Please note that, in this notation, even though $\zeta g'$ is tiny compared to the weak coupling g_W, ϵ can still be fairly large due to the enhancement from small $\frac{M_W}{M_{Z'}}$. The squared momentum transfer is

$$\begin{aligned}q^2 &= (p_\tau-p_\alpha)^2 \;=\; (k_{\nu_\tau}+k_{\nu_\alpha})^2 \\ &= (m_\tau-E_\alpha)^2-\mathbf{p}_\alpha^2 \;=\; 2|\mathbf{k}_{\nu_\tau}||\mathbf{k}_{\nu_\alpha}|(1-\cos\theta)\,, \qquad (8.66)\end{aligned}$$

where the second line is in the rest frame of the decaying τ, and the angle θ is the angle between the momenta of the two outgoing neutrinos in that frame[1]. So with the Z' exchange contribution, the amplitude and its square become

$$\begin{aligned}\mathcal{M}_{\mathrm{SM}}+\mathcal{M}_{Z'} &= \mathcal{M}_{\mathrm{SM}}\left(1+\frac{\epsilon M_{Z'}^2}{q^2-M_{Z'}^2}\right) \\ &\downarrow \\ |\mathcal{M}_{\mathrm{SM}}+\mathcal{M}_{Z'}|^2 &= |\mathcal{M}_{\mathrm{SM}}|^2\left[1+\frac{2\epsilon M_{Z'}^2}{q^2-M_{Z'}^2}+\mathcal{O}(\epsilon^2)\right], \qquad (8.67)\end{aligned}$$

Note that, due to the interference, the Z' exchange contributes an $\mathcal{O}(\epsilon)$ correction, not an $\mathcal{O}(\epsilon^2)$ correction. Also, the correction term blows up at $q^2=M_{Z'}^2$ (which could happen if $M_{Z'}<m_\tau$) so we may need to include the width of the Z' in the Z' propagator:

$$\frac{1}{q^2-M_{Z'}^2}\quad\rightarrow\quad\frac{1}{q^2-M_{Z'}^2+iM_{Z'}\Gamma_{Z'}}\,. \qquad (8.68)$$

in which case the correction term becomes

$$\frac{2\epsilon M_{Z'}^2}{q^2-M_{Z'}^2}\quad\rightarrow\quad\frac{2\epsilon M_{Z'}^2(q^2-M_{Z'}^2)}{(q^2-M_{Z'}^2)^2+M_{Z'}^2\Gamma_{Z'}^2}\,. \qquad (8.69)$$

[1]We treat the neutrinos as massless.

After integrating over k_{ν_τ}, k_{ν_α}, and the angle of p_α, we have the differential decay rate

$$\begin{aligned}\frac{d\Gamma}{dE_\alpha} &= \frac{G_F^2}{\pi^3}\left(1+\frac{2\epsilon M_{Z'}^2(m_\tau^2+m_\alpha^2-M_{Z'}^2-2m_\tau E_\alpha)}{(m_\tau^2+m_\alpha^2-M_{Z'}^2-2m_\tau E_\alpha)^2+M_{Z'}^2\Gamma_{Z'}^2}\right)\\ &\times\left(\frac{1}{4}(m_\tau^2-m_\alpha^2)(m_\tau-E_\alpha)\sqrt{E_\alpha^2-m_\alpha^2}-\frac{1}{4}m_\tau\left((m_\tau-E_\alpha)^2+\frac{1}{3}(E_\alpha^2-m_\alpha^2)\right)\sqrt{E_\alpha^2-m_\alpha^2}\right)\\ &= \frac{G_F^2}{4\pi^3}\left(1+\frac{2\epsilon M_{Z'}^2(m_\tau^2+m_\alpha^2-M_{Z'}^2-2m_\tau E_\alpha)}{(m_\tau^2+m_\alpha^2-M_{Z'}^2-2m_\tau E_\alpha)^2+M_{Z'}^2\Gamma_{Z'}^2}\right)\\ &\times\left(-\frac{4}{3}m_\tau E_\alpha^2+m_\tau^2E_\alpha-\frac{2}{3}m_\alpha^2m_\tau+m_\alpha^2E_\alpha\right)\sqrt{E_\alpha^2-m_\alpha^2}.\end{aligned} \tag{8.70}$$

According to Ref. [504], the Z' mass is chosen to be lighter than $2m_\mu$ to avoid bounds from $Z'\to\mu\mu$. Therefore, for the Z' decay width, we consider $Z'\to\nu\overline{\nu}$, and $Z'\to e^+e^-$ only. The details of the calculation are shown in Appendix E.1.

According to the Particle Data Group, the branching ratio of $\tau^-\to\mu^-\overline{\nu}_\mu\nu_\tau$ is (17.39±0.04)%. Defining r to be the ratio of Γ within this model and taking Γ from the SM prediction, the bounds on $\Gamma(\tau^-\to\mu^-\overline{\nu}_\mu\nu_\tau)$ corresponds to $r=1\pm0.0023$. From this, we infer the bounds on g', $M_{Z'}$, and ζ in Fig. 8.7(a) and on $\varepsilon_{\mu\tau}^{qP}$ in Fig. 8.7(b)(c). It is observed that $\tau\to\mu\nu\nu$ does not impose a strong bound on the NSI in this model. The reason is that ζ stays small and does not run due to the lack of a quantum correction. On the other hand, the dependence of the bound on ζ is the same.

8.4 Constraints from Other Sectors

8.4.1 Nuclear Binding Energy

In order to generate sizable NSI while avoiding constraints from the lepton sector, the coupling between Z' and quarks is set to be large and $M_{Z'}$ to be small. In this case, the Z' exchange between nucleons generates an extra Yukawa potential for the nuclear binding energy. Because u,d quarks share the same $U(1)'$ charge, the mass number dependence of the Yukawa potential is different from the Coulomb potential, both of which are calculable. As a result, the nuclear binding energy profile constrains the coupling g'. In this section, we briefly study the binding energy of the nuclear system using the semi-empirical formula, and draw bounds on g' and $M_{Z'}$.

Semi-empirical Mass Formula

The semi-empirical mass formula is given by

$$E = c_V A - c_S A^{\frac{2}{3}} - c_C \frac{Z(Z-1)}{A^{\frac{1}{3}}} - c_A \frac{(A-2Z)^2}{A} + \delta(A,Z), \tag{8.71}$$

where Z is the atomic number, and A is the mass number. The fitting coefficients c_V, c_S, c_C, c_A are the *volume, surface, Coulomb, asymmetry* terms, respectively. The pairing term $\delta(A,Z)$ is a correction arising from the phenomenon that the nuclear binding energy is lower when neutrons (protons) form pairs. It is expressed in Table 8.2, where k_P is fixed to 1/2 or 3/4

	$(A-Z)$ even	$(A-Z)$ odd
Z even	$+c_P A^{-k_P}$	0
Z odd	0	$-c_P A^{-k_P}$

Table 8.2: Paring term expression in the semi-empirical Mass Formula.

for fitting purpose, such as in the least-squares fit in Ref. [510]. If we assume the error of the energy binding for each element is the same, we can perform a least square fit of the semi-empirical formula to the measured binding energy of nuclei. According to Wikipedia [511], the best fit is given in Table 8.3. Using *Mathematica* isotope data (excluding the first four

k_P	c_V	c_S	c_C	c_A	c_P
$\frac{3}{4}$	15.76	17.81	0.711	23.702	34
$\frac{1}{2}$	15.8	18.3	0.714	23.2	12

Table 8.3: Best fit value of the semi-empirical formula from Wikipedia.

light nuclei, *i.e.* requiring $A > 4$), one of the authors of Ref. [505] finds the fit shown in Table 8.4, which agrees with the result of Table 8.3 within the uncertainties. Since the ref-

	c_V	c_S	c_C	c_A
Best Fit	15.474	17.280	0.694	21.876
1σ error	0.067	0.199	0.006	0.217

Table 8.4: Fitting the nuclear binding energy of the stable isotopes with $4 < A < 293$ using the semi-empirical mass formula. We fix $k_P = \frac{1}{2}$ and $c_P = 12$.

erence of Table 8.3 is not included nor is the error estimated, we refrain from discussing the small disagreement between that and our fit.

Modified Semi-Empirical Mass Formula with Z' Term

The potential of Z' can be modeled with a Yukawa potential, for which

$$\Delta E \propto A^{\frac{5}{3}} f(\mu r_0 A^{\frac{1}{3}}), \tag{8.72}$$

where r_0 is the charge radius of the nucleus, μ is the mass of Z', and

$$f(x) \equiv 1 - \frac{5x}{6} + \frac{3x^2}{7} - \frac{x^3}{6} + ... \tag{8.73}$$

For the derivation of this potential, see Appendix F.2. With the presence of Z', the semi-empirical mass formula is modified by an extra term, as follows

$$E' = c_V A - c_S A^{\frac{2}{3}} - c_C \frac{Z(Z-1)}{A^{\frac{1}{3}}} - c_A \frac{(A-2Z)^2}{A} + \delta(A,Z) + \underbrace{c' A^{\frac{5}{3}} f(\mu r_0 A^{\frac{1}{3}})}_{\Delta E}. \tag{8.74}$$

Because the Coulomb-term coefficient is calculable, we add a penalty term during the fitting to restrict it from floating far away from the calculated value. The constraints on g' are shown in Fig. 8.8.

8.4.2 Neutrino Scattering at IceCube

The IceCube experiment [512] is sensitive to ultra high energy (UHE) neutrinos from sources at cosmological distances. With the presence of Z', it is possible to generate a new contribution to cascade events through deep inelastic scattering (DIS), shown in Fig. 8.9. The current track-to-cascade ratio is already in tension with the null hypothesis of neutrinos at the source being $\nu_e : \nu_\mu : \nu_\tau = 1 : 1 : 1$[2]. The DIS-induced cascade events aggravate this tension.

On the other hand, while the UHE neutrinos propagate to the Earth, the scattering with relic neutrinos may be enhanced by a Z' resonance, as discussed in Ref. [513]. Assuming the relic neutrino has mass $m_{\rm atm} = 0.1$ eV, the resonance requires

$$M_{Z'} = \sqrt{2 m_\nu E_\nu} = \sqrt{2 \cdot 0.1 \cdot 6.3 \times 10^{15}}\ \text{eV} \approx 35\ \text{MeV}, \tag{8.75}$$

which is within the proposed energy range 5 MeV $\sim$ 200 MeV. The non-observation of the Glashow resonance at IceCube might be explained by UHE neutrinos being converted to hadrons by this resonance. Given the current IceCube statistics not being sensitive enough to determine the neutrino source, we leave the detailed analysis for future work.

[2]The current best fit is $\nu_e : \nu_\mu : \nu_\tau = 1 : 2 : 0$.

8.4.3 Neutron-Star Cooling

For neutron-star cooling process [514], the presence of a light long-lived Z' might affect the cooling rate. The radius of a neutron star is of the order of 10 km. Based on our calculations, the lifetime of Z' is around 1.4×10^{-6} s. Depending on the energy of the neutron star, it might be possible for the Z' to travel far enough before it decays into neutrino pair. If Z' decays after it escapes the neutron star, it prevents the produced neutrinos being trapped in the star and hence opens a new channel for neutron-star cooling. We leave the details of the estimation to Ref. [505].

8.4.4 Synchrotron Radiation

When charged particles are moving in a circular orbit, *i.e.*, accelerating, they lose energy through radiation of gauge particles. With the presence of a Z' particle, in principle it is possible to put constraints on the gauge coupling through synchrotron radiation. The energy of photon is calculated through the following formula:

$$E_\gamma = \frac{3\gamma^3 \hbar c}{2R}, \tag{8.76}$$

where R is the radius of the synchrotron and γ is the relativistic factor. For LHC, $R \approx 4.3$ km, $\gamma = 7000/0.938 \approx 7500$, so $E_\gamma \approx 30$ eV. Therefore, it does not apply to this particular model. On the other hand, models that contain ultra-light gauge mediators might be subject to this bound.

8.5 Conclusion

With data from recent long baseline neutrino experiments [515–521] and plans for future experiments [522], models are proposed to produce non-standard interactions (NSI) that can be tested in these experiments. In past studies such as in Refs. [4, 75, 440, 444, 473–475, 480, 481, 523], it is assumed that the NSI is led by dimension-six or -eight operators. Most of the effort was put on directly constraining the effective coupling of such interactions, usually denoted as $\varepsilon\, G_F$. However, it turns out to be non-trivial to achieve such high-order operators with light mediators in the EFT framework while surviving all existing bounds from particle data. In this chapter, we focused on the model from Ref. [504] as an example and study constraints of the model beyond the ones discussed in the original paper.

Based on our analysis, τ decay puts severe constraints on such models utilizing light particles as mediators. In particular, $\tau \to \ell Z'$ two-body decay puts stringent constraints when Z' is long-lived, where ℓ is μ or e, and $\tau \to \mu ee$ puts constraints in the case Z' is short-lived. We point out that in some cases such as the model we analyzed, even if we set certain tree

level couplings to zero, the effective couplings can still be significant due to the quantum loop effect, such as in eeZ' coupling. On the other hand, if there is no such mixing allowed through the loop effect, the coupling can be protected up to one loop even though it is small, such as in $\mu\tau Z'$ coupling.

To close, we discussed other constraints on this model in passing, including the constraints from nuclear binding energy and neutron star dynamics. In addition, synchrotron radiation also puts constraints on super-light mediator fairly model independently, which might be useful for constraining ultra-light mediators.

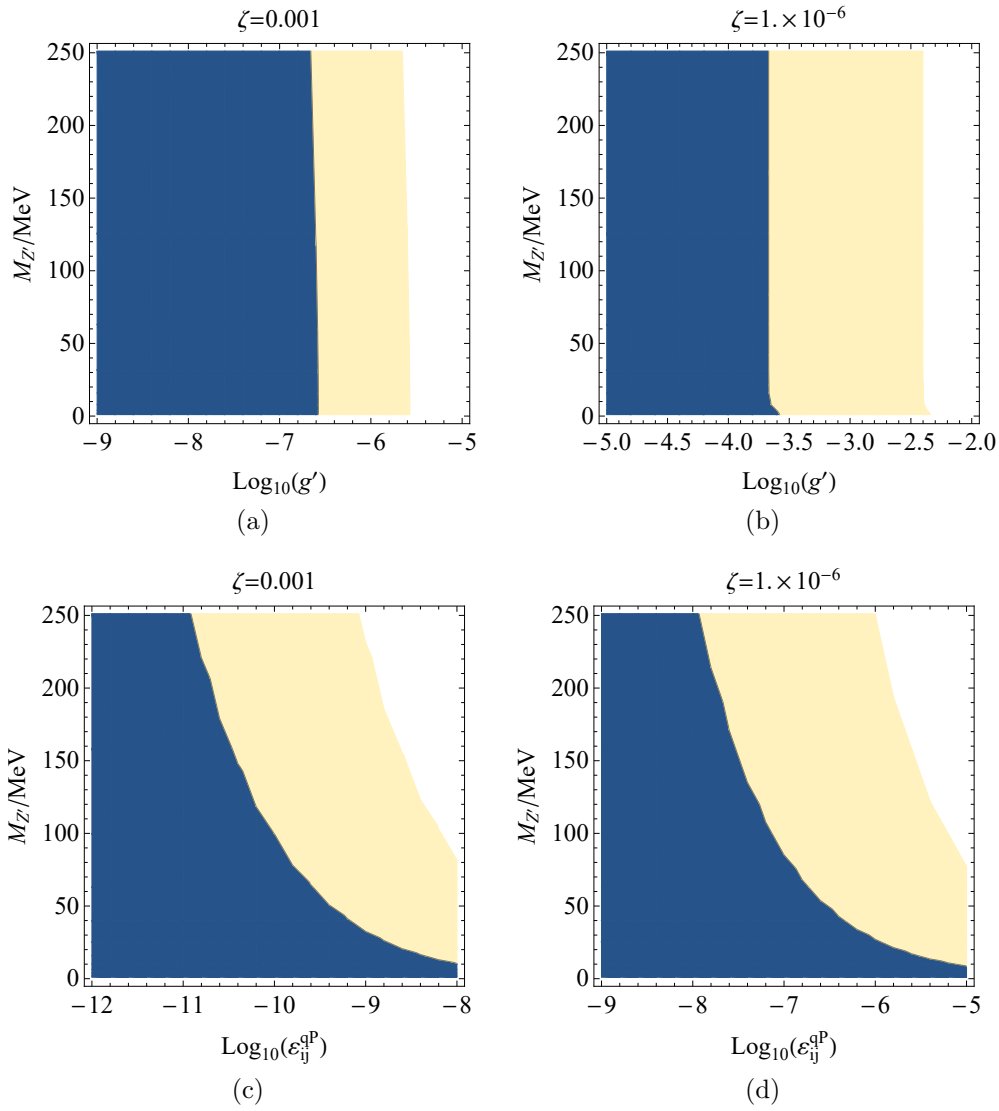

Figure 8.5: Contour (blue shaded region) corresponds to the upper bound of partial decay $\Gamma(\tau \to \mu ee)$. Upper panel: contour on $M_{Z'}, g'$ plane. Lower panel: contour on $M_{Z'}, \varepsilon^{u,d}_{\mu\tau}$ plane.

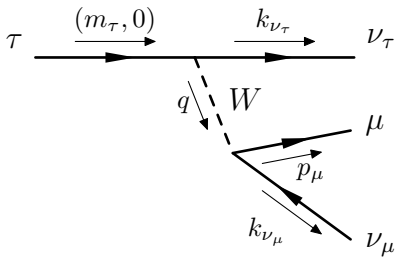

Figure 8.6: The SM process of $\tau^- \to \mu^- \nu_\tau \overline{\nu}_\nu$.

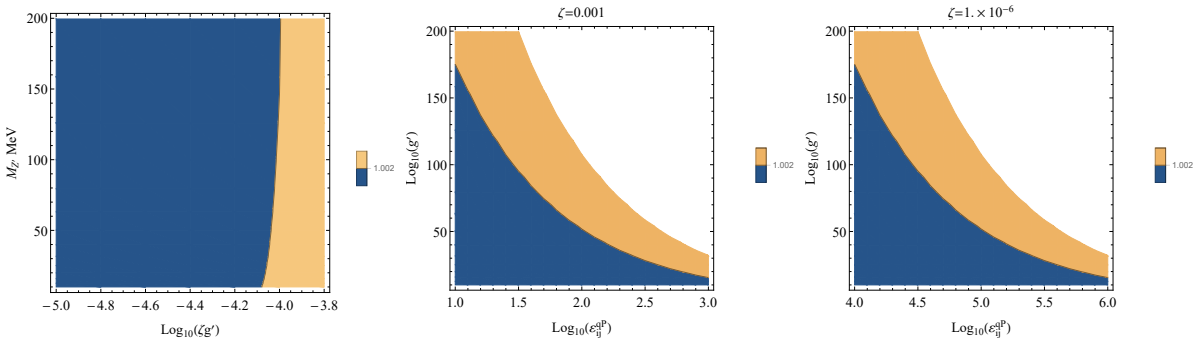

(a) (b) (c)

Figure 8.7: Blue shaded region corresponds to the upper bound of partial decay width $\Gamma(\tau \to \mu\nu\nu)$. Upper panel: contour on $M_{Z'}, g'$ plane. Lower panel: contour on $M_{Z'}, \varepsilon_{\mu\tau}^{u,d}$ plane.

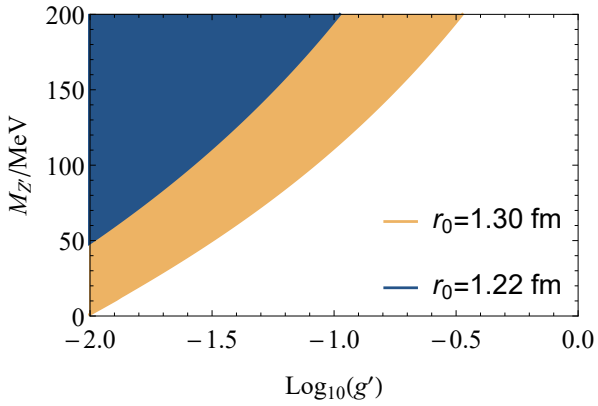

Figure 8.8: Constraints of $g', M_{Z'}$ from nuclear binding energy at 90% confidence level. The blue (orange) shaded region is for $r_0 = 1.22$ fm (1.30 fm).

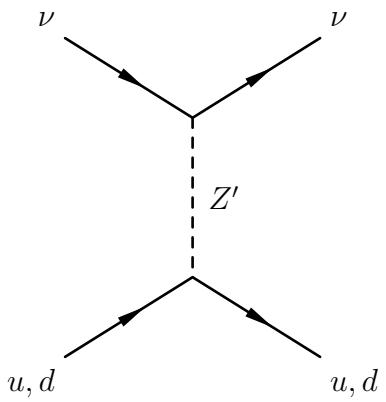

Figure 8.9: DIS process at IceCube.

Conclusions

In this work, we started with discussions on the possibility of new physics not being compatible with a local EFT framework. After summarizing the problems encountered in the SM in the EFT picture, we drew a list of requirements based on what was already known and what was needed to achieve understanding of the new physics. As a first attempt, we found a class of noncommutative theories (NCG) that exhibited the behavior of these requirements quite well. To study the new physics, we investigated the low energy EFT allowed by the NCG, which contained the SM plus a minimal extension. We describe this picture as a quasi-desert due to the lack of proliferation of particles in the extension.

Due to the presence of the NCG, the EFT at low energy is fixed by the boundary condition dictated by the NCG. In Part I, we studied the EFT dictated by NCG type of theories and the collider signatures of the EFT at the TeV scale. To our surprise, it was noticed that this boundary condition of gauge couplings turned out to be very restrictive in accommodating low energy collider signals, if any such signals arise. Therefore, it is possible to use collider signals to test this class of models derived from NCG, and hence improve the way we understand the new physics through NCG. As an example, we used the ephemeral collider anomalies in the diphoton and diboson channels to show how the collider signals favor or rule out such models. In addition, we pointed out in passing that the embedding of the SM in the NCG framework hinted at extensions of the SM through anomaly cancellation. A thorough understanding of the anomaly cancellation condition within the NCG framework and a classification of the NCG framework itself remain open for future study.

Because new field operators at high energy can be parametrized as effective operators of a high mass dimension in the Wilsonian picture, a careful study of low energy EFT is of importance to find clues of new physics. Besides the constraints obtained from the collider experiments, at low energy the neutrino sector has large uncertainty due to the nature of weak interaction. In order to carefully examine the EFT at low energy, in Part II we looked into the neutrino sector and studied the possibilities of finding new physics parametrized as NSI. To be specific, we studied the sensitivity of putting constraints on $\varepsilon_{ee}^{eL,R}$ using the neutron spallation source for the neutrinos and a mineral oil neutrino detector. Because of the pulsed time structure of the proton beam, we separated the ν_μ flux from the $\nu_e, \overline{\nu}_\mu$ flux, which in turn constrained the neutrino flux and NSI separately. We observed that the sensitivity to NSI was strongly affected by the control of the uncertainty in the neutrino

flux. We also mentioned in passing that, at very low energy range ($E_\nu < 50$ MeV), one of the largest backgrounds is still from the theoretical estimate of $\nu - {}^{12}C$ cross section. In Chapter 7, we worked out an analytic approximation of the NSI matter effect for $\varepsilon_{\mu\tau}$. With this expression, the term of the matter effect in the Lagrangian is absorbed into the vacuum oscillation parameters by analogy with the idea of renormalization group flow. In this approach, it is clear to observe the physical effect of NSI. Therefore, it is easy to analyze the degeneracy of parameters such as the proper octant of θ_{23}, the mass hierarchy, and NSI.

In Part III, we studied the models that generate sizable NSI with a light gauge boson. We showed that even though certain interaction terms are turned off at tree level to avoid stringent bounds, it is inevitably pulled back through quantum loop effect. This puts strong bounds on the model, which otherwise is not applicable at tree level. In addition, we briefly discussed bounds from other sectors, such as the change of nuclear binding energy, neutron star cooling, and the high energy neutrino scattering and synchrotron radiation. Although the bounds are model dependent, we observed that, in general, the bounds listed above put strong constraints on models that utilize light mediator particles to generate large NSI. Further investigation on other models are left for future studies.

Part IV

Appendices

Appendix A

Formula for the Superconnection Formalism

A.1 The Ne'eman-Sternberg Rule for Supermatrix Multiplication

As stated in Footnote 11 on Page 29, some papers in the literature treat the superconnection $\mathcal{J}$ as a super-endomorphism of a superspace and calculate the supercurvature $\mathcal{F}$ differently. In this appendix, we derive the multiplication rule for super-endomorphisms with differential forms as elements (or super-endomorphism valued differential forms). We will follow the notation of Sternberg [171] in which the $\mathbb{Z}_2$ gradings with be denoted with $\pm$ superscripts instead of 0, 1 subscripts.

A superspace E is simply a vector space with a $\mathbb{Z}_2$ grading:

$$E \;=\; E^+ \oplus E^- \;. \tag{A.1}$$

We denote the set of all endomorphisms, *i.e.*, linear transformations, on E with $\mathrm{End}(E)$, which is already an associative algebra. In the matrix representation, the product of $\mathrm{End}(E)$ is just standard matrix multiplication.

When E is provided with a $\mathbb{Z}_2$ grading as above, a $\mathbb{Z}_2$ grading can also be introduced into $\mathrm{End}(E)$ by simply letting $\mathrm{End}(E)^+$ consist of all endomorphisms that map $E^\pm$ to $E^\pm$, and $\mathrm{End}(E)^-$ consist of all endomorphisms that map $E^\pm$ to $E^\mp$. That is:

$$\begin{aligned} \mathrm{End}(E)^+ \;&:\; E^+ \to E^+,\;\; E^- \to E^- \;, \\ \mathrm{End}(E)^- \;&:\; E^+ \to E^-,\;\; E^- \to E^+ \;. \end{aligned} \tag{A.2}$$

In matrix representation, the elements of $\mathrm{End}(E)^+$ consist of matrices of the form

$$\begin{bmatrix} A & 0 \\ 0 & B \end{bmatrix}, \quad A : E^+ \to E^+, \quad B : E^- \to E^-, \tag{A.3}$$

while elements of $\mathrm{End}(E)^-$ consist of those of the form

$$\begin{bmatrix} 0 & C \\ D & 0 \end{bmatrix}, \quad C : E^- \to E^+, \quad D : E^+ \to E^-. \tag{A.4}$$

Then, clearly

$$\mathrm{End}(E) \;=\; \mathrm{End}(E)^+ \oplus \mathrm{End}(E)^- \,, \tag{A.5}$$

and $\mathrm{End}(E)$ can be viewed as a superalgebra, its product satisfying Eq. (2.7). Note that the product of the superalgebra here is just the product of the associative algebra from which it was derived, *i.e.*, standard matrix multiplication. So far, nothing has changed by viewing $\mathrm{End}(E)$ as a superalgebra.

The multiplication rule changes when the superalgebra $\mathrm{End}(E) = \mathrm{End}(E)^+ \oplus \mathrm{End}(E)^-$ is tensored with the commutative superalgebra of differential forms $\Omega(M) = \Omega^+(M) \oplus \Omega^-(M)$, yielding a superalgebra of super-endomorphism valued differential forms, or super-endormorphisms with differential forms as elements. The rule depends slightly on whether we view super-endomorphism valued differential forms as elements of the tensor product $\mathrm{End}(E) \otimes \Omega(M)$, or the tensor product $\Omega(M) \otimes \mathrm{End}(E)$, since this affects the sign in the definition of the product for tensored superalgebras, Eq. (2.28).

For elements of $\mathrm{End}(E) \otimes \Omega(M)$, we have the Ne'eman-Sternberg multiplication rule given in Refs. [120, 129, 171, 173] as:

$$\begin{bmatrix} A & C \\ D & B \end{bmatrix} \odot \begin{bmatrix} A' & C' \\ D' & B' \end{bmatrix} := \begin{bmatrix} A \wedge A' + (-1)^{|C|} C \wedge D' & C \wedge B' + (-1)^{|A|} A \wedge C' \\ D \wedge A' + (-1)^{|B|} B \wedge D' & B \wedge B' + (-1)^{|D|} D \wedge C' \end{bmatrix}, \tag{A.6}$$

where A, B, C, D, A', B', C', and D' are all matrices themselves whose elements are differential forms of a definite grading. For the elements of $\Omega(M) \otimes \mathrm{End}(E)$, we have

$$\begin{bmatrix} A & C \\ D & B \end{bmatrix} \odot \begin{bmatrix} A' & C' \\ D' & B' \end{bmatrix} := \begin{bmatrix} A \wedge A' + (-1)^{|D'|} C \wedge D' & A \wedge C' + (-1)^{|B'|} C \wedge B' \\ (-1)^{|A'|} D \wedge A' + B \wedge D' & (-1)^{|C'|} D \wedge C' + B \wedge B' \end{bmatrix}. \tag{A.7}$$

These relations are simple consequences of Eq. (2.28). First, rewrite each matrix in tensor product form, schematically, as

$$\begin{aligned} &\begin{bmatrix} A & C \\ D & B \end{bmatrix} \\ &\quad = \; A \otimes \begin{bmatrix} 1 & 0 \\ 0 & 0 \end{bmatrix} + B \otimes \begin{bmatrix} 0 & 0 \\ 0 & 1 \end{bmatrix} + C \otimes \begin{bmatrix} 0 & 1 \\ 0 & 0 \end{bmatrix} + D \otimes \begin{bmatrix} 0 & 0 \\ 1 & 0 \end{bmatrix}, \\ &\begin{bmatrix} A' & C' \\ D' & B' \end{bmatrix} \\ &\quad = \; A' \otimes \begin{bmatrix} 1 & 0 \\ 0 & 0 \end{bmatrix} + B' \otimes \begin{bmatrix} 0 & 0 \\ 0 & 1 \end{bmatrix} + C' \otimes \begin{bmatrix} 0 & 1 \\ 0 & 0 \end{bmatrix} + D' \otimes \begin{bmatrix} 0 & 0 \\ 1 & 0 \end{bmatrix}. \end{aligned} \tag{A.8}$$

Note that we are using tensor products in $\Omega(M) \otimes \mathrm{End}(E)$ with the differential form on the left and the supermatrix on the right. Then, we multiply the tensor products together, term by term. For instance,

$$\begin{aligned}
&\left(A \otimes \begin{bmatrix} 1 & 0 \\ 0 & 0 \end{bmatrix}\right) \odot \left(A' \otimes \begin{bmatrix} 1 & 0 \\ 0 & 0 \end{bmatrix}\right) \\
&= (-1)^{0 \times |A'|} (A \wedge A') \otimes \left(\begin{bmatrix} 1 & 0 \\ 0 & 0 \end{bmatrix} \cdot \begin{bmatrix} 1 & 0 \\ 0 & 0 \end{bmatrix}\right) \\
&= (A \wedge A') \otimes \begin{bmatrix} 1 & 0 \\ 0 & 0 \end{bmatrix} \\
&= \begin{bmatrix} A \wedge A' & 0 \\ 0 & 0 \end{bmatrix}, \qquad \text{(A.9)}
\end{aligned}$$

and

$$\begin{aligned}
&\left(C \otimes \begin{bmatrix} 0 & 1 \\ 0 & 0 \end{bmatrix}\right) \odot \left(D' \otimes \begin{bmatrix} 0 & 0 \\ 1 & 0 \end{bmatrix}\right) \\
&= (-1)^{1 \times |D'|} (C \wedge D') \otimes \left(\begin{bmatrix} 0 & 1 \\ 0 & 0 \end{bmatrix} \cdot \begin{bmatrix} 0 & 0 \\ 1 & 0 \end{bmatrix}\right) \\
&= (-1)^{|D'|} (C \wedge D') \otimes \begin{bmatrix} 1 & 0 \\ 0 & 0 \end{bmatrix} \\
&= \begin{bmatrix} (-1)^{|D'|} C \wedge D' & 0 \\ 0 & 0 \end{bmatrix}. \qquad \text{(A.10)}
\end{aligned}$$

Summing, we obtain the 1-1 element of Eq. (A.7). All other elements can be derived in a similar fashion.

Appendix B

Formula for LRSM RGE running

B.1 Useful Identities for Higgs Bidoublets

To compare Eq. (2.9) of Ref. [207] and Eq. (A2) of Ref. [208], we need the following identities:

$$\begin{aligned}
\mathrm{Tr}\Big[\big(\Phi^\dagger\Phi\big)^2\Big] &= \Big(\mathrm{Tr}\Big[\Phi^\dagger\Phi\Big]\Big)^2 - \frac{1}{2}\mathrm{Tr}\Big[\Phi^\dagger\widetilde{\Phi}\Big]\mathrm{Tr}\Big[\widetilde{\Phi}^\dagger\Phi\Big]\,, \\
\frac{1}{2}\Big(\mathrm{Tr}\Big[\Phi^\dagger\widetilde{\Phi}\Big] + \mathrm{Tr}\Big[\widetilde{\Phi}^\dagger\Phi\Big]\Big)^2 &= \frac{1}{2}\left\{\Big(\mathrm{Tr}\Big[\Phi^\dagger\widetilde{\Phi}\Big]\Big)^2 + \Big(\mathrm{Tr}\Big[\widetilde{\Phi}^\dagger\Phi\Big]\Big)^2\right\} + \mathrm{Tr}\Big[\Phi^\dagger\widetilde{\Phi}\Big]\mathrm{Tr}\Big[\widetilde{\Phi}^\dagger\Phi\Big]\,, \\
\frac{1}{2}\Big(\mathrm{Tr}\Big[\Phi^\dagger\widetilde{\Phi}\Big] - \mathrm{Tr}\Big[\widetilde{\Phi}^\dagger\Phi\Big]\Big)^2 &= \frac{1}{2}\left\{\Big(\mathrm{Tr}\Big[\Phi^\dagger\widetilde{\Phi}\Big]\Big)^2 + \Big(\mathrm{Tr}\Big[\widetilde{\Phi}^\dagger\Phi\Big]\Big)^2\right\} - \mathrm{Tr}\Big[\Phi^\dagger\widetilde{\Phi}\Big]\mathrm{Tr}\Big[\widetilde{\Phi}^\dagger\Phi\Big]\,, \\
\mathrm{Tr}\Big[\Phi^\dagger\Phi\widetilde{\Phi}^\dagger\widetilde{\Phi}\Big] &= \frac{1}{2}\,\mathrm{Tr}\Big[\Phi^\dagger\widetilde{\Phi}\Big]\mathrm{Tr}\Big[\widetilde{\Phi}^\dagger\Phi\Big]\,, \\
\mathrm{Tr}\Big[\Phi^\dagger\widetilde{\Phi}\Phi^\dagger\widetilde{\Phi}\Big] + \mathrm{Tr}\Big[\widetilde{\Phi}^\dagger\Phi\widetilde{\Phi}^\dagger\Phi\Big] &= \frac{1}{2}\left\{\Big(\mathrm{Tr}\Big[\Phi^\dagger\widetilde{\Phi}\Big]\Big)^2 + \Big(\mathrm{Tr}\Big[\widetilde{\Phi}^\dagger\Phi\Big]\Big)^2\right\}\,, \\
\mathrm{Tr}\Big[\big(\Delta_L^\dagger\Delta_L\big)^2\Big] &= \Big(\mathrm{Tr}\Big[\Delta_L^\dagger\Delta_L\Big]\Big)^2 - \frac{1}{2}\,\mathrm{Tr}\Big[\Delta_L\Delta_L\Big]\mathrm{Tr}\Big[\Delta_L^\dagger\Delta_L^\dagger\Big]\,, \\
\mathrm{Tr}\Big[\widetilde{\Phi}\widetilde{\Phi}^\dagger\Delta_L\Delta_L^\dagger\Big] &= \mathrm{Tr}\Big[\Phi^\dagger\Phi\Big]\mathrm{Tr}\Big[\Delta_L^\dagger\Delta_L\Big] - \mathrm{Tr}\Big[\Phi^\dagger\Phi\Delta_L^\dagger\Delta_L\Big]\,, \\
\mathrm{Tr}\Big[\widetilde{\Phi}^\dagger\widetilde{\Phi}\Delta_R\Delta_R^\dagger\Big] &= \mathrm{Tr}\Big[\Phi\Phi^\dagger\Big]\mathrm{Tr}\Big[\Delta_R^\dagger\Delta_R\Big] - \mathrm{Tr}\Big[\Phi\Phi^\dagger\Delta_R^\dagger\Delta_R\Big]\,. \qquad \text{(B.1)}
\end{aligned}$$

B.2 Derivation of Relations Between Symmetry Breaking Scales

$$\frac{1}{g_1^2(M_Z)} = \frac{1}{g_1^2(M_R)} + \frac{a_1^{\mathrm{I}}}{8\pi^2}\ln\frac{M_R}{M_Z}$$

$$
\begin{aligned}
&= \frac{1}{g_R^2(M_R)} + \frac{1}{g_{BL}^2(M_R)} + \frac{a_1^{\rm I}}{8\pi^2}\ln\frac{M_R}{M_Z} \\
&= \frac{1}{g_R^2(M_C)} + \frac{1}{g_{BL}^2(M_C)} + \frac{(a_R+a_{BL})^{\rm II}}{8\pi^2}\ln\frac{M_C}{M_R} + \frac{a_1^{\rm I}}{8\pi^2}\ln\frac{M_R}{M_Z} \\
&= \frac{1}{g_R^2(M_C)} + \frac{2}{3}\frac{1}{g_4^2(M_C)} + \frac{(a_R+a_{BL})^{\rm II}}{8\pi^2}\ln\frac{M_C}{M_R} + \frac{a_1^{\rm I}}{8\pi^2}\ln\frac{M_R}{M_Z} \\
&= \frac{1}{g_R^2(M_D)} + \frac{2}{3}\frac{1}{g_4^2(M_D)} + \frac{1}{8\pi^2}\left(a_R+\frac{2}{3}a_4\right)^{\rm III}\ln\frac{M_D}{M_C} \\
&\quad + \frac{(a_R+a_{BL})^{\rm II}}{8\pi^2}\ln\frac{M_C}{M_R} + \frac{a_1^{\rm I}}{8\pi^2}\ln\frac{M_R}{M_Z} \\
&= \frac{1}{g_R^2(M_U)} + \frac{2}{3}\frac{1}{g_4^2(M_U)} + \frac{1}{8\pi^2}\left(a_R+\frac{2}{3}a_4\right)^{\rm IV}\ln\frac{M_U}{M_D} \\
&\quad + \frac{1}{8\pi^2}\left(a_R+\frac{2}{3}a_4\right)^{\rm III}\ln\frac{M_D}{M_C} + \frac{(a_R+a_{BL})^{\rm II}}{8\pi^2}\ln\frac{M_C}{M_R} + \frac{a_1^{\rm I}}{8\pi^2}\ln\frac{M_R}{M_Z}\,, \\
\frac{1}{g_2^2(M_Z)} &= \frac{1}{g_2^2(M_R)} + \frac{a_2^{\rm I}}{8\pi^2}\ln\frac{M_R}{M_Z} \\
&= \frac{1}{g_L^2(M_R)} + \frac{a_2^{\rm I}}{8\pi^2}\ln\frac{M_R}{M_Z} \\
&= \frac{1}{g_L^2(M_C)} + \frac{a_L^{\rm II}}{8\pi^2}\ln\frac{M_C}{M_R} + \frac{a_2^{\rm I}}{8\pi^2}\ln\frac{M_R}{M_Z} \\
&= \frac{1}{g_L^2(M_D)} + \frac{a_L^{\rm III}}{8\pi^2}\ln\frac{M_D}{M_C} + \frac{a_L^{\rm II}}{8\pi^2}\ln\frac{M_C}{M_R} + \frac{a_2^{\rm I}}{8\pi^2}\ln\frac{M_R}{M_Z} \\
&= \frac{1}{g_L^2(M_U)} + \frac{a_L^{\rm IV}}{8\pi^2}\ln\frac{M_U}{M_D} + \frac{a_L^{\rm III}}{8\pi^2}\ln\frac{M_D}{M_C} + \frac{a_L^{\rm II}}{8\pi^2}\ln\frac{M_C}{M_R} + \frac{a_2^{\rm I}}{8\pi^2}\ln\frac{M_R}{M_Z}\,, \\
\frac{1}{e^2(M_Z)} &= \frac{1}{g_2^2(M_Z)} + \frac{1}{g_1^2(M_Z)} \\
&= \frac{1}{g_2^2(M_R)} + \frac{1}{g_1^2(M_R)} + \frac{1}{8\pi^2}(a_1+a_2)^{\rm I}\ln\frac{M_R}{M_Z} \\
&= \frac{1}{g_L^2(M_R)} + \frac{1}{g_R^2(M_R)} + \frac{1}{g_{BL}^2(M_R)} + \frac{1}{8\pi^2}(a_1+a_2)^{\rm I}\ln\frac{M_R}{M_Z} \\
&= \frac{1}{g_L^2(M_C)} + \frac{1}{g_R^2(M_C)} + \frac{1}{g_{BL}^2(M_C)} + \frac{1}{8\pi^2}(a_L+a_R+a_{BL})^{\rm II}\ln\frac{M_C}{M_R} \\
&\quad + \frac{1}{8\pi^2}(a_1+a_2)^{\rm I}\ln\frac{M_R}{M_Z} \\
&= \frac{1}{g_L^2(M_C)} + \frac{1}{g_R^2(M_C)} + \frac{2}{3}\frac{1}{g_4^2(M_C)} \\
&\quad + \frac{1}{8\pi^2}(a_L+a_R+a_{BL})^{\rm II}\ln\frac{M_C}{M_R} + \frac{1}{8\pi^2}(a_1+a_2)^{\rm I}\ln\frac{M_R}{M_Z} \\
&= \frac{1}{g_L^2(M_D)} + \frac{1}{g_R^2(M_D)} + \frac{2}{3}\frac{1}{g_4^2(M_D)} + \frac{1}{8\pi^2}\left(a_L+a_R+\frac{2}{3}a_4\right)^{\rm III}\ln\frac{M_D}{M_C}
\end{aligned}
$$

$$
\begin{aligned}
& + \frac{1}{8\pi^2}\left(a_L + a_R + a_{BL}\right)^{\rm II} \ln\frac{M_C}{M_R} + \frac{1}{8\pi^2}\left(a_1 + a_2\right)^{\rm I} \ln\frac{M_R}{M_Z} \\
= \;& \frac{1}{g_L^2(M_U)} + \frac{1}{g_R^2(M_U)} + \frac{2}{3}\frac{1}{g_4^2(M_U)} \\
& + \frac{1}{8\pi^2}\left(a_L + a_R + \frac{2}{3}\,a_4\right)^{\rm IV} \ln\frac{M_U}{M_D} + \frac{1}{8\pi^2}\left(a_L + a_R + \frac{2}{3}\,a_4\right)^{\rm III} \ln\frac{M_D}{M_C} \\
& + \frac{1}{8\pi^2}\left(a_L + a_R + a_{BL}\right)^{\rm II} \ln\frac{M_C}{M_R} + \frac{1}{8\pi^2}\left(a_1 + a_2\right)^{\rm I} \ln\frac{M_R}{M_Z}\,, \\
\frac{1}{g_3^2(M_Z)} = \;& \frac{1}{g_3^2(M_R)} + \frac{a_3^{\rm I}}{8\pi^2}\ln\frac{M_R}{M_Z} \\
= \;& \frac{1}{g_3^2(M_C)} + \frac{a_3^{\rm II}}{8\pi^2}\ln\frac{M_R}{M_Z} + \frac{a_3^{\rm I}}{8\pi^2}\ln\frac{M_R}{M_Z} \\
= \;& \frac{1}{g_4^2(M_C)} + \frac{a_3^{\rm II}}{8\pi^2}\ln\frac{M_C}{M_R} + \frac{a_3^{\rm I}}{8\pi^2}\ln\frac{M_R}{M_Z} \\
= \;& \frac{1}{g_4^2(M_D)} + \frac{a_4^{\rm III}}{8\pi^2}\ln\frac{M_D}{M_C} + \frac{a_3^{\rm II}}{8\pi^2}\ln\frac{M_C}{M_R} + \frac{a_3^{\rm I}}{8\pi^2}\ln\frac{M_R}{M_Z} \\
= \;& \frac{1}{g_4^2(M_U)} + \frac{a_4^{\rm IV}}{8\pi^2}\ln\frac{M_U}{M_D} + \frac{a_4^{\rm III}}{8\pi^2}\ln\frac{M_D}{M_C} + \frac{a_3^{\rm II}}{8\pi^2}\ln\frac{M_C}{M_R} + \frac{a_3^{\rm I}}{8\pi^2}\ln\frac{M_R}{M_Z}\,, \\
\frac{1}{g_R^2(M_R)} = \;& \frac{1}{g_R^2(M_C)} + \frac{a_R^{\rm II}}{8\pi^2}\ln\frac{M_C}{M_R} \\
= \;& \frac{1}{g_R^2(M_D)} + \frac{a_R^{\rm III}}{8\pi^2}\ln\frac{M_D}{M_C} + \frac{a_R^{\rm II}}{8\pi^2}\ln\frac{M_C}{M_R} \\
= \;& \frac{1}{g_R^2(M_U)} + \frac{a_R^{\rm IV}}{8\pi^2}\ln\frac{M_U}{M_D} + \frac{a_R^{\rm III}}{8\pi^2}\ln\frac{M_D}{M_C} + \frac{a_R^{\rm II}}{8\pi^2}\ln\frac{M_C}{M_R}\,. \qquad \text{(B.2)}
\end{aligned}
$$

If we impose the condition

$$
g_L(M_U) \;=\; g_R(M_U) \;=\; g_4(M_U) \;\equiv\; g_U\,, \qquad \text{(B.3)}
$$

then it is straightforward to show that

$$
\begin{aligned}
& 2\pi\left[\frac{3 - 8\sin^2\theta_W(M_Z)}{\alpha(M_Z)}\right] \\
= \;& 8\pi^2\left[\frac{3}{e^2(M_Z)} - \frac{8}{g_2^2(M_Z)}\right] \\
= \;& \left[\left(-5a_L + 3a_R + 2a_4\right)^{\rm IV} \ln\frac{M_U}{M_D} + \left(-5a_L + 3a_R + 2a_4\right)^{\rm III} \ln\frac{M_D}{M_C}\right. \\
& \left. + \left(-5a_L + 3a_R + 3a_{BL}\right)^{\rm II} \ln\frac{M_C}{M_R} + \left(3a_1 - 5a_2\right)^{\rm I} \ln\frac{M_R}{M_Z}\right]\,, \\
& 2\pi\left[\frac{3}{\alpha(M_Z)} - \frac{8}{\alpha_s(M_Z)}\right] \\
= \;& 8\pi^2\left[\frac{3}{e^2(M_Z)} - \frac{8}{g_3^2(M_Z)}\right]
\end{aligned}
$$

$$
\begin{aligned}
&= \left[(3a_L + 3a_R - 6a_4)^{\rm IV} \ln\frac{M_U}{M_D} + (3a_L + 3a_R - 6a_4)^{\rm III} \ln\frac{M_D}{M_C} \right. \\
&\quad \left. + (3a_L + 3a_R + 3a_{BL} - 8a_3)^{\rm II} \ln\frac{M_C}{M_R} + (3a_1 + 3a_2 - 8a_3)^{\rm I} \ln\frac{M_R}{M_Z} \right] , \\
&2\pi \left[\frac{4\pi}{g_R^2(M_R)} - \frac{\sin^2\theta_W(M_Z)}{\alpha(M_Z)} \right] \\
&= 8\pi^2 \left[\frac{1}{g_R^2(M_R)} - \frac{1}{g_2^2(M_Z)} \right] \\
&= 8\pi^2 \left[\frac{1}{g_R^2(M_R)} - \frac{1}{g_L^2(M_R)} \right] + 8\pi^2 \left[\frac{1}{g_2^2(M_R)} - \frac{1}{g_2^2(M_Z)} \right] \\
&= \left[(a_R - a_L)^{\rm III} \ln\frac{M_D}{M_C} + (a_R - a_L)^{\rm II} \ln\frac{M_C}{M_R} - a_2^{\rm I} \ln\frac{M_R}{M_Z} \right] , \\
\frac{8\pi^2}{g_U^2} &= \frac{3}{8} \left[\frac{2\pi}{\alpha(M_Z)} - \left\{ \left(a_L + a_R + \frac{2}{3}\, a_4 \right)^{\rm IV} \ln\frac{M_U}{M_D} + \left(a_L + a_R + \frac{2}{3}\, a_4 \right)^{\rm III} \ln\frac{M_D}{M_C} \right. \right. \\
&\quad \left. \left. + (a_L + a_R + a_{BL})^{\rm II} \ln\frac{M_C}{M_R} + (a_1 + a_2)^{\rm I} \ln\frac{M_R}{M_Z} \right\} \right] \\
&= \frac{2\pi}{\alpha_s(M_Z)} - \left(a_4^{\rm IV}\ \ln\frac{M_U}{M_D} + a_4^{\rm III}\ \ln\frac{M_D}{M_C} + a_3^{\rm II}\ \ln\frac{M_C}{M_R} + a_3^{\rm I}\ \ln\frac{M_R}{M_Z} \right) . \qquad \text{(B.4)}
\end{aligned}
$$

Note that $a_L^{\rm IV} = a_R^{\rm IV}$ since parity is not broken in energy interval IV.

If instead, we impose the conditions

$$
g_L(M_D) \;=\; g_R(M_D) \;\equiv\; g_{LR} \,, \qquad g_4(M_D) \;\equiv\; g_{4D} \,, \qquad \text{(B.5)}
$$

where g_{LR} and g_{4D} are not necessarily equal, then the relations will be

$$
\begin{aligned}
&2\pi \left[\frac{3 - 6\sin^2\theta_W(M_Z)}{\alpha(M_Z)} - \frac{2}{\alpha_s(M_Z)} \right] \\
&= 8\pi^2 \left[\frac{3}{e^2(M_Z)} - \frac{6}{g_2^2(M_Z)} - \frac{2}{g_3^2(M_Z)} \right] \\
&= \left[(-3a_L + 3a_R)^{\rm III} \ln\frac{M_D}{M_C} + (-3a_L + 3a_R + 3a_{BL} - 2a_3)^{\rm II} \ln\frac{M_C}{M_R} \right. \\
&\quad \left. + (3a_1 - 3a_2 - 2a_3)^{\rm I} \ln\frac{M_R}{M_Z} \right] , \\
&2\pi \left[\frac{4\pi}{g_R^2(M_R)} - \frac{\sin^2\theta_W(M_Z)}{\alpha(M_Z)} \right] \\
&= 8\pi^2 \left[\frac{1}{g_R^2(M_R)} - \frac{1}{g_2^2(M_Z)} \right] \\
&= \left[\frac{1}{g_R^2(M_R)} - \frac{1}{g_L^2(M_R)} \right] + \left[\frac{1}{g_2^2(M_R)} - \frac{1}{g_2^2(M_Z)} \right]
\end{aligned}
$$

$$
\begin{aligned}
&= \frac{1}{8\pi^2}\left[(a_R-a_L)^{\rm III}\ln\frac{M_D}{M_C}+(a_R-a_L)^{\rm II}\ln\frac{M_C}{M_R}-a_2^{\rm I}\ln\frac{M_R}{M_Z}\right]\ ,\\
\frac{8\pi^2}{g_{LR}^2} &= \frac{\pi}{\alpha(M_Z)}-\frac{1}{3}\frac{2\pi}{\alpha_s(M_Z)}-\frac{1}{6}\Bigg[\left\{3\left(a_L+a_R\right)\right\}^{\rm III}\ \ln\frac{M_D}{M_C}\\
&\quad +\left\{3\left(a_L+a_R+a_{BL}\right)-2a_3\right\}^{\rm II}\ \ln\frac{M_C}{M_R}+\left\{3\left(a_1+a_2\right)-2a_3\right\}^{\rm I}\ \ln\frac{M_R}{M_Z}\Bigg]\ ,\\
\frac{8\pi^2}{g_{4D}^2} &= \frac{2\pi}{\alpha_s(M_Z)}-\left(a_4^{\rm III}\ \ln\frac{M_D}{M_C}+a_3^{\rm II}\ \ln\frac{M_C}{M_R}+a_3^{\rm I}\ \ln\frac{M_R}{M_Z}\right)\ . \qquad \text{(B.6)}
\end{aligned}
$$

Appendix C

Formula for OscSNS Phenomenology

C.1 Pion and Muon Decay Energy Spectra

At the SNS at the Oak Ridge National Laboratory, a proton beam is shot into a liquid mercury target creating both positively and negatively charged pions. The negatively charged pions are attracted to nuclei and quickly absorbed, while the positively charged pions come to rest in the target and decay:

$$\pi^+ \;\rightarrow\; \mu^+ + \nu_\mu \;. \tag{C.1}$$

The mean lifetime of the charged pions is $\tau_\pi = (2.6033 \pm 0.0005) \times 10^{-8}$ sec ≈ 26 ns. The μ^+ and ν_μ from this decay are mono-energetic and have the energies

$$\begin{aligned} E_\mu &= \frac{m_\pi^2 + m_\mu^2}{2m_\pi} = 109.778 \text{ MeV} \;, \\ E_{\nu_\mu} &= \frac{m_\pi^2 - m_\mu^2}{2m_\pi} = 29.792 \text{ MeV} \;. \end{aligned} \tag{C.2}$$

The momentum of the positive muon is

$$p_\mu = \frac{E_{\nu_\mu}}{c} = 29.792 \text{ MeV/c} \;, \tag{C.3}$$

and its velocity is

$$\beta_\mu = \frac{v_\mu}{c} = \frac{p_\mu c}{E_\mu} = 0.2714 \;. \tag{C.4}$$

These positive muons also come to rest inside the Hg target and decay via

$$\mu^+ \;\rightarrow\; e^+ + \overline{\nu}_e + \nu_\mu \;. \tag{C.5}$$

The mean lifetime of the muon is $\tau_\mu = (2.1969811 \pm 0.0000022) \times 10^{-6}$ sec ≈ 2200 ns. Thus, it lives two orders of magnitude longer than the charged pion. The differential decay widths

are

$$\begin{aligned}\frac{d\Gamma}{dx} &= \frac{G_F^2 m_\mu^5}{\pi^3}\,\frac{x^2(x_{\max}-x)^2}{\left(\frac{1}{2}-x\right)}\,\theta(x_{\max}-x)\;,\\ \frac{d\Gamma}{dy} &= \frac{G_F^2 m_\mu^5}{\pi^3}\,\frac{y^2(y_{\max}-y)^2\left(y^2-\frac{5+\eta}{4}y+\frac{3(1+\eta)}{8}\right)}{3\left(\frac{1}{2}-y\right)^3}\,\theta(y_{\max}-y)\;.\end{aligned} \tag{C.6}$$

where $x = E_{\nu_e}/m_\mu$, $y = E_{\overline{\nu}_\mu}/m_\mu$, $\eta = m_e^2/m_\mu^2 = 2.339\times10^{-5}$, and

$$x_{\max} \;=\; y_{\max} \;=\; \frac{1-\eta}{2} \;\approx\; 0.5\;. \tag{C.7}$$

The total width is

$$\Gamma \;=\; \int_0^{x_{\max}} \frac{d\Gamma}{dx}\,dx \;=\; \int_0^{y_{\max}} \frac{d\Gamma}{dy}\,dy \;=\; \frac{G_F^2 m_\mu^5}{192\pi^3}\,f(\eta)\;, \tag{C.8}$$

where

$$f(\eta) \;=\; \left(1-8\eta+8\eta^3-\eta^4-12\eta^2\ln\eta\right)\approx 1\;. \tag{C.9}$$

Thus, the energy spectra of the ν_e and $\overline{\nu}_\mu$ in μ^+ decay are given by

$$\lambda_{\nu_e}(E_{\nu_e}) \;=\; \frac{1}{m_\mu\Gamma}\,\frac{d\Gamma}{dx}\;,\qquad \lambda_{\overline{\nu}_\mu}(E_{\overline{\nu}_\mu}) \;=\; \frac{1}{m_\mu\Gamma}\,\frac{d\Gamma}{dy}\;. \tag{C.10}$$

These functions are shown in Fig. 6.1.

C.2 SNS Source Timing

The proton beam at the SNS is provided at a pulse length of $T_p = 695\,\text{ns}$ and a repetition rate of 60 Hz (Ref. [401]: Page 11 and Table 3.1 on page 13). According to page 10 of Ref. [401], there is a yield of 0.12 neutrinos per proton on target (POT). However, according to page 23 of Ref. [401], the number of π^+'s created per POT is $0.116 \approx 0.12$, but the resulting yields of ν_e, ν_μ, and $\overline{\nu}_\mu$ are quoted as 0.09. The reason that the pion and neutrino yields on page 23 do not agree remains unclear. As we discussed with Dr. Pilar Coloma in several email exchanges that were shared with the proponents, it was conjectured that 0.09 was the number they used.

On page 37, the proton beam intensity at the SNS with 1.4 MW of power is quoted as 8.7×10^{15} POT/second or 2.74×10^{23} POT/year. Page 10 mentions a planned upgrade to 3 MW, which means that this intensity can be more than doubled in the near future. We will use the value of 1.4 MW in the following.

From the above numbers, we can see that "1 year" for the SNS is defined as

$$\frac{2.74 \times 10^{23}\,\mathrm{POT/year}}{8.7 \times 10^{15}\,\mathrm{POT/second}} \;=\; \frac{3.1 \times 10^{7}\,\mathrm{seconds}}{\mathrm{year}}\;, \tag{C.11}$$

which is basically one full Julian year:

$$\frac{365.25\,\mathrm{days}}{\mathrm{year}} \times \frac{24\,\mathrm{hours}}{\mathrm{day}} \times \frac{60\,\mathrm{minutes}}{\mathrm{hour}} \times \frac{60\,\mathrm{seconds}}{\mathrm{minute}} \;=\; \frac{3.15576 \times 10^{7}\,\mathrm{seconds}}{\mathrm{year}}\;. \tag{C.12}$$

We need to keep this in mind since in many accelerator based experiments "1 year" is defined as 1×10^7 seconds (Europe) or 2×10^7 seconds (USA), not 3×10^7 seconds. The POT per 10^7 seconds (1 European year) is:

$$(8.7 \times 10^{15}\,\mathrm{POT/second}) \times (10^{7}\,\mathrm{seconds}/10^{7}\,\mathrm{seconds}) \;=\; 8.7 \times 10^{22}\,\mathrm{POT}/10^{7}\,\mathrm{seconds}\;. \tag{C.13}$$

Since the pulse rate is 60 Hz, the number of POT per pulse is

$$\frac{8.7 \times 10^{15}\,\mathrm{POT/second}}{60\,\mathrm{pulses/second}} \;=\; 1.5 \times 10^{14}\,\mathrm{POT/pulse}\;, \tag{C.14}$$

which agrees with the number of protons per pulse (ppp) listed in Table 3.1 on page 13. Using a π^+ production rate of 0.12/POT, this leads to the production of $(1.5 \times 10^{14}\,\mathrm{ppp}) \times (0.12/\mathrm{POT}) = (1.8 \times 10^{13}\,\pi\mathrm{pp})$. But since we are only interested in the decays of these pions that lead to neutrinos detected at the detector, we should be using the production rate of 0.09/POT which would give us $(8.7 \times 10^{15}\,\mathrm{POT/second})/(60\,\mathrm{pulse/second}) \times (0.09/\mathrm{POT}) = (1.3 \times 10^{13}\,\pi\mathrm{pp})$. Assuming that the production of π^+ is uniform during the proton pulse duration, the production rate is

$$A_\pi \;=\; \frac{1.3 \times 10^{13}}{695\,\mathrm{ns}} \;=\; 1.9 \times 10^{10}\,/\mathrm{ns}\;. \tag{C.15}$$

If we write the numbers of π^+ and μ^+ in the Hg target at time t as $N_\pi(t)$ and $N_\mu(t)$, their time derivatives are given by

$$\begin{aligned}
\frac{N_\pi(t)}{dt} &= \begin{cases} A_\pi - \dfrac{N_\pi(t)}{\tau_\pi} & \text{if } 0 < t < T_p\;, \\ -\dfrac{N_\pi(t)}{\tau_\pi} & \text{if } T_p < t\;, \end{cases} \\
\frac{N_\mu(t)}{dt} &= \frac{N_\pi(t)}{\tau_\pi} - \frac{N_\mu(t)}{\tau_\mu}\;,
\end{aligned} \tag{C.16}$$

where $\tau_\pi = 26\,\mathrm{ns}$ and $\tau_\mu = 2200\,\mathrm{ns}$. Imposing the initial condition $N_\pi(0) = N_\mu(0) = 0$, the solution to the above pair of differential equations is

$$\frac{N_\pi(t)}{\tau_\pi} \;=\; A_\pi\big(1 - e^{-t/\tau_\pi}\big)\;,$$

$$\frac{N_\mu(t)}{\tau_\mu} \;=\; A_\pi \left[1 - \left(\frac{\tau_\mu}{\tau_\mu - \tau_\pi} \right) e^{-t/\tau_\mu} + \left(\frac{\tau_\pi}{\tau_\mu - \tau_\pi} \right) e^{-t/\tau_\pi} \right] \,, \tag{C.17}$$

in the range $0 < t < T_p$, and

$$\begin{aligned}
\frac{N_\pi(t)}{\tau_\pi} &= \frac{N_\pi(T_p)}{\tau_\pi}\, e^{-(t-T_p)/\tau_\pi} \\
&= A_\pi \big(1 - e^{-T_p/\tau_\pi} \big)\, e^{-(t-T_p)/\tau_\pi} \;=\; A_\pi \big(e^{T_p/\tau_\pi} - 1 \big)\, e^{-t/\tau_\pi} \,, \\
\frac{N_\mu(t)}{\tau_\mu} &= \left[\frac{N_\pi(T_p)}{\tau_\mu - \tau_\pi} + \frac{N_\mu(T_p)}{\tau_\mu} \right] e^{-(t-T_p)/\tau_\mu} - \frac{N_\pi(T_p)}{\tau_\mu - \tau_\pi}\, e^{-(t-T_p)/\tau_\pi} \\
&= A_\pi \left[\left(\frac{\tau_\mu}{\tau_\mu - \tau_\pi} \right) \big(1 - e^{-T_p/\tau_\mu} \big)\, e^{-(t-T_p)/\tau_\mu} + \left(\frac{\tau_\pi}{\tau_\mu - \tau_\pi} \right) \big(1 - e^{-T_p/\tau_\pi} \big)\, e^{-(t-T_p)/\tau_\pi} \right] \\
&= A_\pi \left[\left(\frac{\tau_\mu}{\tau_\mu - \tau_\pi} \right) \big(e^{T_p/\tau_\mu} - 1 \big)\, e^{-t/\tau_\mu} - \left(\frac{\tau_\pi}{\tau_\mu - \tau_\pi} \right) \big(e^{T_p/\tau_\pi} - 1 \big)\, e^{-t/\tau_\pi} \right] \,,
\end{aligned} \tag{C.18}$$

in the range $T_p < t$. The total flux of ν_μ, ν_e, and $\overline{\nu}_\mu$ can be obtained from

$$\phi_{\nu_\mu}(t) \;=\; \frac{N_\pi(t)}{\tau_\pi} \,, \qquad \phi_{\nu_e}(t) \;=\; \phi_{\overline{\nu}_\mu}(t) \;=\; \frac{N_\mu(t)}{\tau_\mu} \,. \tag{C.19}$$

The time-dependence of these fluxes are shown in Fig. 6.2 (*cf.* Figure 3.1 on page 11 of Ref. [401]). As can be seen, there is a clear temporal separation of ν_μ's from π^+ decay, and ν_e and $\overline{\nu}_\mu$'s from μ^+ decay.

The total numbers of neutrinos of each flavor from $t = 0$ to $t = T_p$ are

$$\begin{aligned}
\int_0^{T_p} dt\; \phi_{\nu_\mu}(t) &= A_\pi \left[T_p + \big(e^{-T_p/\tau_\pi} - 1 \big)\, \tau_\pi \right] \,, \\
&= A_\pi \times (669\,\mathrm{ns}) \;=\; 1.3 \times 10^{13} \,, \\
\int_0^{T_p} dt\; \phi_{\nu_e}(t) &= \int_0^{T_p} dt\; \phi_{\overline{\nu}_\mu}(t) \\
&= A_\pi \left[T_p + \big(e^{-T_p/\tau_\mu} - 1 \big)\, \frac{\tau_\mu^2}{\tau_\mu - \tau_e} + \big(1 - e^{-T_p/\tau_\pi} \big)\, \frac{\tau_\pi^2}{\tau_\mu - \tau_e} \right] \\
&= A_\pi \times (92.3\,\mathrm{ns}) \;=\; 1.8 \times 10^{12} \,.
\end{aligned} \tag{C.20}$$

So the ratio of the numbers of ν_e or $\overline{\nu}_\mu$ to ν_μ is

$$\frac{92.3}{669} \;=\; 0.138 \;=\; 14\% \,. \tag{C.21}$$

This is the number quoted on page 10, but we now understand that 14% is not the fraction of ν_e's and $\overline{\nu}_\mu$'s in the total flux but rather the ratio to the ν_μ count alone. The fraction of the total yield is

$$\frac{0.14}{1 + 0.14 + 0.14} \;=\; 0.11 \;=\; 11\% \,. \tag{C.22}$$

So during the time that the proton beam is on, ν_μ's make up 78% of the flux while ν_e's and $\overline{\nu}_\mu$'s make 11% each.

On the other hand, the total numbers of neutrinos of each flavor from $t = T_p$ to $t = \infty$ are

$$\begin{aligned}
\int_{T_p}^{\infty} dt\ \phi_{\nu_\mu}(t) &= A_\pi \left(1 - e^{-T_p/\tau_\pi}\right) \tau_\pi \ , \\
&= A_\pi \times (26.0\,\mathrm{ns}) \ = \ 4.9 \times 10^{11} \ , \\
\int_{T_p}^{\infty} dt\ \phi_{\nu_e}(t) &= \int_{T_p}^{\infty} dt\ \phi_{\overline{\nu}_\mu}(t) \\
&= A_\pi \left[\left(1 - e^{-T_p/\tau_\mu}\right) \frac{\tau_\mu^2}{\tau_\mu - \tau_e} + \left(e^{-T_p/\tau_\pi} - 1\right) \frac{\tau_\pi^2}{\tau_\mu - \tau_e} \right] \\
&= A_\pi \times (603\,\mathrm{ns}) \ = \ 1.1 \times 10^{13} \ .
\end{aligned} \tag{C.23}$$

Thus, the ratio of the numbers of ν_μ to ν_e or $\overline{\nu}_\mu$ during the interval from $t = T_p$ to $t = \infty$ is

$$\frac{26.0}{603} \ = \ 0.043 \ = \ 4\% \ , \tag{C.24}$$

and the fraction of ν_μ's in the total flux is

$$\frac{0.04}{1 + 1 + 0.04} \ = \ 0.02 \ = \ 2\% \ , \tag{C.25}$$

while ν_e and $\overline{\nu}_\mu$ contribute 49% each. The fraction of ν_μ's can be made negligibly small by moving the initial time of the interval away from T_p. For instance, the fraction can be reduced from 2% to 0.04% by moving the start of the interval to 800 ns.

The total number of neutrinos of each flavor from $t = 0$ to $t = \infty$ is, of course,

$$\int_0^{\infty} dt\ \phi_{\nu_\mu}(t) \ = \ \int_0^{\infty} dt\ \phi_{\nu_e}(t) \ = \ \int_0^{\infty} dt\ \phi_{\overline{\nu}_\mu}(t) \ = \ A_\pi T_p \ = \ A_\pi \times (695\,\mathrm{ns}) \ = \ 1.3 \times 10^{13} \ . \tag{C.26}$$

For ν_μ, 96.3% of the total flux is emitted during the duration of the proton pulse, while 3.7% is emitted after the pulse is turned off:

$$\frac{669.0\,\mathrm{ns}}{695\,\mathrm{ns}} \ = \ 0.963 \ , \qquad \frac{26.0\,\mathrm{ns}}{695\,\mathrm{ns}} \ = \ 0.037 \ . \tag{C.27}$$

For ν_e and $\bar{\nu}_\mu$, the percentages are 13.3% and 86.7%:

$$\frac{92.3\,\mathrm{ns}}{695\,\mathrm{ns}} \ = \ 0.133 \ , \qquad \frac{602.7\,\mathrm{ns}}{695\,\mathrm{ns}} \ = \ 0.867 \ . \tag{C.28}$$

C.3 SNS Neutrino Fluxes

The total number of neutrinos of each flavor created per pulse is

$$1.3 \times 10^{13}/\text{pulse} \, . \tag{C.29}$$

With a pulse rate of 60 Hz, the number of neutrinos created per second would be

$$(1.3 \times 10^{13}/\text{pulse}) \times (60 \text{ pulses/second}) \; = \; 7.8 \times 10^{14}/\text{second} \, . \tag{C.30}$$

This is, of course, what one gets from $8.7 \times 10^{15}\,\text{POT/second}$ with a neutrino production rate of 0.09/POT. The number of neutrinos created per 10^7 seconds would be $7.8 \times 10^{21}/10^7\,\text{seconds}$. In one Julian year, the number will be

$$(7.8 \times 10^{14}/\text{second}) \times (3.16 \times 10^7\,\text{seconds/year}) \; = \; 2.5 \times 10^{22}/\text{year} \, . \tag{C.31}$$

These neutrinos are spread out over a sphere of radius 60 meters, so the flux at the detector will be

$$\Phi \; = \; \frac{(2.5 \times 10^{22}/\text{year})}{4\pi(6000\,\text{cm})^2} \; = \; 5.5 \times 10^{13}/\text{year/cm}^2 \, , \tag{C.32}$$

which agrees with the numbers cites on page 37 of Ref. [401]. For 10^7 seconds, the flux would be:

$$\Phi \; = \; \frac{(7.8 \times 10^{21}/10^7\,\text{seconds})}{4\pi(6000\,\text{cm})^2} \; = \; 1.7 \times 10^{13}/10^7\,\text{seconds/cm}^2 \, . \tag{C.33}$$

Appendix D

R Ratio, Self-Energy, Running of Coupling, and All That

In this section we summarize the relation between the R ratio, the self-energy $\Pi^{(h)}(q^2)$, the running of the coupling $\delta\alpha$. The picture can be described by the following relation:

$$\Delta\alpha(q^2) \xleftrightarrow[I]{\text{reparametrizing}} \Pi'(q^2) - \Pi'(0) \xleftrightarrow[II]{\text{dispersion relation}} \int (\text{Im}\Pi'(q^2) - \text{Im}\Pi'(0))$$
$$\xleftrightarrow[III]{\text{optical theorem}} \int \sigma^{(h)} \xleftrightarrow[IV]{\text{write out } \sigma^{\mu\mu}} \int R. \tag{D.1}$$

Next, we show each one of the double arrows.

D.1 $\Delta\alpha(q^2) \leftrightarrow \Pi'(q^2) - \Pi'(0)$

Just as in the usual one loop calculation, the QED coupling constant is shifted by vacuum polarization by

$$\hat{\alpha}(q^2) = \frac{e^2}{4\pi}\left[1 + \frac{\Pi_{\gamma\gamma}(q^2)}{q^2}\right], \tag{D.2}$$

where the blue part is dependent on the vacuum polarization and not necessarily calculable. To write it in the way it is usually formulated,

$$\begin{aligned}\hat{\alpha}(0) &= \frac{e^2}{4\pi}\left(1+\Pi'_{\gamma\gamma}(0)\right)\\ &= \frac{e^2}{4\pi}\left(1+\frac{\Pi_{\gamma\gamma}(q^2)}{q^2}+\underbrace{\Pi'_{\gamma\gamma}(0)-\frac{\Pi_{\gamma\gamma}(q^2)}{q^2}}_{-\Delta\alpha(q^2)}\right)\\ &= \frac{e^2}{4\pi}\left(1+\frac{\Pi_{\gamma\gamma}(q^2)}{q^2}\right)-\frac{e^2}{4\pi}\Delta\alpha(q^2)\\ &= \hat{\alpha}(q^2)(1-\Delta\alpha(q^2))+\mathcal{O}(\alpha^2),\end{aligned} \tag{D.3}$$

which gives us the familiar $\hat{\alpha}(q^2)=\dfrac{\hat{\alpha}(0)}{1-\Delta\alpha(q^2)}$, where $\Delta\alpha(q^2)=\Pi'_{\gamma\gamma}(q^2)-\Pi'_{\gamma\gamma}(0)$.

D.2 $\Pi'(q^2)-\Pi'(0) \leftrightarrow \int(\mathrm{Im}\Pi'(q^2)-\mathrm{Im}\Pi'(0))$

Essentially, this is just a Cauchy integral. It is also referred to as dispersion relation for some reason. The Cauchy integral is the following contour integral:

$$f(a)=\frac{1}{2\pi i}\oint\frac{f(z)}{z-a}\mathrm{d}z. \tag{D.4}$$

Replacing $f(a)$ with $\Pi(x)$, we have

$$\Pi^{(h)}_{\gamma\gamma}(q^2)=\frac{1}{2\pi i}\oint\frac{\Pi^{(h)}(x)}{x-q^2}\mathrm{d}x. \tag{D.5}$$

Due to the cut structure of $\Pi(q^2)$, the contour cannot be closed for the whole q^2 complex plane. The cut on the real axis starting at $4m_\pi^2$ has to be excluded. Due to Jordan's lemma, the contour around infinity vanishes. Therefore, the right side of the above equation becomes a 'C' shaped integral along the ray $[4m_\pi^2,+\infty)$. The nature of the branch cut dictates the discontinuity of Π to be twice the imaginary part of Π, *i.e.*

$$Disc.\ \Pi(q^2)=\Pi(q^2+i\epsilon)-\Pi(q^2-i\epsilon)=2i\mathrm{Im}\Pi(q^2+i\epsilon), \tag{D.6}$$

when $\mathrm{Im}(q^2)\geq 4m_\pi^2$ and $\epsilon\to 0$. Therefore, we have the following expression for $\Pi^{(h)}_{\gamma\gamma}(q^2)$.

$$\begin{aligned}\Pi^{(h)}_{\gamma\gamma}(q^2) &= -\frac{1}{2\pi i}\int_{4m_\pi^2}^{\infty}\frac{1}{q^2-x}(2i)\mathrm{Im}\Pi^{(h)}_{\gamma\gamma}(x+i\epsilon)\mathrm{d}x\\ &= -\frac{1}{\pi}\int_{4m_\pi^2}^{\infty}\frac{1}{q^2-x}\mathrm{Im}\Pi^{(h)}_{\gamma\gamma}(x+i\epsilon)\mathrm{d}x.\end{aligned} \tag{D.7}$$

D.3 $\int(\mathrm{Im}\,\Pi'(q^2)-\mathrm{Im}\,\Pi'(0))\leftrightarrow\int\sigma^{(h)}$

The optical theorem is just unitarity rephrased in field theory language. With the definition of the T matrix, $S=1+iT$, the following statements are equivalent:

$$\begin{aligned} S^\dagger S&=1,\\ (1-iT^\dagger)(1+iT)&=1+i(T-T^\dagger)+T^\dagger T=1,\\ T^\dagger T&=-i(T-T^\dagger). \end{aligned} \tag{D.8}$$

The last equation corresponds to two types of processes. As in Ref. [524], the matrix element corresponding to $T^\dagger T$ can be decomposed by summing over intermediate states,

$$\left\langle \mathbf{p}_1\mathbf{p}_2|T^\dagger T|\mathbf{k}_1\mathbf{k}_2\right\rangle=\sum_n\left(\prod_{i=1}^n\int\frac{\mathrm{d}^3q_i}{(2\pi)^3}\frac{1}{2E_i}\right)\underbrace{\left\langle \mathbf{p}_1\mathbf{p}_2|T^\dagger|\{\mathbf{q}_i\}\right\rangle}_{\mathcal{M}^*(\mathbf{p}_1\mathbf{p}_2\to\{\mathbf{q}_i\})}\underbrace{\left\langle\{\mathbf{q}_i\}|T|\mathbf{k}_1\mathbf{k}_2\right\rangle}_{\mathcal{M}(\mathbf{k}_1\mathbf{k}_2\to\{\mathbf{q}_i\})}, \tag{D.9}$$

which physically corresponds to the matrix element of two particles with momentum $\mathbf{k}_1,\mathbf{k}_2$ going to any arbitrary final states, multiplied by the conjugate of the matrix element of two particles with momentum $\mathbf{p}_1,\mathbf{p}_2$ going to the same arbitrary final states. Letting $|\mathbf{p}_1,\mathbf{p}_2\rangle=|\mathbf{k}_1,\mathbf{k}_2\rangle$, *i.e.*, elastic forward scattering process, the two matrix elements under the curly brackets are conjugate to each other and lead to the differential cross section

$$\frac{\mathrm{d}^n\sigma}{\mathrm{d}q_1...\mathrm{d}q_n}=\left|\mathcal{M}(\mathbf{p}_1\mathbf{p}_2\to\{\mathbf{q}_i\})\right|^2. \tag{D.10}$$

Therefore the right side of Eq.(D.9) is the sum over the final states of total cross section $|\mathbf{p}_1\mathbf{p}_2\rangle\to|\{\mathbf{q}_i\}\rangle$, *i.e.*, an inclusive cross section with initial state $|\mathbf{p}_1\mathbf{p}_2\rangle$. On the other hand, when sandwiched by initial and final states the right side of Eq.(D.8) leads to

$$\begin{aligned} &-i\Big(\left\langle \mathbf{p}_1\mathbf{p}_2|T|\mathbf{k}_1\mathbf{k}_2\right\rangle-\left\langle \mathbf{p}_1\mathbf{p}_2|T^\dagger|\mathbf{k}_1\mathbf{k}_2\right\rangle\Big)\\ =&-i\Big(\mathcal{M}(\mathbf{k}_1\mathbf{k}_2\to\mathbf{p}_1\mathbf{p}_2)-\mathcal{M}^*(\mathbf{p}_1\mathbf{p}_2\to\mathbf{k}_1\mathbf{k}_2)\Big). \end{aligned} \tag{D.11}$$

Again, letting $|\mathbf{p}_1,\mathbf{p}_2\rangle=|\mathbf{k}_1,\mathbf{k}_2\rangle$, we end up with the difference of two matrix elements

$$\begin{aligned} &-i\Big(\mathcal{M}(\mathbf{p}_1\mathbf{p}_2\to\mathbf{p}_1\mathbf{p}_2)-\mathcal{M}^*(\mathbf{p}_1\mathbf{p}_2\to\mathbf{p}_1\mathbf{p}_2)\Big)\\ =&2\mathrm{Im}\mathcal{M}(\mathbf{p}_1\mathbf{p}_2\to\mathbf{p}_1\mathbf{p}_2). \end{aligned} \tag{D.12}$$

Putting them together, we have

$$\begin{aligned} 2\mathrm{Im}\mathcal{M}(\mathbf{p}_1\mathbf{p}_2\to\mathbf{p}_1\mathbf{p}_2)&=\sum_n\left(\prod_{i=1}^n\int\frac{\mathrm{d}^3q_i}{(2\pi)^3}\frac{1}{2E_i}\right)\left|\mathcal{M}(\mathbf{p}_1\mathbf{p}_2\to\{\mathbf{q}_i\})\right|^2\\ &=\sum_X\sigma(\mathbf{p}_1\mathbf{p}_2\to X), \end{aligned} \tag{D.13}$$

which indicates the imaginary part of an amplitude can be related to the total cross section of 'half' of the same process. Next, let us work out an explicit example relevant to our study of the $e^+e^- \to hadrons$ process.

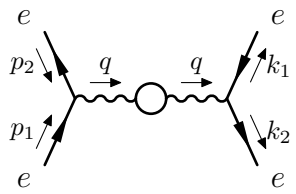

For the above process, we cut it in half and apply the optical theorem. In four-vectors, it is expressed in the following way.

$$\begin{aligned}
\sigma_{tot}(e^+e^- \to had) &= \frac{1}{2E_1 2E_2|v_1 - v_2|}\left(\prod_{i=1}^{n}\int \frac{\mathrm{d}^3 q_i}{(2\pi)^3}\frac{1}{2E_i}\right) \times \frac{1}{4}\sum_{spins}|\mathcal{M}|^2(2\pi)^4\delta^4(k_1+k_2-\sum q_i) \\
&= \frac{1}{2E_1 2E_2|v_1 - v_2|}\left(\frac{1}{4}\sum_{spins}\right)\left(\prod_{i=1}^{n}\int \frac{\mathrm{d}^3 q_i}{(2\pi)^3}\frac{1}{2E_i}\right)|\mathcal{M}|^2(2\pi)^4\delta^4(k_1+k_2-\sum q_i) \\
&= \frac{1}{2E_1 2E_2|v_1 - v_2|}\left(\frac{1}{4}\sum_{spins}\right)(-i)\left(\mathcal{M}-\mathcal{M}^*\right) \\
&= \frac{1}{2E_1 2E_2|v_1 - v_2|}\left(\frac{1}{4}\sum_{spins}\right)2\mathrm{Im}\mathcal{M}(e^+e^- \to e^+e^-).
\end{aligned} \tag{D.14}$$

It is useful to extract the vacuum polarization function out of the hadron process. To express $\mathcal{M}$, we follow the Feynman rules.

$$\begin{aligned}
\sum_{spins} i\mathcal{M} &= \sum_{spins}\overline{\psi}(p_2)\gamma^\mu\psi(p_1)(-ie)\frac{-ig_{\mu\nu}}{q^2}\left(i\Pi^{\nu\rho}(q^2)\right)\frac{-ig_{\rho\sigma}}{q^2}(-ie)\overline{\psi}(k_2)\gamma^\sigma\psi(k_1) \\
&= \sum_{spins}\overline{\psi}(p_2)\gamma^\mu\psi(p_1)(e^2)\frac{1}{q^4}\underbrace{\left(i\Pi_{\mu\sigma}(q^2)\right)}_{iq^2 g_{\mu\sigma}\Pi'_{\gamma\gamma}(q^2)}\overline{\psi}(k_2)\gamma^\sigma\psi(k_1) \\
&= \sum_{spins}\overline{\psi}(p_2)\gamma^\mu\psi(p_1)\overline{\psi}(k_2)\gamma^\sigma\psi(k_1)(e^2)\frac{1}{q^2}i\Pi'_{\gamma\gamma}(q^2) \\
&= -q^2\frac{e^2}{q^2}i\Pi'_{\gamma\gamma}(q^2) \\
&= -ie^2\Pi'_{\gamma\gamma}(q^2).
\end{aligned} \tag{D.15}$$

We list in the following the trick for handling the prefactor in Eq.(D.14). In the CM frame,

$$\begin{aligned} E_1E_2|v_1 - v_2| &= |E_2|\mathbf{p}_1| - E_1|\mathbf{p}_2|| \\ &= (E_2 + E_1)|\mathbf{p}_1| \\ &= E_{cm}|\mathbf{p}_{cm}|. \end{aligned} \tag{D.16}$$

Neglecting the mass of electron, $m_e \approx 0$, we have

$$\begin{aligned} E_{cm} &= 2|\mathbf{p}_1| = \sqrt{q^2}, \\ |\mathbf{p}_{cm}| &= \frac{1}{2}|\mathbf{p}_1 - \mathbf{p}_2| = |\mathbf{p}_1| = \frac{1}{2}\sqrt{q^2}. \end{aligned} \tag{D.17}$$

Substituting Eq.(D.15)-(D.17) into Eq.(D.14), we get

$$\begin{aligned} \sigma_{tot}(e^+e^- \to had)(q^2) &= \frac{1}{q^2}\sum_{spins} \mathrm{Im}\mathcal{M}(e^+e^- \to e^+e^-) \\ &= -\frac{4\pi\alpha}{q^2}\mathrm{Im}\Pi'_{\gamma\gamma}(q^2). \end{aligned} \tag{D.18}$$

Please note that there is a little cheat we have done (and everybody does) in the previous proof. In order to decompose as in Eq.(D.9), the intermediate states $\{\mathbf{q}_i\}$ must form a complete basis. However, when we talk about the 'hadronic intermediate states,' it is not obvious how they form a complete basis. Since there is a mathematical complication in defining quantum field theory with interactions in the first place, we ignored such subtlety even when the perturbation fails for QCD at low energy.

D.4 $\int \sigma^{(h)} \leftrightarrow \int R$

This is the easy part. Write out the $e^+e^- \to \mu^+\mu^-$ total cross section and convert $\sigma^{(h)}$ into R ratio. Up to leading order, we have

$$\sigma(e^+e^- \to \mu^+\mu^-) = \frac{4\pi\alpha^2}{3q^2}\sqrt{1 - \frac{4m_\mu^2}{q^2}}\left(1 + \frac{2m_\mu^2}{q^2}\right). \tag{D.19}$$

Taking $m_\mu \to 0$,

$$\begin{aligned} R &= \frac{\sigma^{(h)}}{\sigma^{\mu\mu}} \\ &= \frac{3q^2\sigma^{(h)}}{4\pi\alpha^2}. \end{aligned} \tag{D.20}$$

D.5 Combinations

Playing with the I - IV relations, we can write out various combinations relating different quantities, some of which are quite powerful. For example, combining III and IV, we have

$$\mathrm{Im}\Pi'_{\gamma\gamma}(x) = -\frac{\alpha}{3}R^{(h)}(x). \tag{D.21}$$

Combining II to IV, we have

$$\begin{aligned}
\Pi'_{\gamma\gamma}(q^2) - \Pi'_{\gamma\gamma}(0) &= -\frac{1}{\pi}\int_{4m_\pi^2}^{\infty}\left(\frac{1}{q^2-x}+\frac{1}{x}\right)\mathrm{Im}\Pi'_{\gamma\gamma}(x)\mathrm{d}x \\
&= -\frac{1}{\pi}\int_{4m_\pi^2}^{\infty}\frac{q^2}{x(q^2-x)}\left(\frac{-x}{4\pi\alpha}\right)\sigma^{(h)}(x)\mathrm{d}x \\
&= -\frac{1}{\pi}\int_{4m_\pi^2}^{\infty}\frac{q^2}{x(q^2-x)}\left(\frac{-x}{4\pi\alpha}\right)\left(\frac{4\pi\alpha^2}{3x}\right)R^{(h)}(x)\mathrm{d}x \\
&= \frac{\alpha}{3\pi}\int_{4m_\pi^2}^{\infty}\frac{q^2}{x(q^2-x)}R^{(h)}(x)\mathrm{d}x \\
&= -\frac{e^2}{12\pi^2}\int_{4m_\pi^2}^{\infty}\frac{q^2}{x(x-q^2)}R^{(h)}(\sqrt{x})\mathrm{d}x,
\end{aligned} \tag{D.22}$$

which is how we extract the vacuum polarization function out of the R ratio. Also, we can combine relations I - IV, which gives the following expression.

$$\Delta\alpha(q^2) = -\frac{e^2}{12\pi^2}\int_{4m_\pi^2}^{\infty}\frac{q^2}{x(x-q^2)}R^{(h)}(\sqrt{x})\mathrm{d}x, \tag{D.23}$$

which enables us to calculate the QED coupling constant running due to hadronic loop effects.

D.6 Remarks

Please note there is a loophole in deriving the above relations. In Eq. (D.7) Π is related to $\mathrm{Im}\,\Pi$, while in Eq. (D.22) the Cauchy integral is applied on Π'. Let us now show it is valid without going through the pole/ cut structure of Π'. In order to do this, we take the

derivative after $\Pi_{\gamma\gamma}(q^2)$ is expressed in the integral form.

$$\begin{aligned}
\Pi'_{\gamma\gamma}(q^2) &= \frac{1}{\pi}\int_{4m_\pi^2}^{\infty}\frac{1}{(q^2-x)^2}\mathrm{Im}\,\Pi_{\gamma\gamma}(x)\mathrm{d}x \\
&\approx \frac{1}{\pi}\int_{4m_\pi^2}^{\infty}\frac{1}{(q^2-x)^2}x\mathrm{Im}\Pi'_{\gamma\gamma}(x)\mathrm{d}x \\
&\approx \frac{1}{\pi}\int_{4m_\pi^2}^{\infty}\frac{1}{(q^2-x)(-x)}x\mathrm{Im}\Pi'_{\gamma\gamma}(x)\mathrm{d}x \\
&= -\frac{1}{\pi}\int_{4m_\pi^2}^{\infty}\frac{1}{(q^2-x)}\mathrm{Im}\Pi'_{\gamma\gamma}(x)\mathrm{d}x. \qquad \text{(D.24)}
\end{aligned}$$

Please note the second and the third line only work for small q^2; thus, only the region of small x matters. On the other hand, for small q^2 we often write Π' as $\Pi(q^2)/q^2$. Let us show that is also compatible.

$$\begin{aligned}
\frac{\Pi_{\gamma\gamma}}{q^2} &= -\frac{1}{\pi}\int_{4m_\pi^2}^{\infty}\frac{1}{q^2(q^2-x)}\mathrm{Im}\,\Pi_{\gamma\gamma}(x)\mathrm{d}x \\
&= -\frac{1}{\pi}\int_{4m_\pi^2}^{\infty}\left(\frac{1}{q^2-x}-\frac{1}{q^2}\right)\frac{1}{x}\mathrm{Im}\,\Pi_{\gamma\gamma}(x)\mathrm{d}x \\
&\approx -\frac{1}{\pi}\int_{4m_\pi^2}^{\infty}\mathrm{Im}\,\Pi'_{\gamma\gamma}(x)\mathrm{d}x + \underbrace{\frac{1}{\pi}\int_{4m_\pi^2}^{\infty}\frac{1}{q^2}\mathrm{Im}\,\Pi'_{\gamma\gamma}(x)\mathrm{d}x}_{=0}. \qquad \text{(D.25)}
\end{aligned}$$

The second term of last line vanishes because of the following.

$$\begin{aligned}
\frac{1}{\pi}\int_{4m_\pi^2}^{\infty}\frac{1}{q^2}\mathrm{Im}\,\Pi'_{\gamma\gamma}(x)\mathrm{d}x &= \frac{1}{q^2}\frac{1}{\pi}\int_{4m_\pi^2}^{\infty}\frac{\mathrm{Im}\,\Pi_{\gamma\gamma}(x)}{x-0}\mathrm{d}x \\
&= \frac{1}{q^2}\Pi_{\gamma\gamma}(0) \\
&= 0. \qquad \text{(D.26)}
\end{aligned}$$

Appendix E

Formulas for Decay Width and Approximation

In this appendix we show the decay width expression of Z', and use the two-body decay formula to approximate three-body decay process in the case where the mediator particle is very long-lived.

E.1 Z' Decay Width

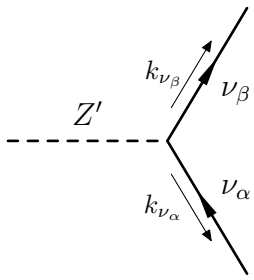

Figure E.1: The process of $Z' \to \nu_\alpha \nu_\beta$.

Assuming $Z' \to \nu\overline{\nu}$ mode only for simplification, we can write out the matrix element as

$$\mathcal{M} = (Q'g')^2 \left[\overline{\nu}_\alpha(k_{\nu_\alpha}) \gamma^\mu \left(\frac{1-\gamma^5}{2} \right) \nu_\beta(k_{\nu_\beta}) \right]. \tag{E.1}$$

The average over final spin reads

$$\begin{aligned}
\sum_{f.\,s.}|\mathcal{M}|^2 =& \sum_{f.\,s.}(Q'g')^2\left[\overline{\nu}_\alpha(k_{\nu_\alpha})\gamma^\mu\left(\frac{1-\gamma^5}{2}\right)\nu_\beta(k_{\nu_\beta})\right]\left[\overline{\nu}_\alpha(k_{\nu_\alpha})\gamma^\mu\left(\frac{1-\gamma^5}{2}\right)\nu_\beta(k_{\nu_\beta})\right]^* \\
=& \sum_{f.\,s.}(Q'g')^2\overline{\nu}_\alpha(k_{\nu_\alpha})\gamma^\mu\left(\frac{1-\gamma^5}{2}\right)\nu_\beta(k_{\nu_\beta})\nu_\beta^\dagger(k_{\nu_\beta})\left(\frac{1-\gamma^5}{2}\right)\gamma^{\mu\dagger}\gamma^{0\dagger}\nu_\alpha(k_{\nu_\alpha})g_{\mu\nu} \\
=& (Q'g')^2\mathrm{Tr}\left(\gamma_\mu \not{k}_{\nu_\alpha}\gamma^0\gamma^{\mu\dagger}\gamma^0\not{k}_{\nu_\beta}\right) \\
=& (Q'g')^2\mathrm{Tr}\left(\gamma_\mu\gamma^\rho\gamma^\mu\gamma^\sigma\right)\left(k_{\nu_\alpha}\right)_\rho\left(k_{\nu_\beta}\right)_\sigma \\
=& (Q'g')^2 g_{\mu\nu}\mathrm{Tr}\left(\gamma^\nu\gamma^\rho\gamma^\mu\gamma^\sigma\right)\left(k_{\nu_\alpha}\right)_\rho\left(k_{\nu_\beta}\right)_\sigma \\
=& (Q'g')^2 g_{\mu\nu}\,4\,\left(g^{\nu\rho}g^{\mu\sigma}-g^{\nu\mu}g^{\rho\sigma}+g^{\nu\sigma}g^{\rho\mu}\right)\left(k_{\nu_\alpha}\right)_\rho\left(k_{\nu_\beta}\right)_\sigma \\
=& (Q'g')^2\,4\,\left(k_{\nu_\alpha}\cdot k_{\nu_\beta}-4k_{\nu_\alpha}\cdot k_{\nu_\beta}+k_{\nu_\alpha}\cdot k_{\nu_\beta}\right) \\
=& -8(Q'g')^2\left(k_{\nu_\alpha}\cdot k_{\nu_\beta}\right).
\end{aligned} \tag{E.2}$$

The decay width of Z' reads

$$\begin{aligned}
\Gamma_{Z'} =& \int\frac{1}{2|\mathbf{k}_{\nu_\beta}|}\frac{1}{2|\mathbf{k}_{\nu_\alpha}|}\frac{\mathrm{d}^3\mathbf{k}_{\nu_\alpha}}{(2\pi)^3}\frac{\mathrm{d}^3\mathbf{k}_{\nu_\beta}}{(2\pi)^3}\frac{S}{2M_{Z'}}(2\pi)^3\delta^{(3)}(\mathbf{k}_{\nu_\beta}+\mathbf{k}_{\nu_\alpha})(2\pi)\delta(M_{Z'}-|\mathbf{k}_{\nu_\alpha}|-\left|\mathbf{k}_{\nu_\beta}\right|)\left\langle|\mathcal{M}|^2\right\rangle \\
=& \int\frac{1}{4|\mathbf{k}_{\nu_\alpha}|^2}\frac{\mathrm{d}^3\mathbf{k}_{\nu_\alpha}}{(2\pi)^3}\frac{1}{2M_{Z'}}(2\pi)\delta(M_{Z'}-2|\mathbf{k}_{\nu_\alpha}|)(Q'g')^2(|\mathbf{k}_{\nu_\alpha}|^2+|\mathbf{k}_{\nu_\alpha}|^2)(8) \\
=& \int\frac{\mathrm{d}^3\mathbf{k}_{\nu_\alpha}}{(2\pi)^3}\frac{1}{2M_{Z'}}(2\pi)\delta(M_{Z'}-2|\mathbf{k}_{\nu_\alpha}|)\frac{1}{2}(Q'g')^2(8) \\
=& \int\frac{1}{2M_{Z'}}(2\pi)\delta(M_{Z'}-2|\mathbf{k}_{\nu_\alpha}|)\frac{1}{2}(Q'g')^2|\mathbf{k}_{\nu_\alpha}|^2\frac{1}{2\pi^2}\mathrm{d}|\mathbf{k}_{\nu_\alpha}|(8) \\
=& \frac{1}{4\pi}(Q'g')^2M_{Z'}.
\end{aligned} \tag{E.3}$$

Next, let us calculate $\Gamma_{Z'}$ taking into account both $Z'\to\nu\overline{\nu}$ and $Z'\to e^+e^-$ processes. Neglecting the electron mass, since $m_e\ll m_{Z'}$ in most cases, we get almost exactly the same result for $Z'\to e_R^+e_L^-$:

$$\Gamma(Z'\to e_R^+e_L^-) = \frac{1}{4\pi}(Q'g')^2M_{Z'}, \tag{E.4}$$

where Q' is the $U(1)'$ effective charge of electrons. It is the same as in $Z'\to e_L^+e_R^-$, modulo a change of the coupling. For example, in the model of Ref. [504], the decay width of Z' is

$$\begin{aligned}
\Gamma_{Z'} =& \Gamma(Z'\to\nu\overline{\nu})+\Gamma(Z'\to e_L^+e_R^-)+\Gamma(Z'\to e_R^+e_L^-) \\
=& \frac{1}{4\pi}(\zeta g')^2M_{Z'}X_{\mu\tau}^L+\frac{1}{4\pi}(Q'_*(M_{Z'},\mathbf{0})g')^2M_{Z'}X_{\mu\tau}^L+\frac{1}{4\pi}(Q'_*(M_{Z'},\mathbf{0})g')^2M_{Z'}X_{\mu\tau}^R.
\end{aligned} \tag{E.5}$$

As we can see, the decay width of Z' is very small compared to its mass. Therefore, the $\tau \to \mu ee$ process with Z' as intermediate particles can be seen as $\tau \to Z'\mu$ with Z' produced on-shell most of the time, followed by $Z' \to ee$. In next section, we show how to do the approximation.

E.2 Approximating $\tau \to \mu ee$ with Two Body Decays

In this section, we show the decay width of τ in the presence of Z'. Since the Z' decay width is very small, as is shown in section E.1, we model $\tau \to \ell\alpha\beta$ by two sequential 2-body decays. First of all, we count the degrees of freedom of different objects to make sure they match. For the $1 \to n$ decay process, we have

$$\mathrm{d}\Gamma = \frac{1}{2m_a}\left(\prod_f \frac{\mathrm{d}^3 p_f}{(2\pi)^3}\frac{1}{2E_f}\right)|\mathcal{M}(1\to n)|^2(2\pi)^4\delta^{(4)}(\sum p_f - p_a), \tag{E.6}$$

from which we get

$$\begin{aligned}[\mathcal{M}(p_a \to p_1 p_2)] &= 1,\\ [\mathcal{M}(p_a \to p_1 p_2 p_3)] &= 0,\\ &\ldots\end{aligned} \tag{E.7}$$

For the $2 \to n$ scattering process, the cross section reads

$$\mathrm{d}\sigma = \frac{1}{2E_aE_b|v_a - v_b|}\left(\prod_f \frac{\mathrm{d}^3 p_f}{(2\pi)^3}\frac{1}{E_f}\right)|\mathcal{M}(2\to n)|^2(2\pi)^4\delta^{(4)}(p_a + p_b - \sum p_f). \tag{E.8}$$

Therefore, the dimension of $\mathcal{M}$ is

$$\begin{aligned}[\mathcal{M}(p_a, p_b \to p_1, p_2)] &= 0,\\ [\mathcal{M}(p_a, p_b \to p_1, p_2, p_3)] &= -1,\\ &\ldots\end{aligned} \tag{E.9}$$

$[\mathcal{M}(p_a, p_b \to p_1, p_2)] = [\mathcal{M}(p_a \to p_1, p_2, p_3)]$ as it should. Next, we show how to decompose the three-body decay into two-body decays.

$$\begin{aligned}\Gamma_{\tau\to\mu\alpha\beta} = \frac{1}{2m_\tau}\int \frac{\mathrm{d}^4 k_\mu}{(2\pi)^4}\frac{\mathrm{d}^4 k_\alpha}{(2\pi)^4}\frac{\mathrm{d}^4 k_\beta}{(2\pi)^4}(2\pi)\delta(k_\mu^2 - m_\mu^2)(2\pi)\delta(k_\alpha^2 - m_\alpha^2)(2\pi)\delta(k_\beta^2 - m_\beta^2)\\ \times (2\pi)^4\delta^{(4)}(k_\mu + k_\alpha + k_\beta - p_\tau)\left\langle|\mathcal{M}(\tau\to\mu\alpha\beta)|^2\right\rangle.\end{aligned} \tag{E.10}$$

In order to decompose $\Gamma_{\tau\to\mu\alpha\beta}$ in terms of $\Gamma_{\tau\to\mu Z'}$ and $\Gamma_{Z'\to\alpha\beta}$, we need to decompose the matrix element $\mathcal{M}$. Suppose the states form a complete basis of the interacting particle space (which is a big 'if' by itself), we have

$$\begin{aligned}
\langle\mu\alpha\beta|\tau\rangle &= \int \frac{\mathrm{d}^4 q_\mu}{(2\pi)^4}\frac{\mathrm{d}^4 q_{Z'}}{(2\pi)^4}\langle\mu\alpha\beta|q_\mu q_{Z'}\rangle\langle q_\mu q_{Z'}|\tau\rangle \\
&= \int \frac{\mathrm{d}^4 q_{Z'}}{(2\pi)^4}\langle\alpha\beta|q_{Z'}\rangle\langle\mu q_{Z'}|\tau\rangle \\
&= \int \frac{\mathrm{d}^4 q_{Z'}}{(2\pi)^4} i\mathcal{M}(q_{Z'}\to\alpha\beta)(2\pi)^4\delta^{(4)}(k_\alpha+k_\beta-q_{Z'}) \\
&\qquad\qquad \times i\mathcal{M}(\tau\to\mu q_{Z'})(2\pi)^4\delta^{(4)}(k_\mu+q_{Z'}-p_\tau) \\
&= i\mathcal{M}(\tau\to\mu q_{Z'})i\mathcal{M}(q_{Z'}\to\alpha\beta)(2\pi)^4\delta^{(4)}(k_\mu+k_\alpha+k_\beta-p_\tau) \\
&= i\mathcal{M}(\tau\to\mu\alpha\beta)(2\pi)^4\delta^{(4)}(k_\mu+k_\alpha+k_\beta-p_\tau),
\end{aligned} \tag{E.11}$$

from which we derive $i\mathcal{M}(\tau\to\mu\alpha\beta) = i\mathcal{M}(\tau\to\mu q_{Z'})i\mathcal{M}(q_{Z'}\to\alpha\beta)$, where $q_{Z'} = k_\alpha + k_\beta$ and may not be on-shell. However, the mass dimension does not add up. By dimensional analysis, the intermediate integral should be replaced with on-shell variables. We change it to

$$\begin{aligned}
\langle\mu\alpha\beta|\tau\rangle &= \int \frac{\mathrm{d}^3\mathbf{q}_\mu}{(2\pi)^3 2E_\mu}\frac{\mathrm{d}^3\mathbf{q}_{Z'}}{(2\pi)^3 2E_{Z'}}\langle\mu\alpha\beta|\mathbf{q}_\mu\mathbf{q}_{Z'}\rangle\langle\mathbf{q}_\mu\mathbf{q}_{Z'}|\tau\rangle \\
&= \int \frac{\mathrm{d}^3\mathbf{q}_{Z'}}{(2\pi)^3 2E_{Z'}}\langle\alpha\beta|\mathbf{q}_{Z'}\rangle\langle\mu\mathbf{q}_{Z'}|\tau\rangle \\
&= \int \frac{\mathrm{d}^4 q_{Z'}}{(2\pi)^4} i\mathcal{M}(Z'\to\alpha\beta)(2\pi)^3\delta^{(4)}(k_\alpha+k_\beta-q_{Z'}) \\
&\qquad\qquad \times i\mathcal{M}(\tau\to\mu Z')(2\pi)^4\delta^{(4)}(k_\mu+q_{Z'}-p_\tau)(2\pi)\delta(q_{Z'}^2-M_{Z'}^2) \\
&= i\mathcal{M}(\tau\to\mu Z')(2\pi)\delta(q_{Z'}^2-M_{Z'}^2)i\mathcal{M}(Z'\to\alpha\beta)(2\pi)^4\delta^{(4)}(k_\mu+k_\alpha+k_\beta-p_\tau) \\
&= i\mathcal{M}(\tau\to\mu\alpha\beta)(2\pi)^4\delta^{(4)}(k_\mu+k_\alpha+k_\beta-p_\tau),
\end{aligned} \tag{E.12}$$

which gives us $i\mathcal{M}(\tau\to\mu\alpha\beta) = i\mathcal{M}(\tau\to\mu Z')(2\pi)\delta(q_{Z'}^2-M_{Z'}^2)i\mathcal{M}(Z'\to\alpha\beta)$, which implies, loosely speaking,

$$|\mathcal{M}(\tau\to\mu\alpha\beta)|^2 = |\mathcal{M}(\tau\to\mu Z')|^2|\mathcal{M}(Z'\to\alpha\beta)|^2(2\pi)^2(\delta(q_{Z'}^2-M_{Z'}^2))^2. \tag{E.13}$$

We cannot just plug it into Eq. (E.10) yet because $\mathcal{M}$ is squared there, while a square of the delta function (distribution) is impossible to define mathematically. That is the reason that generally prevents the factorization of a 3-body decay into 2-body decays. However, because of the small mass and small decay width, the intermediate Z' are mostly produced

on-shell. Because of this, we can factorize out a δ function from $|\mathcal{M}(\tau \to \mu\alpha\beta)|^2$ as follows.

$$\begin{aligned}
\mathcal{M}(\tau \to \mu\alpha\beta) &= \mathcal{M}_0 \left(\frac{\epsilon M_{Z'}^2}{q_{Z'}^2 - M_{Z'}^2 + i\Gamma_{Z'} M_{Z'}} \right), \\
|\mathcal{M}(\tau \to \mu\alpha\beta)|^2 &= |\mathcal{M}_0|^2 \left(\frac{\epsilon^2 M_{Z'}^4}{(q_{Z'}^2 - M_{Z'}^2)^2 + M_{Z'}^2 \Gamma_{Z'}^2} \right) \\
&= |\mathcal{M}_0|^2 \frac{\pi\epsilon^2 M_{Z'}^4}{M_{Z'}\Gamma_{Z'}} \left(\frac{1}{\pi} \frac{M_{Z'}\Gamma_{Z'}}{(q_{Z'}^2 - M_{Z'}^2)^2 + M_{Z'}^2\Gamma_{Z'}^2} \right),
\end{aligned} \tag{E.14}$$

where $\mathcal{M}_0$ is the part that has no poles nor zeroes. One of the definitions of the δ function is expressed as follows:

$$\delta(x) = \frac{1}{\pi} \lim_{\epsilon \to 0} \frac{\epsilon}{x^2 + \epsilon^2}. \tag{E.15}$$

When $M_{Z'}$ and $\Gamma_{Z'}$ are small, Eq. (E.14) is approximated by

$$|\mathcal{M}(\tau \to \mu\alpha\beta)|^2 = |\mathcal{M}_0|^2 \frac{\pi\epsilon^2 M_{Z'}^4}{M_{Z'}\Gamma_{Z'}} \delta(q_{Z'}^2 - M_{Z'}^2). \tag{E.16}$$

Combining with Eq. (E.13) gives

$$\begin{aligned}
|\mathcal{M}(\tau \to \mu\alpha\beta)|^2 &= |\mathcal{M}_0|^2 \frac{\pi\epsilon^2 M_{Z'}^4}{M_{Z'}\Gamma_{Z'}} \delta(q_{Z'}^2 - M_{Z'}^2) \\
&= |\mathcal{M}(\tau \to \mu Z')|^2 |\mathcal{M}(Z' \to \alpha\beta)|^2 (2\pi)^2 (\delta(q_{Z'}^2 - M_{Z'}^2))^2,
\end{aligned} \tag{E.17}$$

which leads to

$$|\mathcal{M}_0|^2 = \frac{2M_{Z'}\Gamma_{Z'}}{\epsilon^2 M_{Z'}^4} |\mathcal{M}(\tau \to \mu Z')|^2 |\mathcal{M}(Z' \to \alpha\beta)|^2 (2\pi) \delta(q_{Z'}^2 - M_{Z'}^2), \tag{E.18}$$

which satisfies a dimensional-analysis check. Substitute into Eq. (E.10):

$$\begin{aligned}
\Gamma_{\tau\to\mu\alpha\beta} &= \frac{1}{2m_\tau}\int \frac{\mathrm{d}^4k_\mu}{(2\pi)^4}\frac{\mathrm{d}^4k_\alpha}{(2\pi)^4}\frac{\mathrm{d}^4k_\beta}{(2\pi)^4}(2\pi)\delta(k_\mu^2-m_\mu^2)(2\pi)\delta(k_\alpha^2-m_\alpha^2)(2\pi)\delta(k_\beta^2-m_\beta^2) \\
&\quad\times(2\pi)^4\delta^{(4)}(k_\mu+k_\alpha+k_\beta-p_\tau)\left\langle|\mathcal{M}_0|^2\right\rangle\left(\frac{\epsilon^2M_{Z'}^4}{(q_{Z'}^2-M_{Z'}^2)^2+M_{Z'}^2\Gamma_{Z'}^2}\right) \\
&\approx \frac{1}{2m_\tau}\int \frac{\mathrm{d}^4k_\mu}{(2\pi)^4}\frac{\mathrm{d}^4k_\alpha}{(2\pi)^4}\frac{\mathrm{d}^4k_\beta}{(2\pi)^4}\frac{\mathrm{d}^4q_{Z'}}{(2\pi)^4} \\
&\quad\times(2\pi)\delta(k_\mu^2-m_\mu^2)(2\pi)\delta(k_\alpha^2-m_\alpha^2)(2\pi)\delta(k_\beta^2-m_\beta^2)(2\pi)\delta(q_{Z'}^2-M_{Z'}^2) \\
&\quad\times(2\pi)^4\delta^{(4)}(k_\mu+q_{Z'}-p_\tau)(2\pi)^4\delta^{(4)}(k_\alpha+k_\beta-p_{Z'})\left\langle|\mathcal{M}(\tau\to\mu Z')|^2\right\rangle\left\langle|\mathcal{M}(Z'\to\alpha\beta)|^2\right\rangle \\
&\quad\times\left(\frac{2M_{Z'}\Gamma_{Z'}}{(q_{Z'}^2-M_{Z'}^2)^2+M_{Z'}^2\Gamma_{Z'}^2}\right) \\
&= \left(\frac{4}{\Gamma_{Z'}}\right)\frac{1}{2M_{Z'}}\frac{1}{2m_\tau}\int \frac{\mathrm{d}^4k_\mu}{(2\pi)^4}\frac{\mathrm{d}^4k_\alpha}{(2\pi)^4}\frac{\mathrm{d}^4k_\beta}{(2\pi)^4}\frac{\mathrm{d}^4q_{Z'}}{(2\pi)^4} \\
&\quad\times(2\pi)\delta(k_\mu^2-m_\mu^2)(2\pi)\delta(k_\alpha^2-m_\alpha^2)(2\pi)\delta(k_\beta^2-m_\beta^2)(2\pi)\delta(q_{Z'}^2-M_{Z'}^2) \\
&\quad\times(2\pi)^4\delta^{(4)}(k_\mu+q_{Z'}-p_\tau)(2\pi)^4\delta^{(4)}(k_\alpha+k_\beta-p_{Z'})\left\langle|\mathcal{M}(\tau\to\mu Z')|^2\right\rangle\left\langle|\mathcal{M}(Z'\to\alpha\beta)|^2\right\rangle \\
&= \frac{4\Gamma(\tau\to\mu Z')\Gamma(Z'\to\alpha\beta)}{\Gamma_{Z'}}. \qquad \text{(E.19)}
\end{aligned}$$

Please note that the above formula only works well when $\Gamma_{Z'}$ is very small due to the definition of the δ function in Eq. (E.15).

Appendix F

Coulomb Potential and Yukawa Potential in the Semi-empirical Mass Formula

F.1 Coulomb Potential

The Coulomb electrostatic term is due to the electrostatic potential energy which, for a uniformly charged sphere of radius R and total charge Q, is given by

$$E \;=\; \frac{3}{5}\left(\frac{1}{4\pi\epsilon_0}\right)\frac{Q^2}{R}\;. \tag{F.1}$$

With the replacements $R = r_0 A^{1/3}$ and $Q^2 = e^2 Z(Z-1)$, we obtain:

$$E \;=\; \frac{3e^2}{20\pi\epsilon_0 r_0}\frac{Z(Z-1)}{A^{1/3}} \;=\; a_C\frac{Z(Z-1)}{A^{1/3}}\;. \tag{F.2}$$

The above expression for the potential energy is obtained via the following integration:

$$\begin{aligned}
E &= \frac{1}{2}\int d^3\mathrm{r}_1 \int d^3\mathrm{r}_2\,\frac{\rho(\mathrm{r}_1)\rho(\mathrm{r}_2)}{|\mathrm{r}_1-\mathrm{r}_2|}\\
&= 4\pi^2\rho^2\int_0^R dr_1 r_1^2\int_0^R dr_2 r_2^2\int_{-1}^1 d\cos\theta\,\frac{1}{\sqrt{r_1^2-2r_1r_2\cos\theta+r_2^2}}\\
&= 4\pi^2\rho^2\int_0^R dr_1 r_1^2\int_0^R dr_2 r_2^2\left[-\frac{1}{r_1r_2}\sqrt{r_1^2-2r_1r_2\cos\theta+r_2^2}\right]_{-1}^{1}\\
&= 4\pi^2\rho^2\int_0^R dr_1 r_1\int_0^R dr_2 r_2\left[\sqrt{(r_1+r_2)^2}-\sqrt{(r_1-r_2)^2}\right]
\end{aligned}$$

$$
\begin{aligned}
&= 4\pi^2\rho^2 \int_0^R dr_1 r_1 \int_0^R dr_2 r_2 \Big[(r_1+r_2) - |r_1-r_2|\Big] \\
&= 8\pi^2\rho^2 \int_0^R dr_1 r_1 \int_0^R dr_2 r_2 \min(r_1,r_2) \\
&= 8\pi^2\rho^2 \int_0^R dr_1 r_1 \left[\int_0^{r_1} dr_2 r_2^2 + r_1 \int_{r_1}^R dr_2 r_2\right] \\
&= 8\pi^2\rho^2 \int_0^R dr_1 r_1 \left[\frac{1}{3}r_1^3 + \frac{1}{2}\left(R^2 - r_1^2\right) r_1\right] \\
&= 8\pi^2\rho^2 \int_0^R dr_1 r_1 \left[\frac{1}{2}R^2 r_1 - \frac{1}{6}r_1^3\right] \\
&= 8\pi^2\rho^2 \left[\frac{1}{2}R^2 \int_0^R dr_1 r_1^2 - \frac{1}{6}\int_0^R dr_1 r_1^4\right] \\
&= 8\pi^2\rho^2 \left[\frac{1}{6}R^5 - \frac{1}{30}R^5\right] \\
&= \frac{16\pi^2\rho^2}{15}R^5 \;=\; \frac{3}{5}\left(\frac{4\pi R^3}{3}\rho\right)^2 \frac{1}{R} \;=\; \frac{3}{5}\frac{Q^2}{R}\,.
\end{aligned}
\tag{F.3}
$$

To use it for a real fit, we need to relate the above parameters to dimensionless couplings e and g', and the mass $m_{Z'}$. First, we wrote the Coulomb electrostatic energy using MKSA units as

$$
E \;=\; \frac{3}{5}\left(\frac{1}{4\pi\epsilon_0}\right)\frac{Q^2}{R} \;=\; \frac{3\tilde{e}^2}{20\pi\epsilon_0 r_0}\frac{Z(Z-1)}{A^{1/3}}\,, \tag{F.4}
$$

where I use the symbol $\tilde{e} = 1.602\times10^{-19}\,\mathrm{C}$ for the proton charge to distinguish it from the dimensionless version which is

$$
e \;=\; \frac{\tilde{e}}{\sqrt{\epsilon_0\hbar c}} \;=\; 0.303\,, \qquad \alpha \;=\; \frac{e^2}{4\pi} \;=\; \frac{1}{137}\,. \tag{F.5}
$$

The constant $r_0 = 1.25\,\mathrm{fm}$ can be converted to MeV^{-1} via

$$
\rho_0 \;\equiv\; \frac{r_0}{\hbar c} \;=\; \frac{(1.25\,\mathrm{fm})}{(197.327\,\mathrm{MeV}\cdot\mathrm{fm})} \;=\; 0.00633\,\mathrm{MeV}^{-1}\,. \tag{F.6}
$$

So the prefactor in Eq. (F.4) can be written as

$$
\frac{3\tilde{e}^2}{20\pi\epsilon_0 r_0} \;=\; \frac{3(\tilde{e}^2/\epsilon_0\hbar c)}{20\pi(r_0/\hbar c)} \;=\; \frac{3e^2}{20\pi\rho_0} \;=\; \frac{3\alpha}{5\rho_0} \;=\; 0.691\,\mathrm{MeV}\,. \tag{F.7}
$$

This agrees with the result in Ref. [511].

F.2 Yukawa Potential

For a Yukawa potential, the above calculation is modified to

$$
\begin{aligned}
E &= \frac{1}{2}\int d^3\mathrm{r}_1 \int d^3\mathrm{r}_2 \, \frac{\rho(\mathrm{r}_1)\rho(\mathrm{r}_2)}{|\mathrm{r}_1-\mathrm{r}_2|}\, e^{-\mu|\mathrm{r}_1-\mathrm{r}_2|} \\
&= 4\pi^2\rho^2 \int_0^R dr_1 r_1^2 \int_0^R dr_2 r_2^2 \int_{-1}^1 d\cos\theta \, \frac{e^{-\mu\sqrt{r_1^2-2r_1r_2\cos\theta+r_2^2}}}{\sqrt{r_1^2-2r_1r_2\cos\theta+r_2^2}} \\
&= 4\pi^2\rho^2 \int_0^R dr_1 r_1^2 \int_0^R dr_2 r_2^2 \left[\frac{1}{\mu r_1 r_2}\, e^{-\mu\sqrt{r_1^2-2r_1r_2\cos\theta+r_2^2}}\right]_{-1}^{1} \\
&= \frac{4\pi^2\rho^2}{\mu} \int_0^R dr_1 r_1 \int_0^R dr_2 r_2 \left[e^{-\mu|r_1-r_2|} - e^{-\mu(r_1+r_2)}\right] \\
&= \frac{4\pi^2\rho^2}{\mu} \left[\int_0^R dr_1 r_1 \int_0^R dr_2 r_2\, e^{-\mu|r_1-r_2|} - \int_0^R dr_1 r_1 \int_0^R dr_2 r_2\, e^{-\mu(r_1+r_2)}\right] \\
&= \frac{4\pi^2\rho^2}{\mu} \left[\int_0^R dr_1 r_1 \left\{e^{-\mu r_1}\int_0^{r_1} dr_2 r_2\, e^{\mu r_2} + e^{\mu r_1}\int_{r_1}^R dr_2 r_2\, e^{-\mu r_2}\right\}\right. \\
&\qquad \left. - \int_0^R dr_1 r_1\, e^{-\mu r_1}\int_0^R dr_2 r_2\, e^{-\mu r_2}\right] \\
&= \frac{4\pi^2\rho^2}{\mu} \left[\int_0^R dr_1 r_1 \left\{e^{-\mu r_1}\left[-\frac{1}{\mu^2}(1-\mu r_2)\, e^{\mu r_2}\right]_0^{r_1} + e^{\mu r_1}\left[-\frac{1}{\mu^2}(1+\mu r_2)\, e^{-\mu r_2}\right]_{r_1}^{R}\right\}\right. \\
&\qquad \left. - \left[-\frac{1}{\mu^2}(1+\mu r_1)\, e^{-\mu r_1}\right]_0^R \left[-\frac{1}{\mu^2}(1+\mu r_2)\, e^{-\mu r_2}\right]_0^R\right] \\
&= \frac{4\pi^2\rho^2}{\mu} \left[\frac{1}{\mu^2}\int_0^R dr_1 r_1 \left\{e^{-\mu r_1} + 2\mu r_1 - (1+\mu R)\, e^{-\mu R} e^{\mu r_1}\right\}\right. \\
&\qquad \left. - \frac{1}{\mu^4}\left\{1-(1+\mu R)\, e^{-\mu R}\right\}^2\right] \\
&= \frac{4\pi^2\rho^2}{\mu} \left[\frac{1}{\mu^2}\left\{\int_0^R dr_1 r_1\, e^{-\mu r_1} + 2\mu\int_0^R dr_1 r_1^2 - (1+\mu R)\, e^{-\mu R}\int_0^R dr_1 r_1\, e^{\mu r_1}\right\}\right. \\
&\qquad \left. - \frac{1}{\mu^4}\left\{1-(1+\mu R)\, e^{-\mu R}\right\}^2\right] \\
&= \frac{4\pi^2\rho^2}{\mu} \left[\frac{1}{\mu^2}\left\{\left[-\frac{1}{\mu^2}(1+\mu r_1)\, e^{-\mu r_1}\right]_0^R + \frac{2\mu R^3}{3} - (1+\mu R)\, e^{-\mu R}\left[-\frac{1}{\mu^2}(1-\mu r_1)\, e^{\mu r_1}\right]_0^R\right\}\right. \\
&\qquad \left. - \frac{1}{\mu^4}\left\{1-(1+\mu R)\, e^{-\mu R}\right\}^2\right]
\end{aligned}
$$

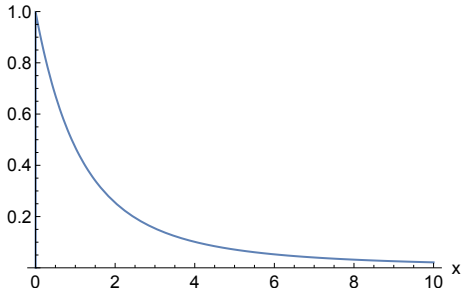

Figure F.1: Plot of the function $f(x)$.

$$
\begin{aligned}
&= \frac{4\pi^2\rho^2}{\mu^5}\left[\left\{\left[1-(1+\mu R)\,e^{-\mu R}\right]+\frac{2(\mu R)^3}{3}-(1+\mu R)\,e^{-\mu R}\left[1-(1-\mu R)\,e^{\mu R}\right]\right\}\right.\\
&\qquad\left.-\left\{1-(1+\mu R)\,e^{-\mu R}\right\}^2\right]\\
&= \frac{4\pi^2\rho^2}{\mu^5}\left[\left\{1-2(1+\mu R)\,e^{-\mu R}+\frac{2(\mu R)^3}{3}+(1+\mu R)(1-\mu R)\right\}\right.\\
&\qquad\left.-\left\{1-2(1+\mu R)\,e^{-\mu R}+(1+\mu R)^2e^{-2\mu R}\right\}\right]\\
&= \frac{4\pi^2\rho^2}{\mu^5}\left[1-(\mu R)^2+\frac{2(\mu R)^3}{3}-(1+\mu R)^2e^{-2\mu R}\right]\\
&= \left[\frac{3}{5}\left(\frac{4\pi R^3}{3}\rho\right)^2\frac{1}{R}\right]\frac{15}{4(\mu R)^5}\left[1-(\mu R)^2+\frac{2(\mu R)^3}{3}-(1+\mu R)^2e^{-2\mu R}\right]\\
&= \frac{3Q^2}{5R}f(\mu R)\,, \qquad\qquad (F.8)
\end{aligned}
$$

where

$$
\begin{aligned}
f(x) &\equiv \frac{15}{4x^5}\left[1-x^2+\frac{2x^3}{3}-(1+x)^2e^{-2x}\right]\\
&= 1-\frac{5x}{6}+\frac{3x^2}{7}-\frac{x^3}{6}+\cdots \qquad\qquad (F.9)
\end{aligned}
$$

The plot of $f(x)$ is shown in Figure F.1.

Since both protons and neutrons have the same $U(1)'$ charge, we have

$$Q \propto A\,, \qquad R \;=\; r_0A^{1/3}\,. \qquad\qquad (F.10)$$

Therefore, the binding energy due to the extra $U(1)'$ interaction would scale as

$$E' \;\propto\; A^{5/3}f(\mu r_0A^{1/3})\,. \qquad\qquad (F.11)$$

Appendix G

Farzan-Shoemaker Model

G.1 Notation of Farzan and Shoemaker

Farzan and Shoemaker express the left-handed leptons with the fields

$$\tilde{L} \equiv \begin{bmatrix} \tilde{L}_\alpha \\ \tilde{L}_\beta \end{bmatrix} \equiv V \begin{bmatrix} L_+ \\ L_- \end{bmatrix}, \qquad V = \frac{1}{\sqrt{2}} \begin{bmatrix} 1 & -1 \\ 1 & 1 \end{bmatrix}. \tag{G.1}$$

Note that $\tilde{L}_\alpha$ and $\tilde{L}_\beta$ do not have definite $U(1)'$ charges. This demands that $\tilde{L}$ transform in the way shown in Eq. (2.2) of Ref. [504]. (I am using the equation numbers from the published JHEP version, not the arXiv eprint.) That is, since

$$\begin{bmatrix} L_+ \\ L_- \end{bmatrix} \quad \to \quad e^{ig'\zeta\sigma_3\alpha} \begin{bmatrix} L_+ \\ L_- \end{bmatrix} \tag{G.2}$$

under a $U(1)'$ phase transformation, we find

$$\tilde{L} \quad \to \quad \left(V e^{ig'\zeta\sigma_3\alpha} V^\dagger \right) \tilde{L} = e^{ig'\zeta\sigma_1\alpha} \tilde{L} \equiv U_1(\alpha) \tilde{L} \,. \tag{G.3}$$

The matrix which relates $\tilde{L}$ to the flavor eigenstates is given in Eq. (2.4) as

$$\begin{bmatrix} L_\alpha \\ L_\beta \end{bmatrix} = \begin{bmatrix} \cos\theta_L & -\sin\theta_L \\ \sin\theta_L & \cos\theta_L \end{bmatrix} \begin{bmatrix} \tilde{L}_\alpha \\ \tilde{L}_\beta \end{bmatrix}. \tag{G.4}$$

Therefore,

$$\begin{aligned} \begin{bmatrix} L_\alpha \\ L_\beta \end{bmatrix} &= \begin{bmatrix} \cos\theta_L & -\sin\theta_L \\ \sin\theta_L & \cos\theta_L \end{bmatrix} \begin{bmatrix} \tilde{L}_\alpha \\ \tilde{L}_\beta \end{bmatrix} \\ &= \begin{bmatrix} \cos\theta_L & -\sin\theta_L \\ \sin\theta_L & \cos\theta_L \end{bmatrix} V \begin{bmatrix} L_+ \\ L_- \end{bmatrix} \end{aligned}$$

$$
\begin{aligned}
&= \begin{bmatrix} \cos\left(\theta_L + \frac{\pi}{4}\right) & -\sin\left(\theta_L + \frac{\pi}{4}\right) \\ \sin\left(\theta_L + \frac{\pi}{4}\right) & \cos\left(\theta_L + \frac{\pi}{4}\right) \end{bmatrix} \begin{bmatrix} L_+ \\ L_- \end{bmatrix} \\
&= U_L \begin{bmatrix} L_+ \\ L_- \end{bmatrix} , \qquad \text{(G.5)}
\end{aligned}
$$

and we find that Farzan and Shoemaker's θ_L is related to our δ_L via

$$\delta_L \;=\; \theta_L + \frac{\pi}{4} \,. \qquad \text{(G.6)}$$

For the right-handed charged leptons Farzan and Shoemaker use two different notations which are actually equivalent. $\tilde{R}$ defined in Eq. (2.6) of Ref. [504] is given by

$$\tilde{R} \;\equiv\; \begin{bmatrix} \tilde{\ell}_{R\alpha} \\ \tilde{\ell}_{R\beta} \end{bmatrix} \;\equiv\; V \begin{bmatrix} \ell_{R+} \\ \ell_{R-} \end{bmatrix} \,. \qquad \text{(G.7)}$$

This transforms as

$$\tilde{R} \quad \to \quad = U_1(\alpha)\tilde{R} \,, \qquad \text{(G.8)}$$

just like $\tilde{L}$. Noting that

$$U_1^\dagger(\alpha)U_1(\alpha) \;=\; 1 \,, \qquad U_1^\dagger(\alpha)\sigma_1 U_1(\alpha) \;=\; \sigma_1 \,, \qquad \text{(G.9)}$$

we can write the $U(1)'$ invariant Yukawa interactions shown in Eq. (2.7) of Ref. [504]:

$$
\begin{aligned}
& b_0 \tilde{R}^\dagger H^\dagger \tilde{L} + b_1 \tilde{R}^\dagger \sigma_1 H^\dagger \tilde{L} \\
&= b_0 \begin{bmatrix} \overline{\ell_{R+}} & \overline{\ell_{R-}} \end{bmatrix} V^\dagger V H^\dagger \begin{bmatrix} L_+ \\ L_- \end{bmatrix} + b_1 \begin{bmatrix} \overline{\ell_{R+}} & \overline{\ell_{R-}} \end{bmatrix} V^\dagger \sigma_1 V H^\dagger \begin{bmatrix} L_+ \\ L_- \end{bmatrix} \\
&= b_0 \begin{bmatrix} \overline{\ell_{R+}} & \overline{\ell_{R-}} \end{bmatrix} H^\dagger \begin{bmatrix} L_+ \\ L_- \end{bmatrix} + b_1 \begin{bmatrix} \overline{\ell_{R+}} & \overline{\ell_{R-}} \end{bmatrix} \sigma_3 H^\dagger \begin{bmatrix} L_+ \\ L_- \end{bmatrix} \\
&= \underbrace{(b_0 + b_1)}_{= f_+} \overline{\ell_{R+}} H^\dagger L_+ + \underbrace{(b_0 - b_1)}_{= f_-} \overline{\ell_{R-}} H^\dagger L_- \,. \qquad \text{(G.10)}
\end{aligned}
$$

The Φ field introduced in the un-numbered equation after Eq. (2.8) is related to our extra Higgs fields via

$$
\begin{aligned}
\Phi \;&\equiv\; \begin{bmatrix} \Phi_{11} & \Phi_{12} \\ \Phi_{21} & \Phi_{22} \end{bmatrix} \\
&\equiv\; V \begin{bmatrix} H^\dagger_{-+} & H^\dagger_{--} \\ H^\dagger_{++} & H^\dagger_{+-} \end{bmatrix} V^\dagger \\
&=\; \frac{1}{2} \begin{bmatrix} H^\dagger_{-+} + H^\dagger_{+-} - H^\dagger_{++} - H^\dagger_{--} & H^\dagger_{-+} - H^\dagger_{+-} - H^\dagger_{++} + H^\dagger_{--} \\ H^\dagger_{-+} - H^\dagger_{+-} + H^\dagger_{++} - H^\dagger_{--} & H^\dagger_{-+} + H^\dagger_{+-} + H^\dagger_{++} + H^\dagger_{--} \end{bmatrix} \,. \qquad \text{(G.11)}
\end{aligned}
$$

This relation can be inverted to give

$$\begin{aligned}\begin{bmatrix} H^\dagger_{-+} & H^\dagger_{--} \\ H^\dagger_{++} & H^\dagger_{+-} \end{bmatrix} &\equiv V^\dagger \begin{bmatrix} \Phi_{11} & \Phi_{12} \\ \Phi_{21} & \Phi_{22} \end{bmatrix} V \\ &= \frac{1}{2}\begin{bmatrix} \Phi_{11}+\Phi_{12}+\Phi_{21}+\Phi_{22} & -\Phi_{11}+\Phi_{12}-\Phi_{21}+\Phi_{22} \\ -\Phi_{11}-\Phi_{12}+\Phi_{21}+\Phi_{22} & \Phi_{11}-\Phi_{12}-\Phi_{21}+\Phi_{22} \end{bmatrix} . \end{aligned} \tag{G.12}$$

The transformation property of Φ can be shown to be

$$\Phi \quad \to \quad U_1(\alpha)\Phi U_1^\dagger(\alpha) \, . \tag{G.13}$$

Four $U(1)'$ invariant Yukawa couplings can be constructed from Φ, $\tilde{L}$, and $\tilde{R}$:

$$\begin{aligned} \tilde{R}^\dagger\Phi\tilde{L} &= \overline{\ell_{R+}}H^\dagger_{-+}L_+ + \overline{\ell_{R-}}H^\dagger_{+-}L_- + \overline{\ell_{R+}}H^\dagger_{--}L_- + \overline{\ell_{R-}}H^\dagger_{++}L_+ \, , \\ \tilde{R}^\dagger\Phi\sigma_1\tilde{L} &= \overline{\ell_{R+}}H^\dagger_{-+}L_+ - \overline{\ell_{R-}}H^\dagger_{+-}L_- - \overline{\ell_{R+}}H^\dagger_{--}L_- + \overline{\ell_{R-}}H^\dagger_{++}L_+ \, , \\ \tilde{R}^\dagger\sigma_1\Phi\tilde{L} &= \overline{\ell_{R+}}H^\dagger_{-+}L_+ - \overline{\ell_{R-}}H^\dagger_{+-}L_- + \overline{\ell_{R+}}H^\dagger_{--}L_- - \overline{\ell_{R-}}H^\dagger_{++}L_+ \, , \\ \tilde{R}^\dagger\sigma_1\Phi\sigma_1\tilde{L} &= \overline{\ell_{R+}}H^\dagger_{-+}L_+ + \overline{\ell_{R-}}H^\dagger_{+-}L_- - \overline{\ell_{R+}}H^\dagger_{--}L_- - \overline{\ell_{R-}}H^\dagger_{++}L_+ \, . \end{aligned} \tag{G.14}$$

Of these, Farzan and Shoemaker only mention the first one:

$$\begin{aligned} c_0\tilde{R}^\dagger\Phi\tilde{L} &= c_0 \begin{bmatrix} \overline{\ell_{R+}} & \overline{\ell_{R-}} \end{bmatrix} V^\dagger V \begin{bmatrix} H^\dagger_{-+} & H^\dagger_{--} \\ H^\dagger_{++} & H^\dagger_{+-} \end{bmatrix} V^\dagger V \begin{bmatrix} L_+ \\ L_- \end{bmatrix} \\ &= c_0\left(\overline{\ell_{R+}}H^\dagger_{-+}L_+ + \overline{\ell_{R-}}H^\dagger_{+-}L_- + \overline{\ell_{R+}}H^\dagger_{--}L_- + \overline{\ell_{R-}}H^\dagger_{++}L_+\right) \, , \end{aligned} \tag{G.15}$$

which includes the redundant couplings with H_{-+} and H_{+-}. The above relations can be inverted to yield

$$\begin{aligned} \overline{\ell_{R+}}H^\dagger_{-+}L_+ &= \frac{1}{4}\left(\tilde{R}^\dagger\Phi\tilde{L} + \tilde{R}^\dagger\Phi\sigma_1\tilde{L} + \tilde{R}^\dagger\sigma_1\Phi\tilde{L} + \tilde{R}^\dagger\sigma_1\Phi\sigma_1\tilde{L}\right) \, , \\ \overline{\ell_{R-}}H^\dagger_{+-}L_- &= \frac{1}{4}\left(\tilde{R}^\dagger\Phi\tilde{L} - \tilde{R}^\dagger\Phi\sigma_1\tilde{L} - \tilde{R}^\dagger\sigma_1\Phi\tilde{L} + \tilde{R}^\dagger\sigma_1\Phi\sigma_1\tilde{L}\right) \, , \\ \overline{\ell_{R+}}H^\dagger_{--}L_- &= \frac{1}{4}\left(\tilde{R}^\dagger\Phi\tilde{L} - \tilde{R}^\dagger\Phi\sigma_1\tilde{L} + \tilde{R}^\dagger\sigma_1\Phi\tilde{L} - \tilde{R}^\dagger\sigma_1\Phi\sigma_1\tilde{L}\right) \, , \\ \overline{\ell_{R-}}H^\dagger_{++}L_+ &= \frac{1}{4}\left(\tilde{R}^\dagger\Phi\tilde{L} + \tilde{R}^\dagger\Phi\sigma_1\tilde{L} - \tilde{R}^\dagger\sigma_1\Phi\tilde{L} - \tilde{R}^\dagger\sigma_1\Phi\sigma_1\tilde{L}\right) \, . \end{aligned} \tag{G.16}$$

So it is always possible to choose the Yukawa couplings in such a way that only the bottom two linear combinations survive, *e.g.*,

$$c_0\left(\overline{\ell_{R+}}H^\dagger_{--}L_- + \overline{\ell_{R-}}H^\dagger_{++}L_+\right) \; = \; \frac{c_0}{2}\left(\tilde{R}^\dagger\Phi\tilde{L} - \tilde{R}^\dagger\sigma_1\Phi\sigma_1\tilde{L}\right) \, . \tag{G.17}$$

Our expression for $\tan(2\delta_L)$ with $c_+ = c_- = c_0$ reads

$$\tan(2\delta_L) \;\approx\; \frac{c_0\langle H^0\rangle\left(f_+\langle H^0_{--}\rangle + f_-\langle H^0_{++}\rangle\right)}{m^2_\beta}$$

$$
\begin{aligned}
&= \frac{c_0\langle H^0\rangle\left[(b_0+b_1)\langle H^0_{--}\rangle + (b_0-b_1)\langle H^0_{++}\rangle\right]}{m_\beta^2} \\
&= \frac{c_0\langle H^0\rangle\left[b_0\langle H^0_{--}+H^0_{++}\rangle + b_1\langle H^0_{--}-H^0_{++}\rangle\right]}{m_\beta^2} \\
&= \frac{2c_0\langle H^0\rangle\left[b_0\langle \Phi^0_{22}-\Phi^0_{11}\rangle + b_1\langle \Phi^0_{12}-\Phi^0_{21}\rangle\right]}{m_\beta^2} \; . \qquad \text{(G.18)}
\end{aligned}
$$

Assuming that δ_L is small, we can argue that

$$
\tan(2\delta_L) \;\approx\; \sin(2\delta_L) \;=\; \sin 2\left(\theta_L+\frac{\pi}{4}\right) \;=\; \sin\left(2\theta_L+\frac{\pi}{2}\right) \;=\; \cos 2\theta_L \; , \qquad \text{(G.19)}
$$

and we recover the expression for $\cos 2\theta_L$ given in the next equation.

The other notation used for the charged right-handed leptons is that given in Eq. (2.12):

$$
\tilde{\ell}_{R\alpha} \;=\; \ell_{R+} \; , \qquad \tilde{\ell}_{R\beta} \;=\; \ell_{R-} \; . \qquad \text{(G.20)}
$$

The Higgs doublets of Eq. (2.13) are related to our fields via

$$
\Phi_1 \;\equiv\; \begin{bmatrix}\phi_{1\alpha}\\ \phi_{1\beta}\end{bmatrix} \;\equiv\; V\begin{bmatrix}H_{-+}\\ H_{--}\end{bmatrix} \; , \qquad \Phi_2 \;\equiv\; \begin{bmatrix}\phi_{2\alpha}\\ \phi_{2\beta}\end{bmatrix} \;\equiv\; V\begin{bmatrix}H_{++}\\ H_{+-}\end{bmatrix} \; . \qquad \text{(G.21)}
$$

These transform as

$$
\Phi_1 \;\to\; e^{-ig'\zeta\alpha}U_1(\alpha)\Phi_1 \; , \qquad \Phi_2 \;\to\; e^{+ig'\zeta\alpha}U_1(\alpha)\Phi_2 \; . \qquad \text{(G.22)}
$$

The transformations shown in Eq. (2.13) are actually incorrect if one wants the Yukawa couplings shown in Eq. (2.14) to be $U(1)'$ invariant:

$$
\begin{aligned}
\tilde{\ell}^\dagger_{R\alpha}\Phi_1^\dagger\tilde{L} &= \overline{\ell_{R+}}\begin{bmatrix}H^\dagger_{-+} & H^\dagger_{--}\end{bmatrix}V^\dagger V\begin{bmatrix}L_+\\ L_-\end{bmatrix} \;=\; \overline{\ell_{R+}}H^\dagger_{-+}L_+ + \overline{\ell_{R+}}H^\dagger_{--}L_- \; , \\
\tilde{\ell}^\dagger_{R\alpha}\Phi_1^\dagger\sigma_1\tilde{L} &= \overline{\ell_{R+}}\begin{bmatrix}H^\dagger_{-+} & H^\dagger_{--}\end{bmatrix}V^\dagger\sigma_1 V\begin{bmatrix}L_+\\ L_-\end{bmatrix} \;=\; \overline{\ell_{R+}}H^\dagger_{-+}L_+ - \overline{\ell_{R+}}H^\dagger_{--}L_- \; , \\
\tilde{\ell}^\dagger_{R\beta}\Phi_2^\dagger\tilde{L} &= \overline{\ell_{R-}}\begin{bmatrix}H^\dagger_{++} & H^\dagger_{+-}\end{bmatrix}V^\dagger V\begin{bmatrix}L_+\\ L_-\end{bmatrix} \;=\; \overline{\ell_{R-}}H^\dagger_{++}L_+ + \overline{\ell_{R-}}H^\dagger_{+-}L_- \; , \\
\tilde{\ell}^\dagger_{R\beta}\Phi_2^\dagger\sigma_1\tilde{L} &= \overline{\ell_{R-}}\begin{bmatrix}H^\dagger_{++} & H^\dagger_{+-}\end{bmatrix}V^\dagger\sigma_1 V\begin{bmatrix}L_+\\ L_-\end{bmatrix} \;=\; \overline{\ell_{R-}}H^\dagger_{++}L_+ - \overline{\ell_{R-}}H^\dagger_{+-}L_- \; . \qquad \text{(G.23)}
\end{aligned}
$$

As we can see, the so called "two solutions" of Ref. [504] are actually exactly the same model which becomes obvious if we write the model in terms of fields with definite $U(1)'$ charges.

G.2 Anomaly Cancellation in the Farzan and Shoemaker Model

When gauging baryon and lepton numbers as a $U(1)$ symmetry with only the SM fermion content, it is known that the anomaly-free combinations are $B-(aL_e+bL_\mu+cL_\tau)$ with

$a+b+c=3$, or $L_\alpha - L_\beta$ for some pair of flavors α and β (see Ref. [491] and references therein). The new $U(1)'$ gauge group considered here corresponds to gauging $3\eta B + \zeta(L_\alpha - L_\beta)$, which is only anomaly-free when $\eta = 0$.

Farzan and Shoemaker propose to cancel the unwanted anomalies by the introduction of new leptons. First, let's see what anomalies need to be canceled. Following Refs. [494] and [496], we use the notation

$$\mathcal{A}(G_1 \otimes G_2 \otimes G_3) \;=\; \frac{1}{2}\mathrm{Tr}\Big[T_1\left\{T_2, T_3\right\}\Big] \;, \tag{G.24}$$

where T_i is the generator of the group G_i. The anomalies in the baryon sector are

$$\begin{aligned}
\mathcal{A}_1\left(SU(3)_C^2 \otimes U(1)'\right) &= 0 \;, \\
\mathcal{A}_2\left(SU(2)_L^2 \otimes U(1)'\right) &= \frac{9\eta}{2} \;, \\
\mathcal{A}_3\left(U(1)_Y^2 \otimes U(1)'\right) &= -\frac{9\eta}{2} \;, \\
\mathcal{A}_4\left(U(1)_Y \otimes U(1)'^2\right) &= 0 \;, \\
\mathcal{A}_5\left(U(1)'\right) &= 0 \;, \\
\mathcal{A}_6\left(U(1)'^3\right) &= 0 \;,
\end{aligned} \tag{G.25}$$

while those in the lepton sector are

$$\begin{aligned}
\mathcal{A}_7\left(SU(3)_C^2 \otimes U(1)'\right) &= 0 \;, \\
\mathcal{A}_8\left(SU(2)_L^2 \otimes U(1)'\right) &= 0 \;, \\
\mathcal{A}_9\left(U(1)_Y^2 \otimes U(1)'\right) &= 0 \;, \\
\mathcal{A}_{10}\left(U(1)_Y \otimes U(1)'^2\right) &= 0 \;, \\
\mathcal{A}_{11}\left(U(1)'\right) &= 0 \;, \\
\mathcal{A}_{12}\left(U(1)'^3\right) &= 0 \;.
\end{aligned} \tag{G.26}$$

So we need to cancel $\mathcal{A}_2$ and $\mathcal{A}_3$ without introducing new ones. Ref. [504] argues that the introduction of one extra lepton generation with charge

$$L_4 = \begin{bmatrix}\nu_{L4} \\ \ell_{L4}\end{bmatrix} \sim \left(1, 2, -\frac{1}{2}, -9\eta\right) \;, \quad \ell_{R4} \sim (1, 1, -1, -9\eta) \;, \tag{G.27}$$

would do the job, but opts for two generations with charges

$$\begin{aligned}
L_4 = \begin{bmatrix}\nu_{L4} \\ \ell_{L4}\end{bmatrix} &\sim \left(1, 2, -\frac{1}{2}, -\frac{9}{2}\eta\right) \;, \quad \ell_{R4} \sim \left(1, 1, -1, -\frac{9}{2}\eta\right) \;, \\
L_5 = \begin{bmatrix}\nu_{L5} \\ \ell_{L5}\end{bmatrix} &\sim \left(1, 2, -\frac{1}{2}, -\frac{9}{2}\eta\right) \;, \quad \ell_{R5} \sim \left(1, 1, -1, -\frac{9}{2}\eta\right) \;,
\end{aligned} \tag{G.28}$$

so that the Witten anomaly [525] is also taken care of. Unfortunately, the introduction of these lepton generations will reintroduce the following anomalies per generation:

$$\mathcal{A}\left(SU(2)_L^2 \otimes U(1)_Y\right) \;=\; -\frac{1}{4}$$

$$\mathcal{A}\left(U(1)_Y^3\right) \;=\; +\frac{3}{4}\,. \tag{G.29}$$

Within the SM, these anomalies are canceled by the quarks. So introducing lepton generations without the corresponding quark generations does not work.

In any case, in order to obtain an anomaly-free theory with $\eta \neq 0$, we need to introduce new fermions which are required to be very heavy to avoid constraints from direct searches.

G.3 Symmetry Breaking in the Farzan and Shoemaker Model

The neutral components of the Higgs doublets H, H_{++}, and H_{--} are assumed to develop VEV's. If we assume the standard Mexican hat potential for each, this will lead to nine Goldstone bosons, of which only four can be absorbed into the $W^{\pm}$, Z, and Z'. So we need a way to make the unwanted Goldstone bosons heavy.

Let's first take a look at what the mass spectrum of the gauge bosons will be. The gauge coupling of the Higgses are given by

$$(D_\mu H)^\dagger (D^\mu H) + (D_\mu H_{++})^\dagger (D^\mu H_{++}) + (D_\mu H_{--})^\dagger (D^\mu H_{--})\,, \tag{G.30}$$

where

$$\begin{aligned}
D_\mu H &= \left(\partial_\mu - i\frac{g_2}{2}\vec{W}_\mu\cdot\vec{\sigma} - i\frac{g_1}{2}B_\mu\right) H\,,\\
D_\mu H_{++} &= \left(\partial_\mu - i\frac{g_2}{2}\vec{W}_\mu\cdot\vec{\sigma} - i\frac{g_1}{2}B_\mu - 2i\zeta g' Z'_\mu\right) H_{++}\,,\\
D_\mu H_{--} &= \left(\partial_\mu - i\frac{g_2}{2}\vec{W}_\mu\cdot\vec{\sigma} - i\frac{g_1}{2}B_\mu + 2i\zeta g' Z'_\mu\right) H_{--}\,.
\end{aligned} \tag{G.31}$$

Write the components of H, H_{++}, and H_{--} as

$$H = \begin{bmatrix} H^+ \\ H^0 \end{bmatrix}\,, \qquad H_{++} = \begin{bmatrix} H^+_{++} \\ H^0_{++} \end{bmatrix}\,, \qquad H_{--} = \begin{bmatrix} H^+_{--} \\ H^0_{--} \end{bmatrix}\,, \tag{G.32}$$

and assume $\langle H^0\rangle = v/\sqrt{2}$, $\langle H^0_{++}\rangle = v_+/\sqrt{2}$, and $\langle H^0_{--}\rangle = v_-/\sqrt{2}$ will be non-zero. Then, the following gauge boson mass terms will be generated:

$$\begin{aligned}
&\frac{g_2^2}{4} W_\mu^+ W^{-\mu}\left(v^2 + v_+^2 + v_-^2\right)\\
&+ \left(\frac{g_2}{2}W_{3\mu} - \frac{g_1}{2}B_\mu\right)\left(\frac{g_2}{2}W_3^\mu - \frac{g_1}{2}B^\mu\right)\frac{v^2}{2}\\
&+ \left(\frac{g_2}{2}W_{3\mu} - \frac{g_1}{2}B_\mu - 2\zeta g' Z'_\mu\right)\left(\frac{g_2}{2}W_3^\mu - \frac{g_1}{2}B^\mu - 2\zeta g' Z'^\mu\right)\frac{v_+^2}{2}
\end{aligned}$$

$$+\left(\frac{g_2}{2}W_{3\mu}-\frac{g_1}{2}B_\mu+2\zeta g'Z'_\mu\right)\left(\frac{g_2}{2}W_3^\mu-\frac{g_1}{2}B^\mu+2\zeta g'Z'^\mu\right)\frac{v_-^2}{2}\,, \tag{G.33}$$

where

$$W_\mu^\pm \;=\; \frac{1}{\sqrt{2}}\left(W_{1\mu}\mp W_{2\mu}\right)\,. \tag{G.34}$$

So the mass of $W^\pm$ in this model is

$$M_W \;=\; \frac{g_2}{2}\sqrt{v^2+v_+^2+v_-^2}\,. \tag{G.35}$$

The mass matrix for the neutral gauge bosons is

$$M \;=\; \frac{1}{4}\begin{bmatrix} g_1^2\left(v^2+v_+^2+v_-^2\right) & -g_1g_2\left(v^2+v_+^2+v_-^2\right) & 4\zeta g_1g'\left(v_+^2-v_-^2\right) \\ -g_1g_2\left(v^2+v_+^2+v_-^2\right) & g_2^2\left(v^2+v_+^2+v_-^2\right) & -4\zeta g_2g'\left(v_+^2-v_-^2\right) \\ 4\zeta g_1g'\left(v_+^2-v_-^2\right) & -4\zeta g_2g'\left(v_+^2-v_-^2\right) & 16\zeta^2g'^2\left(v_+^2+v_-^2\right) \end{bmatrix}\,, \tag{G.36}$$

where the rows and columns correspond to B, W_3, and Z' in this order. If $v_+=v_-\equiv w/\sqrt{2}$, this reduces to

$$M \;=\; \frac{1}{4}\begin{bmatrix} g_1^2\left(v^2+w^2\right) & -g_1g_2\left(v^2+w^2\right) & 0 \\ -g_1g_2\left(v^2+w^2\right) & g_2^2\left(v^2+w^2\right) & 0 \\ 0 & 0 & 16\zeta^2g'^2w^2 \end{bmatrix}\,. \tag{G.37}$$

Note that this would prevent the Z' from mixing with the B or the W_3, and not change the value of the Weinberg angle or the linear combinations of W_3 and B that constitute the photon and the Z.

Indeed, to diagonalize this matrix, we define

$$\tan\theta_W \;=\; \frac{g_1}{g_2}\,, \qquad U \;=\; \begin{bmatrix} \cos\theta_W & -\sin\theta_W & 0 \\ \sin\theta_W & \cos\theta_W & 0 \\ 0 & 0 & 1 \end{bmatrix}\,. \tag{G.38}$$

Then

$$\begin{aligned} M' \;&=\; U^\dagger M U \\ &=\; \frac{1}{4}\begin{bmatrix} 0 & 0 & 0 \\ 0 & \left(g_1^2+g_2^2\right)\left(v^2+w^2\right) & 0 \\ 0 & 0 & 16\zeta^2g'^2w^2 \end{bmatrix} \\ &=\; \begin{bmatrix} 0 & 0 & 0 \\ 0 & M_Z^2 & 0 \\ 0 & 0 & M_{Z'}^2 \end{bmatrix}\,. \end{aligned} \tag{G.39}$$

So the masses of the massive gauge bosons are

$$M_W \;=\; \frac{g_2}{2}\sqrt{v^2+w^2}\,, \quad M_Z \;=\; \frac{\sqrt{g_1^2+g_2^2}}{2}\sqrt{v^2+w^2}\,, \quad M_{Z'} \;=\; 2\zeta g'w\,. \tag{G.40}$$

The mass eigenfields are

$$\begin{bmatrix} A^\mu \\ Z^\mu \\ Z'^\mu \end{bmatrix} = U^\dagger \begin{bmatrix} B^\mu \\ W_3^\mu \\ Z'^\mu \end{bmatrix} = \begin{bmatrix} B^\mu \cos\theta_W + W_3^\mu \sin\theta_W \\ -B^\mu \sin\theta_W + W_3^\mu \cos\theta_W \\ Z'^\mu \end{bmatrix} , \tag{G.41}$$

and the currents that couple to these bosons are

$$\begin{aligned} \begin{bmatrix} eJ_Q^\mu \\ g_Z J_Z^\mu \\ g' J_{Z'}^\mu \end{bmatrix} &= U^\dagger \begin{bmatrix} g_1 J_Y^\mu \\ g_2 J_3^\mu \\ g' J_{Z'}^\mu \end{bmatrix} \\ &= \begin{bmatrix} g_1 J_Y^\mu \cos\theta_W + g_2 J_3^\mu \sin\theta_W \\ -g_1 J_Y^\mu \sin\theta_W + g_2 J_3^\mu \cos\theta_W \\ g' J_{Z'}^\mu \end{bmatrix} \\ &= \begin{bmatrix} \dfrac{g_1 g_2}{\sqrt{g_1^2+g_2^2}} \left(J_Y^\mu + J_3^\mu\right) \\ \sqrt{g_1^2+g_2^2}\left(J_3^\mu - \sin^2\theta_W J_Q^\mu\right) \\ g' J_{Z'}^\mu \end{bmatrix} , \end{aligned} \tag{G.42}$$

that is

$$e = \frac{g_1 g_2}{\sqrt{g_1^2+g_2^2}} , \quad g_Z = \sqrt{g_1^2+g_2^2} , \quad J_Q^\mu = J_3^\mu + J_Y^\mu , \quad J_Z^\mu = J_3^\mu - \sin^2\theta_W J_Y^\mu . \tag{G.43}$$

The only difference from the SM is that the Higgs VEV v is replaced by $\sqrt{v^2+w^2}$.

This is a nice result since the Z' does not mix with the photon or the Z at tree level, and we can make the Z' light by taking $\zeta g' w$ to be small. This can be accomplished by either taking the coupling $\zeta g'$ too be small, or the $U(1)'$-charged Higgs VEV w to be small. However, if ζ is tiny, one may need to take w to be large to obtain the $M_{Z'}$ that one wants.

G.4 Bounds of Z' Studied in the Original Model

In Ref. [504], the experimental bounds considered are in two categories, with Z' being produced on-shell and with virtual Z' being a mediator of the process, respectively. We first look at the on-shell Z' production. Since the coupling constant for the new gauge sector is different for quarks and leptons, being g' and $\zeta g'$ respectively, we need to constrain the quark vertex and lepton vertex separately. Diagrams in the upper panel of Fig. G.1 correspond to the Z' decay processes $Z' \to \ell^+\ell^-$, $Z' \to \nu\overline{\nu}$, and $Z' \to q\overline{q}$. In the lower panel of Fig. G.1, the diagrams correspond to the Z' production processes $\ell_\beta \to \ell_\alpha Z'$ and $\pi^0 \to Z'\gamma$. Not all processes are kinematically allowed when a specific value of $m_{Z'}$ is chosen. As a result, not all the experimental bounds apply to constrain g' and $\zeta g'$. The Z' decay modes kinematically allowed with the choice of $M_{Z'}$ are listed in Table G.1. The corresponding production processes

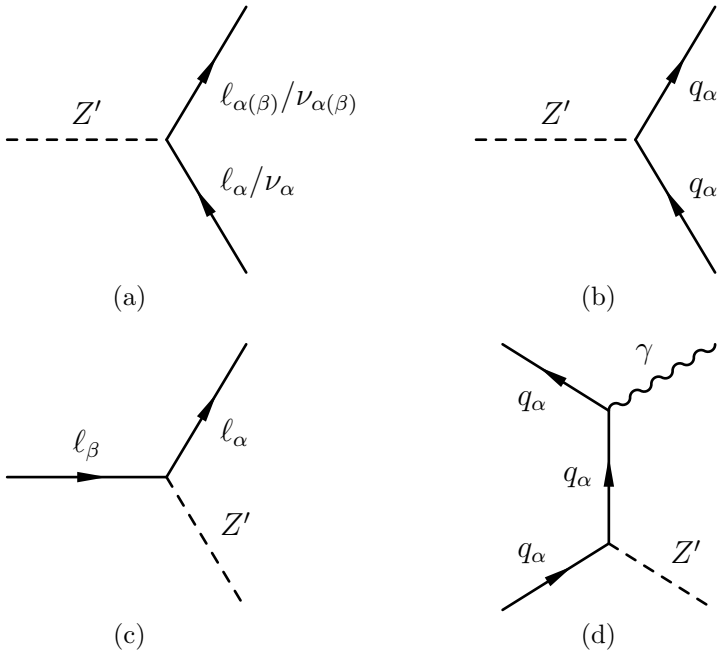

Figure G.1: Upper panel: the vertices responsible for Z' decay. (a) Z' decays to a pair of leptons. (b) Z' decays to hadrons. Lower panel: the vertices for Z' production. (c) lepton decays to Z'. (d) π^0 decays to Z'.

of Z' are listed in Table G.2. The processes that are considered in Ref. [504] are highlighted in red in Tables G.1 and G.2. Combining these production/decay modes, we get the processes that might be affected by the introduction of Z', with expreimental data from Ref. [1].

$$
\begin{aligned}
&\{\alpha,\beta\}=\{e,\mu\},\\
&\qquad m_{Z'}<m_\mu\mu\to Z'e\to eee, && (<10^{-12}, CF=90\%)\\
&\qquad m_{Z'}<m_{\pi^0}\pi^0\to\gamma Z'\to\gamma ee, && (1.174\pm0.035)\%\\
&\{\alpha,\beta\}=\{\mu,\tau\},\\
&\qquad m_{Z'}>2m_\mu\tau\to Z'\mu\to\mu\mu\mu, && (<2.1\times10^{-8}, CL=90\%)\\
&\qquad m_{Z'}<m_{\pi^0}\pi^0\to\gamma Z'\to\gamma+inv., && (<6\times10^{-4})\\
&\qquad \tau\to\mu Z', && (<5\times10^{-3}, CL=95\%)\\
&\{\alpha,\beta\}=\{e,\tau\},\\
&\qquad all\ region\tau\to eZ'\to eee, && (<2.7\times10^{-8})\\
&\qquad \tau\to eZ', && (<2.7\times10^{-3})\\
&\qquad m_{Z'}<m_{\pi^0}\pi^0\to\gamma Z'\to\gamma ee. && (1.174\pm0.035)\%
\end{aligned}
$$

Next, the authors of Ref. [504] translate the bounds to constraints on g', ζ, and ε_{ij}^{qP} at the end, at different $m_{Z'}$. Since $\{\alpha,\beta\}=\{e,\tau\}$ and $\{\alpha,\beta\}=\{e,\mu\}$ are heavily constrained by

	$\alpha = e$ $\beta = \mu$	$\alpha = \mu$ $\beta = \tau$	$\alpha = e$ $\beta = \tau$
$2m_\mu < m_{Z'} \ll m_\tau$	$ee, e\mu, \mu\mu, \nu\nu + had$	$\mu\mu, \nu\nu + had$	$ee, \nu\nu + had$
$m_\mu < m_{Z'} < 2m_\mu$	$ee, e\mu, \nu\nu + had$	$\nu\nu + had$	$ee, \nu\nu + had$
$m_{\pi^0} < m_{Z'} < m_\mu$	$ee, \nu\nu + had$	$\nu\nu + had$	$ee, \nu\nu + had$
$m_{Z'} < m_{\pi^0}$	$ee, \nu\nu$	$\nu\nu$	$ee, \nu\nu$

Table G.1: The decay modes of Z'.

	$\alpha = e$ $\beta = \mu$	$\alpha = \mu$ $\beta = \tau$	$\alpha = e$ $\beta = \tau$
$2m_\mu < m_{Z'} \ll m_\tau$		$\tau \to \mu Z'$	$\tau \to e Z'$
$m_\mu < m_{Z'} < 2m_\mu$		$\tau \to \mu Z'$	$\tau \to e Z'$
$m_{\pi^0} < m_{Z'} < m_\mu$	$\mu \to e Z'$	$\tau \to \mu Z'$	$\tau \to e Z'$
$m_{Z'} < m_{\pi^0}$	$\mu \to e Z'$	$\tau \to \mu Z'$	$\tau \to e Z'$
	$\pi^0 \to \gamma Z'$	$\pi^0 \to \gamma Z'$	$\pi^0 \to \gamma Z'$

Table G.2: The production modes of Z'.

electron final state, the only option is $\{\alpha, \beta\} = \{\mu, \tau\}$.

Bounds on the qqZ' vertex:

- When $m_{Z'} < m_{\pi^0}$, with $\pi^0 \to \gamma Z' \to \gamma\nu\bar{\nu}$, we have

$$\text{Br}(\pi^0 \to \gamma Z') \leq \text{Br}(\pi^0 \to \gamma\nu\bar{\nu}) < 6 \times 10^{-4}. \tag{G.44}$$

  This translates to

$$g' < 2 \times 10^{-3}, \qquad \text{when } m_{Z'} < m_{\pi^0} = 135\text{MeV}. \tag{G.45}$$

- For $m_{\pi^0} < m_{Z'} < 2m_\mu$, all current bounds of g' are for the leptonic coupling $\zeta g'$, so it does not apply. The only requirement is $(g')^2/4\pi < \alpha$, i.e. it is smaller than strong coupling.

- For $m_{Z'} > 2m_\mu$, the bounds are from $Z' \to \mu\mu$, from BaBar and KLOE-2, which is fairly tight.

Bounds on the $\ell\ell Z'$ vertex:

The lepton vertex is determined by the process $\ell_\beta \to Z'\ell_\alpha$, which gives

$$\Gamma(\ell_\beta \to Z'\ell_\alpha) = \frac{(g')^2\zeta^2}{32\pi}\frac{m_{\ell_\beta}^3}{m_{Z'}^2}(\sin^2 2\delta_L + \sin^2 2\delta_R). \tag{G.46}$$

- $m_{Z'} < m_{\pi^0}$, the bound for g' is strong. For example, for $m_{Z'} = 10$ MeV, we can generate $\varepsilon_{\mu\tau}^{qP} \sim 10^{-3}$ and $\left|\varepsilon_{\tau\tau}^{qP} - \varepsilon_{\mu\mu}^{qP}\right| \sim 0.01$.
- $m_{\pi^0} < m_{Z'} < 2m_\mu$, the bound on g' is relaxed quite a bit so we have larger NSI. For example, for $m_{Z'} = 140$ MeV, we can generate $\varepsilon_{\mu\tau}^{qP} \sim 5 \times 10^{-3}$ and $\left|\varepsilon_{\tau\tau}^{qP} - \varepsilon_{\mu\mu}^{qP}\right| \sim 0.05$.
- $m_{Z'} > 2m_\mu$, the bounds on $Z' \to \mu\mu$ is too tight.

Bibliography

[1] C. Patrignani et al. Review of Particle Physics. *Chin. Phys.*, C40(10):100001, 2016.

[2] Ali H. Chamseddine, Alain Connes, and Walter D. van Suijlekom. Grand Unification in the Spectral Pati-Salam Model. *JHEP*, 11:011, 2015.

[3] J. Charles, Andreas Hocker, H. Lacker, S. Laplace, F. R. Le Diberder, J. Malcles, J. Ocariz, M. Pivk, and L. Roos. CP violation and the CKM matrix: Assessing the impact of the asymmetric B factories. *Eur. Phys. J.*, C41(1):1–131, 2005.

[4] Pilar Coloma. Non-Standard Interactions in propagation at the Deep Underground Neutrino Experiment. *JHEP*, 03:016, 2016.

[5] Katsuhiro Asano and Hisakazu Minakata. Large-Theta(13) Perturbation Theory of Neutrino Oscillation for Long-Baseline Experiments. *JHEP*, 1106:022, 2011.

[6] S. I. Dolinsky et al. Summary of experiments with the neutral detector at the e+ e- storage ring VEPP-2M. *Phys. Rept.*, 202:99–170, 1991.

[7] M. Lindner and M. Weiser. Gauge coupling unification in left-right symmetric models. *Phys. Lett.*, B383:405–414, 1996.

[8] R. Slansky. Group Theory for Unified Model Building. *Phys. Rept.*, 79:1–128, 1981.

[9] M.C. Gonzalez-Garcia, Michele Maltoni, Jordi Salvado, and Thomas Schwetz. Global fit to three neutrino mixing: critical look at present precision. 2012.

[10] Mikhail A. Shifman, A. I. Vainshtein, and Valentin I. Zakharov. QCD and Resonance Physics. Theoretical Foundations. *Nucl. Phys.*, B147:385–447, 1979.

[11] Avinash Dhar, R. Shankar, and Spenta R. Wadia. Nambu-Jona-Lasinio Type Effective Lagrangian. 2. Anomalies and Nonlinear Lagrangian of Low-Energy, Large N QCD. *Phys. Rev.*, D31:3256, 1985.

[12] J. Gasser and H. Leutwyler. Low-Energy Theorems as Precision Tests of QCD. *Phys. Lett.*, B125:325–329, 1983.

[13] B. L. Ioffe. QCD at low energies. *Prog. Part. Nucl. Phys.*, 56:232–277, 2006.

[14] Tadakatsu Sakai and Shigeki Sugimoto. Low energy hadron physics in holographic QCD. *Prog. Theor. Phys.*, 113:843–882, 2005.

[15] Robert G. Leigh, Djordje Minic, and Alexandr Yelnikov. Solving pure QCD in 2+1 dimensions. *Phys. Rev. Lett.*, 96:222001, 2006.

[16] William A. Bardeen. On naturalness in the standard model. In *Ontake Summer Institute on Particle Physics Ontake Mountain, Japan, August 27-September 2, 1995*, 1995.

[17] M. Buysse. Natural relations in the standard model. 2001.

[18] Robert Foot, Archil Kobakhidze, and Raymond R. Volkas. Stable mass hierarchies and dark matter from hidden sectors in the scale-invariant standard model. *Phys. Rev.*, D82:035005, 2010.

[19] C. D. Froggatt, L. V. Laperashvili, and H. B. Nielsen. The Fundamental-weak scale hierarchy in the standard model. *Phys. Atom. Nucl.*, 69:67–80, 2006.

[20] Fred Jegerlehner. The hierarchy problem of the electroweak Standard Model revisited. 2013.

[21] J. F. Donoghue, E. Golowich, and Barry R. Holstein. Dynamics of the standard model. *Camb. Monogr. Part. Phys. Nucl. Phys. Cosmol.*, 2:1–540, 1992. [Camb. Monogr. Part. Phys. Nucl. Phys. Cosmol.35(2014)].

[22] A. V. Manohar. Effective field theories. *Lect. Notes Phys.*, 479:311–362, 1997.

[23] David B. Kaplan. Effective field theories. In *Beyond the standard model 5. Proceedings, 5th Conference, Balholm, Norway, April 29-May 4, 1997*, 1995.

[24] H. Georgi. Effective field theory. *Ann. Rev. Nucl. Part. Sci.*, 43:209–252, 1993.

[25] C. P. Burgess. Introduction to Effective Field Theory. *Ann. Rev. Nucl. Part. Sci.*, 57:329–362, 2007.

[26] D. C. Kennedy and B. W. Lynn. Electroweak Radiative Corrections with an Effective Lagrangian: Four Fermion Processes. *Nucl. Phys.*, B322:1–54, 1989.

[27] Michael E. Peskin and Tatsu Takeuchi. A New constraint on a strongly interacting Higgs sector. *Phys.Rev.Lett.*, 65:964–967, 1990.

[28] Michael E. Peskin and Tatsu Takeuchi. Estimation of oblique electroweak corrections. *Phys.Rev.*, D46:381–409, 1992.

[29] Konstantin Matchev. TASI lectures on precision electroweak physics. In *Particle physics and cosmology: The quest for physics beyond the standard model(s). Proceedings, Theoretical Advanced Study Institute, TASI 2002, Boulder, USA, June 3-28, 2002*, pages 51–98, 2004.

[30] James D. Wells. TASI lecture notes: Introduction to precision electroweak analysis. In *Physics in D ¿= 4. Proceedings, Theoretical Advanced Study Institute in elementary particle physics, TASI 2004, Boulder, USA, June 6-July 2, 2004*, pages 41–64, 2005.

[31] Witold Skiba. Effective Field Theory and Precision Electroweak Measurements. In *Physics of the large and the small, TASI 09, proceedings of the Theoretical Advanced Study Institute in Elementary Particle Physics, Boulder, Colorado, USA, 1-26 June 2009*, pages 5–70, 2011.

[32] Georges Aad et al. Observation of a new particle in the search for the Standard Model Higgs boson with the ATLAS detector at the LHC. *Phys. Lett.*, B716:1–29, 2012.

[33] Serguei Chatrchyan et al. Observation of a new boson at a mass of 125 GeV with the CMS experiment at the LHC. *Phys. Lett.*, B716:30–61, 2012.

[34] Christoph Borschensky, Michael Krämer, Anna Kulesza, Michelangelo Mangano, Sanjay Padhi, Tilman Plehn, and Xavier Portell. Squark and gluino production cross sections in pp collisions at $\sqrt{s} = 13$, 14, 33 and 100 TeV. *Eur. Phys. J.*, C74(12):3174, 2014.

[35] Aram Avetisyan et al. Methods and Results for Standard Model Event Generation at $\sqrt{s} = 14$ TeV, 33 TeV and 100 TeV Proton Colliders (A Snowmass Whitepaper). In *Proceedings, Community Summer Study 2013: Snowmass on the Mississippi (CSS2013): Minneapolis, MN, USA, July 29-August 6, 2013*, 2013.

[36] Matthew Low and Lian-Tao Wang. Neutralino dark matter at 14 TeV and 100 TeV. *JHEP*, 08:161, 2014.

[37] Nima Arkani-Hamed, Tao Han, Michelangelo Mangano, and Lian-Tao Wang. Physics opportunities of a 100 TeV proton–proton collider. *Phys. Rept.*, 652:1–49, 2016.

[38] R. Abbasi et al. Measurement of the atmospheric neutrino energy spectrum from 100 GeV to 400 TeV with IceCube. *Phys. Rev.*, D83:012001, 2011.

[39] D. M. Mei, Z. B. Yin, and S. R. Elliott. Cosmogenic Production as a Background in Searching for Rare Physics Processes. *Astropart. Phys.*, 31:417–420, 2009.

[40] Paride Paradisi. Constraints on SUSY lepton flavor violation by rare processes. *JHEP*, 10:006, 2005.

[41] John Foster, Ken-ichi Okumura, and Leszek Roszkowski. Probing the flavor structure of supersymmetry breaking with rare B-processes: A Beyond leading order analysis. *JHEP*, 08:094, 2005.

[42] Stephan J. Huber and Qaisar Shafi. Neutrino oscillations and rare processes in models with a small extra dimension. *Phys. Lett.*, B512:365–372, 2001.

[43] Sacha Davidson, David C. Bailey, and Bruce A. Campbell. Model independent constraints on leptoquarks from rare processes. *Z.Phys.*, C61:613–644, 1994.

[44] B. A. Campbell, John R. Ellis, K. Enqvist, M. K. Gaillard, and Dimitri V. Nanopoulos. Superstring Models Challenged by Rare Processes. *Int. J. Mod. Phys.*, A2:831, 1987.

[45] Tim Brown, Nilendra Deshpande, Sandip Pakvasa, and Hirotaka Sugawara. CP Nonconservation and Rare Processes in S(4) Model of Permutation Symmetry. *Phys. Lett.*, B141:95–99, 1984.

[46] O. W. Greenberg, R. N. Mohapatra, and S. Nussinov. Constraints on Composite Models due to Rare Processes. *Phys. Lett.*, 148B:465, 1984. [Addendum: Phys. Lett.164B,410(1985)].

[47] Andrzej J. Buras. An Upper Bound on the Top Quark Mass from Rare Processes. *Phys. Rev. Lett.*, 46:1354, 1981.

[48] Enrico Fermi. An attempt of a theory of beta radiation. 1. *Z. phys*, 88(161):19, 1934.

[49] Fred L Wilson. Fermi's theory of beta decay. *American Journal of Physics*, 36(12):1150–1160, 1968.

[50] Chen Ning Yang. Fermi's β-decay theory. *Asia Pacific Physics Newsletter*, 1(01):27–30, 2012.

[51] T. D. Lee and Chen-Ning Yang. Question of Parity Conservation in Weak Interactions. *Phys. Rev.*, 104:254–258, 1956.

[52] R. E. Marshak, S. Okubo, and G. Sudarshan. V-A theory and the decay of the hyperon. *Phys. Rev.*, 113:944–954, 1959.

[53] R. P. Feynman and Murray Gell-Mann. Theory of Fermi interaction. *Phys. Rev.*, 109:193–198, 1958.

[54] S. L. Glashow. Partial Symmetries of Weak Interactions. *Nucl. Phys.*, 22:579–588, 1961.

[55] Steven Weinberg. A Model of Leptons. *Phys. Rev. Lett.*, 19:1264–1266, 1967.

[56] Abdus Salam. Weak and Electromagnetic Interactions. *Conf. Proc.*, C680519:367–377, 1968.

[57] G. Arnison et al. Experimental Observation of Lepton Pairs of Invariant Mass Around 95-GeV/c**2 at the CERN SPS Collider. *Phys. Lett.*, 126B:398–410, 1983.

[58] M. Banner et al. Observation of Single Isolated Electrons of High Transverse Momentum in Events with Missing Transverse Energy at the CERN anti-p p Collider. *Phys. Lett.*, 122B:476–485, 1983.

[59] Hideki Yukawa. On the interaction of elementary particles. i. *Nippon Sugaku-Buturigakkwai Kizi Dai 3 Ki*, 17(0):48–57, 1935.

[60] C. M. G. Lattes, G. P. S. Occhialini, and C. F. Powell. Observations on the Tracks of Slow Mesons in Photographic Emulsions. 1. *Nature*, 160:453–456, 1947. [,99(1947)].

[61] C. M. G. Lattes, H. Muirhead, G. P. S. Occhialini, and C. F. Powell. PROCESSES INVOLVING CHARGED MESONS. *Nature*, 159:694–697, 1947. [,42(1947)].

[62] John M. Cornwall, R. Jackiw, and E. Tomboulis. Effective Action for Composite Operators. *Phys. Rev.*, D10:2428–2445, 1974.

[63] E. G. Floratos, D. A. Ross, and Christopher T. Sachrajda. Higher Order Effects in Asymptotically Free Gauge Theories: The Anomalous Dimensions of Wilson Operators. *Nucl. Phys.*, B129:66–88, 1977. [Erratum: Nucl. Phys.B139,545(1978)].

[64] E. G. Floratos, D. A. Ross, and Christopher T. Sachrajda. Higher Order Effects in Asymptotically Free Gauge Theories. 2. Flavor Singlet Wilson Operators and Coefficient Functions. *Nucl. Phys.*, B152:493–520, 1979.

[65] Toru Goto and Takeshi Nihei. Effect of RRRR dimension five operator on the proton decay in the minimal SU(5) SUGRA GUT model. *Phys. Rev.*, D59:115009, 1999.

[66] Thomas Mannel. Operator product expansion for inclusive semileptonic decays in heavy quark effective field theory. *Nucl. Phys.*, B413:396–412, 1994.

[67] K. S. Babu and Chung Ngoc Leung. Classification of effective neutrino mass operators. *Nucl. Phys.*, B619:667–689, 2001.

[68] Vernon Barger, Tao Han, Paul Langacker, Bob McElrath, and Peter Zerwas. Effects of genuine dimension-six Higgs operators. *Phys. Rev.*, D67:115001, 2003.

[69] Andre de Gouvea and James Jenkins. A Survey of Lepton Number Violation Via Effective Operators. *Phys. Rev.*, D77:013008, 2008.

[70] P. J. Ellis and E. Osnes. An introductory guide to effective operators in nuclei. *Rev. Mod. Phys.*, 49:777–832, 1977.

[71] Florian Bonnet, Daniel Hernandez, Toshihiko Ota, and Walter Winter. Neutrino masses from higher than d=5 effective operators. *JHEP*, 10:076, 2009.

[72] J. A. Aguilar-Saavedra. Effective four-fermion operators in top physics: A Roadmap. *Nucl. Phys.*, B843:638–672, 2011. [Erratum: Nucl. Phys.B851,443(2011)].

[73] Benjamin Grinstein and Mark B. Wise. Operator analysis for precision electroweak physics. *Phys. Lett.*, B265:326–334, 1991.

[74] Adam Falkowski and Francesco Riva. Model-independent precision constraints on dimension-6 operators. *JHEP*, 02:039, 2015.

[75] Carla Biggio, Mattias Blennow, and Enrique Fernandez-Martinez. Loop bounds on non-standard neutrino interactions. *JHEP*, 03:139, 2009.

[76] Rodrigo Alonso, Hsi-Ming Chang, Elizabeth E. Jenkins, Aneesh V. Manohar, and Brian Shotwell. Renormalization group evolution of dimension-six baryon number violating operators. *Phys. Lett.*, B734:302–307, 2014.

[77] Sebastian Liem, Gianfranco Bertone, Francesca Calore, Roberto Ruiz de Austri, Tim M. P. Tait, Roberto Trotta, and Christoph Weniger. Effective field theory of dark matter: a global analysis. *JHEP*, 09:077, 2016.

[78] Edward Witten. Mass Hierarchies in Supersymmetric Theories. *Phys. Lett.*, B105:267, 1981.

[79] Benjamin Grinstein. A Supersymmetric SU(5) Gauge Theory with No Gauge Hierarchy Problem. *Nucl. Phys.*, B206:387, 1982.

[80] Riccardo Barbieri, A. Masiero, and G. Veneziano. Hierarchy of Fermion Masses in Supersymmetric Composite Models. *Phys. Lett.*, B128:179, 1983.

[81] Lisa Randall and Raman Sundrum. A Large mass hierarchy from a small extra dimension. *Phys. Rev. Lett.*, 83:3370–3373, 1999.

[82] Nima Arkani-Hamed and Martin Schmaltz. Hierarchies without symmetries from extra dimensions. *Phys. Rev.*, D61:033005, 2000.

[83] Koichi Yoshioka. On fermion mass hierarchy with extra dimensions. *Mod. Phys. Lett.*, A15:29–40, 2000.

[84] Andrew G. Cohen and David B. Kaplan. Solving the hierarchy problem with noncompact extra dimensions. *Phys. Lett.*, B470:52–58, 1999.

[85] Z. Chacko and Ann E. Nelson. A Solution to the hierarchy problem with an infinitely large extra dimension and moduli stabilization. *Phys. Rev.*, D62:085006, 2000.

[86] P. H. Frampton, R. N. Mohapatra, and Sungwook Suh. Prediction of sin**2 theta(W) in a conformal approach to coupling unification. *Phys. Lett.*, B520:331–336, 2001.

[87] Paul H. Frampton and Cumrun Vafa. Conformal approach to particle phenomenology. 1999.

[88] Minako Honda, Yee Kao, Naotoshi Okamura, Alexey Pronin, and Tatsu Takeuchi. The Effect of Topcolor Assisted Technicolor, and other models, on Neutrino Oscillation. pages 278–284, 2007.

[89] Will Loinaz and Tatsu Takeuchi. Constraints on topcolor assisted technicolor models from vertex corrections. *Phys. Rev.*, D60:015005, 1999.

[90] Christopher T. Hill. Topcolor assisted technicolor. *Phys. Lett.*, B345:483–489, 1995.

[91] B. Holdom and J. Terning. Large corrections to electroweak parameters in technicolor theories. *Phys. Lett.*, B247:88–92, 1990.

[92] R. Sekhar Chivukula and Howard Georgi. Composite Technicolor Standard Model. *Phys. Lett.*, B188:99–104, 1987.

[93] Thomas Appelquist and L. C. R. Wijewardhana. Chiral Hierarchies from Slowly Running Couplings in Technicolor Theories. *Phys. Rev.*, D36:568, 1987.

[94] Koichi Yamawaki, Masako Bando, and Ken-iti Matumoto. Scale Invariant Technicolor Model and a Technidilaton. *Phys. Rev. Lett.*, 56:1335, 1986.

[95] Thomas W. Appelquist, Dimitra Karabali, and L. C. R. Wijewardhana. Chiral Hierarchies and the Flavor Changing Neutral Current Problem in Technicolor. *Phys. Rev. Lett.*, 57:957, 1986.

[96] Savas Dimopoulos and John R. Ellis. Challenges for Extended Technicolor Theories. *Nucl. Phys.*, B182:505–528, 1982.

[97] Edward Farhi and Leonard Susskind. Technicolor. *Phys. Rept.*, 74:277, 1981.

[98] Michael Dine, Willy Fischler, and Mark Srednicki. Supersymmetric Technicolor. *Nucl. Phys.*, B189:575–593, 1981.

[99] P. Sikivie, Leonard Susskind, Mikhail B. Voloshin, and Valentin I. Zakharov. Isospin Breaking in Technicolor Models. *Nucl. Phys.*, B173:189–207, 1980.

[100] Keith R. Dienes. Solving the Hierarchy Problem without Supersymmetry or Extra Dimensions: An Alternative Approach. *Nucl. Phys.*, B611:146–178, 2001.

[101] Gerard 't Hooft. Dimensional reduction in quantum gravity. In *Salamfest 1993:0284-296*, pages 0284–296, 1993.

[102] Luis J. Garay. Quantum gravity and minimum length. *Int. J. Mod. Phys.*, A10:145–166, 1995.

[103] Giovanni Amelino-Camelia. An Interferometric gravitational wave detector as a quantum gravity apparatus. *Nature*, 398:216–218, 1999.

[104] V. Alan Kostelecky. Gravity, Lorentz violation, and the standard model. *Phys. Rev.*, D69:105009, 2004.

[105] David Mattingly. Modern tests of Lorentz invariance. *Living Rev. Rel.*, 8:5, 2005.

[106] Claus Kiefer. Quantum gravity: General introduction and recent developments. *Annalen Phys.*, 15:129–148, 2005. [Annalen Phys.518,129(2006)].

[107] Sabine Hossenfelder. Minimal Length Scale Scenarios for Quantum Gravity. *Living Rev. Rel.*, 16:2, 2013.

[108] Stefano Liberati. Tests of Lorentz invariance: a 2013 update. *Class. Quant. Grav.*, 30:133001, 2013.

[109] Francesco Marin et al. Gravitational bar detectors set limits to Planck-scale physics on macroscopic variables. *Nature Phys.*, 9:71–73, 2013.

[110] Muxin Han. Covariant Loop Quantum Gravity, Low Energy Perturbation Theory, and Einstein Gravity with High Curvature UV Corrections. *Phys. Rev.*, D89(12):124001, 2014.

[111] Hikaru Kawai. Low energy effective action of quantum gravity and the naturalness problem. *Int. J. Mod. Phys.*, A28:1340001, 2013.

[112] John F. Donoghue and Barry R. Holstein. Low Energy Theorems of Quantum Gravity from Effective Field Theory. *J. Phys.*, G42(10):103102, 2015.

[113] Alessio Belenchia, Dionigi M. T. Benincasa, Stefano Liberati, Francesco Marin, Francesco Marino, and Antonello Ortolan. Tests of Quantum Gravity-Induced Non-Locality via Opto-mechanical Experiments. *Phys. Rev.*, D95(2):026012, 2017.

[114] Lay Nam Chang, Zachary Lewis, Djordje Minic, and Tatsu Takeuchi. Is Quantum Gravity a Super-Quantum Theory? *Int. J. Mod. Phys.*, D22:1342025, 2013.

[115] Ali H. Chamseddine and Alain Connes. Quantum Gravity Boundary Terms from Spectral Action. *Phys. Rev. Lett.*, 99:071302, 2007.

[116] Ali H. Chamseddine, Alain Connes, and Viatcheslav Mukhanov. Geometry and the Quantum: Basics. *JHEP*, 12:098, 2014.

[117] Alain Connes. Geometry and the Quantum. 2017.

[118] Laurent Freidel, Robert G. Leigh, and Djordje Minic. Quantum Gravity, Dynamical Phase Space and String Theory. *Int. J. Mod. Phys.*, D23(12):1442006, 2014.

[119] Agostino Devastato. Noncommutative geometry, Grand Symmetry and twisted spectral triple. In *Conceptual and Technical Challenges for Quantum Gravity Rome, Italy, September 8-12, 2014*, 2015.

[120] Robert Coquereaux, Gilles Esposito-Farese, and G. Vaillant. Higgs fields as Yang-Mills fields and discrete symmetries. *Nucl. Phys.*, B353:689–706, 1991.

[121] R. Haussling, N. A. Papadopoulos, and F. Scheck. SU(2/1) symmetry, algebraic superconnections and a generalized theory of electroweak interactions. *Phys. Lett.*, B260:125–130, 1991.

[122] Robert Coquereaux, R. Haussling, N. A. Papadopoulos, and F. Scheck. Generalized gauge transformations and hidden symmetry in the standard model. *Int. J. Mod. Phys.*, A7:2809–2824, 1992.

[123] Michel Dubois-Violette, Richard Kerner, and John Madore. Noncommutative Differential Geometry of Matrix Algebras. *J. Math. Phys.*, 31:316, 1990.

[124] Michel Dubois-Violette, Richard Kerner, and John Madore. Noncommutative Differential Geometry and New Models of Gauge Theory. *J. Math. Phys.*, 31:323, 1990.

[125] M. Dubois-Violette, J. Madore, and R. Kerner. Classical Bosons in a Noncommutative Geometry. *Class. Quant. Grav.*, 6:1709, 1989.

[126] M. Dubois-Violette, J. Madore, and R. Kerner. Gauge Bosons in a Noncommutative Geometry. *Phys. Lett.*, B217:485–488, 1989.

[127] J. Madore. Noncommutative geometry for pedestrians. In *Classical and quantum nonlocality. Proceedings, International School of Cosmology and Gravitation, 16th Course, Erice, Italy, April 27-May 4, 1999*, pages 111–139, 1999.

[128] John Madore, Stefan Schraml, Peter Schupp, and Julius Wess. Gauge theory on noncommutative spaces. *Eur. Phys. J.*, C16:161–167, 2000.

[129] Yuval Ne'eman and S. Sternberg. Superconnections and internal supersymmetry dynamics. *Proc. Nat. Acad. Sci.*, 87:7875–7877, 1990.

[130] Dae Sung Hwang, Chang-Yeong Lee, and Yuval Ne'eman. BRST quantization of gauge theory in noncommutative geometry: Matrix derivative approach. *J. Math. Phys.*, 37:3725–3738, 1996.

[131] Raimar Wulkenhaar. The Standard model within nonassociative geometry. *Phys. Lett.*, B390:119–127, 1997.

[132] Thomas Schucker and Jean-Marc Zylinski. Connes' model building kit. *J. Geom. Phys.*, 16:207–236, 1995.

[133] Bruno Iochum, Daniel Kastler, and Thomas Schucker. On the universal Chamseddine-Connes action 1. Details of the action computation. *J. Math. Phys.*, 38:4929–4950, 1997.

[134] Lionel Carminati, Bruno Iochum, Daniel Kastler, and Thomas Schucker. On Connes' new principle of general relativity. Can spinors hear the forces of space-time? 1996.

[135] D. Kastler. Noncommutative geometry and fundamental physical interactions: The Lagrangian level: Historical sketch and description of the present situation. *J. Math. Phys.*, 41:3867–3891, 2000.

[136] Katsusada Morita. Quaternions and noncommutative geometry. *Prog. Theor. Phys.*, 90:219–236, 1993.

[137] Katsusada Morita and Yoshitaka Okumura. Weinberg-Salam theory in noncommutative geometry. *Prog. Theor. Phys.*, 91:959–974, 1994.

[138] Katsusada Morita and Yoshitaka Okumura. Reconstruction of Weinberg-Salam theory in noncommutative geometry on M(4) x Z(2). *Phys. Rev.*, D50:1016–1025, 1994.

[139] Yoshitaka Okumura. Gauge theory and Higgs mechanism based on differential geometry on discrete space M(4) x Z(N). *Phys. Rev.*, D50:1026–1039, 1994.

[140] I. S. Sogami. Generalized covariant derivative with gauge and Higgs fields in the standard model. *Prog. Theor. Phys.*, 94:117–123, 1995.

[141] Shigefumi Naka and Eizou Umezawa. An Approach to electroweak interactions based on noncommutative geometry. *Prog. Theor. Phys.*, 92:189–204, 1994.

[142] Enrique Alvarez, Jose M. Gracia-Bondia, and C. P. Martin. Anomaly cancellation and the gauge group of the standard model in NCG. *Phys. Lett.*, B364:33–40, 1995.

[143] Joseph C. Varilly and Jose M. Gracia-Bondia. Connes' noncommutative differential geometry and the Standard Model. *J. Geom. Phys.*, 12:223–301, 1993.

[144] C. P. Martin, Jose M. Gracia-Bondia, and Joseph C. Varilly. The Standard model as a noncommutative geometry: The Low-energy regime. *Phys. Rept.*, 294:363–406, 1998.

[145] Joseph C. Varilly. An Introduction to noncommutative geometry. 1997.

[146] F. Scheck, W. Werner, and H. Upmeier, editors. *Noncommutative geometry and the standard model of elementary particle physics. Proceedings, Conference, Hesselberg, Gerolfingen, Germany, March 14-19, 1999*, volume 596, 2002.

[147] Alain Connes and John Lott. Particle Models and Noncommutative Geometry (Expanded Version). *Nucl. Phys. Proc. Suppl.*, 18B:29–47, 1991.

[148] Ali H. Chamseddine and Alain Connes. Universal formula for noncommutative geometry actions: Unification of gravity and the standard model. *Phys. Rev. Lett.*, 77:4868–4871, 1996.

[149] Ali H. Chamseddine and Alain Connes. The Spectral action principle. *Commun. Math. Phys.*, 186:731–750, 1997.

[150] Alain Connes. Gravity coupled with matter and foundation of noncommutative geometry. *Commun. Math. Phys.*, 182:155–176, 1996.

[151] Ali H. Chamseddine, Alain Connes, and Matilde Marcolli. Gravity and the standard model with neutrino mixing. *Adv. Theor. Math. Phys.*, 11(6):991–1089, 2007.

[152] Alain Connes. Noncommutative geometry and the standard model with neutrino mixing. *JHEP*, 11:081, 2006.

[153] Ali H. Chamseddine and Alain Connes. Why the Standard Model. *J. Geom. Phys.*, 58:38–47, 2008.

[154] Ali H. Chamseddine and Alain Connes. Noncommutative Geometry as a Framework for Unification of all Fundamental Interactions including Gravity. Part I. *Fortsch. Phys.*, 58:553–600, 2010.

[155] Ali H. Chamseddine and Alain Connes. Resilience of the Spectral Standard Model. *JHEP*, 09:104, 2012.

[156] Ali H. Chamseddine, Alain Connes, and Walter D. van Suijlekom. Beyond the Spectral Standard Model: Emergence of Pati-Salam Unification. *JHEP*, 11:132, 2013.

[157] Denis Perrot. Anomalies and noncommutative index theory. *Contemp. Math.*, 434:125–160, 2007.

[158] E. Langmann. On Anomalies and noncommutative geometry. *Lect. Notes Phys.*, 469:291–298, 1996.

[159] Ufuk Aydemir, Djordje Minic, Chen Sun, and Tatsu Takeuchi. Higgs mass, superconnections, and the TeV-scale left-right symmetric model. *Phys. Rev.*, D91:045020, 2015.

[160] Ufuk Aydemir, Djordje Minic, Chen Sun, and Tatsu Takeuchi. Pati-Salam unification from noncommutative geometry and the TeV-scale W_R boson. *Int. J. Mod. Phys.*, A31(01):1550223, 2016.

[161] Ufuk Aydemir, Djordje Minic, Chen Sun, and Tatsu Takeuchi. The 750 GeV diphoton excess in unified $SU(2)_L \times SU(2)_R \times SU(4)$ models from noncommutative geometry. *Mod. Phys. Lett.*, A31(18):1650101, 2016.

[162] Ufuk Aydemir, Djordje Minic, Chen Sun, and Tatsu Takeuchi. in preparation.

[163] Ufuk Aydemir, Djordje Minic, and Tatsu Takeuchi. The Higgs Mass and the Emergence of New Physics. *Phys. Lett.*, B724:301–305, 2013.

[164] Yuval Ne'eman. Irreducible Gauge Theory of a Consolidated Weinberg-Salam Model. *Phys. Lett.*, B81:190, 1979.

[165] D. B. Fairlie. Two Consistent Calculations of the Weinberg Angle. *J. Phys.*, G5:L55, 1979.

[166] D. B. Fairlie. Higgs' Fields and the Determination of the Weinberg Angle. *Phys. Lett.*, B82:97–100, 1979.

[167] Euan J. Squires. On a Derivation of the Weinberg-Salam Model. *Phys. Lett.*, B82:395–397, 1979.

[168] J. G. Taylor. Electroweak Theory in SU(2/1). *Phys. Lett.*, B83:331–334, 1979.

[169] P. H. Dondi and Peter D. Jarvis. A supersymmetric Weinberg-Salam model. *Phys. Lett.*, B84:75, 1979. [Erratum: Phys. Lett.B87,403(1979)].

[170] Daniel Quillen. Superconnections and the chern character. *Topology*, 24(1):89–95, 1985.

[171] Shlomo Sternberg. *Curvature in mathematics and physics*. Courier Corporation, 2012.

[172] Yuval Ne'eman. Internal Supergroup Prediction for the Goldstone-higgs Particle Mass. *Phys. Lett.*, B181:308–310, 1986.

[173] Dae Sung Hwang, Chang-Yeong Lee, and Yuval Ne'eman. BRST quantization of SU(2/1) electroweak theory in the superconnection approach and the Higgs meson mass. *Int. J. Mod. Phys.*, A11:3509–3522, 1996.

[174] G. Roepstorff. Superconnections and the Higgs field. *J. Math. Phys.*, 40:2698–2715, 1999.

[175] L. Corwin, Yuval Ne'eman, and S. Sternberg. Graded Lie Algebras in Mathematics and Physics (Bose-Fermi Symmetry). *Rev. Mod. Phys.*, 47:573, 1975.

[176] M. Scheunert, W. Nahm, and V. Rittenberg. Graded Lie Algebras: Generalization of Hermitian Representations. *J. Math. Phys.*, 18:146, 1977.

[177] I. Bars and M. Gunaydin. Unitary Representations of Noncompact Supergroups. *Commun. Math. Phys.*, 91:31, 1983.

[178] Itzhak Bars. Supergroups and Superalgebras in Physics. *Physica*, 15D:42, 1985.

[179] N. S. Manton. A New Six-Dimensional Approach to the Weinberg-Salam Model. *Nucl. Phys.*, B158:141–153, 1979.

[180] J. G. Taylor. Superunification in $SU(5|1)$. *Phys. Rev. Lett.*, 43:824–826, 1979.

[181] P. H. Dondi and Peter D. Jarvis. Assignments in Strong Electroweak Unified Models With Internal and Space-time Symmetry. *Z. Phys.*, C4:201, 1980.

[182] Yuval Ne'eman and Shlomo Sternberg. Internal Supersymmetry and Unification. *Proc. Nat. Acad. Sci.*, 77:3127–3131, 1980.

[183] J. G. Taylor. Gauging SU(n/m). *Phys. Lett.*, B84:79–82, 1979.

[184] Jean Thierry-Mieg and Yuval Ne'eman. Exterior Gauging of an Internal Supersymmetry and SU(2/1) Quantum Asthenodynamics. *Proc. Nat. Acad. Sci.*, 79:7068–7072, 1982.

[185] Yuval Ne'eman and Jean Thierry-Mieg. Geometrical Gauge Theory of Ghost and Goldstone Fields and of Ghost Symmetries. *Proc. Nat. Acad. Sci.*, 77:720–723, 1980.

[186] Jean Thierry-Mieg and Yuval Ne'eman. BRS Algebra of the SU(2/1) Electroweak Ghost Gauge Theory. *Nuovo Cim.*, A71:104, 1982.

[187] Shigefumi Naka, Hiroshi Chyujou, and Hitoshi Kan. Electroweak gauge theory out of SU(2/1) gauge theory. *Prog. Theor. Phys.*, 85:643–660, 1991.

[188] R. Ecclestone. A Critique of Supersymmetric Weinberg-Salam Models. *J. Phys.*, A13:1395, 1980.

[189] Alain Connes. *Noncommutative geometry*. 1994.

[190] Alain Connes and Matilde Marcolli. *Noncommutative Geometry, Quantum Fields and Motives*. American Mathematical Society, 2007.

[191] E. Alvarez, Jose M. Gracia-Bondia, and C. P. Martin. Parameter restrictions in a noncommutative geometry model do not survive standard quantum corrections. *Phys. Lett.*, B306:55–58, 1993.

[192] E. Alvarez, Jose M. Gracia-Bondia, and C. P. Martin. A Renormalization group analysis of the NCG constraints m(top) = 2 m(w), m(Higgs) = 3.14 m(W). *Phys. Lett.*, B329:259–262, 1994.

[193] Agostino Devastato, Fedele Lizzi, and Pierre Martinetti. Grand Symmetry, Spectral Action, and the Higgs mass. *JHEP*, 01:042, 2014.

[194] Agostino Devastato, Fedele Lizzi, and Pierre Martinetti. Higgs mass in Noncommutative Geometry. *Fortsch. Phys.*, 62:863–868, 2014.

[195] Jogesh C. Pati and Abdus Salam. Lepton Number as the Fourth Color. *Phys. Rev.*, D10:275–289, 1974. [Erratum: Phys. Rev.D11,703(1975)].

[196] Keith R. Dienes. Statistics on the heterotic landscape: Gauge groups and cosmological constants of four-dimensional heterotic strings. *Phys. Rev.*, D73:106010, 2006.

[197] C. Itzykson and J. B. Zuber. *Quantum Field Theory*. International Series In Pure and Applied Physics. McGraw-Hill, New York, 1980.

[198] Jose M. Gracia-Bondia, J. C. Varilly, and H. Figueroa. *Elements of noncommutative geometry*. 2001.

[199] Paul Langacker. *The standard model and beyond*. 2010.

[200] D. R. T. Jones. The Two Loop beta Function for a G(1) x G(2) Gauge Theory. *Phys. Rev.*, D25:581, 1982.

[201] Rabindra N. Mohapatra and Jogesh C. Pati. Left-Right Gauge Symmetry and an Isoconjugate Model of CP Violation. *Phys. Rev.*, D11:566–571, 1975.

[202] R. N. Mohapatra and Jogesh C. Pati. A Natural Left-Right Symmetry. *Phys. Rev.*, D11:2558, 1975.

[203] G. Senjanovic and Rabindra N. Mohapatra. Exact Left-Right Symmetry and Spontaneous Violation of Parity. *Phys. Rev.*, D12:1502, 1975.

[204] Rabindra N. Mohapatra and Goran Senjanovic. Neutrino Mass and Spontaneous Parity Violation. *Phys. Rev. Lett.*, 44:912, 1980.

[205] Rabindra N. Mohapatra and Goran Senjanovic. Neutrino Masses and Mixings in Gauge Models with Spontaneous Parity Violation. *Phys. Rev.*, D23:165, 1981.

[206] D. Chang, R. N. Mohapatra, and M. K. Parida. Decoupling Parity and SU(2)-R Breaking Scales: A New Approach to Left-Right Symmetric Models. *Phys. Rev. Lett.*, 52:1072, 1984.

[207] J. F. Gunion, J. Grifols, A. Mendez, Boris Kayser, and Fredrick I. Olness. Higgs Bosons in Left-Right Symmetric Models. *Phys. Rev.*, D40:1546, 1989.

[208] N. G. Deshpande, J. F. Gunion, Boris Kayser, and Fredrick I. Olness. Left-right symmetric electroweak models with triplet Higgs. *Phys. Rev.*, D44:837–858, 1991.

[209] Biswajoy Brahmachari, Utpal Sarkar, and K. Sridhar. Ruling out low-energy left-right symmetry in unified theories. *Phys. Lett.*, B297:105–110, 1992.

[210] M. Czakon, M. Zralek, and J. Gluza. Left-right symmetry and heavy particle quantum effects. *Nucl. Phys.*, B573:57–74, 2000.

[211] P. Duka, J. Gluza, and M. Zralek. Quantization and renormalization of the manifest left-right symmetric model of electroweak interactions. *Annals Phys.*, 280:336–408, 2000.

[212] Chang-Hun Lee, P. S. Bhupal Dev, and R. N. Mohapatra. Natural TeV-scale left-right seesaw mechanism for neutrinos and experimental tests. *Phys. Rev.*, D88(9):093010, 2013.

[213] G. Bambhaniya, J. Chakrabortty, J. Gluza, T. Jeliński, and M. Kordiaczynska. Lowest limits on the doubly charged Higgs boson masses in the minimal left-right symmetric model. *Phys. Rev.*, D90(9):095003, 2014.

[214] G. Bambhaniya, J. Chakrabortty, J. Gluza, M. Kordiaczyńska, and R. Szafron. Left-Right Symmetry and the Charged Higgs Bosons at the LHC. *JHEP*, 05:033, 2014.

[215] Goran Senjanović and Vladimir Tello. Right Handed Quark Mixing in Left-Right Symmetric Theory. *Phys. Rev. Lett.*, 114(7):071801, 2015.

[216] M. Nakahara. *Geometry, topology and physics*. 2003.

[217] Joan Elias-Miro, Jose R. Espinosa, Gian F. Giudice, Hyun Min Lee, and Alessandro Strumia. Stabilization of the Electroweak Vacuum by a Scalar Threshold Effect. *JHEP*, 06:031, 2012.

[218] Oleg Lebedev. On Stability of the Electroweak Vacuum and the Higgs Portal. *Eur. Phys. J.*, C72:2058, 2012.

[219] Chian-Shu Chen and Yong Tang. Vacuum stability, neutrinos, and dark matter. *JHEP*, 04:019, 2012.

[220] Matthew Gonderinger, Yingchuan Li, Hiren Patel, and Michael J. Ramsey-Musolf. Vacuum Stability, Perturbativity, and Scalar Singlet Dark Matter. *JHEP*, 01:053, 2010.

[221] Naoyuki Haba and Ryo Takahashi. Higgs inflation with singlet scalar dark matter and right-handed neutrino in light of BICEP2. *Phys. Rev.*, D89(11):115009, 2014. [Erratum: Phys. Rev.D90,no.3,039905(2014)].

[222] Yutaka Hosotani. Dynamical Mass Generation by Compact Extra Dimensions. *Phys. Lett.*, B126:309–313, 1983.

[223] Yutaka Hosotani. Dynamical Gauge Symmetry Breaking as the Casimir Effect. *Phys. Lett.*, B129:193–197, 1983.

[224] Yutaka Hosotani. Dynamics of Nonintegrable Phases and Gauge Symmetry Breaking. *Annals Phys.*, 190:233, 1989.

[225] Hisaki Hatanaka, Takeo Inami, and C. S. Lim. The Gauge hierarchy problem and higher dimensional gauge theories. *Mod. Phys. Lett.*, A13:2601–2612, 1998.

[226] Lawrence J. Hall, Yasunori Nomura, and David Tucker-Smith. Gauge Higgs unification in higher dimensions. *Nucl. Phys.*, B639:307–330, 2002.

[227] Gustavo Burdman and Yasunori Nomura. Unification of Higgs and gauge fields in five-dimensions. *Nucl. Phys.*, B656:3–22, 2003.

[228] Naoyuki Haba, Masatomi Harada, Yutaka Hosotani, and Yoshiharu Kawamura. Dynamical rearrangement of gauge symmetry on the orbifold S1 / Z(2). *Nucl. Phys.*, B657:169–213, 2003. [Erratum: Nucl. Phys.B669,381(2003)].

[229] Erich Kahler. Inner and exterior differential calculus. *Abh. Deutsch. Akad. Wiss. Berlin Kl. Math. Phys. Tech.*, 1960N4:1–32, 1960.

[230] W. Graf. Differential Forms as Spinors. *Ann. Inst. H. Poincare Phys. Theor.*, 29:85–109, 1978.

[231] Tom Banks, Y. Dothan, and D. Horn. Geometric Fermions. *Phys. Lett.*, B117:413–417, 1982.

[232] I. M. Benn and R. W. Tucker. Fermions Without Spinors. *Commun. Math. Phys.*, 89:341, 1983.

[233] Lay Nam Chang, Djordje Minic, Chen Sun, and Tatsu Takeuchi. Observable Effects of Quantum Gravity. 2016.

[234] Lay Nam Chang, Djordje Minic, Ahmed Roman, Chen Sun, and Tatsu Takeuchi. On the Physics of the Minimal Length: The Question of Gauge Invariance. 2016. [Int. J. Mod. Phys.A31,1630012(2016)].

[235] Yue Zhang, Haipeng An, Xiangdong Ji, and Rabindra N. Mohapatra. General CP Violation in Minimal Left-Right Symmetric Model and Constraints on the Right-Handed Scale. *Nucl. Phys.*, B802:247–279, 2008.

[236] G. Beall and A. Soni. Electric Dipole Moment of the Neutron in a Left-right Symmetric Theory of CP Violation. *Phys. Rev. Lett.*, 47:552, 1981.

[237] G. Beall, Myron Bander, and A. Soni. Constraint on the Mass Scale of a Left-Right Symmetric Electroweak Theory from the K(L) K(S) Mass Difference. *Phys. Rev. Lett.*, 48:848, 1982.

[238] Rabindra N. Mohapatra, Goran Senjanovic, and Minh D. Tran. Strangeness Changing Processes and the Limit on the Right-handed Gauge Boson Mass. *Phys. Rev.*, D28:546, 1983.

[239] Frederick J. Gilman and M. H. Reno. Restrictions on Left-right Symmetric Gauge Theories From the Neutral Kaon System and B Decays. *Phys. Lett.*, B127:426–428, 1983.

[240] G. Ecker, W. Grimus, and H. Neufeld. Higgs Induced Flavor Changing Neutral Interactions in SU(2)-l X SU(2)-r X U(1). *Phys. Lett.*, B127:365, 1983. [Erratum: Phys. Lett.B132,467(1983)].

[241] G. Ecker, W. Grimus, and H. Neufeld. The Neutron Electric Dipole Moment in Left-right Symmetric Gauge Models. *Nucl. Phys.*, B229:421–444, 1983.

[242] G. Ecker and W. Grimus. Mass Mixing, CP Violation and Left-right Symmetry for Heavy Neutral Mesons. *Z. Phys.*, C30:293, 1986.

[243] G. Ecker and W. Grimus. CP Violation and Left-Right Symmetry. *Nucl. Phys.*, B258:328–360, 1985.

[244] Miriam Leurer. $K^0\bar{K}0$ Mixing in Minimal and Nonminimal Left-right Symmetric Theories. *Nucl. Phys.*, B266:147–170, 1986.

[245] P. Herczeg. On Muon Decay in Left-right Symmetric Electroweak Models. *Phys. Rev.*, D34:3449, 1986.

[246] Xiao-Gang He, Bruce H. J. McKellar, and Sandip Pakvasa. Epsilon-prime / Epsilon and the Electric Dipole Moment of the Neutron in Left-right Symmetric Models. *Phys. Rev. Lett.*, 61:1267–1270, 1988.

[247] Paul Langacker and S. Uma Sankar. Bounds on the Mass of W(R) and the W(L)-W(R) Mixing Angle xi in General SU(2)-L x SU(2)-R x U(1) Models. *Phys. Rev.*, D40:1569–1585, 1989.

[248] David London and D. Wyler. Left-right Symmetry and CP Violation in the B System. *Phys. Lett.*, B232:503–508, 1989.

[249] Darwin Chang, Chong Sheng Li, and Tzu Chiang Yuan. Larger neutron electric dipole moment in left-right symmetric models. *Phys. Rev.*, D42:867–870, 1990.

[250] M. Aquino, A. Garcia, and A. Fernandez. Bounds on manifest left-right symmetry from neutron beta decay. *Phys. Lett.*, B261:280–284, 1991.

[251] G. Barenboim, J. Bernabeu, and M. Raidal. Spontaneous CP violation in the left-right model and the kaon system. *Nucl. Phys.*, B478:527–543, 1996.

[252] Patricia Ball and Robert Fleischer. An Analysis of B_s decays in the left-right symmetric model with spontaneous CP violation. *Phys. Lett.*, B475:111–119, 2000.

[253] Ken Kiers, Jeff Kolb, John Lee, Amarjit Soni, and Guo-Hong Wu. Ubiquitous CP violation in a top inspired left-right model. *Phys. Rev.*, D66:095002, 2002.

[254] Martti Raidal. CP asymmetry in $B \to \phi K(S)$ decays in left-right models and its implications on B(s) decays. *Phys. Rev. Lett.*, 89:231803, 2002.

[255] M. Czakon, J. Gluza, and J. Hejczyk. Muon decay to one loop order in the left-right symmetric model. *Nucl. Phys.*, B642:157–172, 2002.

[256] Chuan-Hung Chen and Soo-hyeon Nam. Left-right mixing on leptonic and semileptonic $b \to u$ decays. *Phys. Lett.*, B666:462–466, 2008.

[257] Panying Chen, Hongwei Ke, and Xiangdong Ji. Direct CP Violation in K-decay and Minimal Left-Right Symmetry Scale. *Phys. Lett.*, B677:157–159, 2009.

[258] Fanrong Xu, Haipeng An, and Xiangdong Ji. Neutron Electric Dipole Moment Constraint on Scale of Minimal Left-Right Symmetric Model. *JHEP*, 03:088, 2010.

[259] Alessio Maiezza, Miha Nemevsek, Fabrizio Nesti, and Goran Senjanovic. Left-Right Symmetry at LHC. *Phys. Rev.*, D82:055022, 2010.

[260] R. Bayes et al. Experimental Constraints on Left-Right Symmetric Models from Muon Decay. *Phys. Rev. Lett.*, 106:041804, 2011.

[261] J. Chakrabortty, J. Gluza, R. Sevillano, and R. Szafron. Left-Right Symmetry at LHC and Precise 1-Loop Low Energy Data. *JHEP*, 07:038, 2012.

[262] Stefano Bertolini, Alessio Maiezza, and Fabrizio Nesti. Present and Future K and B Meson Mixing Constraints on TeV Scale Left-Right Symmetry. *Phys. Rev.*, D89(9):095028, 2014.

[263] K. S. Babu, Kazuo Fujikawa, and Atsushi Yamada. Constraints on left-right symmetric models from the process $b \to s\gamma$. *Phys. Lett.*, B333:196–201, 1994.

[264] Thomas G. Rizzo. Constraints from $b \to s\gamma$ on the left-right symmetric model. *Phys. Rev.*, D50:3303–3309, 1994.

[265] T. G. Rizzo. $b \to s\ell^+\ell^-$ in the left-right symmetric model. In *B physics and CP violation. Proceedings, 2nd International Conference, Honolulu, USA, March 24-27, 1997*, pages 457–461, 1997.

[266] C. S. Kim and Yeong Gyun Kim. $b \to s\gamma$ decays in the left-right symmetric model. *Phys. Rev.*, D61:054008, 2000.

[267] G. Couture, M. Frank, and H. Konig. Doubly charged Higgsino contribution to the decays $\mu \to e\gamma$ and $\mu \to 3e$ and to the anomalous magnetic moment of the muon Delta a(mu) within the left-right supersymmetric model. *Phys. Rev.*, D56:4219–4225, 1997.

[268] Mariana Frank and Shu-quan Nie. Delta M(K) and epsilon(K) in the left-right supersymmetric model. *Phys. Rev.*, D67:115008, 2003.

[269] Yue Zhang, Haipeng An, and Xiang-dong Ji. Constraining the right-handed scale through kaon mixing in the supesymmetric left-right model. *Phys. Rev.*, D78:035006, 2008.

[270] Bhaskar Dutta and Yukihiro Mimura. Constraint from $D - \bar{D}$ Mixing in Left-Right Symmetric Models. *Phys. Rev.*, D77:051701, 2008.

[271] Wai-Yee Keung and Goran Senjanovic. Majorana Neutrinos and the Production of the Right-handed Charged Gauge Boson. *Phys. Rev. Lett.*, 50:1427, 1983.

[272] Georges Aad et al. Search for heavy neutrinos and right-handed W bosons in events with two leptons and jets in pp collisions at $\sqrt{s} = 7$ TeV with the ATLAS detector. *Eur. Phys. J.*, C72:2056, 2012.

[273] Vardan Khachatryan et al. Search for heavy neutrinos and W bosons with right-handed couplings in proton-proton collisions at $\sqrt{s} = 8\,\text{TeV}$. *Eur. Phys. J.*, C74(11):3149, 2014.

[274] Georges Aad et al. Search for doubly-charged Higgs bosons in like-sign dilepton final states at $\sqrt{s} = 7$ TeV with the ATLAS detector. *Eur. Phys. J.*, C72:2244, 2012.

[275] Serguei Chatrchyan et al. A search for a doubly-charged Higgs boson in pp collisions at $\sqrt{s} = 7$ TeV. *Eur. Phys. J.*, C72:2189, 2012.

[276] M. Hirsch, H. V. Klapdor-Kleingrothaus, and O. Panella. Double beta decay in left-right symmetric models. *Phys. Lett.*, B374:7–12, 1996.

[277] Vladimir Tello, Miha Nemevsek, Fabrizio Nesti, Goran Senjanovic, and Francesco Vissani. Left-Right Symmetry: from LHC to Neutrinoless Double Beta Decay. *Phys. Rev. Lett.*, 106:151801, 2011.

[278] Werner Rodejohann. Neutrino-less Double Beta Decay and Particle Physics. *Int. J. Mod. Phys.*, E20:1833–1930, 2011.

[279] V. Cirigliano, A. Kurylov, M. J. Ramsey-Musolf, and P. Vogel. Neutrinoless double beta decay and lepton flavor violation. *Phys. Rev. Lett.*, 93:231802, 2004.

[280] P. S. Bhupal Dev, Srubabati Goswami, Manimala Mitra, and Werner Rodejohann. Constraining Neutrino Mass from Neutrinoless Double Beta Decay. *Phys. Rev.*, D88:091301, 2013.

[281] S. P. Das, F. F. Deppisch, O. Kittel, and J. W. F. Valle. Heavy Neutrinos and Lepton Flavour Violation in Left-Right Symmetric Models at the LHC. *Phys. Rev.*, D86:055006, 2012.

[282] James Barry and Werner Rodejohann. Lepton number and flavour violation in TeV-scale left-right symmetric theories with large left-right mixing. *JHEP*, 09:153, 2013.

[283] Peter Minkowski. $\mu \to e\gamma$ at a Rate of One Out of 10^9 Muon Decays? *Phys. Lett.*, B67:421–428, 1977.

[284] J. Adam et al. New constraint on the existence of the $\mu^+ \to e^+\gamma$ decay. *Phys. Rev. Lett.*, 110:201801, 2013.

[285] D. N. Dinh, A. Ibarra, E. Molinaro, and S. T. Petcov. The $\mu - e$ Conversion in Nuclei, $\mu \to e\gamma, \mu \to 3e$ Decays and TeV Scale See-Saw Scenarios of Neutrino Mass Generation. *JHEP*, 08:125, 2012. [Erratum: JHEP09,023(2013)].

[286] U. Bellgardt et al. Search for the Decay $\mu^+ \to e^+e^+e^-$. *Nucl. Phys.*, B299:1–6, 1988.

[287] C. Dohmen et al. Test of lepton flavor conservation in $\mu \to e$ conversion on titanium. *Phys. Lett.*, B317:631–636, 1993.

[288] W. Honecker et al. Improved limit on the branching ratio of $\mu \to e$ conversion on lead. *Phys. Rev. Lett.*, 76:200–203, 1996.

[289] J. Kaulard et al. Improved limit on the branching ratio of $\mu \to e$ conversion on titanium. *Phys. Lett.*, B422:334–338, 1998.

[290] Wilhelm H. Bertl et al. A Search for muon to electron conversion in muonic gold. *Eur. Phys. J.*, C47:337–346, 2006.

[291] V. Cirigliano, A. Kurylov, M. J. Ramsey-Musolf, and P. Vogel. Lepton flavor violation without supersymmetry. *Phys. Rev.*, D70:075007, 2004.

[292] K. Hayasaka et al. New Search for $\tau \to \mu\gamma$ and $\tau \to e\gamma$ Decays at Belle. *Phys. Lett.*, B666:16–22, 2008.

[293] Bernard Aubert et al. Searches for Lepton Flavor Violation in the Decays $\tau \to e\gamma$ and $\tau \to \mu\gamma$. *Phys. Rev. Lett.*, 104:021802, 2010.

[294] Y. Miyazaki et al. Search for Lepton Flavor Violating tau Decays into Three Leptons. *Phys. Lett.*, B660:154–160, 2008.

[295] J. P. Lees et al. Limits on tau Lepton-Flavor Violating Decays in three charged leptons. *Phys. Rev.*, D81:111101, 2010.

[296] R Aaij et al. Searches for violation of lepton flavour and baryon number in tau lepton decays at LHCb. *Phys. Lett.*, B724:36–45, 2013.

[297] A. G. Akeroyd, Mayumi Aoki, and Yasuhiro Okada. Lepton Flavour Violating tau Decays in the Left-Right Symmetric Model. *Phys. Rev.*, D76:013004, 2007.

[298] A. G. Akeroyd et al. Physics at super B factory. 2004.

[299] M. Bona et al. SuperB: A High-Luminosity Asymmetric e+ e- Super Flavor Factory. Conceptual Design Report. 2007.

[300] Y. G. Cui et al. Conceptual design report for experimental search for lepton flavor violating mu- - e- conversion at sensitivity of 10**(-16) with a slow-extracted bunched proton beam (COMET). 2009.

[301] R. J. Abrams et al. Mu2e Conceptual Design Report. 2012.

[302] G. Senjanovic and A. Sokorac. Effects of Heavy Higgs Scalars at Low-energies. *Phys. Rev.*, D18:2708, 1978.

[303] Shiraz Minwalla, Mark Van Raamsdonk, and Nathan Seiberg. Noncommutative perturbative dynamics. *JHEP*, 02:020, 2000.

[304] Laurent Freidel, Robert G. Leigh, and Djordje Minic. Born Reciprocity in String Theory and the Nature of Spacetime. *Phys. Lett.*, B730:302–306, 2014.

[305] Harald Grosse and Raimar Wulkenhaar. Renormalization of phi**4 theory on noncommutative R**4 in the matrix base. *Commun. Math. Phys.*, 256:305–374, 2005.

[306] Georges Aad et al. Observation of a new particle in the search for the Standard Model Higgs boson with the ATLAS detector at the LHC. *Phys. Lett.*, B716:1–29, 2012.

[307] Serguei Chatrchyan et al. Observation of a new boson at a mass of 125 GeV with the CMS experiment at the LHC. *Phys. Lett.*, B716:30–61, 2012.

[308] Georges Aad et al. Search for high-mass diboson resonances with boson-tagged jets in proton-proton collisions at $\sqrt{s} = 8$ TeV with the ATLAS detector. *JHEP*, 12:055, 2015.

[309] Vardan Khachatryan et al. Search for resonances and quantum black holes using dijet mass spectra in proton-proton collisions at $\sqrt{s} = 8$ TeV. *Phys. Rev.*, D91(5):052009, 2015.

[310] Georges Aad et al. Search for new phenomena in the dijet mass distribution using $p-p$ collision data at $\sqrt{s} = 8$ TeV with the ATLAS detector. *Phys. Rev.*, D91(5):052007, 2015.

[311] CMS Collaboration. Search for massive WH resonances decaying to $\ell\nu\mathrm{b\bar{b}}$ final state in the boosted regime at $\sqrt{s} = 8\,\mathrm{TeV}$. 2015.

[312] Vardan Khachatryan et al. Search for massive resonances decaying into pairs of boosted bosons in semi-leptonic final states at $\sqrt{s} = 8$ TeV. *JHEP*, 08:174, 2014.

[313] The ATLAS collaboration. Search for WW, WZ, and ZZ resonances in pp collisions at $\sqrt{s} = 8$ TeV with the ATLAS detector. 2015.

[314] D. Chang, R. N. Mohapatra, J. Gipson, R. E. Marshak, and M. K. Parida. Experimental Tests of New SO(10) Grand Unification. *Phys. Rev.*, D31:1718, 1985.

[315] M. K. Parida and C. C. Hazra. Superheavy Higgs Scalar Effects in Effective Gauge Theories From SO(10) Grand Unification With Low Mass Right-handed Gauge Bosons. *Phys. Rev.*, D40:3074–3085, 1989.

[316] N. G. Deshpande, E. Keith, and Palash B. Pal. Implications of LEP results for SO(10) grand unification. *Phys. Rev.*, D46:2261–2264, 1993.

[317] Stefano Bertolini, Luca Di Luzio, and Michal Malinsky. Intermediate mass scales in the non-supersymmetric SO(10) grand unification: A Reappraisal. *Phys. Rev.*, D80:015013, 2009.

[318] K. S. Babu and R. N. Mohapatra. Coupling Unification, GUT-Scale Baryogenesis and Neutron-Antineutron Oscillation in SO(10). *Phys. Lett.*, B715:328–334, 2012.

[319] Ram Lal Awasthi, M. K. Parida, and Sudhanwa Patra. Neutrino masses, dominant neutrinoless double beta decay, and observable lepton flavor violation in left-right models and SO(10) grand unification with low mass W_R, Z_R bosons. *JHEP*, 08:122, 2013.

[320] Triparno Bandyopadhyay, Biswajoy Brahmachari, and Amitava Raychaudhuri. Implications of the CMS search for W_R on grand unification. *JHEP*, 02:023, 2016.

[321] Ufuk Aydemir. SO(10) grand unification in light of recent LHC searches and colored scalars at the TeV-scale. *Int. J. Mod. Phys.*, A31:1650034, 2016.

[322] N. G. Deshpande, E. Keith, and T. G. Rizzo. SO(10) grand unification with a low-energy M(R). *Phys. Rev. Lett.*, 70:3189–3192, 1993.

[323] Swarup Kumar Majee, Mina K. Parida, Amitava Raychaudhuri, and Utpal Sarkar. Low intermediate scales for leptogenesis in SUSY SO(10) GUTs. *Phys. Rev.*, D75:075003, 2007.

[324] M. K. Parida. Intermediate left-right gauge symmetry, unification of couplings and fermion masses in SUSY SO(10) x S(4). *Phys. Rev.*, D78:053004, 2008.

[325] Mina K. Parida and Amitava Raychaudhuri. Inverse see-saw, leptogenesis, observable proton decay and $\Delta_{\mathrm{R}}^{\pm\pm}$ in SUSY SO(10) with heavy W_R. *Phys. Rev.*, D82:093017, 2010.

[326] Keith R. Dienes. Statistics on the heterotic landscape: Gauge groups and cosmological constants of four-dimensional heterotic strings. *Phys. Rev.*, D73:106010, 2006.

[327] Frank F. Deppisch, Tomas E. Gonzalo, Sudhanwa Patra, Narendra Sahu, and Utpal Sarkar. Signal of Right-Handed Charged Gauge Bosons at the LHC? *Phys. Rev.*, D90(5):053014, 2014.

[328] Frank F. Deppisch, Tomas E. Gonzalo, Sudhanwa Patra, Narendra Sahu, and Utpal Sarkar. Double beta decay, lepton flavor violation, and collider signatures of left-right symmetric models with spontaneous D-parity breaking. *Phys. Rev.*, D91(1):015018, 2015.

[329] Johann Brehmer, JoAnne Hewett, Joachim Kopp, Thomas Rizzo, and Jamie Tattersall. Symmetry Restored in Dibosons at the LHC? *JHEP*, 10:182, 2015.

[330] Frank F. Deppisch, Lukas Graf, Suchita Kulkarni, Sudhanwa Patra, Werner Rodejohann, Narendra Sahu, and Utpal Sarkar. Reconciling the 2 TeV excesses at the LHC in a linear seesaw left-right model. *Phys. Rev.*, D93(1):013011, 2016.

[331] S. Schael et al. Precision electroweak measurements on the Z resonance. *Phys. Rept.*, 427:257–454, 2006.

[332] Bogdan A. Dobrescu and Zhen Liu. W' Boson near 2 TeV: Predictions for Run 2 of the LHC. *Phys. Rev. Lett.*, 115(21):211802, 2015.

[333] Bogdan A. Dobrescu and Zhen Liu. Heavy Higgs bosons and the 2 TeV W$'$ boson. *JHEP*, 10:118, 2015.

[334] Giacomo Cacciapaglia, Aldo Deandrea, and Michio Hashimoto. Scalar Hint from the Diboson Excess? *Phys. Rev. Lett.*, 115(17):171802, 2015.

[335] Hidenori S. Fukano, Shinya Matsuzaki, and Koichi Yamawaki. Conformal Barrier for New Vector Bosons Decay to the Higgs. *Mod. Phys. Lett.*, A31(09):1630009, 2016.

[336] Chuan-Hung Chen and Takaaki Nomura. 2 TeV Higgs boson and diboson excess at the LHC. *Phys. Lett.*, B749:464–468, 2015.

[337] Yuji Omura, Kazuhiro Tobe, and Koji Tsumura. Survey of Higgs interpretations of the diboson excesses. *Phys. Rev.*, D92(5):055015, 2015.

[338] Kenneth Lane and Lukas Pritchett. Heavy Vector Partners of the Light Composite Higgs. *Phys. Lett.*, B753:211–214, 2016.

[339] Pere Arnan, Domenec Espriu, and Federico Mescia. Interpreting a 2 TeV resonance in WW scattering. *Phys. Rev.*, D93(1):015020, 2016.

[340] P. S. Bhupal Dev and R. N. Mohapatra. Unified explanation of the $eejj$, diboson and dijet resonances at the LHC. *Phys. Rev. Lett.*, 115(18):181803, 2015.

[341] Pilar Coloma, Bogdan A. Dobrescu, and Jacobo Lopez-Pavon. Right-handed neutrinos and the 2 TeV W' boson. *Phys. Rev.*, D92(11):115023, 2015.

[342] J. A. Aguilar-Saavedra. Triboson interpretations of the ATLAS diboson excess. *JHEP*, 10:099, 2015.

[343] Matti Heikinheimo, Martti Raidal, and Christian Spethmann. Testing Right-Handed Currents at the LHC. *Eur. Phys. J.*, C74(10):3107, 2014.

[344] D. Chang, R. N. Mohapatra, and M. K. Parida. A New Approach to Left-Right Symmetry Breaking in Unified Gauge Theories. *Phys. Rev.*, D30:1052, 1984.

[345] F. del Aguila and Luis E. Ibanez. Higgs Bosons in SO(10) and Partial Unification. *Nucl. Phys.*, B177:60–86, 1981.

[346] Rabindra N. Mohapatra and Goran Senjanovic. Higgs Boson Effects in Grand Unified Theories. *Phys. Rev.*, D27:1601, 1983.

[347] Rabindra N. Mohapatra and R. E. Marshak. Local B-L Symmetry of Electroweak Interactions, Majorana Neutrinos and Neutron Oscillations. *Phys. Rev. Lett.*, 44:1316–1319, 1980. [Erratum: Phys. Rev. Lett. 44, 1643 (1980)].

[348] Laurent Freidel, Robert G. Leigh, and Djordje Minic. Metastring Theory and Modular Space-time. *JHEP*, 06:006, 2015.

[349] Search for resonances decaying to photon pairs in 3.2 fb^{-1} of pp collisions at $\sqrt{s} = 13$ TeV with the ATLAS detector. 2015. ATLAS-CONF-2015-081.

[350] Search for new physics in high mass diphoton events in proton-proton collisions at 13 TeV. 2015. CMS-PAS-EXO-15-004.

[351] Ufuk Aydemir and Tanumoy Mandal. Interpretation of the 750 GeV diphoton excess with colored scalars in $\mathbf{SO(10)}$ grand unification. 2016.

[352] Arnab Dasgupta, Manimala Mitra, and Debasish Borah. Minimal Left-Right Symmetry Confronted with the 750 GeV Di-photon Excess at LHC. 2015.

[353] Georges Aad et al. Combination of searches for WW, WZ, and ZZ resonances in pp collisions at $\sqrt{s} = 8$ TeV with the ATLAS detector. *Phys. Lett.*, B755:285–305, 2016.

[354] Vardan Khachatryan et al. Search for massive WH resonances decaying into the $\ell\nu\mathrm{b\bar{b}}$ final state at $\sqrt{s} = 8$ TeV. 2016.

[355] R. N. Mohapatra. *Unification and Supersymmetry – The Frontiers of Quark-Lepton Physics*. Springer, 3rd edition, 2002.

[356] Lincoln Wolfenstein. Parametrization of the Kobayashi-Maskawa Matrix. *Phys. Rev. Lett.*, 51:1945, 1983.

[357] Debasish Borah, Sudhanwa Patra, and Prativa Pritimita. Sub-dominant type-II seesaw as an origin of non-zero θ_{13} in SO(10) model with TeV scale Z' gauge boson. *Nucl. Phys.*, B881:444–466, 2014.

[358] K. S. Babu, B. Bajc, and Z. Tavartkiladze. Realistic Fermion Masses and Nucleon Decay Rates in SUSY SU(5) with Vector-Like Matter. *Phys. Rev.*, D86:075005, 2012.

[359] Ram Lal Awasthi and Mina K. Parida. Inverse Seesaw Mechanism in Nonsupersymmetric SO(10), Proton Lifetime, Nonunitarity Effects, and a Low-mass Z' Boson. *Phys. Rev.*, D86:093004, 2012.

[360] Lawrence J. Hall and Yasunori Nomura. Grand Unification and Intermediate Scale Supersymmetry. *JHEP*, 02:129, 2014.

[361] Junji Hisano, Takumi Kuwahara, and Natsumi Nagata. Grand Unification in High-scale Supersymmetry. *Phys. Lett.*, B723:324–329, 2013.

[362] Carolina Arbeláez, Martin Hirsch, Michal Malinský, and Jorge C. Romão. LHC-scale left-right symmetry and unification. *Phys. Rev.*, D89(3):035002, 2014.

[363] Ilja Dorsner, Svjetlana Fajfer, Admir Greljo, and Jernej F. Kamenik. Higgs Uncovering Light Scalar Remnants of High Scale Matter Unification. *JHEP*, 11:130, 2012.

[364] Junji Hisano, Daiki Kobayashi, Takumi Kuwahara, and Natsumi Nagata. Decoupling Can Revive Minimal Supersymmetric SU(5). *JHEP*, 07:038, 2013.

[365] Zurab Berezhiani, Marco Chianese, Gennaro Miele, and Stefano Morisi. Chances for SUSY-GUT in the LHC Epoch. *JHEP*, 08:083, 2015.

[366] T. Daniel Brennan. Two Loop Unification of Non-SUSY SO(10) GUT with TeV Scalars. *Phys. Rev.*, D95(6):065008, 2017.

[367] Triparno Bandyopadhyay and Amitava Raychaudhuri. Left-right model with TeV fermionic dark matter and unification. 2017.

[368] K. Hayasaka et al. Search for Lepton Flavor Violating Tau Decays into Three Leptons with 719 Million Produced Tau+Tau- Pairs. *Phys. Lett.*, B687:139–143, 2010.

[369] J. Adam et al. New limit on the lepton-flavour violating decay $\mu^+ \to e^+\gamma$. *Phys. Rev. Lett.*, 107:171801, 2011.

[370] R. D. Bolton et al. Search for Rare Muon Decays with the Crystal Box Detector. *Phys. Rev.*, D38:2077, 1988.

[371] R. D. Bolton et al. Search for the Decay $\mu^+ \to e^+\gamma$. *Phys. Rev. Lett.*, 56:2461–2464, 1986.

[372] D. Grosnick et al. Search for the Rare Decay $\mu^+ \to e^+\gamma\gamma$. *Phys. Rev. Lett.*, 57:3241, 1986.

[373] A. Abada, C. Biggio, F. Bonnet, M. B. Gavela, and T. Hambye. $\mu \to e\gamma$ and $\tau \to \ell\gamma$ decays in the fermion triplet seesaw model. *Phys. Rev.*, D78:033007, 2008.

[374] K. Abe et al. Search for proton decay via $p \to e^+\pi^0$ and $p \to \mu^+\pi^0$ in 0.31 megaton years exposure of the Super-Kamiokande water Cherenkov detector. *Phys. Rev.*, D95(1):012004, 2017.

[375] Warren Wright. Oscillation degeneracy in non-standard neutrino interactions. *AIP Conf. Proc.*, 1743:030010, 2016.

[376] Tsutomu Yanagida. Horizontal Symmetry And Masses Of Neutrinos. *Conf. Proc.*, C7902131:95–99, 1979.

[377] S. L. Glashow. The Future of Elementary Particle Physics. *NATO Sci. Ser. B*, 61:687, 1980.

[378] Murray Gell-Mann, Pierre Ramond, and Richard Slansky. Complex Spinors and Unified Theories. *Conf. Proc.*, C790927:315–321, 1979.

[379] D. Wyler and L. Wolfenstein. Massless Neutrinos in Left-Right Symmetric Models. *Nucl. Phys.*, B218:205–214, 1983.

[380] R. N. Mohapatra and J. W. F. Valle. Neutrino Mass and Baryon Number Nonconservation in Superstring Models. *Phys. Rev.*, D34:1642, 1986.

[381] M. C. Gonzalez-Garcia, A. Santamaria, and J. W. F. Valle. Isosinglet Neutral Heavy Lepton Production in Z Decays and Neutrino Mass. *Nucl. Phys.*, B342:108–126, 1990.

[382] M. C. Gonzalez-Garcia and J. W. F. Valle. Fast Decaying Neutrinos and Observable Flavor Violation in a New Class of Majoron Models. *Phys. Lett.*, B216:360–366, 1989.

[383] F. Deppisch and J. W. F. Valle. Enhanced lepton flavor violation in the supersymmetric inverse seesaw model. *Phys. Rev.*, D72:036001, 2005.

[384] Sin Kyu Kang and C. S. Kim. Extended double seesaw model for neutrino mass spectrum and low scale leptogenesis. *Phys. Lett.*, B646:248–252, 2007.

[385] Joachim Kopp, Pedro A. N. Machado, Michele Maltoni, and Thomas Schwetz. Sterile Neutrino Oscillations: The Global Picture. *JHEP*, 05:050, 2013.

[386] K.N. Abazajian, M.A. Acero, S.K. Agarwalla, A.A. Aguilar-Arevalo, C.H. Albright, et al. Light Sterile Neutrinos: A White Paper. 2012.

[387] Heinrich Päs and Philipp Sicking. Discriminating sterile neutrinos and unitarity violation with CP invariants. *Phys. Rev.*, D95(7):075004, 2017.

[388] Ernest Ma. Deciphering the Seesaw Nature of Neutrino Mass from Unitarity Violation. *Mod. Phys. Lett.*, A24:2161–2165, 2009.

[389] J. A. Aguilar-Saavedra and G. C. Branco. Unitarity triangles and geometrical description of CP violation with Majorana neutrinos. *Phys. Rev.*, D62:096009, 2000.

[390] V. Barger, D. Marfatia, and K. Whisnant. Breaking eight fold degeneracies in neutrino CP violation, mixing, and mass hierarchy. *Phys. Rev.*, D65:073023, 2002.

[391] Monojit Ghosh, Pomita Ghoshal, Srubabati Goswami, Newton Nath, and Sushant K. Raut. New look at the degeneracies in the neutrino oscillation parameters, and their resolution by T2K, NOνA and ICAL. *Phys. Rev.*, D93(1):013013, 2016.

[392] Suprabh Prakash, Sushant K. Raut, and S. Uma Sankar. Getting the Best Out of T2K and NOvA. *Phys. Rev.*, D86:033012, 2012.

[393] Sanjib Kumar Agarwalla, Suprabh Prakash, and S. Uma Sankar. Resolving the octant of theta23 with T2K and NOvA. *JHEP*, 07:131, 2013.

[394] Sanjib Kumar Agarwalla, Sabya Sachi Chatterjee, and Antonio Palazzo. Degeneracy between θ_{23} octant and neutrino non-standard interactions at DUNE. *Phys. Lett.*, B762:64–71, 2016.

[395] Monojit Ghosh, Shivani Gupta, Zachary M. Matthews, Pankaj Sharma, and Anthony G. Williams. Study of parameter degeneracy and hierarchy sensitivity of NOνA in presence of sterile neutrino. 2017.

[396] Irina Mocioiu and Warren Wright. Non-standard neutrino interactions in the mu?tau sector. *Nucl. Phys.*, B893:376–390, 2015.

[397] A.M. Gago, H. Minakata, H. Nunokawa, S. Uchinami, and R. Zukanovich Funchal. Resolving CP Violation by Standard and Nonstandard Interactions and Parameter Degeneracy in Neutrino Oscillations. *JHEP*, 1001:049, 2010.

[398] Sanjib Kumar Agarwalla, Yee Kao, Chen Sun, and Tatsu Takeuchi. Running of Oscillation Parameters in Matter in the presence of Flavor-Off-Diagonal Non-Standard Interactions of the Neutrino. 2017.

[399] Sanjib Kumar Agarwalla, Yee Kao, Chen Sun, and Tatsu Takeuchi. Running of Oscillation Parameters in Matter in the presence of Flavor-Off-Diagonal Non-Standard Interactions of the Neutrino, Part 2. 2017. In preparation.

[400] Pilar Coloma, Chen Sun, Tatsu Takeuchi, and Vishvas Pandey. Constraining the Interactions of the Neutrino with Spallation Neutron Sources. 2017. In preparation.

[401] I. Stancu et al. The OscSNS White Paper, October 6, 2008. `http://www.phys.ufl.edu/research/oscsns/wiki/pmwiki.php/Main/OscSNSHomePage`.

[402] I. Habib et al. The OscSNS White Paper, April 30, 2012. http://www.phys.ufl.edu/research/oscsns/wiki/pmwiki.php/Main/OscSNSHomePage.

[403] Heather Ray. OscSNS: Precision Neutrino Measurements at the Spallation Neutron Source. *J.Phys.Conf.Ser.*, 136:022029, 2008.

[404] Geoffrey B. Mills. Neutrino physics at OscSNS. *AIP Conf.Proc.*, 1189:94–96, 2009.

[405] William C. Louis. Searching for physics beyond the standard model with accelerator neutrino experiments. *J.Phys.Conf.Ser.*, 173:012017, 2009.

[406] http://neutrons.ornl.gov/facilities/SNS/.

[407] Heinrich Pas, Sandip Pakvasa, and Thomas J. Weiler. Sterile-active neutrino oscillations and shortcuts in the extra dimension. *Phys.Rev.*, D72:095017, 2005.

[408] Michele Maltoni and Thomas Schwetz. Sterile neutrino oscillations after first MiniBooNE results. *Phys.Rev.*, D76:093005, 2007.

[409] Joachim Kopp, Michele Maltoni, and Thomas Schwetz. Are there sterile neutrinos at the eV scale? *Phys.Rev.Lett.*, 107:091801, 2011.

[410] Particle Data Group. Atomic and nuclear properties of materials for more than 300 materials, 2012. http://pdg.lbl.gov/2012/AtomicNuclearProperties/.

[411] Donald E. Groom, Nikolai V. Mokhov, and Sergei I. Striganov. Muon stopping power and range tables 10-MeV to 100-TeV. *Atom.Data Nucl.Data Tabl.*, 78:183–356, 2001.

[412] S. Agostinelli et al. Geant4: A Simulation toolkit. *Nucl.Instrum.Meth.*, A506:250–303, 2003. http://geant4.cern.ch/.

[413] John Allison, K. Amako, J. Apostolakis, H. Araujo, P.A. Dubois, et al. Geant4 developments and applications. *IEEE Trans.Nucl.Sci.*, 53:270, 2006.

[414] M. Fukugita, Y. Kohyama, and K. Kubodera. NEUTRINO REACTION CROSS-SECTIONS ON C-12 TARGET. *Phys.Lett.*, B212:139, 1988.

[415] J. Engel, E. Kolbe, K. Langanke, and P. Vogel. Neutrino induced transitions between the ground states of the A=12 triad. *Phys.Rev.*, C54:2740–2744, 1996.

[416] F. Ajzenberg-Selove. Energy levels of light nuclei A = 11-12. *Nucl.Phys.*, A506:1–158, 1990.

[417] C. Athanassopoulos et al. Measurements of the reactions C-12 (electron-neutrino, e-) N-12 (g.s.) and C-12 (electron-neutrino, e-) N*-12. *Phys.Rev.*, C55:2078–2091, 1997.

[418] Gaby Radel and Rolf Beyer. Neutrino electron scattering. *Mod. Phys. Lett.*, A8:1067–1088, 1993.

[419] Natalie Jachowicz, Vishvas Pandey, Marco Martini, Raúl González-Jiménez, Tom Van Cuyck, and Nils Van Dessel. CRPA Calculations for Neutrino-Nucleus Scattering: From Very Low Energies to the Quasielastic Peak. *JPS Conf. Proc.*, 12:010018, 2016.

[420] B.E. Bodmann et al. Neutrino interactions with carbon: Recent measurements and a new test of electron-neutrino, anti-muon-neutrino universality. *Phys.Lett.*, B332:251–257, 1994.

[421] B. Armbruster, I. Blair, B.A. Bodmann, N.E. Booth, G. Drexlin, et al. KARMEN limits on electron-neutrino → tau-neutrino oscillations in two neutrino and three neutrino mixing schemes. *Phys.Rev.*, C57:3414–3424, 1998.

[422] L.B. Auerbach et al. Measurements of charged current reactions of nu(e) on 12-C. *Phys.Rev.*, C64:065501, 2001.

[423] D.A. Krakauer, R.L. Talaga, R.C. Allen, H.H. Chen, R. Hausammann, et al. Experimental study of neutrino absorption on carbon. *Phys.Rev.*, C45:2450–2463, 1992.

[424] B. Armbruster et al. Measurement of the weak neutral current excitation C-12(nu(mu) nu'(mu))C*-12(1+,1,15.1-MeV) at E(nu(mu)) = 29.8-MeV. *Phys.Lett.*, B423:15–20, 1998.

[425] G. Drexlin et al. First observation of the neutral current nuclear excitation C-12 (nu, nu-prime) C-12* (1+, 1). *Phys.Lett.*, B267:321–324, 1991.

[426] B. Zeitnitz. KARMEN: Neutrino physics at ISIS. *Prog.Part.Nucl.Phys.*, 32:351–373, 1994.

[427] G. Bellini et al. The Borexino experiment and the results of the Counting Test Facility. *Nucl.Phys.Proc.Suppl.*, 48:363–369, 1996.

[428] V. Pandey, N. Jachowicz, M. Martini, R. González-Jiménez, J. Ryckebusch, T. Van Cuyck, and N. Van Dessel. Impact of low-energy nuclear excitations on neutrino-nucleus scattering at MiniBooNE and T2K kinematics. *Phys. Rev.*, C94(5):054609, 2016.

[429] B. Pontecorvo. Inverse beta-processes and non-conservation of lepton charge. *Sov. Phys. JETP*, 7:172–173, 1958.

[430] Ziro Maki, Masami Nakagawa, and Shoichi Sakata. Remarks on the unified model of elementary particles. *Prog. Theor. Phys.*, 28:870–880, 1962.

[431] B. Pontecorvo. Neutrino Experiments and the Problem of Conservation of Leptonic Charge. *Sov. Phys. JETP*, 26:984–988, 1968.

[432] Sanjib Kumar Agarwalla, Yee Kao, Debashis Saha, and Tatsu Takeuchi. Running of Oscillation Parameters in Matter in the presence of Flavor-Diagonal Non-Standard Interactions of the Neutrino. 2015.

[433] S. T. Petcov and S. Toshev. Three Neutrino Oscillations in Matter: Analytical Results in the Adiabatic Approximation. *Phys. Lett.*, B187:120, 1987.

[434] S. T. Petcov. An Analytic Description of Three Neutrino Oscillations in Matter With Varying Density. *Phys. Lett.*, B214:259, 1988.

[435] P. I. Krastev and S. T. Petcov. Resonance Amplification and T Violation Effects in Three Neutrino Oscillations in the Earth. *Phys. Lett.*, B205:84–92, 1988.

[436] H.W. Zaglauer and K.H. Schwarzer. The Mixing Angles in Matter for Three Generations of Neutrinos and the MSW Mechanism. *Z. Phys.*, C40:273, 1988.

[437] Minako Honda, Yee Kao, Naotoshi Okamura, and Tatsu Takeuchi. A Simple parameterization of matter effects on neutrino oscillations. 2006.

[438] Sanjib Kumar Agarwalla, Yee Kao, and Tatsu Takeuchi. Analytical approximation of the neutrino oscillation matter effects at large θ_{13}. *JHEP*, 1404:047, 2014.

[439] Carl Gustav Jacob Jacobi. Über ein leichtes Verfahren, die in der Theorie der Säkularstörangen vorkommenden Gleichungen numerisch Aufzuloösen. *Crelle's Journal*, 30:51–94, 1846.

[440] S. Davidson, C. Pena-Garay, N. Rius, and A. Santamaria. Present and future bounds on nonstandard neutrino interactions. *JHEP*, 03:011, 2003.

[441] J. Barranco, O.G. Miranda, C.A. Moura, and J.W.F. Valle. Constraining non-standard neutrino-electron interactions. *Phys.Rev.*, D77:093014, 2008.

[442] Carla Biggio, Mattias Blennow, and Enrique Fernandez-Martinez. General bounds on non-standard neutrino interactions. *JHEP*, 0908:090, 2009.

[443] F.J. Escrihuela, M. Tortola, J.W.F. Valle, and O.G. Miranda. Global constraints on muon-neutrino non-standard interactions. *Phys. Rev.*, D83:093002, 2011.

[444] Tommy Ohlsson. Status of non-standard neutrino interactions. *Rept. Prog. Phys.*, 76:044201, 2013.

[445] P. Vilain et al. Flavor universality of neutrino couplings with the Z. *Phys. Lett.*, B320:203–205, 1994.

[446] P. Vilain et al. Precision measurement of electroweak parameters from the scattering of muon-neutrinos on electrons. *Phys.Lett.*, B335:246–252, 1994.

[447] G.P. Zeller et al. A Precise determination of electroweak parameters in neutrino nucleon scattering. *Phys. Rev.Lett.*, 88:091802, 2002.

[448] Richard D. Ball et al. Precision determination of electroweak parameters and the strange content of the proton from neutrino deep-inelastic scattering. *Nucl. Phys.*, B823:195–233, 2009.

[449] W. Bentz, I.C. Cloet, J.T. Londergan, and A.W. Thomas. Reassessment of the NuTeV determination of the weak mixing angle. *Phys. Lett.*, B693:462–466, 2010.

[450] R. Barate et al. Searches for supersymmetry in the photon(s) plus missing energy channels at $\sqrt{s} = 161$-GeV and 172-GeV. *Phys. Lett.*, B420:127–139, 1998.

[451] R. Barate et al. Single photon and multiphoton production in e^+e^- collisions at a center-of-mass energy of 183-GeV. *Phys. Lett.*, B429:201–214, 1998.

[452] A. Heister et al. Single photon and multiphoton production in e^+e^- collisions at $\sqrt{s}$ up to 209-GeV. *Eur.Phys.J.*, C28:1–13, 2003.

[453] M. Acciarri et al. Single and multiphoton events with missing energy in e^+e^- collisions at 161-GeV $< \sqrt{s} <$ 172-GeV. *Phys. Lett.*, B415:299–310, 1997.

[454] M. Acciarri et al. Single and multiphoton events with missing energy in e^+e^- collisions at $\sqrt{s} = 183$-GeV. *Phys. Lett.*, B444:503–515, 1998.

[455] M. Acciarri et al. Single and multiphoton events with missing energy in e^+e^- collisions at $\sqrt{s} = 189$-GeV. *Phys. Lett.*, B470:268–280, 1999.

[456] K. Ackerstaff et al. Photonic events with large missing energy in e^+e^- collisions at $\sqrt{s} = 161$-GeV. *Phys. Lett.*, B391:210–220, 1997.

[457] K. Ackerstaff et al. Search for anomalous production of photonic events with missing energy in e^+e^- collisions at $\sqrt{s} = 130$-GeV to 172-GeV. *Eur.Phys.J.*, C2:607–625, 1998.

[458] G. Abbiendi et al. Search for anomalous photonic events with missing energy in e^+e^- collisions at $\sqrt{s} = 130$-GeV, 136-GeV and 183-GeV. *Eur.Phys.J.*, C8:23–40, 1999.

[459] G. Abbiendi et al. Photonic events with missing energy in e^+e^- collisions at $\sqrt{s} = 189$-GeV. *Eur.Phys.J.*, C18:253–272, 2000.

[460] J. Abdallah et al. Photon events with missing energy in e^+e^- collisions at $\sqrt{s} = 130$-GeV to 209-GeV. *Eur.Phys.J.*, C38:395–411, 2005.

[461] G. Mitsuka et al. Study of Non-Standard Neutrino Interactions with Atmospheric Neutrino Data in Super-Kamiokande I and II. *Phys. Rev.*, D84:113008, 2011.

[462] M. Ambrosio et al. Measurements of atmospheric muon neutrino oscillations, global analysis of the data collected with MACRO detector. *Eur. Phys. J.*, C36:323–339, 2004.

[463] S. Abe et al. Precision Measurement of Neutrino Oscillation Parameters with KamLAND. *Phys. Rev. Lett.*, 100:221803, 2008.

[464] B. Aharmim et al. An Independent Measurement of the Total Active B-8 Solar Neutrino Flux Using an Array of He-3 Proportional Counters at the Sudbury Neutrino Observatory. *Phys. Rev. Lett.*, 101:111301, 2008.

[465] P. Adamson et al. Search for flavor-changing non-standard neutrino interactions by MINOS. *Phys. Rev.*, D88(7):072011, 2013.

[466] Andreas Gross. Atmospheric Neutrino Oscillations in IceCube. *Nucl. Phys. Proc. Suppl.*, 237-238:272–274, 2013.

[467] R. Abbasi et al. The Design and Performance of IceCube DeepCore. *Astropart. Phys.*, 35:615–624, 2012.

[468] M. Maltoni. Standard and nonstandard physics in neutrino oscillations. *Nucl. Phys. Proc. Suppl.*, 114:191–196, 2003.

[469] M.C. Gonzalez-Garcia, Michele Maltoni, and Jordi Salvado. Testing matter effects in propagation of atmospheric and long-baseline neutrinos. *JHEP*, 1105:075, 2011.

[470] Arman Esmaili and Alexei Yu. Smirnov. Probing Non-Standard Interaction of Neutrinos with IceCube and DeepCore. *JHEP*, 1306:026, 2013.

[471] Stefan Antusch, Jochen P. Baumann, and Enrique Fernandez-Martinez. Non-Standard Neutrino Interactions with Matter from Physics Beyond the Standard Model. *Nucl.Phys.*, B810:369–388, 2009.

[472] Jordi Salvado, Olga Mena, Sergio Palomares-Ruiz, and Nuria Rius. Non-standard interactions with high-energy atmospheric neutrinos at IceCube. *JHEP*, 01:141, 2017.

[473] M. B. Gavela, D. Hernandez, T. Ota, and W. Winter. Large gauge invariant non-standard neutrino interactions. *Phys. Rev.*, D79:013007, 2009.

[474] Zurab Berezhiani and Anna Rossi. Limits on the nonstandard interactions of neutrinos from e+ e- colliders. *Phys. Lett.*, B535:207–218, 2002.

[475] Zurab Berezhiani, R. S. Raghavan, and Anna Rossi. Probing nonstandard couplings of neutrinos at the Borexino detector. *Nucl. Phys.*, B638:62–80, 2002.

[476] Davide Meloni, Tommy Ohlsson, Walter Winter, and He Zhang. Non-standard interactions versus non-unitary lepton flavor mixing at a neutrino factory. *JHEP*, 1004:041, 2010.

[477] Michal Malinsky, Tommy Ohlsson, and He Zhang. Non-Standard Neutrino Interactions from a Triplet Seesaw Model. *Phys.Rev.*, D79:011301, 2009.

[478] Tommy Ohlsson, Thomas Schwetz, and He Zhang. Non-standard neutrino interactions in the Zee-Babu model. *Phys.Lett.*, B681:269–275, 2009.

[479] Davide Meloni, Tommy Ohlsson, and He Zhang. Exact and Approximate Formulas for Neutrino Mixing and Oscillations with Non-Standard Interactions. *JHEP*, 0904:033, 2009.

[480] Maria Archidiacono and Steen Hannestad. Updated constraints on non-standard neutrino interactions from Planck. *JCAP*, 1407:046, 2014.

[481] Enrique Fernandez Martinez. Are there consistent models giving observable NSI? *J. Phys. Conf. Ser.*, 408:012031, 2013.

[482] Robert Foot, Girish C. Joshi, and H. Lew. Gauged Baryon and Lepton Numbers. *Phys. Rev.*, D40:2487–2489, 1989.

[483] Subhash Rajpoot. Electroweak Interactions With Gauged Baryon and Lepton Numbers. *Phys. Rev.*, D40:2421, 1989.

[484] Christopher D. Carone and Hitoshi Murayama. Possible light U(1) gauge boson coupled to baryon number. *Phys. Rev. Lett.*, 74:3122–3125, 1995.

[485] Christopher D. Carone and Hitoshi Murayama. Realistic models with a light U(1) gauge boson coupled to baryon number. *Phys. Rev.*, D52:484–493, 1995.

[486] Ernest Ma. Gauged $B - 3L_\tau$ and radiative neutrino masses. *Phys. Lett.*, B433:74–81, 1998.

[487] Ernest Ma and Utpal Sarkar. Gauged $B-3L_\tau$ and baryogenesis. *Phys. Lett.*, B439:95–102, 1998.

[488] Ernest Ma, D.P. Roy, and Utpal Sarkar. A Seesaw model for atmospheric and solar neutrino oscillations. *Phys. Lett.*, B444:391–396, 1998.

[489] Ernest Ma and D.P. Roy. Phenomenology of the $B - 3L_\tau$ gauge boson. *Phys. Rev.*, D58:095005, 1998.

[490] Ernest Ma and D.P. Roy. Minimal seesaw model for atmospheric and solar neutrino oscillations. *Phys. Rev.*, D59:097702, 1999.

[491] Lay Nam Chang, Oleg Lebedev, Will Loinaz, and Tatsu Takeuchi. Constraints on gauged $B - 3L_\tau$ and related theories. *Phys. Rev.*, D63:074013, 2001.

[492] Ernest Ma, D. P. Roy, and Sourov Roy. Gauged L(mu) - L(tau) with large muon anomalous magnetic moment and the bimaximal mixing of neutrinos. *Phys. Lett.*, B525:101–106, 2002.

[493] Seungwon Baek, N. G. Deshpande, X. G. He, and P. Ko. Muon anomalous g-2 and gauged L(muon) - L(tau) models. *Phys. Rev.*, D64:055006, 2001.

[494] Pavel Fileviez Perez and Mark B. Wise. Baryon and lepton number as local gauge symmetries. *Phys. Rev.*, D82:011901, 2010. [Erratum: Phys. Rev.D82,079901(2010)].

[495] Julian Heeck and Werner Rodejohann. Gauged $L_\mu - L_\tau$ Symmetry at the Electroweak Scale. *Phys. Rev.*, D84:075007, 2011.

[496] Michael Duerr, Pavel Fileviez Perez, and Mark B. Wise. Gauge Theory for Baryon and Lepton Numbers with Leptoquarks. *Phys. Rev. Lett.*, 110:231801, 2013.

[497] R. A. Malaney, G. D. Starkman, and S. Tremaine. Time delays of Supernova neutrinos from new long range interactions. *Phys. Rev.*, D51:324–327, 1995.

[498] Alexandre D. Dolgov and Georg G. Raffelt. Screening of long range leptonic forces by cosmic background neutrinos. *Phys. Rev.*, D52:2581–2582, 1995.

[499] Anjan S. Joshipura and Subhendra Mohanty. Constraints on flavor dependent long range forces from atmospheric neutrino observations at super-Kamiokande. *Phys. Lett.*, B584:103–108, 2004.

[500] J. A. Grifols and E. Masso. Neutrino oscillations in the sun probe long range leptonic forces. *Phys. Lett.*, B579:123–126, 2004.

[501] M. C. Gonzalez-Garcia, P. C. de Holanda, E. Masso, and R. Zukanovich Funchal. Probing long-range leptonic forces with solar and reactor neutrinos. *JCAP*, 0701:005, 2007.

[502] Hooman Davoudiasl, Hye-Sung Lee, and William J. Marciano. Long-Range Lepton Flavor Interactions and Neutrino Oscillations. *Phys. Rev.*, D84:013009, 2011.

[503] Sabya Sachi Chatterjee, Arnab Dasgupta, and Sanjib Kumar Agarwalla. Exploring Flavor-Dependent Long-Range Forces in Long-Baseline Neutrino Oscillation Experiments. *JHEP*, 12:167, 2015.

[504] Yasaman Farzan and Ian M. Shoemaker. Lepton Flavor Violating Non-Standard Interactions via Light Mediators. *JHEP*, 07:033, 2016.

[505] Sofiane M. Boucenna, David V. Forero, Patick Huber, Chen Sun, and Tatsu Takeuchi. Constraining Models with Large NSI. 2017. In preparation.

[506] H. Albrecht et al. A Search for lepton flavor violating decays $\tau \to e\alpha$, $\tau \to \mu\alpha$. *Z. Phys.*, C68:25–28, 1995.

[507] Toshiki Yoshinobu and Kiyoshi Hayasaka. MC study for the lepton flavor violating tau decay into a lepton and an undetectable particle. 2016. Poster presentation by Yoshinobu at the 14th International Workshop on Tau Lepton Physics (Tau2016), 19-23 September 2016, IHEP, Beijing, China.

[508] Stephan Narison. New evaluation of the QED running coupling and of the muonium hyperfine splitting. 2001.

[509] A. Abashian et al. The Belle Detector. *Nucl. Instrum. Meth.*, A479:117–232, 2002.

[510] M. Alonso. *QUANTUM PHYSICS. (IN GERMAN)*. 1988.

[511] Semi-empirical mass formula. `https://en.wikipedia.org/wiki/Semi-empirical_mass_formula`. Accessed: 2017-05-04.

[512] M. G. Aartsen et al. Observation of High-Energy Astrophysical Neutrinos in Three Years of IceCube Data. *Phys. Rev. Lett.*, 113:101101, 2014.

[513] John F. Cherry, Alexander Friedland, and Ian M. Shoemaker. Short-baseline neutrino oscillations, Planck, and IceCube. 2016.

[514] Dima G. Yakovlev and C. J. Pethick. Neutron star cooling. *Ann. Rev. Astron. Astrophys.*, 42:169–210, 2004.

[515] M. H. Ahn et al. Measurement of Neutrino Oscillation by the K2K Experiment. *Phys. Rev.*, D74:072003, 2006.

[516] R. Acciarri et al. Long-Baseline Neutrino Facility (LBNF) and Deep Underground Neutrino Experiment (DUNE). 2015.

[517] T. Fukuda. Discovery of Tau Neutrino Appearance and Recent Results from OPERA. In *30th Rencontres de Physique de La Vallée d'Aoste La Thuile, Aosta valley, Italy, March 6-12, 2016*, 2016.

[518] M. Antonello et al. Search for anomalies in the ν_e appearance from a ν_μ beam. *Eur. Phys. J.*, C73:2599, 2013.

[519] K. Abe et al. Indication of Electron Neutrino Appearance from an Accelerator-produced Off-axis Muon Neutrino Beam. *Phys. Rev. Lett.*, 107:041801, 2011.

[520] P. Adamson et al. First measurement of muon-neutrino disappearance in NOvA. *Phys. Rev.*, D93(5):051104, 2016.

[521] P. Adamson et al. First measurement of electron neutrino appearance in NOvA. *Phys. Rev. Lett.*, 116(15):151806, 2016.

[522] Alexandre B. Sousa. First MINOS+ Data and New Results from MINOS. *AIP Conf. Proc.*, 1666:110004, 2015.

[523] Sanjib Kumar Agarwalla, Yee Kao, Debashis Saha, and Tatsu Takeuchi. Running of Oscillation Parameters in Matter with Flavor-Diagonal Non-Standard Interactions of the Neutrino. *JHEP*, 11:035, 2015.

[524] Michael E. Peskin and Daniel V. Schroeder. *An Introduction to quantum field theory.* 1995.

[525] Edward Witten. An SU(2) Anomaly. *Phys. Lett.*, B117:324–328, 1982.